

**NM1 - 57**

**PART 36**

**PERMIT**

**APPLICATION**

**Volume III Part 4**

**November 7, 2013**

**APPLICATION FOR PERMIT  
DNCS ENVIRONMENTAL SOLUTIONS**

**VOLUME III: ENGINEERING DESIGN AND CALCULATIONS  
SECTION 6: GEOSYNTHETICS APPLICATION AND  
COMPATIBILITY DOCUMENTATION**

**ATTACHMENT III.6.F  
PVC PIPE REFERENCE DOCUMENTATION**

## PVC Chemical Resistance

KEY — E = Excellent    G = Good    L = Limited    U = Unsuitable    O = No test

Chemical	PVC I		PVC II		Chemical	PVC I		PVC II	
	72°F.	140°F.	72°F.	140°F.		72°F.	140°F.	72°F.	140°F.
Acetaldehyde	U	U	U	U	Beet - Sugar Liquor	E	E	E	E
Acetamide	O	O	U	U	Benzaldehyde	U	U	U	U
Acetate Solvents - Crude	U	U	U	U	Benzene	U	U	U	U
Acetate Solvents - Pure	U	U	U	U	Benzenesulfonic Acid - 10%	E	E	E	E
Acetic Acid 0-10%	E	E	G	L	Benzenesulfonic Acid	U	U	U	U
Acetic Acid 10-20%	E	E	G	L	Benzoic Acid	E	E	E	E
Acetic Acid 20-30%	E	G	G	L	Benzol	U	U	U	U
Acetic Acid 30-60%	E	E	G	L	Bismuth Carbonate	E	E	E	E
Acetic Acid 80%	G	L	L	L	Black Liquor (Paper Industry)	E	E	E	E
Acetic Acid - Glacial	G	U	L	U	Bleach - 12.5% Active Cl <sub>2</sub>	E	G	G	L
Acetic Acid - Vapors	E	U	U	U	Borax	E	E	E	E
Acetic Anhydride	U	U	U	U	Borax Liquors	E	E	E	E
Acetone	U	U	U	U	Boric Acid	E	E	E	E
Acetylene	L	L	U	U	Boron, TriFluoride	E	E	E	E
Adipic Acid	E	E	E	E	Breeder Pellets - Fish Deriv.	E	E	E	E
Alcohol - Allyl - 96%	G	L	L	U	Brine	E	E	E	E
Alcohol - Amyl	E	L	L	U	Bromic Acid	E	E	E	E
Alcohol - Butyl	E	G	L	U	Bromine - Liquid	U	U	U	U
Alcohol - Ethyl	E	E	L	G	Bromine (Gas) - 25%	U	U	U	U
Alcohol - Methyl	E	E	E	E	Bromine - Water	E	E	L	U
Alcohol - Propargyl	E	E	E	E	Butadiene	E	E	E	E
Alcohol - Propyl	E	E	E	G	Butane	E	E	E	E
Allyl - Chloride	U	U	U	U	Butane, Butylene	E	E	E	E
Alum	E	E	E	E	Butane, Diol	E	E	E	E
Alum, Ammonium	E	E	E	E	Butanol	E	U	U	U
Alum, Chrome	E	E	E	E	Butanol - Primary	E	E	U	U
Alum, Potassium	E	E	E	E	Butanol - Secondary	E	L	U	U
Aluminum Chloride	E	E	E	E	Butter milk	E	E	E	E
Aluminum Fluoride	E	E	E	E	Butyl Acetate	U	U	U	U
Aluminum Hydroxide	E	E	E	E	Butyl Phenol	E	U	L	U
Aluminum Oxychloride	E	E	E	E	Butylene	E	O	E	O
Aluminum Nitrate	E	E	E	E	Butynediol (Erthritol)	E	U	U	U
Aluminum Sulfate	E	E	E	E	Butyric Acid 20%	G	U	U	U
Ammonia - Dry Gas	E	E	E	E	Butyric Acid	E	U	L	U
Ammonia, Aqua (10%)	E	E	E	E	Calcium Bisulfide	E	E	E	E
Ammonia - Liquid	L	U	O	O	Calcium Bisulfite	E	E	E	E
Ammonium Acetate	E	E	E	E	Calcium Carbonate	E	E	E	E
Ammonium BiFluoride	E	E	E	E	Calcium Chlorate	E	E	E	E
Ammonium Carbonate	E	E	E	E	Calcium Chloride	E	E	E	E
Ammonium Chloride	E	E	E	E	Calcium Hydroxide	E	E	E	E
Ammonium Fluoride - 25%	E	L	U	U	Calcium Hypochlorite	E	E	E	E
Ammonium Hydroxide - 28%	E	E	E	E	Calcium Nitrate	E	E	E	E
Ammonium Metaphosphate	E	E	E	E	Calcium Oxide	E	E	E	U
Ammonium Monophosphate	E	E	E	E	Calcium Sulfate	E	E	E	E
Ammonium Nitrate	E	E	E	E	Cane Sugar Liquors	E	E	E	E
Ammonium Persulfate	E	E	E	E	Carbic Acid	E	U	E	U
Ammonium Phosphatel (Ammoniacal)	E	E	O	O	Carbon Bisulfide	U	U	U	U
Ammonium Phosphate - Neutral	E	E	E	E	Carbon Dioxide (Aqueous S.L.)	E	E	E	E
Ammonium Sulfate	E	E	E	E	Carbon Dioxide Gas (Wet)	E	E	E	E
Ammonium Sulfide	E	E	E	E	Carbon Monoxide	E	E	E	E
Ammonium Thiocyanate	U	U	U	U	Carbon Tetrachloride	L	U	U	U
Amyl Acetate	U	U	U	U	Carbonated Water	E	E	E	E
Amyl Chloride	U	U	U	U	Carbonic Acid	E	E	E	E
Aniline	U	U	U	U	Casein	E	E	E	E
Aniline Chlorohydrate	U	U	U	U	Castor Oil	E	E	E	E
Aniline Dyes	U	U	U	U	Caustic Potash	E	E	E	E
Aniline Hydrochloride	U	U	U	U	Caustic Soda	E	E	E	E
Anthraquinone	E	E	E	L	Cellosolve	G	L	L	U
Anthraquinonesulfonic Acid	E	E	E	E	Chloracetic Acid	E	E	E	E
Antimony Trichloride	E	E	E	E	Chloral Hydrate	E	E	E	E
Aqua Regia	E	L	U	U	Chloric Acid 20%	E	E	E	E
Arsenic Acid - 80%	E	G	U	G	Chlorinated Solvents	U	U	U	U
Arylsulfonic Acid	E	E	L	E	Chlorine (Dry)	E	L	L	L
Asphalt	E	E	E	E	Chlorine Gas (Moist)	G	L	L	L
Barium Carbonate	E	E	E	E	Chlorine Water	E	E	E	E
Barium Chloride	E	E	E	E	Chloroacetic Acid	E	E	E	E
Barium Hydroxide	E	E	E	E	Chlorobenzene	U	U	U	U
Barium Sulfate	E	E	E	E	Chlorobenzyl Chloride	U	U	U	U
Barium Sulfide	E	E	E	E	Chloro Form	U	U	U	U
Beer	E	E	E	E	Chlorosulfonic Acid (100%)	E	U	O	O
					Chrome Alum	E	E	E	E

# CertainTeed EI

Chemical	PVC I		PVC II		Chemical	PVC I		PVC II	
	72 °F.	140 °F.	72 °F.	140 °F.		72 °F.	140 °F.	72 °F.	140 °F.
Chromic Acid 10%	E	E	E	E	Gas - Natural (Wet)	E	E	E	E
Chromic Acid 25%	E	L	G	L	Gasoline (Leaded)	E	E	E	E
Chromic Acid 30%	E	L	G	L	Gasoline (unleaded)	E	E	E	E
Chromic Acid 40%	E	L	L	L	Gasoline - Refined	E	E	E	E
Chromic Acid 50%	E	L	L	L	Gasoline - Sour	E	E	E	E
Citric Acid	E	E	E	E	Gelatin	E	E	E	E
Coconut Oil	E	E	E	E	Glucose	E	E	E	E
Coke Oven Gas	E	E	E	E	Glycerine (Glycerol)	E	E	E	E
Copper Carbonate	E	E	E	E	Glycol	E	E	E	E
Copper Chloride	E	E	E	E	Glue	E	E	E	E
Copper Cyanide	E	E	E	E	Glycolic Acid 30%	E	E	E	E
Copper Fluoride	E	E	E	E	Green Liquor (Paper Industry)	E	E	E	E
Copper Nitrate	E	E	E	E	Heptane	E	G	L	U
Copper Sulfate	E	E	E	E	Hexane	E	L	L	U
Care Oils	E	E	E	E	Hexanol Tertiary	E	L	L	U
Corn Oil	E	E	E	E	Hydrobromic Acid - 20%	E	E	E	E
Corn Syrup	E	E	E	E	Hydrochloric Acid - 0-25%	E	G	E	E
Cottonseed Oil	E	E	E	E	Hydrochloric Acid - 25-40%	E	E	E	E
Cresol	U	U	U	U	Hydrocyanic Acid or				
Cresylic Acid 50%	U	U	L	U	Hydrogen Cyanide	E	E	E	E
Croton Aldehyde	U	U	U	U	Hydrofluoric Acid 4%	E	L	E	E
Crude Oil - Sour	E	E	E	E	Hydrofluoric Acid 10%	E	L	L	E
Crude Oil - Sweet	E	E	E	E	Hydrofluoric Acid 48%	E	L	L	E
Cuprous Chloride	E	E	E	E	Hydrofluoric Acid 60%	E	L	L	E
Cyclohexane	U	U	U	U	Hydrofluoric Acid 100%	G	L	L	E
Cyclohexanol	U	U	U	U	Hydrogen	E	E	E	E
Cyclohexanon	U	U	U	U	Hydrogen Peroxide - 30%	E	E	E	E
Demineralized Water	E	E	E	E	Hydrogen Peroxide - 50%	E	E	E	E
Dextrin	E	E	E	E	Hydrogen Peroxide - 90%	E	E	E	E
Dextrose	E	E	E	E	Hydrogen Sulfide - Aqueous			U	U
Diazo Salts	E	E	E	E	Solution	E	E	E	E
Diesel Fuels	E	E	E	E	Hydrogen Sulfide - Dry	E	E	E	E
Diethy Amine	U	U	U	U	Hydroquinone	E	E	E	E
Diethylphthalate	U	U	U	U	Hydroxylamine Sulfate	E	E	E	E
Disodium Phosphate	U	U	U	U	Hypochlorous Acid	E	E	E	E
Diethyl Ether	U	U	U	U	Hypo-(Sodium Thiosulfate)	E	E	E	E
Diglycolic Acid	E	E	E	E	Iodine	U	U	U	U
Dioxane - 1,4	O	O	O	O	Iodine (in Alcohol)	U	U	U	U
Divinyl Benzene	O	O	O	O	Iodine Solution (10%)	U	U	U	U
Drying Oil	O	O	O	O	Iodoform	O	O	O	O
Ethers	U	U	U	U	Isopropylalcohol	E	E	E	E
Ethyl Acetate	U	U	U	U	Jet Fuels, JP4 & JP5	E	E	E	E
Ethyl Acrylate	U	U	U	U	Kerosene	E	E	E	E
Ethyl Chloride	U	U	U	U	Ketones	U	U	U	U
Ethyl Ether	U	U	U	U	Kraft Liquor (Paper Industry)	E	E	E	E
Ethylene Bromide	U	U	U	U	Lacquer Thinners	L	U	L	U
Ethylene Chlorohydrin	U	U	U	U	Lactic Acid 28%	E	E	E	E
Ethylene Dichloride	U	U	U	U	Lard Oil	E	E	E	E
Ethylene Glycol	E	E	E	E	Lauric Acid	E	E	E	E
Ethylene Oxide	U	U	U	U	Lauryl Chloride	E	E	E	E
Fatty Acide	E	E	E	E	Lauryl Sulfate	E	E	E	E
Ferric Chloride	E	E	E	E	Lead Acetate	E	E	E	E
Ferric Nitrate	E	E	E	E	Lime Sulfur	E	E	E	E
Ferric Sulfate	E	E	E	E	Linoleic Acid	E	E	E	E
Ferrous Nitrate	E	E	E	E	Linseed Oil	E	E	E	E
Fish Solubles	E	E	E	E	Liquers	E	E	E	E
Flourine Gas - Dry	L	U	U	U	Liquors	E	E	E	E
Flourine Gas - Wet	L	U	U	U	Lithium Bromide	E	E	E	E
Fluoroboric Acid - 25%	E	E	E	E	Lubricating Oil	E	E	E	E
Fluorosilicic Acid	E	E	E	E	Machine Oil	E	E	E	E
Formaldehyde	E	G	G	L	Magnesium Carbonate	E	E	E	E
Food Products such as Milk, Buttermilk, Molasses, Salad Oils, Fruit	E	E	E	E	Magnesium Chloride	E	E	E	E
Formic Acid	E	U	E	U	Magnesium Citrate	E	E	E	E
Freon - 12	E	G	E	G	Magnesium Hydroxide	E	E	E	E
Fructose	E	E	E	E	Magnesium Nitrate	E	E	E	E
Fruit Pulps and Juices	E	E	E	E	Magnesium Sulfate	E	E	E	E
Fuel Oil (containing H <sub>2</sub> SO <sub>4</sub> )	E	E	E	E	Maleic Acid	E	E	E	E
Furfural	U	U	U	U	Malic Acid	E	E	E	E
Gallic Acid	E	E	E	E	Mercuric Chloride	E	E	G	G
Gas - Coke Oven	E	E	G	G	Mercuric Cyanide	E	E	G	G
Gas - Manufactured	U	U	U	U	Mercurous Nitrate	E	E	G	G
Gas - Natural (Dry)	E	E	E	E	Mercury	E	E	G	G

Chemical	PVC I		PVC II		Chemical	PVC I		PVC II	
	72 °F.	140 °F.	72 °F.	140 °F.		72 °F.	140 °F.	72 °F.	140 °F.
Methane	E	E	E	E	Photographic Solutions	E	E	E	E
Methyl Bromide	U	U	U	U	Phthalic Acid	O	O	O	O
Methyl Cellosolve	U	U	U	U	Picric Acid	U	U	U	U
Methyl Chloride	U	U	U	U	Plating Solutions:				
Methyl Chloroform	U	U	U	U	Brass	E	E	E	E
Methyl Ethyl Ketone	U	U	U	U	Cadium	E	E	E	E
Methyl Iso-Butyl Ketone	U	U	U	U	Chromium	E	E	E	E
Methyl Salicylate	E	E	E	E	Copper	E	E	E	E
Methyl Sulfate	E	E	E	E	Gold	E	E	E	E
Methyl Sulfonic Acid	E	E	E	E	Iron	E	E	E	E
Methyl Sulfuric Acid	E	E	E	E	Judium	E	E	E	E
Methylene Chloride	E	E	E	E	Lead	E	E	E	E
Milk	E	E	E	E	Nickel	E	E	E	E
Mineral Oils	E	E	E	E	Rhodium	E	E	E	E
*Mixed Acids (H <sub>2</sub> SO <sub>4</sub> & HNO <sub>3</sub> )	E	E	E	E	Silver	E	E	E	E
Molasses	E	E	E	E	Tin	E	E	E	E
Monoethanolamine	E	E	E	E	Zinc	E	E	E	E
Muriatic Acid	E	E	E	E	Potassium Acid Sulfate	E	E	E	E
Naptha	E	E	E	E	Potassium Aluminum Sulfate	E	E	E	E
Napthalene	U	U	U	U	Potassium Alum	E	E	E	E
Natural Gas, Dry & Wet	E	E	E	E	Potassium Antimonate	E	E	E	E
Nickel Acetate	E	E	E	E	Potassium Bicarbonate	E	E	E	E
Nickel Chloride	E	E	E	E	Potassium Bichromate	E	E	E	E
Nickel Nitrate	E	E	E	E	Potassium Bisulfite	E	E	E	E
Nickel Sulfate	E	E	E	E	Potassium Borate 1%	E	E	E	E
Nickel Sulphate	E	E	E	E	Potassium Borate	E	E	E	E
Nicotine	E	E	E	E	Potassium Bromate 10%	E	E	E	E
Nicotine Acid	E	E	E	E	Potassium Bromate	E	E	E	E
Nitric Acid Anhydrous	U	U	U	U	Potassium Bromide	E	E	E	E
Nitric Acid 10%	E	E	E	E	Potassium Carbonate	E	E	E	E
Nitric Acid 20%	E	E	E	E	Potassium Chlorate (ag)	E	E	E	E
Nitric Acid 35%	E	E	E	E	Potassium Chlorate	E	E	E	E
Nitric Acid 40%	E	E	E	E	Potassium Chloride	E	E	E	E
Nitric Acid 60%	E	E	E	E	Potassium Chromate (Aln)	E	E	E	E
Nitric Acid 68%	E	E	E	E	Potassium Chromate (Neut.)	E	E	E	E
Nitric Acid 70%	E	E	E	E	Potassium Chromate 40%	E	E	E	E
Nitric Acid 100%	E	E	E	E	Potassium Cuprocyanide	E	E	E	E
Nitric Acid, Red Fuming	U	U	U	U	Potassium Cyanide	E	E	E	E
Nitrobenzene	U	U	U	U	Potassium Dichromate 40%	E	E	E	E
Nitropropane	U	U	U	U	Potassium Dichromate	E	E	E	E
Nitrous Acid (10%)	E	E	E	E	Potassium Dichrom (Alkaline)	E	E	E	E
Nitrous Oxide	E	E	E	E	Potassium Dichrom (Neutral)	E	E	E	E
Oenol (Unsaturated Alcohol)	E	E	E	E	Potassium Diphosphate	E	E	E	E
Oil and Fats	E	E	E	E	Potassium Ferricyanide	E	E	E	E
Oleic Acid	E	E	E	E	Potassium Ferrocyanide	E	E	E	E
Oleum	U	U	U	U	Potassium Fluoride	E	E	E	E
Oxalic Acid	E	E	E	E	Potassium Hydroxide	E	E	E	E
Oxygen	E	E	E	E	Potassium Hypochlorite	E	E	E	E
Ozone	G	L	U	U	Potassium Iodide	E	E	E	E
Palmitic Acid 10%	E	E	E	E	Potassium Nitrate	E	E	E	E
Palmitic Acid 70%	E	E	E	E	Potassium Perborate	E	E	E	E
Paraffin	E	E	E	E	Potassium Perchlorate	E	E	E	E
Pentane	O	O	O	O	Potassium Perchlorite	E	E	E	E
Paracetic Acid 40%	E	E	E	E	Potassium Permanganate 10%	E	E	E	E
Perchloric Acid 10%	E	E	E	E	Potassium Permanganate 25%	G	L	U	U
Perchloric Acid 15%	E	E	E	E	Potassium Persulfate	E	E	E	E
Perchloric Acid 70%	E	E	E	E	Potassium Sulfate	E	E	E	E
Perchloroethylene	O	O	O	O	Potassium Sulfide	E	E	E	E
Petrolatum	E	E	E	E	Potassium Thiosulfate	E	E	E	E
Phenol	E	E	E	E	Propane	E	E	E	E
Phenol (90%)	L	U	U	U	Propylene Dichloride	U	U	U	U
Phenylhydrazine	U	U	U	U	Propylene Glycol	E	E	E	E
Phenylhydrazine Hydrochloride	E	U	L	U	Pyrogalllic Acid	O	O	O	O
Phosgene (Gas)	E	U	L	U	Rayon Coagulating Bath	E	E	E	E
Phosgene (Liquid)	E	U	L	U	Rachelle Salts	E	E	E	E
Phosphoric Acid 0-25%	E	E	E	E	Sea Water	E	E	E	E
Phosphoric Acid 25-50%	E	E	E	E	Salen's Acid (Aqueous)	O	O	O	O
Phosphoric Acid 50-75%	E	E	E	E	Salicylaldehyde	O	O	O	O
Phosphoric Acid - 85%	E	E	E	E	Salt Water	E	E	E	E
Phosphorous (Yellow)	E	E	E	E	Selenic Acid	E	E	E	E
Phosphorous (Red)	E	E	E	E	Sewage	E	E	E	E
Phosphorous Pentoxide	E	E	E	E	Sillicic Acid	E	E	E	E
Phosphorous Trichloride	E	E	E	E	Silver Cyanide	E	E	E	E
Photographic Chemicals	E	E	E	E	Silver Nitrate	E	E	E	E
					Silver Sulfate	E	E	E	E
					Soap Solution	E	E	E	E

\*Use PVC 1120

# CertainTeed

Chemical	PVC I		PVC II		Chemical	PVC I		PVC II	
	72°F.	140°F.	72°F.	140°F.		72°F.	140°F.	72°F.	140°F.
Soaps	E	E	E	E	Sulphuric Acid 50-75%	E	E	E	G
Sodium Acetate	E	E	E	E	Sulphuric Acid 75-90%	E	E	L	L
Sodium Alum	E	E	E	E	Sulphuric Acid 95%	E	G	U	U
Sodium Acid Sulfate	E	E	E	E	Sulphurous Acid	G	U	L	U
Sodium Aluminate	E	E	E	E	Tan Oil	E	E	E	E
Sodium Antimonate	E	E	E	E	Tannic Acid	E	E	E	E
Sodium Arsenite	E	E	E	E	Tanning Liquors	E	E	E	E
Sodium Benzoate	E	E	E	E	Tartaric Acid	E	E	E	E
Sodium Bicarbonate	E	E	E	E	Tetrachloroethane	O	O	O	O
Sodium Bisulfate	E	E	E	E	Tetraethyl Lead	E	G	G	L
Sodium Bisulfite	E	E	E	E	Tetrahydro Furane	U	U	U	U
Sodium Borate	E	E	E	E	Thionyl Chloride	U	U	U	U
Sodium Bromide	E	E	E	E	Tepineol	G	L	G	L
Sodium Carbonate (Soda Ash)	E	E	E	E	Tin Chloride	E	E	E	E
Sodium Chlorate	E	G	G	L	Titanium Tetrachloride	E	U	U	U
Sodium Chloride	E	E	E	E	Toluol or Toluene	U	U	U	U
Sodium Chlorite	E	E	O	O	Toxaphene (90%)	O	O	O	O
Sodium Cyanide	E	E	E	E	Tributyl Phosphate	U	U	U	U
Sodium Dichromate	E	E	E	E	Trichloroacetic Acid	E	E	E	E
Sodium Dichromate (Neutral)	E	E	E	E	Trichloroethylene	U	U	U	U
Sodium Ferricyanide	E	E	E	E	Tricresylphosphate	U	U	U	U
Sodium Ferrocyanide	E	E	E	E	Triethanolamine	E	E	G	G
Sodium Fluoride	E	E	E	E	Triethylamine	E	G	G	L
Sodium Hydroxide 10%	E	E	E	E	Trimethyl Propane	E	E	E	E
Sodium Hydroxide 15%	E	E	E	E	Trisodium Phosphate	E	E	E	E
Sodium Hydroxide 35%	E	E	E	E	Turpentine	E	E	E	U
Sodium Hydroxide 70%	E	E	O	O	Urea	E	E	E	E
Sodium Hydroxide (Satr)	E	E	E	E	Urine	E	E	E	E
Sodium Hypochlorite	E	E	E	E	Vegetable Oil	E	E	E	E
Sodium Iodide	E	E	E	E	Vinegar	E	E	E	U
Sodium Nitrate	E	E	E	E	Vinyl Acetate	U	U	U	U
Sodium Nitrite	E	E	E	E	Water - Acid Mine	E	E	E	E
Sodium Perborate	E	E	O	O	Water - Distilled	E	E	E	E
Sodium Peroxide	E	E	E	E	Water - Fresh	E	E	E	E
Sodium Phosphate	E	E	E	E	Water - Salt	E	E	E	E
Sodium Phosphate - Acid	E	E	E	G	Water - Sewage	E	E	E	E
Sodium Silicate	E	E	E	E	Whiskey	E	E	E	E
Sodium Sulfate	E	E	E	E	White Gasoline	E	E	E	E
Sodium Sulfide	E	E	E	E	White Liquor (Paper Industry)	E	E	E	E
Sodium Sulfite	E	E	E	E	Wines	E	E	E	E
Sodium Thiosulfate (Hypo)	E	E	E	E	Xylene or Xylol	U	U	U	U
Sour Crude Oil	E	E	E	E	Zinc Chloride	E	E	E	E
Stannic Chloride	E	E	E	E	Zinc Chromate	E	E	E	E
Stannous Chloride (50%)	E	E	E	E	Zinc Cyanide	E	E	E	E
Stannous Chloride	E	G	E	E	Zinc Nitrate	E	E	E	E
Starch	E	E	E	E	Zinc Sulfate	E	E	E	E
Stearic Acid	E	E	E	E	Mixtures of Acids:				
Stoddards Solvent	E	E	U	U	Nitric 15% -				
Sulfated Detergents	E	E	E	E	Hydrofluoric 4%	E	E	E	G
Sulfur	E	E	E	E	Sodium Dichromate 13% -				
Sulfur Dioxide Gas - Dry	E	E	E	E	Nitric Acid 16				
*Sulfur Dioxide Gas - Wet	E	L	U	U	Water 71%	E	E	E	G
Sulfur Trioxide	E	E	E	G					
Sulphur Dioxide - Liquid	G	U	L	U					
Sulphuric Acid 0-10%	E	E	E	G					
Sulphuric Acid 10-30%	E	E	E	G					
Sulphuric Acid 30-50%	E	E	E	G					

\*Use PVC 1120

This information has been obtained from reliable sources and can be used as a guide to assist in the proper application of PVC pipe. CertainTeed, however, cannot warrant its accuracy. It is suggested that you run your own tests for critical applications.

## Pipe & Plastics Group

CertainTeed Corporation  
P.O. Box 860  
Valley Forge, PA 19482  
(610) 341-6820  
(610) 341-6837 Fax

Code No. 40-10-29

Printed in U.S.A.  
0398

**APPLICATION FOR PERMIT  
DNCS ENVIRONMENTAL SOLUTIONS**

**VOLUME III: ENGINEERING DESIGN AND CALCULATIONS  
SECTION 7: TENSILE STRESS ANALYSIS**

**TABLE OF CONTENTS**

<b>Section No.</b>	<b>Title</b>	<b>Page</b>
1.0	INTRODUCTION .....	III.7-1
1.1	Description .....	III.7-1
2.0	DESIGN CRITERIA .....	III.7-1
3.0	CALCULATION OF TENSILE STRESSES IN GEOSYNTHETICS AND SIDESLOPE LINER STABILITY .....	III.7-3
4.0	CALCULATION OF TENSILE STRESSES IN GEOSYNTHETICS DUE TO EQUIPMENT LOADING .....	III.7-10
5.0	ANCHOR TRENCH PULLOUT ANALYSIS.....	III.7-12
5.1	Geonet – Double-Sided Textured Geomembrane Interface.....	III.7-13
6.0	GEOSYNTHETIC SLIPPAGE ANALYSIS.....	III.7-14

**LIST OF FIGURES**

<b>Figure No.</b>	<b>Title</b>	<b>Page</b>
III.7.1	SIDEWALL AND FLOOR LINER SYSTEM DETAIL .....	III.7-20
III.7.2	GEOSYNTHETIC FRICTION FORCES.....	III.7-21
III.7.3	SLIPPAGE ANALYSIS LOCATION.....	III.7-22
III.7.4	GEOSYNTHETIC SLIPPAGE ANALYSIS.....	III.7-23

**LIST OF TABLES**

<b>Table No.</b>	<b>Title</b>	<b>Page</b>
III.7.1	GEOSYNTHETIC INTERFACE FRICTION ANGLES AND ADHESION – SIDESLOPE NORMAL LOAD.....	III.7-4
III.7.2	GEOSYNTHETIC INTERFACE FRICTION ANGLES AND ADHESION – FLOOR NORMAL LOAD.....	III.7-4
III.7.3	GEOSYNTHETIC INTERFACE FRICTION ANGLES AND ADHESION – SIDESLOPE LINER SYTEM.....	III.7-5
III.7.4	GEOSYNTHETIC INTERFACE FRICTION ANGLES AND ADHESION – FLOOR LINER SYSTEM .....	III.7-5
III.7.5	SOILS INTERNAL FRICTION ANGLE AND COHESION.....	III.7-6

**APPLICATION FOR PERMIT  
DNCS ENVIRONMENTAL SOLUTIONS**

**VOLUME III: ENGINEERING DESIGN AND CALCULATIONS  
SECTION 7: TENSILE STRESS ANALYSIS**

III.7.6	TRANSLATIONAL FAILURE ANALYSIS.....	III.7-15
III.7.7	GEOSYNTHETIC SLIPPAGE ANALYSIS FACTOR OF SAFETY SUMMARY .....	III.7-18

**LIST OF ATTACHMENTS**

Attachment No.	Title
III.7.A	KOERNER, ROBERT M. 2005. <i>DESIGNING WITH GEOSYNTHETICS, 5<sup>TH</sup> EDITION</i> . NEW JERSEY: PEARSON PRENTICE HALL.
III.7.B	SHARMA, HARI D. AND LEWIS, SANGEETA, P. 1994. <i>WASTE CONTAINMENT SYSTEMS, WASTE STABILIZATION, AND LANDFILLS: DESIGN AND EVALUATION</i> . NEW YORK: JOHN WILEY AND SONS.
III.7.C	QIAN, XUEDE; KOERNER, ROBERT M.; AND GRAY, DONALD H. 2002. <i>GEOTECHNICAL ASPECTS OF LANDFILL DESIGN AND CONSTRUCTION</i> . NEW YORK: PRETENCE HALL.
III.7.D	CETCO® LINING TECHNOLOGIES, 2009. <i>BENTOMAT® GCL DIRECT SHEAR DATABASE (TR-114BM)</i>
III.7.E	KOERNER, ROBERT M. AND KOERNER, GEORGE R. 2007. <i>INTERPETATION(S) OF LABORATORY GENERATED INTERFACE SHEAR STRENGTH DATA FOR GEOSYNTHETIC MATERIALS WITH EMPHISIS ON THE ADHESION VALUE</i> . GRI WHITE PAPER #11. GEOSYNTHETICS INSTITUTE.
III.7.F	THIEL, RICHARD. <i>A TECHNICAL NOTE REGARDING INTERPRETATION OF COHESION (OR ADHESION) AND FRICTION ANGLE IN DIRECT SHEAR TESTS</i> . GEOSYNTHETICS, APRIL MAY 2009 VOLUME 27: PAGES 10-19.
III.7.G	THIEL, RICHARD. <i>PEAK VS RESIDUAL SHEAR STRENGTH FOR LANDFILL BOTTOM LINER STABILITY ANALYSES</i> . THIEL ENGINEERING, OREGON HOUSE, CA, USA.
III.7.H	BOWLES, JOSEPH E. 1977. <i>FOUNDATION ANALYSIS AND DESIGN, 2<sup>ND</sup> EDITION</i> . UNITED STATES: MCGRAW HILL BOOK COMPANY.
III.7.I	RICHARDSON, CLINTON P., PHD, PE. 2009. <i>MUNICIPAL LANDFILL DESIGN CALCULATIONS: AN ENTRY LEVEL MANUAL OF PRACTICE</i> . CALIFORNIA: UBUILDABOOK, LLC.
III.7.J	GSE LINING TECHNOLOGY, INC., <i>GSE HD TEXTURED PRODUCT DATA SHEET</i>

**APPLICATION FOR PERMIT  
DNCS ENVIRONMENTAL SOLUTIONS**

**VOLUME III: ENGINEERING DESIGN AND CALCULATIONS  
SECTION 7: TENSILE STRESS ANALYSIS**

**1.0 Introduction**

DNCS Environmental Solutions (DNCS Facility) is a proposed Surface Waste Management Facility for oil field waste processing and disposal services. The proposed DNCS Facility is subject to regulation under the New Mexico Oil and Gas Rules, specifically 19.15.36 NMAC, administered by the Oil Conservation Division (OCD). The Facility has been designed in compliance with 19.15.36 NMAC, and will be constructed and operated in compliance with a Surface Waste Management Facility Permit issued by the OCD. The Facility is owned by, and will be constructed and operated by, DNCS Properties, LLC.

**1.1 Description**

The DNCS site is comprised of a 562-acre  $\pm$  tract of land located south of NM 529 in portions of Section 31, Township 17 South, Range 33 East; and in the northern half of Section 6, Township 18 South, Range 33 East, Lea County, NM. A portion of the 562-acre tract is a drainage feature that will be excluded from development. The drainage feature includes a 500-ft setback and totals 67 acres  $\pm$ . The DNCS Facility will include two main components; a liquid oil field waste Processing Area (177 acres  $\pm$ ), and an oil field waste Landfill (318 acres  $\pm$ ); therefore the DNCS Facility comprises 495 acres  $\pm$ . Oil field wastes are anticipated to be delivered to the DNCS Facility from oil and gas exploration and production operations in southeastern NM and west Texas. The Site Development Plan provided in the **Permit Plans, Sheet 3**, identifies the locations of the Processing Area and Landfill facilities.

**2.0 DESIGN CRITERIA**

The liner system for the DNCS Landfill is designed to meet the requirements of the New Mexico Energy, Minerals and Natural Resource Department, Oil and Gas Rules (i.e., 19.15.36 NMAC). More specifically, 19.15.36.14.D.(1)(b) NMAC requires:

*“Liners shall be able to withstand projected loading stresses, settling and disturbances from overlying oil field waste, cover materials and equipment operations.”*

and further 19.15.36.14.D.(2)(b) NMAC requires:

*“Geosynthetic material the operator installs on a slope greater than 25 percent shall be designed to withstand the calculated tensile forces acting upon the material. The design shall consider the maximum friction angle of the geosynthetic with regard to a soil-geosynthetic or geosynthetic-geosynthetic interface and shall ensure that overall slope stability is maintained.”*

The interior (excavation) sideslopes of the DNCS Landfill are designed at 4H:1V, and the depth of waste is greater than 100 feet (ft). Tensile stresses in liner components were evaluated using guidelines provided in the following documents:

1. Koerner, Robert M. 2005. *Designing with Geosynthetics 5<sup>th</sup> Edition*. New Jersey: Pearson Prentice Hall (**Attachment III.7.A**).
2. Sharma, Hari D. and Lewis, Sangeeta, P. 1994. *Waste Containment Systems, Waste Stabilization and Landfills: Design and Evaluation*. New York: John Wiley and Sons (**Attachment III.7.B**).
3. Qian, Xuede; Koerner, Robert M.; and Gray, Donald H. 2002. *Geotechnical Aspects of Landfill Design and Construction*. New York: Prentice Hall (**Attachment III.7.C**).
4. CETCO<sup>®</sup> Lining Technologies, 2009. *Bentomat<sup>®</sup> GCL Direct Shear Database (TR-114BM)* (**Attachment III.7.D**).
5. Koerner, Robert M. and Koerner, George R. 2007. *Interpretation(s) of Laboratory Generated Interface Shear Strength Data for Geosynthetic Materials with Emphasis on the Adhesion Value*. GRI White Paper #11. Geosynthetic Institute (**Attachment III.7.E**).
6. Thiel, Richard. *A Technical Note Regarding Interpretation of Cohesion (or Adhesion) and Friction Angle in Direct Shear Tests*. Geosynthetics, April May 2009 Volume 27: Pages 10-19 (**Attachment III.7.F**).
7. Thiel, Richard. *Peak vs Residual Shear Strength for Landfill Bottom Liner Stability Analyses*. Thiel Engineering, Oregon House, CA, USA (**Attachment III.7.G**).
8. Bowles, Joseph E. 1977. *Foundation Analysis and Design, 2<sup>nd</sup> Edition*. United States: McGraw Hill Book Company (**Attachment III.7.H**).
9. Richardson, Clinton P., PhD., PE. 2009. *Municipal Landfill Design Calculations: An Entry Level Manual of Practice*. California: UBuildABook, LLC (**Attachment III.7.I**).
10. GSE Lining Technology, Inc., *GSE HD Textured Product Data Sheet* (**Attachment III.7.J**).

The liner design for the landfill sideslopes (**Figure III.7.1**), from top to bottom, consists of the following components below the waste:

- 24-inches (in.) protective soil layer (on-site soils)
- 60-mil double-sided textured high density polyethylene (HDPE) liner
- 200-mil geonet
- 60-mil double-sided textured HDPE liner
- Geosynthetic clay liner (GCL)
- 6-in. compacted subgrade

The liner design for the landfill floor (**Figure III.7.1**), from top to bottom, consists of the following components below the waste:

- 24-in. protective soil layer (on-site soils)
- 60-mil smooth HDPE liner
- 200-mil geonet
- 60-mil smooth HDPE liner
- Geosynthetic clay liner
- 6-in. compacted subgrade

### **3.0 CALCULATION OF TENSILE STRESSES IN GEOSYNTHETICS AND SIDESLOPE LINER STABILITY**

External shear forces will develop on the 4H:1V sideslopes assuming the placement of an initial 2-ft lift of protective soil, and 8-ft lift of waste; assuming the lifts are unsupported and no adhesion (**Attachment III.7.A**, **Attachment III.7.B**, **Attachment III.7.C** and **Attachment III.7.D**). The unbalanced forces, due to the assumed unsupported placement of the 2-ft protective soil layer and 10-ft waste layer, must be supported by the liner components above the interface with the least amount of frictional resistance. Based on the review of the six references listed in Section 2.0 above, **Tables III.7.1**, **III.7.2**, **III.7.3**, **III.7.4** and **III.7.5** present the interface friction angles and soil internal friction angles to be used to determine the tensile stresses in the geosynthetics that will be installed at the DNCS Landfill.

Interface friction angles ( $\Phi$ ) and adhesion (as determined by direct shear testing) for geosynthetics will vary depending on the normal load applied to the geosynthetics. For DNCS, the maximum normal load applied to the floor and sideslope varies. The interface friction angle and adhesion for the geosynthetic interfaces is determined for the sideslope and floor as follows:

**TABLE III.7.1**  
**Geosynthetic Interface Friction Angles and Adhesion – Sideslope Normal Load**  
**DNCS Environmental Solutions**

Normal Load	Thickness (ft)	Unit Weight (lbs/ft <sup>3</sup> )	Total Weight (lbs/ft <sup>2</sup> )	Range of Shear Testing Loads <sup>1</sup> per ASTM D 5321 (lbs/in <sup>2</sup> )
1. Final Cover Soil	3	110	330	0.25 (23.2) = 5.8 0.50 (23.2) = 11.6 1.0 (23.2) = 23.2
2. Intermediate Cover Soils	1	110	110	
3. Oil Field Waste <sup>2</sup>	37.5	74	2,775	
4. Protective Soil Layer	2	110	220	
Design Vertical Load:		Total:	3,435 lbs/ft <sup>2</sup> (23.9 lbs/in <sup>2</sup> )	
Design Normal Load: = [(23.9 lbs/in <sup>2</sup> ) (cos 14.04°)] = 23.2 lbs/in <sup>2</sup>		Total:	44.3 lbs/in <sup>2</sup>	5.8    11.6    23.2

Notes: 1. Shear testing loads based on ASTM D 5321 = 0.25 (maximum normal load); 0.5 (maximum normal load); 1.0 (maximum normal load)  
2. Oil field waste on the sideslope varies from 0 to approximately 75 feet in depth; averaging 37.5 feet at the centroid of the sideslope waste mass.

**TABLE III.7.2**  
**Geosynthetic Interface Friction Angles and Adhesion – Floor Normal Load**  
**DNCS Environmental Solutions**

Normal Load	Thickness (ft)	Unit Weight (lbs/ft <sup>3</sup> )	Total Weight (lbs/ft <sup>2</sup> )	Range of Shear Testing Loads <sup>1</sup> per ASTM D 5321 (lbs/in <sup>2</sup> )
1. Final Cover Soil	4	110	330	0.25 (87.6) = 21.9 0.50 (87.6) = 43.8 1.0 (87.6) = 87.6
2. Intermediate Cover Soils	1	110	110	
3. Oil Field Waste	160	74	11,840	
4. Protective Soil Layer	2	110	220	
Design Vertical/Normal Load:		Total:	12,610 lbs/ft <sup>2</sup> (87.6 lbs/in <sup>2</sup> )	21.9    43.8    87.6

Note: 1. Shear testing loads based on ASTM D 5321 = 0.25 (maximum normal load); 0.5 (maximum normal load); 1.0 (maximum normal load)

**TABLE III.7.3**  
**Geosynthetic Interface Friction Angles and Adhesion<sup>1</sup> – Sideslope Liner System**  
**DNCS Environmental Solutions**

Geosynthetic to Geosynthetic Interface	Normal Stresses (lbs/in <sup>2</sup> )	Mohr-Coulomb Failure Envelope <sup>2</sup>	
		$\Phi$	Adhesion
Protective Soil Layer (SM) <sup>2</sup> to Double-Sided Textured HDPE FML	Reference 1	26°	ND
HDPE Geonet to Double-Sided Textured HDPE FML	Reference 2	7.0° – 25° Assume $\frac{3}{4}$ = 20°	ND
Double-Sided Textured HDPE FML to Nonwoven Geotextile of GCL	Reference 2	15° - 32° Average = 24°	ND
Nonwoven Geotextile of GCL to Subgrade Soil (undrained)	5.8    11.6    23.2 Reference 4	24.3°	92 lbs/ft <sup>2</sup>

- Notes: 1. Values reported for  $\Phi$  and Adhesion are based on review of available literature and are used to predict the performance of the liner system. Site specific shear strength testing should be conducted using actual liner system components and soils specified by the Engineer for the facility prior to construction.
2. Geotechnical laboratory testing of on-site soils show predominately SP-SC soils within the top 35 feet. For the purposes of these calculations, it was assumed these soils would behave similar to SM soils.
3. As recommended in Reference 7, the values for  $\Phi$  and Adhesion (when available in the literature) represent “Residual Shear Strength” values.
4. ND = not determined

**TABLE III.7.4**  
**Geosynthetic Interface Friction Angles and Adhesion<sup>1</sup> – Floor Liner System**  
**DNCS Environmental Solutions**

Geosynthetic to Geosynthetic Interface	Normal Stresses (lbs/in <sup>2</sup> )	Mohr-Coulomb Failure Envelope <sup>2</sup>	
		$\Phi$	Adhesion
Protective Soil Layer (SM) to Smooth HDPE FML	Reference 1	18°	ND
HDPE Geonet to Smooth HDPE FML	Reference 2	5° – 19° Average = 12°	ND
Smooth HDPE FML to Nonwoven Geotextile of GCL	Reference 2	8° – 12° Average = 10°	ND
Nonwoven Geotextile of GCL to Subgrade Soil (undrained)	21.9    43.8    87.6 Reference 4	32°	61 lbs/ft <sup>2</sup>

- Notes: 1. Values reported for  $\Phi$  and Adhesion are based on review of available literature and are used to predict the performance of the liner system. Site specific shear strength testing should be conducted using actual liner system components and soils specified by the Engineer for the facility prior to construction.
2. Geotechnical laboratory testing of on-site soils show predominately SP-SC soils within the top 35 feet. For the purposes of these calculations, it was assumed these soils would behave similar to SM soils.
3. As recommended in Reference 6, the values for  $\Phi$  and Adhesion (when available in the literature) represent “Peak Shear Strength” values.
4. ND = not determined

**TABLE III.7.5**  
**Soils Internal Friction Angle and Cohesion<sup>1,2</sup>**  
**DNCS Environmental Solutions**

Material	Density	$\Phi$	Cohesion [Assumed]
Protective Soil Layer (Relative Density, Medium)	110 lbs/ft <sup>3</sup>	33°	0 lbs/ft <sup>2</sup>
Oil Field Stabilized Waste (Relative Density, Medium)	74 lbs/ft <sup>3</sup>	33°	0 lbs/ft <sup>2</sup>
Compacted Subgrade (Relative Density, Medium to Dense)	112 lbs/ft <sup>3</sup>	35°	0 lbs/ft <sup>2</sup>
Natural Foundation Soils (Relative Density, Medium to Dense)	110 lbs/ft <sup>3</sup>	35°	0 lbs/ft <sup>2</sup>

- Notes: 1. Values reported for  $\Phi$  and Cohesion are based on review of available literature and are used to predict the performance of the liner system. Site specific shear strength testing should be conducted on soils specified by the Engineer for the facility prior to construction.
2. Geotechnical laboratory testing of on-site soils show predominately SP-SC soils within the top 35 feet. For the purposes of these calculations, the values of  $\Phi$  are based on the “blow counts” recorded during the drilling of borings B-3 through B-5 (average range 27 – 45); and using information contained in Reference 8. No cohesion was assumed providing an additional factor of safety to these calculations.

Based on the sideslope liner system design, the interface with the least amount of frictional resistance occurs at the geonet to double-sided textured interface ( $\Phi = 20^\circ$ ) [Table III.7.3 as referenced in Attachment III.7.B, p. 149]. The unbalanced forces, due to the assumed unsupported oil field waste and protective soil layer, are based on the sideslope liner stability calculations presented in Reference 9; *Municipal Landfill Design Calculations: An Entry Level Manual of Practice* (Richardson, 2009) [Attachment III.7.I]:

Where given the following:

- $\beta$  = slope angle for 4H:1V sideslope = 14.04°
- $F_x$  = Shear forces that are equal to the product of the normal force ( $W_w \cos \beta$ ) and the tangent of the friction angle between the two neighboring materials.
- $W_w$  = Weight of Waste.
- $T_w$  = Friction force on edge of waste.
- $W_{net}$  = Net weight of waste acting upon the liner system ( $W_w - T_w$ )
- $h_{waste}$  = Height of waste layer = 10 ft
- $h_{soil}$  = Height of protective soil layer = 2 ft
- $\Phi_{waste}$  = Waste internal angle of friction = 33°
- $\Phi_{soil}$  = Soil Internal angle of friction = 33°

$$\begin{aligned} \text{Density of waste} &= 74 \text{ lbs/ft}^3 \\ \text{Density of protective soil} &= 110 \text{ lbs/ft}^3 \text{ dry density} \end{aligned}$$

**A. Determine weight of waste and protective soil layer on sideslope:**

Weight of waste and protective soil layer = [ ½ (base)(height)] x (density of material)]

$$W_{\text{waste/soil}} = 0.5 (h_{\text{waste}}) [(h_{\text{waste}})(\text{slope factor})] (\text{density of waste}) + 0.5 (h_{\text{soil}}) [(h_{\text{soil}})(\text{slope factor})] (\text{density of protective soil layer})$$

$$W_{\text{waste/soil}} = 0.5 (8 \text{ ft}) [(8 \text{ ft})(4)] (74 \text{ lbs/ft}^3) + 0.5 (2 \text{ ft}) [(2 \text{ ft})(4)] (110 \text{ lbs/ft}^3)$$

$$W_{\text{waste/soil}} = 9,472.0 \text{ lbs/ft} + 880 \text{ lbs/ft} = 10,352.0 \text{ lbs/ft}$$

**B. Determine friction force on edge of waste and protective soil layer:**

$$T_W = (K_o) (\sigma_v) (\tan (\Phi_{\text{waste}}) (h_{\text{lift}}) + (K_o) (\sigma_v) (\tan (\Phi_{\text{soil}}) (h_{\text{lift}}))$$

Where:

$$\begin{aligned} K_o &= 1 - \sin (\Phi_{\text{waste}}) = 1 - \sin (33^\circ) = 0.455 \\ K_o &= 1 - \sin (\Phi_{\text{soil}}) = 1 - \sin (33^\circ) = 0.455 \\ \sigma_v &= (0.5) (h_{\text{waste}}) (\text{density of waste}) = (0.5)(8 \text{ ft})(74 \text{ lbs/ft}^3) = 296 \text{ lbs/ft}^2 \\ \sigma_v &= (0.5) (h_{\text{soil}}) (\text{density of soil}) = (0.5)(2 \text{ ft})(110 \text{ lbs/ft}^3) = 110 \text{ lbs/ft}^2 \\ \Phi_{\text{waste}} &= \text{Internal friction angle of waste} = 33^\circ \\ \Phi_{\text{soil}} &= \text{Internal friction angle of protective soil} = 33^\circ \\ h_{\text{waste}} &= \text{height of lift of waste} = 8 \text{ ft} \\ h_{\text{soil}} &= \text{height of lift of soil} = 2 \text{ ft} \end{aligned}$$

$$T_W = (0.455)(296 \text{ lbs/ft}^2)(\tan (33^\circ)) (8 \text{ ft}) + (0.455)(110 \text{ lbs/ft}^2)(\tan (33^\circ)) (2 \text{ ft})$$

$$T_W = 699.7 \text{ lbs/ft} + 65.0 \text{ lbs/ft}$$

$$T_W = 764.7 \text{ lbs/ft}$$

**C. Net weight of waste and protective soil layer**

$$W_{\text{net}} = W_{\text{waste/soil}} - T_W$$

$$W_{\text{net}} = 9,472 \text{ lbs/ft} - 764.7 \text{ lbs/ft}$$

$$W_{\text{net}} = 8,707.3 \text{ lbs/ft}$$

**D. Determine weight force component**

$$N_A = (W_{\text{net}}) (\cos (\text{slope angle}))$$

Where  $N_A$  is the normal force perpendicular to the sideslope (**Figure III.7.2**)

$$N_A = 8,707.3 \text{ lbs/ft} (\cos 14.04^\circ)$$

$$N_A = 8,447.2 \text{ lbs/ft}$$

**E. Calculate shear forces on geosynthetics (Figure III.7.2)**

Determine friction forces:

1. Interface friction angle between protective soil layer and double-sided, textured HDPE FML and,  $\Phi = 26^\circ$ .

$$F_1 = N_A (\tan 26^\circ)$$

$$F_1 = 8,447.2 \text{ lbs/ft} (0.487)$$

$$F_1 = 4,113.8 \text{ lbs/ft}$$

2. Interface friction angle between double-sided textured HDPE and the geonet,  $\Phi = 20^\circ$

$$F_2 = N_A (\tan 20^\circ)$$

$$F_2 = 8,447.2 \text{ lbs/ft} (0.364)$$

$$F_2 = 3,074.8 \text{ lbs/ft}$$

$$\text{Geomembrane tension} = 4,113.8 \text{ lbs/ft} - 3,074.8 \text{ lbs/ft.}$$

$$\text{Geomembrane tension} = 1,039.0 \text{ lbs/ft} = 86.5 \text{ lbs/in.}$$

$F_1 > F_2$ , therefore the geomembrane is in tension.

The force difference must be carried by the geomembrane. The actual stress in the geomembrane is given by:

$$\sigma_{\text{actual}} = (F_1 - F_2)/t_{\text{geomembrane}}$$

$\sigma_{\text{actual}}$  = actual stress in geomembrane

$t_{\text{geomembrane}}$  = geomembrane thickness = 60 mil = 0.06in.

$$\sigma_{\text{actual}} = 86.5 \text{ lbs/in} / 0.06 \text{ in}$$

$$\sigma_{\text{actual}} = 1,441.7 \text{ lbs/in}^2$$

The factor of safety for the geomembrane against failure in tension is:

$$FS_{\text{geomembrane}} = \sigma_{\text{yield}} / \sigma_{\text{actual}}$$

The tensile stress in the 60-mil geomembrane is 1,441.7 lbs/ft. This positive value indicates that the 60-mil geomembrane is in tension. The strength at yield for the geomembrane is 126 lbs/in-width (**Attachment III.7.J**) which results in a 60-mil geomembrane yield stress ( $\sigma_{\text{yield}}$ ) of 2,100 lbs/in<sup>2</sup>. Therefore a geomembrane with a strength at yield of 126 lbs/in or greater will not be

adversely affected if a 8-ft lift of waste and 2-ft lift of PSL is placed on the sideslope as calculated below:

$$FS_{\text{geomembrane}} = 2,100 \text{ lbs/in}^2 / 1,441.7 \text{ lbs/in}^2$$

$$FS_{\text{geomembrane}} = 1.4$$

3.  $F_3 = F_2 = 3,074.8 \text{ lbs/ft}$  for static no-slip condition.

4. Interface friction angle between double-side textured HDPE FML and geonet,  $\Phi = 20^\circ$ .

$$F_4 = N_A (\tan 20^\circ)$$

$$F_4 = 8,447.2 \text{ lbs/ft (0.364)}$$

$$F_4 = 3,074.8 \text{ lbs/ft}$$

$$\text{Geonet tension} = 3,074.8 \text{ lbs/ft} - 3,074.8 \text{ lbs/ft}$$

$$\text{Geonet tension} = 0 \text{ lbs/ft} = 0 \text{ lbs/in.}$$

$$F_3 = F_4, \text{ therefore the geonet is not in tension.}$$

5.  $F_4 = F_5 = 3,074.8 \text{ lbs/ft}$  for static no-slip condition.

6. Interface friction angle between geonet and double-side textured HDPE FML,  $\Phi = 20^\circ$ .

$$F_6 = N_A (\tan 20^\circ)$$

$$F_6 = 8,447.2 \text{ lbs/ft (0.364)}$$

$$F_6 = 3,074.8 \text{ lbs/ft}$$

$$\text{Geomembrane tension} = 3,074.8 \text{ lbs/ft} - 3,074.8 \text{ lbs/ft}$$

$$\text{Geomembrane tension} = 0 \text{ lbs/ft} = 0 \text{ lbs/in.}$$

$$F_5 = F_6, \text{ therefore the geomembrane is not in tension.}$$

7.  $F_6 = F_7 = 3,074.8 \text{ lbs/ft}$  for static no-slip condition.

8. Interface friction angle between double-side textured HDPE FML and nonwoven geotextile of GCL,  $\Phi = 24^\circ$ .

$$F_8 = N_A (\tan 24^\circ)$$

$$F_8 = 8,447.2 \text{ lbs/ft (0.435)}$$

$$F_8 = 3,674.5 \text{ lbs/ft}$$

$$\text{Geomembrane tension} = 3,074.8 \text{ lbs/ft} - 3,674.5 \text{ lbs/ft}$$

$$\text{Geomembrane tension} = - 599.7 \text{ lbs/ft} = - 49.9 \text{ lbs/in.}$$

$$F_7 < F_8, \text{ therefore the geomembrane is not tension.}$$

9.  $F_8 = F_9 = 3,674.5$  lbs/ft for static no-slip condition.
10. Interface friction angle between nonwoven geotextile of GCL and subgrade soils,  $\Phi = 24.3^\circ$ .

$$F_{10} = N_A (\tan 24.3^\circ)$$

$$F_{10} = 8,447.2 \text{ lbs/ft (0.452)}$$

$$F_{10} = 3,818.1 \text{ lbs/ft}$$

$$\text{GCL tension} = 3,674.5 \text{ lbs/ft} - 3,818.1 \text{ lbs/ft}$$

$$\text{GCL tension} = - 143.6 \text{ lbs/ft} = - 11.9 \text{ lbs/in.}$$

$F_9 < F_{10}$  , therefore the GCL is not tension.

## F. Conclusion

The unbalanced forces due to the assumed unsupported placement of the 2-ft protective soil layer and 8-ft waste layer is supported by the 60-mil double-sided textured HDPE primary liner; the geosynthetics below the HDPE primary liner are not in tension. The stress in the primary geomembrane due to the unbalanced force is 1,441.7 lbs/in<sup>2</sup>; and provides a factor of safety of 1.4 against failure in tension.

## 4.0 CALCULATION OF TENSILE STRESSES IN GEOSYNTHETICS DUE TO EQUIPMENT LOADING

A Caterpillar D6E dozer or equivalent will be used to place the protective soil layer up the sideslope a sufficient distance to accommodate an approximate 8 ft lift of waste placed on the floor of the landfill. The maximum unsupported length of protective soil to accommodate this lift will be 33 ft for a 4H:1V sideslope. Parameters to be used in the analysis include:

- Unit weight of protective soil = 110 lbs/ft<sup>3</sup> Dry Density.
- Internal friction angle of protective soil = 33 degrees .
- Critical liner interface friction angle occurs between the HDPE Geonet and the double-sided textured HDPE liner = 20° (**Table III.7.3**).
- Equipment loading assuming a D6E dozer: (CAT Performance Handbook, Edition 29)
  - Weight = 32,000 lbs.
  - Track width = 22 in. = 1.83 ft.
  - Pressure distribution: Assume a 2H:1V distribution, therefore width acting on geomembrane = 9.83 ft.
- Tensile forces acting on Geomembrane:

- Protective soil layer,  $F_{\text{soil}}$
- D6E dozer,  $F_{\text{dozer}}$
- Total resisting forces:
  - Geonet interface friction,  $F_{\text{geonet}}$
  - Soil buttress friction at toe of slope,  $F_{\text{buttress}}$

The minimum interface friction angle for the liner system is 20° and occurs between the HDPE geonet and the double-sided textured geomembrane (**Table III.7.3**).

Tensile forces acting on geomembrane:

$$F_{\text{soil}} = h_{\text{lift}} (\text{unsupported slope length}) (\text{unit weight of protective soil}) (\sin (\text{slope angle}))$$

$$F_{\text{soil}} = (2 \text{ ft}) (33 \text{ ft}) (110 \text{ lbs/ft}^3) (\sin (14.04^\circ))$$

$$F_{\text{soil}} = 1,761.3 \text{ lbs/ft}$$

$$F_{\text{dozer}} = [0.5 (\text{dozer weight}) / (\text{width acting on geocomposite})] (\sin (14.04^\circ))$$

$$F_{\text{dozer}} = [0.5 (32,000 \text{ lbs}) / 9.83 \text{ ft}] (\sin (14.04^\circ))$$

$$F_{\text{dozer}} = [16,000 \text{ lbs} / 9.83 \text{ ft}] (0.243)$$

$$F_{\text{dozer}} = 395.5 \text{ lbs/ft}$$

Total tensile force acting on geocomposite = 1,761.3 lbs/ft + 395.5 lbs/ft = 2,156.8 lbs/ft

Total Resisting Forces acting on geomembrane:

$$F_{\text{geomembrane}} = (\text{Weight of protective soil} + \text{Weight of Dozer}) (\cos (\text{slope angle})) (\tan (\text{interface friction angle}))$$

$$F_{\text{geomembrane}} = [(2 \text{ ft}) (33 \text{ ft}) (110 \text{ lbs/ft}^3) + (16,000 \text{ lbs} / 9.83 \text{ ft})] (\cos 14.04^\circ) (\tan 20^\circ)$$

$$F_{\text{geomembrane}} = (7,260.0 \text{ lbs/ft} + 1,627.7 \text{ lbs/ft}) (0.97) (0.364)$$

$$F_{\text{geomembrane}} = 3,138.1 \text{ lbs/ft}$$

$$F_{\text{buttress}} = \left[ \frac{\cos (\text{internal friction angle of soil})}{\cos (\text{internal friction angle of soil} + \text{slope angle})} \right] \left[ \frac{(\text{Unit weight of soil}) (\text{thickness of soil})^2}{\sin 2 (\text{slope angle})} \tan (\text{internal friction angle of soil}) \right]$$

$$F_{\text{buttress}} = \left[ \frac{\cos (33^\circ)}{\cos (33^\circ + 14.04^\circ)} \right] \left[ \frac{(110 \text{ lbs/ft}^3 (2 \text{ ft})^2)}{\sin 2 (14.04^\circ)} \right] [\tan (33^\circ)]$$

$$F_{\text{buttress}} = [0.839 / 0.682] [440 \text{ lbs/ft} / 0.471] [0.649]$$

$$F_{\text{butress}} = [1.23] [934.2] [0.649]$$

$$F_{\text{butress}} = 745.7 \text{ lbs/ft}$$

Total resisting force acting on geomembrane = 3,138.1 lbs/ft + 745.7 lbs/ft = 3,883.8 lbs/ft

Tensile forces (2,156.8 lbs/ft) < Resisting forces (3,883.8 lbs/ft); therefore geomembrane is not in tension.

### Summary

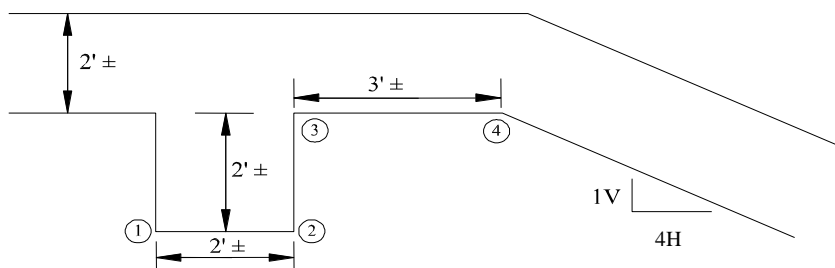
Tensile stress in the geomembrane = 2,156.8 lbs/ft – 3,883.8 lbs/ft = - 1,727.0 lbs/ft = - 143.9 lbs/in. The negative tensile stress indicates that the geocomposite is not in tension. Therefore, placing the protective soil layer 10 ft up the sideslope will not adversely impact the geomembrane.

### Conclusion

The tensile stress upon the geocomposite due to equipment loading is – 143.9 lbs/in. This value is less than the tensile (yield) strength for the geocomposite of 270 lbs/in, as previously referenced.

## 5.0 ANCHOR TRENCH PULLOUT ANALYSIS

Anchor trench configuration:



The anchor trench consists of extending the geosynthetics along the trench bottom to increase resistance force. In order to establish the static equilibrium equation, two imaginary and frictionless pulleys are assumed at the top edge and the bottom corner of the anchor trench (**Attachment III.7.C, page 111, Equation 4-28**). The friction force above a runout geosynthetic is always neglected in the anchor trench. Based on the calculation in Section 3.0, the primary geomembrane is in tension and, the interface friction angle between the geonet and the double-

sided textured geomembrane is the minimum interface friction angle of the liner system; therefore, any pull out will occur at this interface.

### 5.1 Geonet – Double-Sided Textured Geomembrane Interface

$\Sigma F_H = 0$  yields the following equation for the calculation of T (where T = geocomposite tensile force per unit width lbs/ft):

$$T = \frac{(\gamma_s)(d_{cs})(L_{ro})(\tan \delta_c) + [(1 - \sin \theta)((\gamma_s)(d_{cs} + 0.5d_{AT}))d_{AT} + \gamma_s(d_{cs} + d_{AT})L_{AT}](\tan \delta_c + \tan \delta_F)}{\cos \beta - (\sin \beta)(\tan \delta_c)}$$

Where:

- $\gamma_s$  = unit weight of cover and backfill soil = 110 lbs/cf dry density
- $d_{cs}$  = depth of cover soil = 2 ft
- $L_{ro}$  = runout length = 3 ft
- $\delta_c$  = friction angle between the geomembrane and underlying HDPE geonet = 20°
- $\theta$  = internal friction angle of compacted backfill soil in anchor trench = 35° (**Table III.7.5**)
- $d_{AT}$  = depth of anchor trench = 2 ft
- $L_{AT}$  = width of anchor trench = 2 ft
- $\delta_F$  = interface friction angle between the geomembrane and the compacted backfill soil = 26°
- $\beta$  = sideslope angle, measured from horizontal = 14.04°

$$T = \frac{(110 \text{ lbs/cf})(2')(3')(\tan 20^\circ) + [(1 - \sin 35^\circ)((110 \text{ lbs/cf})(2'+0.5(2'))(2') + 110 \text{ lbs/cf}(2'+2')2')](\tan 20^\circ + \tan 26^\circ)}{\cos 14.04^\circ - (\sin 14.04^\circ)(\tan 20^\circ)}$$

$$T = \frac{(240.2 \text{ lbs/ft}) + [(0.426)(110 \text{ lbs/cf})(3.0 \text{ ft})(2 \text{ ft}) + 110 \text{ lb/cf}(8 \text{ sf})](0.852)}{0.882}$$

$$T = \frac{240.2 \text{ lbs/ft} + [281.2 \text{ lbs/ft} + 880 \text{ lbs/ft}]0.852}{0.882}$$

$$T = \frac{240.2 \text{ lbs/ft} + 989.3 \text{ lbs/ft}}{0.882}$$

$$T = \frac{1,229.5 \text{ lbs/ft}}{0.882}$$

$$T = 1,394 \text{ lbs/ft} = 116.2 \text{ lbs/in}/0.06 \text{ in (Geomembrane Thickness)} = 1,936.7 \text{ lbs/in}^2$$

Ultimate Strength > Anchor Trench Resistance > Allowable Strength

Assume Allowable Strength = Ultimate Strength/Assumed Factor of Safety

Assumed Factor of Safety = 3

$2,100 \text{ lbs/in}^2 > 1,936.7 \text{ lbs/in}^2 > 700 \text{ lbs/in}^2$

The results indicate that the anchor trench, as designed, provides sufficient capacity such that the anchor trench capacity lies between the geomembrane yield stress and allowable stress.

## 6.0 GEOSYNTHETIC SLIPPAGE ANALYSIS

In order to determine the factor of safety for slippage and subsequent tension in the liner geosynthetics, the method of active and passive wedges developed by Qian et al. (2002) was used (**Attachment III.7.C, pg. 521**). This calculation utilizes the passive wedge that supports the active wedge on the sideslope, consistent with actual conditions in the field. These calculations were performed along the geomembrane covered slope shown on the cross section (**Figure III.7.3**). To be conservative, the lowest interface friction angles (residual strength values) for the sideslope liner system; and peak strength values for the floor liner system were used. These values taken from **Table III.7.3** are  $\delta_A = 20^\circ$ , for the interface friction angle between the geonet and double-sided textured HDPE geomembrane on the sideslope; and  $\delta_P = 10^\circ$  for the interface friction angle between the geonet and smooth HDPE geomembrane on the floor. The total height of the active wedge is the maximum height of waste over the sloped portion of liner system.

For the purposes of this calculation, the following assumptions and nomenclature (**Table III.7.6**) were used from the literature (**Attachment III.7.C, pg. 521**):

**TABLE III.7.6**  
**Translational Failure Analysis**  
**DNCS Environmental Solutions**

$W_P =$	total weight of the passive wedge
$N_P =$	normal force acting on the bottom of the passive wedge
$F_P =$	Frictional force acting on the bottom of the passive wedge ( parallel to the bottom of the passive wedge)
$E_{HP} =$	normal force from the active wedge acting on the passive wedge
$E_{VP} =$	frictional force acting on the side of the passive wedge
$FS_P =$	Factor of safety for the passive wedge
$\delta_P =$	Minimum interface friction angle of multi-layer liner components beneath the passive wedge = $10^\circ$ (assumed interface friction angle between the geotextile of the GCL and the smooth HDPE geomembrane, from <b>Table III.7.4</b> )
$\Phi_S =$	friction angle of the solid waste = $33^\circ$
$\alpha =$	angle of the waste slope, measured from horizontal
$\theta =$	angle of the landfill cell subgrade, measured from horizontal = $1.15^\circ$
$W_A =$	weight of the active wedge
$W_T =$	total weight of active and passive wedges
$N_A =$	normal force acting on the bottom of the active wedge
$F_A =$	Frictional force acting on the bottom of the active wedge (parallel to the bottom of the active wedge)
$E_{HA} =$	normal force from the active wedge acting on the active wedge, $E_{HA} = E_{HP}$
$E_{VA} =$	frictional force acting on the side of the active wedge, $E_{VA} = E_{VP}$
$FS_A =$	factor of safety for the active wedge
$b =$	Horizontal length of the Active Wedge (cell sideslope at its maximum depth) = 200 ft
$b_p =$	Horizontal length of the Passive Wedge = 285 ft
$h_t =$	Total Height of the Wedges = 95 ft
$\delta_A =$	minimum interface friction angle of multi-layer liner components beneath the active wedge = $20^\circ$ ( <b>Table III.7.3</b> )
$\beta =$	angle of sideslope, measured from the horizontal = $14.04^\circ$
$FS =$	factor of safety for the entire solid waste mass

**Figure III.7.4** also shows measured values for  $b$ ,  $b_p$ , and  $h_t$ .

The active wedge is considered first:

$$W_A = \frac{1}{2}((b * h_a * \gamma) + (b * h_b * \gamma))$$

$$W_A = \frac{1}{2} \left( 200 \text{ ft} * 45 \text{ ft} * 74 \left( \frac{\text{lbs}}{\text{ft}^3} \right) + 200 \text{ ft} * 50 \text{ ft} * 74 \left( \frac{\text{lbs}}{\text{ft}^3} \right) \right) = 703,000 \frac{\text{lbs}}{\text{ft}}$$

The passive wedge is then considered by multiplying the cross sectional area by the unit weight of waste.

$$W_P = \frac{1}{2}(b_P * h_t * \gamma) = W_P = \frac{1}{2} \left( 285 \text{ ft} * 95 \text{ ft} * 74 \left( \frac{\text{lbs}}{\text{ft}^3} \right) \right) = 1,001,775 \frac{\text{lbs}}{\text{ft}}$$

$$W_T = 703,000 \frac{\text{lbs}}{\text{ft}} + 1,001,775 \frac{\text{lbs}}{\text{ft}} = 1,704,775 \frac{\text{lbs}}{\text{ft}}$$

From **Attachment III.7.C, equation 13.62, pg. 524**, is used to determine the factor of safety.

$$aFS^3 + bFS^2 + cFS + d = 0$$

Where:

$$\begin{aligned} a &= W_A \sin \beta \cos \theta + W_P \cos \beta \sin \theta \\ b &= (W_A \tan \delta_P + W_P \tan \delta_A + W_T \tan \varphi_s) \sin \beta \sin \theta - (W_A \tan \delta_A + W_P \tan \delta_P) \cos \beta \cos \theta \\ c &= - [W_T \tan \varphi_s (\sin \beta \cos \theta \tan \delta_P + \cos \beta \sin \theta \tan \delta_A) + (W_A \cos \beta \sin \theta + W_P \sin \beta \cos \theta) \tan \delta_A \tan \delta_P] \\ d &= W_T \cos \beta \cos \theta \tan \delta_A \tan \delta_P \tan \varphi_s \end{aligned}$$

and:

$$\begin{aligned} \beta &= 14.04^\circ - \text{sideslope angle; } \sin 14.04^\circ = 0.243, \cos 14.04^\circ = 0.970 \\ \theta &= 1.15^\circ - \text{subgrade angle; } \sin 1.15^\circ = 0.020, \cos 1.15^\circ = 1.000 \\ \delta_P &= 10^\circ - \text{minimum friction angle of bottom liner system; } \tan 10^\circ = 0.176 \\ \delta_A &= 20^\circ - \text{minimum friction angle of sideslope liner system; } \tan 20^\circ = 0.364 \\ \varphi_s &= 33^\circ - \text{friction angle of waste; } \tan 33^\circ = 0.649 \end{aligned}$$

Compute values for a, b, c and d:

$$a = W_A \sin \beta \cos \theta + W_P \cos \beta \sin \theta$$

$$a = 703,000 \text{ lbs/ft} (0.243)(1.000) + 1,001,775 \text{ lbs/ft} (0.970)(0.020)$$

$$a = 170,829 \text{ lbs/ft} + 19,434.4 = 190,263.4 \text{ lbs/ft}$$

$$b = (W_A \tan \delta_P + W_P \tan \delta_A + W_T \tan \phi_s) \sin \beta \sin \theta - (W_A \tan \delta_A + W_P \tan \delta_P) \cos \beta \cos \theta$$

$$b = [703,000 \text{ lbs/ft } (0.176) + 1,001,775 \text{ lbs/ft } (0.364) + 1,704,775 \text{ lbs/ft } (0.649)] (0.243)(0.020) - [703,000 \text{ lbs/ft } (0.364) + 1,001,775 \text{ lbs/ft } (0.176)] (0.970) (1.000)$$

$$b = 1,594,773.1 \text{ lbs/ft } (0.243)(0.020) - 432,204.4 \text{ lbs/ft } (0.970)(1.000)$$

$$b = 7,750.6 \text{ lbs/ft} - 419,238.3 \text{ lbs/ft} = - 411,487.7 \text{ lbs/ft}$$

$$c = - [W_T \tan \phi_s (\sin \beta \cos \theta \tan \delta_P + \cos \beta \sin \theta \tan \delta_A) + (W_A \cos \beta \sin \theta + W_P \sin \beta \cos \theta) \tan \delta_A \tan \delta_P]$$

$$c = - [1,704,775 \text{ lbs/ft } (0.649) [(0.243)(1.000)(0.176) + (0.970)(0.020)(0.364)] + [703,000 \text{ lbs/ft } (0.970)(0.020) + 1,001,775 \text{ lbs/ft } (0.243)(1.000)] (0.364)(0.176)]$$

$$c = - [1,704,775 \text{ lbs/ft } (0.649)[0.0428 + 0.0071] + [(13,638.2 \text{ lbs/ft} + 243,431.3 \text{ lbs/ft}) (0.364)(0.176)]]$$

$$c = - [1,106,399 \text{ lbs/ft } [0.0499] + [257,069.5 \text{ lbs/ft } (0.364)(0.176)]]$$

$$c = - [55,209.3 \text{ lbs/ft} + 16,468.9 \text{ lbs/ft}]$$

$$c = - 71,678.2 \text{ lbs/ft}$$

$$d = W_T \cos \beta \cos \theta \tan \delta_A \tan \delta_P \tan \phi_s$$

$$d = 1,704,775 \text{ lbs/ft } (0.970)(1.000)(0.364)(0.176)(0.649)$$

$$d = 68,753.9 \text{ lbs/ft}$$

$$aFS^3 + bFS^2 + cFS + d = 0$$

$$190,263.4 FS^3 - 411,487.7 FS^2 - 71,678.2 FS + 68,468.9 = 0$$

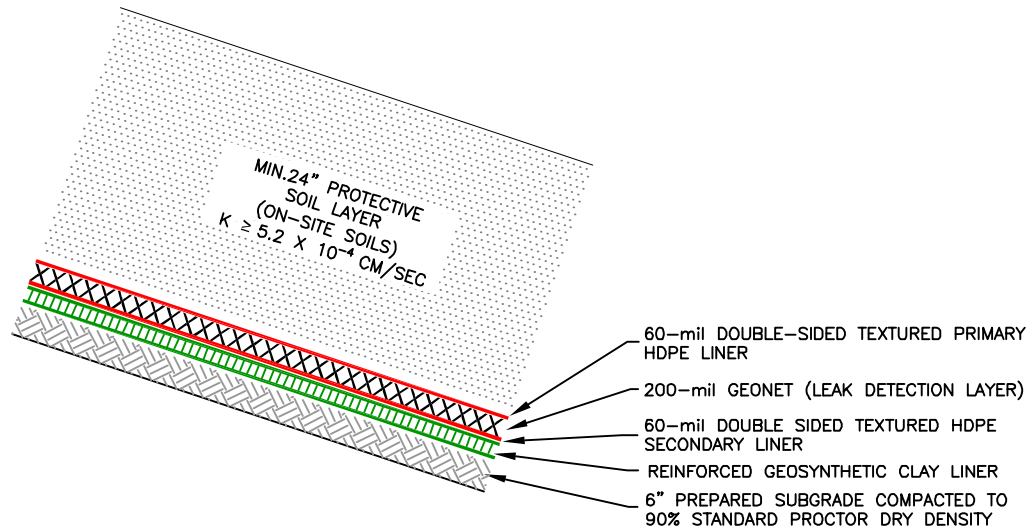
$$190,263.4 FS^3 + 68,468.9 = 411,487.7 FS^2 + 71,678.2 FS$$

This equation is then solved by trial and error as provided in **Table III.7.7**.

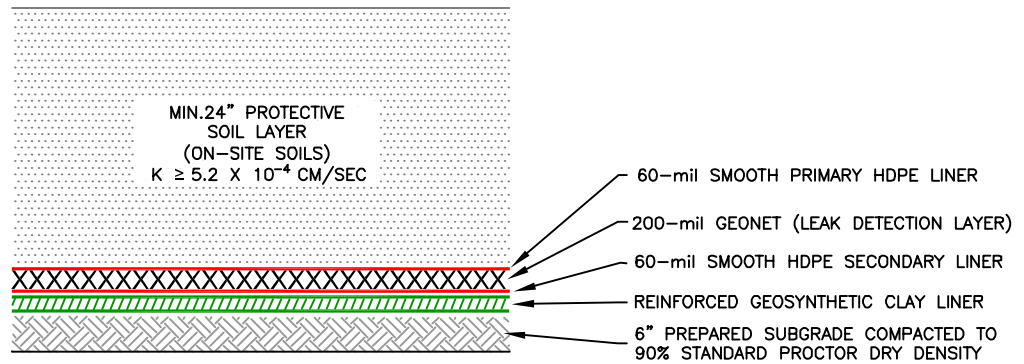
**TABLE III.7.7**  
**Geosynthetic Slippage Analysis Factor of Safety Summary**  
**DNCS Environmental Solutions**

<b>Assumed FS</b>	<b>190,263.4 FS<sup>3</sup> + 68,468.9</b>	<b>411,487.7 FS<sup>2</sup>+ 71,678.2 FS</b>	<b>Closure</b>
(1)	(2)	(3)	(2) – (3)
2.0	1,590,576.10	1,789,307.20	-198,731.10
2.5	3,041,334.53	2,750,993.63	290,340.90
2.3	2,383,403.69	2,341,629.79	41,773.90
2.2	2,094,393.58	2,149,292.50	-54,898.92
2.25	2,235,687.94	2,244,432.43	-8,744.49
2.27	2,293,995.68	2,283,064.48	10,931.20

The factor of safety against translational geosynthetic failure considering active and passive soil wedges is 2.26, which indicates that the passive wedge will more than adequately support the active wedge on the sideslopes without slipping and the geosynthetic liner system is not in tension. Therefore, the proposed liner system design is compatible with calculated external forces.



SIDEWALL LINER SYSTEM



FLOOR LINER SYSTEM

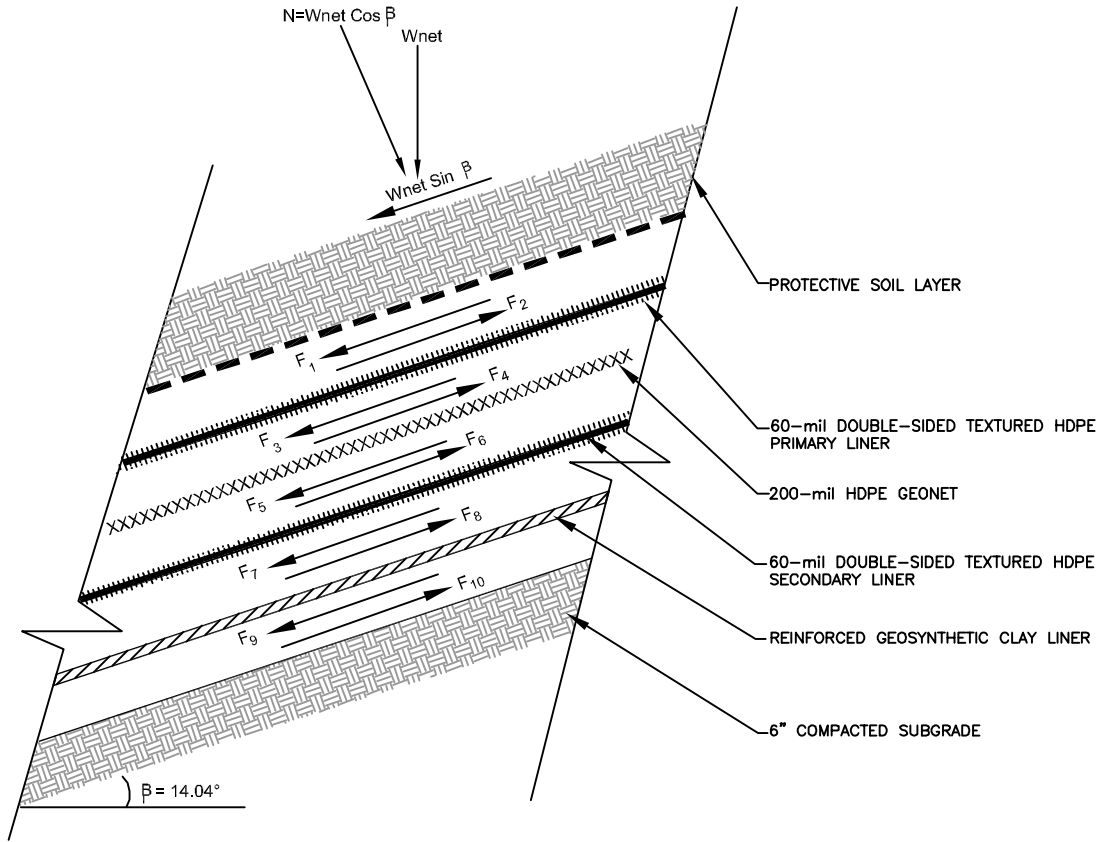
## SIDEWALL AND FLOOR LINER SYSTEM DETAIL

DNCS ENVIRONMENTAL SOLUTIONS  
LEA COUNTY, NEW MEXICO



Gordon Environmental, Inc.  
Consulting Engineers

213 S. Camino del Pueblo  
Bernalillo, New Mexico, USA  
Phone: 505-867-6990  
Fax: 505-867-6991



**FREE BODY DIAGRAM**

NOT TO SCALE

**GEOSYNTHETIC  
 FRICTION FORCES**  
 DNCS ENVIRONMENTAL SERVICES  
 LEA COUNTY, NEW MEXICO



Gordon Environmental, Inc.

Consulting Engineers

213 S. Camino del Pueblo  
 Bernalillo, New Mexico, USA  
 Phone: 505-867-6990  
 Fax: 505-867-6991

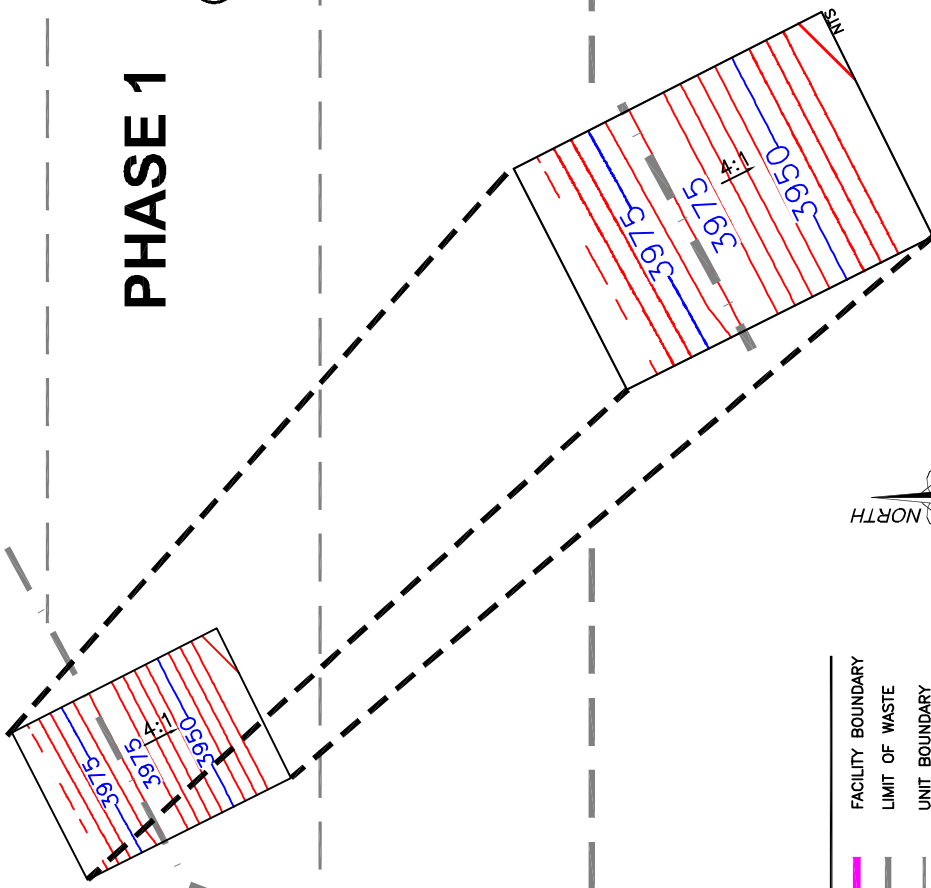
DATE: 10/22/2013	CAD: FRICTION.dwg	PROJECT #: 542.01.01
DRAWN BY: DMI	REVIEWED BY: MRH	FIGURE III.7.2
APPROVED BY: IKG	gei@gordonenvironmental.com	

UNIT 1  
(13.5 ACRES±)

**PHASE 1**

UNIT 2  
(19.8 ACRES±)

UNIT 3  
(22.2 ACRES±)



- LEGEND**
- FACILITY BOUNDARY
  - LIMIT OF WASTE
  - UNIT BOUNDARY



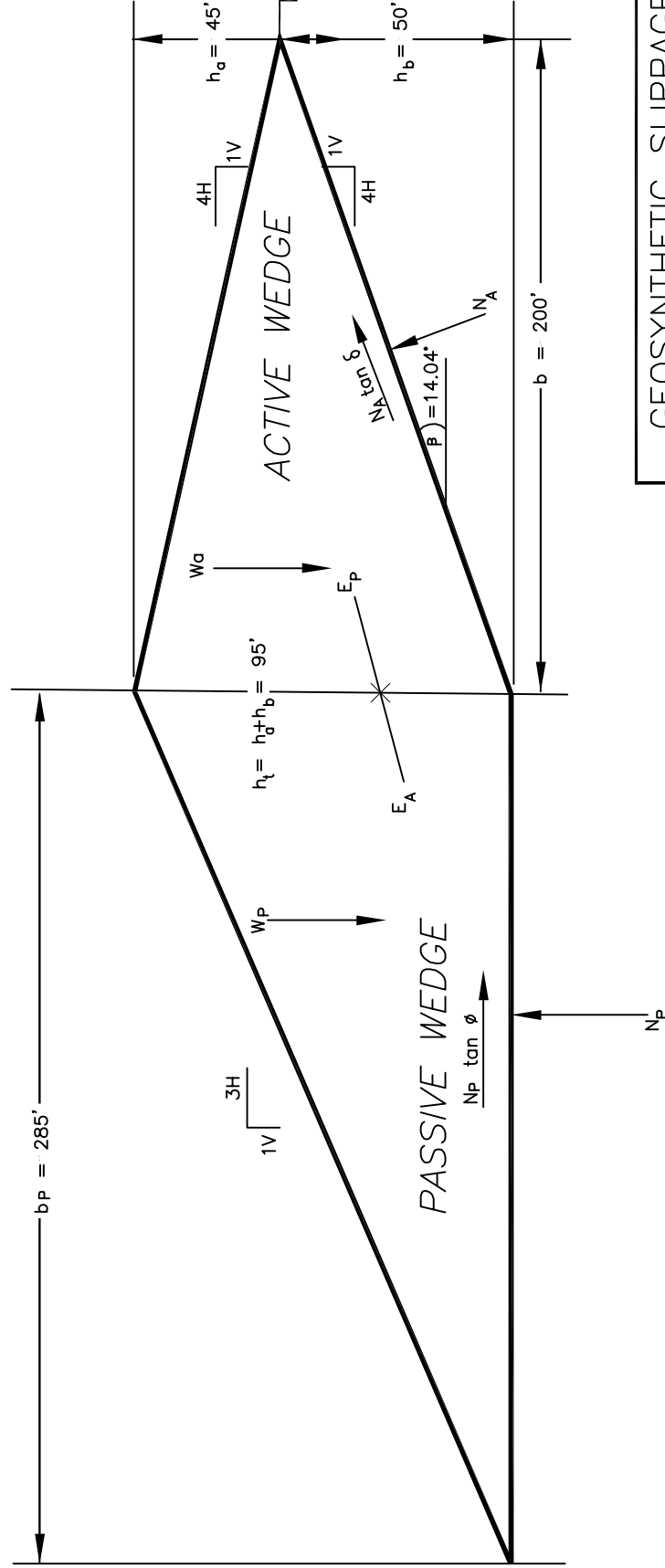
**SLIPPAGE ANALYSIS  
LOCATION**

DNCS ENVIRONMENTAL SOLUTIONS  
LEA COUNTY, NEW MEXICO

Gordon Environmental, Inc.  
*Consulting Engineers*

213 S. Camino del Pueblo  
Bernalillo, New Mexico, USA  
Phone: 505-867-6900  
Fax: 505-867-6991

DATE: 10/29/2013	CAD: SLIP.dwg	PROJECT #: 542.01.01
DRAWN BY: DMI	REVIEWED BY: GEI	<b>FIGURE III.7.3</b>
APPROVED BY: IKG	gei@gordonenvironmental.com	



# GEOSYNTHETIC SLIPPAGE ANALYSIS

DNCS ENVIRONMENTAL SOLUTIONS  
LEA COUNTY, NEW MEXICO



213 S. Camino del Pueblo  
Bernalillo, New Mexico, USA  
Phone: 505-867-6990  
Fax: 505-867-6891

DATE: 10/29/2013	CAD: GEO ANALYSIS.dwg	PROJECT #: 542.01.01
DRAWN BY: DMI	REVIEWED BY: MRH	FIGURE III.7.4
APPROVED BY: IKG	gkelt@gordonenvironmental.com	

NO SCALE

DrawingPath:acad 2003\542.01.01\PERMIT FIGURES\GEO ANALYSIS.dwg  
Date/Time:Oct. 29, 2013-15:27:12  
Copyright © All Rights Reserved, Gordon Environmental, Inc. 2013

**APPLICATION FOR PERMIT  
DNCS ENVIRONMENTAL SOLUTIONS**

**VOLUME III: ENGINEERING DESIGN AND CALCULATIONS  
SECTION 7: TENSILE STRESS ANALYSIS**

**ATTACHMENT III.7.A**

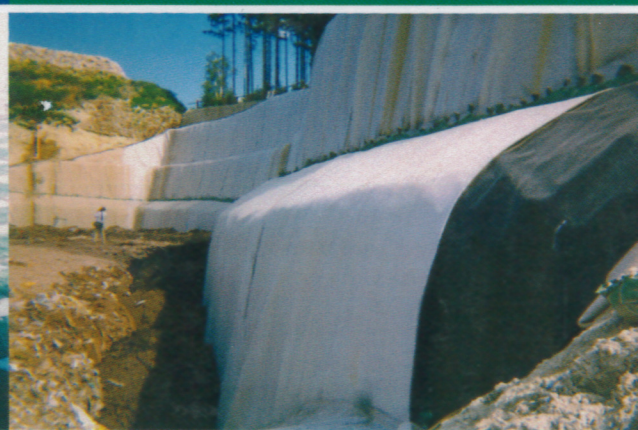
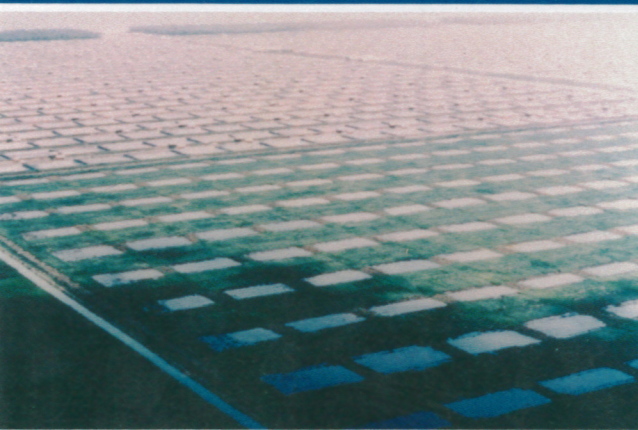
**KOERNER, ROBERT M. 2005.**

***DESIGNING WITH GEOSYNTHETICS, 5<sup>th</sup> EDITION***

**NEW JERSEY: PEARSON PRENTICE HALL.**

# DESIGNING WITH GEOSYNTHETICS

FIFTH EDITION



ROBERT M. KOERNER

**TABLE 5.7** PEAK FRICTION VALUES AND EFFICIENCIES OF VARIOUS GEOSYNTHETIC INTERFACES\*

<b>(a) Soil-to-Geomembrane Friction Angles</b>						
Geomembrane	Soil type					
	Concrete Sand ( $\phi = 30^\circ$ )		Ottawa Sand ( $\phi = 28^\circ$ )		Mica Schist Sand ( $\phi = 26^\circ$ )	
HDPE						
Textured	30°	(100%)	26°	(92%)	22°	(83%)
Smooth	18°	(56%)	18°	(61%)	17°	(63%)
PVC						
Rough	27°	(88%)	—	—	25°	(96%)
Smooth	25°	(81%)	—	—	21°	(79%)
CSPE-R	25°	(81%)	21°	(72%)	23°	(87%)

<b>(b) Geomembrane-to-Geotextile Friction Angles</b>					
Geotextile	Geomembrane				
	HDPE		PVC		CSPE-R
	Textured	Smooth	Rough	Smooth	Undulating
Nonwoven needle-punched	32°	8°	23°	21°	15°
Nonwoven heat-bonded	28°	11°	20°	18°	21°
Woven monofilament	19°	6°	11°	10°	9°
Woven slit-film	32°	10°	28°	24°	13°

<b>(c) Soil-to-Geotextile Friction Angles</b>						
Geotextile	Soil type					
	Concrete Sand ( $\phi = 30^\circ$ )		Ottawa Sand ( $\phi = 28^\circ$ )		Mica Schist Sand ( $\phi = 26^\circ$ )	
Nonwoven needle-punched	30°	(100%)	26°	(92%)	25°	(96%)
Nonwoven heat-bonded	26°	(84%)	—	—	—	—
Woven monofilament	26°	(84%)	—	—	—	—
Woven slit-film	24°	(77%)	24°	(84%)	23°	(87%)

\*Efficiency percentages (in parentheses) are based on Equations (5.8) at (5.9).

Source: Extended from Martin et al. [18].

harder geomembranes being the lowest. A much more extensive and recent paper is by Narejo and Koerner [19].

The frictional behavior of geomembranes placed on clay soils is of considerable importance for composite liners containing solid or liquid wastes. The current requirements are for the clay to have a hydraulic conductivity equal to or less than  $1 \times 10^{-7}$  cm/s and for the geomembrane to be placed directly upon the clay. While an indication of the shear strength parameters has been investigated (e.g., Narejo and Koerner [19] and Koerner et al. [20]), the data are so sensitive to the variables discussed

**APPLICATION FOR PERMIT  
DNCS ENVIRONMENTAL SOLUTIONS**

**VOLUME III: ENGINEERING DESIGN AND CALCULATIONS  
SECTION 7: TENSILE STRESS ANALYSIS**

**ATTACHMENT III.7.B**

**SHARMA, HARI D. AND LEWIS, SANGEETA, P. 1994.  
*WASTE CONTAINMENT SYSTEMS, WASTE STABILIZATION,  
AND LANDFILLS: DESIGN AND EVALUATION.*  
NEW YORK: JOHN WILEY AND SONS.**

---

# WASTE CONTAINMENT SYSTEMS, WASTE STABILIZATION, AND LANDFILLS: DESIGN AND EVALUATION

---

**HARI D. SHARMA, Ph.D, P.E.**

Chief Engineer and Director  
EMCON Associates  
San Jose, California

**SANGETTA P. LEWIS, P.E.**

Project Manager  
CH<sub>2</sub>M Hill  
Oakland, California



A Wiley-Interscience Publication

**JOHN WILEY & SONS, INC.**

New York / Chichester / Toronto / Brisbane / Singapore

stress cracking may occur. The recommended elongation for shear test acceptance is greater than 50 percent (Rollin et al., 1991; Giroud and Peggs, 1990; Carlson et al., 1993).

Destructive testing procedures other than shear and peel tests are available to evaluate geomembrane seams, although their use has not yet been widely accepted. Several researchers (Peggs and Charron, 1989; Rollin et al., 1989, 1991; Halse et al., 1991b; Carlson et al., 1993) have suggested the use of microtomes (microscopic evaluation of thin geomembrane sections) to evaluate possible initiation of stress cracking in seams. Another reported method is impact testing (Rollin et al., 1993).

Geomembrane seams may also be tested using nondestructive test methods. These test methods do not measure the seam strength, but rather, detect whether holes exist in the seams. The most commonly used methods are the vacuum test, pressure test, and copper wire spark test. The vacuum test procedure involves placing a soapy solution over a seam approximately 1 to 2 feet in length. A vacuum box with a clear viewing window is placed over the seam length and a vacuum pressure of approximately 5 psi is applied. If a stream of soap bubbles is detected through the viewing window, a leak exists and must be repaired.

Pressure tests can be performed only on double-wedge weld seams. These tests are performed by sealing both ends of an unobstructed double-wedge weld length and then applying approximately 30 psi of air pressure in the channel between the welds through a fine needle. A pressure gage is attached to the needle, and the pressure is monitored for approximately 5 minutes. A reduction in pressure greater than 2 psi during the 5-minute period usually indicates that air is escaping through a leak in the seam. This leak must be located and repaired. In the copper wire spark test, a copper wire is welded into the seam. A current is passed through the copper wire, and any sparks indicate that a hole is present.

## 3.2 GEOTEXTILES

### 3.2.1 Types and Functions

Geotextiles are synthetic fabrics used in geotechnical engineering for various applications. The majority of geotextiles are composed of polypropylene or polyester fibers; a small percentage are composed of polyamide or polyethylene. Among the geosynthetics, geotextiles appear to have the most associated terminology and the widest ranging properties. This is due in part to the numerous types of fibers and geotextile manufacturing processes.

The types of fibers used in the manufacture of geotextiles include monofilament, staple, and slit<sup>20</sup> film. If fibers are twisted or spun together, they are known as a yarn. Monofilament fibers are created by extruding molten polymer through an apparatus containing several small-diameter holes, known as a spinnaret. The extruded polymer strings are then cooled and stretched to align the polymers and give

<sup>20</sup>Slit-film fibers are also known as split-film fibers.

the fiber increased strength. Staple fibers are also manufactured by extruding polymer through a spinnaret; however, the extruded strings are twisted together and cut into 1- to 4-inch lengths. The staple fibers are then spun into longer fibers known as staple yarns. Finally, slit-film fibers are manufactured by extruding a continuous sheet of polymer and cutting it into fibers by knives or lanced air jets. Slit-film fibers are rectangular in cross section rather than the circular cross sections of the monofilament and staple fibers.

The fibers or yarns are formed into geotextiles using either woven or nonwoven (spunbonded) methods. Woven geotextiles are formed using traditional weaving methods and a variety of weave types. Common terminology associated with woven geotextiles include machine direction, cross machine direction, selvage, warp, and weft. The machine direction refers to the direction in the plane of fabric parallel to the direction of manufacture, and conversely, the cross machine direction refers to the direction in the plane of fabric perpendicular to the direction of manufacture. The machine direction is also known as the warp, since warp yarns are those yarns placed lengthwise on the weaving loom; and the cross machine direction is known as the weft, since weft yarns are woven between and perpendicular to the warp yarns. The selvage is the finished area on both sides of the geotextile width that prevents the yarns from unraveling.

To create nonwoven geotextiles, the manufactured fibers are placed and oriented on a moving conveyor belt. The fibers are bonded by needle punching, melt bonding, or resin bonding. The needle-punching process consists of pushing numerous barbed needles through the fiber web. The fibers are thus mechanically interlocked into a stable configuration. As the name implies, the melt bonding process consists of melting and pressurizing fibers together at their crossover points. In resin bonding, an acrylic resin is applied to the fiber web to form the geotextile.

In waste containment facilities, geotextiles are most commonly used for filtration, separation, reinforcement, cushioning, and drainage. A relatively new application for geotextiles is an alternative daily cover over refuse. Typically, nonwoven geotextiles are used in waste containment facilities for filtration, separation, cushioning, and drainage. Woven geotextiles are usually used for reinforcement. Both woven and nonwoven geotextiles may be used for alternative daily cover.

### 3.2.2 Material Properties

As with geomembranes, there are numerous tests that may be performed on geotextiles. However, geotextiles have numerous different applications where geomembranes are used almost exclusively as a barrier material. In developing geotextile specifications, it is important that the designer understand the material tests and specify material properties important for the geotextiles' intended use. The following sections therefore indicate the geotextile application for which the material test is significant. Index or quality control tests are also discussed.

The material properties generally specified for waste containment system applications are thickness, mass per unit area, uniaxial tensile strength, multiaxial tensile strength, puncture resistance, trapezoid tear strength, apparent opening size, per-

mittivity, transmissivity, and ultraviolet resistance. In specifying geotextile material properties, the designer should be aware that many reported material properties and test methods were borrowed from the textile industry. Many tests are therefore more applicable to evaluating fabric for clothing rather than for engineering fabrics. Most geotextile properties reported by manufacturers are index or quality control tests and are not intended for engineering design. Hopefully, as further research on geotextiles is performed, material tests to evaluate engineering properties will be developed.

*Thickness (ASTM D 177,<sup>21</sup> D 5199).* The average thickness of a geotextile is measured using a thickness gage under a gradually applied, specified pressure. The pressure to be applied depends on the material type. For geotextiles, a pressure of approximately 0.3 psi is typically used. The thickness of a geotextile alone is generally not critical for design. It is, however, related to other material properties, such as mass per unit area, tensile strength, puncture resistance, and tear resistance. Thickness is also important if the geotextile is used for cushioning and in calculating permeability coefficients.

*Mass per Unit Area (ASTM D 5261<sup>22</sup>).* The mass per unit area of a geotextile is determined by weighing several test specimens of known area, taken from various locations of the fabric sample. The calculated values are averaged to obtain the mean mass per unit area of the sample. Geotextiles, especially nonwoven geotextiles, are commonly referred to by an abbreviated form of their mass per unit area. For example, a nonwoven geotextile that is 8 ounces per square yard is commonly referred to as an 8-ounce geotextile. Although this is obviously incorrect, the problem is not as much in the terminology as it is in specifying the mass per unit area as a design value. Many specifiers attribute a certain mass per unit area to a certain set of mechanical and hydraulic properties, such as puncture resistance, tear resistance, apparent opening size, and tensile strength. While the mass per unit area is related to these properties, there is not a direct correlation. Therefore, geotextiles with a mass per unit area of 8 oz/yd<sup>2</sup> can have widely varying mechanical and hydraulic properties. A certain mass per unit area may be required, however, if the geotextile is to be used as a cushion.

*Uniaxial Tensile Strength (ASTM D 4632,<sup>23</sup> D 4595<sup>24</sup>).* The uniaxial tensile strength of geotextiles is measured in a tensile testing machine by applying a continually increasing load along the longitudinal length of a specimen. The specimen is grasped within clamps, specially designed to prevent slippage (Figure 3.33). The distance between clamps (called the gage dimension) and the specimen dimensions

<sup>21</sup> ASTM D 1777: Standard Method for Measuring Thickness of Textile Materials.

<sup>22</sup> ASTM D 5261: Standard Test Method for Measuring Mass per Unit Area of Geotextiles.

<sup>23</sup> ASTM D 4632: Standard Test Method for Breaking Load and Elongation of Geotextiles (Grab Method).

<sup>24</sup> ASTM D 4595: Standard Test Method for Tensile Properties by the Wide-Width Strip Method.

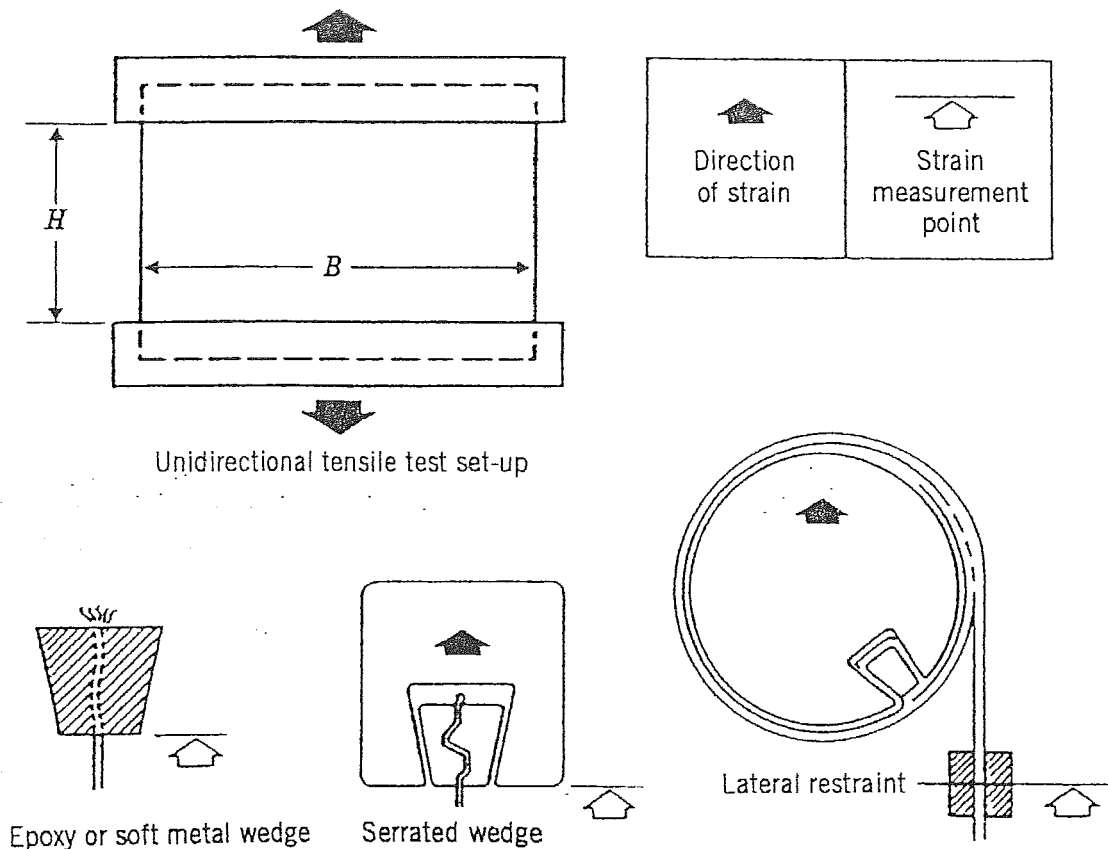


Figure 3.33 Clamping systems for uniaxial tension test. (From Myles, 1987.)

are standardized. While the test values typically reported are the breaking load (reported in pounds) and apparent elongation (reported as a percentage increase in length), a load elongation curve or a stress-strain curve can also be produced (Figure 3.34). The stress-strain curve is generated by dividing the load by the width and thickness of the geotextile specimen. Since the thickness of the geotextile typically decreases as tensile load is applied and is also variable throughout the specimen, the "stress" is often reported as the load divided by the specimen width (in lb/in.). This curve is important in assessing geotextile strength, particularly for strain compatibility in soil reinforcement applications.

Researchers throughout the world have studied the factors affecting the uniaxial tensile strength of geotextiles (Shrestha and Bell, 1982; Moritz and Murray, 1982; Richards and Scott, 1986; Rowe and Ho, 1986; Cazzuffi et al., 1986; Myles, 1987; deGroot et al., 1990; Anjiang et al., 1990; Wayne et al., 1993). These factors include specimen size, aspect ratio (width-to-length ratio), stain rates, gage length, clamping conditions, fabric type and construction, and anisotropic conditions. This research has led to the standardization of uniaxial tension testing procedures and the following general trends:

- The breaking force per unit width measured in a uniaxial tensile test is not affected significantly by the sample width (Moritz and Murray, 1982; Shrestha and Bell, 1982; Richards and Scott, 1986; Rowe and Ho, 1986; Cazzuffi et

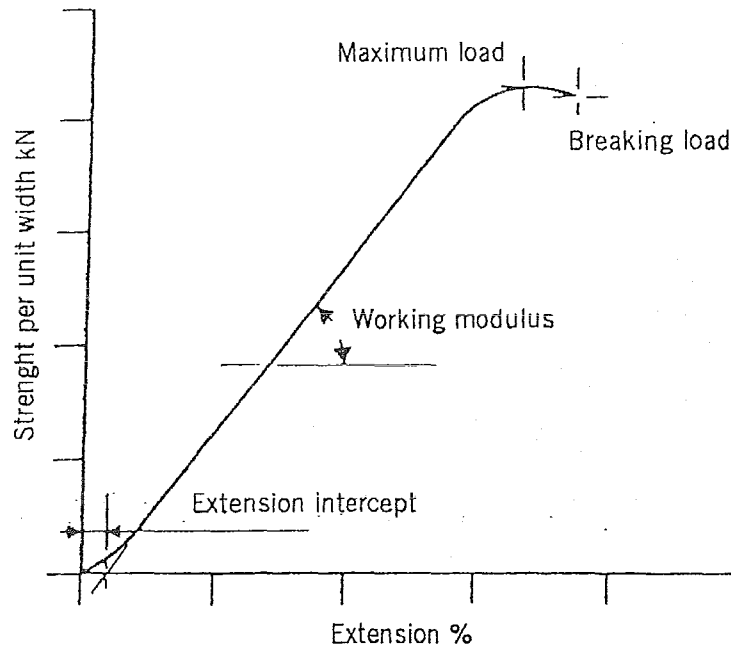


Figure 3.34 Strength per unit width versus extension curve for uniaxial tension test. (From Myles, 1987.)

al., 1986; Wayne et al., 1993) but may be influenced by the gage length<sup>25</sup> (Shrestha and Bell, 1982; Richards and Scott, 1986; Montalvo and Sickler, 1993).

- Depending on the type of geotextile, the modulus and elongation properties may vary with specimen width and gage length (Shrestha and Bell, 1982; Rowe and Ho, 1986; Richards and Scott, 1986; Wayne et al., 1993).
- Both woven and nonwoven geotextiles show anisotropic behavior. The anisotropic behavior in woven geotextile is expected due to the machine and cross directions. For nonwoven geotextiles, anisotropy is due to potential fluctuations and irregularity in the manufacturing process (Novais-Ferreira and Quarasma, 1982; Richards and Scott, 1986; Cazzuffi et al., 1986).
- Fabric structure has a significant influence on the stress-stain behavior. Woven and heat-bonded geotextiles show high strength and modulus and low elongation; needle-punched geotextiles have low strength and modulus and high elongation (Moritz and Murray, 1982; Shrestha and Bell, 1982; Richards and Scott, 1986).

Standard test methods have been developed for uniaxial geotextile tensile testing. The two commonly used standards include the grab (ASTM D 4632) and wide-width (ASTM D 4595) methods. The strip test is also often used and reported in the literature. Figure 3.35 shows various tensile test specimen sizes.

The strip and grab tensile tests utilize procedures originally established for the

<sup>25</sup>The gage length is defined as the length of the specimen between clamps.

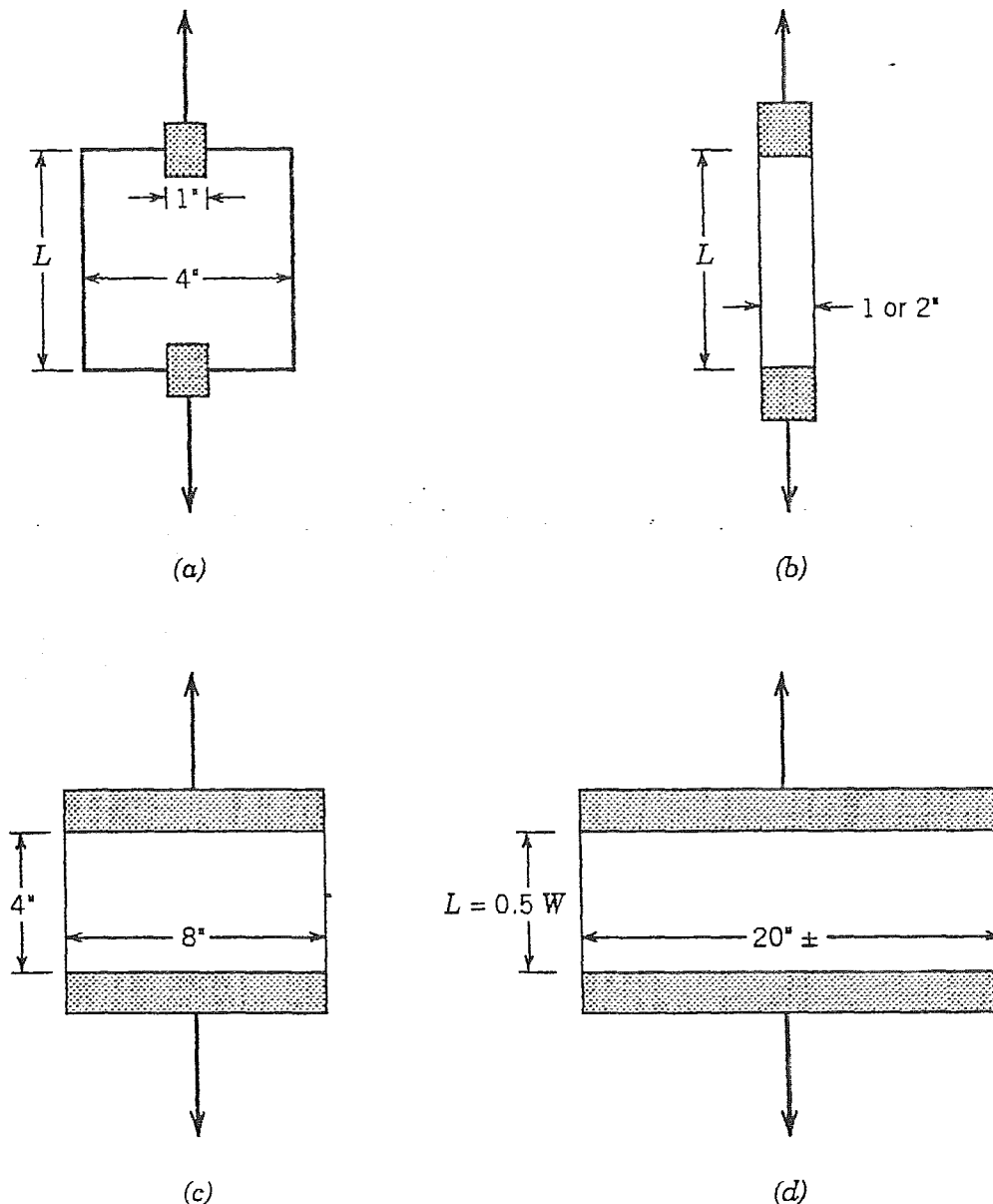


**Figure 3.35** Various tensile test specimen sizes: (a) ASTM D4632 grab; (b) "narrow" strip; (c) ASTM D4595 wide width; (d) very wide width. (From Koerner, 1990.)

textile industry. The *strip tensile test* is typically performed on a 1- to 2-inch-wide specimen. As the tensile load is applied to this specimen, the specimen necks in its central region. These edge effects have significant influence on the tensile strength. In the *grab tensile test*, as shown in Figure 3.35, the clamps holding the specimen do not hold the entire width of the specimen. The grab method measures the "effective strength" of the geotextile, that is, the strength of the material in a specific width, together with the additional strength contributed by adjacent material. Both the grab and strip tests are useful as quality control or acceptance tests but have limited usefulness for design. Table 3.9 presents a range of typical grab tensile strength values for some nonwoven geotextiles.

The recommended tensile test for design is the *wide-width tensile test*, ASTM D 4595. This test was developed specifically for geotextiles and uses an 8-inch-wide

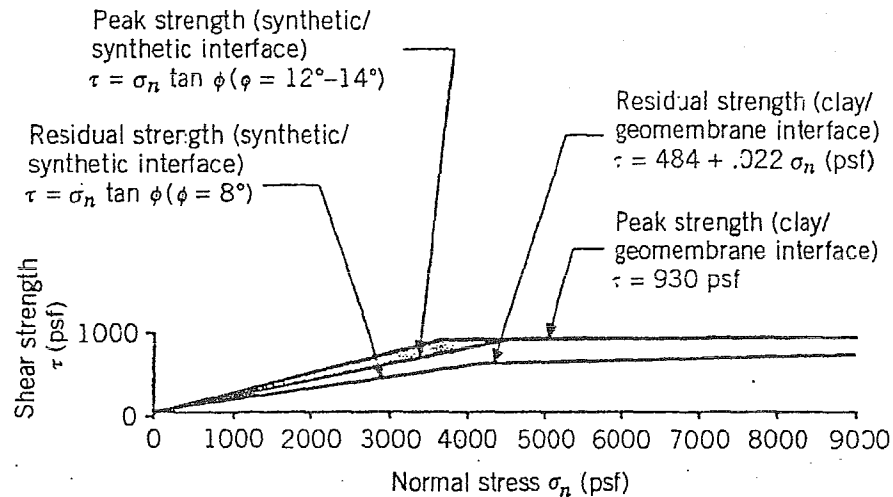


Figure 3.61 Liner strength relations. (From Byrne et al., 1992. Reproduced by permission of ASCE.)

1987; Soil and Material Engineers, 1987; Leach et al., 1987; Koutsourais et al., 1990; Swan et al., 1990; O'Rourke et al., 1990; Mitchell et al., 1990; Ojeshina, 1990; Druschel and O'Rourke, 1991; Somasundaram and Khilnani, 1991; Sharma and Hullings, 1993). The results are highly variable due to the large range of soil types and testing conditions. Both peak and residual values are included within the reported range. Table 3.14 also includes recommended soil geomembrane interface strengths.

As shown in Figure 3.61, the interface strength of clay–geomembrane exhibits a linear shear strength ( $\tau$ ) and normal stress ( $\sigma_n$ ) relationship at lower normal stresses. The interface friction angles ( $\delta$ ) reported in Table 3.14 represent this behavior. At higher normal loads, the interface friction angle becomes very low and for all practical purposes  $\tau$  tends to become independent of  $\sigma_n$ . The authors' experience on various low-plasticity (CL) and high-plasticity (CH) clays tested against both smooth and textured HDPE geomembrane confirms this  $\tau$ – $\sigma_n$  behavior. Recommended values presented in Table 3.14 should be used only as a guide in feasibility studies. Tests on site-specific materials and selected geomembranes should be conducted for final design purposes.

### 3.6.3 Geosynthetic-to-Geosynthetic Shear Strength

Several researchers have tested various geosynthetic-to-geosynthetic interfaces (Martin et al., 1984; Williams and Houlihan, 1986; Koutsourais et al., 1990; Mitchell et al., 1990; Lydick and Zagorski, 1990; Ojeshina, 1990; Somasundaram and Khilnani, 1991). The results of these studies are summarized in Table 3.15. The primary components of interface friction between multiple layers of geosynthetics are sliding between layers and dilation at the geosynthetic surface (Williams and Houlihan, 1986).

TABLE 3.15 Typical Range of Reported Geosynthetic to Geosynthetic Friction Angles (Degrees)

	PVC	HDPE Smooth	HDPE Textured	Geonet
Woven Geotextile	10–28	7–11	9–17	9–18
Nonwoven, needle-punched Geotextile	16–26	8–12	15–33	10–27
Nonwoven, resin/heat-bonded Geotextile	18–21	9–11	15–16	17–21
Geonet	11–24	5–19	7–25	—

The testing conditions may also have a significant effect on results. Mitchell et al. (1990) noted that polishing of geomembrane surfaces by geotextiles reduced interface friction. Also, the orientation of geonet strands can affect the interface strength between geonets and geomembranes (Geotek, 1987; Mitchell et al., 1990). Site-specific tests should therefore be performed using the actual materials and anticipated shear conditions.

### 3.6.4 Geosynthetic Clay Liner Shear Strength

Limited information is currently available on the internal shear strength of GCLs, due primarily to their relatively short history. The tests that have been performed are also difficult to compare, due to the numerous variations in test conditions. Many of these variations, such as strain rate, normal load, sample size, and consolidation conditions, are similar to the variations experienced when comparing shear strength testing of other geosynthetics. An additional variation of GCLs, however, is the hydrating conditions, including the hydrating liquid. Hydration can occur under free swell, constrained swell, or partially constrained swell, or the sample may be tested unhydrated. Even if hydrated under free-swell conditions, it may be difficult to assess whether full hydration has occurred since the bentonite may be restricted from free swell by the bonded geotextiles. Also, due to the large water absorption of bentonite, most shear strength test results will incorporate some immeasurable pore pressure effects unless the test is performed at extremely low displacement rates.

Table 3.16 presents the results of direct shear testing performed under various hydration conditions. The tests were performed at a strain rate of 9 mm/min and at normal stresses up to 60 kPa. Although these test results provide some information on the internal shear strength of GCLs, it is highly recommended that project specific testing be performed.

since creases in the geomembrane caused by sharp corners may lead to environmental stress cracking.

**8.3.3.6 Placement of Soils over Geomembranes.** As discussed in Section 8.3.3.2, soil should be “floated” over geomembranes such that a minimum 12 inches of this material exists between the construction equipment and the geomembrane at all times. This minimizes the possibility of geomembrane puncture and impact damage since the effective stress exerted by the construction equipment is reduced and the soil is not dumped on top of the geomembrane.

Soil placement over polyethylene geomembranes should occur in the early morning when there is adequate lighting and the geomembrane is contracted. By midday, wrinkles often develop in polyethylene geomembranes, making soil placement difficult. On days where the temperature exceeds 100°F, the wrinkles can be as large as 1 to 2 feet high. Even in the morning, 6-inch-high wrinkles can easily develop. If it cannot be avoided, soils may be placed over geomembrane wrinkles by placing the soil directly on top of the wrinkle such that it forms two smaller wrinkles. By continuously placing soil directly above the wrinkle, the wrinkle will eventually work itself out. Therefore, if possible, the geomembrane should not be permanently anchored until the soil overlying the geomembrane has been placed. In no situation should the geomembrane wrinkle be allowed to fold over under the weight of the overlying soil. These folds will crease the geomembrane and provide a preferential location for stress cracking and eventual leakage.

Placement of soils over geomembranes on slopes should occur from the bottom of slope upward. This will minimize the stresses on the geomembrane from construction equipment. Soils should be placed over geomembranes as soon as possible following geomembrane installation. This prevents UV degradation of the geomembrane and damage from ongoing construction activities, and also provides for good contact between the geomembrane and underlying material.

### 8.3.4 Structural Details

**8.3.4.1 Anchorage.** Anchor trenches are used at the top of side-slope liners to hold installed geosynthetics in place against applied loads and to prevent potential tears caused by wind intrusion beneath the geosynthetics. As shown in Figure 8.19, anchor trenches can generally be classified as flat, rectangular, or V-shaped. Selection of the appropriate anchor trench configuration for any particular site depends on the required holding capacity, access considerations, dimensional constraints, and available construction equipment. Often, a contractor may request that the anchor trench configuration be modified based on the equipment available. All such modifications should be checked and approved by the designer.

The holding capacity of anchor trenches is developed by the applied normal load of the soil placed above the geosynthetics, which creates frictional resistance between the geosynthetics and the underlying soil; there is minimal friction resistance developed between the upper soil and the geosynthetic since the soil above the

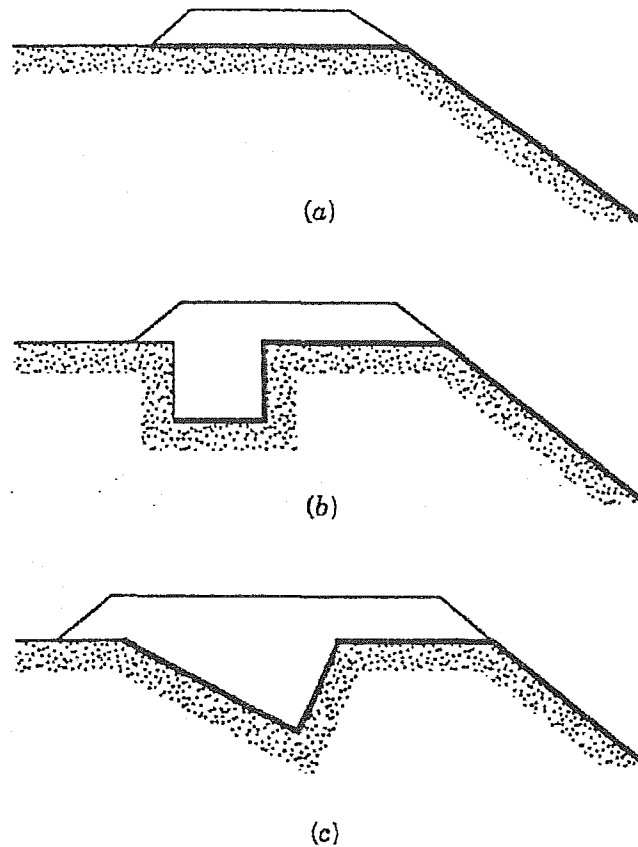


Figure 8.19 Typical anchor trench configurations: (a) flat anchor; and (b) rectangular anchor; and (c) V-shaped anchor.

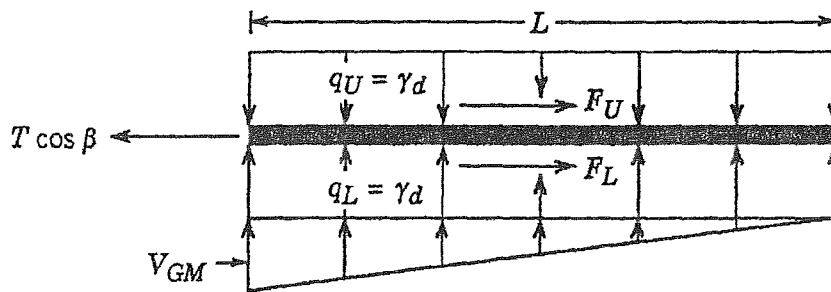
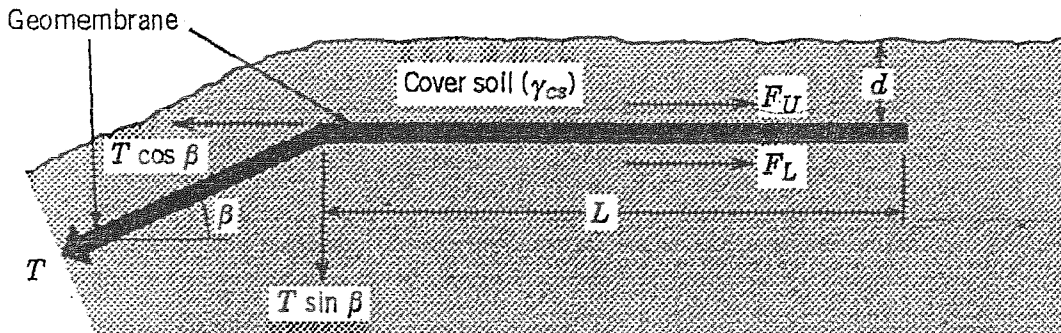
geosynthetic is likely to move with the geosynthetic. The soil depth, type of soil or other material underlying the geosynthetics, and geosynthetic anchorage length are therefore the key factors in developing the required anchor trench holding capacity.

The easiest anchor trench configuration to analyze is the flat anchor. The free-body diagram for the flat anchor and the development of equation (8.14) for anchorage length is shown in Figure 8.20.

$$L = \frac{T \cos \beta - T \sin \beta \tan \delta_L}{\gamma d \tan \delta_L} \quad (8.14)$$

There is no ideal solution for rectangular or V trenches. Koerner (1990) recommends that the problem be solved using imaginary, frictionless pulleys, as shown in Figure 8.21.

The anchor trench should be designed to resist pullout loads ( $T$ ) caused by the self-weight of the geosynthetics. For geomembranes that may be exposed to severe temperature and wind loading conditions, stresses caused by these forces should also be evaluated. Ideally, the anchor trench should be designed to allow the geosynthetics to pull out slightly rather than cause tearing of the geosynthetics. The reasoning for this is that even if complete pullout occurred, it would usually be easier to replace pulled-out materials than to repair torn geosynthetics. The maxi-



$$F_U = q_U \tan \delta_U(L) \text{ (neglected since cover soil moves with geomembrane)}$$

$$F_L = q_L + 0.5 v_{GM} \tan \delta_L(L)$$

$$= \left[ q_U + 0.5 \left( \frac{2 T \sin \beta}{L} \right) \right] \tan \delta_L(L)$$

$$T \cos \beta = q_L \tan \delta_L(L) + T \sin \beta \tan \delta_L$$

$$L = \frac{T \cos \beta - T \sin \beta \tan \delta_L}{\gamma_d \tan \delta_L}$$

Where:  $V_{GM}$  = vertical force due to geomembrane

$F_U$  = friction force above geomembrane

$F_L$  = friction force below geomembrane

$q_U$  = stress above geomembrane due to cover soil weight

$q_L$  = stress below geomembrane due to cover soil weight

$T$  = tensile force in geomembrane

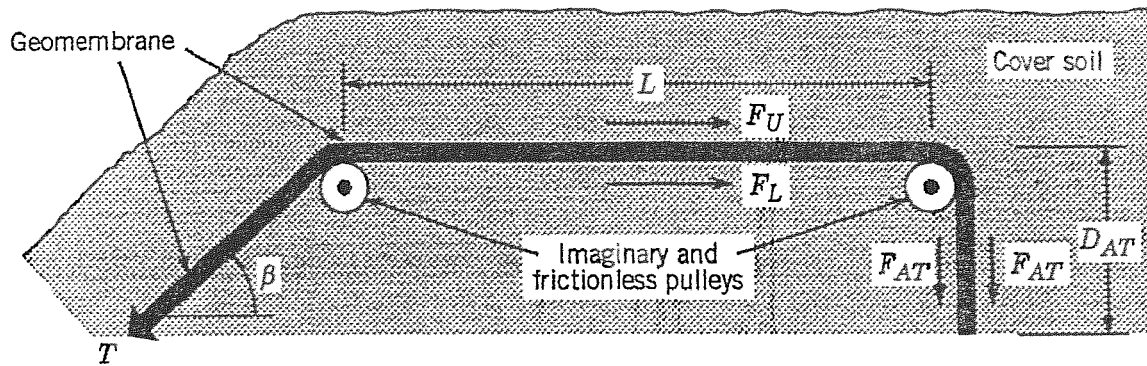
$\beta$  = slope angle

$d$  =

= unit weight of cover soil

$\delta$  = interface friction angle

Figure 8.20 Design of a flat anchor. (From Koerner, 1990.)



$$T = F_U + F_L + 2F_{AT}$$

Where:  $T$  = tensile stress in geomembrane

$F_U$  = friction force above geomembrane  
(assumed to be negligible since cover soil likely moves with geomembrane)

$$F_L = q \tan \delta (L)$$

$q$  = surcharge pressure =  $\gamma d$

$d$  = depth of cover soil

$\gamma$  = unit weight of cover soil

$\delta$  = interface friction angle

$L$  = runout length

$$F_{AT} = (\sigma_h \text{ ave}) \tan \delta (d_{AT})$$

$\sigma_h$  = average horizontal stress in anchor trench

$$= k_o \sigma_v$$

$$\sigma_v = \gamma H_{ave}$$

$H_{ave}$  = average depth of anchor trench (requires an estimate)

$$k_o = 1 - \sin \phi$$

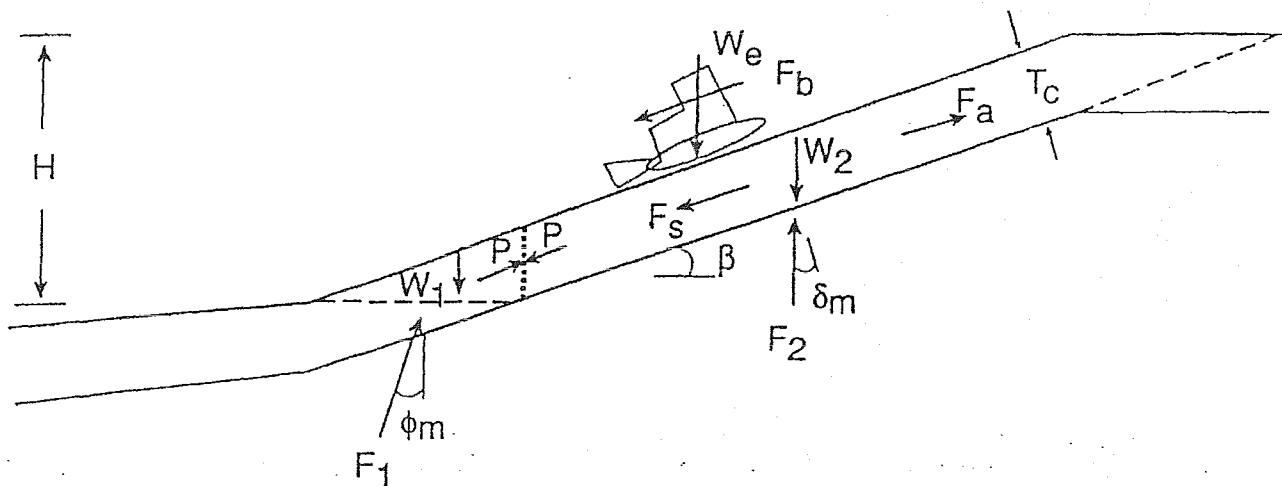
$\phi$  = angle of shearing resistance of backfill soil

$d_{AT}$  = depth of anchor trench (unknown)

**Figure 8.21** Design of a rectangular and V anchor trenches. (From Koerner, 1990.)

imum holding capacity of the anchor trench should therefore be slightly less than the ultimate tensile strength of the geosynthetic to be anchored, irrespective of the applied loads. If the applied loads are greater than the tensile strength of the geosynthetics, measures should be taken to reduce the applied loads or higher-strength geosynthetics should be used.

If soil materials are placed above side-slope geosynthetics, the load caused by soil, seepage forces, and construction equipment should be assessed. Often, a high-strength reinforcing geotextile or geogrid is required to hold the soil on the slopes. Druschel and Underwood (1993) used a force equilibrium method to assess the required anchorage force for these high-strength materials. The free-body and force vector diagram for this method are illustrated in Figures 8.22 and 8.23, respectively. As shown, the items<sup>4</sup> to be evaluated include the toe buttress resistance, soil



Note:  $P$ ,  $F_s$ ,  $F_a$ , and  $F_b$ , are assumed to be parallel to  $\beta$

Figure 8.22 Free-body diagram of side-slope forces. (From Druschel and Underwood, 1993.)

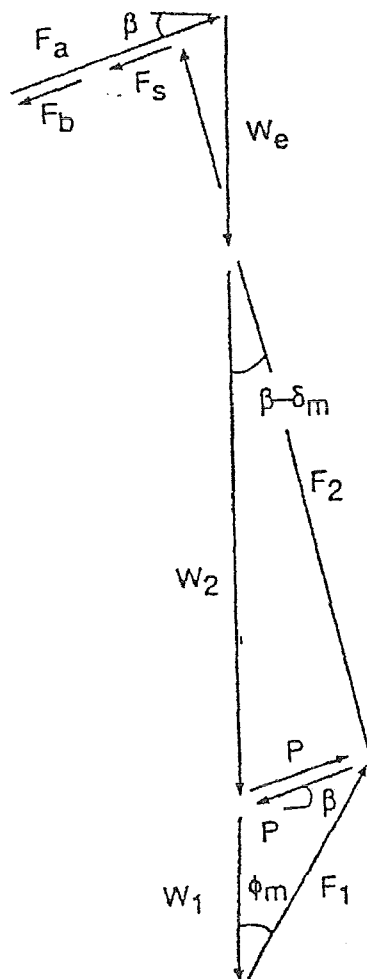


Figure 8.23 Force vector diagram. (From Druschel and Underwood, 1993.)

cover, equipment load, and seepage forces. The equation for the required anchorage force is

$$F_a = \frac{\gamma_w T_w^2}{2 \tan \beta} \left( \frac{\tan \phi_m}{\cos^2 \beta} + \frac{2H \tan \delta_m}{\cos \beta} - \frac{\tan \delta_m}{\cos \beta} \right) + W_e \left[ 0.3 + \frac{\sin(\beta - \delta_m)}{\cos \delta_m} \right] \quad (8.15)$$

$$\frac{\gamma_c T_c^2 \sin(\beta - \delta_m)}{2 \sin \beta \cos \beta \cos \delta_m} \left[ \frac{\sin \phi_m \cos \delta_m}{\cos(\beta + \phi_m) \sin(\beta - \delta_m)} + 1 - \frac{2H \cos \beta}{T_c} \right]$$

where  $H$  = side-slope height

$T_c$  = cover soil thickness

$\beta$  = side-slope angle

$\gamma_w$  = unit weight of water

$\gamma_c$  = unit weight of cover soil

$\delta$  = interface friction angle

$\delta_m$  = interface friction angle (mobilized)

$\phi$  = soil shear strength angle

$\phi_m$  = soil shear strength angle (mobilized)

$W_2$  = weight of side slope soil

$W_1$  = weight of toe buttress soil

$W_e$  = weight of equipment on the sideslope (equipment weight divided by equipment width)

$F_b$  = equipment braking force (approximately 30 percent of equipment's weight acting downslope and parallel to interface)

$T_w$  = thickness of seepage

$W_{w1}$  = weight of seepage water in toe buttress

$W_{w2}$  = weight of seepage water in side-slope soil

$F_a$  = geosynthetic anchorage force

$F_s$  = seepage force

$F_1$  = toe buttress reaction force

$F_2$  = side-slope reaction force

$P$  = side slope/toe buttress reaction force

Although this equation may seem complex, it is relatively straightforward and easily adaptable to a computer spreadsheet. Figures 8.24 and 8.25 present the variation in anchorage force with slope height assuming an interface friction angle of 9 and 12°, respectively. The reinforcing geotextile or geogrid selected should have a yield strength greater than the required anchorage force and should be able to attain the required anchorage force at a strain level of approximately 2 percent.

<sup>4</sup>Further discussion of these forces is provided in Chapter 10.

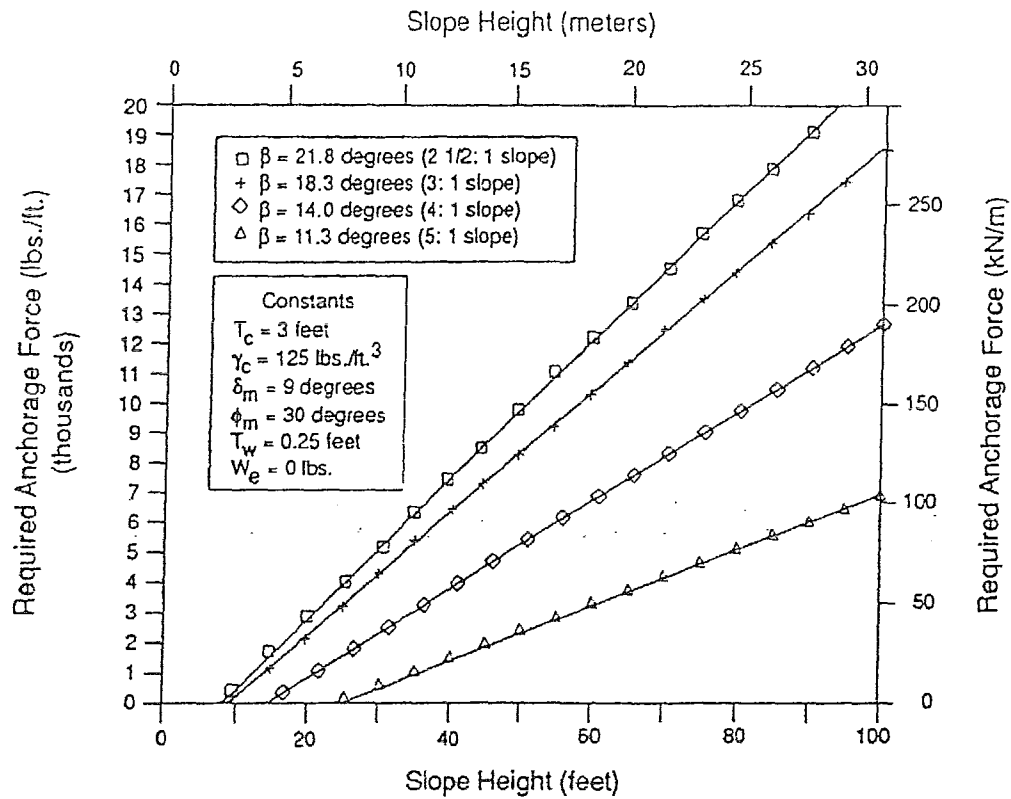


**Figure 8.24** Anchorage force required for slope with  $9^\circ$  interface friction angle. (From Druschel and Underwood, 1993.)

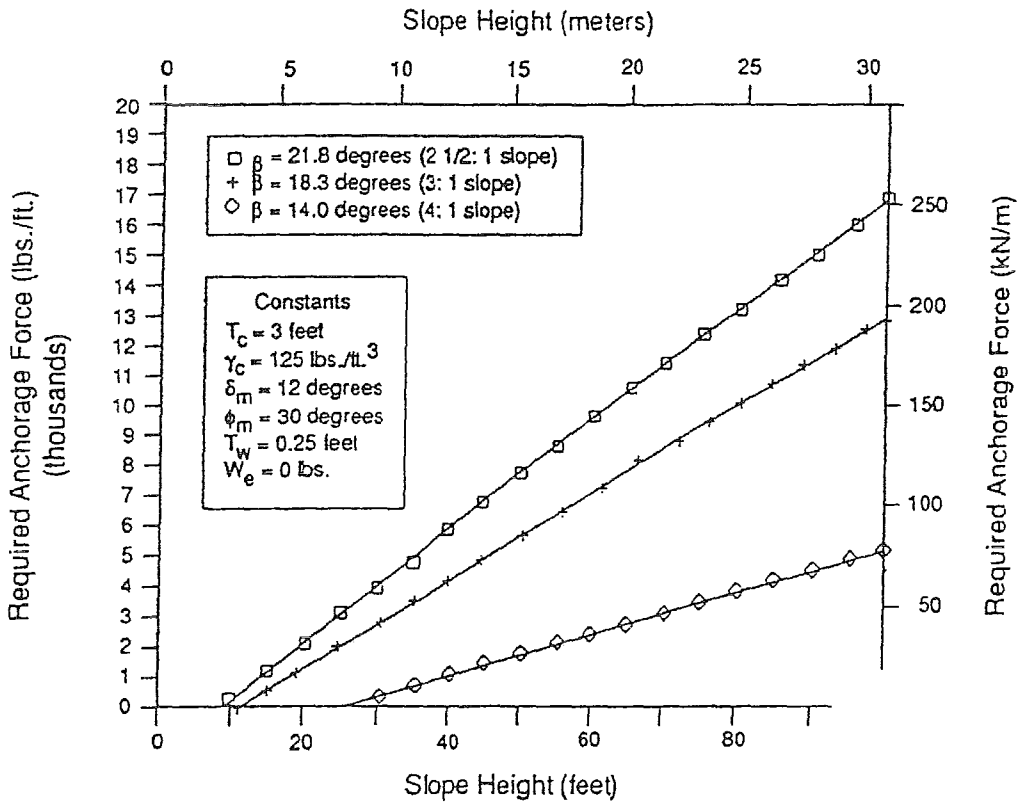


**Figure 8.25** Anchorage force required for slope with  $12^\circ$  interface friction angle. (From Druschel and Underwood, 1993.)

*Example 8.4.* A 50-foot-high 3H:1V side slope is lined with 60-mil single sided textured HDPE (textured side down against underlying clay and smooth side facing up). Calculate various stresses in the liner and determine the anchor trench capacity assuming that it is 3 feet deep and 2 feet wide. At the base, a 3-foot thickness of soil, consisting of a 1-foot drainage layer and a 2-foot-thick operations layer, is already in place.

### SOLUTION

A. *Forces on Geomembrane.* The forces on the geomembrane include those due to self-weight, temperature, and wind.

1. *Force ( $F_w$ ) per foot width due to self-weight ( $W$ ).*

$$F_w = W \sin \beta - F$$

where

$$W = L t \gamma = \frac{H}{\sin \beta} t \gamma$$

and where

$$F = W \cos \beta \tan \beta$$

$$H = \text{exposed height of geomembrane} = 50 - 3 = 47 \text{ ft}$$

$$\sin \beta = \sin [\tan^{-1}(1/3)] = \sin 18.3^\circ = 0.314$$

$$\cos \beta = \cos 18.3^\circ = 0.95$$

$$t = \text{geomembrane thickness} = \frac{60}{1000 \times 12} = 0.005 \text{ ft}$$

$$\gamma = \text{unit weight of geomembrane} = SG \cdot \gamma_w = (0.94)(62.4 \text{ lb/ft}^3) = 59 \text{ lb/ft}^3$$

Therefore,

$$W = \frac{47}{0.314} (0.005)(59) = 44.1 \text{ lb/ft width}$$

and assuming that  $\delta = 15^\circ$  yields

$$F = (44.1)(0.95)(\tan 15^\circ) = 11.23 \text{ lb/ft width}$$

and

$$\begin{aligned} F_w &= 44.1(0.314) - 11.23 \\ &= 2.62 \text{ lb/ft width} \end{aligned}$$

2. *Thermal forces ( $F_t$ ) per foot width due to temperature change ( $\Delta T$ ).* Assume that the coefficient of thermal expansion  $\mu = 1 \times 10^{-4}/^\circ\text{F}$  and the temperature fluctuations of the geomembrane during the day and the night are  $120^\circ\text{F}$  and  $60^\circ\text{F}$ , respectively. From equation (8.12),

$$\Delta L = \mu L \Delta T$$

which in terms of thermal strain may be written as

$$\epsilon_t = \mu \Delta T$$

Therefore,

$$\epsilon_t = 1 \times 10^{-4} \times (120 - 60) = 6 \times 10^{-3}$$

From the geomembrane stress-strain curve (test data sheet),  $\sigma$  corresponding to  $\epsilon_t = 6 \times 10^{-3}$  is  $\sim 300$  psi.

$$F_t = \sigma A = 300 \times 144 \times \frac{0.06}{12} = 216 \text{ lb/ft}$$

3. Forces ( $F_{\text{wind}}$ ) per foot width due to wind loading. From equation (8.13)

$$q = 0.002556 V^2$$

Assuming that  $V = 50$  miles/h, we have

$$q = 0.002556(50)^2 = 6.39 \text{ lb/ft}^2$$

Assuming that half of this force is supported by the drainage and operations layer and the other half is supported by the anchor trench gives us

$$F_{\text{wind}} = \frac{1}{2} q L = (6.39)(\frac{1}{2})(149.7) = 478 \text{ lb/ft width}$$

4. Total design forces ( $F_d$ )

$$\begin{aligned} F_d &= F_w + F_t + F_{\text{wind}} \\ &= 3 + 216 + 478 = 697 \text{ lb/ft width} \end{aligned}$$

B. Anchor Trench Capacity. From Figure 8.21.

$$\begin{aligned} T &= F_U + F_L + 2F_{\text{AT}} \\ &= 0 + \gamma d \tan \delta L + 2\sigma_{\text{have}} \tan \delta(d_{\text{AT}}) \end{aligned}$$

Assuming that  $d = 3$  ft,  $\delta = 15^\circ$ ,  $L = 3$  ft,  $\phi = 30^\circ$ ,  $d_{\text{AT}} = 3$  ft yields

$$\sigma_{\text{have}} = k_0 \left( \frac{\gamma h}{2} \right) = (1 - \sin \phi) \left( \frac{125 \times 3}{2} \right) = 94$$

$$T = 125(2) \tan 15(3) + 2(94) \tan 15(3) = 352 \text{ lb/ft width}$$

$$\text{additional resistance due to backfill soil} = (3 + 3) \times 2 \times 125 (\tan 20^\circ + \tan 15^\circ) = 948 \text{ lb/ft}$$

$$\text{total } T = 352 + 948 = 1300 \text{ lb/ft}$$

### C. Allowable Stress

Minimum allowable stress at yield = 2000 psi:

$$\begin{aligned} F_{\text{all}} &= \sigma t \\ &= 2000(0.06) = 120 \text{ lb/in.} = 1440 \text{ lb/ft} \end{aligned}$$

### D. Comparison of Various Forces

$$\begin{aligned} F_d &= \text{design force} = 697 \text{ lb/ft width} \\ T &= \text{anchor trench capacity} = 1300 \text{ lb/ft width} \\ F_{\text{all}} &= \text{allowable force} = 1440 \text{ lb/ft width} \end{aligned}$$

The anchor trench should be designed to:

- Resist the design force = 697 lb/ft
- Allow the geomembrane to slip out before the allowable stress is reached

Therefore,

$$\begin{aligned} F_d &< T < F_{\text{all}} \\ 697 &< 1300 < 1440 \text{ lb/ft width} \quad \text{OK} \end{aligned}$$

$$\text{FS against pullout} = \frac{T}{F_d} = \frac{1300}{697} = 1.87$$

$$\text{FS against geomembrane failure} = \frac{F_{\text{all}}}{F_d} = \frac{1440}{697} = 2.07$$

**8.3.4.2 Connection/Termination.** As discussed in Section 8.3.1, most landfill liners are constructed in phases. Adequate liner connection and termination details are therefore critical in maintaining liner continuity between phases. To provide satisfactory connection/termination details, the designer must first envision how the connection will be constructed, the required construction equipment access, and how much overlap is necessary between the lining systems. Typically a 4- to 5-foot overlap is sufficient for the clay liner and 2 to 3 feet for the geosynthetics. To avoid a preferential leachate flow path, the connection between clay liners should not be vertical but rather, stair-stepped at an angle (Figure 8.26). This requires some reworking of the existing clay liners but will lead to a continuous bond between the existing and future clay liners. For future connection of geomembrane liners, the edge of the existing geomembrane liner should be kept as clean as possible for proper seaming. This is often achieved by wrapping the final leading edge of the geomembrane with a nonwoven geotextile prior to placing any cover materials over the geomembrane.

Connection/termination details parallel to landfill sideslopes should also be considered, especially for geomembranes. Often the edge of a geomembrane is left

**APPLICATION FOR PERMIT  
DNCS ENVIRONMENTAL SOLUTIONS**

**VOLUME III: ENGINEERING DESIGN AND CALCULATIONS  
SECTION 7: TENSILE STRESS ANALYSIS**

**ATTACHMENT III.7.C**

**QIAN, XUEDE; KOERNER, ROBERT M.; AND GRAY, DONALD H. 2002.  
*GEOTECHNICAL ASPECTS OF LANDFILL DESIGN AND CONSTRUCTION.*  
NEW YORK: PRETENCE HALL.**

# GEOTECHNICAL ASPECTS OF LANDFILL DESIGN AND CONSTRUCTION

**Xuede Qian**

*Geotechnical Engineering Specialist  
Michigan Department of Environmental Quality*

**Robert M. Koerner**

*H. L. Bowman Professor of Civil Engineering, Drexel University  
Director, Geosynthetic Research Institute*

**Donald H. Gray**

*Professor of Civil and Environmental Engineering  
The University of Michigan*



PRENTICE HALL  
Upper Saddle River, New Jersey 07458

**Solution:**

Assume the runout resistance force is equal to the geomembrane allowable tensile force. From the design equations just presented,

$$\begin{aligned} T \cdot (\cos \beta) &= 350(144)(0.030/12) \cos 18.4^\circ \\ &= 120 \text{ lb/ft (1.75 kN/m)} \end{aligned}$$

$$T \cdot (\sin \beta) = 39.8 \text{ lb/ft (0.58 kN/m)}$$

$$q_B = \gamma_s \cdot d_{CS} = (100)(1.0) = 100 \text{ lb/ft (1.46 kN/m)}$$

which, when substituted into Equation 4.11, gives

$$\begin{aligned} T \cdot (\cos \beta) &= q_B \cdot \tan \delta_C (L_{RO}) + T \cdot \sin \beta \cdot \tan \delta_C \\ 120 &= 100(\tan 20^\circ)(L_{RO}) + 39.8(\tan 20^\circ) \end{aligned} \quad (4.11)$$

$$120 = 36.4 \cdot L_{RO} + 14.5$$

from which it follows that

$$L_{RO} = 2.9 \text{ ft (0.88 m); use 3.0 ft (use 1 m)}$$


---

Note that the runout length is strongly dependent on the value of allowable stress used in the analysis. To mobilize the full strength of the geomembrane would require a longer runout length or an anchor trench. However, this might not be desirable. Pullout, without geomembrane failure, might be preferable to tensile rupture and separation of the geomembrane. Thus, the design runout or anchor resistance capacity should fall between the ultimate strength and allowable strength of a geosynthetic liner (Qian, 1995). That is,

Ultimate Strength > Runout and/or Anchor Resistance Capacity > Allowable Strength

$$\text{Runout and/or Anchor Resistance Capacity} = T/t$$

$$\sigma_{\text{allow}} = \sigma_{\text{ult}}/FS, \text{ and } T_{\text{allow}} = \sigma_{\text{allow}} \cdot t,$$

where  $T$  = geomembrane tensile force (i.e., runout or anchor resistance force) per unit width;

$t$  = geomembrane thickness;

$\sigma_{\text{ult}}$  = ultimate geomembrane stress (e.g., yield or break);

$FS$  = factor of safety based on geomembrane strength;

$\sigma_{\text{allow}}$  = allowable geomembrane stress; and

$T_{\text{allow}}$  = allowable geomembrane force per unit width.

#### 4.7.2 Design of Rectangular Anchor Trench

The situation with a rectangular anchor trench in place at the end of the runout section is illustrated in Figure 4.9. The configuration requires some important assumptions regarding the state of stress within the anchor trench and its resistance mechanism. In order to establish static equilibrium, an imaginary and frictionless pulley is assumed at

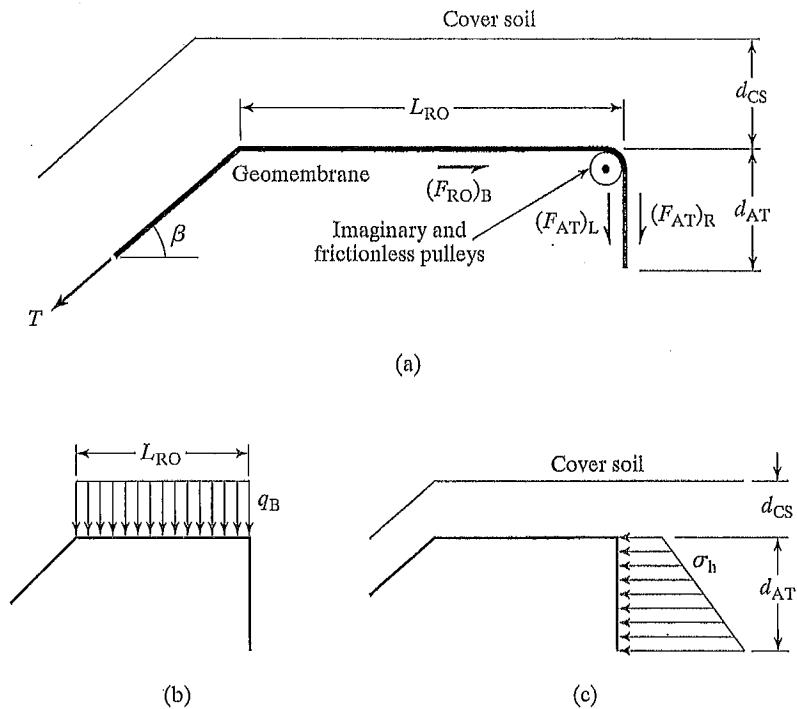


FIGURE 4.9 Cross Section of Geomembrane Runout Section with a Rectangular Anchor Trench and Related Stresses and Forces Involved

the top edge of the anchor trench, as shown in Figure 4.9 (Qian, 1995), which allows the geomembrane to be considered as a continuous member along its entire length.

From Figure 4.9, the following force summations lead to the appropriate design equations:

From  $\sum F_V = 0$ ,

$$T \cdot (\sin \beta) = 0.5 \cdot V_{GM} L_{RO}$$

The cover soil pressure on the runout length is

$$q_B = \gamma_s \cdot d_{CS}$$

The lateral earth force acting on both sides of the geomembrane buried in the anchor trench is

$$P_L = P_R = K_o \cdot \gamma_s \cdot (d_{CS} + 0.5 \cdot d_{AT}) \cdot d_{AT}$$

The vertical force due to the geomembrane force is

$$V_{GM} = \frac{2 \cdot T \cdot \sin \beta}{L_{RO}}$$

The friction force above the runout geomembrane is always neglected in the anchor trench design, since the cover soil probably moves along with the geomembrane as it deforms.

From  $\Sigma F_H = 0$ ,

$$T \cdot (\cos \beta) = (F_{RO})_B + (F_{AT})_L + (F_{AT})_R \quad (4.13)$$

$$\begin{aligned} \text{and} \quad (F_{RO})_B &= q_B \cdot L_{RO} \cdot \tan \delta_C + 0.5 \cdot V_{GM} \cdot L_{RO} \cdot \tan \delta_C \\ &= q_B \cdot L_{RO} \cdot \tan \delta_C + 0.5 \cdot (2 \cdot T \cdot \sin \beta / L_{RO}) \cdot L_{RO} \cdot \tan \delta_C \end{aligned}$$

$$\text{or} \quad (F_{RO})_B = q_B \cdot L_{RO} \cdot \tan \delta_C + T \cdot \sin \beta \cdot \tan \delta_C \quad (4.14)$$

Because  $q_B = \gamma_s \cdot d_{CS}$ , the friction force beneath the runout geomembrane is

$$(F_{RO})_B = \gamma_s \cdot d_{CS} \cdot L_{RO} \cdot \tan \delta_C + T \cdot \sin \beta \cdot \tan \delta_C \quad (4.15)$$

The friction force between the left side of the geomembrane and the side wall of the anchor trench is

$$(F_{AT})_L = (\sigma_h)_{ave} \cdot d_{AT} \cdot \tan \delta_C$$

The friction force between the right side of the geomembrane and the side wall of the anchor trench is

$$(F_{AT})_R = (\sigma_h)_{ave} \cdot d_{AT} \cdot \tan \delta_F$$

where  $(\sigma_h)_{ave} = K_o \cdot (\sigma_v)_{ave}$

Because  $K_o = 1 - \sin \phi$  and  $(\sigma_v)_{ave} = \gamma_s \cdot (d_{CS} + 0.5 \cdot d_{AT})$

$$(\sigma_h)_{ave} = (1 - \sin \phi) \cdot \gamma_s \cdot (d_{CS} + 0.5 d_{AT}) \quad (4.16)$$

$$\text{So} \quad (F_{AT})_L = (1 - \sin \phi) \cdot \gamma_s \cdot (d_{CS} + 0.5 \cdot d_{AT}) \cdot d_{AT} \cdot \tan \delta_C \quad (4.17)$$

$$\text{and} \quad (F_{AT})_R = (1 - \sin \phi) \cdot \gamma_s \cdot (d_{CS} + 0.5 \cdot d_{AT}) \cdot d_{AT} \cdot \tan \delta_F \quad (4.18)$$

Substituting Equations 4.15, 4.17, and 4.18 into Equation 4.13 gives

$$\begin{aligned} T \cdot (\cos \beta - \sin \beta \cdot \tan \delta_L) &= \gamma_s \cdot d_{CS} \cdot L_{RO} \cdot \tan \delta_C + \\ &\quad (1 - \sin \phi) \cdot \gamma_s \cdot (d_{CS} + 0.5 \cdot d_{AT}) \cdot d_{AT} \cdot (\tan \delta_C + \tan \delta_F) \end{aligned}$$

which leads to

$$T = \frac{\gamma_s \cdot d_{CS} \cdot L_{RO} \cdot \tan \delta_C + (1 - \sin \phi) \cdot \gamma_s \cdot (d_{CS} + 0.5 \cdot d_{AT}) \cdot d_{AT} \cdot (\tan \delta_C + \tan \delta_F)}{\cos \beta - \sin \beta \cdot \tan \delta_C} \quad (4.19)$$

or

$$T = \frac{q_B \cdot L_{RO} \cdot \tan \delta_C + K_o \cdot (\sigma_v)_{ave} \cdot d_{AT} \cdot (\tan \delta_C + \tan \delta_F)}{\cos \beta - \sin \beta \cdot \tan \delta_C} \quad (4.20)$$

When  $\delta_C = \delta_F = \delta$ , Equation 4.19 becomes

$$T = \frac{\gamma_s \cdot d_{CS} \cdot L_{RO} \cdot \tan \delta + 2 \cdot (1 - \sin \phi) \cdot \gamma_s \cdot 0.5 \cdot d_{AT} \cdot \tan \delta}{\cos \beta - \sin \beta \cdot \tan \delta} \quad (4.21)$$

and Equation 4.20 becomes

$$T = \frac{q_B \cdot L_{RO} \cdot \tan \delta + 2 \cdot K_o \cdot (\sigma_v)_{ave} \cdot d_{AT} \cdot \tan \delta}{\cos \beta - \sin \beta \cdot \tan \delta} \quad (4.22)$$

where  $T$  = geomembrane tensile force (i.e., anchor trench resistance force) per unit width;

$(F_{RO})_B$  = friction force beneath runout geomembrane;

$(F_{AT})_L$  = friction force between the left side of the geomembrane and the side wall of the anchor trench;

$(F_{AT})_R$  = friction force between the right side of the geomembrane and the side wall of the anchor trench;

$(\sigma_h)_{ave}$  = average horizontal stress in anchor trench;

$(\sigma_v)_{ave}$  = average vertical stress in anchor trench;

$H_{ave}$  = average depth of anchor trench;

$K_o$  = coefficient of at-rest earth pressure;

$L_{RO}$  = runout length;

$d_{CS}$  = depth of cover soil;

$d_{AT}$  = anchor trench depth;

$\gamma_s$  = unit weight of cover and backfill soil;

$\phi$  = friction angle of backfill soil in anchor trench;

$\delta_C$  = friction angle between geomembrane and underlying soil;

$\delta_F$  = friction angle between geomembrane and backfill soil;

$\delta$  = friction angle between geomembrane and soil; and

$\beta$  = sideslope angle, measured from horizontal.

Note that because this situation results in one equation with two unknowns, thus a choice of  $L_{RO}$  or  $d_{AT}$  is necessary to calculate the other.

#### EXAMPLE 4.4

A 60-mil (1.5-mm) HDPE geomembrane of allowable stress 840 lb/in<sup>2</sup> (5,800 kN/m<sup>2</sup>) is placed on a 3(H) to 1(V) sideslope. There is a cover soil of 12 inches (0.3 m) placed over the geomembrane. The unit weight of cover soil and backfill soil in the anchor trench is 110 lb/ft<sup>3</sup> (17.3 kN/m<sup>3</sup>). The friction angle between the geomembrane and the underlying soil is 18 degrees, and the friction angle between the geomembrane and the backfill soil in the anchor trench is 22 degrees. The friction of the backfill soil is 30 degrees. Determine the required runout length for a 24-inch-deep (0.6-meter-deep) anchor trench.

#### Solution:

Assume the anchor resistance force is equal to the geomembrane allowable tensile force. Using the previously developed design equation from Figure 4.9,

$$T \cdot (\cos \beta) = (F_{RO})_B + (F_{AT})_L + (F_{AT})_R \quad (4.13)$$

where  $T = T_{allow} = \sigma_{allow} \cdot t$

From Equation 4.19, we have

$$T = \frac{\gamma_s \cdot d_{CS} \cdot L_{RO} \cdot \tan \delta_C + (1 - \sin \phi) \cdot \gamma_s \cdot (d_{CS} + 0.5 \cdot d_{AT}) \cdot d_{AT} \cdot (\tan \delta_C + \tan \delta_F)}{\cos \beta - \sin \beta \cdot \tan \delta_C} \quad (4.19)$$

and

$$\sigma_{\text{allow}} \cdot t \cdot (\cos\beta - \sin\beta \cdot \tan\delta_C) = \gamma_s \cdot d_{\text{CS}} \cdot L_{\text{RO}} \cdot \tan\delta_C + (1 - \sin\phi) \cdot \gamma_s \cdot (d_{\text{CS}} + 0.5 \cdot d_{\text{AT}}) \cdot d_{\text{AT}} \cdot (\tan\delta_C + \tan\delta_F)$$

so that

$$\sigma_{\text{allow}} \cdot t = (840)(144)(0.060)/12 = 605 \text{ lb/ft (8.83 kN/m) and } (605)[(\cos 18.4^\circ) - (\sin 18.4^\circ)(\tan 18^\circ)] = (110)(1)(\tan 18^\circ)(L_{\text{RO}}) + (0.5)(110)(2)(2)(\tan 18^\circ + \tan 22^\circ)$$

or

$$(605)(0.846) = (35.74) \cdot L_{\text{RO}} + (220)(0.729) \text{ which yields } 512.83 = (35.74) \cdot L_{\text{RO}} + 160.38 \text{ or } L_{\text{RO}} = 9.86 \text{ ft (2.96 m)}$$

Thus, use the runout length  $L_{\text{RO}} = 10 \text{ ft (3 m)}$ .

The geomembrane can also be extended along the trench bottom to increase resistance force, which is called an L-shaped rectangular anchor trench. A typical layout in an L-shaped rectangular anchor trench, which is widely used in landfill projects, is shown in Figure 4.10. In order to establish the static equilibrium equation, two imaginary and frictionless pulleys are assumed at the top edge and the bottom corner of the anchor trench, as shown in Figure 4.10 (Qian, 1995). This assumption again allows the geomembrane to be considered as a continuous member.

The friction force above a runout geomembrane is always neglected in the anchor trench design, since the cover soil probably moves together with the geomembrane as it deforms.

From  $\Sigma F_H = 0$

$$T \cdot (\cos\beta) = (F_{\text{RO}})_B + (F_{\text{AT}})_L + (F_{\text{AT}})_R + (F_{\text{AB}})_B + (F_{\text{AB}})_U \quad (4.23)$$

The friction force between the geomembrane and the underlying soil at the bottom of the anchor trench is

$$(F_{\text{AB}})_B = \sigma_{\text{vB}} \cdot L_{\text{AT}} \cdot \tan\delta_C \quad (4.24)$$

The friction force between the geomembrane and the overlying soil at the bottom of the anchor trench is

$$(F_{\text{AB}})_U = \sigma_{\text{vB}} \cdot L_{\text{AT}} \cdot \tan\delta_F \quad (4.25)$$

Because  $\sigma_{\text{vB}} = \gamma_s \cdot (d_{\text{CS}} + d_{\text{AT}})$ ,

$$(F_{\text{AB}})_B = \gamma_s \cdot (d_{\text{CS}} + d_{\text{AT}}) \cdot L_{\text{AT}} \cdot \tan\delta_C \quad (4.26)$$

and

$$(F_{\text{AB}})_U = \gamma_s \cdot (d_{\text{CS}} + d_{\text{AT}}) \cdot L_{\text{AT}} \cdot \tan\delta_F \quad (4.27)$$

Substituting Equations 4.15, 4.17, 4.18, 4.26, and 4.27 into Equation 4.23 gives

$$T \cdot (\cos\beta - \sin\beta \cdot \tan\delta_L) = \gamma_s \cdot d_{\text{CS}} \cdot L_{\text{RO}} \cdot \tan\delta_C + \gamma_s \cdot (\tan\delta_C + \tan\delta_F) [(1 - \sin\phi) \cdot \gamma_s \cdot (d_{\text{CS}} + 0.5 \cdot d_{\text{AT}}) \cdot d_{\text{AT}} + (d_{\text{CS}} + d_{\text{AT}}) \cdot L_{\text{AT}}]$$

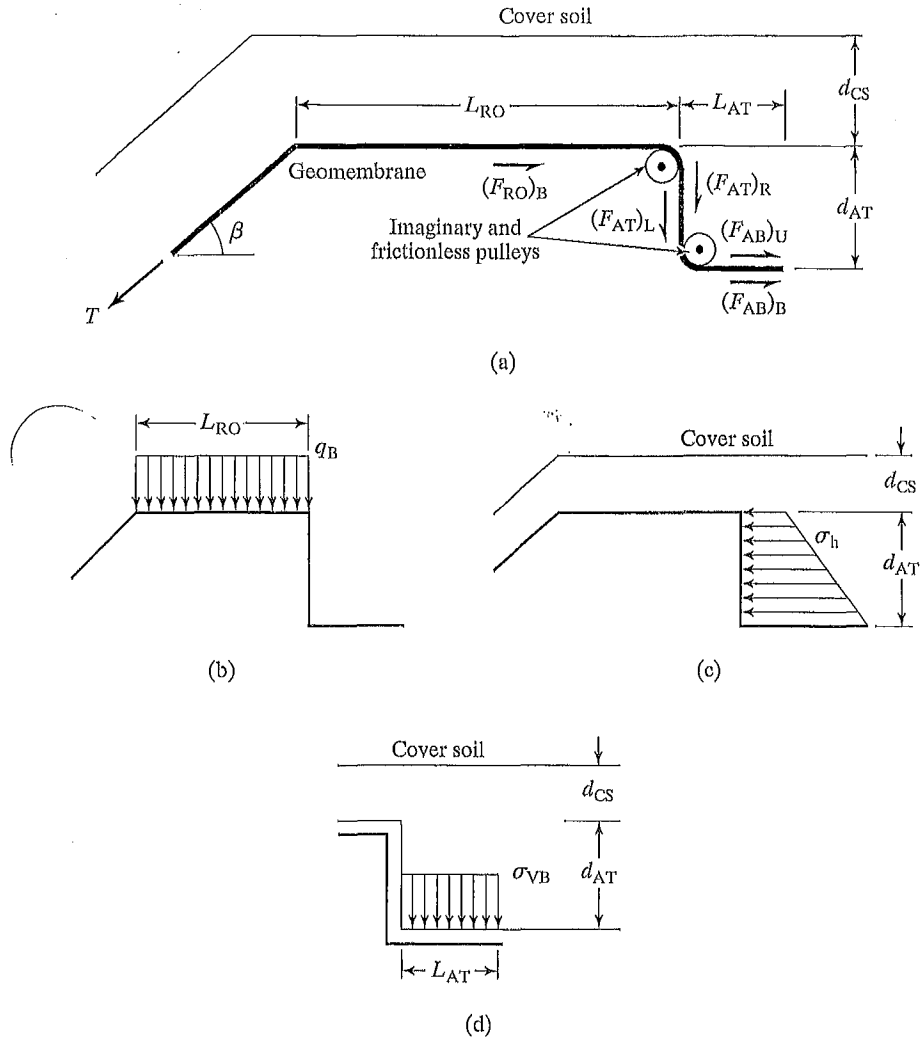


FIGURE 4.10 Cross Section of Geomembrane Runout Section with an L-Shaped Rectangular Anchor Trench and Related Stresses and Forces Involved

which leads to

$$T = \frac{\gamma_s \cdot d_{CS} \cdot L_{RO} \cdot \tan \delta_C + \gamma_s \cdot [(1 - \sin \phi) \cdot \gamma_s \cdot (d_{CS} + 0.5 \cdot d_{AT}) \cdot d_{AT} + (d_{CS} + d_{AT}) \cdot L_{AT}] (\tan \delta_C + \tan \delta_F)}{\cos \beta + \sin \beta \cdot \tan \delta_C} \quad (4.28)$$

or

$$T = \frac{q_B \cdot L_{RO} \cdot \tan \delta_C + [K_o \cdot (\sigma_v)_{ave} \cdot d_{AT} + \sigma_{vB} \cdot L_{AT}] (\tan \delta_C + \tan \delta_F)}{\cos \beta - \sin \beta \cdot \tan \delta_C} \quad (4.29)$$

When  $\delta_C = \delta_F = \delta$ , Equation 4.28 becomes

$$T = \frac{\gamma_s \cdot d_{CS} \cdot L_{RO} \cdot \tan \delta + 2 \cdot \gamma_s \cdot [(1 - \sin \phi) \cdot \gamma_s \cdot (d_{CS} + 0.5 \cdot d_{AT}) \cdot d_{AT} + (d_{CS} + d_{AT}) \cdot L_{AT}] \cdot \tan \delta}{\cos \beta - \sin \beta \cdot \tan \delta} \quad (4.30)$$

and Equation 4.29 becomes

$$T = \frac{q_B \cdot L_{RO} \cdot \tan \delta + 2 \cdot [K_o \cdot (\sigma_v)_{ave} \cdot d_{AT} + \sigma_{vB} \cdot L_{AT}] \cdot \tan \delta}{\cos \beta - \sin \beta \cdot \tan \delta} \quad (4.31)$$

where  $T$  = geomembrane tensile force (i.e., anchor trench resistance force) per unit width;

$(F_{RO})_B$  = friction force beneath runout geomembrane;

$(F_{AT})_L$  = friction force between the left side of the geomembrane and the side wall of the anchor trench;

$(F_{AT})_R$  = friction force between the right side of the geomembrane and the side wall of the anchor trench;

$(F_{AB})_B$  = friction force between the geomembrane and the underlying soil at the bottom of the anchor trench;

$(F_{AB})_U$  = friction force between the geomembrane and the overlying soil at the bottom of the anchor trench;

$(\sigma_v)_{ave}$  = average vertical stress in anchor trench;

$K_o$  = coefficient of at-rest earth pressure;

$L_{RO}$  = runout length;

$d_{CS}$  = depth of cover soil;

$d_{AT}$  = anchor trench depth;

$\gamma_s$  = unit weight of cover and backfill soil;

$\phi$  = friction angle of backfill soil in anchor trench;

$\delta_C$  = friction angle between the geomembrane and the underlying soil;

$\delta_F$  = friction angle between the geomembrane and the backfill soil;

$\delta$  = friction angle between the geomembrane and the soil; and

$\beta$  = sideslope angle, measured from horizontal.

The design of an anchor trench is considered to be adequate if mobilized stress lies between the yield stress and allowable stress of the geosynthetic components. It should be mentioned that many manufacturers specify 1.5-foot- (0.45-m)-deep anchor trenches and a 3.0-foot- (0.90-m)-long runout section.

#### EXAMPLE 4.5

Calculate the resistant capacity of a given geomembrane in a L-shaped rectangular anchor trench of known dimensions. The geomembrane is 60-mil (1.5-mm) HDPE with an ultimate strength (at yield) 2,100 lb/in<sup>2</sup> (14,500 kN/m<sup>2</sup>) and an allowable strength 840 lb/in<sup>2</sup> (5,800 kN/m<sup>2</sup>).

The runout length is 3 feet (0.9 m). The cover soil is 1 foot (0.3 m). The anchor trench is 2 feet (0.6 m) wide and 2 feet (0.6 m) deep. The side slope angle is 18.4 degrees [3(H):1(V)]. The unit weight of soil is 110 lb/ft<sup>3</sup> (17.3 kN/m<sup>3</sup>). The soil friction angle is 30 degrees. The friction angle between the soil and the geomembrane is 20 degrees.

**Solution:**

The resistance capacity of the geomembrane in the anchor can be calculated from Equation 4.31 as

$$T = \frac{q_B \cdot L_{RO} \cdot \tan \delta + 2 \cdot [K_o \cdot (\sigma_v)_{ave} \cdot d_{AT} + \sigma_{vB} \cdot L_{AT}] \cdot \tan \delta}{\cos \beta - \sin \beta \cdot \tan \delta}$$

where

$$q_B = \gamma_s \cdot d_{CS} = 110 \times 1 = 110 \text{ lb/ft}^2 \text{ (5.27 kN/m}^2\text{)}$$

$$K_o = 1 - \sin \phi = 1 - 0.5 = 0.5$$

$$(\sigma_v)_{ave} = \gamma_s \cdot (d_{cs} + 0.5 \cdot d_{AT})$$

$$= 110 \times (1 + 0.5 \times 2) = 110 \times 2 = 220 \text{ lb/ft}^2 \text{ (10.53 kN/m}^2\text{)}$$

$$\sigma_{vB} = \gamma_s \cdot (d_{cs} + d_{AT}) = 110 \times (1 + 2) = 330 \text{ lb/ft}^2 \text{ (15.80 kN/m}^2\text{)}$$

Substituting these calculated values into Equation 4.31 yields

$$\begin{aligned} T &= \frac{q_B \cdot L_{RO} \cdot \tan \delta + 2 \cdot [K_o \cdot (\sigma_v)_{ave} \cdot d_{AT} + \sigma_{vB} \cdot L_{AT}] \cdot \tan \delta}{\cos \beta - \sin \beta \cdot \tan \delta} \\ &= \frac{(110)(2)(\tan 20^\circ) + 2[(0.5)(220)(2) + (330)(2)](\tan 20^\circ)}{\cos 18.4^\circ - (\sin 18.4^\circ)(\tan 20^\circ)} \\ &= \frac{(110)(2)(0.364) + 2(220 + 660)(0.364)}{0.949 - (0.316)(0.364)} \\ &= \frac{80.08 + 640.64}{0.834} \\ &= \frac{720.72}{0.834} \\ &= 864 \text{ lb/ft (12.61 kN/m)} \end{aligned}$$

So,

Anchor Resistance Capacity = 864 lb/ft = 72 lb/in ÷ 0.06 in = 1,200 lb/in<sup>2</sup> (8,270 kN/m<sup>2</sup>), which leads to the following inequalities:

$$\begin{aligned} \text{Ultimate Strength} &> \text{Anchor Resistance Capacity} > \text{Allowable Strength} \\ 2,100 \text{ lb/in}^2 &> 1,200 \text{ lb/in}^2 > 840 \text{ lb/in}^2 \\ (14,500 \text{ kN/m}^2) &> 8,270 \text{ kN/m}^2 > 5,800 \text{ kN/m}^2 \end{aligned}$$

The results of the calculation indicate the design anchor resistance capacity falls between the yield stress and allowable stress of a geosynthetic membrane liner. Therefore, the anchor trench dimensions are acceptable.

By using a model as presented here, any set of conditions can be used to analyze and arrive at an acceptable design solution. Even situations in which geotextiles and geonets or geocomposites are used in conjunction with a geomembrane can be analyzed in a similar manner.

be normally consolidated under the surcharge of about 4 m of fill. The soft clay layer, however, was underconsolidated below the fill layer. The excess pore pressures caused by the placement of the fill in the 1970s and 1980s had experienced very little dissipation—particularly between elevations of -10 and -20 m—at the time waste placement started. In the middle zone of the soft clay layer, the difference between the actual undrained strength and the one used in the stability analyses was of the order of 10 kN/m<sup>2</sup>. The original short-term stability analysis did not consider the possibility of failure surfaces extending to the river (like the one that actually happened), where there was no fill layer over the soft clay, and, hence, the soft clay did not have the undrained strength assumed in the stability calculations.

As noted, this case history had a geosynthetic lining system that failed along with the rotational movement. However, the lining system could not (and was not) a contributing issue to the failure. The little reinforcement benefit that may have been provided by the geosynthetic layer is negligible in the context of this large of a waste mass. This, as with the previous two case histories, was completely a geotechnical-related failure of the classical rotational failure mode except now a portion of the failure surface passes through waste materials.

### 13.5.3 General Remarks

It should be obvious from these three case histories that proper site characterization during the design stage and well before waste placement is critical. Irrespective of the high shear strength of waste materials, if the soil foundation fails, it will eventually propagate through the waste mass and cause the entire system to fail. Once a crack is observed on the surface of the waste mass, the entire failure surface beneath it has been mobilized. Failure of the mass is then imminent.

The situation is obviously important when dealing with soft, fine-grained soils. Typically, but certainly not always, such soils are near rivers, harbors, and estuaries. Best available geotechnical practice must be followed (recall Section 13.3.3). Even beyond site investigation, laboratory testing, and design which lead to site-specific plans and specifications, one should consider field instrumentation. Piezometers placed in the subsoil and inclinometers placed at the toe of the waste slope (and beyond) could be most valuable in providing an instantaneous assessment of the landfill as waste is being placed. Unfortunately, such instrumentation is rarely provided, even for sensitive site situations.

## 13.6 WASTE MASS FAILURES

The relatively low interface shear strengths of components within liner systems can lead to translational failures of the type shown in Figure 13.1(f). However, failure can only occur if the toe of the waste mass is unsupported by an opposing slope or large soil berm. Unfortunately, unsupported toe conditions are often the case. Canyon landfills are very common in areas of mountainous or rolling topography. Even when an excavation is dug for a landfill, the waste mass during filling is generally left unsupported at its toe. This section deals with the instability of such situations.

13.6.1 Translational Failure Analysis

While the approach to translational failures is generally similar to that described in Section 13.5.1, the failure surface is not circular, but usually piecewise linear. Thus, the simplified Bishop method is not applicable. A translational (or two-wedge) failure analysis is used to calculate the factor of safety for the landfill against possible mass movement of the type of “translational (or wedge) failure along liner” [Figure 13.1(f)] in the interim filling condition.

The waste mass shown in Figure 13.24(a) can be divided into two discrete parts, one active wedge lying on the side slope and tending to cause failure, and another passive wedge lying on the cell bottom floor and tending to resist failure. The forces acting on the active and passive wedges are shown in Figure 13.24(a). The individual forces, friction angles, and slope angles involved in the analysis are listed as follows:

- $W_P$  = weight of the passive wedge;
- $N_P$  = normal force acting on the bottom of the passive wedge;
- $F_P$  = frictional force acting on the bottom of the passive wedge (parallel to the bottom of the passive wedge);
- $E_{HP}$  = normal force from the active wedge acting on the passive wedge (unknown in magnitude, but with the direction perpendicular to the interface of the active and passive wedges);

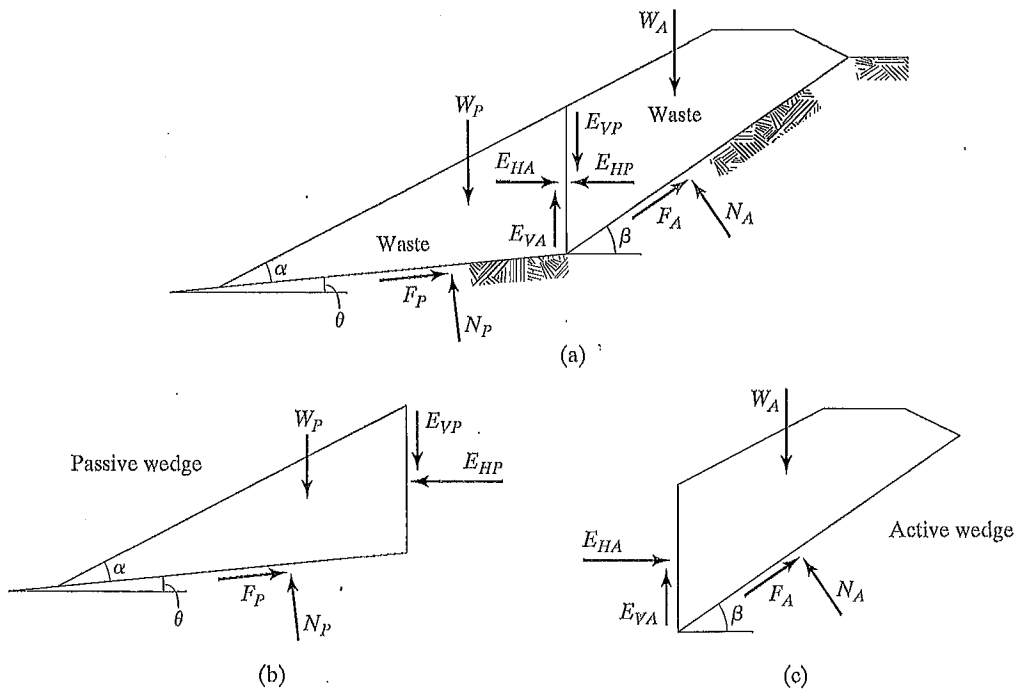


FIGURE 13.24 Forces Acting on Two adjacent Wedges for Solid Waste Filled in Landfill

$E_{VP}$  = frictional force acting on the side of the passive wedge (unknown in magnitude, but with the direction parallel to the interface of the active and passive wedges);

$FS_P$  = factor of safety for the passive wedge;

$\delta_P$  = minimum interface friction angle of multi-layer liner components beneath the passive wedge;

$\phi_s$  = friction angle of the solid waste;

$\alpha$  = angle of the solid waste slope, measured from horizontal, degrees;

$\theta$  = angle of the landfill cell subgrade, measured from horizontal, degrees;

$W_A$  = weight of the active wedge;

$W_T$  = total weight of the active and passive wedges;

$N_A$  = normal force acting on the bottom of the active wedge;

$F_A$  = frictional force acting on the bottom of the active wedge (parallel to the bottom of the active wedge);

$E_{HA}$  = normal force from passive wedge acting on the active wedge (unknown in magnitude, but with the direction perpendicular to the interface of the active and passive wedges),  $E_{HA} = E_{HP}$ ;

$E_{VA}$  = frictional force acting on the side of the active wedge (unknown in magnitude, but with the direction parallel to the interface of the active and passive wedges),  $E_{VA} = E_{VP}$ ;

$FS_A$  = factor of safety for the active wedge;

$\delta_A$  = minimum interface friction angle of multi-layer liner components beneath the active wedge;

$\beta$  = angle of the side slope, measured from horizontal, degrees;

$FS$  = factor of safety for the entire solid waste mass.

Considering the force equilibrium of the passive wedge [Figure 13.24(b)], the forces acting on it are

$$\Sigma F_Y = 0:$$

$$W_P + E_{VP} = N_P \cdot \cos \theta + F_P \cdot \sin \theta \quad (13.47)$$

$$F_P = N_P \cdot \tan \delta_P / FS_P \quad (13.48)$$

$$E_{VP} = E_{HP} \cdot \tan \phi_s / FS_P \quad (13.49)$$

Substituting Equations 13.48 and 13.49 into Equation 13.47 gives

$$W_P + E_{HP} \cdot \tan \phi_s / FS_P = N_P \cdot (\cos \theta + \sin \theta \cdot \tan \delta_P / FS_P), \text{ and} \quad (13.50)$$

when  $\Sigma F_X = 0$ ,

$$F_P \cdot \cos \theta = E_{HP} + N_P \cdot \sin \theta \quad (13.51)$$

Substituting Equation (13.48) into Equation (13.51) gives

$$N_P \cdot \cos \theta \cdot \tan \delta_P / FS_P = E_{HP} + N_P \cdot \sin \theta$$

$$N_P \cdot (\cos \theta \cdot \tan \delta_P / FS_P - \sin \theta) = E_{HP}$$

$$N_P = \frac{E_{HP}}{\cos\theta \cdot \tan\delta_P/FS_P - \sin\theta} \quad (13.52)$$

Substituting Equation 13.52 into Equation 13.50 gives

$$\begin{aligned} W_P + E_{HP} \cdot \tan\phi_s/FS_P &= \frac{E_{HP} \cdot (\cos\theta + \sin\theta \cdot \tan\delta_P/FS_P)}{\cos\theta \cdot \tan\delta_P/FS_P - \sin\theta} \\ E_{HP} \cdot (\cos\theta + \sin\theta \cdot \tan\delta_P/FS_P) &= W_P \cdot (\cos\theta \cdot \tan\delta_P/FS_P - \sin\theta) \\ &\quad + E_{HP} \cdot (\cos\theta \cdot \tan\delta_P/FS_P - \sin\theta) \cdot \tan\phi_s/FS_P \\ E_{HP} \cdot (\cos\theta + \sin\theta \cdot \tan\delta_P/FS_P - \cos\theta \cdot \tan\delta_P \cdot \tan\phi_s/FS_P^2 + \sin\theta \cdot \tan\phi_s/FS_P) &= W_P \cdot (\cos\theta \cdot \tan\delta_P/FS_P - \sin\theta) \\ E_{HP} &= \frac{W_P \cdot (\cos\theta \cdot \tan\delta_P/FS_P - \sin\theta)}{\cos\theta + (\tan\delta_P + \tan\phi_s) \cdot \sin\theta/FS_P - \cos\theta \cdot \tan\delta_P \cdot \tan\phi_s/FS_P^2} \quad (13.53) \end{aligned}$$

Considering the force equilibrium of the active wedge [Figure 13.12(c)] yields

$$\Sigma F_Y = 0:$$

$$W_A = F_A \cdot \sin\beta + N_A \cdot \cos\beta + E_{VA} \quad (13.54)$$

$$F_A = N_A \cdot \tan\delta_A/FS_A \quad (13.55)$$

$$E_{VA} = E_{HA} \cdot \tan\phi_s/FS_A \quad (13.56)$$

Substituting Equations 13.55 and 13.56 into Equation 13.54 gives

$$W_A = N_A \cdot (\cos\beta + \sin\beta \cdot \tan\delta_A/FS_A) + E_{HA} \cdot \tan\phi_s/FS_A \quad (13.57)$$

$$\Sigma F_X = 0:$$

$$F_A \cdot \cos\beta + E_{HA} = N_A \cdot \sin\beta \quad (13.58)$$

Substituting Equation 13.55 into Equation 13.58 gives

$$\begin{aligned} E_{HA} &= N_A \cdot (\sin\beta - \cos\beta \cdot \tan\delta_A/FS_A) \\ N_A &= \frac{E_{HA}}{\sin\beta - \cos\beta \cdot \tan\delta_A/FS_A} \quad (13.59) \end{aligned}$$

Substituting Equation 13.59 into Equation 13.57 gives

$$\begin{aligned} W_A &= E_{HA} \cdot \frac{\cos\beta + \sin\beta \cdot \tan\delta_A/FS_A}{\sin\beta - \cos\beta \cdot \tan\delta_A/FS_A} + E_{HA} \cdot \tan\phi_s/FS_A \\ E_{HA} \cdot \frac{\cos\beta + \sin\beta \cdot \tan\delta_A/FS_A + \sin\beta \cdot \tan\phi_s/FS_A - \cos\beta \cdot \tan\delta_A \cdot \tan\phi_s/FS_A^2}{\sin\beta - \cos\beta \cdot \tan\delta_A/FS_A} &= W_A \\ E_{HA} &= \frac{W_A \cdot (\sin\beta - \cos\beta \cdot \tan\delta_A/FS_A)}{\cos\beta + (\tan\delta_A + \tan\phi_s) \cdot \sin\beta/FS_A - \cos\beta \cdot \tan\delta_A \cdot \tan\phi_s/FS_A^2} \quad (13.60) \end{aligned}$$

Because  $E_{HLA} = E_{HP}$  and  $FS_A = FS_P = FS$ , Equation 13.60 must equal Equation 13.53, giving

$$\frac{W_A \cdot (\sin \beta - \cos \beta \cdot \tan \delta_A / FS)}{\cos \beta + (\tan \delta_A + \tan \phi_s) \cdot \sin \beta / FS - \cos \beta \cdot \tan \delta_A \cdot \tan \phi_s / FS^2} = \frac{W_P \cdot (\cos \theta \cdot \tan \delta_P / FS - \sin \theta)}{\cos \theta + (\tan \delta_P + \tan \phi_s) \cdot \sin \theta / FS - \cos \theta \cdot \tan \delta_P \cdot \tan \phi_s / FS^2}$$

$$\begin{aligned} & W_A \cdot (\sin \beta - \cos \beta \cdot \tan \delta_A / FS) [\cos \theta + (\tan \delta_P + \tan \phi_s) \cdot \sin \theta / FS - \cos \theta \cdot \tan \delta_P \cdot \tan \phi_s / FS^2] \\ &= W_P \cdot (\cos \theta \cdot \tan \delta_P / FS - \sin \theta) [\cos \beta + (\tan \delta_A + \tan \phi_s) \cdot \sin \beta / FS - \cos \beta \cdot \tan \delta_A \cdot \tan \phi_s / FS^2] \\ & (W_A \cdot \sin \beta - W_A \cdot \cos \beta \cdot \tan \delta_A / FS) [\cos \theta + (\tan \delta_P + \tan \phi_s) \cdot \sin \theta / FS - \cos \theta \cdot \tan \delta_P \cdot \tan \phi_s / FS^2] \\ &= (W_P \cdot \cos \theta \cdot \tan \delta_P / FS - W_P \cdot \sin \theta) [\cos \beta + (\tan \delta_A + \tan \phi_s) \cdot \sin \beta / FS - \cos \beta \cdot \tan \delta_A \cdot \tan \phi_s / FS^2] \\ & W_A \cdot \sin \beta \cdot \cos \theta + W_A \cdot (\tan \delta_P + \tan \phi_s) \cdot \sin \beta \cdot \sin \theta / FS - W_A \cdot \sin \beta \cdot \cos \theta \cdot \tan \delta_P \cdot \tan \phi_s / FS^2 \\ & - W_A \cdot \cos \beta \cdot \cos \theta \cdot \tan \delta_A / FS - W_A \cdot (\tan \delta_P + \tan \phi_s) \cdot \cos \beta \cdot \sin \theta \cdot \tan \delta_A / FS^2 \\ & + W_A \cdot \cos \beta \cdot \cos \theta \cdot \tan \delta_A \cdot \tan \delta_P \cdot \tan \phi_s / FS^3 = W_P \cdot \cos \beta \cdot \cos \theta \cdot \tan \delta_P / FS \\ & + W_P \cdot (\tan \delta_A + \tan \phi_s) \cdot \sin \beta \cdot \cos \theta \cdot \tan \delta_P / FS^2 - W_P \cdot \cos \beta \cdot \cos \theta \cdot \tan \delta_A \cdot \tan \delta_P \cdot \tan \phi_s / FS^3 \\ & - W_P \cdot \cos \beta \cdot \sin \theta - W_P \cdot (\tan \delta_A + \tan \phi_s) \cdot \sin \beta \cdot \sin \theta / FS + W_P \cdot \cos \beta \cdot \sin \theta \cdot \tan \delta_A \cdot \tan \phi_s / FS^2 \\ & (W_A \cdot \sin \beta \cdot \cos \theta + W_P \cdot \cos \beta \cdot \sin \theta) \cdot FS^3 + [W_A \cdot (\tan \delta_P + \tan \phi_s) \cdot \sin \beta \cdot \sin \theta \\ & + W_P \cdot (\tan \delta_P + \tan \phi_s) \cdot \sin \beta \cdot \sin \theta - W_A \cdot \cos \beta \cdot \cos \theta \cdot \tan \delta_A - W_P \cdot \cos \beta \cdot \cos \theta \cdot \tan \delta_P] \cdot FS^2 \\ & - [W_A \cdot (\tan \delta_P + \tan \phi_s) \cdot \cos \beta \cdot \sin \theta \cdot \tan \delta_A + W_P \cdot (\tan \delta_A + \tan \phi_s) \cdot \sin \beta \cdot \cos \theta \cdot \tan \delta_P \\ & + W_A \cdot \sin \beta \cdot \cos \theta \cdot \tan \delta_P \cdot \tan \phi_s + W_P \cdot \cos \beta \cdot \sin \theta \cdot \tan \delta_A \cdot \tan \phi_s] \cdot FS \\ & + (W_A \cdot \cos \beta \cdot \cos \theta \cdot \tan \delta_A \cdot \tan \delta_P \cdot \tan \phi_s + W_P \cdot \cos \beta \cdot \cos \theta \cdot \tan \delta_A \cdot \tan \delta_P \cdot \tan \phi_s) = 0 \\ & (W_A \cdot \sin \beta \cdot \cos \theta + W_P \cdot \cos \beta \cdot \sin \theta) \cdot FS^3 + [(W_A \cdot \tan \delta_P + W_P \cdot \tan \delta_A + W_T \cdot \tan \phi_s) \cdot \sin \beta \cdot \sin \theta \\ & - (W_A \cdot \tan \delta_A + W_P \cdot \tan \delta_P) \cdot \cos \beta \cdot \cos \theta] \cdot FS^2 - [W_T \cdot \tan \phi_s \cdot (\sin \beta \cdot \cos \theta \cdot \tan \delta_P \\ & + \cos \beta \cdot \sin \theta \cdot \tan \delta_A) + (W_A \cdot \cos \beta \cdot \sin \theta + W_P \cdot \sin \beta \cdot \cos \theta) \cdot \tan \delta_A \cdot \tan \delta_P] \cdot FS \\ & + W_T \cdot \cos \beta \cdot \cos \theta \cdot \tan \delta_A \cdot \tan \delta_P \cdot \tan \phi_s = 0 \end{aligned} \quad (13.61)$$

Equation 13.61 is now solved as follows:

$$a \cdot FS^3 + b \cdot FS^2 + c \cdot FS + d = 0 \quad (13.62)$$

$$\begin{aligned} a &= W_A \cdot \sin \beta \cdot \cos \theta + W_P \cdot \cos \beta \cdot \sin \theta \\ b &= (W_A \cdot \tan \delta_P + W_P \cdot \tan \delta_A + W_T \cdot \tan \phi_s) \cdot \sin \beta \cdot \sin \theta \\ & \quad - (W_A \cdot \tan \delta_A + W_P \cdot \tan \delta_P) \cdot \cos \beta \cdot \cos \theta \\ c &= -[W_T \cdot \tan \phi_s \cdot (\sin \beta \cdot \cos \theta \cdot \tan \delta_P + \cos \beta \cdot \sin \theta \cdot \tan \delta_A) \\ & \quad + (W_A \cdot \cos \beta \cdot \sin \theta + W_P \cdot \sin \beta \cdot \cos \theta) \cdot \tan \delta_A \cdot \tan \delta_P] \\ d &= W_T \cdot \cos \beta \cdot \cos \theta \cdot \tan \delta_A \cdot \tan \delta_P \cdot \tan \phi_s \end{aligned}$$

When the cell subgrade is very small (i.e.,  $\theta \approx 0$ ),  $\sin \theta \approx 0$ , and  $\cos \theta \approx 1$ , Equation 13.62 then becomes

$$a \cdot FS^3 + b \cdot FS^2 + c \cdot FS + d = 0 \quad (13.63)$$

$$\begin{aligned} \text{where } a &= W_A \cdot \sin \beta \\ b &= -(W_A \cdot \tan \delta_A + W_P \cdot \tan \delta_P) \cdot \cos \beta \end{aligned}$$

$$c = -(W_T \cdot \tan \phi_s + W_P \cdot \tan \delta_A) \cdot \sin \beta \cdot \tan \delta_P$$

$$d = W_T \cdot \cos \beta \cdot \tan \delta_A \cdot \tan \delta_P \cdot \tan \phi_s$$

In the conventional translational (or two-wedge) failure analysis method, the direction of the resultant force  $E_P$  of  $E_{HP}$  and  $E_{VP}$  (or the resultant force  $E_A$  of  $E_{HA}$  and  $E_{VA}$ ), which acts on the interface between the passive wedge and active wedge, is usually assumed to be parallel to waste filling slope. The effect of the waste property of the interface between the active and passive wedges (i.e., shear strength of the waste) on the stability is not considered for this assumption. Actually, the real direction of the resultant force  $E_A$  of  $E_{HA}$  and  $E_{VA}$  (or the direction of the interwedge force) should be calculated as

$$\begin{aligned} \tan \omega &= E_{VP}/E_{HP} \\ &= (E_{HP} \cdot \tan \phi_s / FS) / E_{HP} \\ &= \tan \phi_s / FS \\ \omega &= \tan^{-1}(\tan \phi_s / FS) \end{aligned} \quad (13.64)$$

where  $\omega$  = inclination angle of the interwedge force (i.e., the resultant force of  $E_{HP}$  and  $E_{VP}$ ), measured from horizontal, degrees;  
 $\phi_s$  = friction angle of solid waste;  
 $FS$  = factor of safety for the entire solid waste mass.

Municipal solid waste usually settles a considerable amount during the filling operation. Review of field settlements from several landfills indicates that municipal solid waste landfills usually settle approximately 15 to 30% of the initial height because of placement and decomposition. The large settlement of the waste fill induces shear stresses in the liner system on the side slope, all of which tends to displace the liner downslope. The large settlement of the waste fill also causes the large deformation of the landfill cover to induce shear stresses in the final cover system. These shear stresses induce shear displacements along specific interfaces in the liner and cover systems that may lead to the mobilization of a residual interface strength. In addition, thermal expansion and contraction of the side slope liner and cover systems during construction and filling may also contribute to the accumulation of shear displacements and the mobilization of a residual interface shear strength in the liner system (Qian, 1994; Stark and Poeppel, 1994).

Earthquake loading can provide permanent displacements along landfill liner interfaces, resulting in a permanent reduction in their available shear resistance following the completion of the dynamic loading. Post-earthquake static stability must therefore be evaluated using shear strengths that are compatible with the shear displacements predicted to be experienced during the earthquake. In areas of high seismicity, this probably implies that the static stability of the final configuration of the landfill should be assured assuming the mobilization of full residual strength conditions (Byrne, 1994).

Landfill stability should be considered not only during construction and operation periods, but also for the duration of the closure period. Land development of closed landfills should be also considered in the future. Thus, the shear strengths (e.g.,  $\delta_p$ ,  $\delta_A$ , and  $\phi_s$ ) used in stability analysis must be carefully selected based on actual site-specific conditions.

**EXAMPLE 13.8**

Calculate the factor of safety for a landfill filling shown in Figure 13.25. Use a translational failure analysis and the following information:

- Minimum interface friction angle of bottom liner system,  $\delta_p = 20^\circ$ ;
- Minimum interface residual friction angle of side slope liner system,  $\delta_A = 14^\circ$ ;
- Friction angle of solid waste,  $\phi_s = 33^\circ$ ;
- Waste unit weight =  $10.2 \text{ kN/m}^3$ ;
- Landfill subgrade is 2% [50(H) : 1(V)];
- Waste filling slope is 25% [4(H) : 1(V)];
- Side slope angle,  $\beta = 18.4^\circ$ ;
- Height of side slope is 30 m;
- Distance between the top edge of waste and the top edge of side slope is 20 m.

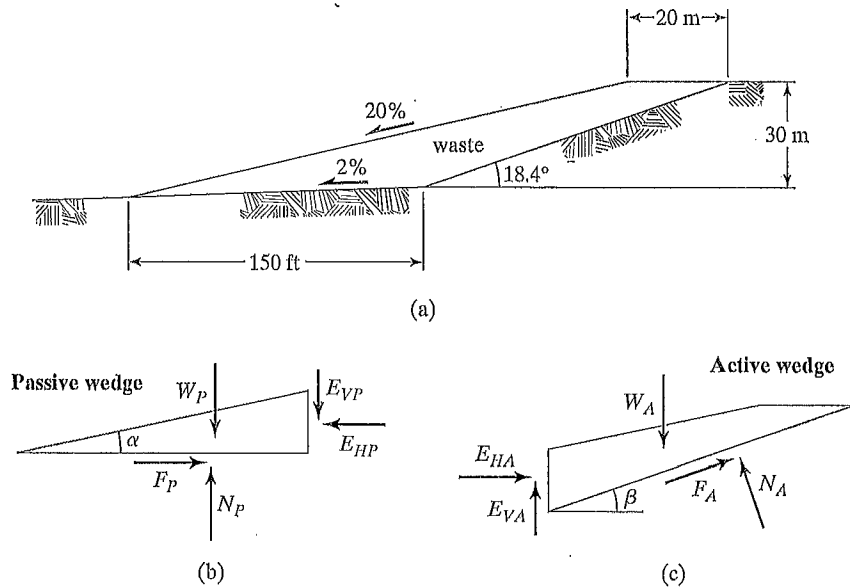


FIGURE 13.25 Cross Section of a Solid Waste Landfill during Filling Condition

**Solution** The forces acting on the solid waste mass are shown in Figure 13.25. The side slope angle is at  $18.4^\circ$  and the slope angle of cell subgrade is  $1.15^\circ$  according to a 2% slope; hence,

$$\begin{aligned}\sin\beta &= \sin(18.4^\circ) = 0.3162, \cos\beta = \cos(18.4^\circ) = 0.9487, \\ \sin\theta &= \sin(1.15^\circ) = 0.0200, \cos\theta = \cos(1.15^\circ) = 0.9998 \\ \tan\delta_A &= \tan(14^\circ) = 0.2493, \tan\delta_P = \tan(20^\circ) = 0.3640, \\ \tan\phi_s &= \tan(33^\circ) = 0.6494.\end{aligned}$$

The total weight of solid waste mass is

$$W_T = 10,987 \text{ kN/m}$$

The weight of the passive wedge is

$$W_P = 3,465 \text{ kN/m}$$

The weight of the active wedge is

$$W_A = W_T - W_P = 10,987 - 3,465 = 7,522 \text{ kN/m}$$

Use Equation 13.62 to calculate  $FS$ .

Calculate the coefficients of  $a$ ,  $b$ ,  $c$ , and  $d$  in Equation 13.62:

$$\begin{aligned}a &= W_A \cdot \sin\beta \cdot \cos\theta + W_P \cdot \cos\beta \cdot \sin\theta \\ &= 7,522 \times 0.3162 \times 0.9998 + 3,465 \times 0.9487 \times 0.0200 \\ &= 2,444 \text{ kN/m} \\ b &= (W_A \cdot \tan\delta_P + W_P \cdot \tan\delta_A + W_T \cdot \tan\phi_s) \cdot \sin\phi \cdot \sin\theta - (W_A \cdot \tan\delta_A + W_P \cdot \tan\delta_P) \cdot \cos\beta \cdot \cos\theta \\ &= (7,522 \times 0.3640 + 3,465 \times 0.2493 + 10,987 \times 0.6494) \times 0.3162 \times 0.0200 - \\ &\quad (7,522 \times 0.2493 + 3,465 \times 0.3640 \times 0.9487 \times 0.9998) \\ &= -2,907 \text{ kN/m} \\ c &= -[W_T \cdot \tan\phi_s \cdot (\sin\beta \cdot \cos\theta \cdot \tan\delta_P + \cos\beta \cdot \sin\theta \cdot \tan\delta_A) + \\ &\quad (W_A \cdot \cos\beta \cdot \sin\theta \cdot W_P \cdot \sin\beta \cdot \cos\theta) \cdot \tan\delta_A \cdot \tan\delta_P] \\ &= -[10,987 \times 0.6494 \times (0.3162 \times 0.9998 \times 0.3640 + 0.9487 \times 0.0200 \times 0.2493) + \\ &\quad (7,522 \times 0.9487 \times 0.0200 + 3,465 \times 0.3162 \times 0.9998) \times 0.2493 \times 0.3640] \\ &= -967 \text{ kN/m} \\ d &= W_T \cdot \cos\beta \cdot \cos\theta \cdot \tan\delta_A \cdot \tan\delta_P \cdot \tan\phi_s \\ &= 10,987 \times 0.9487 \times 0.9998 \times 0.2493 \times 0.3640 \times 0.6494 \\ &= 614 \text{ kN/m} \\ a \cdot FS^3 + b \cdot FS^2 + c \cdot FS + d &= 0 \tag{13.62} \\ 2,444 \cdot FS^3 - 2,907 \cdot FS^2 - 967 \cdot FS + 614 &= 0 \\ FS^3 - 1.189 \cdot FS^2 - 0.396 \cdot FS + 0.251 &= 0 \\ FS^3 + 0.251 &= 1.189 \cdot FS^2 + 0.396 \cdot FS\end{aligned}$$

which is solved by trial and error as in the following table:

Assumed $FS$	$FS^3 + 0.251$	$1.189 \cdot FS^2 + 0.396 \cdot FS$	Closure
(1)	(2)	(3)	(2) - (3)
1.5	3.626	3.269	0.357
1.4	2.995	2.885	0.110
1.3	2.448	2.524	-0.076
1.35	2.711	2.702	0.009
1.34	2.657	2.666	-0.009
1.345	2.684	2.684	0

Thus,  $FS = 1.345$ .

The direction of the resultant force of  $E_{HP}$  and  $E_{VP}$  (i.e., direction of the interwedge force) can be calculated from Equation 13.34 as

$$\begin{aligned}
 \tan \omega &= \tan \phi_s / FS & (13.64) \\
 &= \tan(33^\circ) / 1.345 \\
 &= 0.649 / 1.345 \\
 &= 0.483 \\
 \omega &= 25.8^\circ
 \end{aligned}$$

Recall that the inclination of waste filling slope is 20%, which is only 11.3°. Thus, the direction of the resultant force of  $E_{HP}$  and  $E_{VP}$  is definitely not parallel to the waste filling slope as is often assumed in these types of calculations (Corps of Engineers, 1960).

### 13.6.2 Case Histories

Alternatively, for the analysis of the case histories that follow, which failed in a translational manner, the simplified Janbu method was used. (See Koerner and Soong, 2000.) This derivation is also readily available in the literature and leads to a similar equation for the  $FS$ -value, but it is now modified with an  $f_o$ -value. The resulting equation is

$$FS = (f_o) \cdot \frac{\sum_{i=1}^n [c \cdot \Delta b_i + (W_i - u_i \cdot \Delta b_i) \cdot \tan \phi] / m_i}{\sum_{i=1}^n W_i \cdot \sin \theta_i} \quad (13.65)$$

where  $m_i$  is defined in Equation 13.31, and  $f_o$  is a function of the curvature ratio of the failure surface and the type of soil. Since these surfaces are linear, however, the depth-to-length ratio is zero and the value of  $f_o = 1.0$ . The analysis becomes quite straightforward. (See Schuster and Krizek, 1978.)

To illustrate the seriousness of translational failures (they have represented the largest waste mass failures to date), three case histories are presented next.

**APPLICATION FOR PERMIT  
DNCS ENVIRONMENTAL SOLUTIONS**

**VOLUME III: ENGINEERING DESIGN AND CALCULATIONS  
SECTION 7: TENSILE STRESS ANALYSIS**

**ATTACHMENT III.7.D**

**CETCO® LINING TECHNOLOGIES, 2009.**

***BENTOMAT® GCL DIRECT SHEAR DATABASE (TR-114BM)***

## BENTOMAT<sup>®</sup> DIRECT SHEAR TESTING SUMMARY

The following table summarizes the direct shear testing on Bentomat that has been performed by CETCO and other laboratories on a project-specific basis for the past several years. This data will give the designer some general information about the shear strength of commonly used GCL interfaces and should be the first step in evaluating a proposed liner system where slope stability is a concern.

The variables in any direct shear test are numerous, including specimen preparation; hydration pressures, liquids, and sequencing, and rate of shear, and others. Test results will vary accordingly, which is partially accountable for the wide range of data reported even for similar interfaces.

This data is for informational purposes only and is not intended to replace project-specific interface testing, which CETCO emphatically recommends. CETCO makes no warranty as to the usefulness of the data. Individual test reports for most of the summarized data can be provided upon request.

BENTOMAT GCL DIRECT SHEAR DATABASE  
TR-114BM

Lab <sup>1</sup>	Report Date	GCL Tested	Interface Tested <sup>2</sup>		Testing Conditions				Mohr-Coulomb Failure Envelopes <sup>6</sup>			Comments <sup>8</sup>		
			GCL	Other	Normal Stresses (psi)	Hydratn. <sup>3</sup> psf	Consol. <sup>4</sup> hrs	SDR <sup>5</sup> (in/min)	Angle (deg)	Peak adhesion (psf)	Large Displacement Angle (deg)		adhesion (psf)	
<b>Internal Shear Results</b>														
SGI	Oct-08	200R		Internal	75	200	24	48 hrs @ load	0.04	23 °	0	7 °	0	
SGI	Apr-09	ST		Internal	1.4	200	24	48 hrs @ load	0.004	73 °	0	--	--	sliding at gripping surface
PGL	Feb-08	ST		Internal	1.4		48 hrs @ load		0.004	77 °	0	--	--	sliding at gripping surface
SGI	Jun-06	ST		Internal	34.7	200	24	24 hrs	0.04	27 °	0	7 °	0	
SGI	Jun-06	ST		Internal	34.7	200	24	24 hrs	0.04	31 °	0	8 °	0	
SGI	Jun-06	ST		Internal	34.7	200	24	24 hrs	0.04	38 °	0	9 °	0	
SGI	Jun-06	ST		Internal	34.7	200	24	24 hrs	0.04	31 °	0	7 °	0	
SGI	Jun-06	ST		Internal	34.7	200	24	24 hrs	0.04	42 °	0	9 °	0	
SGI	Jun-06	ST		Internal	34.7	200	24	24 hrs	0.04	34 °	0	7 °	0	
SGI	Jun-06	ST		Internal	34.7	200	24	24 hrs	0.04	26 °	0	7 °	0	
SGI	Oct-06	ST		Internal	34.7	200	24	24 hrs	0.04	37 °	0	8 °	0	
PGL	Feb-03	ST		Internal	5 20 45	432	7 days	48 hrs @ load	0.004	22.7 °	1146	19.3 °	676	
SGI	Aug-01	ST		Internal	10 30 50		24 hrs @ load		0.001	32 °	1645	13 °	160	
SGI	Aug-01	ST		Internal	10 30 50		24 hrs @ load		0.001	39 °	1050	15 °	220	
SGI	Aug-01	ST		Internal	10 30 50		24 hrs @ load		0.001	38 °	1105	17 °	190	
SGI	Apr-09	ST		Internal	75	200	24	48 hrs @ load	0.004	32 °	0	8 °	0	

# BENTOMAT GCL DIRECT SHEAR DATABASE

## TR-114BM

Lab <sup>1</sup>	Report Date	GCL Tested	Interface Tested <sup>2</sup>		Testing Conditions							Mohr-Coulomb Failure Envelopes <sup>6</sup>				Comments <sup>8</sup>
					Normal Stresses (psi)	Hydration. <sup>3</sup>		Consol. <sup>4</sup>	SDR <sup>5</sup> (in/min)	Peak adhesion (psf)	Angle (deg)	Large Displacement <sup>7</sup> adhesion (psf)	Angle (deg)			
						psf	hrs									
SGI	Jan-09	ST		Internal	75	200	24	48 hrs @ load	0.04	0	32 °	0	7 °	0		
SGI	Feb-08	ST		Internal	75	200	24	48 hrs @ load	0.04	0	38 °	0	8 °	0		
SGI	Jan-07	ST		Internal	75	200	24	48 hrs @ load	0.004	0	33 °	0	11 °	0		
SGI	Oct-98	ST		Internal	36 75 145	167	6 days	step-load	0.00006	1545	22 °	1545	6 °	731		
SGI	Jan-09	ST		Internal	150	200	24	48 hrs @ load	0.04	0	24 °	0	6 °	0		
SGI	Feb-01	ST		Internal	50 100 150		48 hrs @ load	0.04	1195	15 °	1195	8 °	-310			
SGI	Feb-01	ST		Internal	150 250 400		48 hrs @ load	0.04	2875	11 °	2875	5 °	1080			
SGI	Feb-01	ST		Internal	50 to 400 psi		48 hrs @ load	0.04	2095	12 °	2095	6 °	275			
SGI	Apr-09	DN		Internal	1.4	200	24	48 hrs @ load	0.004	0	75 °	0	--	--	sliding at gripping surface	
SGI	Feb-08	DN		Internal	1.4		24 hrs @ load	0.004	0	77 °	0	0	--	--	sliding at gripping surface	
TRI	Apr-03	DN		Internal	0.7 1.7 3.5		24 hrs @ load	0.04	2813	47.3 °	2813	26.6 °	392			
SGI	Jun-01	DN		Internal	1.0 2.6 6.5	72	120	step-load	0.004	215	46 °	215	42 °	120		
PGL	Jul-06	DN		Internal	7 21	200	48	24 hrs @ load	0.04	2326	14.5 °	2326	0.5 °	1436		
SGI	Sep-08	DN		Internal	5 25 50	200	24	24 hrs	0.04	1155	34 °	1155	7 °	425		
SGI	Sep-08	DN		Internal	5 25 50	200	24	24 hrs	0.04	1260	33 °	1260	8 °	425		
SGI	Sep-08	DN		Internal	5 25 50	200	24	24 hrs	0.04	990	35 °	990	8 °	430		

**BENTOMAT GCL DIRECT SHEAR DATABASE**  
**TR-114BM**

Lab <sup>1</sup>	Report Date	GCL Tested	Interface Tested <sup>2</sup>		Testing Conditions						Mohr-Coulomb Failure Envelopes <sup>6</sup>				Comments <sup>8</sup>		
			GCL	Other	Normal Stresses (psi)		Hydrat. <sup>3</sup>		Consol. <sup>4</sup>	SDR <sup>5</sup> (in/min)	Angle (deg)	adhesion (psf)	Angle (deg)	Large Displacement <sup>7</sup> adhesion (psf)			
SGI	Sep-08	DN	Internal		5	25	50	200	24	24	24 hrs	0.04	32 °	1185	8 °	380	
SGI	Sep-08	DN	Internal		5	25	50	200	24	24	24 hrs	0.04	35 °	1120	7 °	385	
SGI	Sep-08	DN	Internal		5	25	50	200	24	24	24 hrs	0.04	33 °	1190	8 °	380	
SGI	Sep-08	DN	Internal		5	25	50	200	24	24	24 hrs	0.04	34 °	1150	7 °	410	
SGI	Sep-00	DN	Internal		10	25	50		24 hrs @ load			0.001	31 °	1000	12 °	770	GCL peel = 45 lbs
SGI	Sep-00	DN	Internal		10	25	50		24 hrs @ load			0.001	30 °	1155	10 °	170	GCL peel = 27 lbs
SGI	Mar-01	DN	Internal		15	30	60		48 hrs @ load			0.04	24 °	1655	7 °	180	
SGI	Apr-09	DN	Internal			75		200	24	48 hrs @ load		0.004	33 °	0	8 °	0	
SGI	Feb-08	DN	Internal			75		200	24	48 hrs @ load		0.04	40 °	0	8 °	0	
SGI	Jan-07	DN	Internal			75		200	24	48 hrs @ load		0.004	36 °	0	12 °	0	
SGI	Jun-08	DN	Internal			150		200	24	48 hrs @ load		0.04	28 °	0	7 °	0	
SGI	Sep-02	DN	Internal		34.7	150		As-received (21.6%)			0.04	23 °	1715	13 °	1100		
SGI	Apr-09	SDN	Internal			1.4		200	24	48 hrs @ load		0.004	76 °	0	--	--	sliding at gripping surface
GT	Nov-08	SDN	Internal			1.4		200	24	48 hrs @ load		0.004	74 °	0	--	--	
SGI	Aug-09	SDN	Internal		10	30	70	144	48	24 hrs @ load		0.004	34 °	1248	6 °	1020	
SGI	Apr-09	SDN	Internal			75		200	24	48 hrs @ load		0.004	37 °	0	8 °	0	

# BENTOMAT GCL DIRECT SHEAR DATABASE

## TR-114BM

Lab <sup>1</sup>	Report Date	GCL Tested	Interface Tested <sup>2</sup>		Testing Conditions					Mohr-Coulomb Failure Envelopes <sup>6</sup>			Comments <sup>8</sup>		
			GCL	Other	Normal Stresses (psi)	Hydration: <sup>3</sup>		Consol. <sup>4</sup>	SDR <sup>5</sup> (in/min)	Peak adhesion (psf)	Angle (deg)	Large Displacement <sup>7</sup> adhesion (psf)		Angle (deg)	
SGI	Feb-08	SDN		Internal	75	200	24	48 hrs @ load		0.04	34 °	0	7 °	0	
SGI	Jan-07	SDN		Internal	75	200	24	48 hrs @ load		0.004	36 °	0	12 °	0	
TRI	Apr-08	SDN		Internal	90		24 hrs @ load		0.04	39.1 °	0	0	15.5 °	0	
SGI	Oct-06	SDN		Internal	5 20 90	115	24	step-load		0.004	22 °	755	5 °	435	
TRI	Oct-07	SDN		Internal	41.7 83.3 125	200	24	step-load		0.04	27.2 °	680	17.1 °	0	
SGI	Jun-03	SDN		Internal	150 250 400		48 hrs @ load		0.04	12 °	1390	5 °	1715		
SGI	Aug-08	STM		Internal	1.4		48 hrs @ load		0.004	73 °	0	--	--		sliding at gripping surface
SGI	Feb-01	CL		Internal	139	144	21	168 hrs @ load		0.04	25 °	0	7 °	0	
<b>Interface Shear Results (with geomembranes)</b>															
TRI	May-09	200R		40-mil smooth LLDPE	1 2 4		24 hrs @ load		0.04	11.2 °	4	10 °	4		
SGI	Mar-05	ST	W	60-mil text. HDPE	0.7		48 hrs @ load		0.04	34 °	0	25 °	0		co-extruded textured geomembrane
PGL	Feb-01	ST	white NW	40-mil text. LLDPE	0.35 0.69 1.39	50	24	24 hrs @ load		0.04	29 °	196	16 °	176	co-extruded textured geomembrane
SGI	Dec-08	ST	W	60-mil text. HDPE	2.8	200	24	48 hrs @ load		0.04	40 °	0	26 °	0	co-extruded textured geomembrane
SGI	Apr-07	ST	W	30-mil PVC	1 2 3	100	24	24 hrs @ load		0.04	16 °	5	15 °	5	smooth side
SGI	Apr-07	ST	NW	30-mil PVC	1 2 3	100	24	24 hrs @ load		0.04	14 °	0	14 °	0	smooth side
SGI	Jan-06	ST	W	30-mil PVC	1 2 3	200	48	--		0.04	15 °	5	15 °	0	failure side
SGI	Jan-96	ST	W	30-mil PVC	2 4 6		24 hrs @ load		0.04	17 °	24	17 °	24		

**BENTOMAT GCL DIRECT SHEAR DATABASE**  
**TR-114BM**

Lab <sup>1</sup>	Report Date	GCL Tested	Interface Tested <sup>2</sup>		Testing Conditions						Mohr-Coulomb Failure Envelopes <sup>6</sup>			Comments <sup>8</sup>		
					Normal Stresses (psi)		Hydration. <sup>3</sup>		Consol. <sup>4</sup>	SDR <sup>5</sup> (in/min)	Peak		Large Displacement <sup>7</sup>			
					psf	hrs	Angle (deg)	adhesion (psf)			Angle (deg)	adhesion (psf)				
PGL	Jun-01	ST	NW	40-mil text. LLDPE	1.3	2.6	6.3	72	72	step-load	0.001	24.8 °	230	18.9 °	203	embossed textured geomembrane
TRI	Apr-08	ST		60-mil text. HDPE	0.7	3.5	6.9	100	24	step-load	0.04	23.9 °	107	16.4 °	62	co-extruded textured geomembrane
TRI	Feb-06	ST	NW	60-mil text. HDPE	1.7	3.5	6.9	200	48	24 hrs @ load	0.04	26.7 °	0	23.9 °	0	co-extruded textured geomembrane
TRI	Sep-05	ST	NW	60-mil text. HDPE	2	5	10		24 hrs @ load		0.04	33.8 °	223	20.2 °	181	embossed textured geomembrane
TRI	Aug-06	ST	W	60-mil text. HDPE	3.5	6.9	13.9		48 hrs @ load		0.04	28 °	50	23.6 °	9	embossed textured geomembrane
TRI	Aug-09	ST	W	60-mil text. HDPE	6.9	13.9	20.8		24 hrs @ load		0.04	21.5 °	291	15.1 °	129	embossed textured geomembrane
PGL	Feb-03	ST	W	80-mil text. HDPE	5	20	45	432	7 days	48 hrs @ load	0.004	22.5 °	83	13.6 °	130	embossed textured geomembrane
PGL	Mar-06	ST	W	80-mil text. HDPE	5	20	45	432	7 days	48 hrs @ load	0.004	20 °	379	13.3 °	413	embossed textured geomembrane
PGL	Mar-07	ST	NW	60-mil text. HDPE	13.9	27.8	55.6	500	6 days	24 hrs @ load	0.04	18.1 °	70.5	12.2 °	222.5	
EMCON	Jun-05	ST	NW	60-mil text. HDPE	13.9	34.7	69.4	300	48	24 hrs @ load	0.04	20.6 °	426	8.1 °	738	embossed textured geomembrane
SGI	Jun-09	ST	W	60-mil text. HDPE		75		200	24	48 hrs @ load	0.04	24 °	0	10 °	0	co-extruded textured geomembrane
SGI	Jun-09	ST	W	60-mil text. HDPE		75		200	24	48 hrs @ load	0.04	23 °	0	11 °	0	co-extruded textured geomembrane
SGI	Dec-08	ST	W	60-mil text. HDPE		75		200	24	48 hrs @ load	0.04	22 °	0	11 °	0	co-extruded textured geomembrane
EMCON	Jul-05	ST	NW	60-mil text. HDPE	13.9	55.6	83.3	300	48	24 hrs @ load	0.04	17.8 °	404.9	6.4 °	463.6	
JLT	Oct-04	ST		60-mil text. HDPE	20	45	90	108	3 days	step-load	0.001	24.3 °	323	15.3 °	243	co-extruded textured geomembrane
TRI	Apr-08	ST		60-mil text. HDPE	6.9	69.4	139	100	24	step-load	0.04	18.9 °	0	7.6 °	192	co-extruded textured geomembrane

**BENTOMAT GCL DIRECT SHEAR DATABASE**  
**TR-114BM**

Lab <sup>1</sup>	Report Date	GCL Tested	Interface Tested <sup>2</sup>		Testing Conditions					Mohr-Coulomb Failure Envelopes <sup>6</sup>			Comments <sup>8</sup>
			GCL	Other	Normal Stresses (psi)	Hydration. <sup>3</sup> psf hrs	Consol. <sup>4</sup>	SDR <sup>5</sup> (in/min)	Peak adhesion (psf)	Angle (deg)	Large Displacement <sup>7</sup> adhesion (psf)	Angle (deg)	
SGI	2003	ST	W	60-mil text. HDPE	139	Hydrated		0.04		14.5 °	0	0	Encapsulated design
SGI	Sep-09	ST	NW	60-mil text. HDPE	13.9 139	200 24	step-load	0.04		21 °	550	590	co-extruded textured geomembrane
SGI	Sep-09	ST	W	60-mil text. HDPE	13.9 139	200 24	step-load	0.04		18 °	575	385	co-extruded textured geomembrane
VE	Jun-09	ST		60-mil text. LLDPE	39 78 156	96 hrs @ load		0.04		18 °	990	1600	embossed textured geomembrane
SGI	2003	ST	W	60-mil text. HDPE	208	Hydrated		0.04		13.7 °	0	0	Encapsulated design
GA	Oct-08	ST		60-mil smooth LLDPE	75 150 300	24 hrs @ load		0.04		15 °	662	3355	GCL internal failure @ 300 psi
SGI	Mar-09	DN	white NW	60-mil text. HDPE	1 2 3	240 48	24 hrs @ load	0.04		33 °	65	30	embossed textured geomembrane
SGI	Mar-09	DN	white NW	60-mil text. HDPE	1 2 3	240 48	24 hrs @ load	0.04		36 °	50	45	embossed textured geomembrane
SGI	Mar-09	DN	white NW	60-mil text. HDPE	1 2 3	240 48	24 hrs @ load	0.04		35 °	60	40	embossed textured geomembrane
SGI	Jan-06	DN	black NW	30-mil PVC	1 2 3	200 48	--	0.04		15 °	0	0	failure side
PGL	Jun-01	DN	black NW	Textured HDPE	1.3 2.6 6.3	216 72	step-load	0.001		21.4 °	225	184	2-inch displacement
PGL	Jun-01	DN	black NW	Textured HDPE	1.3 2.6 6.3	72 72	step-load	0.001		24.8 °	230	203	2-inch displacement
SGI	May-01	DN	black NW	40-mil text. LLDPE	1 2.6 6.5	72 120	step-load	0.004		32 °	5	5	embossed textured geomembrane
PGL	Mar-08	DN	white NW	60-mil text. HDPE	5 7 9	24 hrs @ load		0.04		22.5 °	309	305	
EMCON	May-03	DN		Textured HDPE	13.9	Partially hydrated b/w 2 GMs with 0.3" holes		0.04		18.8 °	0	0	Encapsulated b/w GMs with 0.3" holes
GT	Aug-07	DN	black NW	60-mil text. HDPE	18	Hydrated		0.04		26.6 °	0	0	embossed textured geomembrane

**BENTOMAT GCL DIRECT SHEAR DATABASE**  
**TR-114BM**

Lab <sup>1</sup>	Report Date	GCL Tested	Interface Tested <sup>2</sup>		Testing Conditions						Mohr-Coulomb Failure Envelopes <sup>6</sup>			Comments <sup>8</sup>		
					Normal Stresses (psi)		Hydration. <sup>3</sup>		Consol. <sup>4</sup>	SDR <sup>5</sup> (in/min)	Peak adhesion (psf)		Large Displacement <sup>7</sup>			
							psf	hrs			Angle (deg)	adhesion (psf)	Angle (deg)		adhesion (psf)	
SGL	Feb-00	DN	black NW	60-mil text. HDPE	7	14	35	72	72	step-load	0.0016	29 °	370	18 °	375	
PGL	Jul-05	DN		60-mil text. HDPE	13.9	27.8	41.7	48 hrs @ load		0.04	17.2 °	359	15.4 °	275		
SGL	Jul-03	DN	black NW	60-mil text. HDPE	10.4	20.8	41.7	48 hrs @ load		0.04	27 °	60	18 °	25		co-extruded textured geomembrane
SGL	Feb-08	DN	black NW	60-mil text. HDPE	15	30	50	1440	48	24 hrs @ load	0.04	27 °	530	16 °	390	
PGL	Jan-05	DN	white NW	80-mil text. HDPE	15	30	50	1440	48	24 hrs @ load	1	17.2 °	151	8.5 °	303	
PGL	Feb-07	DN		60-mil text. HDPE	10	30	60	24 hrs @ load		0.02	24 °	254	22.6 °	65		
PGL	Dec-06	DN		60-mil text. HDPE	10	30	60	24 hrs @ load		0.02	19.2 °	155	15.5 °	147		
PGL	Dec-06	DN		60-mil text. HDPE	10	30	60	24 hrs @ load		0.02	18.5 °	342	18.6 °	108		
SGL	Jul-02	DN	white NW	60-mil text. HDPE	6.9	34.7	69.4	125	24	48 hrs @ load	0.04	23 °	520	12 °	380	
SGL	Jun-03	DN		40- and 60-mil textured HDPE	69.4		Partially hydrated b/w 2 GMs with 0.25" holes		0.04	29 °	0	21 °	0	0		co-extruded textured geomembrane
EMCON	Jun-03	DN		Textured HDPE	69.4		Partially hydrated b/w 2 GMs with 0.3" holes		0.04	19.6 °	0	6.5 °	0	0		Encapsulated b/w GMs with 0.25" holes
SGL	Feb-08	DN	white NW	60-mil text. HDPE	25	50	75	1440	48	24 hrs @ load	0.04	23 °	570	10 °	420	
SGL	Feb-08	DN	white NW	60-mil text. HDPE	25	50	75	1440	48	24 hrs @ load	0.04	28 °	345	13 °	415	
PGL	Mar-08	DN	black NW	60-mil text. HDPE	25	50	75	24 hrs @ load		0.04	23.6 °	0	22.2 °	0		
SGL	Apr-09	DN	black NW	60-mil text. HDPE	75		200		24	step-load	0.04	30 °	0	14 °	0	
TRI	Oct-07	DN	black NW	60-mil textured HDPE	25	50	75	24 hrs @ load		0.04	22.7 °	52	11.9 °	409		

**BENTOMAT GCL DIRECT SHEAR DATABASE**  
**TR-114BM**

Lab <sup>1</sup>	Report Date	GCL Tested	Interface Tested <sup>2</sup>		Testing Conditions						Mohr-Coulomb Failure Envelopes <sup>6</sup>				Comments <sup>8</sup>
					Normal Stresses (psi)		Hydration. <sup>3</sup>		Consol. <sup>4</sup>	SDR <sup>5</sup> (in/min)	Peak adhesion (psf)	Angle (deg)	Large Displacement <sup>7</sup> adhesion (psf)	Angle (deg)	
					psf	hrs	psf	hrs							
TRI	Oct-07	DN	black NW	60-mil textured HDPE	25	50	75	24 hrs @ load	0.04	1516	10.8 °	5.4 °	1194	co-extruded textured geomembrane	
TRI	Oct-07	DN	black NW	60-mil textured HDPE	25	50	75	24 hrs @ load	0.04	455	20.4 °	9.6 °	644	co-extruded textured geomembrane	
PGL	Mar-07	DN	white NW	60-mil text. LLDPE	25	50	75	24 hrs @ load	0.04	0	23 °	22 °	0	embossed textured geomembrane	
PGL	Mar-06	DN	white NW	60-mil text. LLDPE	25	50	75	24 hrs @ load	0.04	334	20 °	8.6 °	1216	embossed textured geomembrane	
GA	Mar-02	DN	black NW	80-mil text. LLDPE	20.8	41.7	83.3	288 24	10 minutes	789	21.7 °	11.7 °	559	co-extruded textured geomembrane	
GA	Mar-02	DN	black NW	60-mil text. LLDPE	20.8	41.7	83.3	288 24	10 minutes	361	21.5 °	6.7 °	880.5	embossed textured geomembrane	
PGL	Apr-07	DN		60-mil text. HDPE	20.8	41.7	83.3	48 hrs @ load	0.04	0	20.9 °	12.3 °	545		
JLT	May-07	DN	black NW	60-mil text. HDPE	20	45	90	115 4 days	step-load	77	22.1 °	13 °	239	co-extruded textured geomembrane	
SGL	May-08	DN	black NW	60-mil text. HDPE	1.4	100		200 24	48 hrs @ load	130	24 °	12 °	80	co-extruded textured geomembrane	
TRI	Jul-08	DN		60-mil text. HDPE	139			144 24	step-load	0	22 °	10.2 °	0	co-extruded textured geomembrane	
VE	May-03	DN		40- and 60-mil text. HDPE	13.9	27.8	55.6 111	250 48	16 hrs @ load	260	24 °	10 °	650	Encapsulated design	
SGL	Jul-09	DN	black NW	60-mil text. HDPE	13.9	27.8	55.6 111	144 24	24 hrs @ load	560	22 °	11 °	585	co-extruded textured geomembrane	
VE	May-03	DN		40- and 60-mil text. HDPE	27.8	111		As-received (25% moisture)	0.04	0	26 °	16 °	140	Encapsulated design	
EMCON	Nov-02	DN		60-mil text. HDPE	27.8	55.6	111	48 hrs @ load	0.04	0	26 °	16.8 °	0	co-extruded textured geomembrane	
SGL	2003	DN		40- and 80-mil HDPE	5	20	80 120	wetted conditions (not fully hydrated)	0.04	150	27 °	19 °	95	Encapsulated design (slip b/w 80-mil + GCL)	
SGL	2003	DN		40- and 80-mil HDPE	5	20	80 120	wetted conditions (not fully hydrated)	0.04	270	29 °	19 °	120	Encapsulated design (slip b/w 80-mil + GCL)	

# BENTOMAT GCL DIRECT SHEAR DATABASE

## TR-114BM

Lab <sup>1</sup>	Report Date	GCL Tested	Interface Tested <sup>2</sup>		Testing Conditions						Mohr-Coulomb Failure Envelopes <sup>6</sup>			Comments <sup>8</sup>			
					Normal Stresses (psi)		Hydration. <sup>3</sup>		Consol. <sup>4</sup>	SDR <sup>5</sup> (in/min)	Peak adhesion (psf)	Angle (deg)	Large Displacement <sup>7</sup> adhesion (psf)		Angle (deg)		
					5	20	80	120								psf	hrs
SGI	2003	DN		GCL	Other	40- and 80-mil HDPE	5	20	80	120	wetted conditions (not fully hydrated)	0.04	140	28 °	20 °	20	Encapsulated design (slip b/w 80-mil + GCL)
SGI	2003	DN			HDPE	40- and 80-mil HDPE	5	20	80	120	wetted conditions (not fully hydrated)	0.04	145	29 °	19 °	50	Encapsulated design (slip b/w 80-mil + GCL)
SGI	2003	DN			HDPE	40- and 80-mil HDPE	5	20	80	120	wetted conditions (not fully hydrated)	0.04	580	27 °	20 °	70	Encapsulated design (slip b/w 80-mil + GCL)
SGI	2003	DN			HDPE	40- and 80-mil HDPE	5	20	80	120	wetted conditions (not fully hydrated)	0.04	235	27 °	19 °	95	Encapsulated design (slip b/w 80-mil + GCL)
SGI	Jun-08	DN		black NW	60-mil text. HDPE	60-mil text. HDPE	41.7	83.3	125	24 hrs @ load	24 hrs @ load	0.04	105	26 °	15 °	620	2-inch displacement
SGI	Jun-08	DN		black NW	60-mil text. HDPE	60-mil text. HDPE	41.7	83.3	125	24 hrs @ load	24 hrs @ load	0.04	165	25 °	13 °	870	2-inch displacement
SGI	Jun-08	DN		black NW	60-mil text. HDPE	60-mil text. HDPE	41.7	83.3	125	24 hrs @ load	24 hrs @ load	0.04	110	26 °	16 °	485	2-inch displacement
SGI	Jun-08	DN		black NW	60-mil text. HDPE	60-mil text. HDPE	41.7	83.3	125	24 hrs @ load	24 hrs @ load	0.04	20	26 °	16 °	350	2-inch displacement
SGI	Jun-08	DN		black NW	60-mil text. HDPE	60-mil text. HDPE	41.7	83.3	125	24 hrs @ load	24 hrs @ load	0.04	50	26 °	15 °	165	2-inch displacement
SGI	Jul-08	DN		black NW	60-mil text. HDPE	60-mil text. HDPE	125	125	125	24 hrs @ load	24 hrs @ load	0.04	0	25.1 °	16.4 °	0	2-inch displacement
SGI	Aug-03	DN		white NW	60-mil text. HDPE	60-mil text. HDPE	41.7	83.3	125	0	24	48 hrs @ load	835	22 °	15 °	40	2-inch displacement
SGI	Aug-03	DN		white NW	60-mil text. HDPE	60-mil text. HDPE	41.7	83.3	125	0	24	48 hrs @ load	315	25 °	16 °	255	2-inch displacement
TRI	Jun-09	DN			60-mil text. HDPE	60-mil text. HDPE	20.8	55.6	104	139	125	20	24 hrs @ load	24.9 °	8.7 °	617	embossed textured geomembrane
GTX	Apr-07	DN			HDPE	HDPE	34.7	69.4	104	139	48 hrs @ load	0.04	588	26 °	12 °	398	
SGI	Feb-00	DN		black NW	60-mil text. HDPE	60-mil text. HDPE	7 to 150 psi			72	72	step-load	760	22 °	11 °	710	
SGI	Oct-02	DN			80-mil text. HDPE	80-mil text. HDPE	15	25	100	150	1440	48	24 hrs @ load	23 °	14 °	330	co-extruded textured geomembrane

**BENTOMAT GCL DIRECT SHEAR DATABASE**  
**TR-114BM**

Lab <sup>1</sup>	Report Date	GCL Tested	Interface Tested <sup>2</sup>		Testing Conditions						Mohr-Coulomb Failure Envelopes <sup>6</sup>			Comments <sup>8</sup>
					Normal Stresses (psi)	Hydration. <sup>3</sup>		Consol. <sup>4</sup>	SDR <sup>5</sup> (in/min)	Peak adhesion		Large Displacement <sup>7</sup> adhesion (psf)		
						psf	hrs			Angle (deg)	Angle (deg)			
SGI	Nov-02	DN	GCL	Other	25	100	150	As-received (25% moisture)	0.04	24 °	335	18 °	120	co-extruded textured geomembrane
SGI	Feb-00	DN	black NW	HDPE	35	100	150	72	0.0016	21 °	1305	9 °	1105	
GTX	Jul-05	DN	white NW	HDPE	69.4	111	167	24 hrs @ load	0.04	16 °	102	5 °	707	
SGI	Apr-09	DN	black NW	HDPE	75	150	250	200	0.04	18 °	2450	5 °	2220	embossed textured geomembrane
SGI	Jul-09	DN	black NW	HDPE	150	250	400	200	0.04	17 °	3705	4 °	3435	GCL internal failure @ 400 psi
TRI	Mar-07	SDN	black NW	LLDPE	0.7	2.8	4.9	100	0.04	32.6 °	148	22.5 °	83	embossed textured geomembrane
TRI	Mar-07	SDN	black NW	HDPE	0.7	2.8	4.9	24 hrs @ load	0.04	39.3 °	31	26.7 °	44	embossed textured geomembrane
TRI	Mar-07	SDN	black NW	LLDPE	0.7	2.8	4.9	24 hrs @ load	0.04	44.3 °	97	44.5 °	0	structured GM/Drainage Liner
TRI	Mar-07	SDN	black NW	LLDPE	0.7	2.8	4.9	100	0.04	32.6 °	148	22.5 °	83	embossed textured geomembrane
SGI	May-03	SDN	black NW	HDPE	0.7	3.5	6.9	100	0.04	30 °	25	19 °	20	co-extruded textured geomembrane
TRI	Jul-08	SDN	Black NW	HDPE	3.5	13.9	31.3	200	0.04	15.8 °	243	6.5 °	303	co-extruded textured geomembrane
TRI	May-07	SDN		HDPE	6.9	41.7	83.3	250	0.04	23.8 °	467	10.6 °	365	embossed textured geomembrane
SGI	Oct-06	SDN	white NW	HDPE	5	20	90	115	0.04	23 °	695	8 °	425	co-extruded textured geomembrane
PGL	Apr-04	SDN		HDPE	25	60	100	24 hrs @ load	0.04	24.7 °	308	14.1 °	155	
PGL	Sep-04	SDN		HDPE	25	60	100	24 hrs @ load	0.04	22.6 °	0	14.5 °	203	
PGL	Sep-04	SDN		HDPE	25	60	100	24 hrs @ load	0.04	18.9 °	387	15.2 °	333	

**BENTOMAT GCL DIRECT SHEAR DATABASE**  
**TR-114BM**

Lab <sup>1</sup>	Report Date	GCL Tested	Interface Tested <sup>2</sup>		Testing Conditions				Mohr-Coulomb Failure Envelopes <sup>6</sup>			Comments <sup>8</sup>			
			GCL	Other	Normal Stresses (psi)	Hydrat <sup>3</sup> psf hrs	Consol. <sup>4</sup>	SDR <sup>5</sup> (in/min)	Peak Angle (deg)	adhesion (psf)	Large Displacement <sup>7</sup> Angle (deg)		adhesion (psf)		
PGL	Sep-04	SDN		60-mil text. HDPE	25	60	100	24 hrs @ load		0.04	26.4 °	0	24.1 °	0	
PGL	Sep-04	SDN		60-mil text. HDPE	25	60	100	24 hrs @ load		0.04	22.6 °	0	14.5 °	203	
PGL	Sep-04	SDN		60-mil text. HDPE	25	60	100	24 hrs @ load		0.04	18.9 °	387	15.2 °	333	
PGL	Sep-04	SDN		60-mil text. HDPE	25	60	100	24 hrs @ load		0.04	26.4 °	0	24.1 °	0	
EMCON	Dec-02	SDN	white NW	60-mil text. HDPE	27.8	55.6	111	24 hrs @ load	24 hrs @ load	0.04	21.2 °	0	11.4 °	0	co-extruded textured geomembrane
TRI	Oct-07	SDN	black NW	60-mil text. HDPE	41.7	83.3	125	24 hrs @ load	step-load	0.04	22.7 °	0	10.5 °	0	embossed textured geomembrane
GA	Oct-08	SDN		60-mil smooth LLDPE	75	150	300	24 hrs @ load		0.04	18.3 °	662	12.4 °	2246	
SGL	Jun-03	SDN		80-mil text. LLDPE	150	250	400	48 hrs @ load		0.04	11 °	540	7 °	325	co-extruded textured geomembrane
TRI	Jun-07	STM	white NW	60-mil text. LLDPE		100		24 hrs @ load	step-load	0.04	20.1 °	0	11.5 °	0	co-extruded textured geomembrane
SGL	May-07	STM	white NW	40-mil text. LLDPE		100		24 hrs @ load	48 hrs @ load	0.04	24 °	0	10 °	0	co-extruded textured geomembrane
SGL	Aug-09	STM	white NW	60-mil text. LLDPE	39	78	156	96 hrs @ load		0.04	21 °	720	9 °	1185	embossed textured geomembrane
<b>Interface Shear Results (with soil)</b>															
ARD	Aug-01	ST	W	SOIL	2.3	3	3.75	24 hrs @ load		0.04	38.7 °	0	38.7 °	0	CIDCO Pit sand
ARD	Aug-01	ST	NW	SOIL	2.3	3	3.75	24 hrs @ load		0.04	36.5 °	0	36.5 °	0	CIDCO Pit sand
ARD	Aug-01	ST	W	SOIL	2.3	3	3.75	24 hrs @ load		0.04	38.1 °	0	38.1 °	0	Michigan Pit sand
ARD	Aug-01	ST	NW	SOIL	2.3	3	3.75	24 hrs @ load		0.04	36.7 °	0	35.6 °	0	Michigan Pit sand
STS	Jan-00	ST	W	SOIL	1	2	4	48 hrs @ load		0.04	28.6 °	293	28 °	241	Topsol: 62 pcf, 15%

# BENTOMAT GCL DIRECT SHEAR DATABASE

## TR-114BM

Lab <sup>1</sup>	Report Date	GCL Tested	Interface Tested <sup>2</sup>		Testing Conditions					Mohr-Coulomb Failure Envelopes <sup>6</sup>				Comments <sup>8</sup>
			GCL	Other	Normal Stresses (psi)	Hydration. <sup>3</sup>		Consol. <sup>4</sup>	SDR <sup>5</sup> (in/min)	Angle (deg)	adhesion (psf)	Angle (deg)	Large Displacement <sup>7</sup> adhesion (psf)	
TRI	Nov-03	ST	NW	SOIL	1.4	3.6	7.1	24 hrs @ load	0.04	17.7 °	139	18.2 °	135	Soil: 99 pcf, 17%
TRI	Oct-05	ST	W	SOIL	2	5	10	24 hrs @ load	0.04	23.2 °	134	19.9 °	117	Soil: 114 pcf, 14%
TRI	Aug-09	ST	NW	SOIL	7.4	15.4	23.5	24 hrs @ load	0.04	28.1 °	5	25.9 °	0	
PGL	Mar-07	ST	W	SOIL	13.9	27.8	55.6	500 6 days	0.04	21.4 °	279	8.7 °	926	Soil: 110 pcf, 15.2%
TRI	Jul-08	ST	NW	SOIL	3.5	13.9	55.6	24 hrs @ load	0.04	28.7 °	176	16.1 °	474	Soil: 94 pcf, 14.2%
TRI	Nov-06	ST	NW	SOIL	8.1	27.8	55.7	24 hrs @ load	0.04	21.6 °	0	21.6 °	0	Soil: 110 pcf, 12.4%
SGI	Jul-04	ST	W	SOIL	1	20	40	60	0.04	23 °	145	22 °	120	
SGI	Aug-08	ST	NW	SOIL	10	35	60	100 24	0.04	7 °	475	7 °	360	
SGI	Feb-04	ST	W	SOIL	20.8	52.1	79.9	72 7 days	0.0016	9.9 °	930	6.7 °	500	Clay
SGI	Feb-04	ST	W	SOIL	20.8	52.1	79.9	72 7 days	0.0016	10 °	1025	7 °	590	Clay
EMCON	Jul-05	ST	W	SOIL	13.9	55.6	83.3	300 48	0.04	15.6 °	561.1	15.6 °	435.8	
NTH	2005	ST	NW	SOIL	25	50	100	144 24	0.04	11.9 °	0	7.9 °	0	Clay: 95 pcf, 8%
SGI	Apr-06	ST	W	SOIL	20.8	79.9	139	72 7 days	0.004	12 °	905	--	--	Clay: GCL internal failure at 139 psi load
JLT	Jan-03	DN		SOIL	0.3	0.7	1.4	24 hrs @ load	0.04	36.3 °	2	29 °	1	Angular gravel
CETCO	Mar-00	DN	black NW	SOIL	0.7	1.4	2.1	24 hrs @ load	0.04	25.2 °	315	--	--	SP, 108 pcf, 11%
GTX	Jul-05	DN	black NW	SOIL	0.7	1.4	2.8	24 hrs @ load 24 hrs @ load	0.04	31 °	60	18 °	27	

# BENTOMAT GCL DIRECT SHEAR DATABASE

## TR-114BM

Lab <sup>1</sup>	Report Date	GCL Tested	Interface Tested <sup>2</sup>		Testing Conditions					Mohr-Coulomb Failure Envelopes <sup>6</sup>			Comments <sup>8</sup>			
			GCL	Other	Normal Stresses (psi)	Hydration. <sup>3</sup>		Consol. <sup>4</sup>	SDR <sup>5</sup> (in/min)	Peak adhesion (psf)	Angle (deg)	Large Displacement <sup>7</sup> adhesion (psf)		Angle (deg)		
TRI	Nov-08	DN	white NW	SOIL	0.8	1.6	2.9	24 hrs @ load		0.04	41.1 °	0	28.4 °	29	Soil: 105 pcf, 13.5%	
SGI	Nov-08	DN	black NW	SOIL	1	2	3	240	48	24 hrs @ load	0.04	32 °	25	31 °	5	
SGI	Nov-08	DN	black NW	SOIL	1	2	3	240	48	24 hrs @ load	0.04	31 °	25	31 °	5	
TRI	Nov-08	DN	black NW	SOIL	0.7	1.5	3	24 hrs @ load		0.04	18.9 °	70	10.9 °	82	Soil: 105 pcf, 14.1%	
PGL	Jun-01	DN	white NW	SOIL	1.3	2.6	6.3	72	72	step-load	0.001	21.2 °	207	21.6 °	184	2-inch displacement: soil: 103 pcf, 17%
PGL	Jun-01	DN	white NW	SOIL	1.3	2.6	6.3	216	72	step-load	0.001	23.2 °	206	20.8 °	194	2-inch displacement: soil: 103 pcf, 17%
SGI	Jun-01	DN	white NW	SOIL	1.0	2.6	6.5	72	120	step-load	0.004	35 °	65	34 °	40	
PGL	Mar-08	DN	black NW	SOIL	5	7	9	24 hrs @ load		0.04	33.6 °	342	33.6 °	337	Soil: 107 pcf, 13.4%	
ARD	Oct-05	DN	white NW	SOIL	2	5	9.9	48 hrs @ load		0.04	28.2 °	64	28.4 °	47	Medium to fine silty sand: 117 pcf, 9.5%	
ARD	Oct-05	DN	black NW	SOIL	2	5	9.9	48 hrs @ load		0.04	29.3 °	42	29.4 °	38	Medium to fine silty sand: 117 pcf, 9.5%	
SGI	Apr-01	DN	black NW	SOIL	1	5	10	48 hrs @ load		0.04	36 °	35	35 °	10	Soil: 124 pcf, 9 %	
GT	Aug-07	DN	white NW	SOIL	3	5	10	18	Hydrated		0.04	25.8 °	81	24.3 °	92	Soil: 100 pcf, 19.4%
GT	Aug-07	DN	white NW	SOIL	3	5	10	18	Hydrated		0.04	25.1 °	96	16.1 °	135	Soil: 93 pcf, 20.9%
SGI	Jul-03	DN	white NW	SOIL	10.4	20.8	41.7	48 hrs @ load		0.04	28 °	40	26 °	10		
SGI	Mar-01	DN	white NW	SOIL	55.6			1000	24	24 hrs @ load	0.04	26 °	0	23 °	0	
PGL	Dec-06	DN		SOIL	10	30	60	24 hrs @ load		0.02	32.5 °	491	7.5 °	1319	Soil: 92 pcf, 17.5%	

BENTOMAT GCL DIRECT SHEAR DATABASE  
TR-114BM

Lab <sup>1</sup>	Report Date	GCL Tested	Interface Tested <sup>2</sup>		Testing Conditions					Mohr-Coulomb Failure Envelopes <sup>6</sup>				Comments <sup>8</sup>
			GCL	Other	Normal Stresses (psi)	Hydration: <sup>3</sup> psf hrs	Consol. <sup>4</sup>	SDR <sup>5</sup> (in/min)	Angle (deg)	Peak adhesion (psf)	Large Displacement <sup>7</sup> Angle (deg)	adhesion (psf)		
PGL	Dec-06	DN		SOIL	10 30 60	24 hrs @ load		0.02	36.9 °	305	23.2 °	751		
PGL	Aug-04	DN	white NW	SOIL	6.9 41.7 69.4	125 20 16 hrs @ load		0.04	28.6 °	312	15.6 °	854	Soil: 120 pcf, 12%	
PGL	Aug-04	DN	white NW	SOIL	6.9 34.7 69.4	125 20 16 hrs @ load		0.04	20.8 °	177	17.3 °	190	Soil: 114 pcf, 14.9%	
PGL	Aug-04	DN	white NW	SOIL	6.9 41.7 69.4	125 20 16 hrs @ load		0.04	28.6 °	312	15.6 °	854	Soil: 120 pcf, 12%	
PGL	Aug-04	DN	white NW	SOIL	6.9 34.7 69.4	125 20 16 hrs @ load		0.04	20.8 °	177	17.3 °	190	Soil: 114 pcf, 14.9%	
PGL	Mar-06	DN	black NW	SOIL	25 50 75	24 hrs @ load		0.04	32 °	61	32 °	0	Soil: 109 pcf, 14.9%	
PGL	Apr-07	DN		SOIL	20.8 41.7 83.3	48 hrs @ load		0.04	32.2 °	0	31.9 °	0		
PGL	Jul-03	DN		SOIL	3.5 20.8 41.7 83.3	125 24 16 hrs @ load		0.04	22.3 °	320	19 °	322	Soil: 91 pcf, 22%; GCL internal failure at 83 psi	
GTX	Apr-07	DN		SOIL	34.7 69.4 104 139	48 hrs @ load		0.04	20 °	1940	-3 °	3247	Brown silty gravel	
GTX	Jul-05	DN	black NW	SOIL	69.4 111 167	24 hrs @ load		0.04	11 °	1833	4 °	975	Brown clay with silt: 69 pcf, 45%	
OSU	Jan-05	SDN	white NW	SOIL	0.8	Dry		0.04	40.5 °	0	33.2 °	0	Topsoil: 93 pcf, 18%	
OSU	Jan-05	SDN	white NW	SOIL	0.8	2 days @ load		0.04	36.1 °	0	25.5 °	0	Topsoil: 93 pcf, 37.8%	
OSU	Jan-05	SDN	black NW	FGD	0.8	Dry		0.04	44.8 °	0	41.5 °	0	FGD: 93 pcf, 68.4%	
OSU	Jan-05	SDN	black NW	FGD	0.8	2 days @ load		0.04	38.3 °	0	35.3 °	0	FGD: 93 pcf, 68.4%	
OSU	Jan-05	SDN	white NW	SOIL	0.8	2 days @ load		0.04	36.3 °	0	14.3 °	0	Topsoil: 93 pcf, 38.2%	
JLT	Feb-07	SDN		SOIL	0.7 2.1	12 hrs @ load		0.04	27 °	44	17 °	41	Soil: 116 pcf, 16.4%	

# BENTOMAT GCL DIRECT SHEAR DATABASE

## TR-114BM

Lab <sup>1</sup>	Report Date	GCL Tested	Interface Tested <sup>2</sup>		Testing Conditions						Mohr-Coulomb Failure Envelopes <sup>6</sup>					
					Normal Stresses (psi)	Hydration. <sup>3</sup>		Consol. <sup>4</sup>	SDR <sup>5</sup> (in/min)	Peak adhesion (psf)	Angle (deg)	Large Displacement <sup>7</sup>		Comments <sup>8</sup>		
						psf	hrs					Angle (deg)	adhesion (psf)			
SGI	2/205	SDN	black NW	COAL REFUSE	0.7	2.8	144	24	24 hrs @ load	0.04	40	32 °	31 °	40	Coal Refuse	
SGI	Jul-06	SDN	black NW	SOIL	0.7	2.8	24 hrs @ load		0.04	5	34 °	33 °	0	Gravel (34R)		
SGI	Jul-06	SDN	white NW	SOIL	0.7	2.8	24 hrs @ load		0.04	30	32 °	31 °	10	Fine brown sand		
TRI	Apr-07	SDN	white NW	SOIL	0.9	5.2	100	24	24 hrs @ load	0.04	108	25.3 °	23.6 °	117	Soil: 103 pcf, 19.6%	
ARD	Jul-03	SDN	white NW	SOIL	2	5.9	24 hrs @ load		0.04	72	28.5 °	27.7 °	79	Fine brown sand with silt		
ARD	Jul-03	SDN	black NW	SOIL	2	5.9	24 hrs @ load		0.04	43	33.5 °	33.5 °	43	Fine brown sand with silt		
TRI	Jul-08	SDN	Black NW	SOIL	3.5	31.3	62.5	24	step-load	0.04	587	19.3 °	19.1 °	561	Soil: 112 pcf, 17%	
SGI	2/205	SDN	white NW	SOIL	83		144	24	24 hrs @ load	0.04	0	27 °	22 °	0	Compacted Subgrade	
SGI	2/205	SDN	white NW	SOIL	13.9	34.7	55.6	83.3	24	24 hrs @ load	0.04	365	18 °	18 °	485	Compacted Subgrade
SGI	Oct-06	SDN	black NW	SOIL	5	20	90	24	step-load	0.04	245	17 °	9 °	140	Compacted clay	
TRI	May-07	SDN	SOIL	SOIL	9.3	52.3	91.6	24	step-load	0.04	317	21.6 °	6.6 °	1270	Soil: 102 pcf, 12.9%	
EMCON	Dec-02	SDN	white NW	SOIL	27.8	55.6	111	24	24 hrs @ load	0.04	1320	26.8 °	2.7 °	3140	Sand	
TRI	Oct-07	SDN	white NW	SOIL	41.7	83.3	125	24	step-load	0.04	0	28.8 °	5.8 °	2935	Soil: 100 pcf, 12.9%	
SGI	Feb-02	CL	smooth plastic	SOIL	0.7	1.4	2.8	24 hrs @ load		0.04	50	20 °	20 °	40	Graded Aggregate Base	
SGI	Feb-02	CL	smooth plastic	SOIL	0.7	1.4	2.8	24 hrs @ load		0.04	40	18 °	16 °	40	Silty sand	
SGI	Feb-02	CL	smooth plastic	SOIL	0.7	1.4	2.8	24 hrs @ load		0.04	70	19 °	18 °	70	Clay	

**BENTOMAT GCL DIRECT SHEAR DATABASE**  
**TR-114BM**

Lab <sup>1</sup>	Report Date	GCL Tested	Interface Tested <sup>2</sup>		Testing Conditions					Mohr-Coulomb Failure Envelopes <sup>6</sup>				Comments <sup>8</sup>	
			GCL	Other	Normal Stresses (psi)	Hydration. <sup>3</sup>		Consol. <sup>4</sup>	SDR <sup>5</sup> (in/min)	Peak adhesion (psf)	Angle (deg)	Large Displacement <sup>7</sup> adhesion (psf)	Angle (deg)		
						psf	hrs								
PGL	Dec-05	CL	smooth plastic	SOIL	0.7	1.4	2.8	Interface sprayed with water	0.04	67	29.6 °	24.4 °	54	Clayey sand: 113 pcf, 14%	
PGL	Dec-05	CL	smooth plastic	SOIL	0.7	1.4	2.8	Interface sprayed with water	0.04	14	37 °	33 °	8	Silty sand: 115 pcf, 11.5%	
PGL	Dec-05	CL	smooth plastic	SOIL	0.7	1.4	2.8	Interface sprayed with water	0.04	66	25 °	18.5 °	71	CL: 102 pcf, 17.5%	
PGL	Dec-05	CL	smooth plastic	SOIL	0.7	1.4	2.8	Interface sprayed with water	0.04	78	22.9 °	21.8 °	49	CH: 92.8 pcf, 22.6%	
PGL	Dec-05	CL	smooth plastic	SOIL	0.7	1.4	2.8	Interface sprayed with water	0.04	57	22.9 °	22.5 °	58	SP: 106.5 pcf, 5%	
SGL	May-00	CL	W	SOIL	0.5	1.0	2.1	24 hrs @ load	0.04	10	36 °	36 °	10		
CETCO	Mar-00	CLT	W	SOIL	0.7	1.4	2.1	24 hrs @ load	0.04	278	24.9 °	--	--	SP, 108 pcf, 11%	
CETCO	Feb-00	CLT	20-mil text. HDPE	SOIL	0.7	1.4	2.1	24 hrs @ load	0.04	108	41.7 °	--	--	SP, 108 pcf, 11%	
SGL	Mar-01	CLT	20-mil text. HDPE	SOIL		55.6		1000	0.04	0	24 °	21 °	0		
<b>Interface Shear Results (with drainage geocomposites, geonets, and geotextiles)</b>															
GT	Dec-00	ST	W	drainage geocomposite	1.4	2.8	4.2	100	24	--	0.04	25 °	20.7 °	0	1
EMCON	Jul-05	ST	W	drainage geocomposite	13.9	55.6	83.3	300	48	24 hrs @ load	0.04	19.7 °	8.3 °	0	331
PGL	Sep-03	ST	NW	drainage geocomposite	5	19.4	60	83.3	144	24 hrs @ load	0.04	19.8 °	13.6 °	129	164
PGL	Jul-06	ST	W	geonet	1.5	3	6		24 hrs @ load		0.04	23.5 °	23.6 °	33.5	29
GT	Dec-00	DN	black NW	drainage geocomposite	1.4	2.8	4.2	100	24	--	0.04	28 °	21.9 °	0	0
TRI	Sep-06	DN		drainage geocomposite	1.4	2.8	5.6		24 hrs @ load		0.04	30.1 °	27.2 °	14	0
PGL	Sep-09	DN	white NW	drainage geocomposite	0.35	2.78	6.94		24 hrs @ load		0.04	21.7 °	13.8 °	96	68

**BENTOMAT GCL DIRECT SHEAR DATABASE**  
**TR-114BM**

Lab <sup>1</sup>	Report Date	GCL Tested	Interface Tested <sup>2</sup>		Testing Conditions					Mohr-Coulomb Failure Envelopes <sup>6</sup>			Comments <sup>8</sup>		
			GCL	Other	Normal Stresses (psi)	Hydration. <sup>3</sup>		Consol. <sup>4</sup>	SDR <sup>5</sup> (in/min)	Peak Angle (deg)	adhesion (psf)	Large Displacement Angle (deg)		adhesion (psf)	
GTX	Oct-00	DN	black NW	drainage geocomposite	10	30	70	144	72	24 hrs @ load	0.04	22 °	144	18 °	0
GT	Aug-08	DN	white NW	drainage geocomposite	20.8	41.7	83.3	200	24	48 hrs @ load	0.04	28.7 °	152	16.5 °	515
PGL	Dec-06	DN		Nonwoven geotextile	2	3.5	5	24 hrs @ load		0.04	20.7 °	160	6.3 °	167	
GT	Dec-04	SDN	black NW	drainage geocomposite	0.7	1.4	2.8	Hydrated		0.04	21.6 °	9	17.2 °	10	
TRI	Jun-07	SDN		drainage geocomposite	6.9	41.7	83.3	250	24	step-load	0.04	21.4 °	0	9.5 °	278
TRI	Oct-07	SDN	white NW	drainage geocomposite	41.7	83.3	125	200	24	step-load	0.04	27.5 °	0	21.6 °	0
SGL	Jul-06	SDN	white NW	Nonwoven geotextile	0.7	1.4	2.8	24 hrs @ load		0.04	27 °	35	20 °	20	
TRI	Jun-07	CL	smooth plastic	drainage geocomposite	0.7	1.4	2.8	200	24	24 hrs @ load	0.04	19.2 °	33	10.8 °	46
ATT	Dec-98	CL	smooth plastic	drainage geocomposite	1	2	3	72	48	--	0.04	14 °	72	11.6 °	72
SGL	Mar-01	CLT	20-mil text. HDPE	drainage geocomposite		55.6		1000	48	24 hrs @ load	0.04	23 °	0	19 °	0

# BENTOMAT GCL DIRECT SHEAR DATABASE

## TR-114BM

### Notes:

#### (1) Laboratories:

ARD = Ardaman and Associates, Orlando FL  
ATT = Advanced Terra Testing, inc. Lakewood, CO  
CETCO = CETCO, Hoffman Estates, IL  
EMCON = Emcon Assoc. (now Shaw Group), Mahwah, NJ  
GA = Golder Associates, Atlanta, Georgia  
GT = Geotechnics, East Pittsborough, PA  
GTX = Geotesting Express, Boxborough, MA  
JLT = J&L Testing, Canonsburg, PA  
OSU = Ohio State University, Columbus, OH  
PGL = Precision Laboratory, Orange, CA  
SGI = SGI Testing Services LLC, Atlanta, GA (formerly GeoSyntec)  
STS = STS Consultants, Ltd., Vernon Hills, IL  
TRI = TRI Laboratory, Austin, TX  
VE = Vector Engineering, Grass Valley, CA

(2) Internal = Failure forced within the GCL (between the geotextiles).

NW = Non-woven geotextile of Bentomat.

W = Woven geotextile of Bentomat.

(3) Hydrated = specimen was soaked under the specified load for the specified duration prior to testing. Hydration methods may vary

Dry = specimen was tested in the as-received moisture (typically 25-30 percent).

Wetted = specimen was partially hydrated.

(4) Consolidation. If the hydration load does not equal the ultimate normal load for shearing, the normal load is increased in steps.

(5) SDR = Shear Displacement Rate.

(6) Mohr-Coulomb failure envelope,  $\tau = c_0 + \sigma \tan \phi$ , determined by a least-squares, "best-fit" straight line through the shear strength-normal stress test results. Two shear strength components are shown:  $\zeta =$  adhesion and  $\phi =$  friction angle. Caution should be exercised in using these strength parameters for applications involving normal stresses outside the range of the stresses covered. Refer to TR-264 for discussion of cohesion (or adhesion) and friction angle in direct shear tests.

(7) Measured at 3" displacement, unless otherwise noted.

(8) Including information on: geomembrane type; soil type, density, and moisture content; observed GCL internal failure during interface shearing; and any other unique testing conditions.

**APPLICATION FOR PERMIT  
DNCS ENVIRONMENTAL SOLUTIONS**

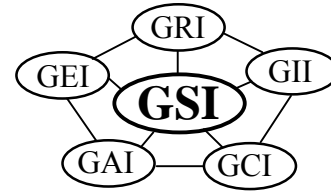
**VOLUME III: ENGINEERING DESIGN AND CALCULATIONS  
SECTION 7: TENSILE STRESS ANALYSIS**

**ATTACHMENT III.7.E**

**KOERNER, ROBERT M. AND KOERNER, GEORGE R. 2007.  
*INTERPETATION(S) OF LABORATORY GENERATED INTERFACE  
SHEAR STRENGTH DATA FOR GEOSYNTHETIC MATERIALS WITH  
EMPHASIS ON THE ADHESION VALUE.*  
GRI WHITE PAPER #11. GEOSYNTHETICS INSTITUTE**

***Geosynthetic Institute***

475 Kedron Avenue  
Folsom, PA 19033-1208 USA  
TEL (610) 522-8440  
FAX (610) 522-8441



**GRI White Paper #11**

**Interpretation(s) of Laboratory Generated Interface Shear Strength  
Data for Geosynthetic Materials With Emphasis on the Adhesion Value**

by

**Robert M. Koerner and George R. Koerner  
Geosynthetic Institute  
475 Kedron Avenue  
Folsom, PA 19033 USA**

**Phone (610) 522-8440  
Fax (610) 522-8441**

**E-mail:  
robert.koerner@coe.drexel.edu  
gkoerner@dca.net**

**September 11, 2007**

## Interpretation(s) of Laboratory Generated Interface Shear Strength Data for Geosynthetic Materials With Emphasis on the Adhesion Value

The beginning point of this White Paper is based on the assumption that a designer has a credible set of laboratory generated shear stress versus shear displacement curves on the desired geosynthetic-to-geosynthetic or geosynthetic-to-soil interface tested per ISO 12957 or ASTM D5321, or ASTM D6243 if geosynthetic clay liners are involved. In this regard we are considering having such data as shown in Figure 1. It is clearly seen that many behavioral trends are possible.

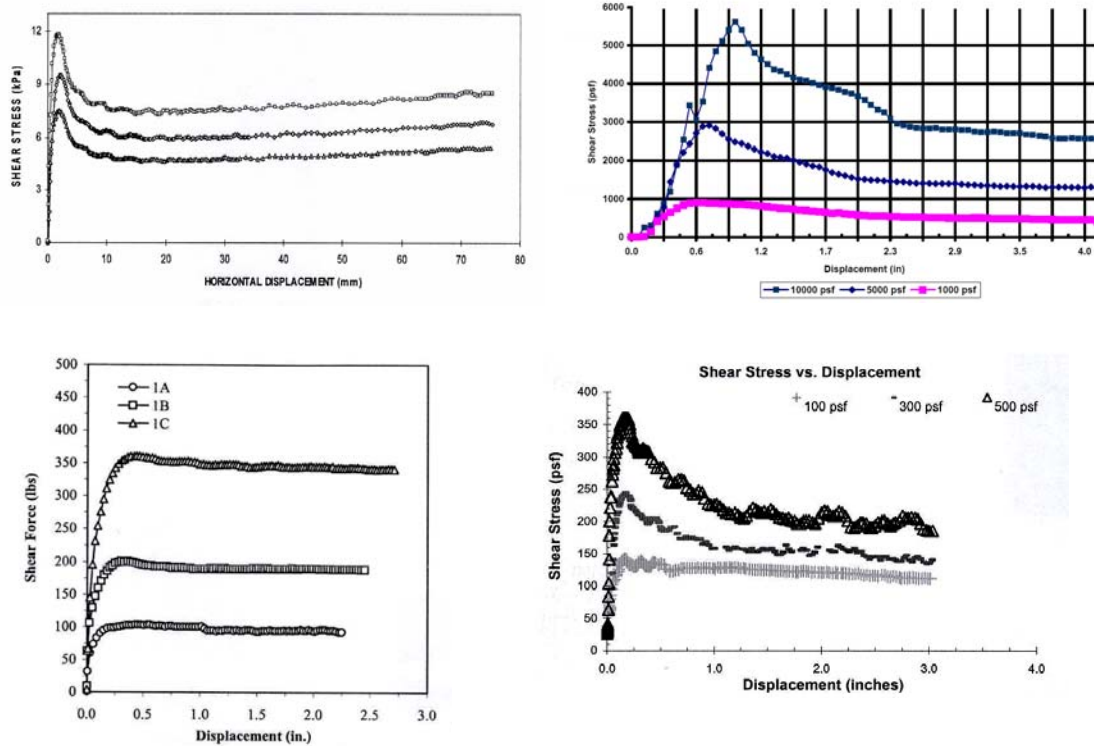


Figure 1 – Various stress versus displacement curves for different geosynthetic materials. (Data compliments of TRI, Golder, Precision and SGI Laboratories)

Either the designer or the testing laboratory will have to generate the Mohr-Coulomb failure envelope from these curves by selecting one point on each normal stress curve and plotting the results on a normal stress versus shear stress curve as shown in Figure 2a. A least squares fit of the data point produces the failure envelope. Even further, one might have more than one such failure envelopes; peak, large displacement and/or residual. Please note, however, that this White Paper is not about the selection of peak, large displacement or residual values and the technical literature is abundant on that subject.

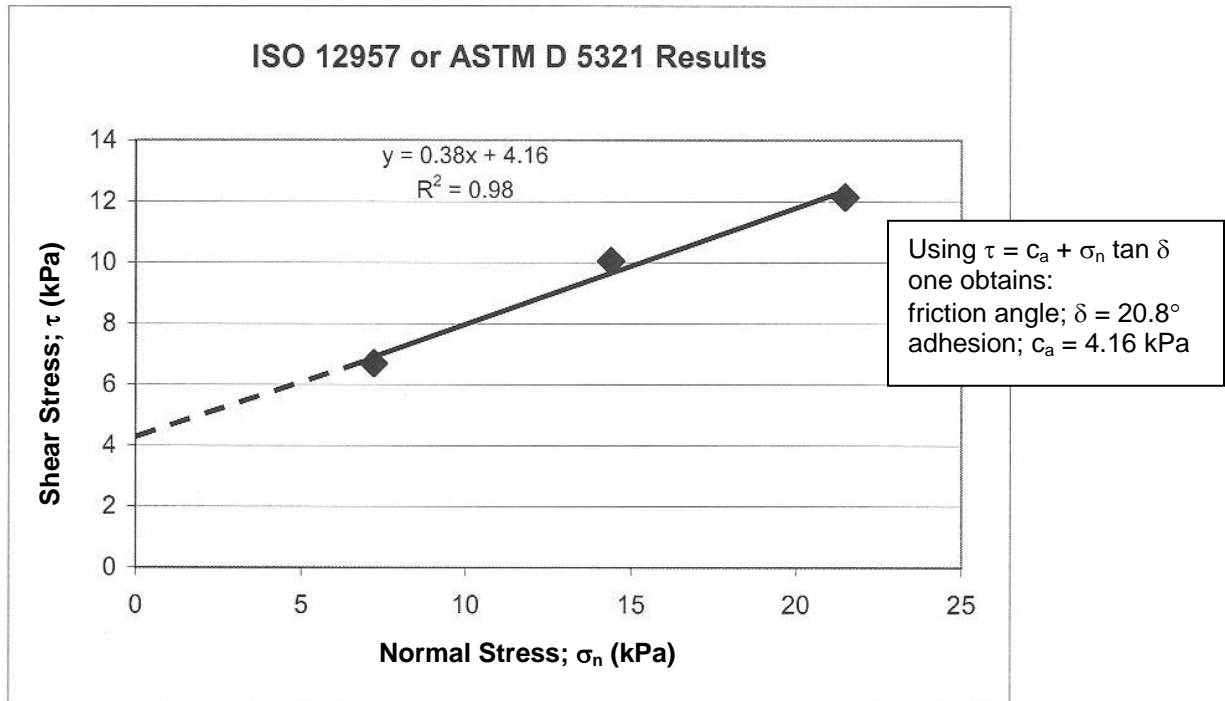


Figure 2a – Three point laboratory data leading to the drawing of a failure envelope and subsequent measurement of friction angle and shear strength intercept (or adhesion) values.

At any rate, to begin the present discussion on the interpretation of the selected failure envelope, the designer is confronted with something like that shown Figure 2a. Here the data points are clearly identified and the failure envelope is usually generated by a least squares fitting procedure. The dashed extension to the y-axis is often the general assumption particularly for low normal stresses as indicated. Note that there are indeed exceptions to this situation such as curved failure envelopes within the normal stress range tested, or zero normal stress tests. They are special cases and will be discussed later.

#### Interpretation #1 – Use of full “ $c_a$ ” and full “ $\delta$ ” values

Assuming that the previous failure envelope is based on credible laboratory procedures, properly simulated insofar as representative samples, normal stress selection, moisture conditions, strain rate, etc., our recommended approach is to use the shear strength parameters directly in your slope stability analysis and, if found to be adequate, for your materials specification criteria as well. For landfill cover veneer stability problems all GSI Members and Associate Members should have our spreadsheet calculation program which is extremely easy to use. For others, there are many computer codes available. For a hypothetical veneer slope stability example using the two shear strength parameters ( $c_a$  and  $\delta$ ) from Figure 2a, the input information is as follows:

- cover soil thickness  $h = 0.3$  m
- slope angle  $\beta = 18.4^\circ$  (3-to-1)
- length of slope  $L = 30.0$  m
- unit weight of cover soil  $\gamma = 18.0$  kN/m<sup>3</sup>
- friction angle of cover soil  $\phi = 30.0$  deg
- cohesion of cover soil  $c = 0.0$  kN/m<sup>2</sup>
- friction angle of interface  $\delta = 20.8$  deg
- adhesion of interface  $c_a = 4.16$  kPa (= 87 psf)

By using the program just mentioned or similar procedure, the resulting slope factor-of-safety value is;  $FS = 3.62$ . This is a relatively high value and would generally be considered quite conservative. One point worth mentioning, however, is the strong influence of the adhesion value on factor-of-safety. To illustrate this, we now vary the  $c_a$ -value between zero and ten while holding everything else the same. This procedure results in the following table; clearly illustrating the sensitivity of the FS-value to this particular parameter.

Adhesion; " $c_a$ "		Resulting FS-value
kPa	lb/ft <sup>2</sup>	
0	0	1.18
2	42	2.35
4	84	3.53
6	125	4.70
8	167	5.80
10	209	7.05

Presented now is the heart of this White Paper concerning the *issue of how reliable is this laboratory generated  $c_a$ -value?* The ultimate decision is yours as the designer, but our opinions on different geosynthetic materials and related interfaces are as follows:

- For textured geomembranes against geotextiles or soil, the asperities (be they manufactured as structured, blown film, or impinged) are on the material giving rise to the high adhesion values, so we recommend using the adhesion value accordingly. Only by continuously rubbing the surfaces against one another can asperity reorientation occur and we feel this is an artifact of aggressive laboratory testing as has been done (and reported) using the ring shear testing device in particular. Alternatively, concern has been expressed when testing at very high normal stresses. The thought in both instances is that if you eliminate adhesion from textured geomembranes you are essentially assuming smooth geomembrane sheet. This is a designer's prerogative, but be prepared to have very gentle slopes in so doing.
- For smooth geomembranes against other geosynthetics or soil, a small adhesion is often observed. This is particularly the case for LLDPE, fPP, EPDM, and PVC. Each of these geomembranes are less hard than HDPE, and thus an indentation can be visualized (particularly dealing with soil) which is clearly a function of the

- applied normal stress. Assuming that the appropriate normal stresses were used in the direct shear test, we feel that one is generally justified in its use.
- (c) For geotextiles thermally bonded to geonets or other types of drainage cores, we feel that the full value of adhesion should be used. Most of these geocomposites can barely be “delaminated” in the conducting of the test and we have never heard of a field delamination problem from a properly manufactured geocomposite interface in this regard.
  - (d) For the internal shear strength of reinforced GCLs, the fibers would have to pull-out or break (or both) for a loss of adhesion. While you can force this to happen in the lab, we have no evidence of this occurring in the field. Test results invariably show high adhesion values. Furthermore, longevity (durability) of the fibers in a hydrated bentonite atmosphere promises 100-year lifetime, or longer. We have a creep-related paper in this regard. Thus, we see no reason not to use the laboratory generated value of adhesion for reinforced GCLs manufactured by either needlepunching or stitching. Of course, the upper and lower interfaces of the GCLs must be independently evaluated.
  - (e) For certain geosynthetic-to-soil interfaces, the interface shear behavior may force the failure plane into the soil. This results in the identification of the soil’s shear strength and if there is a shear strength intercept it is a cohesion value and can be used accordingly.

Thus, if adhesion from short-term testing is indicated by the failure envelope and the long-term permanence of the physical or mechanical mechanism giving rise to this adhesion is logical to anticipate, its use in a stability analysis and subsequent material’s specification is felt to be generally justified.

#### Interpretation #2 – Use of zero “ $c_a$ ” and full “ $\delta$ ” value

For the situation where an adhesion is indicated by the failure envelope and you as the designer feel that its long-term existence is not justified, the most conservative approach you can take is to simply translate the entire failure envelope in a parallel manner down by the amount of adhesion indicated on the original data-generated graph; see Figure 2b.

The effect of this very conservative approach on the FS-value of the slope is substantial. The shear strength is now represented by a friction angle alone and the site-specific result will be very flat slopes. For example, the 3-to-1 slope in the hypothetical example given previously with an adhesion of zero, now has a FS = 1.18 using this approach. For the interfaces mentioned previously, we do not recommend this approach.

Alternatively, one could also decrease the adhesion slightly, but not entirely. That said, we really don’t know how to comment on this type of “compromise” situation?

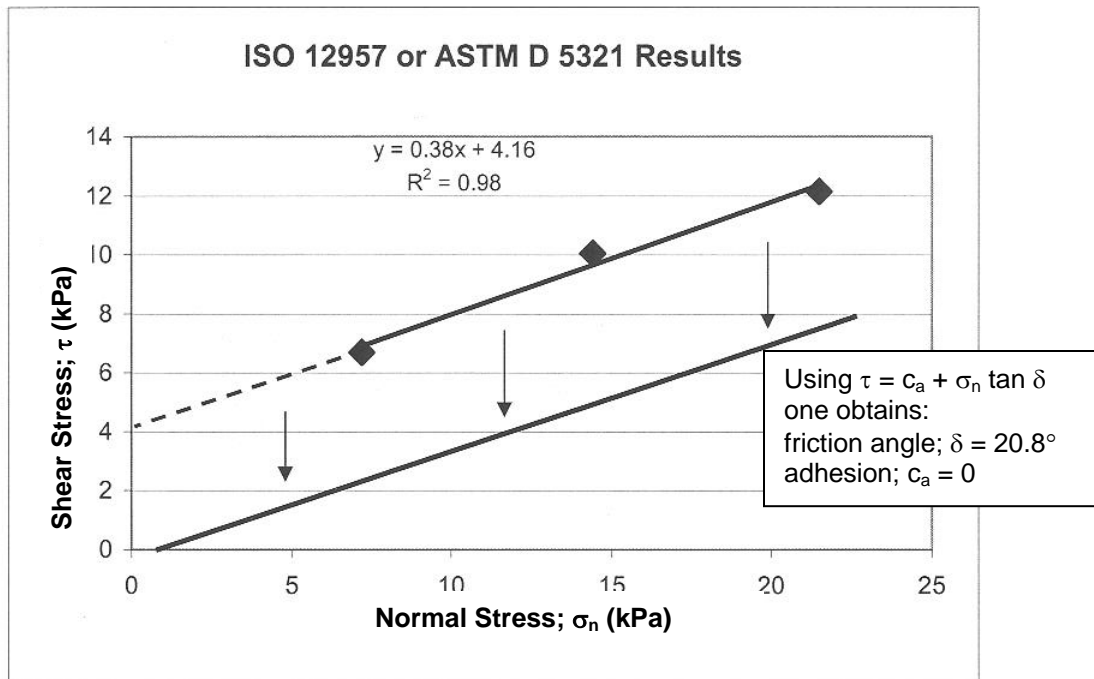


Figure 2b – Parallel translation downward of the entire laboratory generated failure envelope by an amount equal to the y-axis intercept, i.e., the adhesion.

Interpretation #3 – Use of zero “c<sub>a</sub>” at zero normal stress only

A hybrid interpretation somewhere between the interpretations just presented is sometimes suggested, but its logic is somewhat difficult to fathom. In essence, the adhesion is lost only at zero normal stress but not at higher normal stresses. Thus, the failure envelope is forced through the origin but thereafter it is based on a least squares fit of the laboratory tested points as they were generated. Figure 3 illustrates the situation where the resulting friction angle is seen to be 32.2°. For our hypothetical example, this results in FS = 1.93. Alternatively, and equally difficult to fathom, is when only one laboratory point is generated and the failure envelope is forced through it and the origin. Both approaches are the least conservative of those mentioned in this White Paper giving rise to a rotation of the failure envelope and the highest friction angle possible. The angle resulting from this practice has been variously called “secant friction angle”, “secant angle”, or “modulus angle”. Of the group, secant angle is probably the best description for this interpretation since it shouldn’t be confused with the Mohr-Coulomb friction angle, and modulus brings with it completely other test procedures like tension testing.

We generally do not recommend such approaches for the reason that adhesion should be an intrinsic property of the interface involved and not be arbitrarily eliminated or used on the basis of a particular normal stress, or stresses. (That stated, if the interface is tested at

zero normal stress and found to have zero adhesion, the origin is a valid point and should then be used accordingly).

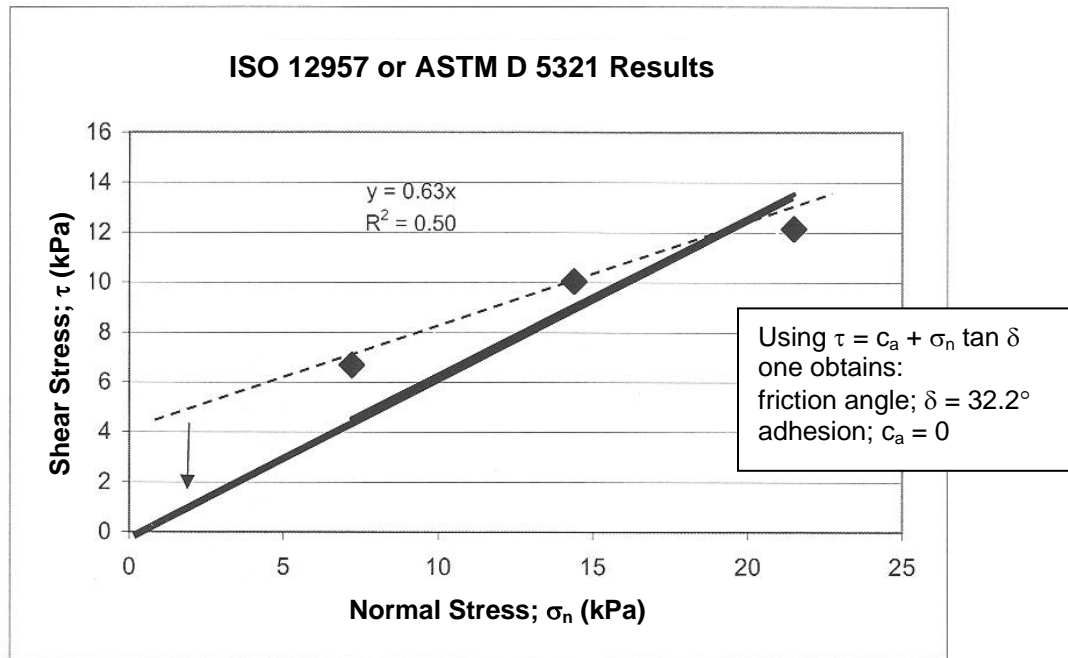


Figure 3 – Elimination of adhesion at zero normal stress but not at any of the three laboratory measured data points.

#### Interpretation #4 – Use of the total shear strength at a particular normal stress

A very straightforward approach to a specification value is to require a certain shear strength value at a particular normal stress. This is particularly the case if the failure envelope is curved as mentioned previously. In so doing, a specifier is requiring a single point to be taken from the failure envelope which is targeted at the expected field normal stress. Figure 4 suggests that if the field normal stress is 17.2 kPa it results in a required shear strength of 10.7 kPa, or greater. The shear strength value is thereby reflective of both a frictional component and adhesion, neither of which are specifically identified.

In so doing one avoids specifying individual “ $c_a$ ” and “ $\delta$ ” values and much of the previous discussion is altogether avoided. The method can be extended to give two, or more, values of shear strength (or even the equation of the failure envelope) at different normal stresses in the form of a “required” table.

This approach has been used by a select few designers but is far from common practice. There is nothing of a fundamental nature which says it cannot be done and it would avoid some of the other complications inherent with different approaches.

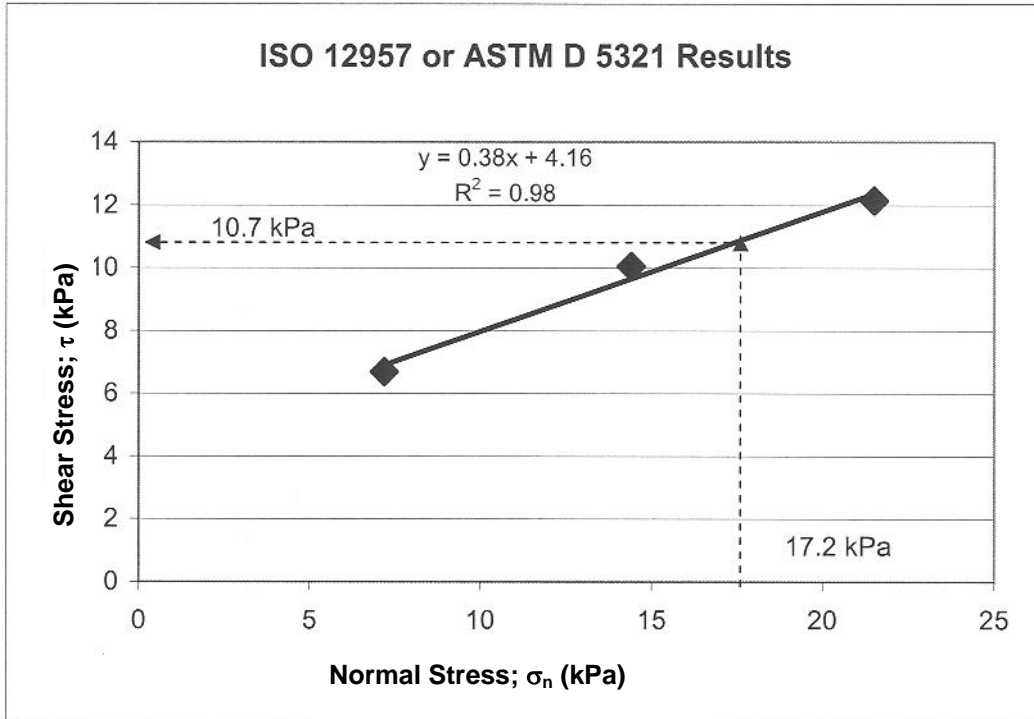


Figure 4 – Use of a laboratory generated failure envelope by specifying a site-specific normal stress and requiring a minimum value of shear strength taken directly off of the y-axis.

In summary, there are probably other or intermediate interpretations of an interface shear strength failure envelope for use in design and then a subsequent specification, but those presented here are felt to be the most common.

**APPLICATION FOR PERMIT  
DNCS ENVIRONMENTAL SOLUTIONS**

**VOLUME III: ENGINEERING DESIGN AND CALCULATIONS  
SECTION 7: TENSILE STRESS ANALYSIS**

**ATTACHMENT III.7.F**

**THIEL, RICHARD. *A TECHNICAL NOTE REGARDING INTERPRETATION OF  
COHESION (OR ADHESION) AND FRICTION ANGLE IN DIRECT SHEAR TESTS.*  
GEOSYNTHETICS, APRIL MAY 2009 VOLUME 27: PAGES 10-19.**

# A technical note regarding interpretation of cohesion (or adhesion) and friction angle in direct shear tests

By Richard Thiel

## Introduction

Direct shear testing with geosynthetics is generally performed in accordance with ASTM D5321, *Standard Test Method for Determining the Coefficient of Soil to Geosynthetic or Geosynthetic to Geosynthetic Friction by the Direct Shear Method*. There is also a related standard, D6243, *Standard Test Method for Determining the Internal and Interface Shear Resistance of Geosynthetic Clay Liner by the Direct Shear Method*. This technical note applies to both equally.

## Interpreting lab results

There is often confusion expressed in the industry regarding how laboratory results should be interpreted, specifically: whether one should use both the friction angle and cohesion (or adhesion) parameters; whether cohesion should be ignored; whether secant friction angles are more appropriate; what to do if the data are nonlinear; and how the data should be interpolated or extrapolated.

The goal of this technical note is to provide some guidance to take the mystery out of these questions. In the end, all data should be evaluated by an experienced practitioner qualified to use the test results properly.

What this note will not do is go into the subtleties of requesting, setting up, calibrating, and performing a direct shear test. That would be the subject of additional articles.

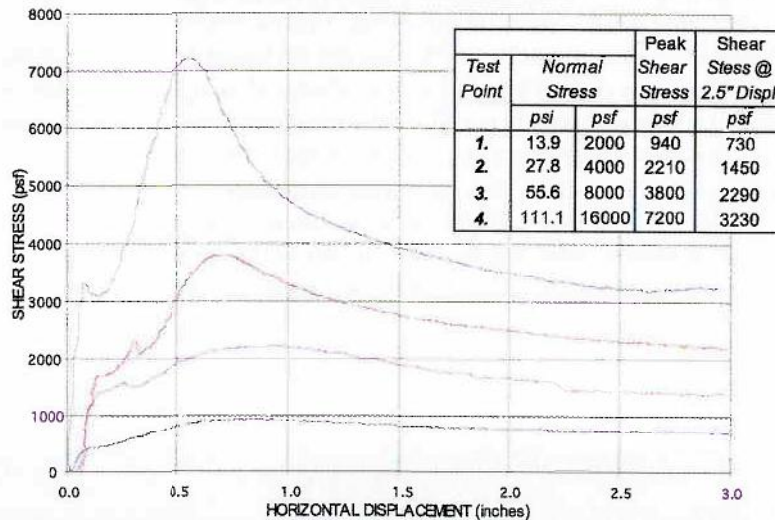
This article will also not definitively describe how direct shear test data should be interpreted. That is the responsibility of a professional with specific expertise, and one article could never presume to cover all of the considerations that might apply to any unique design problem that might arise. That is why professionals are trained and mentored in basic geotechnical principles: so they can appropriately account for

the various factors affecting a design and make appropriate decisions regarding test data interpretations.

The typical sequence of events related to direct shear testing includes the following:

1. An engineer requests a direct shear test series to obtain data to help solve a problem. The request should be very specific with regard to all the necessary details regarding

Material 1:	GSE 40 mil HDPE Tex / Tex (White side towards GCL)
Material 2:	Bentomat DN GCL (black side up) Roll # 00000481
Substrate:	GSE 60 mil HDPE Tex-white / Tex-black (Black side toward GCL)



The "gap" between shear boxes was set at 80 mil (2.0 mm)
The test specimens were flooded during testing.
High Normal Stresses, >5psi (35 kPa) was applied using air pressure.
Low Normal Stresses, <5psi (35 kPa) was applied using dead weights.
The tests were terminated after 3.0" (75 mm) of displacement unless otherwise noted.
Tests were performed in general accordance with ASTM procedure D-5321 using a Brainard-Killman LG-112 direct shear machine with an effective area of 12" x 12" (300 x 300 mm).
Each specimen of 60 mil geomembrane was cut to 14" x 20" and clamped to the lower shear box. Avg. Asperity = 0.025"
Each specimen of 40 mil geomembrane was cut to 14" x 16" and clamped to the upper shear box. Avg. Asperity = 0.016"
Each GCL specimen was Hydrated for 48 hrs at the 250 psf, then placed, unclamped between upper & lower HDPEs
The grouped specimens were consolidated 16 hrs. under the specified normal stress, then sheared
Shearing occurred at the interface of the GCL's and 40 mil geomembrane specimens.
Extrusion of bentonite was noted on the surface of the 40 mil & white side of the GCL contact area for points 2, 3 & 4
The Friction Angle and Adhesion (or Cohesion) results given here are based on a mathematically determined best fit line.
Further interpretation should be conducted by a qualified professional experienced in geosynthetic and geotechnical engineering.

| Richard Thiel is a senior project manager at Vector Engineering Inc. in Grass Valley, Calif.

The Designer's Forum column is refereed by Greg Richardson, Ph.D., P.E., a principal at RSG & Associates, Raleigh, N.C., [www.rsgengineers.com](http://www.rsgengineers.com)

sampling, specimen preparation and setup in the testing device, and test execution in accordance with both project-specific conditions and industry standards.

2. A competent and certified laboratory performs the test series in accordance with the request and the industry standard test method (e.g., ASTM D5321 or D6243). The laboratory reports results to the engineer.

3. The engineer interprets and applies the results to the project design.

**What we are measuring in the direct shear test is shear strength as a function of normal load. The test does not measure "friction" or "cohesion," as these are simply mathematical parameters derived from the laboratory test results.**

Ideally the engineer who originally specified and required the shear test would be the same one who reviews and interprets the results. Sometimes, such as in a third-party construction quality assurance (CQA) project, an engineer other than the original designer will commission and review the testing. Interactions with test laboratories and other engineers over time have shown that there are often misconceptions and misunderstandings related to the interpretation of direct shear test data. Thus, this article is intended to serve the purpose of helping project participants avoid confusion. The key point of this article is that what we are measuring in the direct shear test is shear strength as a function of normal load. The test does not measure "friction" or "cohesion," as these are simply mathematical parameters derived from the laboratory test results.

**Figure 1** presents shear test results of a 4-point test for an interface between a textured geomembrane and a reinforced GCL. Three shear points, each at a different normal stress, are the most common number of points used to run a test series, but the number of points could

vary from as few as one, to perhaps as many as six points, depending on many factors beyond the scope of this article. The figure shows: (a) a table of the normal stresses vs. peak and large-displacement shear strengths measured at 2.5in. of displacement, (b) graphs of the shear stress vs. displacement measurements, and (c) notes describing test conditions and observations.

There is adequate information in this figure for a trained practitioner to evaluate and use the data. The laboratory has performed its duty, which is to measure and report the shear strength under specified normal stresses (we are simplifying the dis-



cussion here by not elaborating on other factors such as hydration, consolidation, etc.), showing how the shear strength changed with displacement of the two surfaces, and providing descriptive and observational notes.

Figure 2 shows additional information that can be provided by a laboratory in the form of a graph of the peak and large-displacement strengths plotted as a function of normal stress. Best-fit straight lines, called Mohr-Coulomb strength envelopes, named after the gentlemen who first publicized the relationship between shear strength and normal stress, have been drawn through the two sets (peak and large-displacement) of data points.

Equations can be written for these lines, as we learned in first-year algebra class, in the form of  $y = mx + b$ . In this case we define  $y$  as the shear strength ( $S$ );  $m$  as the slope of the line that we call the "coefficient of friction" and whose angle is  $\phi$  ( $\phi$ ), which we call the "friction angle" (and thus  $\tan[\phi]$  is the slope of the line);  $x$  is the normal stress ( $N$ ); and  $b$  is the  $y$ -intercept of the line that we call either "adhesion" ( $a$ , usually used for geosynthetics-only tests) or "cohesion" ( $c$ , usually used for tests involving soils, which will be used for the remainder of this article).

### Mohr-Coulomb

In geotechnical engineering, we write the Mohr-Coulomb equation for these lines as:

$$S = N \cdot \tan(\phi) + c$$

This equation is written for peak, large-displacement, or residual shear strength conditions. The fundamental points in this article regarding the presentation of the data in Figure 2 include the following:

1. **The Mohr-Coulomb envelope should not be extrapolated beyond the limits of the normal stresses under which the testing was conducted.** To do so would never be conservative and, in fact, may be significantly nonconservative. The reason that simple extension-extrapolations of the Mohr-Coulomb

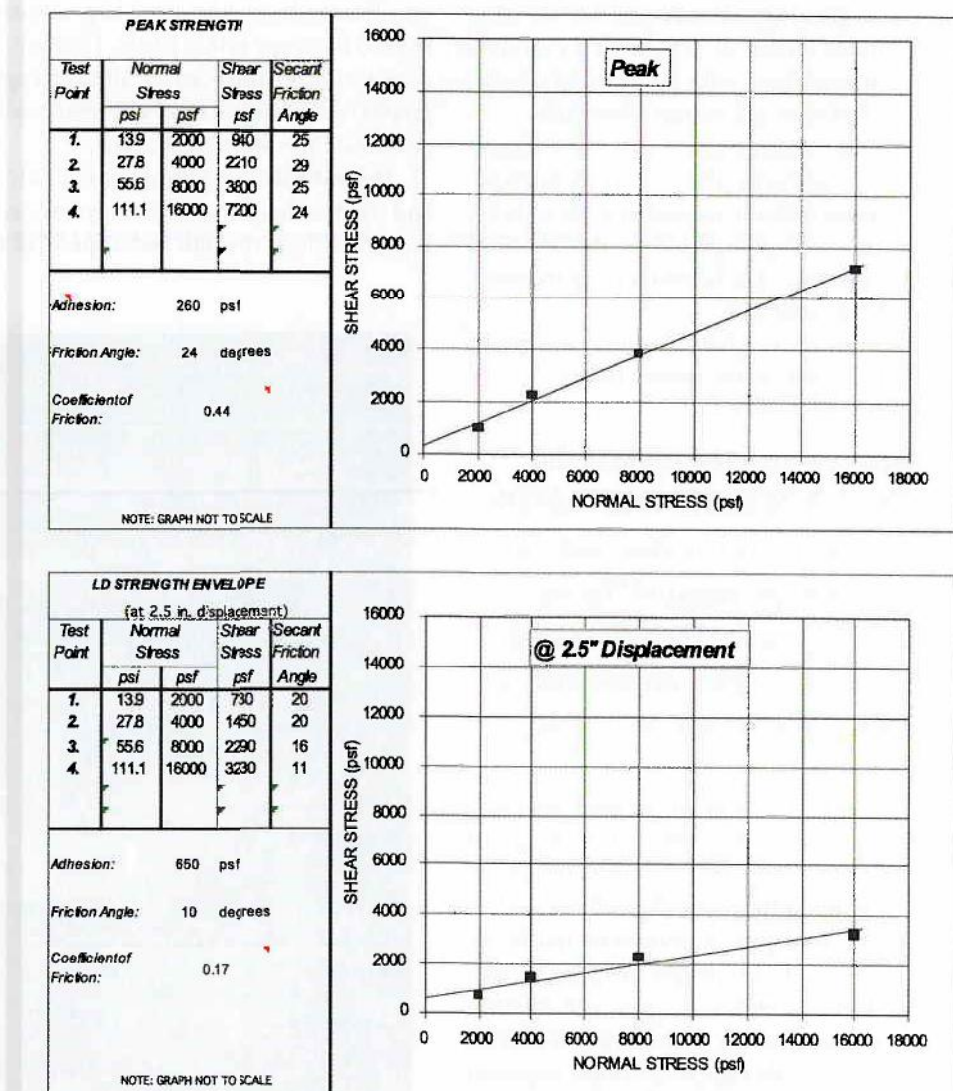


Figure 2 | Example of supplemental data interpretation provided by the laboratory.

envelope are nonconservative is presented in Figure 3. Most shear strength envelopes are truly curved (nonlinear). This tendency for a curved failure envelope is exaggerated in Figure 3, but can clearly be identified for the real-life strength envelopes presented in Figure 2, in particular for large-displacement conditions.

The Mohr-Coulomb model is merely a linear simplification of a portion of the entire envelope over a limited range of normal stresses. If testing were performed over a large enough range of normal stresses the curvature would become

more apparent. True shear strength envelopes are found to be most accurately described by hyperbolic functions. Giroud et al. (1993) provides a good method to describe hyperbolic strength envelopes.

2. **The values of  $\phi$  and  $c$  should be considered nothing more than mathematical parameters to describe the shear strength vs. normal stress over the normal-load range the test was conducted.** It is perhaps better not to think of "friction" and "cohesion" as real material properties, but simply as mathematical parameters to describe the failure envelope.

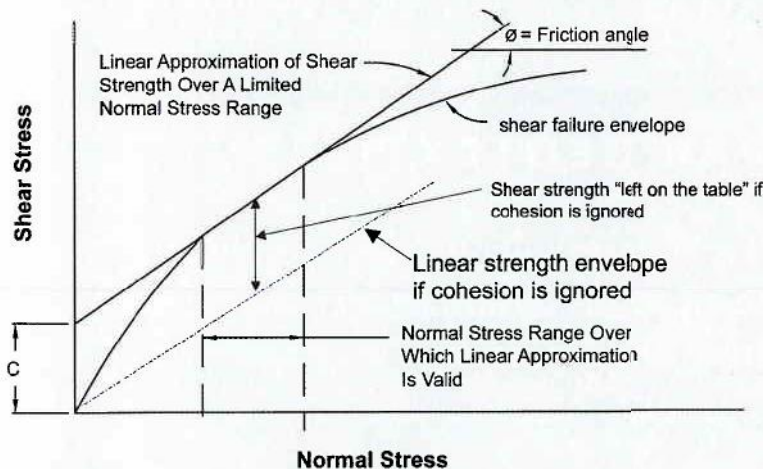


Figure 3 | Exaggerated schematic of true curvilinear shear strength envelope, linear interpretation over a selected normal stress range, and the penalty for ignoring cohesion.

### Example Safe Shear Strength Results Extrapolations

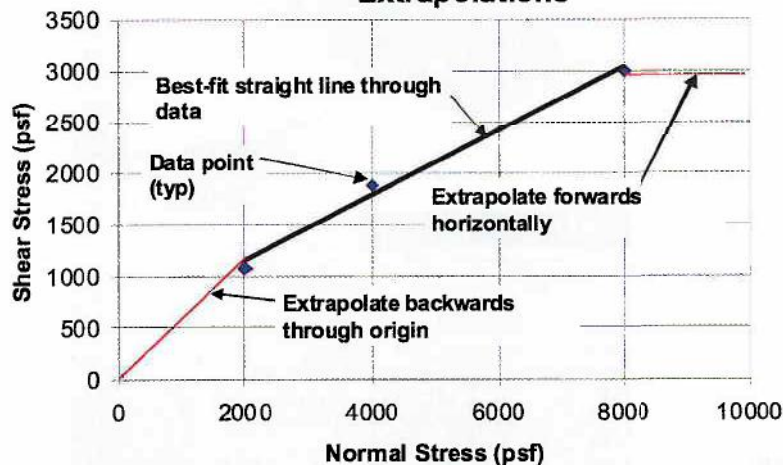


Figure 4 | Example of safe shear strength extrapolation.

In geotechnical practice with soils, there are situations and examples where the cohesion parameter is evaluated separately from the friction parameter, but these are sophisticated considerations that involve very project-specific materials and conditions and should only be done by experienced professionals.

For many geosynthetic interfaces and in the context of many types of projects, there is absolutely no reason to dissociate the slope of the line from its y-intercept, and the shear strength should be taken as

a whole in those cases. Other situations may occur, however, where it is appropriate, but those considerations are beyond the scope of this article.

3. In many, if not most, cases with geosynthetics where there is no reason to ignore the cohesion value, it is important to re-emphasize that shear strength should only be defined within the range of normal stresses for which the Mohr-Coulomb envelope was derived. Ignoring the cohesion may be unjustifiably penalizing the shear strength values that

were measured in the test, as illustrated in Figure 3.

Using the cohesion value at normal stresses extrapolated below the range of testing, however, could have dire consequences on the safety of a design project. This problem may occur when designers consider only the operational or final build-out of a facility and they ignore the construction condition. Several failures have occurred during construction because of this. For example, an embossed geomembrane against a geotextile may perform well under high normal loads by providing a good friction angle and a modest y-intercept for operating and final build-out conditions. However, under the low normal loads experienced during construction of a thin soil veneer on a steep sideslope, testing might reveal that the adhesion extrapolated from the high-normal load results do not exist at low normal loads. In this case, a more aggressive texturing that exhibits a “Velcro”-effect type of adhesion, or a very high friction angle, at low normal loads may be needed and should be verified at the proper normal loads.

4. Figures 1 and 2 also report secant friction angles for each point. These are the angles of the straight lines from each point drawn back to the origin. A key concept regarding secant friction angles is that you should never extrapolate a secant angle line beyond the normal load for which it is measured. Secant values are conservative as long as the secant values are derived from a test whose normal stress was greater than the normal stresses of the design. They can quickly become nonconservative if the same friction angle is used for higher normal loads.

5. If users wish to extrapolate shear strength data, Figure 4 illustrates the only “safe” way to accomplish this. Going from the low end of the Mohr-Coulomb envelope and extrapolating backward, the data can be extrapolated by drawing a straight line back to the origin. Going from the high end of the Mohr-Coulomb envelope and extrapolating forward, the data can be extrapolated by drawing a straight line

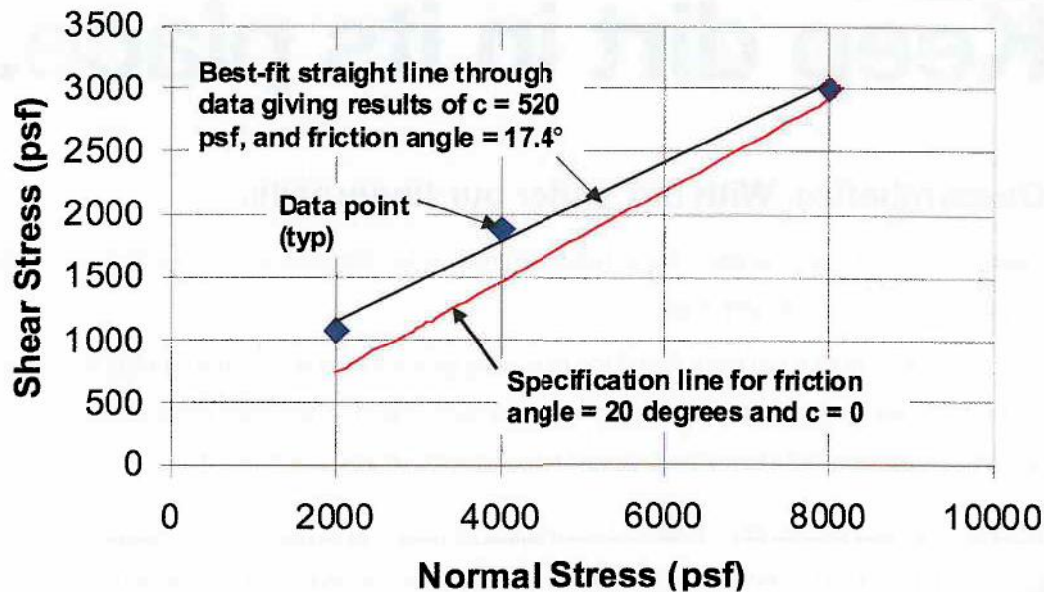


**Figure 5** | Example project results where interpretation of test data results in lower friction angle than specified value, even though shear strength results are higher than the failure envelope implied by the specifications.

horizontally forward. This extrapolation rule is safe only when considering a single interface. When multiple interfaces are involved, it is not safe to extrapolate a multi-layered system on the high side of the Mohr-Coulomb envelope.

From the discussion above, we can now look at the ASTM standard D5321 with more understanding and critical thought. The first thing to note is that the title of that standard is poorly worded. The title is “*Determining the Coefficient of...Friction...*” This is somewhat misleading because it implies that the designer is simply after a coefficient of friction. In fact, what designers need is a relationship between shear strength and normal stress. Therefore, a more appropriate title for this method would be “*Determining the Relationship between Shear Strength and Normal Stress for Soil-to-Geosynthetic or Geosynthetic-to-Geosynthetic Interfaces Using the Direct Shear Method.*” Note that ASTM D6243 has already rectified this problem in its title.

Another misleading element in ASTM D5321 is the definition of *adhesion* (which applies equally to cohesion), which it states as: “The shearing resistance between two adjacent materi-

als *under zero normal stress* (emphasis added). Practically, this is determined as the y-intercept to a straight line relating the limiting value of shear stress that resists slippage between two materials and the normal stress across the contact surface of the two materials.”

This is actually *two separate definitions*, which are most likely not the intent of the standard. The first part of this definition, which defines the adhesion as the shear strength at zero normal stress, is not applicable relative to the test method. It *could be true* if we proposed to test the interface at zero normal load, but that is rarely done and generally of no use. The industry would be better served by deleting the first part of the definition. In reality, the second part of the definition is the controlling aspect of the definition, and the “y-intercept” concept is the true nature of the adhesion value which, as stated above, is simply a mathematical parameter.

Note that ASTM D6243 has a different set of definitions, and it is not clear if those definitions are unique to that standard, or are intended to be industry norms. ASTM D6243 suggests that adhesion is the true shear strength when

there is truly zero normal load, and that cohesion is the mathematical parameter of the y-intercept obtained from the Mohr-Coulomb envelope. In the author’s opinion these definitions are acceptable as stated, but the audience should know that the definition of *adhesion* may conflict with other definitions put forward in the industry. Also, other authors have introduced other terms for the measurable shear strength under zero normal load, such as Lambe and Whitman’s (1969) “*true cohesion*.” Interested readers can research ASTM D6243 and the literature and judge for themselves.

### Example problem 1

The following situation illustrates a common example of a problem that occurs with shear test data interpretation:

- A specification is written that requires a certain minimum interface friction angle to be achieved between a textured geomembrane and a GCL. For purposes of this example, the requirement is 20° peak shear strength for normal loads tested between 2,000 and 8,000 pounds per square foot (psf).
- The laboratory results, shown as an

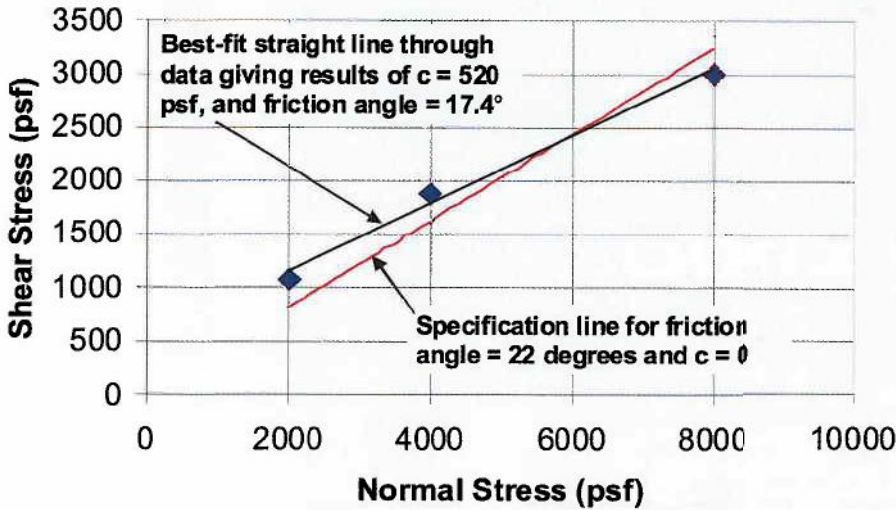


Figure 6 | Example project results where the two lower points are above the specification and the upper point is below the specification.

example in Figure 5, report a best-fit Mohr-Coulomb peak strength envelope with shear strength parameters of 500 psf cohesion and 15° friction. Figure 5 also shows the line representing the minimum project specification.

Inspection of Figure 5 shows that the shear strengths achieved in the direct shear test plot above the shear strength envelope required by the specification. Even though the plot appears to clearly indicate that the minimum required shear strength is achieved by the products tested, the author has experienced several projects where one of the project parties (e.g., the design engineer or perhaps a regulator) have declared the test a failure because the reported Mohr-Coulomb friction angle was less than the specified friction angle.

In the author's opinion, in many cases involving this particular interface, there is no reason to consider this a failing test.

This example illustrates the confusion that might arise when specification is written in terms of a shear-strength parameter, when the real objective is to achieve a certain value of absolute shear strength. Even though the materials provided the shear strength required by the specification, there is some confusion because one of the strength parameters did not meet the specified value for that parameter.

It is possible that the original specifier had taken into account the potential for cohesion, and had wished to discount cohesion, and really wanted a true minimum friction angle of 20°. If the specifier were truly that sophisticated and had such complex reasoning, then more than likely the specification would have also been more sophisticated in explaining these constraints on the test results.

In the author's experience it is rare that other designers and specifiers are discounting cohesion with geosynthetic interfaces, and usually it is simply a matter of proper interpretation and communication of the design intent compared to the actual test results. Nevertheless, as stated at the beginning of this article, it is not the intent of this article to provide guidance and suggestions on interpreting test results. Rather, the intent is to shed light on some common misunderstandings.

### Example problem 2

The following problem has the same laboratory shear strength results as Problem 1, but the specification requirement is increased to 22° peak shear strength.

The relationship between the test results and the specification is shown in Figure 6. In this example, the two lower-normal load shear strength test results plot above the specification line, while the up-

per-normal load shear strength test result plots below the specification line. Based on the failing result of the upper-normal load test, most reviewers would initially say that this is a noncompliant test result and fails to meet the specification.

In the author's experience, curved failure envelopes are common, and the tendency for the highest normal-load result to fall beneath a straight-line friction-based specification is not unusual.

In this case, a more detailed review by the design engineer might reveal that the shear strength results provide an acceptable factor of safety for the intended purpose. It may be that the additional strength capacity provided in the lower normal load range that is above the specification more than offsets the reduced strength capacity in the upper normal load range that is below the specification. Clearly, the only person who can evaluate this issue, and who carries the requisite authority and responsibility, is the design engineer.

The following lessons can be gleaned from this example:

- Design engineers often attempt to specify a unique set of shear strength parameters as a minimum requirement for a given design. In reality, there may be an infinite combination of shear strength variations over the applicable range of normal loads that may satisfy the stability and shear resistance requirements, and many of these combinations may have a portion of their failure envelopes that fall below the specification.
- The tendency for natural and geosynthetic interfaces to yield curved failure envelopes can present a challenge to engineers, owners, and manufacturers who wish to optimize a design using simple straight-line shear strength specifications.
- A learned interpretation of direct shear testing data by an experienced practitioner may allow acceptance of apparently failing test results. This can occur because overly simplistic specification parameters may not ac-

count for other combinations of shear strength results that could provide acceptable overall shear resistance.

### Summary

The direct shear test measures shear strengths as a function of normal stress. Period.

The test does not measure “friction angle” or “cohesion,” as these values are parameters that are derived from the test results. Consideration of “friction angle” and “cohesion” simply as mathematical parameters used to describe shear strength data is of great benefit to practitioners for the following four reasons:

1. Interpretation of laboratory shear strength data should not be confused with the mathematical parameters used to describe it.

2. Proper data interpretation may avoid unnecessary penalization of the results by arbitrarily reducing the measured values.

3. This understanding can improve a designer's sensitivity to how important it is that shear strength is measured within the range of normal stresses that represent the design. Thus, the only defensible extrapolation of data should be: (a) back through the origin from the lowest normal stress, and (b) horizontally from the highest normal stress.

4. Laboratory shear strength data should be interpreted by a qualified practitioner experienced in the use and application of the results.

Often of much more importance than deciding whether to include or omit the cohesion (or adhesion) parameter is the

decision of whether to use peak, post-peak, or residual shear strength. This discussion is beyond the scope of this technical note, and anyone commissioning and interpreting shear strength testing should be well versed in the issues surrounding this topic, as well.

### Acknowledgements

The author would like to thank Richard Erickson and Chris Athanassopoulos for their review of this article.

### References

- Giroud, J.P., Darrasse, J., and Bachus, R.C., (1993). “Hyperbolic Expression for Soil-Geosynthetic or Geosynthetic-Geosynthetic Interface Shear Strength”, *Geotextiles and Geomembranes*, Vol. 12, No.3, pp. 275–286.
- Lambe, T.W. and Whitman, R.V., (1969). *Soil Mechanics*. John Wiley & Sons, New York, NY. 

**APPLICATION FOR PERMIT  
DNCS ENVIRONMENTAL SOLUTIONS**

**VOLUME III: ENGINEERING DESIGN AND CALCULATIONS  
SECTION 7: TENSILE STRESS ANALYSIS**

**ATTACHMENT III.7.G**

**THIEL, RICHARD. *PEAK VS RESIDUAL SHEAR STRENGTH FOR BOTTOM  
LINER STABILITY ANALYSES.***

**THIEL ENGINEERING. OREGON HOUSE, CALIFORNIA, USA**

# PEAK VS RESIDUAL SHEAR STRENGTH FOR LANDFILL BOTTOM LINER STABILITY ANALYSES

Richard Thiel  
Thiel Engineering, Oregon House, CA, USA

## ABSTRACT

The decision whether to use peak or residual shear strengths for a stability analysis must be made in the context of a specific design situation. Yet even when the specific situation is defined, the decision of whether to use peak or residual shear strength is often unclear. In general, if there are potential construction, operation, or design conditions that might cause relative displacement between layers, then a post-peak or residual shear strength for the layer having the lowest peak strength is appropriate. If seismic analyses predict deformation on a given interface, then the design should use the post-peak or residual shear strength for that interface. For bottom liner systems, where stress distribution along the liner system is very complex, it is advisable to verify that the slope stability has a factor of safety greater than unity for residual shear strength conditions along the critical interface.

## INTRODUCTION

---

This paper is concerned with the forces that support a landfill on its liner system, and the shear strength of geosynthetic interfaces that keep the mass from sliding. Figure 1 schematically portrays the shear forces that work to keep the waste mass from sliding. If sliding occurs, the surface along which sliding would occur is called the critical surface, or potential slip plane. Bottom liner systems that use geosynthetics often have their critical surface along one of the geosynthetic interfaces. The shear strength of these interfaces can usually be measured by means of laboratory testing. These interfaces often realize their peak shear strength within a small amount of relative displacement (on the order of 25 mm), after which their shear strength decreases. Typically, after 50 to 300 mm of relative displacement, the shear strength is reduced to a steady minimum value, which is called the residual shear strength of that interface. Figure 2 shows a typical shear stress-displacement curve for a geosynthetic interface.

Over the life of a landfill the following activities occur: the liner system is built; waste is placed; settlement occurs; a final cover system is installed; and settlement and degradation of the waste continues. Each of these phases of the landfill's life produces different combinations of normal and shear stresses on the liner system. Landfill leachate and gas, which can create destabilizing pore pressures, are by-products of the landfill, and are removed with varying degrees of efficiency. The primary questions addressed in this paper are:

- Should a designer use peak or residual shear strengths, something in between, or a combination of peak and residual strengths, when evaluating a landfill design?
- What does the profession really know about the mobilized shear stresses? (This paper will focus on bottom liner systems.)
- Should the same choice whether to use peak or residual shear strengths be applied along the entire lining system, or should slopes and base liners be treated differently?
- Is there a preferred design approach?
- What factors of safety are appropriate for design?

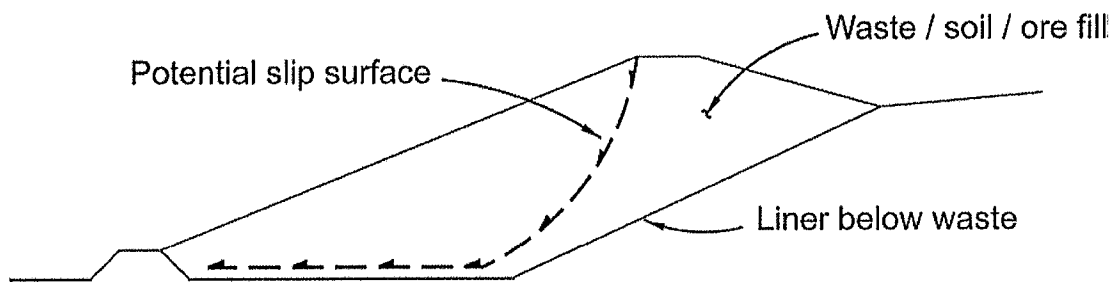


Figure 1 – Schematic of Shear Forces Along Critical Slip Plane

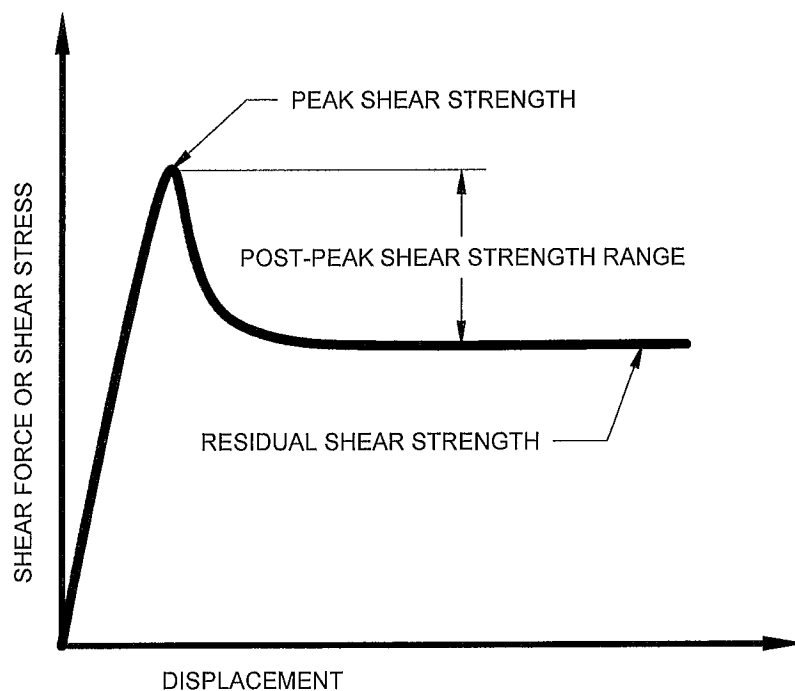


Figure 2 – Example Graph of Shear Force vs. Deformation for Geosynthetic Interface

## **ORGANIZATION OF THIS PAPER**

Part 1 of the paper describes general considerations in performing slope stability analyses. It begins with a discussion of different types of slope stability analyses, including limit equilibrium, finite element, and 2-dimensional (2-D) vs. 3-dimensional (3-D) analyses. Understanding how the state-of-the-practice has developed, and the limitations of the analytical approach, both contribute strongly to making the right selection of appropriate shear strengths and factors of safety.

2-D limit-equilibrium analyses are by far the most common approach for evaluating slope stability. Part 1 discusses practical guidelines and common pitfalls that affect the results of these analyses, especially the selection of the critical shear plane on which the peak or residual shear strength will be modeled. Part 1 also discusses how pore pressures might cause a surface to exceed its peak shear strength and induce progressive failure. Selecting the appropriate shear strength requires an understanding of the effective normal stress range. Also, commissioning direct shear testing from a laboratory requires that one understand the proper testing parameters needed to obtain appropriate peak and/or residual shear strength values.

Part 2 of the paper directly addresses the question of peak vs. residual shear strength, and begins by discussing ductile vs. brittle behavior. Progressive failure, which occurs with brittle materials, then emerges as the chief concern of this paper. The discussion that follows considers conditions that could cause a brittle material to exceed its peak strength in the context of a landfill bottom liner, followed by a brief summary of field observations in this regard.

Part 3 discusses possible design approaches in terms of the selection of peak strength, residual strength, and hybrid approaches, and then considers the appropriate factors of safety for these different approaches.

Part 4 then presents conclusions reached from the preceding discussions. It also provides recommendations for practical design approaches based on the author's experience, as well as recommendations for further research.

This paper surveys the key considerations one employs when deciding whether to use peak or residual shear strength for bottom liner systems in landfills. It does not presume to make that decision, but rather seeks to outline and discuss all considerations that are necessary and pertinent to that process. Although many of the considerations this paper presents may be general enough to apply to cover (veneer) systems, it has been written solely with bottom liner systems in mind, and does not consider the long-term issues related to cover systems.

## PART 1 – GENERAL CONSIDERATIONS

### LIMIT-EQUILIBRIUM VS FINITE-ELEMENT ANALYSES

Limit-equilibrium analyses, whether 2-D or 3-D, are the most common methods of assessing slope stability. These methods can be performed by hand or, more commonly, by using a computer program. Such analyses evaluate the force and moment equilibrium of a slope on an assumed slip plane given assumed shear strength, unit weight, and pore pressure parameters. The result of these analyses is then presented as a factor of safety (*FS*) defined as:

$$FS = \frac{\text{Shear strength along the slip surface}}{\text{Shear stress along the slip surface}}$$

One defining characteristic of the limit-equilibrium approach is that it presumes that the factor of safety is the same everywhere along the slip plane. Therefore, the mobilized shear stress distribution along the slip plane is simplistically assumed to be a constant ratio of the shear strength along that plane. Such analyses also do not take into account elastic or plastic deformation. These are both significant considerations when deciding whether to use peak or residual shear strength.

Finite-element analyses attempt to calculate the stress distribution and deformations in a soil mass. In addition to considering force and moment equilibrium, these analyses also typically consider the materials' elastic modulus and Poisson's ratio, and some models can also calculate the change in shear strength with displacement for various materials. The result of these analyses is usually presented as a distribution of mobilized shear stress and displacements.

At first glance it would seem that finite-element analyses offer more of what we wish from a slope stability analysis as opposed to limit-equilibrium analyses. So much so, that we might even ask ourselves why we continue to bother with limit-equilibrium analyses. The fact remains, however, that the limit-equilibrium approach has been and will continue to be the basis of standard practice in the industry. The reasons for this, some of which also appear in the next section that considers 2-D vs. 3-D, are:

- Limit-equilibrium approaches have been performed and “calibrated” through industry experience for the past 80 years. Properly performed limit-equilibrium analyses have been proven to be adequate.
- Finite-element analyses are sophisticated and complicated to perform. The average design practitioner often is not adequately trained to perform such analyses, and the low frequency of projects that require their use do not justify the

resources needed to keep an engineer qualified to perform them on every landfill-design firm's staff.

- In the past few years the author has peer-reviewed a number of slope stability analyses. On four major landfill projects for which calculations had been prepared by separate reputable nationwide and local design firms, the author found fundamental errors in 2-D limit-equilibrium analyses. Some of these projects had already been built and were, in the author's opinion, at serious risk of large-scale failure. If such fundamental errors continue to be made with analyses as simple as 2-D limit-equilibrium, the prospects of universalizing a finite-element approach for the solid waste industry is not very promising. Finite-element analyses epitomize the expression "garbage-in garbage-out", so strict quality control and quality assurance is in order whenever they are employed.

## **2-D vs. 3-D ANALYSES**

One issue that is periodically debated in the literature and at professional gatherings is the use of 2-D as opposed to 3-D analyses. Soong et al. (1998) question whether 2-D analyses are appropriate for landfills, and suggest it would be more appropriate to use 3-D analyses with residual strengths. From a pragmatic point of view, the everyday stability analysis has been, and will continue to be, 2-D in actual practice. There are three main reasons for this, clearly laid out by Duncan (1996):

- **Inherent Conservatism.** Properly performed 2-D analyses always give a factor of safety that is equal to or less than those given by 3-D analyses. 2-D analyses, therefore, are more conservative.
- **Ease of Application.** The average professional consulting engineer is interested in the amount of time it will take to arrive at an answer, the frequency of projects that will require special attention, and the effort it will take to organize the results in a final report. 3-D applications are simply not as easy to use as 2-D.
- **Avoidance of Errors.** As illustrated above, analyses are prone to errors, and 3-D analyses are more complicated than 2-D analyses. The author believes that the emphasis in the profession needs to be on performing solid, fundamental engineering, rather than on increased sophistication that invites more errors.

3-D analyses have mostly been used for forensic studies, and for those few complex situations that involve a very unusual geometry and/or distribution of shear strengths in the potential sliding mass. Examples of these can be found in Stark and Eid (1998). In the author's 16 years of experience performing stability analyses on dams, embankments, cut slopes, and landfills, there were only three situations where a 3-D analysis was warranted during design, and all three were satisfactorily accomplished using multiple 2-D sections. One of these projects was given as an example in the Stark

and Eid (1998) paper. In that case Stark and Eid (1998) felt that a 2-D slope stability analysis could not anticipate the combined effects of the project's complicated geometry and shear strength zones. After discussion of the project's complexity, they reported a minimum 3-D factor of safety of 1.65 using a 3-D analysis program. In fact, the original design team, of which the author was a part, had two years earlier calculated a factor of safety of 1.60 using weighted averages of several 2-D cross-sections. Thus, even in this circumstance that had unusually complicated geometry and shear strength conditions, a modified-2-D approach gave results one would expect relative to the 3-D analysis results.

Notwithstanding the reservations given above, 3-D analyses will well serve those who have the time and budget to perform them.

To summarize, the refinements in accuracy offered by 3-D analyses are rarely matched by the average practitioner's understanding of basic slope stability mechanics, much less the level of confidence ordinarily offered by assumed shear-strength and pore-pressure parameters. Most often, the differences in shear strength and pore-pressure assumptions made by different engineers will substantially outweigh the refinements obtained by favoring 3-D over 2-D analyses. Compare, for example, the different conclusions reached by Schmucker and Hendron (1998) versus Stark et al. (2000) regarding the cause of a major landfill failure; or the difference in 2-D vs. 3-D comparisons for a landfill failure described by Soong et al. (1998), from those made by Stark et al. (1998). These case histories, recently published by experienced professionals, do not provide a compelling argument that 3-D analyses should be preferred. They do, however, reinforce the notion that the major factors contributing to uncertainty in a slope's performance are shear strengths and fluid pressures, and that this is where our attention should be focused. The purpose of this paper is to focus specifically on one of these issues, namely, when it is appropriate to use residual vs. peak shear strength for geosynthetic interfaces at the base of a waste containment facility.

## **GENERAL DISCUSSION OF 2-D ANALYSIS APPROACH**

### Method of Analysis

Slope stability analyses are most commonly assessed using computer programs that evaluate the limit equilibrium of a 2-D cross-section. Less sophisticated limit equilibrium analyses can be performed using hand-calculation methods or charts. Hand calculations are an effective analysis tool because they often provide a clearer understanding of the critical aspects of the problem, and mistakes in geometry and assumed failure planes are less likely. A common approach is to perform a hand check on the most critical surface that has been analyzed by a computer program. A good summary of slope stability approaches using hand calculations is provided by Abramson et al. (1996).

Limit-equilibrium analyses of varying complexity that have been developed are available to design practitioners. One of the first approaches was the Ordinary Method of Slices developed by Fellenius. Later refinements were presented by Bishop, Janbu, Morgenstern and Price, Spencer, and others. A review of these methods is beyond the scope of this paper, and the reader is referred to Abramson et al. (1996) and Duncan (1996) as a starting place for a comparison of the various limit-equilibrium methods. The author would, however, offer three points from his own practice as to which method to use for performing stability analyses of bottom liner systems:

- The Bishop method is generally not applicable when analyzing bottom liner system geometries because it was developed for circular failure surfaces. The critical slip plane for liner systems is often a translational block that is non-circular.
- Spencer's method, which is now commonly available in computer codes, is considered more rigorous and complete in its analysis than the simplified Janbu method, which is commonly used for block analyses. Spencer's method is computationally more intensive, however, and may be difficult to use for random searches for a critical failure surface, even with modern computers. It is also less stable and can yield incorrect results unless the line of thrust results are checked by the user. Therefore, a good practice is to search for the critical surface using Janbu's simplified approach, and then perform a final check on the stability using Spencer's method. Usually, but not always, Janbu's method will result in a slightly higher factor of safety.
- The approach developed by NAVFAC (1982) for translational block analyses is often a good and appropriate method for performing a hand-check on the computer results for a 2-D translational block failure along a bottom liner system.

### Identification of Critical Slip Plane

The most typical requirement for static stability is to meet a specified factor of safety. Just what constitutes an appropriate factor of safety will be discussed later in this paper. The idea is that if the stability analysis is performed correctly with the proper input variables, the factor of safety should provide a level of confidence that the slope will in fact be stable.

The essential operative words in the above paragraph relating to stability analyses is that they are "*performed correctly*". The safety margin in a factor of safety exists to account for unknown or unpredicted deviations from the original design assumptions. It is not, however, supposed to account for errors in the analysis, or incorrect geometric and material property assumptions.

When performing a correct analysis the critical slip plane for analysis must be identified correctly. An experienced geotechnical engineer is usually required in order to

select the critical cross-sections for analysis of a slope. Even for experienced practitioners, though, it is not always obvious which section is the most critical, and several trials generally need to be performed. For very complicated geometries, as described in the previous section, multiple 2-D sections may need to be weighted in order to simulate a 3-D analysis, or the more complex 3-D analysis can actually be performed.

In addition to selecting the proper cross-section, it is also important to search for and select the correct critical slip plane within that cross-section. In peer-reviewing slope stability analyses performed by others, the author has found errors in which the designer had correctly identified the critical cross-section, but incorrectly identified the critical slip plane within that cross-section. He found others, too, in which the designer had conceptually identified the correct slip plane, but failed to code the computer program to correctly place the slip plane at the correct interface within the liner system. The effects of such errors was to drop from an ignorantly-blissful factor of safety of 2 to 3, to an uncomfortable factor of safety of less than 1.1.

When the critical slip plane is along the liner system, the critical surface is always the one that has the lowest peak strength. If residual strengths are used in the analysis, they should reflect the surface that has the lowest peak shear strength, because that is the one that will govern deformations.

### Pore Pressures

Next to gravity, pore pressures (most pervasively those caused by liquid as opposed to gas) are the single most prevalent factor contributing to slope stability failures. They are also among the most overlooked elements in slope stability analyses. Schmucker and Hendron (1998) illuminate this problem when they state that "Very little is known at this time regarding the generation and distribution of pore pressures in MSW landfills."

The one area where evaluating the influence of pore pressures on slope stability has been well focused has been in the design of dams. For this reason there have been few dam failures due to the neglect of pore pressures, with dam failures in the past century generally being caused by other factors (e.g. liquefaction or piping). Pore pressures are not commonly included in landfill analyses. Yet most (or at least many) of the dramatic landfill failures reported in the industry can be attributed to pore pressures that built up either in the foundation, due to waste loading, or in the waste itself, due to leachate buildup or leachate injection. Examples are the Rumpke landfill failure (see Schmucker and Hendron, 1998, who attributed the failure in part to leachate buildup caused by an ice dam at the toe), and the Dona Juana landfill failure (see Hendron et al., 1999, who attributed the failure to high-pressure leachate injection).

When performing slope stability analyses, designers should consider the potential for unanticipated pore pressures. Unanticipated conditions may occur in landfills due to clogging of the leachate collection systems, or aggressive leachate recirculation in the waste mass. Additional discussion of this issue is provided by Koerner and Soong (2000). Further discussion later in this paper describes how pore pressures could lead to a localized exceedence of peak strength, leading ultimately to a progressive failure.

### Selecting and Measuring Material Shear Strengths

*Shear Strength Definition.* Figure 3 illustrates a non-linear shear strength envelope, which is typical for many soil and geosynthetic interfaces. Sometimes the non-linearity is slight, and a straight-line approximation over the entire load range under consideration can be valid. This is often true for very narrow load ranges such as those considered for cover veneer systems. At other times this non-linearity is quite significant, especially when shear strength characteristics are evaluated over the broad range of normal loads indicative of bottom lining systems.

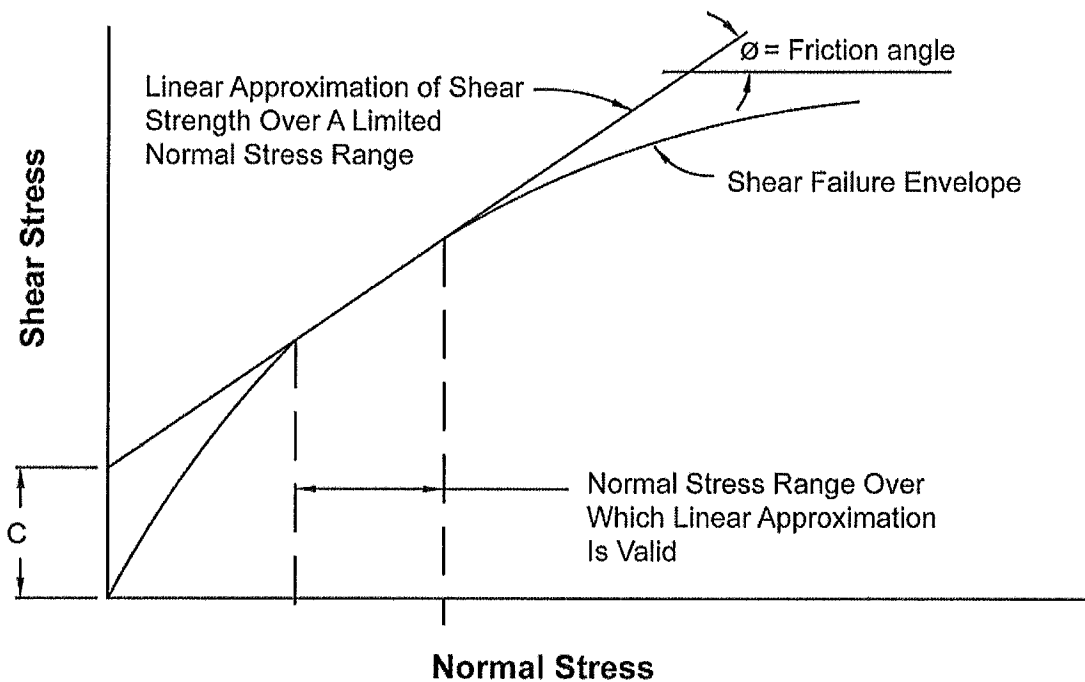


Figure 3 - Typical Shear Failure Envelope for Soil and Geosynthetic Materials.

If the shear strength curve of the evaluated materials is non-linear with respect to normal load, then special consideration should be given to defining the shear strength parameters within a specific normal load range. Many computer programs only allow the input of linear shear strength parameters. These parameters are normally identified as a friction parameter ( $\phi$ ) and a cohesion (or adhesion) parameter ( $c$ ). It is useful to

recognize that these are often only mathematical parameters that describe the shear strength of a material or interface over a specific normal load range. The shear strength parameters are demonstrated in Figure 3.

Draft European Standards, and other publications (e.g. Koerner and Daniel, 1997) suggest that the apparent cohesion of a shear strength envelope can be ignored. As stated by Jones and Dixon (1998): “This assumption can have a significant effect in that the shear strength for any particular normal stress will be quoted as being lower than measured... It is possible that the failure envelope may curve to the origin at very low normal stresses, in which case ignoring the apparent cohesion will result in over conservative results.” If we recognize that the values of the parameters  $\phi$  and  $c$  are only mathematical tools used to describe the measured or estimated shear strength over a given normal load range, we can discount statements that advocate that cohesion can be ignored.

The friction parameter ( $\phi$ ) is related to the slope of the line (slope =  $\tan\phi$ ), the cohesion parameter ( $c$ ) is the y-intercept, and the normal load range is the abscissa range over which the straight-line approximation of the shear strength envelope is valid. Use of the shear strength parameters outside of the normal load range for which they were defined is generally non-conservative, as illustrated in Figure 3.

If the computer program only allows the consideration of linear shear strength envelopes, the shear strength envelope for non-linear materials should be discretized into a series of straight-line approximations for different normal load ranges. Furthermore, where the critical slip surface runs through a material or interface that exhibits a non-linear strength envelope, the designer should either use a computer code that allows input of a non-linear shear strength envelope, or assign different strength parameters to different zones of the material or interface according to the normal loading it theoretically experiences. For computer codes that do not allow non-linear shear strength envelopes, the delineation of different normal-load zones for non-linear materials is usually calculated by hand. This procedure is outlined in detail by Thiel et al. (2001).

*Shear Strength Measurement.* For geosynthetic lining systems, the internal and interface shear strength is normally determined by using the direct shear test in accordance with ASTM D 5321. For GCL internal and interface shear strength evaluation, direct shear testing is conducted in accordance with ASTM D 6243. In these direct shear tests, the geosynthetic material and one or more contact surfaces, such as soil or other geosynthetics, are placed within a direct shear box. The specimens are hydrated, consolidated, and placed under a constant normal load in accordance with the ASTM procedures, along with any project-specific testing clarifications/instructions from the design engineer. A tangential (shear) force is applied to the materials, causing one section of the box to move in relation to the other section. The shear force needed to cause movement is recorded as a function of horizontal displacement.

The test is normally performed for several different normal loads. Typically a series of at least three individual tests are performed at specified normal load conditions. The normal load and shear forces are converted to stresses by the given area over which shear occurred, typically a 12 in x 12 in (300 mm x 300 mm) sample. The peak and post-peak (or residual, if deformation is taken far enough) shear strengths are plotted on a graph, and a best-fit straight line or curve is fit through the data to represent the shear strength envelope. Several factors can influence the interface shear strength of geosynthetics. The most important of these are discussed below.

*Valid Testing Technique.* While not offering any endorsements, the author can state that he trusts very few laboratories in the nation to provide high quality direct shear test data. Initial ASTM round-robin testing of even the most simple interface (nonwoven geotextile against a smooth HDPE geomembrane) produced a shot-gun scatter of results with very poor correlation. Unless the initial test data has integrity, most of the further considerations offered in this paper become meaningless. It is imperative that the designer screen the testing laboratory in order to obtain test data of assured accuracy.

*Rate of Shear Displacement.* The typical default shear rate for direct shear testing with geosynthetics as presented in ASTM D 5321 is 0.04 in/min (1.0 mm/min). For testing hydrated GCLs, ASTM D 6243 provides guidance on attaining consolidated drained conditions that should preclude the build-up of excess pore pressures.

In general the rate of shear displacement affects peak strength more than residual strength. Depending on the interface being tested, the strain rate of the test should be slow enough to give results representative of long-term (slow) shear conditions.

*Hydration.* The moisture content, degree of saturation, and degree of consolidation of adjacent soils and geosynthetics can all exert an influence on the shear strength results. It is important to direct the testing laboratory as to the sequence of hydration and consolidation. With clay soils adjacent to geosynthetics, it is generally more conservative to hydrate under low normal loads before consolidating. Thus far, the type of hydrating fluid has not been reported in the literature as affecting shear strength results, especially in regard to typical landfill leachates.

*Normal Stress.* The most common strength-related errors in computer slope stability analyses stem from using strength parameters that do not correspond to the normal load conditions at the surface being analyzed (Lambe et al., 1989). It is generally unconservative to extrapolate linear strength envelopes beyond the limits for which they were defined. It is, therefore, important that shear test data be acquired under normal loading conditions that are representative of the conditions being analyzed. For base liners this is zero to full height of the waste mass.

*Utilization of Representative Materials.* Designers often tend to use either published literature values or previously obtained test results for shear strengths. In such cases, their experience and judgment may assist them in selecting shear strength parameters for the purposes of preliminary design. It is highly recommended, however, that material-specific testing be performed to assist in preparing the final construction specifications, and/or to verify the actual materials delivered as part of a CQA program. The reason for this is that the variation in geosynthetic manufacturing parameters from job to job can have a significant effect on shear strength. The most significant of these is the degree of texturing on coextruded geomembranes. Figure 4 presents a graph showing the difference in peak and post-peak shear strengths obtained with two different degrees of texturing. Designers can use this concept to their advantage, as will be discussed later. Designers unaware of this issue may test a manufacturer's sample and obtain passing results, and then use GRI-GM 13 as a texturing specification. This would provide an extremely low-level requirement for texturing that may not achieve the same interface shear strength as the nice sample provided for initial testing by the manufacturer. The same principle may hold for geotextile-based products, whose fiber denier size, fiber type, degree of needling, etc. can influence its interface shear strength properties. The only way to be sure is to test the actual materials provided for construction.

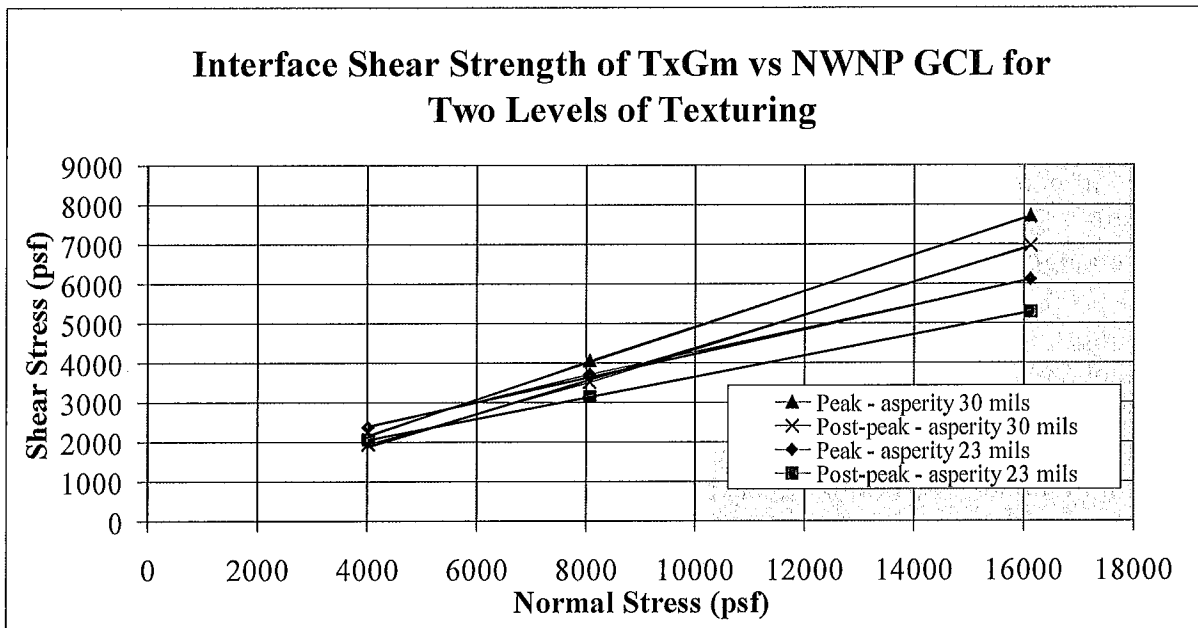


Figure 4 – Variation of Interface Shear Strength with Different Degrees of Geomembrane Texturing

*Adjacent Materials and Consolidation Time.* Using representative materials for direct shear testing refers not just to the materials for the interface being tested, but also to the adjacent materials. The use of realistic adjacent soil materials will typically provide slightly higher interface shear strengths than will, for example, the use of steel plates. In

the same vein, Breitenbach and Swan (1999) show that longer load consolidation times result in a significant increase in interface shear strengths, apparently due to micro-scale load-induced deformation of the interface materials. Jones and Dixon (1998) question the use of the ring-shear apparatus for testing, because the narrow specimen of limited surface area on hard, smooth boundaries may not be representative of field conditions. These factors can affect both the peak and post-peak shear strength results.

*Peak vs. Post-Peak vs. Residual Shear Strength.* The highest level of shear strength measured in a direct shear test under a given normal load is defined as the peak strength. With continued shear displacement there is typically a loss of strength. The shear strength at any given displacement past the point of peak strength is referred to as “post-peak strength”. The strength at which there is no further strength loss with continued displacement is called the “residual strength”. Many of the most common direct shear devices do not allow enough displacement to occur that would enable true residual strength to be measured (e.g., see Stark et al., 1996). Therefore, in some cases it is not technically correct to refer to end-of-test conditions as representing the “residual” strength, but rather, to refer to “post-peak” strength while also specifying the amount of displacement. For the purposes of this paper, the lowest expected shear strength after significant deformation (typically more than 3-6 inches [70-150 mm]) is described as the residual shear strength. Shear strengths between the peak and residual shear strength are referred to as post-peak. This brings us then, to the main focus of this paper, which is whether it is appropriate to use peak or residual shear strengths (or something in between).

## **PART 2 – PEAK vs. RESIDUAL: THEORETICAL AND PRACTICAL CONSIDERATIONS**

### **BACKGROUND DISCUSSION ON BRITTLE MATERIALS AND PROGRESSIVE FAILURE**

Many, but not all, geosynthetic interfaces are strain softening. This highlights the essence of the peak vs. residual question. With a relatively short amount of deformation (typically less than 25 mm), the materials pass beyond peak strength into a lower post-peak shear strength, ultimately becoming what we call residual. In geotechnical engineering these shear strength characteristics are also sometimes called ‘brittle’ – brittle meaning that the material substantially decreases in strength after it is “broken”, that is, has gone past peak strength. (Note that this has nothing to do with the tensile behavior of the material.) This behavior is in contrast to a ductile shear interface, which continues to deform after reaching its peak strength, but retains its strength close to the peak. An example of a brittle geosynthetic interface is an HDPE textured geomembrane against a geotextile, which produces a dramatic drop in strength after the peak strength is

exceeded. An example of a ductile geosynthetic interface is a smooth PVC geomembrane against a geotextile (see data published by Hillman and Stark, 2001). Also, MSW waste is generally considered a ductile material in terms of shear strength (Kavazanjian, 2001).

As a progressive failure develops, the shear stresses are redistributed within the slope. This often involves the slow deformation of the failing mass over time, followed by an abrupt slide. If the critical plane supporting a slope is brittle, and for some reason part of it is stressed past its peak strength, then that part quickly becomes significantly weaker, which means it can carry less of the load. That in turn puts more of the load on other parts of the critical plane, which may in turn cause another part of that plane to become overstressed and exceed its peak strength. The continuation of this process is called progressive failure. At some point the entire system becomes overstressed and an abrupt failure occurs. This is the concern when there is a brittle interface.

Progressive failures have been characteristically noted for stiff clays, as described by LaRoche (1989): “We have come to realize that we cannot count on the peak strength in this strain-softening material either for short- or long-term stability.” Past landfill failures have been attributed to this same phenomenon (Schmucker and Hendron, 1998; Mazzucato et al., 1999; Stark et al., 2000), which holds significant potential for future failures (Gilbert and Byrne, 1996).

## **POTENTIAL CONDITIONS THAT MAY LEAD TO PROGRESSIVE FAILURE**

Several reasons are provided below which explain why the peak strength of a bottom liner interface might unexpectedly be exceeded.

### Non-Uniform Stress Distribution and Strain Incompatibility

Perhaps one of the most compelling reasons to be concerned about progressive failure in liner systems is that the stress distribution along the liner interface is not known. “It is impossible to obtain all of the necessary information in most cases” to perform a rigorous analysis of a progressive failure process (Tiande et al. 1999). “It is difficult to determine the available shear resistance along an interface exhibiting strain-softening behavior. It may be unsafe to assume that peak strength is available, while it may be excessively conservative and costly to assume that only the residual strength is available” (Gilbert and Byrne, 1996).

The complexities of stress distribution are affected by the type of loading and by pore pressures. According to Li and Lam (2001) “.. the development of progressive failure will also be different depending on whether failure is triggered by a rise in water table [*insert by author: namely, leachate*] or an increase in external loading [*insert by author: namely, continued waste stacking*]”.

Reddy et al. (1996) present a most interesting finite-element modeling study that evaluates the stress distribution and deformations along a landfill liner system for an assumed landfill geometry. Their study compares smooth and textured interfaces for different stiffnesses of waste. Although their analysis did not model strain-softening behavior of the interfaces, the results provide valuable insight into stress and strain distribution. Some of the conclusions from their study are:

- The stiffness of the waste influences the distribution of interface stress and shear displacements. Stiffer waste puts more stress and strain on side slopes (especially the lower part of the slope). Softer (more compressible) waste puts more stress on the base liner below the highest part of the waste, and more strain accumulation towards the toe. The overall factor of safety, however, is not affected by the waste stiffness, assuming that no strain-softening of the interface shear strength occurs.
- The smooth interface with  $11^\circ$  friction reached its peak strength in a number of places along the interface in their example, even though the global factor of safety was 1.5. The textured interface did not approach its peak strength anywhere along the interface in their example, but had a factor of safety of over 4. This means that a typical stability evaluation that results in a factor of safety of 1.5 may actually result in areas of the critical interface achieving their peak strength and possibly going into a reduced post-peak strength.

A finite element study was performed by Filz et al. (2001) who reached conclusions similar to those obtained by Reddy et al. (1996). Filz et al. (2001) provided a compelling demonstration that a smooth clay-geomembrane interface exhibiting strain-softening characteristics might be inappropriate to analyze based on peak shear strengths. They showed that the distribution of mobilized shear stresses was not uniform along the base and side slope, and would result in progressive exceedence of peak strength. Their comparative analyses demonstrated that whereas a limit-equilibrium analysis based on peak strengths might result in  $FS = 1.6$ , the finite-element analysis would suggest impending failure (i.e.  $FS = 1.0$ ). The same problems analyzed using residual shear strengths in limit-equilibrium analyses resulted in an average  $FS = 0.94$ . Furthermore, for a finite-element analysis to show  $FS = 1.5$ , the limit-equilibrium analysis based on peak strengths needed to show a  $FS$  of about 2.2, and the limit-equilibrium analyses using residual shear strength resulted in  $FS = 1.3$ .

Differences in the relative stiffnesses of the overlying waste as compared to that of the liner interface are also cited by Gilbert and Byrne (1996) as a significant potential cause of deformations along the liner interface that could lead to residual shear strengths.

Similar suppositions are made by Stark et al. (2000), who postulate that strain incompatibility between MSW and underlying interfaces can lead to progressive failure, as they believe was the underlying cause of the Rumpke landfill failure. The weaker lower interfaces may achieve post-peak strengths before the MSW ever achieves peak

strength. After peak strength of the interfaces is achieved, the peak strength of the MSW may be mobilized at a time when the strength of the interfaces is reduced to the residual value. They state: "The greater the difference between the stress-strain characteristics of the MSW and the foundation soil or geosynthetic interfaces, the smaller the percentage of [peak] strength mobilized in the MSW and underlying materials." <sup>1</sup>

### Unexpected Increases in Pore Pressure

The typical effect of pore pressures is to decrease the effective normal stress, which in turn decreases the effective shear strength, even as the shear stress that is driving instability remains unchanged. When pore pressures are introduced, the effective shear strength may be reduced to the point that the peak shear strength at that location is exceeded, at which point progressive failure can begin. This was what Schmucker and Hendron (1998) concluded was the triggering mechanism for the Rumpke landfill failure.

### Seismic Loading

With seismic loading there is certainly the potential for deformation to occur along the critical failure plane, which can reduce the strength of the critical interface below its peak strength. In this regard the design practitioner needs to assess the potential for this type of deformation and, if the design earthquake is expected to produce deformation greater than about 20 mm, then the residual strength of that interface must be considered.

### Construction Deformation

Construction conditions frequently result in temporary stability conditions with lower factors of safety than the completed fill scenario. To the author's knowledge, the effect of preliminary interface deformation at low normal loads on the subsequent shear strength at higher normal loads has only been documented in one recent study by Esterhuizen et al. (2001). They showed that for a smooth clay-geomembrane interface, deformations at low normal loads would partially, but not fully, reduce the peak strength of the interface at higher normal loads. They provide a very interesting "work-softening" model to describe this behavior in a manner that can be used in a finite-element analysis. Although their model fits the data very well, it is only applicable to the specific clay and geomembrane used for their study, and it is not known at this time how well their approach would work for other interfaces. This is an area for further research.

---

<sup>1</sup> For years now the author has heard the statement that the strain incompatibility between waste and liner systems could be a major consideration in selecting appropriate shear strengths. It is interesting, however, that some of the literature reports surprisingly low amounts of deformation required to reach the peak strength of the waste; on the order of only 40 mm for rigid-body deformation. See, for example, Eid et al. (2000), Stark et al. (1998), Mazzucato et al. (1999). Also Kavazanjian (2001) states his belief that strain compatibility with MSW is not nearly as significant an issue as has generally been supposed, based on direct- and simple-shear test results that show that the strains and deformations required to reach peak strength are comparable to those required for most soils.

## Waste and Foundation Settlement

Over time there is substantial deformation and settlement of the waste that may cause unknown redistribution of stresses. The settlement of waste adjacent to a sideslope has often been noted as a source of downdrag forces, which may become great enough to exceed the peak strength of one of the slope liner interfaces. This phenomenon was cited by Stark and Poeppel (1994) as a mechanism contributing to the Kettleman Hills landfill failure, and is echoed in Gilbert and Byrne's (1996) theoretical study: "...it is more likely that the residual strength will be mobilized along the side slope rather than the buttress [bottom liner]", and they even go so far as to say "...it is unlikely that an average stress greater than the residual value could be mobilized along a typical side slope in a containment system." Likewise, foundation settlement has the potential to cause differential movements of the liner system.

## Aging and Creep

Geosynthetic durability has been the subject of many papers and studies which address the ability of geosynthetics to maintain their physical properties as containment barriers, and to some extent as tensile reinforcement. Little has been published, however, regarding the long-term durability of shear interfaces such as, for example, the long-term dependence on the strength of geotextile fibers at interfaces with textured geomembranes, or within reinforced GCLs. Quantitative predictions regarding the long-term aging and creep potential of geosynthetic interfaces are certainly beyond the author's capacity, but are noted as an additional potential mechanism whereby the assumed peak strength of an interface might be reduced.

## **FIELD OBSERVATIONS**

From the author's experience and his informal polling of industry representatives, two general field observations that have been made regarding deformations along geosynthetic interfaces on slopes:

- Slopes that were designed with robust interfaces using textured geomembrane or granular materials against geosynthetics, have not been observed to undergo tension or deformation.
- Slopes that had less brittle, but also less strong interfaces, such as a geotextile over a smooth geomembrane, have been observed to result in tension in the upper geosynthetic, presumably due to slippage along the interface which occurred as a result of downdrag forces.

It is worthwhile to note in the Gilbert and Byrne (1996) model that strain softening on the slope would generally only occur if the slope angle was greater than the peak friction angle of the lining material. Although unverified by the author, this may be a

general guideline for estimating whether or not peak or residual shear strength would occur on a slope (excluding seismic forces). For example, on a 3(H):1(V) slope, perhaps a peak interface strength of 18° or more would maintain its peak strength, and an interface strength of less than that would have a higher potential for going into residual.

Given the large number of landfills constructed with geosynthetic bottom liner systems, it is quite surprising how few failures have actually been reported. Furthermore, none of the reported failures, to the author's knowledge, involved the progressive failure of a substantially brittle geosynthetic interface. Most of those failures have involved soil (including bentonite failures associated with unreinforced GCLs, which are ductile relative to shear strength). The best example of a pure geosynthetic failure that involved some degree of strain softening is the notorious Kettleman Hills failure, but the interfaces in that failure were fairly weak to begin with (all against smooth HDPE), and the initial factor of safety, even assuming peak strengths of the interfaces as they existed, was low, and below standard industry guidelines.

The conclusion of industry observations is that actual industry experience has not shown degradation of peak strength (i.e. progressive failure) to be a pervasive problem. Nonetheless, it definitely presents a potential problem that has on occasion bloomed into an unfortunate reality. It is, therefore, worth taking it into account by means of design and analysis considerations, which are discussed in the next section.

## **PART 3 - DESIGN APPROACHES**

### **THE PEAK vs. RESIDUAL ISSUE IN THE CONTEXT OF THE DESIGN PROCESS**

Many elements of a landfill are not designed, per se, but are largely dictated either by the owner's desires or by regulatory constraints. For example, the geometry of a landfill (boundaries, slopes, height, etc.) is often governed by an attempt to maximize the resource (i.e. volume) while meeting the constraints presented by conditional use permits, property line setbacks, maximum slope regulations and the like. Furthermore, the liner system is usually prescribed by regulation, at least in its fundamental requirements, and oftentimes by a default regulatory configuration.

In many cases then, the two major elements that influence a stability analysis are largely predetermined. That is, both the preferred landfill geometry and the liner system are more or less given to the "designer", who is charged with producing the "final design". From the point of view of slope stability, what is there left to do? Obviously the slope stability should be checked and verified. What does this mean and how is it done?

The first step in performing a slope stability analysis is to define the basis of the analysis. This is often documented in the project files as a Design Basis Memorandum (DBM), in which the following kinds of determinations are made:

- Will the analysis look at only the final configuration, or at interim operational configurations as well? (The latter option is highly recommended for risk management.)
- What unit weight will be assumed for the waste?
- What material strength values will be assumed for the different materials, and how will they be determined?
- Which pore-pressure scenarios will be evaluated?
- What will be the minimum acceptable factors of safety?
- Are seismic analyses required? If so, what approach will be used? How is the design earthquake defined? If a deformation approach is used, what is the maximum allowable deformation?

The results of the slope stability analyses will be:

- A static factor of safety (for each configuration analyzed).
- If a seismic analysis is required, the results will present either a potential magnitude of deformation along the critical slip plane, or a factor of safety for a simplified pseudo-static analysis.
- A description of the minimum required interface shear strength properties for the liner system construction.

It is this last point that makes slope stability analyses a design function rather than a mere geotechnical engineering exercise. It is essential that a clear linkage be made between the slope stability calculations and the ultimate project specifications, to ensure that the proper materials are provided during construction to meet the slope stability requirements. If the analysis results do not meet expectations, iterations of laboratory testing and/or alterations in slope geometry and/or liner materials may be required in order to achieve an acceptable design that can be adequately specified.

The design aspect of slope stability analyses becomes even more interesting when an additional constraint is put on the design criteria, namely to position the critical slip surface above the primary geomembrane. This is a common practice in Germany that is also employed by several design practitioners in the United States (and likely in other places as well, given the author's limited knowledge of practices worldwide). This design approach helps to ensure that, if for any reason slippage does occur, the barrier liner system will remain intact. Ensuring that the slip plane is above the primary geomembrane is not necessarily a simple matter; laboratory shear testing programs and

iterations of slope stability analyses are often required in order to achieve acceptable results.

Implicit in the slope stability design and analysis process is the need to decide whether peak or residual shear strengths should be used. Though this is not generally an issue for waste materials, which are usually considered ductile, it is often a significant issue for liner system interfaces. This decision will significantly influence the calculated factor of safety. For seismic analyses, the influence is often less significant, because if the seismic analysis indicates deformation will occur, a prudent designer will use a post-peak shear strength (even as the question remains whether to use a deformation-based post-peak strength, or a true residual strength).

### **WHAT IS AN APPROPRIATE FACTOR OF SAFETY?**

The author previously co-authored a paper whose title posed this same question concerning cover systems (Liu et al., 1997). That paper discussed assessing the degree of confidence in each of the variables that went into assessing the factor of safety, and assessing the potential risk and cost of a failure. This approach is espoused by Gilbert (pers. comm.) who believes that the factor of safety should be based on “uncertainties, assumptions, and the consequences of failure.”

It is common in the literature to see geotechnical references that reiterate the idea that the greatest degree of uncertainty in performing slope stability analyses is the shear strength of the materials (e.g. Liu et al, 1997; Stark and Poeppel, 1994; Duncan, 1996). Given that the factor of safety is a reflection of uncertainty, it should logically reflect the degree of uncertainty in the shear strength properties. This was clearly noted by Terzaghi and Peck (1948, pg. 106):

“The practical consequences of the observed differences between real soils and their ideal substitutes must be compensated by adequate factors of safety.”

A commonly accepted value for the factor of safety in geotechnical engineering slope stability analyses is  $FS \geq 1.5$ . Many engineers blindly accept this value while remaining ignorant of its basis. The origin of this value was the empirical result of analyzing the relative success and failure of dams that have been constructed over the past century. Experience proved that when an analysis was performed correctly, assuming reasonable and prudent material properties, an earthen structure with a factor of safety of 1.5 can be expected to remain stable even when some of its structural geometry and material properties have varied from those assumed in the analysis. Similarly, other values for an acceptable factor of safety have been established as general industry practice for other types of problems, such as bearing capacity (required FS generally between 2 and 5) or drainage applications (FS generally ranging from 1 to 20 depending on the problem).

It is also fundamental to the establishment of generally accepted factors of safety that analyses are performed correctly, and are based on prudent assumptions regarding material properties, geometry, unit weights, and pore pressures. Factors of safety are not intended to compensate for engineering errors or omissions. Indeed, the author has evaluated failures where the design factor of safety exceeded 1.5, which means that the original design neglected to take into account one or more critical factors.

With containment lining systems we meet a unique opportunity. We have a greater ability to know where the potential critical slip plane is, and can measure its shear strength characteristics more accurately than we can in a number of traditional geotechnical problems. We have far more knowledge of the geometry and shear strengths than when we are confronted with a natural slope, for example. Knowing where slippage is most likely to occur, we have to assess the implications for deformation. As described previously in this paper, we often don't really know if some deformation will occur, but experience from many analogous failures, along with the process of deduction, tells us that it *could* occur. Knowing this, we should at least be prepared to use the post-peak shear strength of the surface having the lowest peak strength.

## **SPECIFIC APPROACHES**

Some specific design approaches, which the author has himself employed, are summarized below. This does not imply that others approaches do not exist, but simply that this paper is based on the author's experience.

1. The Most Conservative Approach – Force the Slip Plane Above the Geomembrane and Use Residual Shear Strengths Everywhere the Slip Plane Occurs in the Liner System. A simple and common way of achieving this objective is to use single-side textured geomembrane for the primary liner, and then cover it with a geotextile or geonet product. In nearly every case the author has been involved with (save a few inevitable exceptions), single-sided textured geomembrane (textured side down, of course) always caused whatever slippage occurred to take place on the top surface of the geomembrane, if it was covered with another geosynthetic. Even when directly covered by a granular material, it was often possible to make the bottom (textured) interface stronger than the smooth geomembrane/granular soil interface. In our experience there is often not a large difference between the peak and residual shear strength on smooth geomembrane interfaces with either other geosynthetics or granular soils, and these interfaces would not be considered very brittle. There may be some exceptions, such as a smooth HDPE geomembrane against a wet clay as described by Filz et al. (2001) for the Kettleman Hills failure analysis.

Some designs may need greater shear strength for interim construction and operational conditions than can be provided by a smooth geomembrane surface, so a double-sided textured geomembrane may be required. In this case the design condition of having the weak interface above the primary geomembrane may still be achieved by specifying a more aggressive texturing on the lower side of the geomembrane (see shear data presented in Figure 4).

If a designer is able to use the residual shear strength of the upper geomembrane interface and achieve acceptable factors of safety, this design can be very safe from the point of view of both stability and environmental containment. This approach is favored by Hullings and Sansome (1997), who recommend: "If possible, provide a slip plane and a stress-free geomembrane."

If true residual shear strengths are used for the analysis, and those strengths are measured with a degree of confidence that they represent worst case for the liner system interfaces, it follows that a lower-than-typical factor of safety can be allowed. Gilbert and Byrne (1996) suggest that a factor of safety simply greater than unity may be an adequate design criterion for analyses that assume residual shear strengths are the only strengths mobilized along the entire slip surface. Part of Gilbert's rationale (personal communication, 2001) is that even if a failure were induced for a slope analyzed with this criterion, things could not degenerate quickly, presuming the analysis were properly performed. The slope could subsequently be monitored and measures taken to reduce the deformation rate, if deemed necessary.

A similar recommendation is given by Stark et al. (1998): "...strain incompatibility can facilitate the development of slope instability because the geosynthetic interface may mobilize a post-peak or residual strength while the waste is mobilizing a strength that is significantly below the peak strength. This can be incorporated into a design by assigning a residual strength to the critical interface or slip surface and requiring a factor of safety,  $FS > 1$ ...Because field interface displacements and *effect(s) of progressive failure are not known [emphasis by author]*, a factor of safety,  $FS > 1$  with a ring shear residual interface strength assigned to all potential slip surfaces should be satisfied in addition to meeting regulatory requirements."

Filz et al. (2001) suggest that if true residual shear strengths are used for the analysis, then whatever factor of safety would normally be deemed appropriate for a given project could be reduced by the following reduction factor ( $RF$ ):

$$RF = \tau_r / [\tau_r + 0.1(\tau_p - \tau_r)]$$

Where  $\tau_r$  = residual shear strength, and  $\tau_p$  = peak shear strength. They imply that the normally appropriate factor of safety would be determined based on considerations of uncertainty and consequences as described by Duncan (2000). Also, it should be noted that their discussion and recommendations were restricted to smooth-geomembrane/clay interfaces.

2. Safe Approach – Use Residual Shear Strength of the Interface with the Lowest Peak Strength. This approach could be the same as the above approach if the interface having the lowest shear strength happens to be above the primary geomembrane. If, due to overall slope stability constraints, the interface with the lowest peak strength is below the primary geomembrane (e.g. weak subgrade interface), this approach will still result in a very safe design relative to slope stability. It could, however, be less conservative in terms of environmental containment should deformation occur, causing a tear in the primary geomembrane. This approach is recommended by Gilbert and Byrne (1996) who “strongly recommended that the potential for instability be explored in a limit equilibrium analysis using residual strengths along all interfaces....It is strongly recommended that a factor of safety greater than one be achieved in all containment system slope designs, assuming residual strengths are mobilized along the entire slip surface.”

The same degree of factor of safety for this approach would apply as for Approach # 1 above. Holley et al. (1997) reported using residual shear strengths for a critical surface below the primary geomembrane in a steep canyon landfill, and obtaining operating factors of safety of 1.2 and an ultimate factor of safety of 1.4 for the final build-out. It is not clear if these were their minimum design criteria, or simply the results that they accepted.

3. Brute Strength Approach – This approach would employ very aggressive texturing to achieve high interface strengths, although the assumed strengths may be prorated by some factor to account for variability. The need to occasionally use this approach is suggested by Hullings and Sansome (1997): “Overall slope stability conditions often do not allow low interface strengths, so the interface strengths above the geomembrane cannot be much lower than the interface strength on the underside of the geomembrane.”

If the approach of high interface strength is used everywhere, and seismic analysis shows no deformation, an acceptable design basis may be to use peak shear strength with an adequately high factor of safety. How high is adequate is difficult to say, because the theoretical possibility of progressive failure still exists. The finite-element study performed by Filz et al. (2001) indicates that  $FS > 2$  should be required for analyses based on peak strength of smooth-geomembrane/clay interfaces.

We have only the record of successful designs that were constructed based on peak strength to testify that the brute strength approach may be valid, but this does not demonstrate that it is conservative. The analysis should account for potential leachate build-up under worst case assumptions, for example after a post-closure maintenance period with substantial leachate still being generated, and the operations or leachate-collection layer completely clogged. Check that a submerged condition at the toe does not result in a reduction in shear strength (due to reduction in effective normal stresses) to the point that it fails the peak strength at the toe, which could lead to progressive failure through the rest of the fill (such as that discussed by Schmucker and Hendron, 1998).

#### 4. Hybrid Approaches

- a) *Use Residual on the Side Slope and Peak on the Base.* To the author's knowledge, this approach was first documented in the literature by Stark and Poepfel (1994) in their review of the notorious Kettleman Hills failure. As they so aptly stated: "...it appears that peak and residual interface strengths should be assigned to the base and sideslopes, respectively, for design purposes." This was later echoed by Jones and Dixon (1998) from the U.K., who stated: "In some instances residual values may be appropriate on the side slope where large displacements are anticipated, used together with peak values on the base." In the author's opinion, this approach is a strong qualifier for accepting a traditional factor of safety in the range of 1.5 for ultimate build-out conditions (assuming unexpected pore-pressure scenarios are included in the evaluation), and 1.3 for operations.
- b) *Use Post-Peak Strength Values that Anticipate a Limited Amount of Deformation.* Shear strength reductions may occur due to relative deformations during construction, landfill operations, and waste settlement, but these deformations may be less than those which would lead to the minimum residual shear strength conditions. Also, based on their observation of numerous apparently successful facilities, design practitioners may consider peak shear strengths with an adequate factor of safety to be valid designs, while still wishing to incorporate an additional degree of conservatism by reducing the measured peak strength of the geosynthetic interfaces. These strength reductions would be applied to the side slope as well as the base. Use of this approach is suggested by Filz et al. (2001), who suggest using a mobilized strength that is higher than the residual by about 10% of the increment from residual to peak strength, and applying an appropriate factor of safety to this based on reliability concepts as described by Duncan (2000).

- c) *Use Lower Waste Shear Strengths.* From the observation of trends published in the literature, shear strengths of 30° or more are commonly used for municipal solid waste. This level of shear strength has been documented as being generally conservative (e.g. Kavazanjian, 2001), but may require some amount of strain to become fully mobilized. As an approach to stability analyses designers may wish to reduce the mobilized strength of the waste material to more closely match the strain compatibility of the liner system.

The author has used all the above approaches in his own practice, which over the years has been based on improved levels of understanding. Currently (subject to change!) the author employs a combination of Approach #1 and #4 as his standard practice. That is, he usually defines a “design condition” which he believes will be the actual long-term conditions that interface shear strengths will experience. The decision as to what long-term shear strengths he selects is project-specific (there are many variations), and a complete discussion of this is beyond the scope of this paper. Suffice it to say that the decision is usually related to the criteria described for Approach #4. Next, the author follows the advice of Gilbert and Byrne (1996) and checks that the stability under the worst-case shear strength conditions (e.g. hydrated residual shear strength) results in  $FS > 1.0$ . This latter test is often the more significant.

A good example of the above approach is for bottom liner designs that involve the encapsulation of unreinforced bentonite between two geomembranes. The design scenario argues that most of the bentonite will remain dry for at least several centuries, and the basic slope stability analysis is performed on this basis. A second analysis is performed, however, to verify that the stability factor of safety is greater than unity even when all of the bentonite is under fully hydrated residual shear strength conditions. This example is more fully described in Thiel et al. (2001).

## **PART 4 – CONCLUSIONS AND RECOMMENDATIONS**

### **CONCLUSIONS**

- Many geosynthetic interfaces are highly strain-softening (i.e. “brittle”). The most common example is a textured geomembrane against some form of geotextile (whether it be a cushion, part of a geonet composite, or a GCL).
- There are mechanisms that can lead to exceedence of peak strength even though a correctly-performed slope stability analysis predicts a factor of safety greater than one. Examples of these mechanisms include:
  - Non-uniform mobilized stress distribution.

- Relative differences in stiffness between waste and liner materials.
  - Unexpected pore pressures.
  - Seismic loading.
  - Deformation during construction.
  - Waste settlement.
  - Foundation settlement.
  - Aging and creep of the geosynthetics.
- Exceedence of peak strength in a brittle interface can result in progressive failure.
- Based on field observation, most facilities designed with aggressive interface shear strengths are not experiencing post-peak shear strength, which means that the working shear stress is probably less than or equal to the peak strength. Only a few examples of progressive failure along geosynthetic interfaces have occurred in the industry, and these have not been along highly brittle interfaces, which means that the projects did not have high factors of safety to begin with, even assuming peak interface strengths.
- Several design approaches have been used over the years and the standard-of-practice is evolving. In the United States a preferred approach has not yet clearly emerged.

## **RECOMMENDATIONS FOR PRACTICE**

- Designers and CQA firms should conduct material-specific testing of interfaces to verify that the materials specified and/or supplied for a project are realistic and meet the design requirements. Whoever commissions the testing should possess a skilled familiarity with the design objectives as well as the testing technique.
- Designers should attempt to position the critical slip plane above the primary geomembrane to the extent feasible for a given project. If a double-sided textured geomembrane is required for construction or operational stability, attempt to specify more aggressive texturing on the under side of the geomembrane.
- Using peak shear strengths on the landfill base, and residual shear strengths on the side slopes appears to be a successful state-of-the-practice in many situations.
- Designers should consider evaluating all facilities for stability using the residual shear strength along the geosynthetic interface that has the lowest peak strength. This would be an advisable risk-management practice for designers, even if the FS under these conditions is simply greater than unity.

- Regardless of the design assumptions, specify soil spreading by pushing up-slope only, and require close monitoring of LCRS and operations soil placement on slopes during construction to verify that relative shear displacement does not occur during construction. Exceptions to this practice should be allowed only with field tests and CQA verification.
- If LCRS or operations soils are placed as part of landfill operations, designers should assume the worst and automatically assume residual side-slope shear strength conditions will occur (and extra leakage rates as well). The reason for this is that construction by landfill operators is usually not controlled and monitored closely.
- Check stability for a potential leachate buildup, especially near the toe of the landfill.

## **RECOMMENDATIONS FOR FURTHER RESEARCH**

- More finite element analyses at an academic level, such as those performed by Reddy et al. (1996) and Filz et al. (2001) would be warranted, to gain a better understanding of the threshold beyond which localized stress distributions might cause exceedence of peak shear resistance. Refinements in the analyses would include modeling the strain-softening behavior of the geosynthetic interfaces, and checking different types of interfaces and geometries. The results of these analyses might prove useful for establishing guidelines as to when peak strengths might be exceeded and when they might be maintained. Ultimately, the author envisions correlations between the FS determined by limit equilibrium analyses, ratios of peak interface strengths to waste fill strengths, and relative stiffnesses (somewhat as proposed by Gilbert and Byrne (1996), but more specific and less general), being used to estimate when and where peak vs. post-peak strengths would be reached at the interfaces.
- The monitoring of slope deformation on geosynthetic interfaces that are being buried by waste is recommended. One fairly easy way to do this would be to use the simple tell-tale technique employed for the Cincinnati cover demonstration project (Koerner et al., 1996), though this would require participation by landfill owners and operators. This avenue of research echoes that suggested by Gilbert and Byrne (1996), who state: "Future research should focus on measuring deformations and mobilized shear resistances in existing waste containment facilities."
- The monitoring of pore pressures in the LCRS above liner systems, with the reporting of the worst-case conditions, would provide valuable information regarding long term conditions in landfills. Unfortunately, any high pressures would likely result in a permit violation at many facilities, so it is improbable that

an existing owner will voluntarily monitor high pressures, much less report them. We are therefore left with only orphan or Superfund sites as a possible basis for monitoring. Because of this limitation, participation in international waste conferences is increasingly valuable.

- Additional laboratory testing, conducted on various types of interfaces, would be useful to assess the impact of interface deformations at low normal loads on the peak strength reductions at higher normal loads.

## REFERENCES

Abramson, L.W., Lee, T.S., Sharma, S., and Boyce, G.M. (1996). Slope Stability and Stabilization Methods. John Wiley & Sons, Inc. New York.

Breitenbach, A.J. (1997) "Overview Study of Several Geomembrane Liner Failures Under High Fill Load Conditions." Proc. of Geosynthetics '97, IFAI, Vol. 2, pp. 1045-1061.

Breitenbach, A.J. and Swan, R.H. (1999) "Influence of High Load Deformations on Geomembrane Liner Interface Strengths." Proc. of Geosynthetics '99, IFAI, Vol. 1, pp. 517-529.

Brink, D., Day, P.W. and DuPreez, L. (1999) "Failure and Remediation of Bulbul Drive Landfill: Kwazulu-Natal, South Africa." Proc. Sardinia '99 Seventh International Waste Management and Landfill Symposium, CISA, Vol. III, pp. 555-562.

Duncan, J.M. (1996) "State of the Art: Limit Equilibrium and Finite-Element Analyses of Slopes." J. of Geotechnical Engineering, ASCE, Vol. 122, No. 7, May, pp. 577-596.

Duncan, J.M. (2000) "Factors of Safety and Reliability in Geotechnical Engineering" J. of Geotechnical and Geoenvironmental Engineering, ASCE, Vol. 126, No. 4, Apr., pp. 307-316.

Eid, H.T., Stark, T.D., Evans, W.D. and Sherry, P.E. (2000) "Municipal Solid Waste Slope Failure. I: Waste and Foundation Soil Properties." J. of Geotechnical and Geoenvironmental Engineering, ASCE, Vol. 126, No. 5, May, pp. 397-407.

Esterhuizen, J.B., Filz, G.M., and Duncan, J.M. (2001) "Constitutive Behavior of Geosynthetic Interfaces" J. of Geotechnical and Geoenvironmental Engineering, ASCE, Vol. 127, No. 10, Oct., pp. 834-840.

Filz, G.M., Esterhuizen, J.B., and Duncan, J.M. (2001) "Progressive Failure of Lined Waste Impoundments" J. of Geotechnical and Geoenvironmental Engineering, ASCE, Vol. 127, No. 10, Oct., pp. 841-848.

Gilbert, R.B. and Byrne, R.J. (1996) "Strain-Softening Behavior of Waste Containment System Interfaces." *Geosynthetics International, IFAI*, Vol. 3, No. 2, pp. 181-203.

Gilbert, R.B. (2001) Personal communication with the author.

Hendron, D.M., Fernandez, G., Prommer, P.J., Giroud, J.P., and Orozco, L.F. (1999) "Investigation of the Cause of the 27 September 1997 Slope Failure at the Dona Juana Landfill" *Proc. Sardinia '99 Seventh International Waste Management and Landfill Symposium, CISA*, Vol. III, pp. 545-554.

Hillman, R.P. and Stark, T.D. (2001) "Shear Strength Characteristics of PVC Geomembrance-Geosynthetic Interfaces." *Geosynthetics International, IFAI*, Vol. 8, No. 2, pp. 135-162.

Holley, K., Richardson, J., and Sadlier, M. (1997) "Design and Construction to Optimise Landfill Stability at the Nent Landfill, Hong Kong." *Proc. Sardinia '99 Seventh International Waste Management and Landfill Symposium, CISA*, Vol. III, pp. 565-574.

Hullings, D.E. and Sanome, L.J. (1997) "Geomembrane Anchor Trenches." *J. of Geotextiles and Geomembranes, Elsevier*, Vol. 15, Nos. 4-6, pp. 403-417.

Jones, D.R.V. and Dixon, N. (1998) "Shear Strength Properties of Geomembrane/Geotextile Interfaces." *J. of Geotextiles and Geomembranes, Elsevier*, Vol. 16, Nos. 1, pp. 45-71.

Kavazanjian, E. (2001) "Mechanical Properties of Solid Waste." *Proc. Sardinia '01 Eighth International Waste Management and Landfill Symposium, CISA*, Vol. III, pp. .

Koerner, R.M., Carson, D.A., Daniel, D.E., and Bonaparte, R. (1996) "Current Status of the Cincinnati GCL Test Plots" *Proceedings of the 10<sup>th</sup> GRI Conference, Field Performance of Geosynthetics and Geosynthetic Related Systems. Geosynthetic Research Institute, Drexel University, Philadelphia, PA*, pp. 147-175.

Koerner, R.M. and Daniel, D.E. (1997) Final Covers for Solid Waste Landfill and Abandoned Dumps. ASCE Press, Reston, VA.

Koerner, R.M. and Soong, T.Y. (2000) "Leachate in Landfills: The Stability Question." *Geotextiles and Geomembranes, Elsevier*, Vol. 18, pp. 293-309.

LaRochelle, P. (1989) "Problems of Stability: Progress and Hopes." The Art and Science of Geotechnical Engineering. Ed. by Corning et al., Prentice Hall, N.J., pp. 269-290.

Li, K.S. and Lam, J. (2001) Discussion of "Evolution of Progressive Failure of Landslides." J. of Geotechnical and Geoenvironmental Engineering, ASCE, Vol. 127, No. 1, Jan., pg. 98.

Liu, C.N., Gilbert, R.B., Thiel, R.S., and Wright, S.G. (1997). "What is an Appropriate Factor of Safety for Landfill Cover Slopes?" Conference Proceedings from Geosynthetics '97. IFAI, Roseville, MN, pp. 481-496.

Mazzucato, A., Somonini, P. and Colombo, S. (1999) "Analysis of Block Slide in a MSW Landfill." Proc. Sardinia '99 Seventh International Waste Management and Landfill Symposium, CISA, Vol. III, pp. 537-544.

NAVFAC (1982) Soil Mechanics. Design Manual 7.1, Department of the Navy, Naval Facilities Engineering Command, Alexandria, VA.

Reddy, K.R., Kosgi, S. and Motan, S. (1996) "Interface Shear Behavior of Landfill Composite Liner Systems: A Finite Element Analysis." Geosynthetics International, IFAI, Vol. 3, No. 2, pp. 247-275.

Schmucker, B.O. and Hendron, D.M. (1998) "Forensic Analysis of the 9 March 1996 Landslide at the Rumpke Sanitary Landfill, Hamilton County, Ohio." Proc. of the 12<sup>th</sup> GRI Conference, Lessons Learned from Geosynthetic Case Histories, Geosynthetic Institute, Folsom, PA, pp. 269-295.

Soong, T.Y., Hungr, O., and Koerner, R.M. (1998) "Stability Analyses of Selected Landfill Failures by 2-D and 3-D Methods" Proc. of the 12<sup>th</sup> GRI Conference, Lessons Learned from Geosynthetic Case Histories, Geosynthetic Institute, Folsom, PA, pp. 296-329.

Stark, T.D. and Eid, H.T. (1998) "Performance of Three-Dimensional Slope Stability Methods in Practice" J. of Geotechnical and Geoenvironmental Engineering, ASCE, Vol. 124, No.11, Nov., pp. 1049-1060.

Stark, T.D., Arellano, D., Evans, W.D., Wilson, V.L., and Gonda, J.M. (1998) "Unreinforced Geosynthetic Clay Liner Case History." Geosynthetics International, IFAI, Vol. 5, No. 5, pp. 521-544.

Stark, T.D., Eid, H.T., Evans, W.D. and Sherry, P.E. (2000) "Municipal Solid Waste Slope Failure. II: Stability Analyses." J. of Geotechnical and Geoenvironmental Engineering, ASCE, Vol. 126, No. 5, May, pp. 408-419.

Stark, T.D., and Poeppel, A.R. (1994) "Landfill Liner Interface Strengths from Torsional Ring Shear Tests." J. of Geotechnical Engineering, ASCE, Vol. 120, No. 3, March, pp. 597-615.

Terzaghi, K. and Peck, R. (1948) Soil Mechanics in Engineering Practice. John Wiley & Sons, New York, NY.

Thiel, R., Daniel, D.E., Erickson, R., Kavazanjian, E., and Giroud, J.P. (2001) *GundSeal GCL Design Manual*. Published by GSE, Houston, TX.

Tiande, M., Chongwu, M, and Shengzhi, W. (1999) "Evolution Model of Progressive Failure of Landslides." J. of Geotechnical and Geoenvironmental Engineering, ASCE, Vol. 125, No. 10, Oct., pp. 827-831.

**APPLICATION FOR PERMIT  
DNCS ENVIRONMENTAL SOLUTIONS**

**VOLUME III: ENGINEERING DESIGN AND CALCULATIONS  
SECTION 7: TENSILE STRESS ANALYSIS**

**ATTACHMENT III.7.H**

**BOWLES, JOSEPH E. 1977. *FOUNDATION ENGINEERING ANALYSIS AND DESIGN*,  
2<sup>ND</sup> EDITION. UNITED STATES: MCGRAW HILL BOOK COMPANY**

# FOUNDATION ANALYSIS AND DESIGN

Joseph E. Bowles

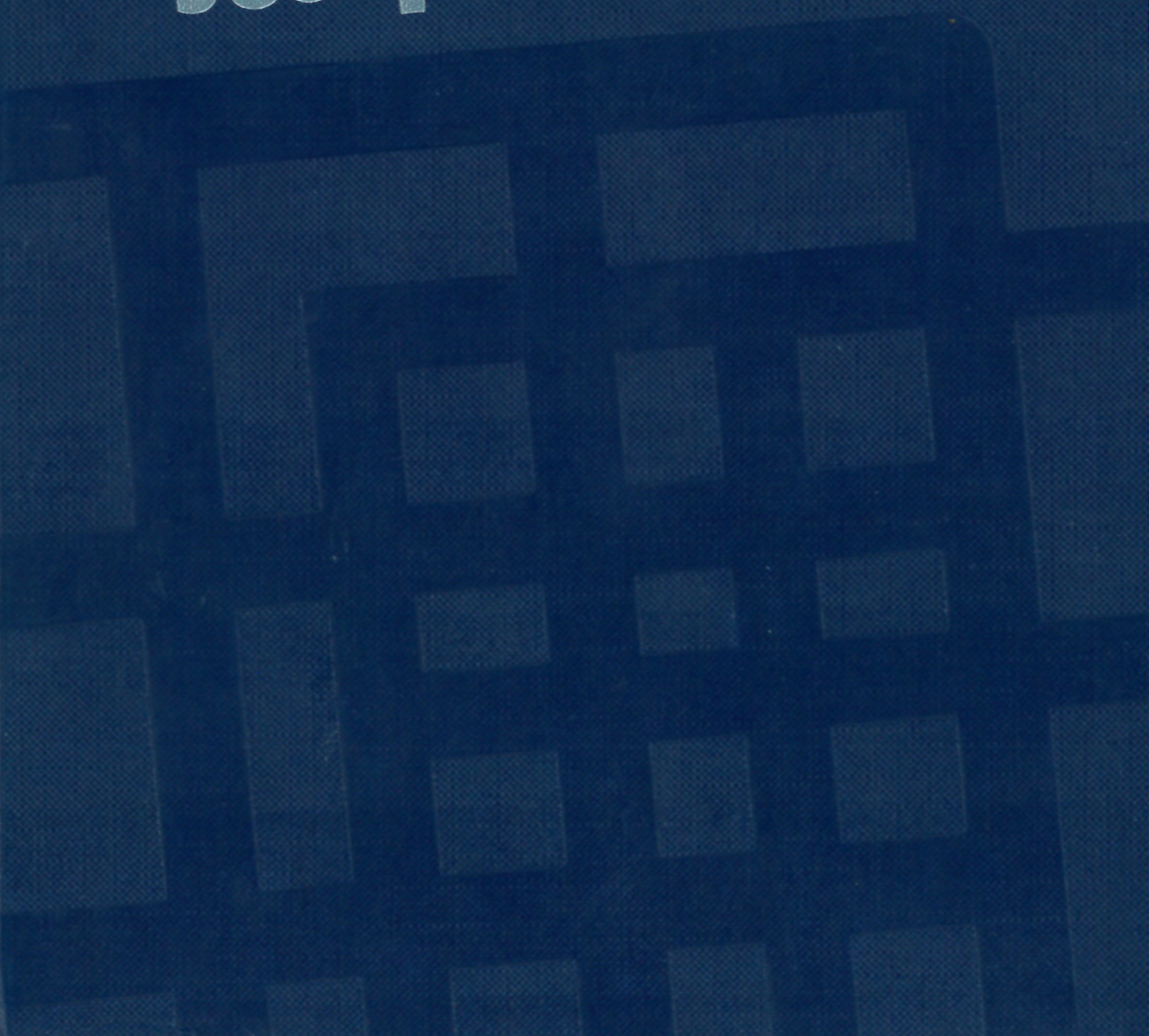


Table 3-2. Standard designation and sizes for drill rods and casing

Drill rod	OD, in	Casing and core barrel	Core-barrel-bit OD, in	Approx. diam of borehole,* in	Diam of core sample, in
E	$1\frac{5}{16}$	EX	$1\frac{7}{16}$	$1\frac{1}{2}$	$\frac{7}{8}$
A	$1\frac{3}{8}$	AX	$1\frac{7}{8}$	2	$1\frac{1}{8}$
B	$1\frac{7}{8}$	BX†	$2\frac{3}{8}$	$2\frac{1}{2}$	$1\frac{3}{8}$
N	$2\frac{3}{8}$	NX	$1\frac{5}{16}$	3	$2\frac{1}{8}$

\* Diameter of borehole is very nearly the ID of the casing.

† In soft or fractured rock, BX or larger cores are preferred.

The SPT was originally developed for cohesionless soils so that samples would not have to be taken. The test has evolved to the current practice of routinely determining  $N$  for all soils. In the zones of particular interest from about 2.5 ft or 1 m below ground surface to considerable depth below the estimated base of the foundation the test is performed every 2.5 ft or 1 m depth increment. At considerable depths where the boring becomes more informational the depth increment for testing is often increased to 5 ft or 2 m.

Empirical correlations between  $N$  and various soil properties have been attempted for cohesionless soils (Table 3-3). Table 3-3 should be used cautiously; for example, a "loose" soil with a range of  $D_r$  between 15 and 35 percent places rather arbitrary numbers on a rather tenuous description of a soil.

Table 3-3. Empirical values for  $\phi$ ,  $D_r$ , and unit weight of granular soils based on the standard penetration number with corrections for depth and for fine saturated sands

Description	Very loose	Loose	Medium	Dense	Very dense	
Relative density $D_r$ ,*	0	0.15	0.35	0.65	0.85	1.00
Standard penetration no. $N$		4	10	30	50	
Approx. angle of internal friction $\phi^\circ$ †	$25^\circ-30^\circ$	$27-32^\circ$	$30-35^\circ$	$35-40^\circ$	$38-43^\circ$	
Approx. range of moist unit weight, ( $\gamma$ ) pcf ( $\text{kN/m}^3$ )	70-100‡ (11-16)	90-115 (14-18)	110-130 (17-20)	110-140 (17-22)	130-150 (20-23)	

\* USBR [Gibbs and Holtz (1957)].

† After Meyerhof (1956).  $\phi = 25 + 25D_r$ , with more than 5 percent fines and  $\phi = 30 + 25D_r$ , with less than 5 percent fines. Use larger values for granular material with 5 percent or less fine sand and silt.

‡ It should be noted that excavated material or material dumped from a truck will weigh 70 to 90 pcf. Material must be quite dense and hard to weigh much over 130 pcf. Values of 105 to 115 pcf for nonsaturated soils are common.

**APPLICATION FOR PERMIT  
DNCS ENVIRONMENTAL SOLUTIONS**

**VOLUME III: ENGINEERING DESIGN AND CALCULATIONS  
SECTION 7: TENSILE STRESS ANALYSIS**

**ATTACHMENT III.7.I**

**RICHARDSON, CLINTON P., PHD., PE 2009.**

***MUNICIPAL LANDFILL DESIGN CALCULATIONS: AN ENTRY LEVEL MANUAL OF  
PRACTICE. CALIFORNIA: UBUILDABOOK, LLC.***

# **Municipal Landfill Design Calculations**

An Entry Level Manual  
of Practice

Clinton P. Richardson, PhD. PE.



# Chapter 28 Side-slope Liner Stability

## Problem Statement

Liner stability or side-slope slippage is complicated for multi-layered liner and collection system. A unit load of waste gravitationally induces shear stress and a portion of stress is transmitted by means of friction to the geosynthetic components beneath. The difference between frictional components must be carried by the particular component in the form of tensile stress and then compared to the component's yield stress for the resulting factor of safety. The portion transmitted to upper component is then propagated to the next component in the multilayered sequence. An unbalanced portion is eventually transmitted to the subgrade soil beneath the lower geosynthetic. If mass failure is going to occur, it will seek the interface with the lowest friction angle. The liner stability method is simply a resolution of shear stresses Koerner, 1994).

## Design Objective

Calculate the tensile stresses and shear stresses carried by the upper and lower geosynthetic components and estimate the factor of safety.

## Design Equations

Figure 1 shows a schematic of a multi-layered liner and resolution of forces assuming a single waste lift thickness.

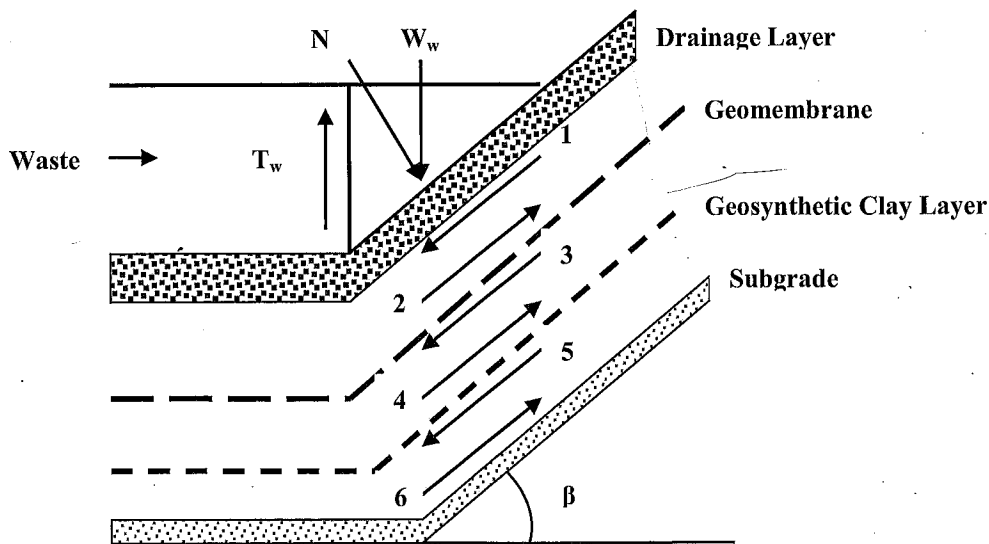


Figure 1: Resolution of Shear Forces in A Multi-layered Landfill Barrier Liner (adapted from Koerner, 1990).

The simple barrier system consists of a geomembrane underlain by a geosynthetic clay liner (GCL). The procedure may be extended to any number of interfaces, such as a geotextile, geomembrane, clay

liner, etc. Time is assumed to be sufficiently long between waste lifts that system readjustment will occur and either equilibrium or failure will exist. A unit width is assumed. The numbers 1 through 6 shown in the figure represent the forces that must be resolved sequentially.

The weight of a unit width of compacted waste is given by

$$W_w = \frac{1}{2} \gamma_w H \frac{H}{\tan \beta} \quad \text{Eq. 1}$$

where

$W_w$  = weight of waste per unit width (lb<sub>f</sub>/ft or kN/m)

$H$  = lift height (ft or m)

$\beta$  = slope angle (°)

$\gamma_w$  = unit weight of waste (lb<sub>f</sub>/ft<sup>3</sup> or kN/m<sup>3</sup>)

The frictional resistance along the waste edge is given by

$$T_w = \sigma_h \tan \phi_w H = K_o \sigma_v \tan \phi_w H \quad \text{Eq. 2}$$

$$K_o = (1 - \sin \phi_w) \quad \text{Eq. 3}$$

$$\sigma_v = \frac{1}{2} \gamma_w H \quad \text{Eq. 4}$$

where

$T_w$  = frictional resistance force per unit width (lb<sub>f</sub>/ft or kN/m)

$\sigma_h$  = horizontal stress of waste lift (lb<sub>f</sub>/ft<sup>2</sup> or kN/m<sup>2</sup>)

$\phi_w$  = waste friction angle (°)

$K_o$  = coefficient of earth pressure at rest (unitless)

$\sigma_v$  = vertical stress of waste lift (lb<sub>f</sub>/ft<sup>2</sup> or kN/m<sup>2</sup>)

The net weight of the waste is the difference between the downward acting waste weight and the upward acting resistance force, or

$$W_{net} = W_w - T_w \quad \text{Eq. 5}$$

The net weight can now be resolved into its two components: a normal force component acting perpendicular to the slope and a parallel force component acting downslope, or

$$N = W_{net} \cos \beta \quad \text{Eq. 6}$$

$$P = W_{net} \sin \beta \quad \text{Eq. 7}$$

where

N = normal force component of net weight (lb<sub>f</sub>/ft or kN/m)

P = parallel force component of net weight (lb<sub>f</sub>/ft or kN/m)

This latter force component is assumed to be dissipated through the drainage layer (Koerner, 1990). The forces that must be determined are a function of the normal force and the frictional resistance provided by the respective interface; for example, in the first force couple, the following relationships hold:

$$F_1 = N \tan \delta_1 = (W_{net} \cos \beta) \tan \delta_1 \quad \text{Eq. 8}$$

$$F_2 = N \tan \delta_2 = (W_{net} \cos \beta) \tan \delta_2 \quad \text{Eq. 9}$$

where

$\delta_1$  = drainage layer friction angle with respect to the upper geomembrane surface (°)

$\delta_2$  = lower geomembrane surface friction angle with respect to the upper GCL surface (°)

If  $F_1$  exceeds  $F_2$ , then the geomembrane is in tension. The force difference must be carried by the geomembrane. The actual stress in the geomembrane is given by

$$\sigma_{\text{actual geomembrane}} = \left( \frac{F_1 - F_2}{t_{\text{geo}}} \right) \quad \text{Eq. 10}$$

where

$\sigma_{\text{actual geomembrane}}$  = actual stress in geomembrane (lb<sub>f</sub>/ft<sup>2</sup> or kN/m<sup>2</sup>)

$t_{\text{geo}}$  = geomembrane thickness (ft or m)

The factor of safety for the geomembrane against failure in tension is

$$FS_{\text{geomembrane}} = \frac{\sigma_{\text{yield}}}{\sigma_{\text{actual geomembrane}}} \quad \text{Eq. 11}$$

where

$\sigma_{\text{yield}}$  = allowable geomembrane stress at yield (lb<sub>f</sub>/ft<sup>2</sup> or kN/m<sup>2</sup>)

The allowable geomembrane stress at yield is usually given in terms of lb<sub>f</sub>/in<sup>2</sup> or kN/m<sup>2</sup> or kPa based on a wide-width tensile test (ASTM D 4885-01 Determining Performance Strength of Geomembranes by the Wide Width Strip Tensile Method).

The frictional shear force acting on the lower geomembrane surface, or  $F_2$ , is equal and opposite to the frictional shear force above the GCL surface, or  $F_3$ ; thus,

$$F_2 = N \tan \delta_2 = F_3 \quad \text{Eq. 12}$$

The frictional shear force acting on the lower GCL is given by

$$F_4 = N \tan \delta_4 \quad \text{Eq. 13}$$

where

$\delta_4$  = friction angle between the lower GCL surface and the subgrade soil

The difference between  $F_3$  and  $F_4$  determines the tensile force carried by the GCL. If negative, the GCL is not in tension. If positive, then the GCL is in tension and a factor of safety must be evaluated based on the wide width strength test (ASTM D 6768-04 Standard Test Method for Tensile Strength of Geosynthetic Clay Liners). The force difference must be carried by the geomembrane. The actual stress in the GCL is given by

$$\sigma_{\text{actual GCL}} = \left( \frac{F_3 - F_4}{t_{\text{GCL}}} \right) \quad \text{Eq. 14}$$

where

$\sigma_{\text{actual GCL}}$  = actual stress in GCL (lb<sub>f</sub>/ft<sup>2</sup> or kN/m<sup>2</sup>)

$t_{\text{geo}}$  = GCL thickness (ft or m)

The factor of safety for the GCL against failure is

$$FS_{\text{GCL}} = \frac{\sigma_{\text{yield}}}{\sigma_{\text{actual GCL}}} \quad \text{Eq. 15}$$

where

$\sigma_{\text{yield}}$  = allowable GCL stress at yield (lb<sub>f</sub>/ft<sup>2</sup> or kN/m<sup>2</sup>)

If  $\delta_2 = \delta_4$ , then  $F_4 = F_2 = F_3$ . If the lower frictional shear force exceeds the upper frictional shear force for a given interface, then the factor of safety is infinite and only a value of the upper frictional shear force will be mobilized at the upper surface of the next interface below. This procedure is repeated for multiple interfaces until the lower most interface is encountered, i.e. a

compacted subgrade or compacted clay. For compacted clay, special attention must be paid to its short-term friction angle *versus* its long-term friction angle with respect to the interface above. Compacted clay can consolidate with overburden stress and expel moisture, which can reduce the friction between it and the contact surface above, potentially placing the upper geosynthetic in tension.

### Design Example #1

Evaluate the maximum stresses, if any, in the landfill liner system described in Figure 1 consisting of a textured 60 mil HDPE/non-woven, needle-punched Bentomat<sup>®</sup> GCL/USCS SP compacted subgrade sequence. The following data may be assumed:

$$H = 10 \text{ ft (3.0 m)}$$

$$\beta = 18.43^\circ \text{ (3H:1V)}$$

$$\gamma_w = 60 \text{ lb}_f/\text{ft}^3 \text{ or (9.4 kN/m}^3\text{)}$$

$$\phi_w = 20^\circ$$

$$\delta_1 = 18^\circ$$

$$\delta_2 = 16^\circ$$

$$\delta_4 = 30^\circ$$

$$\sigma_{\text{allow geomembrane}} = 2100 \text{ lb}_f/\text{in}^2 \text{ (14,478 kN/m}^2\text{)}$$

$$T_{\text{GCL}} = 100 \text{ lb}_f/\text{in (17.5 kN/m)}$$

$$t_{\text{GCL}} = 0.25 \text{ in (6.4 mm)}$$

Solution:

The critical interface lies between the HDPE geomembrane and the GCL based on the magnitude of the respective friction angles. The following parameters are calculated:

$$W_w = 9.0 \times 10^3 \text{ lb}_f/\text{ft (131 kN/m)} \quad \text{Eq. 1}$$

$$K_o = 0.658 \quad \text{Eq. 3}$$

$$\sigma_v = 300 \text{ lb}_f/\text{ft}^2 \text{ (14.4 kN/m}^2\text{)} \quad \text{Eq. 4}$$

$$\sigma_h = 197 \text{ lb}_f/\text{ft}^2 \text{ (9.4 kN/m}^2\text{)} \quad \text{Eq. 2}$$

$$T_w = 718 \text{ lb}_f/\text{ft (10.5 kN/m)} \quad \text{Eq. 2}$$

$$W_{\text{net}} = 8282 \text{ lb}_f/\text{ft (120.9 kN/m)} \quad \text{Eq. 5}$$

$$N = 7857 \text{ lb}_f/\text{ft (114.7 kN/m}^2\text{)} \quad \text{Eq. 6}$$

$$F_1 = 2553 \text{ lb}_f/\text{ft (37.3 kN/m)} \quad \text{Eq. 8}$$

**APPLICATION FOR PERMIT  
DNCS ENVIRONMENTAL SOLUTIONS**

**VOLUME III: ENGINEERING DESIGN AND CALCULATIONS  
SECTION 7: TENSILE STRESS ANALYSIS**

**ATTACHMENT III.7.J  
GSE LINING TECHNOLOGY, INC.,  
*GSE HD TEXTURED PRODUCT DATA SHEET***



## *Appendix B - Minimum Testing Frequencies and Properties for GSE Geomembranes*

### MINIMUM PROPERTIES FOR GSE HD TEXTURED

TESTED PROPERTY	TEST METHOD	FREQUENCY	MINIMUM VALUE				
<b>Product Code</b>			HDT 030G000	HDT 040G000	HDT 060G000	HDT 080G000	HDT 100G000
Thickness, (minimum average) mil (mm)	ASTM D 5994	every roll	29 (0.73)	38 (0.96)	57 (1.45)	76 (1.93)	95 (2.41)
Lowest individual for 8 out of 10 values			27 (0.69)	36 (0.91)	54 (1.40)	72 (1.80)	90 (2.30)
Lowest individual for any of the 10 values			26 (0.66)	34 (0.86)	51 (1.30)	68 (1.73)	85 (2.16)
Density, g/cm <sup>3</sup>	ASTM D 1505	200,000 lb	0.94	0.94	0.94	0.94	0.94
Tensile Properties (each direction) <sup>(1)</sup>	ASTM D 6693, Type IV Dumbbell, 2 ipm  G.L. = 2.0 in (51 mm) G.L. = 1.3 in (33 mm)	20,000 lb	45 (8)	60 (11)	90 (16)	120(21)	150 (27)
Strength at Break, lb/in-width (N/mm)			63 (11)	84 (15)	126 (22)	168 (29)	210 (37)
Strength at Yield, lb/in-width (N/mm)			100	100	100	100	100
Elongation at Break, %			12	12	12	12	12
Elongation at Yield, %							
Tear Resistance, lb (N)	ASTM D 1004	45,000 lb	21 (93)	28 (125)	42 (187)	56 (249)	70 (311)
Puncture Resistance, lb (N)	ASTM D 4833	45,000 lb	45 (200)	60 (267)	90 (400)	120 (534)	150 (667)
Carbon Black Content, %	ASTM D 1603*/4218	20,000 lb	2.0	2.0	2.0	2.0	2.0
Carbon Black Dispersion	ASTM D 5596	45,000 lb	+Note 1	+Note 1	+Note 1	+Note 1	+Note 1
Asperity Height	GRI GM 12	second roll	+Note 2	+Note 2	+Note 2	+Note 2	+Note 2
Notched Constant Tensile Load <sup>(2)</sup> , hr	ASTM D 5397, Appendix	200,000 lb	300	300	300	300	300
REFERENCE PROPERTY	TEST METHOD	FREQUENCY	NOMINAL VALUE				
Oxidative Induction Time, min	ASTM D 3895, 200° C; O <sub>2</sub> , 1 atm	200,000 lb	>100	>100	>100	>100	>100
Roll Length <sup>(3)</sup> (approximate), ft (m)	Standard Textured		830 (253)	700 (213)	520 (158)	400 (122)	330 (101)
Roll Width <sup>(3)</sup> , ft (m)			22.5 (6.9)	22.5 (6.9)	22.5 (6.9)	22.5 (6.9)	22.5 (6.9)
Roll Area, ft <sup>2</sup> (m <sup>2</sup> )			18,674 (1,735)	15,750 (1,463)	11,700 (1,087)	9,000 (836)	7,425 (690)

**NOTES:**

- +Note 1: Dispersion only applies to near spherical agglomerates. 9 of 10 views shall be Category 1 or 2. No more than 1 view from Category 3.
- +Note 2: 10 mil average. 8 of 10 readings ≥ 7 mils. Lowest individual ≥ 5 mils.
- GSE HD Standard Textured is available in rolls weighing about 4,000 lb (1,800 kg).
- <sup>(1)</sup>The combination of stress concentrations due to coextrusion texture geometry and the small specimen size results in large variation of test results. Therefore, these tensile properties are minimum average values.
- <sup>(2)</sup>NCTL for HD Textured is conducted on representative smooth membrane samples.
- All GSE geomembranes have dimensional stability of ±2% when tested with ASTM D 1204 and LTb of <-77° C when tested with ASTM D 746.
- <sup>(3)</sup>Roll lengths and widths have a tolerance of ± 1%.
- \*Modified.

**APPLICATION FOR PERMIT  
DNCS ENVIRONMENTAL SOLUTIONS**

**VOLUME III: ENGINEERING DESIGN AND CALCULATIONS  
SECTION 8: EROSION CALCULATIONS**

**TABLE OF CONTENTS**

Section No.	Title	Page
1.0	INTRODUCTION .....	III.8-1
1.1	Description .....	III.8-1
2.0	DESIGN CRITERIA .....	III.8-1
3.0	RAINFALL EROSION LOSS CALCULATIONS .....	III.8-2
4.0	WIND EROSION LOSS CALCULATIONS .....	III.8-5

**LIST OF FIGURES**

Figure No.	Title	Page
III.8.1	DRAINAGE PLAN – LANDFILL COMPLETION .....	III.8-4
III.8.2	WIND ROSE.....	III.8-7

**LIST OF TABLES**

Table No.	Title	Page
III.8.1	RAINFALL EROSION LOSSES .....	III.8-3

**LIST OF ATTACHMENTS**

Attachment No.	Title
III.8.A	NORTH AMERICAN GREEN, INC. 2011. <i>EROSION CONTROL MATERIALS DESIGN SOFTWARE (ECMDS™), VERSION 5.0</i> . INDIANA: NORTH AMERICAN GREEN, INC.
III.8.B	NATURAL RESOURCES CONSERVATION SERVICE. 2002. <i>NATIONAL AGRONOMY MANUAL, 190-V-NAM, THIRD EDITION, OCTOBER 2002, EXHIBIT 502-2, WIND EROSION</i> . WASHINGTON, D.C.: UNITED STATES DEPARTMENT OF AGRICULTURE.
III.8.C	NATURAL RESOURCES CONSERVATION SERVICE. 1997. <i>APPENDIX 3: GLOSSARY OF SELECTED TERMS</i> . WASHINGTON, D.C.: UNITED STATES DEPARTMENT OF AGRICULTURE.
III.8.D	NATURAL RESOURCES CONSERVATION SERVICE. 1992. FIGURE 14 - ANNUAL “C” VALUES OF THE WIND EROSION EQUATION NEW MEXICO IN <i>AGRONOMY TECH NOTE 27, JUNE 22, 1992</i> . WASHINGTON, D.C.: UNITED STATES DEPARTMENT OF AGRICULTURE.

**APPLICATION FOR PERMIT  
DNCS ENVIRONMENTAL SOLUTIONS**

**VOLUME III: ENGINEERING DESIGN AND CALCULATIONS  
SECTION 8: EROSION CALCULATIONS**

- III.8.E                   NATURAL RESOURCES CONSERVATION SERVICE. 2002. FIGURE 7 - FLAT SMALL GRAIN EQUIVALENTS OF UNGRAZED BLUE GRAMA AND BUFFALOGRASS IN *NATIONAL AGRONOMY MANUAL*, 190-V-NAM, THIRD EDITION, OCTOBER 2002, PART 502, WIND EROSION. WASHINGTON, D.C.: UNITED STATES DEPARTMENT OF AGRICULTURE.
- III.8.F                   NATURAL RESOURCES CONSERVATION SERVICE. 1998. SUBPART G – EXHIBITS (C=150, I=134, K=1.0) IN *NATIONAL AGRONOMY MANUAL*, 190-V-NAM, THIRD EDITION, JANUARY 1998. WASHINGTON, D.C.: UNITED STATES DEPARTMENT OF AGRICULTURE.

**APPLICATION FOR PERMIT  
DNCS ENVIRONMENTAL SOLUTIONS**

**VOLUME III: ENGINEERING DESIGN AND CALCULATIONS  
SECTION 8: EROSION CALCULATIONS**

**1.0 INTRODUCTION**

DNCS Environmental Solutions (DNCS Facility) is a proposed Surface Waste Management Facility for oil field waste processing and disposal services. The proposed DNCS Facility is subject to regulation under the New Mexico Oil and Gas Rules, specifically 19.15.36 NMAC, administered by the Oil Conservation Division (OCD). The Facility has been designed in compliance with 19.15.36 NMAC, and will be constructed and operated in compliance with a Surface Waste Management Facility Permit issued by the OCD. The Facility is owned by, and will be constructed and operated by, DNCS Properties, LLC.

**1.1 Description**

The DNCS site is comprised of a 562-acre  $\pm$  tract of land located south of NM 529 in portions of Section 31, Township 17 South, Range 33 East; and in the northern half of Section 6, Township 18 South, Range 33 East, Lea County, NM. A portion of the 562-acre tract is a drainage feature that will be excluded from development. The drainage feature includes a 500-ft setback and totals 67 acres  $\pm$ . The DNCS Facility will include two main components; a liquid oil field waste Processing Area (177 acres  $\pm$ ), and an oil field waste Landfill (318 acres  $\pm$ ); therefore the DNCS Facility comprises 495 acres  $\pm$ . Oil field wastes are anticipated to be delivered to the DNCS Facility from oil and gas exploration and production operations in southeastern NM and west Texas. The Site Development Plan provided in the **Permit Plans, Sheet 3**, identifies the locations of the Processing Area and Landfill facilities.

**2.0 DESIGN CRITERIA**

The purpose of the Erosion Calculations is to determine potential soil losses due to wind and rainfall erosion for the DNCS Facility Landfill during operations and following final cap installation. Erosion calculations project that the soil loss from rainfall is approximately 4.96 tons per acre per year, which is below the established criterion of 5.0 tons/acre/year. The wind erosion loss from the site is estimated at 1.2 tons per acre per year, which is also below the

established criterion of 2.5 tons/acre/year. The total soil loss from the site potentially caused by water and wind erosion is calculated at 6.16 tons per acre per year.

The attached calculations were used to assess the potential for wind and rainfall erosion at the DNCS Facility. These conservative calculations were also used to determine if additional erosion control measures are required. Evaluation of erosion of the final cover surface was based on the following design criteria:

1. The New Mexico Energy, Minerals, and Natural Resources Department Oil and Gas Rules, 19.15.36 NMAC, Surface Waste Management Facilities Closure and Post-Closure Requirements. More specifically, 19.15.36.18.D.(2)(a) NMAC states:  
*“The operator shall properly close landfill cells, covering the cell with a top cover pursuant to Paragraph (8) of Subsection C of 19.15.36.14 NMAC, with soil contoured to promote drainage of precipitation; side slopes shall not exceed a 25 percent grade (four feet horizontal to one foot vertical), such that the final cover of the landfill’s top portion has a gradient of two percent to five percent, and the slopes are sufficient to prevent the ponding of water and erosion of the cover material.”*
2. The final cover crown of the landfill consists of a minimum 5% slope.
3. The sideslopes of the landfill consist of a 4H:1V slope with drainage benches.
4. The longevity of any temporary erosion protection shall be a minimum of 24 months for the 5% slope and 36 months for the 4H:1V slope.
5. The design erosion rate shall not exceed the 12-inch soil thickness of the landfill erosion/vegetative layer of the final cover.
6. The final cover has been conservatively assumed to have poor vegetation (50% coverage) established.
7. A soil loss tolerance target erosion rate is established at 5.0 tons/acre/year for rainfall erosion; and 2.5 tons/acre/year for wind erosion. The target values represent the erosion at which a management system is or is not sustainable. The target values are typical for non-farm application of erosion calculations (NRCS, 1962).
8. The Operations, Inspection, and Maintenance Plan (**Volume II.1**) provides routine corrective measures to address cover erosion when the site is under construction. The Closure/Post-closure Plan details specific plans to address potential erosion of the final cap.

### **3.0 RAINFALL EROSION LOSS CALCULATIONS**

North American Green, Inc. Slope Erosion Protection Module (**Attachment III.8.A**) was used to model the soil erosion rate from the DNCS Landfill final cover due to rainfall. The City of Alamogordo database was selected based on its similar climate to the DNCS site. This program uses the Revised Universal Soil Loss Equation (RUSLE). The equation is as follows:

$$A = R \times K \times LS \times C$$

Where:

**A** is the soil loss per unit area, typically in tons per acre per year.

**R** is the rainfall/runoff factor which varies with location and climate.

**K** is the soil erodibility factor, which depends on the soil type

**LS** is the topographic factor which accounts for the site slope gradient and slope length.

**C** is the cover factor that accounts for ground cover (bare slope=1).

NOTE: The Slope Erosion Protection Module calculates these factors based on the assumptions input.

The RUSLE was used to determine the loss of soil from each drainage area (**Figure III.8.1**) of the final cover. The values of final cover erosion and their sum are provided on **Table III.8.1**:

**TABLE III.8.1**  
**Rainfall Erosion Losses**  
**North American Green Output**  
**DNCS Environmental Solutions**

Area ID	Area (ac)	Slope Length (ft)	Average Slope (ft/ft)	Slope Gradient (H:1)	Average Soil Loss with Vegetation (in)	Tons/year with Vegetation
A	8.0	761	0.16	6.25	0.029	46.3
B	36.0	1462	0.11	9.1	0.025	165.3
C	104.0	1579	0.10	10	0.023	519.1
D	43.0	1072	0.13	7.7	0.027	231.8
E	39.0	1076	0.13	7.7	0.027	210.2
F	89.0	1645	0.10	10	0.023	408.7
<b>Sum</b>	<b>319.0</b>				<b>0.154</b>	<b>1,581.7</b>

**Conclusion:** When a 50% vegetative cover is considered, the soil loss is 4.96 tons per acre per year.



#### 4.0 WIND EROSION LOSS CALCULATIONS

##### **Purpose:**

To estimate the quantity of soil lost as a result of wind using the Wind Erosion Equation (WEQ).

Wind Erosion Equation:

$$E = f(I, K, C, L, V)$$

Where:

- E** = The potential average annual soil loss (tons per acre per year).
- I** = The soil erodibility index (tons per acre per year).
- K** = The ridge roughness factor (0.5-1.0).
- C** = The Climactic Factor.
- L** = The unsheltered distance along the prevailing wind erosion direction across the area to be evaluated.
- V** = Equivalent Vegetative Cover.

##### Find I:

The soil on-site primarily consists of silty sands of the soil type SM. The I value for silty sands is listed in **Attachment III.8.B** as 134 Tons/Acre/Year (T/A/Y).

$$I = 134$$

##### Find K:

The ridge roughness factor (K) is a measure of the effect from tilled ridges and planting implements. These reduce erosion by absorbing and deflecting wind energy and by trapping blown particles. No wind-breaking ridges are planned for the final cover, therefore a conservative K value of 1.0 has been chosen (**Attachment III.8.C, page 7 of 11**).

$$K = 1.0$$

##### Find C:

The Climactic Factor (C) is based on the average wind velocity and the precipitation – evaporation index (PE Index). The Isolinear map of New Mexico (**Attachment III.8.D**) was used to find the C – value of 150 for the site.

$$C = 150$$

Find L:

L represents the longest unsheltered distance along the prevailing wind direction for the area to be evaluated. The prevailing wind direction was determined using data obtained from the New Mexico Climate Center at Hobbs Lea County Airport, 29 miles east of the site. At the Hobbs Lea County Airport, the prevailing wind is from the south (see **Figure III.8.2, Wind Rose**). The maximum unsheltered distance across the site is from the north end of Unit 1 to the south end of Unit 9. The longest unsheltered distance is approximately 3,400 feet (ft), therefore:

$$L = 3,400 \text{ ft.}$$

Find V:

The equivalent vegetative cover is a value that relates the kind, amount, and orientation of vegetative material to its equivalent in pounds per acre of a small grain residue reference condition. This reference condition is defined as 10-inch long stalks of small grain lying flat in rows spaced 10-inches apart, perpendicular to the direction of the wind.

The vegetation plan for the landfill calls for the cover to be seeded per NRCS recommendations with blue and sideoats grama grasses, as well as dropseed varieties. This plan will yield between 1,500 and 2,000 pounds per acre of vegetative cover (assuming good germination and adequate precipitation). When this value is converted to the Blue Gamma equivalent (See **Attachment III.8.E**) it yields an equivalent vegetative factor of over 10,000 pounds per acre. The tables used to determine soil loss extend only to 3,000 pounds per acre (**Attachment III.8.F**). A highly conservative factor of 3,000 pounds per acre is therefore used for V.

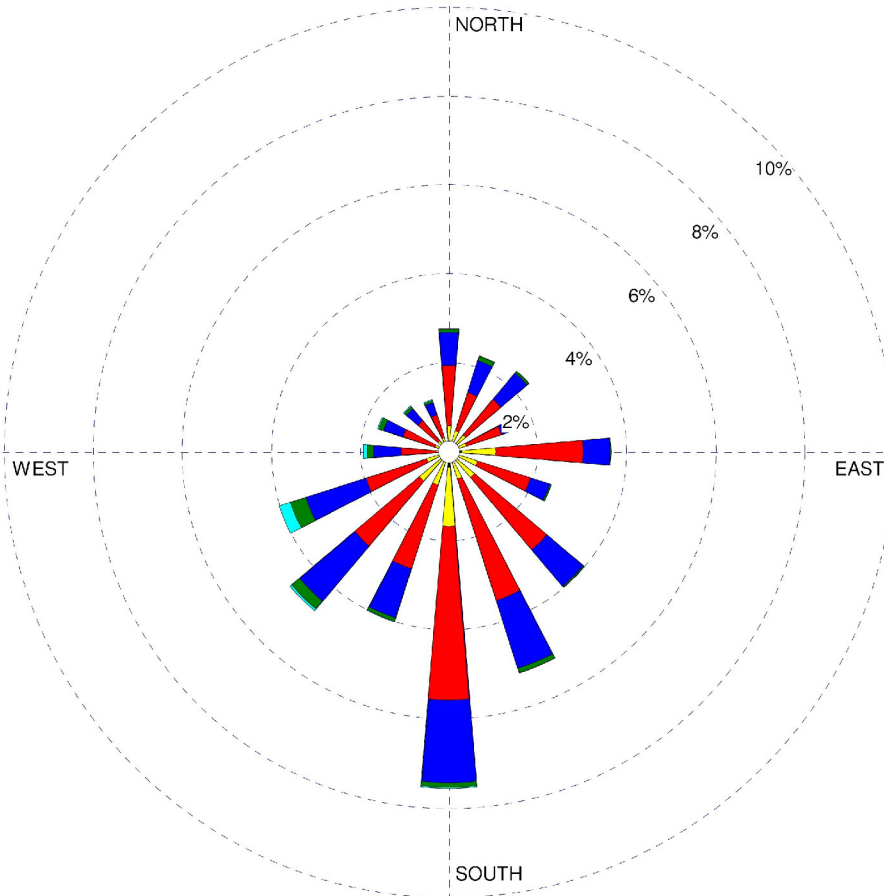
$$V = 3,000 \text{ pounds per acre.}$$

Solve for E:

Using the table in **Attachment III.8.F**, a value of E=1.2 tons per acre per year of soil loss due to wind erosion is expected. This value is less than the recommended maximum value of 2.5 tons per acre per year.

WIND ROSE PLOT:  
**Hobbs Lea County Airport**

DISPLAY:  
**Wind Speed  
 Direction (blowing from)**



DATA PERIOD: JAN 1, 2002–OCT 22, 2009  
 CALM WINDS: 49.41%  
 AVERAGE WIND SPEED: 5.05 KNOTS (1MPH = 0.86897 KNOTS)

## WIND ROSE

DNCS ENVIRONMENTAL SOLUTIONS  
 LEA COUNTY, NEW MEXICO



213 S. Camino del Pueblo  
 Bernalillo, New Mexico, USA  
 Phone: 505-867-6990  
 Fax: 505-867-6991

DATE: 11/04/13	CAD: WIND ROSE.dwg	PROJECT #: 542.01.01
DRAWN BY: MLH	REVIEWED BY: IKG	<b>FIGURE III.8.2</b>
APPROVED BY: IKG	gei@gordonenvironmental.com	

**APPLICATION FOR PERMIT  
DNCS ENVIRONMENTAL SOLUTIONS**

**VOLUME III: ENGINEERING DESIGN AND CALCULATIONS  
SECTION 8: EROSION CALCULATIONS**

**ATTACHMENT III.8.A**

**NORTH AMERICAN GREEN, INC. 2011.**

***EROSION CONTROL MATERIALS DESIGN SOFTWARE (ECMDS™), VERSION 5.0.***

**INDIANA: NORTH AMERICAN GREEN, INC.**



**NORTH  
AMERICAN  
GREEN®**

Tensar International Corporation  
5401 St. Wendel-Cynthiana Road  
Poseyville, Indiana 47633  
Tel. 800.772.2040  
Fax 812.867.0247  
www.nagreen.com

**Erosion Control Materials Design Software  
Version 5.0**

**Project Name: DNCS Environmental Solutions  
Project Number: 33989  
Project Location: Hobbs, New Mexico  
Slope Name: Area A**

Country	United States
State/Region	New Mexico
City	Alamogordo
Annual R Factor	20
Adjusted R Factor	60
Total Slope Length	761
Protection Type	Permanent
Protection Period	36
Beginning Month	January
Slope Gradient (H:1)	6.25
Soil Type	Sandy Loam
K Factor	0.190

**Reach 1**

Start: 0ft End: 761ft

Vegetation Type: Bunch Type(<=50%)

Material	ASL bare	ASL mat	MSL bare	MSL mat	Soil Loss Tolerance	SF	Remarks	Staple / App Rate
C350	0.822 in	0.029 in	1.376 in	0.048 in	0.25 in	5.19	STABLE	D
C350 Reinf. Veg	0.128 in	0.003 in	0.178 in	0.004 in	0.03 in	11.686	STABLE	D
P300	0.822 in	0.058 in	1.376 in	0.096 in	0.25 in	2.595	STABLE	D
P300 Reinf. Veg	0.128 in	0 in	0.178 in	0 in	0.03 in	99.9	STABLE	D
P550	0.822 in	0.028 in	1.376 in	0.047 in	0.25 in	5.265	STABLE	D
P550 Reinf. Veg	0.128 in	0 in	0.178 in	0 in	0.03 in	99.9	STABLE	D
SC250	0.822 in	0.037 in	1.376 in	0.063 in	0.25 in	3.992	STABLE	D
SC250 does not meet the longevity requirements you have specified.								
SC250 Reinf. Veg	0.128 in	0.004 in	0.178 in	0.005 in	0.03 in	7.79	STABLE	D



**NORTH  
AMERICAN  
GREEN®**

Tensar International Corporation  
5401 St. Wendel-Cynthiana Road  
Poseyville, Indiana 47633  
Tel. 800.772.2040  
Fax 812.867.0247  
www.nagreen.com

**Erosion Control Materials Design Software  
Version 5.0**

**Project Name: DNCS Environmental Solutions  
Project Number: 33989  
Project Location: Hobbs, New Mexico  
Slope Name: Area B**

Country	United States
State/Region	New Mexico
City	Alamogordo
Annual R Factor	20
Adjusted R Factor	60
Total Slope Length	1462
Protection Type	Permanent
Protection Period	36
Beginning Month	January
Slope Gradient (H:1)	9.1
Soil Type	Sandy Loam
K Factor	0.190

**Reach 1**

**Start: 0ft End: 1462ft**

**Vegetation Type: Bunch Type(<=50%)**

Material	ASL bare	ASL mat	MSL bare	MSL mat	Soil Loss Tolerance	SF	Remarks	Staple / App Rate
C350	0.727 in	0.025 in	1.189 in	0.042 in	0.25 in	6.008	STABLE	D
C350 Reinf. Veg	0.09 in	0.002 in	0.12 in	0.002 in	0.03 in	16.744	STABLE	D
P300	0.727 in	0.051 in	1.189 in	0.083 in	0.25 in	3.004	STABLE	D
P300 Reinf. Veg	0.09 in	0 in	0.12 in	0 in	0.03 in	99.9	STABLE	D
P550	0.727 in	0.025 in	1.189 in	0.041 in	0.25 in	6.095	STABLE	D
P550 Reinf. Veg	0.09 in	0 in	0.12 in	0 in	0.03 in	99.9	STABLE	D
SC250	0.727 in	0.033 in	1.189 in	0.054 in	0.25 in	4.621	STABLE	D
SC250 does not meet the longevity requirements you have specified.								
SC250 Reinf. Veg	0.09 in	0.003 in	0.12 in	0.004 in	0.03 in	11.163	STABLE	D



**NORTH  
AMERICAN  
GREEN®**

Tensar International Corporation  
5401 St. Wendel-Cynthiana Road  
Poseyville, Indiana 47633  
Tel. 800.772.2040  
Fax 812.867.0247  
www.nagreen.com

**Erosion Control Materials Design Software  
Version 5.0**

**Project Name: DNCS Environmental Solutions  
Project Number: 33989  
Project Location: Hobbs, New Mexico  
Slope Name: Area C**

Country	United States
State/Region	New Mexico
City	Alamogordo
Annual R Factor	20
Adjusted R Factor	60
Total Slope Length	1579
Protection Type	Permanent
Protection Period	36
Beginning Month	January
Slope Gradient (H:1)	10
Soil Type	Sandy Loam
K Factor	0.190

**Reach 1**

Start: 0ft End: 1579ft

Vegetation Type: Bunch Type(<=50%)

Material	ASL bare	ASL mat	MSL bare	MSL mat	Soil Loss Tolerance	SF	Remarks	Staple / App Rate
C350	0.648 in	0.023 in	1.053 in	0.037 in	0.25 in	6.785	STABLE	D
C350 Reinf. Veg	0.078 in	0.002 in	0.103 in	0.002 in	0.03 in	19.327	STABLE	D
P300	0.648 in	0.045 in	1.053 in	0.074 in	0.25 in	3.392	STABLE	D
P300 Reinf. Veg	0.078 in	0 in	0.103 in	0 in	0.03 in	99.9	STABLE	D
P550	0.648 in	0.022 in	1.053 in	0.036 in	0.25 in	6.883	STABLE	D
P550 Reinf. Veg	0.078 in	0 in	0.103 in	0 in	0.03 in	99.9	STABLE	D
SC250	0.648 in	0.029 in	1.053 in	0.048 in	0.25 in	5.219	STABLE	D
SC250 does not meet the longevity requirements you have specified.								
SC250 Reinf. Veg	0.078 in	0.002 in	0.103 in	0.003 in	0.03 in	12.885	STABLE	D



**NORTH  
AMERICAN  
GREEN®**

Tensar International Corporation  
5401 St. Wendel-Cynthiana Road  
Poseyville, Indiana 47633  
Tel. 800.772.2040  
Fax 812.867.0247  
www.nagreen.com

**Erosion Control Materials Design Software  
Version 5.0**

**Project Name: DNCS Environmental Solutions  
Project Number: 33989  
Project Location: Hobbs, New Mexico  
Slope Name: Area D**

Country	United States
State/Region	New Mexico
City	Alamogordo
Annual R Factor	20
Adjusted R Factor	60
Total Slope Length	1072
Protection Type	Permanent
Protection Period	36
Beginning Month	January
Slope Gradient (H:1)	7.7
Soil Type	Sandy Loam
K Factor	0.190

**Reach 1**

**Start: 0ft End: 1072ft**

**Vegetation Type: Bunch Type(<=50%)**

Material	ASL bare	ASL mat	MSL bare	MSL mat	Soil Loss Tolerance	SF	Remarks	Staple / App Rate
C350	0.771 in	0.027 in	1.274 in	0.045 in	0.25 in	5.605	STABLE	D
C350 Reinf. Veg	0.106 in	0.002 in	0.144 in	0.003 in	0.03 in	14.137	STABLE	D
P300	0.771 in	0.054 in	1.274 in	0.089 in	0.25 in	2.802	STABLE	D
P300 Reinf. Veg	0.106 in	0 in	0.144 in	0 in	0.03 in	99.9	STABLE	D
P550	0.771 in	0.027 in	1.274 in	0.044 in	0.25 in	5.686	STABLE	D
P550 Reinf. Veg	0.106 in	0 in	0.144 in	0 in	0.03 in	99.9	STABLE	D
SC250	0.771 in	0.035 in	1.274 in	0.058 in	0.25 in	4.311	STABLE	D
SC250 does not meet the longevity requirements you have specified.								
SC250 Reinf. Veg	0.106 in	0.003 in	0.144 in	0.004 in	0.03 in	9.425	STABLE	D



**NORTH  
AMERICAN  
GREEN®**

Tensar International Corporation  
5401 St. Wendel-Cynthiana Road  
Poseyville, Indiana 47633  
Tel. 800.772.2040  
Fax 812.867.0247  
www.nagreen.com

**Erosion Control Materials Design Software  
Version 5.0**

**Project Name: DNCS Environmental Solutions  
Project Number: 33989  
Project Location: Hobbs, New Mexico  
Slope Name: Area E**

Country	United States
State/Region	New Mexico
City	Alamogordo
Annual R Factor	20
Adjusted R Factor	60
Total Slope Length	1076
Protection Type	Permanent
Protection Period	36
Beginning Month	January
Slope Gradient (H:1)	7.7
Soil Type	Sandy Loam
K Factor	0.190

**Reach 1**

**Start: 0ft End: 1076ft**

**Vegetation Type: Bunch Type(<=50%)**

Material	ASL bare	ASL mat	MSL bare	MSL mat	Soil Loss Tolerance	SF	Remarks	Staple / App Rate
C350	0.773 in	0.027 in	1.278 in	0.045 in	0.25 in	5.59	STABLE	D
C350 Reinf. Veg	0.106 in	0.002 in	0.144 in	0.003 in	0.03 in	14.117	STABLE	D
P300	0.773 in	0.054 in	1.278 in	0.089 in	0.25 in	2.795	STABLE	D
P300 Reinf. Veg	0.106 in	0 in	0.144 in	0 in	0.03 in	99.9	STABLE	D
P550	0.773 in	0.027 in	1.278 in	0.044 in	0.25 in	5.671	STABLE	D
P550 Reinf. Veg	0.106 in	0 in	0.144 in	0 in	0.03 in	99.9	STABLE	D
SC250	0.773 in	0.035 in	1.278 in	0.058 in	0.25 in	4.3	STABLE	D
SC250 does not meet the longevity requirements you have specified.								
SC250 Reinf. Veg	0.106 in	0.003 in	0.144 in	0.004 in	0.03 in	9.411	STABLE	D



**NORTH  
AMERICAN  
GREEN®**

Tensar International Corporation  
5401 St. Wendel-Cynthiana Road  
Poseyville, Indiana 47633  
Tel. 800.772.2040  
Fax 812.867.0247  
www.nagreen.com

**Erosion Control Materials Design Software  
Version 5.0**

**Project Name: DNCS Environmental Solutions**  
**Project Number: 33989**  
**Project Location: Hobbs, New Mexico**  
**Slope Name: Area F**

Country	United States
State/Region	New Mexico
City	Alamogordo
Annual R Factor	20
Adjusted R Factor	60
Total Slope Length	1645
Protection Type	Permanent
Protection Period	36
Beginning Month	January
Slope Gradient (H:1)	10
Soil Type	Sandy Loam
K Factor	0.190

**Reach 1**

**Start: 0ft End: 1645ft**

**Vegetation Type: Bunch Type(<=50%)**

Material	ASL bare	ASL mat	MSL bare	MSL mat	Soil Loss Tolerance	SF	Remarks	Staple / App Rate
C350	0.666 in	0.023 in	1.083 in	0.038 in	0.25 in	6.598	STABLE	D
C350 Reinf. Veg	0.079 in	0.002 in	0.104 in	0.002 in	0.03 in	19.052	STABLE	D
P300	0.666 in	0.047 in	1.083 in	0.076 in	0.25 in	3.299	STABLE	D
P300 Reinf. Veg	0.079 in	0 in	0.104 in	0 in	0.03 in	99.9	STABLE	D
P550	0.666 in	0.023 in	1.083 in	0.037 in	0.25 in	6.694	STABLE	D
P550 Reinf. Veg	0.079 in	0 in	0.104 in	0 in	0.03 in	99.9	STABLE	D
SC250	0.666 in	0.03 in	1.083 in	0.049 in	0.25 in	5.075	STABLE	D
SC250 does not meet the longevity requirements you have specified.								
SC250 Reinf. Veg	0.079 in	0.002 in	0.104 in	0.003 in	0.03 in	12.702	STABLE	D

**Tensar**

**NORTH  
AMERICAN  
GREEN®**



**Erosion Control Materials Design Software**  
*ECMDS Version 5.0*

**Design Manual**  
**Erosion Control Materials Design Software**  
**(ECMDS®) Version 5.0**

© Copyright 2011 North American Green, Inc.

**Tensar International Corporation** | 5401 St. Wendel Cynthiana Road |  
Poseyville, Indiana 47633 | Tel. 800-772-2040 | Direct 812-867-6632 |  
[www.nagreen.com](http://www.nagreen.com)

Erosion Control Materials Design Software  
Version 5.0  
**Table of Contents**

- 1.0 Design Module Overview
  - 1.1 Slope Design Module
  - 1.2 Channel Design Module
  - 1.3 User Defined Channel Design Module
  - 1.4 Spillway Design Module
  - 1.5 Outlet Design Module
  - 1.6 Drop Structure Design Module
  - 1.7 Vegetation Selection Module
  
- 2.0 Design Module Methodology
  - 2.1 Slope Design Module
    - 2.1.1 Terminology and Definitions
    - 2.1.2 Slope Design Methodology
  - 2.2 Channel Design Module
    - 2.2.1 Terminology and Definitions
    - 2.2.2 Channel Design Methodology
    - 2.2.3 User-defined Channel Methodology
    - 2.2.4 Channel Methodology using Mattress products
  - 2.3 Spillway Design Module
    - 2.3.1 Terminology and Definitions
    - 2.3.2 Spillway Design Methodology
  - 2.4 Outlet Design Module
    - 2.4.1 Terminology and Definitions
    - 2.4.2 Outlet Design Methodology
  - 2.5 Drop Structure Module
    - 2.5.1 Terminology and Definitions
    - 2.5.2 Drop Structure Methodology
  - 2.6 Vegetation Selection Module
    - 2.6.1 Terminology and Definitions
  
- 3.0 Appendix
  - 3.1 Soil Textural Triangle
  - 3.2 C-Factors for Erosion Control Products
  - 3.3 Hydraulic Roughness Coefficients for Erosion Control Products
  - 3.4 Permissible Shear Stress of Vegetation – Based on Plant Height and Density
  - 3.5 Permissible Shear Stress of Unvegetated Erosion Control Products
  - 3.6 Permissible Shear Stress of Vegetated TRMs
  - 3.7 Permissible Shear Stress of Soils
  - 3.8 Mattress Unit Thickness Guidelines
  - 3.9 Hydraulic Roughness Coefficients for Pipe/ Culvert Outlet Types
  - 3.10 Mattress Rock Fill Densities
  
- 4.0 References

## 1.0 Design Module Overview

North American Green's Erosion Control Materials Design Software (ECMDS) 5.0 is designed to offer the most complete resource for analyzing erosion control products and their performance in specific project parameters. This section will give you a basis for the analytical ability of each design module. For specific design methodology reference section 2.0.

### 1.1 Slope Design Module

The Slope Design Module of ECMDS 5.0 provides recommendations in the selection of effective temporary and/or permanent erosion protection for a uniform slope face under rainfall induced sheet/rill flow conditions. The materials analysis and performance evaluation are conducted using equations and data from the USDA's Revised Universal Soil Loss Equation (RUSLE)<sup>13</sup> and the NCHRP Report 22<sup>4</sup>. The stability check for slope protection materials is based on the material's capability to provide the necessary degree of erosion protection against rainfall induced erosion for a specified time period. The effectiveness of North American Green erosion control products have been determined based on 3<sup>rd</sup> party research performed at Texas Transportation Institute, Purdue University, Utah State University, San Diego State University, and Texas Research International / Environmental.

### 1.2 Channel Design Module

The Channel Design Module provides recommendations for effective temporary and/or permanent erosion protection of swales and channels conveying intermittent concentrated uniform water flows. The channel lining analysis and performance evaluations are conducted using the maximum shear stress (tractive force) method as outlined in the Federal Highway Administrations' Hydraulic Engineering Circular #15<sup>1</sup> and the USDA's Agricultural Handbook #667<sup>20</sup>. The effectiveness of North American Green erosion control products have been determined based on 3<sup>rd</sup> party research performed at Colorado State University, Texas Transportation Institute, Utah State University, and Texas Research International / Environmental. The stability check for channel lining materials is based on the product's capability to effectively control soil loss on the channel surface under the calculated shear stresses for a specified flow period.

*This section should be used for channel designs when the known values include discharge (Q) and channel dimensions.*

### 1.3 User Defined Channel Design Module

The User Defined Channel Design Module provides recommendations for effective temporary and/or permanent erosion protection of swales and channels conveying intermittent concentrated uniform water flows. The channel lining analysis and performance evaluations are conducted using the maximum shear stress (tractive force) method as outlined in the Federal Highway Administrations' HEC #15<sup>1</sup> and the USDA's Agricultural Handbook #667<sup>20</sup>. The effectiveness of North American Green erosion control products have been determined based on 3<sup>rd</sup> party research performed at Colorado State University, Texas Transportation Institute, Utah State University, and Texas Research International / Environmental. The stability check for channel lining materials is based on the product's capability to effectively control soil loss on the channel surface under the calculated shear stresses for a specified flow period.

*This section varies from the Channel Design Module based on the input parameters and the method of calculating the manning's n.*

*This module should be used when the known input parameters are flow depth and velocity.*

#### **1.4 Spillway Design Module**

The Spillway Design Module provides recommendations for effective temporary and/or permanent erosion protection of spillways conveying intermittent uniform water flows. The spillway analysis and performance evaluations are conducted using the maximum shear stress and the manning's n equation. The stability check for spillway materials is based on the product's capability to effectively control soil loss on the spillway surface under the calculated shear stresses for a specified flow period.

#### **1.5 Outlet Design Module**

The Outlet Design Module provides recommendations for effective temporary and/or permanent erosion protection of pipe and culvert outlets conveying intermittent water flows. The outlet analysis and performance evaluations are conducted using the maximum shear stress and the manning's n equation, based on full or half flow conditions. The stability check for outlet materials is based on the product's capability to effectively control soil loss and scour at the outlet structure under the calculated shear stresses for a specified flow period. Protective dimensions for outlet erosion control products are based on standard pipe and scour apron designs relative to outlet sizing.

#### **1.6 Drop Structure Design Module**

The Drop Structure Design Module provides recommendations for effective temporary and/or permanent erosion protection in drop structures conveying intermittent water flows. The drop structure analysis and performance evaluations are conducted using the maximum shear stress and the manning's n equation, based on manning's equations, drop height and basin length. The stability check for drop structure materials is based on the product's capability to effectively control soil loss and scour at the drop structure under the calculated shear stresses for a specified flow period.

#### **1.7 Vegetation Selection Module**

The Vegetation Selection Module provides recommendations for suitable grasses and legumes species for erosion control for the continental U.S and parts of Canada. The recommendations are based on soil type, moisture regime, planned site maintenance, and regional location of the project site. Due to additional factors not considered in this module, this module only provides general recommendations for species types and monocultural seeding rates. A soil fertility test is recommended before selecting vegetation.

## 2.0 Design Module Methodology

### 2.1 Slope Design Module

#### 2.1.1 Terminology and Definitions

The Revised Universal Soil Loss Equation accounts for the primary factors affecting soil erosion by water and is used to predict soil loss within the Slope Design Module.

**RUSLE:** The Revised Universal Soil Loss Equation is a mathematical model used to describe soil erosion processes. The equation was developed by the USDA-NRCS Soil Conservation Service, and is the main methodology for predicting soil erosion from rainfall induced runoff.

The RUSLE uses the following factors to calculate the average soil loss from a slope:

**R factor:** The annual rainfall/runoff factor for a given location through a given time period

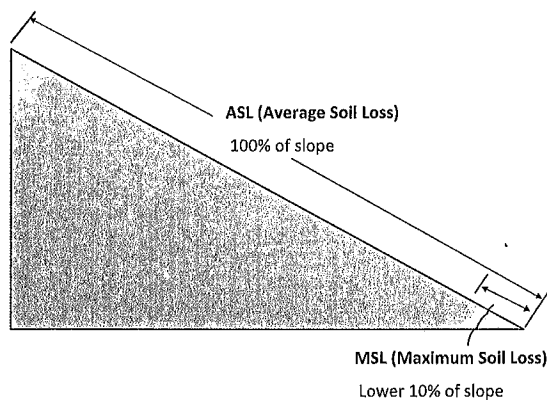
**K factor:** The slope erodibility factor. A value between 0 and 1 assigned to specific soil types.

**LS factor:** Slope length and gradient factor, a value affecting the erodibility of the slope face. Longer, steeper slopes are typically more erodible.

**C factor:** Cover factor, a value assigned to a particular type of erosion control cover based on the product's ability to provide cover and erosion protection.

**Average Soil Loss (A):** The resulting value from the RUSLE equation, calculated in uniform inches (cm) (depth of soil loss) for the slope.

In addition, the RUSLE equation can be used more specifically to evaluate the average soil loss or maximum soil loss from bare (unprotected slopes) or from protected slopes.



**ASL<sub>Bare</sub>:** The average soil loss (in or cm) from the bare unprotected slope.

**ASL<sub>Mat</sub>:** The average soil loss (in or cm) from a slope protected with a material

**MSL<sub>Bare</sub>:** the maximum soil loss (in or cm) from a bare unprotected slope, averaging the soil loss from the lower 10% of the slope.

**MSL<sub>Mat</sub>**: the maximum soil loss (in or cm) from a slope protected with a material, averaging the soil loss from the lower 10% of the slope.

Stability of a slope is determined by calculating a:

**Safety Factor (SF)**: A value assigned to determine the stability of slope with or without erosion protection. The safety factor is determined by comparing the Soil Loss Tolerance to the MSL<sub>Bare</sub> when looking at unprotected slopes, or the MSL<sub>Mat</sub> when analyzing protected slopes.

**Soil Loss Tolerance (SLT)**: The tolerable amount of soil that can be lost under specified time frames. ECMDS 5.0 will use an SLT of 0.25 inches for temporary protection, and an SLT of 0.03 inches for permanent protection. The 0.03 inch SLT is based on the USDA's tolerable average annual soil loss for many different soil types. These limits are based on the soil's capacity for regeneration.

### 2.1.2 Slope Design Methodology

The Slope Design Module is based on the methodology established by the USDA's RUSLE.

$$A = R \times K \times LS \times C \times 0.00595 \quad \text{where,}$$

0.00595 = conversion factor for soil loss rate from tons/acre to uniform inches

The RUSLE can also be used to solve for:

$$ASL_{Bare} = R \times K \times LS \times C \times 0.00595 \quad \text{where,}$$

C = 1.0, or an unprotected state

$$ASL_{Mat} = ASL_{Bare} \times C \quad \text{where,}$$

C = value assigned to a specific cover material, (See appendix 3.2)

$$MSL_{Bare} = ASL_{Bare} \times 1.7 \quad \text{where,}$$

1.7 = factor based on the erodibility of lower 10% of slope

$$MSL_{Mat} = MSL_{Bare} \times C \quad \text{where,}$$

C = value assigned to a specific cover material

Stability is determined from a Safety factor

$$SF = SLT / MSL_{Mat \text{ or } Bare}$$

If SF > 1.0 = Stable Design,  
If SF < 1.0 = Unstable Design

## 2.2 Channel Design Module

### 2.2.1 Terminology and Definitions

The Channel Design Module analysis is conducted using the maximum shear stress method outlined in the FHWA's HEC #15 Design for Roadside Channels with Flexible Liners and the USDA's Handbook #667.

**Shear Stress:** The amount of force developed along the interface of the flowing water and surface material in the direction of flow. Factors effecting shear stress include gravity, water flow along a material and roughness of lining material.

**Maximum Permissible Shear Stress:** The maximum force along the flowing water and surface material interface where any further increase in force will cause movement of lining material or allow more than the tolerable amount of soil loss.

Channel designs using the shear stress method are found to be more accurate than using simple velocity calculations.

**Velocity:** Rate of water flow typically expressed in feet per second, or the time rate of displacement of a fluid particle from one point to another.

To ultimately evaluate a channel liner's stability, a safety factor is calculated.

**Channel Liner:** A material used to line the channel and offer stabilization for the underlying soil. Channel liners are classified as rigid (such as concrete) or flexible (such as vegetation, erosion mattings, and rock).

**Manning's n:** A coefficient for the hydraulic roughness of the surface of a channel (or channel liner). The values for 'n' will vary with depth of water flowing in the channel.

**Safety Factor (SF):** A value assigned to determine the stability of a channel. The safety factor is determined by comparing the calculated shear stress in the channel to the maximum permissible shear stress of the channel lining material.

### 2.2.2 Channel Design Methodology

The Channel Design Module utilizes the manning's n equation and the given channel input parameters and discharge rates to back calculate the cross sectional area, wetted perimeter and the hydraulic radius of the channel. These values are then used in the Continuity Equation to calculate the channel velocity.

**Manning's n equation:**

$$\text{Flow (Q)} = \frac{1.486}{n} * A * R^{2/3} * S^{1/2} \text{ where,}$$

A = Cross-Sectional Area

R = Hydraulic Radius

S = Channel Slope or Energy Gradient (averaged under uniform flow conditions)  
n = hydraulic roughness coefficient of channel liner (See Appendix 3.3)

**The Cross sectional area (A):**

$$A = A_L + A_B + A_R \quad \text{where,}$$

$$\text{Area of Left (A}_L\text{)} = \frac{1}{2} * d^2 * Z_L \quad \text{where,}$$

d = depth of channel  
Z<sub>L</sub> = slope grade of left side slope

$$\text{Area of Base (A}_B\text{)} = W_B * d \quad \text{where,}$$

W<sub>B</sub> = Bottom width of channel

$$\text{Area of Right (A}_R\text{)} = \frac{1}{2} * d^2 * Z_R \quad \text{where,}$$

Z<sub>R</sub> = slope grade of right side slope

**Wetted Perimeter (P):**

$$P = P_L + P_B + P_R \quad \text{where,}$$

$$\text{Left Perimeter (P}_L\text{)} = d * (Z_L + 1)^{0.5}$$

$$\text{Base Perimeter (P}_B\text{)} = W_B$$

$$\text{Right Perimeter (P}_R\text{)} = d * (Z_R + 1)^{0.5}$$

**Hydraulic Radius (R):**

$$R = A / P$$

**Continuity Equation:**

$$\text{Velocity (V)} = Q / A$$

**Calculated Channel Shear Stress (T<sub>d</sub>):**

$$T_d = \gamma * d * S \quad \text{where,}$$

γ = unit weight of water or (62.4 lbs/ft<sup>3</sup>)

**Channel Liner Safety Factor (SF<sub>L</sub>):**

$$SF_L = T_p / T_d \quad \text{where,}$$

T<sub>p</sub> = Permissible shear of channel liner (see Appendix 3.4 , 3.5 or 3.6)

**Effective Shear Stress on Liner (T<sub>e</sub>):**

$$T_e = T_d * (1 - C_f) * (n_s / n)^2 \quad \text{where,}$$

C<sub>f</sub> = Cover factor of channel liner (see Appendix 3.2)

n<sub>s</sub> = hydraulic roughness of underlying soil (0.0156 for most soil types)

n = hydraulic roughness of channel liner (see Appendix 3.3)

**Soil Safety Factor (SF<sub>s</sub>):**

$$SF_s = T_a / T_e \quad \text{where,}$$

T<sub>a</sub> = Permissible shear of soil (see Appendix 3.7)

**Calculated Channel Shear Stress in Bend Areas (T<sub>db</sub>):**

$$T_{db} = K_b * T_d \quad \text{where,}$$

$$\text{Bend coefficient } (K_b) = R_c / W_B \quad \text{where,}$$

$$R_c = \text{Radius of bend curvature}$$

$$W_B = \text{Channel bottom width}$$

**Safety Factor of Channel Liner in Bend Area (SF<sub>LB</sub>):**

$$SF_{LB} = T_p / T_{db}$$

**Effective Shear Stress on Liner in Bend (T<sub>eb</sub>):**

$$T_{eb} = T_{db} * (1-C_f) * (n_s/n)^2$$

**Soil Safety Factor in Bend (SF<sub>sb</sub>):**

$$SF_{sb} = T_a / T_{eb}$$

2.2.3 User-defined Channel Methodology

The User-defined Channel Module, follows the same design methodology that is outlined for the Channel module in 2.2.2. The difference in this module is the starting point for input parameters. Where the channel module uses channel dimensions and discharge rate (Q), the User-defined module starts with the continuity equation with Velocity (V) and channel Depth (d) as the starting inputs.

2.2.4 Channel Methodology using Mattress products

Mattress selection is performed by following the basic channel design steps outlined in 2.2.2. These basic design steps cover the case of a straight channel section as well as a channel with a bend.

The roughness characteristics of mattresses are governed by the size of the stone in the mattress. Therefore, the manning's n should be determined using the D50 of the stone.

**Manning's roughness coefficient for Mattresses (n):**

$$n = \frac{\alpha_c d_a^{1/6}}{2.25 + 5.23 \log\left(\frac{d_a}{D_{50}}\right)} \quad \text{where,}$$

n = Manning's roughness coefficient, s/ft<sup>1/3</sup>

d<sub>a</sub> = Average flow depth in the channel, ft

D<sub>50</sub> = median diameter of stone infill, in

α<sub>c</sub> = Unit of conversion constant, 0.262

This equation is applicable for the range of conditions where 1.5 ≤ d<sub>a</sub> / D<sub>50</sub> ≤ 185. For small channel applications, flow depths should not exceed the upper end of the above range.

Channels that experience conditions below the lower end of the range where protrusions of individual stone elements can affect the roughness, the equation below is used.

$$n = \frac{\alpha d_a^{1/6}}{\sqrt{gf(Fr)f(REG)f(CG)}} \quad \text{where,}$$

$d_a$  = average flow depth of channel, ft

$g$  = acceleration due to gravity (3202 ft/s<sup>2</sup>)

$f(Fr)$  = relates to the Froude number, see equation below

$\alpha$  = unit conversion constant, 1.49

$f(REG)$  = function of roughness element geometry, see equation below

$f(CG)$  = function of channel geometry, see equation below

$$f(Fr) = \left( \frac{0.28Fr}{b} \right)^{\log(0.755/b)}$$

$$f(REG) = 13.434 \left( \frac{T}{D_{50}} \right)^{0.492} b^{1.025} \left( \frac{T}{D_{50}} \right)^{0.118}$$

$$f(CG) = \left( \frac{T}{d_a} \right)^{-b} \quad \text{where,}$$

$T$  = Top width of the channel

$b$  = parameter describing the effective roughness concentration, where

$$b = 1.14 \left( \frac{D_{50}}{T} \right)^{0.453} \left( \frac{d_a}{D_{50}} \right)^{0.814}$$

Analysis of the mattress follows the same shear stress calculations as presented in section 2.2.2. The mattress channel is analyzed with three calculations: the channel, the side slopes, and the bend.

The applicable shear stress is  $1.5 < Z < 5$  (lbs/ft<sup>2</sup>) and stability analysis is determined by

Section Safety Factor = Application Shear / Maximum Permissible Shear Stress.

#### **Mattress sizing:**

Mattress unit thickness: is a function of velocity and specified  $D_{50}$ , (see Appendix 3.8)

Maximum  $D_{50}$  = 1/3 the Unit thickness

Maximum Gradation Size = 1/2 the Unit thickness

**Total Project Stability:** The total project is considered stable when the Channel, Side Slopes, and Bend safety factors are all calculated to be below 1.5.

## 2.3 Spillway Design Module

### 2.3.1 Terminology and Definitions

**Spillway:** A structure used to provide for the controlled release of flows from a dam or levee into a downstream area. A spillway can be a controlled or uncontrolled spillway depending on the design of the water release.

For the purposes of this program's design module, the spillway is assumed to be wide, with negligible side slope gradients.

### 2.3.2 Spillway Design Methodology

The spillway design module calculates the flow depth based on the Manning's n equation.

**Manning's n equation:**

$$\text{Flow (Q)} = \frac{1.486}{n} * A * R^{2/3} * S^{1/2} \quad \text{where,}$$

A = Cross-Sectional Area

R = Hydraulic Radius

S = Channel Slope (averaged under uniform flow conditions)

n = hydraulic roughness of channel liner (see Appendix 3.3)

Since we assume a wide spillway, side slopes are negligible so we can calculate the **Cross-sectional area**,

$$A = D * W \quad \text{where,}$$

D = depth of water over spillway

W = width of spillway

**Hydraulic Radius (R):**

$$R = D * W / (W + 2D)$$

Therefore solve for depth (d),

$$d * \left( \frac{dW}{W + 2d} \right)^{2/3} = \frac{nQ}{1.486S^{1/2}}$$

## 2.4 Outlet Design Module

### 2.4.1 Terminology and Definitions

Culvert outlets are a point of critical erosion potential, due to the change in flow velocities from pipe to open channel areas. To prevent scour, a scour apron is often selected. Generally scour aprons should be used only when the outlet velocity is no more than 10% greater than the downstream velocity. When this requirement is not met, a series of drop structures may be required.

## 2.4.2 Outlet Design Methodology

The average outlet velocity on the scour apron is dependent on the flow transition at the end of the culvert. For circular pipes, the program uses flow depth at full or half capacity, and calculates the pipe area to achieve the outlet velocity.

### Flow Depth at Full Capacity ( $D_{Full}$ ):

$$D_{Full} = 1.335 * \left( \frac{nQ}{S^{0.5}} \right)^{3/8} \quad \text{where,}$$

$n$  = manning's value (hydraulic roughness) of the pipe, (see Appendix 3.9)

$Q$  = Discharge rate (cfs)

$S$  = Slope of the pipe (ft/ft)

### Flow Depth at Half Capacity ( $D_{Half}$ ):

$$D_{Half} = 1.731 * \left( \frac{nQ}{S^{0.5}} \right)^{3/8}$$

### Flow Area at Full Capacity ( $A_{Full}$ ):

$$A_{Full} = 0.07854 * D_{Full}^2$$

### Flow Area at Half Capacity ( $A_{Half}$ ):

$$A_{Half} = 0.07854 * D_{Half}^2$$

### Initial Velocity of Outlet ( $V$ ):

$$V = Q / A$$

### Estimated Outlet Shear Stress ( $T_d$ ):

$$T_d = Y * D * n \quad \text{where,}$$

$Y$  = Unit weight of water (62.4)

### Recommended Design Shear Stress ( $T_{dr}$ ):

$$T_{dr} = 2 * T_d$$

### Safety Factor of Outlet Scour Apron ( $SF_{apron}$ ):

$$SF_{apron} = T_p / T_{dr} \quad \text{where,}$$

$T_p$  = Permissible shear stress of scour apron system (see Appendix 3.5, 3.6)

### Transition Mat Protective Dimensions:

Minimum Transverse Dimension (ft) =  $4 * \text{Diameter}_{\text{pipe (in)}} / 12$

Minimum Longitudinal Dimension (ft) =  $5 * \text{Diameter}_{\text{pipe (in)}} / 12$

## 2.5 Drop Structure Module

### 2.5.1 Terminology and Definitions

**Drop Structure:** A structure designed to check channel erosion by controlling the effective gradient and to provide for abrupt changes in gradient by means of a vertical drop within the channel at intervals along the channel reach.

A drop structure effectively changes a steep bed slope into a series of gentle slopes and vertical drops. Instead of slowing down high velocity water, they are designed to prevent water from reaching erosive velocities.

**Vertical drop structure** is the most basic type and most often used in channel systems. This structure is characterized by flow through a rectangular weir followed by a drop into a stilling basin.

### 2.5.2 Drop Structure Methodology

To evaluate the stability of a mattress or scour apron in the drop structure, the program uses the Manning's n equation, by first determining the Manning's n value.

#### Determining the Manning's n:

##### Channel Top Width ( $W_t$ ):

$$W_t = W_B + (S_L * d) + (S_R * d) \quad \text{where,}$$

$W_B$  = bottom channel width

$S_L$  = Left Side Slope

$S_R$  = Right Side Slope

$d$  = channel depth

##### Average Depth ( $d_a$ ):

$$d_a = A / W_t \quad \text{where,}$$

$A$  = cross-sectional area

#### Manning's roughness coefficient for drop structures (n):

$$n = \frac{\alpha_c d_a^{1/6}}{2.25 + 5.23 \log\left(\frac{d_a}{D_{50}}\right)} \quad \text{where,}$$

$n$  = Manning's roughness coefficient, s/ft<sup>1/3</sup>

$d_a$  = Average flow depth in the channel

$D_{50}$  = median diameter of stone infill

$\alpha_c$  = Unit of conversion constant, 0.262

This equation is applicable for the range of conditions where  $1.5 \leq d_a / D_{50} \leq 185$ .

For small channel applications, flow depths should not exceed the upper end of the above range.

Channels that experience conditions below the lower end of the range where  $0.3 < d_a/D_{50} < 1.5$ , where protrusions of individual stone elements can effect the roughness, the equation below is used.

$$n = \frac{\alpha d_a^{1/6}}{\sqrt{gf(Fr)f(REG)f(CG)}} \quad \text{where,}$$

$d_a$  = average flow depth of channel

$g$  = acceleration due to gravity (32.2 ft/s<sup>2</sup>)

$f(Fr)$  = relates to the Froude number, see equation below

$\alpha$  = unit conversion constant, 1.49

$f(REG)$  = function of roughness element geometry, see equation below

$f(CG)$  = function of channel geometry, see equation below

$$f(Fr) = \left( \frac{0.28Fr}{b} \right)^{\log(0.755/b)}$$

$$f(REG) = 13.434 \left( \frac{T}{D_{50}} \right)^{0.492} b^{1.025} \left( \frac{T}{D_{50}} \right)^{0.118}$$

$$f(CG) = \left( \frac{T}{d_a} \right)^{-b} \quad \text{where,}$$

$T$  = Top width of the channel

$b$  = parameter describing the effective roughness concentration, where

$$b = 1.14 \left( \frac{D_{50}}{T} \right)^{0.453} \left( \frac{d_a}{D_{50}} \right)^{0.814}$$

#### The Cross sectional area (A):

$$A = A_L + A_B + A_R \quad \text{where,}$$

$$\text{Area of Left (A}_L\text{)} = \frac{1}{2} * d^2 * Z_L \quad \text{where,}$$

$d$  = depth of channel

$Z_L$  = slope grade of left side slope

$$\text{Area of Base (A}_B\text{)} = W_B * d \quad \text{where,}$$

$W_B$  = Bottom width of channel

$$\text{Area of Right (A}_R\text{)} = \frac{1}{2} * d^2 * Z_R \quad \text{where,}$$

$Z_R$  = slope grade of right side slope

**Wetted Perimeter (P):**

$P = P_L + P_B + P_R$  where,

Left Perimeter ( $P_L$ ) =  $d * (Z_L + 1)^{0.5}$

Base Perimeter ( $P_B$ ) =  $W_B$

Right Perimeter ( $P_R$ ) =  $d * (Z_R + 1)^{0.5}$

**Hydraulic Radius (R):**

$R = A / P$

**Continuity Equation:**

Velocity ( $V$ ) =  $Q / A$

**Critical Depth ( $y_c$ ):**

$$y_c = \left( \frac{\left( \frac{Q_{des}}{B} \right)^2}{g} \right)^{1/3}$$
 where,

$Q_{des}$  = design discharge ( $ft^3/s$ )

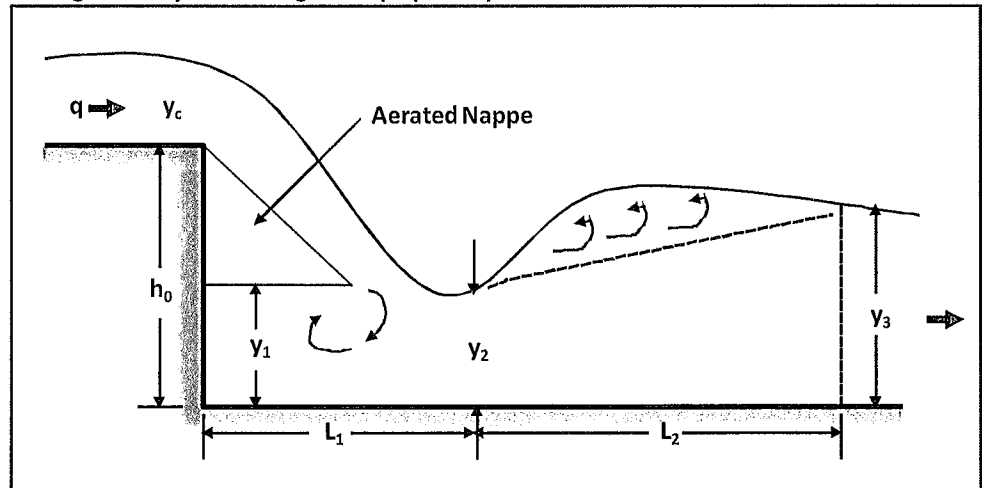
$B$  = Upstream channel width

$g$  = acceleration due to gravity ( $32.2 ft/s^2$ )

**Drop Structure Design Outputs:**

The drop structure design used in this program is based on an aerated nappe and subcritical flow in the upstream as well as downstream channel. This assumption has been made in order to represent the greatest flow conditions in order to properly size the drop geometry. The stilling basin protects the channel against erosion below the drop and dissipates energy. This is accomplished through the impact of the falling water on the floor, redirection of the flow, and turbulence.

**Flow geometry of a straight drop spillway**



**Tailwater Depth ( $y_3$ ):**

Since the tailwater must maintain the proper height within the basin, the required depth above the floor is calculated as follows:

$$y_3 = 2.15 * y_c$$

The tailwater needs to be a distance below the crest to maintain an aerated nappe. Using the crest as a reference point, this distance is calculated as:

$$h_2 = - (h - y_0) \quad \text{where,}$$

$h_2$  = vertical distance of the tailwater below the crest, ft

$h$  = vertical drop between the approach and tailwater channels, ft

$y_0$  = normal depth in the tailwater channel, ft

**Total drop ( $h_0$ ) :**

To achieve sufficient tailwater and adequate drop from the crest to tailwater, it is sometimes necessary to depress the flow below the elevation of the downstream channel. The total drop from the crest to the stilling basin floor is:

$$h_0 = h_2 - y_3$$

If  $h_0 >$  than  $h$ , then depress the basin floor by the difference of Delta:

$$\Delta = h + h_0$$

**Drop Number ( $N_d$ ):**

$$N_d = \frac{q^2}{gh_0^3} \quad \text{where,}$$

$q$  = unit discharge ( $\text{ft}^2/\text{s}$ )

Drops for which  $N_d$  is greater than 1 are considered "low drop" structures. Only low drop structures should be designed with mattresses.

For a given drop height ( $h_0$ ) and discharge ( $q$ ) the subsequent depth ( $y_3$ ) in the downstream channel and the drop length ( $L_1$ ) may be computed.

$$L_1 = 4.30 h_0 N_d^{0.27}$$

$$L_2 = 6.9 (y_3 - y_2)$$

$$y_1 = 1.0 h_0 N_d^{0.22}$$

$$y_2 = 0.54 h_0 N_d^{0.425}$$

$$y_3 = 1.66 h_0 N_d^{0.27} \quad \text{where,}$$

$L_1$  = drop length, the distance from the drop wall to the position of the  $y_2$ , ft

$L_2$  = hydraulic jump length for mattress, ft  
 $y_1$  = pool depth under the nappe, ft  
 $y_2$  = depth of flow at the toe of the nappe or the beginning of the hydraulic jump, ft  
 $y_3$  = tailwater depth sequent to the  $y_2$ , ft

## 2.6 Vegetation Selection Module

### 2.6.1 Terminology and Definitions

The Vegetation Selection Module uses several project site parameters to evaluate and assign appropriate grass and legume species for the site from a database. The following parameters will determine the resulting vegetation.

**Soil Type:** Refers to the classification of soil by its predominate texture. Refer to the Soil Texture chart in Appendix 3.1.

**Moisture Regime:** the determination of the general moisture content of the soil on site. Moisture regime in the ECMD5 5.0 is defined as:

**Wet:** Typical of wetlands and pond shorelines, low gradient channels with poorly drained soils and or areas with common high water table.

**Normal:** Site with adequate but not excessive drainage, not subject to a high water table

**Dry:** Typical of elevated, excessively drained sites with light, course textured soils as well as arid climates.

**Vegetation Maintenance:** the long-term expected maintenance planned for the site in reference to activities such as (mowing, fertilization, irrigation, etc.). Maintenance regimes are defined in this program as:

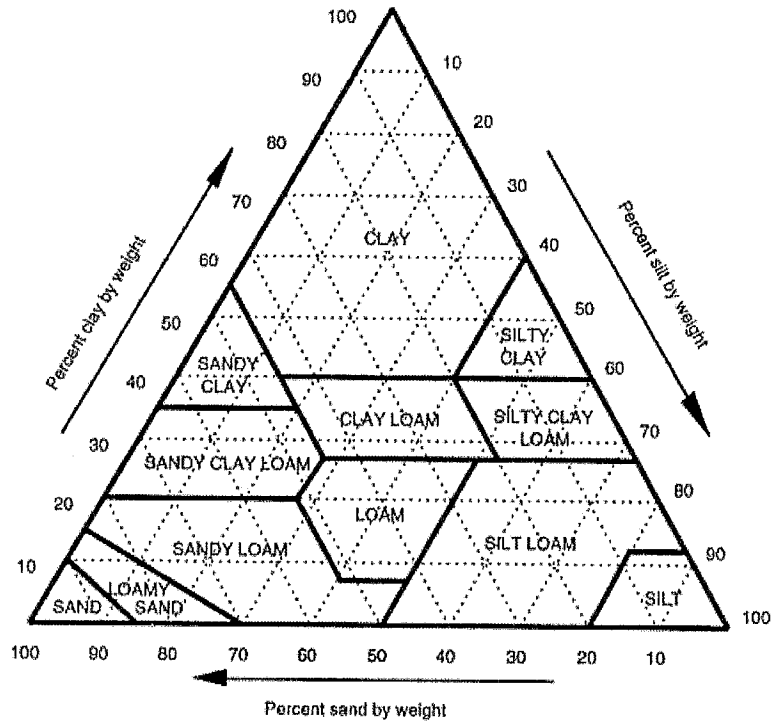
**Low - Medium:** Typical of roadsides, mine reclamation and other large areas where vegetation is considered more functional than aesthetic. Site often receives little to no supplemental fertilization or irrigation.

**Medium - High:** Typical for areas bordering or functioning as residential lawns and recreational turf. Site often requires a high degree of aesthetics necessitating increased mowing, fertilization, and irrigation.

**Project Location:** determine the adaptation zone the project site is located in using the Vegetal Adaptation Zone Map. The zones 1-8 are areas of known vegetation adaptation to regional climates and biological associations.

### 3.0 Appendix

#### 3.1 Soil Texture Triangle



#### 3.2 C-Factors for Erosion Control Products

		Slope Length and Gradient								
		Length ≤ 20 ft.			Length 20 - 50 ft.			Length ≥ 50 ft.		
		≤ 3:1	3:1 – 2:1	≥ 2:1	≤ 3:1	3:1 – 2:1	≥ 2:1	≤ 3:1	3:1 – 2:1	≥ 2:1
Unvegetated Rolled Erosion Control Products	DS75	0.029	0.11	0.23	0.11	0.21	0.45	0.19	0.30	0.66
	S75	0.029	0.11	0.23	0.11	0.21	0.45	0.19	0.30	0.66
	S75BN	0.029	0.11	0.23	0.11	0.21	0.45	0.19	0.30	0.66
	DS150	0.004	0.106	0.13	0.062	0.118	0.17	0.12	0.18	0.22
	S150	0.004	0.106	0.13	0.062	0.118	0.17	0.12	0.18	0.22
	S150BN	.00014	0.039	0.086	0.010	0.07	0.118	0.02	0.10	0.15
	SC150	0.001	0.048	0.10	0.051	0.079	0.145	0.10	0.11	0.19
	SC150BN	.00009	0.029	0.063	0.005	0.055	0.092	0.01	0.08	0.12
	C125	0.001	0.029	0.082	0.036	0.060	0.096	0.07	0.09	0.11
	C125BN	.00009	0.018	0.05	0.003	0.04	0.06	0.007	0.07	0.07
	P300	0.001	0.029	0.082	0.036	0.06	0.096	0.07	0.09	0.11
	SC250	0.001	0.021	0.051	0.023	0.039	0.068	0.0455	0.0555	0.0810
	C350	0.0005	0.015	0.043	0.018	0.031	0.050	0.035	0.047	0.057
	P550	.00045	0.0145	0.0425	0.0173	0.0305	.0495	0.0345	0.0465	0.0565
Hydraulic Erosion Control Products	HydraCX <sup>2</sup>	0.001	0.001	0.01	0.001	0.001	0.02	0.003	0.01	0.02
	HydraCM	0.003	0.003	0.03	0.003	0.003	0.04	0.006	0.06	0.12
	GeoSkinXT	0.04	0.06	0.2	0.1	0.15	0.25	0.2	0.35	0.75
	GeoSkin	0.08	0.12	0.4	0.25	0.5	0.75	0.65	0.85	1.0

### 3.3 Hydraulic Roughness Coefficient for Erosion Control Products

		Manning's n for Flow Depth ft (m)		
		≤ 0.50 (0.15)	0.50 – 2.00 (0.15-0.60)	≥ 2.00 (0.60)
Unvegetated Rolled Erosion Control Products	DS75	0.055	0.055 – 0.021	0.021
	S75	0.055	0.055 – 0.021	0.021
	S75BN	0.055	0.055 – 0.021	0.021
	DS150	0.055	0.055 – 0.021	0.021
	S150	0.055	0.055 – 0.021	0.021
	S150BN	0.055	0.055 – 0.021	0.021
	SC150	0.050	0.050 – 0.018	0.018
	SC150BN	0.050	0.050 – 0.018	0.018
	C125	0.022	0.022 – 0.014	0.014
	C125BN	0.022	0.022 – 0.014	0.014
	P300	0.034	0.034 – 0.020	0.020
	SC250	0.040	0.040 – 0.011	0.011
	C350	0.041	0.041 – 0.012	0.012
	P550	0.041	0.041 – 0.013	0.013
	ShoreMax w/ TRM	0.040	0.040 – 0.026	0.026
	Rock Riprap	0.032 – 0.010		
	Concrete	0.013 – 0.03		

### 3.4 Permissible Shear Stress of Vegetation – Based on Plant Height and Density

		Maximum Permissible Shear lbs/ft <sup>2</sup> (Pa)	
		Short Duration (≤ 2 hours peak flow)	Long Duration (> 2 hours peak flow)
FHWA HEC 15	Class A	3.70 (177)	3.70 (177)
	Class B	2.10 (100)	2.10 (100)
	Class C	1.00 (48)	1.00 (48)
	Class D	0.60 (29)	0.60 (29)
	Class E	0.35 (17)	0.35 (17)
USDA AG Hbk 667	Class A	7.50 (359)	7.50 (359)
	Class B	5.73 (274)	5.73 (274)
	Class C	4.20 (201)	4.20 (201)
	Class D	3.33 (159)	3.33 (159)
	Class E	2.16 (103)	2.16 (103)

### 3.5 Permissible Shear Stress of Unvegetated Erosion Control Products

		Maximum Permissible Shear lbs/ft <sup>2</sup> (Pa)	
		Short Duration (≤ 2 hours peak flow)	Long Duration (> 2 hours peak flow)
Unvegetated Rolled Erosion Control Products	DS75	1.55 (74)	1.55 (74)
	S75	1.55 (74)	1.55 (74)
	S75BN	1.60 (76)	1.60 (76)
	DS150	1.75 (84)	1.75 (84)
	S150	1.75 (84)	1.75 (84)
	S150BN	1.85 (88)	1.85 (88)
	SC150	2.00 (96)	2.00 (96)
	SC150BN	2.10 (100)	2.10 (100)
	C125	2.25 (108)	2.25 (108)
	C125BN	2.35 (112)	2.35 (112)
	P300	3.00 (144)	2.00 (96)
	SC250	3.00 (144)	2.50 (120)
	C350	3.20 (153)	3.00 (144)
	P550	4.00 (191)	3.25 (156)
	ShoreMax w/ SC250	7.50 (359)	7.50 (359)
	ShoreMax w/ C350	8.00(383)	8.00(383)
ShoreMax w/ P550	8.50 (407)	8.50 (407)	

### 3.6 Permissible Shear Stress of Vegetated TRMs

			Maximum Permissible Shear lbs/ft <sup>2</sup> (Pa)		
			Partially Vegetated	Fully Vegetated	
				Short Duration (≤ 2 hours peak flow)	Long Duration (> 2 hours peak flow)
Vegetated Rolled Erosion Control Products	P300	Class A	8.0 (383)	8.0 (383)	8.0 (383)
		Class B	8.0 (383)	8.0 (383)	8.0 (383)
		Class C	8.0 (383)	8.0 (383)	8.0 (383)
		Class D	7.0 (335)	7.0 (335)	7.0 (335)
		Class E	6.0 (287)	6.0 (287)	6.0 (287)
	SC250	Class A	8.0 (383)	10.0 (480)	8.0 (383)
		Class B	8.0 (383)	10.0 (480)	8.0 (383)
		Class C	8.0 (383)	10.0 (480)	8.0 (383)
		Class D	7.0 (335)	9.0 (430)	7.0 (335)
		Class E	6.0 (287)	8.0 (383)	6.0 (287)
	C350	Class A	10.0 (480)	12.0 (576)	10.0 (480)
		Class B	10.0 (480)	12.0 (576)	10.0 (480)
		Class C	10.0 (480)	12.0 (576)	10.0 (480)
		Class D	9.0 (430)	11.0 (335)	9.0 (430)
		Class E	8.0 (383)	10.0 (480)	8.0 (383)
	P550	Class A	12.0 (576)	14.0 (672)	12.0 (576)
		Class B	12.0 (576)	14.0 (672)	12.0 (576)
		Class C	12.0 (576)	14.0 (672)	12.0 (576)
		Class D	11.0 (335)	13.0 (622)	11.0 (335)
		Class E	10.0 (480)	12.0 (576)	10.0 (480)
ShoreMax w/ SC250 (Class A-E)		10.0 (480)	10.0 (480)	10.0 (480)	
ShoreMax w/ C350 (Class A-E)		12.0 (576)	12.0 (576)	12.0 (576)	
ShoreMax w/ P550 (Class A-E)		14.0 (672)	14.0 (672)	14.0 (672)	
Rock Rip Rap		NA	4 x D <sub>50</sub>		
Concrete		NA	~ 100 (4780)		

### 3.7 Permissible Shear Stress of Soils

		Maximum Permissible Shear lbs/ft <sup>2</sup> (Pa)	
		Partially Vegetated	Fully Vegetated
Soil Classifications (USDA)	Fine Sand	0.02 (0.96)	0.02 (0.96)
	Sand	0.02 (0.96)	0.02 (0.96)
	Sandy Loam	0.035 (1.7)	0.035 (1.7)
	Silt Loam	0.035 (1.7)	0.035 (1.7)
	Loam	0.035 (1.7)	0.035 (1.7)
	Clay Loam	0.05 (2.4)	0.05 (2.4)
	Clay	0.07 (3.3)	0.07 (3.3)

### 3.8 Mattress Unit Thickness

Type	Thickness (in)	Filling Stone Size Range (diameter, in)	D <sub>50</sub> (in)	Design Velocities (ft/s)
Mattress	6	3-5	4	9
	9	3-5	4	12
Gabion	12	4-8	6	15
	18	4-8	6	19

### 3.9 Hydraulic Roughness Coefficients for Pipe/Culvert Outlet Types

Type	Manning's n
Concrete or Asbestos-Cement Pipe	0.013
Plastic Pipe - Smooth	0.013
Plastic Pipe - Corrugated	0.024
12" Corrugated Metal Pipe	0.013
15" Corrugated Metal Pipe	0.014
18" Corrugated Metal Pipe	0.015
21" Corrugated Metal Pipe	0.016
24" Corrugated Metal Pipe	0.017
27" Corrugated Metal Pipe	0.018
30" Corrugated Metal Pipe	0.019
33" Corrugated Metal Pipe	0.02
36" Corrugated Metal Pipe	0.021
42" Corrugated Metal Pipe	0.022
48" Corrugated Metal Pipe	0.023
> 48" Corrugate Metal Pipe	0.0255
Black Wrought Iron	0.014
Galvanized Wrought Iron	0.016
Coated Cast Iron	0.013
Uncoated Cast Iron	0.014

### 3.10 Mattress Rock Fill Densities

Type	V <sub>stone</sub> (lbs/ft <sup>3</sup> )
Basalt	185
Granite	165
Hard Limestone	165
Trachytes	159
Sandstone	146
Soft Limestone	140
Crushed Concrete	150

#### 4.0 References

1. Chen, G.Y. and g. Cotton. 1988. Design of Roadside Channels with Flexible Linings. Federal Highway Administration Hydraulic Engineering Circular #15, Simons, Li and Associates.
2. Fifield, J.S., et. al., "Field Testing Erosion Control Products to Control Sediment and to Establish Dryland Grasses under Arid conditions". 1987. HydroDynamics Corp., Parker CO.
3. Foster, G. R., D.K. McCool, K.G. Renard, and W.C. Moldenhauer. 1981. Conversion of the Universal Soil Loss Equation to SI metric Units. Journal of Soil and Water Conservation.
4. Israelsen, C.E. et. al., 1980. National Cooperative Highway Research Program Report 221, "Erosion Control during Highway Construction", Utah State University, Logan, Utah.
5. Lipscomb, C.M., C.I. Thornton, D.E. Buchwald. 2002. "Hydraulic Testing of SC250 and P550 Vegetated with Kentucky Bluegrass. Colorado State University for North American Green. Fort Collins, Colorado.
6. Lipscomb, C.M., C.I. Thornton, B.A. Smith, M.D. Robeson. 2001. "Turf Reinforcement Mattress Performance Testing Phase I, Phase II, and Phase III Data Report", Colorado State University for North American Green, Fort Collins, Colorado.
7. North American Green, Inc. 1986. "A Comparative Study of Erosion Control Materials," North American Green, Purdue University.
8. North American Green, Inc. 1994. "Comparative Testing of S75, C125, C350, and P300 Erosion Control Blankets Under Simulated Rain", Utah State Water Research Laboratory, Logan, Utah.
9. North American Green, Inc. 1993. "Evaluation of Selected Erosion Control Products Using Three Different Slopes and Various Rates of Simulated Rainfall", Utah State Water Research Laboratory, Logan, Utah.
10. North American Green, Inc. 1994. "High Velocity Flow Tests of C350 and P300 Reinforced Sod", Utah State Water Research Laboratory. Logan, Utah.
11. North American Green, Inc. 1993. "High Velocity Flow Test of Two Root-Reinforcing Materials under Bare and Sodded Conditions". Utah State Water Research Laboratory. Logan, Utah.
12. Northcutt, P. and J. McFalls. 1991-2010. Texas Department of Transportation and Texas Transportation Institute Field Testing Program for Slope Erosion Control Products, Texas A&M University, College Station, TX.
13. Renard, K.G., G.R. Foster, G.A. Weesies, D.K. McCool, and D.C. Yoder. 1997. Predicting Soil Erosion by Water: A Guide to Conservation Planning with the Revised Universal Soil Loss Equation (RUSLE). USDA-ARS, Agricultural Handbook No. 703.
14. Rosewell, Colin J. and the Department of Conservation and Land Management, Soil Conservation Service. 1993. Technical Handbook No. 11, 2<sup>nd</sup> Edition, SOILOSS Version 5.1: A program to assist in the selection of management practices to reduce erosion.

15. Sanders, T.G., Abt. And P. Clopper. 1989. A Quantitative Test of Erosion Control Materials. Colorado State University and North American Green, Colorado State Engineering Research Laboratory, Fort Collins, Colorado.
16. Sprague, C.J. et. al. 2010. "GeoSkin, Hydraulic Mulch over Sandy Loam", AASHTO's National Transportation Product Evaluation Program. TRI/Environmental. Austin, TX.
17. Sprague, C.J. et. al. 2010. "HydraCM over Sandy Loam", AASHTO's National Transportation Product Evaluation Program. TRI/Environmental. Austin, TX.
18. Sprague, C.J. et. al. 2010. "HydraCX2 over Sandy Loam", AASHTO's National Transportation Product Evaluation Program. TRI/Environmental. Austin, TX.
19. Sprague, C.J. et. al. 2010. "North American Green's ShoreMax Mats over P550-TRM over Sandy Loam", AASHTO's National Transportation Product Evaluation Program. TRI/Environmental. Austin, TX.
20. Temple, D., et. al. 1987. "Stability Design of Grass-Lined Channels", Agricultural Handbook No. 667, United States Department of Agriculture, Agricultural Research Service.
21. Thornton, C.I., A.L. Cox, M.D. Turner. 2009. "Hydraulic Testing and Data Report for Six-Inch Triton Filter Mattress", Colorado State University for Tensar International Corporation, Fort Collins, Colorado.
22. Toy, T.J., G.R. Foster, and J.R. Galetovic. 1998. Guidelines for the Use of the Revised Universal Soil Loss Equation (RUSLE) Version 1.06 on Mined Lands, Construction Sites, and Reclaimed Lands. Office of Technology Transfer – Office of Surface Mining and Reclamation (OSM), Western Region Coordination Center.
23. Wall, G.J., D.R. Coote, E.A. Pringle, and I.J. Shelton (editors). 1997. RUSLEFAC: Revised Universal Soil Loss Equation for Application in Canada. A handbook for Estimating Soil Loss from Water Erosion in Canada.
24. Wayne, M.H., S.L. Dunlap (editor). 2009. "Design, Installation, and Maintenance Manual for Gabion Structures", Version 1.2, Harris County Flood Control District, Houston, Texas.
25. Wischmeier, W.H. and D.D. Smith. 1978. Predicting rainfall erosion losses: A guide to conservation planning. U.S. Department of Agriculture. Agriculture Handbook No. 537.

**APPLICATION FOR PERMIT  
DNCS ENVIRONMENTAL SOLUTIONS**

**VOLUME III: ENGINEERING DESIGN AND CALCULATIONS  
SECTION 8: EROSION CALCULATIONS**

**ATTACHMENT III.8.B**

**NATURAL RESOURCES CONSERVATION SERVICE. 2002.  
*NATIONAL AGRONOMY MANUAL*, 190-V-NAM, THIRD EDITION,  
OCTOBER 2002, EXHIBIT 502-2, WIND EROSION. WASHINGTON, D.C.:  
UNITED STATES DEPARTMENT OF AGRICULTURE.**

## Exhibit 502-2

# Wind erodibility groups and wind erodibility index

Soil texture <sup>1</sup>	EWE texture wetness factor <sup>2</sup>	Predominant soil texture class of surface layer	Wind Erodibility Group <sup>3</sup> (WEG)	Soil Erodibility Index (I) <sup>4,5</sup> (ton/ac/yr)	Soil Erodibility Index (I) for irrigated soils (ton/ac/yr) <sup>4</sup>
C	1	Very fine sand, fine sand, sand, or coarse sand	1	310 <sup>4</sup>	310
				250	250
				220	220
				180	160
				160	134
C	1	Loamy very fine sand, loamy fine sand, loamy sand, loamy coarse sand, sapric organic soil materials, and all horizons that meet andic <sup>6</sup> soil properties as per Criteria 2 in Soil Taxonomy, regardless of the fine earth texture	2	134	104
C	1	Very fine sandy loam, fine sandy loam, sandy loam, coarse sandy loam, and noncalcareous silt loam with 35 to 50% very fine sand and <10% clay	3	86	56
F	3	Clay, silty clay, non-calcareous clay loam, or silty clay loam with more than 35% clay	4	86	56
M	2	Calcareous <sup>7</sup> loam and silt loam or calcareous clay loam and silty clay loam	4L	86	56
M	2	Non-calcareous loam and silt loam with more than 20% clay (but does not meet WEG 3 criteria), or sandy clay loam, sandy clay, and hemic organic soil materials	5	56	38
M	2	Non-calcareous loam and silt loam with more than 20% clay, or non-calcareous clay loam with less than 35% clay or silty clay loam with less than 35% clay	6	48	21
M	2	Silt and fibric organic soil material	7	38	21
—	—	Soils not susceptible to wind erosion because of surface rock and pararock fragments or wetness	8	—	—

1/ Soil texture, C = Coarse; M = Medium; F = Fine

2/ Texture wetness factor for adjustment of Erosive Wind Energy (EWE) for the period (Irrigated fields only).

3/ For all WEGs except sand and loamy sand textures, if percent rock and pararock fragments (>2mm) by volume is 15-35, reduce I value by one group with more favorable rating. If percent rock and pararock fragments by volume is 35-60, reduce I value by two favorable groups except for sands and loamy sand textures which are reduced by one group with more favorable rating. If percent rock and pararock fragments by volume is more than 60, use I value of zero for all textures except sands and loamy sand textures which are reduced by three groups with more favorable rating.

4/ The wind erodibility index is based on the relationship of dry soil aggregates greater than 0.84 millimeters to potential soil erosion. Value for irrigated soils is applicable throughout the year. Values for irrigated soils determined by Dr. E.L. Skidmore, USDA, ARS, Wind Erosion Research Unit, Manhattan, Kansas.

5/ The I factor for WEG 1 vary from 160 for coarse sands to 310 for very fine sands. Use an I value of 220 as an average figure.

6/ Vitrandic, Vitritorrandic, and Vitixerandic Subgroups with ashy textural modifiers move one group with less favorable rating.

7/ Calcareous is a strongly or violently effervescent reaction of the fine-earth fraction to cold dilute (1N) HCL.

**APPLICATION FOR PERMIT  
DNCS ENVIRONMENTAL SOLUTIONS**

**VOLUME III: ENGINEERING DESIGN AND CALCULATIONS  
SECTION 8: EROSION CALCULATIONS**

**ATTACHMENT III.8.C**

**NATURAL RESOURCES CONSERVATION SERVICE. 1997.**

***APPENDIX 3: GLOSSARY OF SELECTED TERMS.***

**WASHINGTON, D.C.: UNITED STATES DEPARTMENT OF AGRICULTURE.**

**[HTTP://WWW.IA.NRCS.USDA.GOV/PROGRAMS/NRI/GLOSSARY97.HTML](http://www.ia.nrcs.usda.gov/programs/nri/glossary97.html)**



## APPENDIX 3. Glossary of Selected Terms

**Aerial photograph.** A photograph of the earth's surface taken from airborne equipment. Sometimes called aerial photo or air photograph.

**Artificial and modified surfaces.** A General cover category consisting of roads and right-of-ways, buildings, parking lots, farmsteads and ranch headquarters, urban and built-up areas, small built-up areas, rural transportation, and any other buildings that have a surface area greater than 1,000 square feet.

**Barren.** A General cover category consisting of nonvegetated lands, including alkaline barrens, unreclaimed mined land, and other barren areas incapable of supporting vegetation. Barren areas are nonvegetated either because the substrate will not support plant growth or because the area is subject to frequent disturbance (e.g., scouring, flooding) that prevents plant growth.

**Barren land.** A Land cover/use category used to classify lands with limited capacity to support life and having less than 5 percent vegetative cover. Vegetation, if present, is widely spaced.

- Typically, the surface of barren land is sand, rock, exposed subsoil, or salt-affected soils. Subcategories include salt flats; sand dunes; mud flats; beaches; bare exposed rock; quarries, strip mines, gravel pits, and borrow pits; riverwash; oil wasteland; mixed barren lands; and other barren land.

**Beach.** A Barren land subcategory. Includes the area adjacent to the shore of an ocean, sea, large river, or lake that is washed by the tide or waves.

**Built-up land.** See Urban and built-up areas.

**C factor (USLE).** See Cover and management factor.

**C factor (WEQ).** See Climatic factor.

**Census water.** Includes water bodies of at least 40 acres and perennial streams at least 1/8 mile wide. Also referred to as Large water bodies and Large streams.

**Climatic factor (C factor - WEQ).** Characterizes climatic erosivity, specifically wind speed and surface soil moisture. The factor for any given locality is expressed as a percentage of the C factor for Garden City, Kansas, which has a value of 100.

**Close-grown crops.** Crops that are generally drill-seeded or broadcast, such as wheat, oats, rice, barley, and flax.

**Conservation practice.** A specific treatment, such as a structural or vegetative measure or management technique commonly used to meet specific needs in planning and conservation, for which standards and specifications have been developed. Conservation practices are in the NRCS Field Office Technical Guide, Section IV, which is based on the National Handbook of Conservation Practices.

- The practices recorded for NRI have been applied to the area of land in which the NRI point falls or the portion of the field that would be used in conservation planning. The point need not fall on a specific practice.

Conservation Reserve Program (CRP). A federal program established under the Food Security Act of 1985 to assist private landowners to convert highly erodible cropland to vegetative cover for 10 years.

Conservation Reserve Program (CRP) land. A Land cover/use category that includes land under a CRP contract.

Cover and management factor (C factor - USLE). The ratio of soil loss from an area with specific cover and management to that from an identical area in tilled continuous fallow.

Cowardin system. A classification system of wetlands and deepwater habitats of the United States, officially adopted by the U.S. Fish and Wildlife Service (FWS) used to develop wetland data bases. The system was developed by Lewis M. Cowardin of the U.S. Fish and Wildlife Service and others. The five major systems are Estuarine, Lacustrine, Marine, Palustrine, and Riverine.

Cropland. A Land cover/use category that includes areas used for the production of adapted crops for harvest. Two subcategories of cropland are recognized: cultivated and noncultivated. Cultivated cropland comprises land in row crops or close-grown crops and also other cultivated cropland, for example, hayland or pastureland that is in a rotation with row or close-grown crops. Noncultivated cropland includes permanent hayland and horticultural cropland.

Cropping history. A record of the crop that was on the land during each of the 3 years preceding the current inventory year. These data are recorded on cropland, pastureland, and CRP land cover/uses only. Data are used to determine some of the values used to calculate water and wind erosion rates.

Cultivated cropland. See Cropland.

Deepwater habitat. Any open water area in which the mean water depth exceeds 6.6 feet in nontidal areas or at mean low water in freshwater tidal areas, or is covered by water during extreme low water at spring tides in salt and brackish tidal areas, or covers the deepest emerging vegetation, whichever is deeper.

Developed land. A combination of land cover/use categories, Large urban and built-up areas, Small built-up areas, and Rural transportation land.

Erodibility index (EI). A numerical expression of the potential of a soil to erode, considering the physical and chemical properties of the soil and climatic conditions where it is located. The higher the index, the greater the investment needed to maintain the sustainability of the soil resource base if intensively cropped. EI scores above 8 are equated to highly erodible land.

Erosion. The wearing away of the land surface by running water, waves, or moving ice and wind, or by such processes as mass wasting and corrosion (solution and other chemical processes). The term "geologic erosion" refers to natural erosion processes occurring over long (geologic) time spans. "Accelerated erosion" generically refers to erosion that exceeds what is presumed or estimated to be naturally occurring levels, and which is a direct result of human activities (e.g., cultivation and logging).

Estuarine Wetland. Wetlands occurring in the Estuarine System, one of five systems in the classification of wetlands and deepwater habitats (see Wetlands, Cowardin et al. 1979). Estuarine wetlands are tidal

wetlands that are usually semienclosed by land but have open, partly obstructed or sporadic access to the open ocean, and in which ocean water is at least occasionally diluted by freshwater runoff from the land. The most common example is where a river flows into the ocean.

Farmsteads and ranch headquarters. A Land cover/use category that includes dwellings, outbuildings, barns, pens, corrals and feedlots next to buildings, farmstead or feedlot windbreaks, and family gardens associated with operating farms and ranches. (Commercial feedlots, greenhouses, poultry facilities, overnight pastures for livestock, and field windbreaks are not considered part of farmsteads.)

Federal land. See Ownership.

Field. A cultivated area of land that is marked out for a particular crop or cropping sequence.

Forest land. A Land cover/use category that is at least 10 percent stocked by single-stemmed woody species of any size that will be at least 4 meters (13 feet) tall at maturity. Also included is land bearing evidence of natural regeneration of tree cover (cut over forest or abandoned farmland) and not currently developed for nonforest use. Ten percent stocked, when viewed from a vertical direction, equates to an areal canopy cover of leaves and branches of 25 percent or greater. The minimum area for classification as forest land is 1 acre, and the area must be at least 100 feet wide.

General cover. Nine general cover categories are defined, based upon vegetative structure (e.g., canopy cover percentage) or substrate characteristics (e.g., barren land/artificial surfaces). They are:

Crop; Herbaceous; Open canopy short woody plants; Short woody plants; Open canopy tall woody plants; Tall woody plants; Barren; Artificial and modified surfaces; Water

- See also Habitat composition and Habitat configuration.

Growing season. The period and/or number of days between the last freeze in the spring and the first frost in the fall for the freeze threshold temperature of the crop or other designated temperature threshold.

Habitat composition. The makeup or relative proportion of the General cover categories occurring about a point (see Primary sample unit).

Habitat configuration. The arrangement of the nine General cover categories occurring about a point (see Primary sample unit).

Habitat patch. A term used to describe an area displaying a relatively uniform General cover type. Nine General cover categories are used to classify areas of relatively uniform cover. Each individual area is referred to as a habitat patch.

Hayland. A subcategory of Cropland managed for the production of forage crops that are machine harvested. The crop may be grasses, legumes, or a combination of both. Hayland also includes land in set-aside or other short-term agricultural programs.

Herbaceous. A General cover category consisting of predominantly perennial herbaceous plants or noncultivated annuals or both. The tall woody canopy cover is less than 5 percent, and the short woody canopy cover is also less than 5 percent. Arid rangeland and desert can fall into this category although vegetation density and percentage of ground cover may be low.

Horticultural cropland. A subcategory of Cropland used for growing fruit, nut, berry, vineyard, and other bush fruit and similar crops. Nurseries and other ornamental plantings are included.

I factor (WEQ). See Soil erodibility index.

Irrigated land. Land that shows evidence of being irrigated during the year of the inventory or of having been irrigated during 2 or more of the last 4 years. Water is supplied to crops by ditches, pipes, or other conduits. For the purposes of the NRI, water spreading is not considered irrigation.

K factor (USLE). See Soil erodibility factor (USLE).

K factor (WEQ). See Ridge roughness factor (WEQ).

L factor (USLE). See Slope-length factor (USLE).

L factor (WEQ). See Unsheltered distance factor (WEQ).

Lacustrine System. Wetlands and deepwater habitats occurring in the Lacustrine System, one of five systems in the classification of wetlands and deepwater habitats (see Wetlands, Cowardin et al. 1979). The Lacustrine System includes wetlands and deepwater habitats with all of the following characteristics: (1) situated in a topographic depression or a dammed river channel; (2) lacking trees, shrubs, persistent emergent plants, emergent mosses or lichens with greater than 30% areal coverage; and (3) total area exceeding 20 acres. Similar habitats totaling less than 20 acres are included if an active wave-formed or bedrock shoreline feature makes up all or part of the boundary, or if the water depth in the deepest part of the basin exceeds 6.6 feet at low water.

Lake. A natural inland body of water, fresh or salt, extending over 40 acres or more and occupying a basin or hollow on the earth's surface, which may or may not have a current or single direction of flow.

Land capability classification (class and subclass). Land capability classification is a system of grouping soils primarily on the basis of their capability to produce common cultivated crops and pasture plants without deteriorating over a long period. Land capability classification is subdivided into capability class and capability subclass nationally.

Capability class. The broadest category in the system. Class codes I to VIII indicate progressively greater limitations and narrower choices for agriculture. The numbers are used to represent both irrigated and nonirrigated land capability.

Capability subclass. The second category in the system. Class codes e (erosion problems), w (wetness problems), s (root zone limitations), and c (climatic limitations) are used for land capability subclasses.

Land cover/use. A term that includes categories of land cover and categories of land use. Land cover is the vegetation or other kind of material that covers the land surface. Land use is the purpose of human activity on the land; it is usually, but not always, related to land cover. The NRI uses the term land cover/use to identify categories that account for all the surface area of the United States.

Large streams. Perennial streams at least 1/8 mile (660 feet) wide.

Large urban and built-up areas. A Land cover/use category composed of developed tracts of at least 10

acres—meeting the definition of Urban and built-up areas.

Large water bodies. Water bodies of at least 40 acres.

Marine System. The open ocean overlying the continental shelf and its associated high energy coastline. Marine habitats are exposed to the waves and currents of the open ocean and the water regimes are determined primarily by the ebb and flow of oceanic tides.

Marshland. A subcategory of the Land cover/use category Other rural land, described as a nonforested area of land partly or intermittently covered with water and usually characterized by the presence of such monocotyledons as sedges and rushes. These areas are usually in a wetland class and are not placed in another NRI land cover/use category, such as rangeland or pastureland.

Mines, quarries, and pits. Uses of land for extraction of ores, minerals, and rock materials; a subcategory of the Land cover/use category Barren land.

Minor land cover/uses. See Other rural land. A miscellaneous group of land cover/uses that is sometimes used in NRI tables and reports but not in data collection.

Mud flat. A Land cover/use subcategory under Barren land. A mud area with less than 5 percent vegetative cover.

Noncultivated cropland. See Cropland.

Open canopy short woody plants. A General cover category consisting of short woody canopy cover of 5 to 25 percent and tall woody canopy cover of less than 5 percent. The distinction between short (< 4 meters) and tall (> 4 meters) woody plants is made for current conditions, not potential. Arid rangeland and desert can fall into this category although vegetation density and percentage of ground cover may be low.

Open canopy tall woody plants. A General cover category consisting of tall woody canopy cover of 5 to 25 percent and short woody canopy cover of less than 25 percent. The distinction between tall (> 4 meters) and short (< 4 meters) woody plants is made for current conditions, not potential. Arid rangeland and desert can fall into this category although vegetation density and percentage of ground cover may be low.

Other aquatic habitats. Includes wetlands and deepwater habitats occurring in the Riverine, Lacustrine, or Marine Systems, and deepwater habitats occurring in the Estuarine System as defined by Cowardin et al. 1979 (see Wetlands).

Other rural land. A Land cover/use category that includes farmsteads and other farm structures, field windbreaks, barren land, and marshland.

Ownership. The separation of federal and nonfederal lands and the distinction between administrative units of land. Water areas are not classified according to ownership. The six categories of ownership are:

Private. A type of ownership pertaining to land belonging to an individual person or persons, a partnership, or a corporation (all of which are persons in the legal sense), as opposed to the public or the government; private property.

Municipal. A type of ownership pertaining to land belonging to the local government of a town or city.

County or parish. A type of ownership pertaining to land belonging to an administrative subdivision of a state in the United States, which is identified as a county or an equivalent administrative unit in areas where counties do not exist; examples are parishes in Louisiana and boroughs in Alaska.

State. A type of ownership pertaining to land belonging to one of the states, commonwealths, or territories of the United States of America.

Federal land. A land ownership category designating land that is owned by the federal government. It does not include, for example, trust lands administered by the Bureau of Indian Affairs or Tennessee Valley Authority (TVA) land. No data are collected for any year that land is in this ownership.

Indian tribal and individual Indian trust lands. A type of ownership of land administered by officially constituted Indian tribal or individual Indian trust entities.

P factor. See Practice factor.

Palustrine Wetland. Wetlands occurring in the Palustrine System, one of five systems in the classification of wetlands and deepwater habitats (see Wetlands, Cowardin et al. 1979). Palustrine wetlands include all nontidal wetlands dominated by trees, shrubs, persistent emergent plants, or emergent mosses or lichens, as well as small, shallow open water ponds or potholes. Palustrine wetlands are often called swamps, marshes, potholes, bogs, or fens.

Pastureland. A Land cover/use category of land managed primarily for the production of introduced forage plants for livestock grazing. Pastureland cover may consist of a single species in a pure stand, a grass mixture, or a grass-legume mixture. Management usually consists of cultural treatments: fertilization, weed control, reseeding or renovation, and control of grazing. For the NRI, includes land that has a vegetative cover of grasses, legumes, and/or forbs, regardless of whether or not it is being grazed by livestock.

Perennial stream. A stream or reach of a stream that normally flows continuously throughout the year.

Personal Digital Assistant (PDA). A hand-held, computer-assisted survey collection tool used to record NRI data.

Photographic interpretation. The act of examining photography images for the purpose of identifying objects and judging their significance.

Practice factor (P factor - USLE). The ratio of soil loss with a support practice like contouring, stripcropping, or terracing, to soil loss with straight-row farming up and down the slope.

Primary sample unit (PSU). An area of land, typically square to rectangular in shape, that is approximately 40, 100, 160, or 640 acres in size. Within the PSU, sample points are assigned. Certain data elements are collected for the entire PSU, while others are collected at the PSU points.

- The size of the PSU is based on the shape, size, and complexity of the resources being inventoried. In 34 states, PSU's are often 160-acre square parcels measuring 0.5 mile on each side. In the western United States, PSU's are often 40-acre or 640-acre square areas; the 40-acre units are used in most irrigated areas, and the larger PSU's are used in relatively homogeneous areas containing large tracts of rangeland, forest land, or barren land. In the 13 northeastern states, PSU's are defined to be 20 seconds of latitude by 30 seconds of longitude, ranging from 97 acres in Maine to 114 acres in southern Virginia. In Louisiana and parts of northwestern Maine, PSU's are 0.5 kilometer squares

(61.8 acres).

Prime farmland. Land that has the best combination of physical and chemical characteristics for producing food, feed, forage, fiber, and oilseed crops and is also available for these uses.

Railroads. A category of Rural transportation areas that includes all operational rail systems and their rights-of-way. Abandoned railroad beds are not included as railroad areas.

Rainfall and runoff (R factor - USLE). The number of rainfall erosion index units, plus a factor for runoff from snowmelt or applied water where such runoff is significant.

Rangeland. A Land cover/use category on which the climax or potential plant cover is composed principally of native grasses, grasslike plants, forbs or shrubs suitable for grazing and browsing, and introduced forage species that are managed like rangeland. This would include areas where introduced hardy and persistent grasses, such as crested wheatgrass, are planted and such practices as deferred grazing, burning, chaining, and rotational grazing are used, with little or no chemicals or fertilizer being applied. Grasslands, savannas, many wetlands, some deserts, and tundra are considered to be rangeland. Certain communities of low forbs and shrubs, such as mesquite, chaparral, mountain shrub, and pinyon-juniper, are also included as rangeland.

Remote sensing. The science and art of obtaining information about an object, area, or phenomenon through the analysis of data acquired by a device that is not in contact with the object, area, or phenomenon under investigation.

Reservoir. A pond, lake, basin, or other space, created in whole or in part by the building of engineering structures, that is used for the storage, regulation, and control of water.

Ridge roughness (K factor - WEQ). A measure of the effect of ridges made by tillage and planting implements. It is expressed as a decimal from 0.5 to 1.0.

- Ridges, especially those at right angles to the prevailing wind direction, absorb and deflect wind energy and trap moving soil particles. See Wind erosion equation (WEQ).

Riverine System. All wetland and deepwater habitats contained within a channel, with two exceptions (1) wetlands dominated by trees, shrubs, persistent emergents, emergent mosses, or lichens; and (2) habitats with water containing ocean derived salts.

Riverwash. A subcategory of Barren land. Barren alluvial areas, usually coarse-textured, exposed along streams at low water and subject to shifting during normal high water.

Row crops. A subset of the Land cover/use category Cropland (subcategory, Cultivated) comprising land in row crops, such as corn, soybeans, peanuts, potatoes, sorghum, sugar beets, sunflowers, tobacco, vegetables, and cotton.

Rural transportation land. A Land cover/use category which consists of all highways, roads, railroads and associated right-of-ways outside urban and built-up areas; also includes private roads to farmsteads or ranch headquarters, logging roads, and other private roads (field lanes are not included).

S factor. See Slope-steepness factor.

Saline deposits. Precipitated salts or salt found in or on the soil surface that result in reduced vegetative production or in the elimination of crops and grasses on agricultural lands.

Salt flats. Undrained areas in closed basins in arid regions. In these areas, 10 to 75 cm (4 to 30 in) of crystalline salt overlies stratified, very strongly saline sediment. The water table may be within 20 cm (8 in) of the surface at some period during the year.

Sample point. The second-stage sample unit in the NRI two-stage sampling scheme. See also Primary sample unit.

Sand dunes. A Land cover/use subcategory under Barren land. A sand area with less than 5 percent vegetative cover. An accumulation of loose sand heaped by the wind, commonly found along low-lying seashores above high-tide level, more rarely on the border of large lakes or river valleys, as well as in various desert regions, where there is abundant dry surface sand during some part of the year.

Sheet and rill erosion. The removal of layers of soil from the land surface by the action of rainfall and runoff. It is the first stage in water erosion.

Short woody plants. A General cover category consisting of short woody canopy cover of greater than 25 percent, while tall woody canopy cover is less than 25 percent. Short woody plants are less than 4 meters (about 13 feet) tall and often multi-stemmed, e.g., shrubs and seedlings. The distinction between tall (>4m) and short (<4m) is made according to current conditions, not potential.

Silviculture. A branch of forestry dealing with the management and cultivation of forest trees.

Slope. The inclination of the soil surface from the horizontal. Slope percent is the vertical distance divided by the horizontal distance, then multiplied by 100.

Slope length. The distance from the point of origin of overland flow to the point where either the slope gradient decreases enough that deposition begins, or the runoff water enters a well-defined channel that may be part of a drainage network or a constructed channel. For the NRI, length of slope is taken through the sample point.

Slope-length factor (L factor - USLE). The ratio of soil loss from the field slope length to that from a 72.6-foot length under identical conditions.

Slope-steepness factor (S factor - USLE). The ratio of soil loss from the field slope gradient to that from a 9 percent slope under otherwise identical conditions. Used in Universal soil loss equation (USLE) calculations of sheet and rill erosion.

Small built-up areas. A Land cover/use category consisting of developed land units of 0.25 to 10 acres, which meet the definition of Urban and built-up areas.

Small streams. Perennial streams less than 1/8 mile (660 feet) wide.

Small water bodies. Inland bodies of water with a water surface area of less than 40 acres.

Soil erodibility factor (K factor - USLE). An erodibility factor which quantifies the susceptibility of soil particles to detachment and movement by water. This factor is used in the Universal soil loss equation (USLE) to calculate soil loss by water.

Soil erodibility index (I factor - WEQ). The potential soil loss, in tons per acre per year, from a wide, level, unsheltered, isolated field with a bare, smooth, loose, and noncrusted surface, under climatic conditions like those in the vicinity of Garden City, Kansas.

Soil loss tolerance factor (T factor - USLE). The maximum rate of annual soil loss that will permit crop productivity to be sustained economically and indefinitely on a given soil.

Soil survey. The systematic examination, description, classification, and mapping of soils in an area. The USDA- NRCS Soil Survey Program produces Soil Survey Reports, which generally consist of four principal parts: (1) maps, (2) a map legend, (3) a description of the soils in the survey area, and (4) a use and management report. The survey area commonly is a single county but may comprise parts of counties, physiographic regions, or other management areas.

Stream. A flow of water in a channel or bed, as a brook, rivulet, or small river.

T factor (USLE). See Soil loss tolerance factor.

Tall woody plants. A General cover category consisting of tall woody canopy cover of greater than 25 percent. Tall plants are 4 meters (about 13 feet) or more tall, usually single-stemmed trees. The distinction between tall (> 4m) and short (< 4m) is made according to current conditions, not potential. Thus, a 3-meter-tall Douglas-fir is a short woody plant.

Universal soil loss equation (USLE). An erosion model designed to predict the long-term average soil losses in runoff from specific field areas in specified cropping and management systems.

The equation is:  $A = RKLSCP$

where A = Computed soil loss per unit area

R = Rainfall and runoff factor

K = Soil erodibility factor

L = Slope-length factor

S = Slope-steepness factor

C = Cover and management factor

P = Support practice factor

The NRI calculations use location-specific data for the field in which the NRI sample point falls or that portion of the field surrounding the point that would be considered in conservation planning.

Unsheltered distance (L factor - WEQ). The unsheltered distance along the prevailing wind erosion direction across the field or area to be evaluated.

- For NRI, the unsheltered distance is expressed in feet, measured through the sample point, parallel to the prevailing wind direction during the critical wind erosion period.

Uplands. All land not classified as wetland or deepwater habitat (see Wetlands, Cowardin et al. 1979).

Urban and built-up areas. A Land cover/use category consisting of residential, industrial, commercial, and institutional land; construction sites; public administrative sites; railroad yards; cemeteries; airports; golf courses; sanitary landfills; sewage treatment plants; water control structures and spillways; other land used for such purposes; small parks (less than 10 acres) within urban and built-up areas; and highways, railroads, and other transportation facilities if they are surrounded by urban areas. Also included are tracts of less than 10 acres that do not meet the above definition but are completely surrounded by Urban and built-up land. Two size categories are recognized in the NRI: areas of 0.25 acre to 10 acres, and areas of at least 10 acres.

V factor. See Vegetative cover.

Vegetative cover (V factor - WEQ). The effect of vegetative cover in the Wind erosion equation is expressed by relating the kind, amount, and orientation of vegetative material to its equivalent in pounds per acre of small grain residue in reference condition (small grain equivalent).

Water. A General cover category consisting of permanent water, such as a perennial stream, lake, or pond with at least 25 percent open water. If the vegetative canopy obscures more than 75 percent of the water surface from view, the area is recorded under the category appropriate for the canopy vegetation. Four types of water areas are large streams, large water bodies, small streams, and small water bodies.

Water areas. A Land cover/use category comprising water bodies and streams that are permanent open water.

Water body. A type of (permanent open) water area that includes ponds, lakes, reservoirs, bays or gulfs, and estuaries. There are three size categories: less than 2 acres, 2 to 40 acres, and at least 40 acres.

Water spreading. Diverting or collecting runoff from natural channels, gullies, or streams with a system of dams, dikes, ditches, or other means, and spreading it over a relatively flat area.

Wetlands. Lands transitional between terrestrial and aquatic systems where the water table is usually at or near the surface or the land is covered by shallow water. For purposes of this classification wetlands must have one or more of the following three attributes: (1) at least periodically, the land supports predominantly hydrophytes; (2) the substrate is predominantly undrained hydric soil; and (3) the substrate is nonsoil and is saturated with water or covered by shallow water at some time during the growing season of each year. (Cowardin, L. M., V. Carter, F. C. Golet, E. T. LaRoe. 1979. Classification of wetlands and deepwater habitats of the United States. FWS/OBS-79/31. U.S. Department of the Interior, Fish and Wildlife Service.)

Wetland losses. Wetland losses are described in terms of gross and net. Net change is defined as the gross gain minus the gross loss, and can be either positive (net gain) or negative (net loss) for a given region. Wetland losses were attributed to one of the following categories:

- a. Development. Loss occurring on land cover/use category of urban and built-up or rural transportation.
- b. Agriculture. Loss occurring on land cover/use category of cropland, pastureland, CRP land, farmsteads or other farmland.
- c. Silviculture. Loss occurring on forest land.
- d. Miscellaneous. Loss occurring on all other land cover/use categories including mined land, rangeland, and other barren lands. Natural variations in climatic cycles and hydrology are responsible for the

majority of these losses.

Wind erodibility group (WEG). A grouping of soils that have similar properties affecting their resistance to wind erosion.

Wind erosion. The process of detachment, transport, and deposition of soil by wind.

Wind erosion equation (WEQ). An erosion model designed to predict long-term average annual soil losses from a field having specific characteristics.

The equation is:  $E = f(IKCLV)$

where E = Estimated average annual soil loss expressed in tons per acre per year

I = Soil erodibility index

K = Soil ridge roughness factor

C = Climatic factor

L = Equivalent unsheltered distance across the field along the prevailing wind erosion direction

V = Equivalent vegetative cover

**APPLICATION FOR PERMIT  
DNCS ENVIRONMENTAL SOLUTIONS**

**VOLUME III: ENGINEERING DESIGN AND CALCULATIONS  
SECTION 8: EROSION CALCULATIONS**

**ATTACHMENT III.8.D**

**NATURAL RESOURCES CONSERVATION SERVICE. 1992.**

**FIGURE 14 - ANNUAL "C" VALUES OF THE WIND EROSION EQUATION NEW  
MEXICO IN *AGRONOMY TECH NOTE 27*, JUNE 22, 1992. WASHINGTON, D.C.:**

**UNITED STATES DEPARTMENT OF AGRICULTURE.**

Annual "C" Values  
 Of The Wind Erosion Equation  
 New Mexico

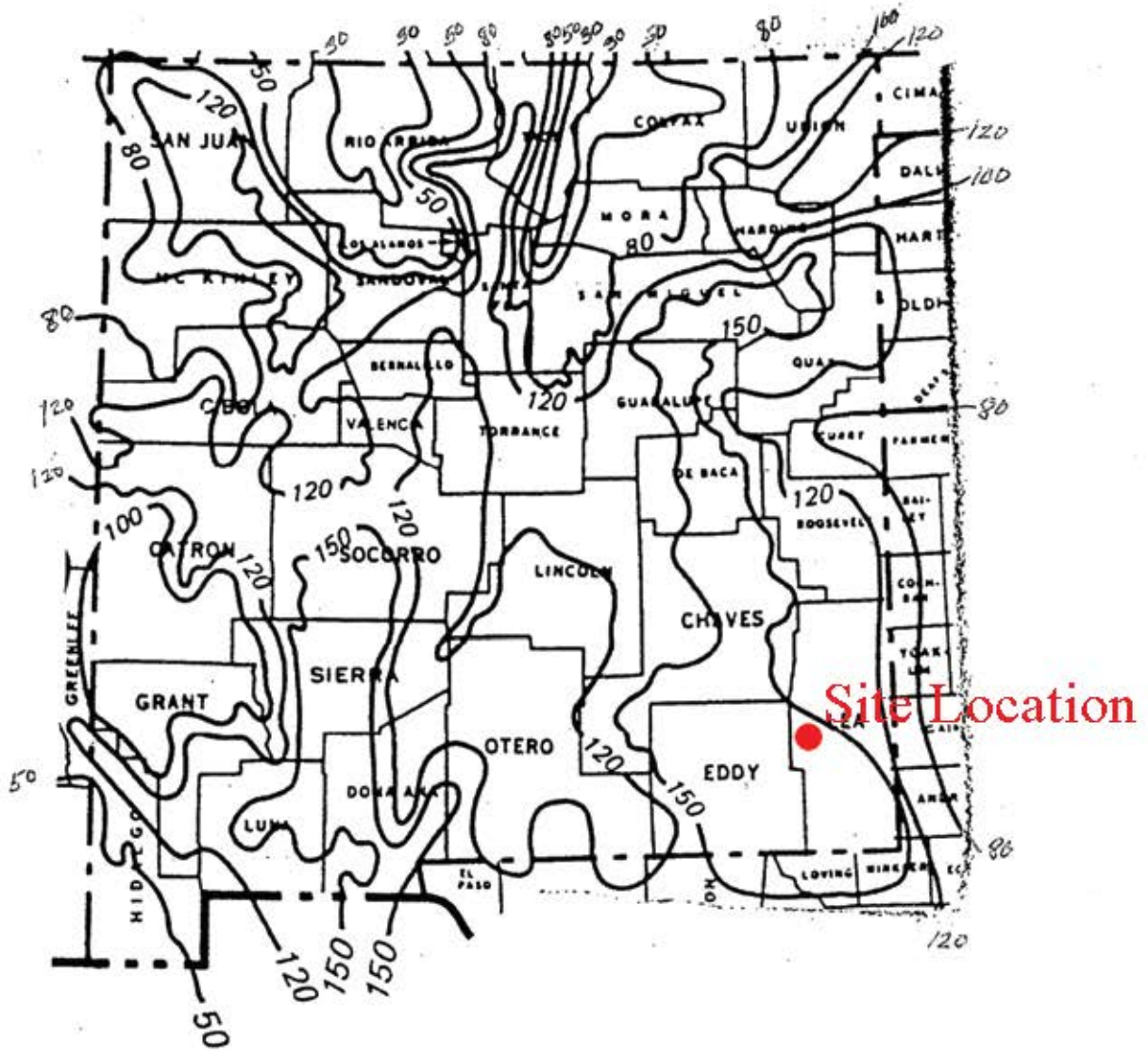


Figure 14

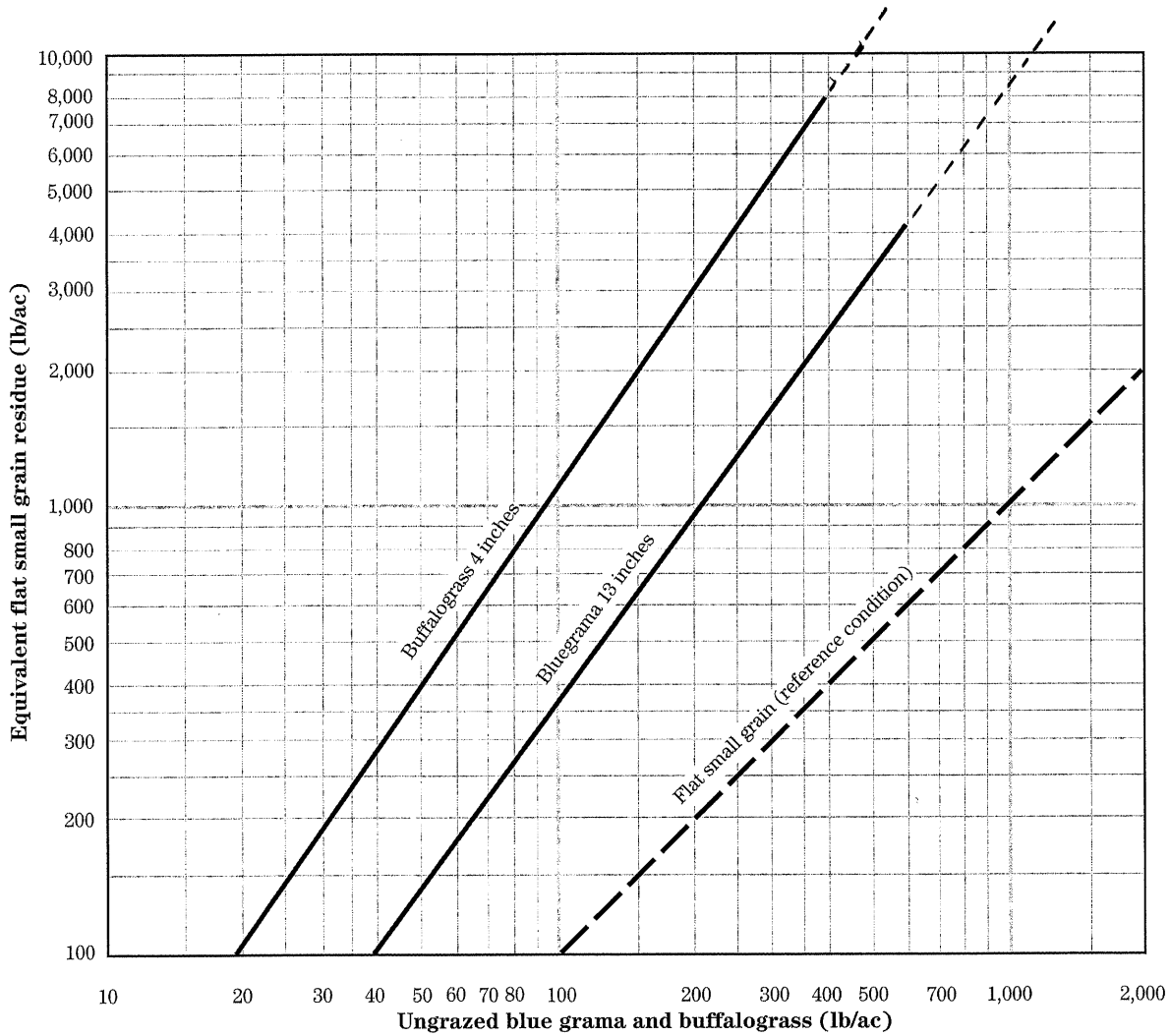
**APPLICATION FOR PERMIT  
DNCS ENVIRONMENTAL SOLUTIONS**

**VOLUME III: ENGINEERING DESIGN AND CALCULATIONS  
SECTION 8: EROSION CALCULATIONS**

**ATTACHMENT III.8.E**

**NATURAL RESOURCES CONSERVATION SERVICE. 2002. FIGURE 7 - FLAT  
SMALL GRAIN EQUIVALENTS OF UNGRAZED BLUE GRAMA AND  
BUFFALOGRASS IN *NATIONAL AGRONOMY MANUAL*, 190-V-NAM, THIRD  
EDITION, OCTOBER 2002, PART 502, WIND EROSION. WASHINGTON, D.C.:  
UNITED STATES DEPARTMENT OF AGRICULTURE.**

**Figure d-7** Flat small grain equivalents of ungrazed blue grama and buffalograss



Reference condition: Dry small grain stalks 10 inches long, lying flat on the soils surface in 10 inch rows perpendicular to wind direction, stalks oriented to wind direction.

Source: Lyles and Allison, 1980, Journal Range Management, 33(2), pages 143-146.

**APPLICATION FOR PERMIT  
DNCS ENVIRONMENTAL SOLUTIONS**

**VOLUME III: ENGINEERING DESIGN AND CALCULATIONS  
SECTION 8: EROSION CALCULATIONS**

**ATTACHMENT III.8.F**

**NATURAL RESOURCES CONSERVATION SERVICE. 1998.**

**SUBPART G – EXHIBITS (C=120, I=134, K=1.0) IN *NATIONAL AGRONOMY  
MANUAL, 190-V-NAM, THIRD EDITION, JANUARY 1998. WASHINGTON, D.C.:***

**UNITED STATES DEPARTMENT OF AGRICULTURE.**

SUBPART G - EXHIBITS

502.60(a)

(E)\* SOIL LOSS FROM WIND EROSION IN TONS PER ACRE PER YEAR JANUARY, 1998  
 C = 150  
 I = 134

SURFACE - K =1.00

(L) (V)\*\* - FLAT SMALL GRAIN RESIDUE IN POUNDS PER ACRE

UNSHeltered	0	250	500	750	1000	1250	1500	1750	2000	2250	2500	2750	3000
DISTANCE													
IN FEET													
10000	201.0	182.4	157.7	134.1	96.9	72.7	46.8	31.6	21.5	12.7	7.7	1.9	1.2
8000	201.0	182.4	157.7	134.1	96.9	72.7	46.8	31.6	21.5	12.7	7.7	1.9	1.2
6000	201.0	182.4	157.7	134.1	96.9	72.7	46.8	31.6	21.5	12.7	7.7	1.9	1.2
4000	201.0	182.4	157.7	134.1	96.9	72.7	46.8	31.6	21.5	12.7	7.7	1.9	1.2
3000	201.0	182.4	157.7	134.1	96.9	72.7	46.8	31.6	21.5	12.7	7.7	1.9	1.2
2000	201.0	182.4	157.7	134.1	96.9	72.7	46.8	31.6	21.5	12.7	7.7	1.9	1.2
1000	192.4	174.3	150.1	127.0	91.0	67.4	43.0	28.6	19.2	11.2	6.7	1.6	1.0
800	190.0	172.0	148.0	124.9	89.3	65.9	41.9	27.8	18.6	10.8	6.4	1.5	1.0
600	183.2	165.5	142.0	119.3	84.7	61.9	39.0	25.6	17.0	9.7	5.7	1.3	0.7
400	173.7	156.6	133.8	111.7	78.4	56.5	35.1	22.7	14.9	8.3	4.8	1.1	0.6
300	166.6	149.9	127.6	106.0	73.8	52.5	32.3	20.6	13.4	7.4	4.2	0.9	0.5
200	152.8	137.0	115.8	95.1	65.2	45.2	27.2	17.0	10.8	5.7	3.1	0.7	0.4
150	142.9	127.8	107.5	87.5	59.2	40.3	23.9	14.6	9.1	4.7	2.5	0.2	
100	133.6	119.1	99.6	80.4	53.6	35.8	20.9	12.5	7.7	3.9	2.0	0.2	
80	125.4	111.5	92.8	74.3	49.0	32.1	18.4	10.8	6.6	3.2	1.6	0.1	
60	113.6	100.6	83.0	65.7	42.5	27.1	15.2	8.7	5.1	2.4	1.2	0.1	
50	107.4	94.9	78.0	61.3	39.2	24.6	13.6	7.6	4.5	2.0	1.0	0.1	
40	102.0	89.9	73.6	57.4	36.4	22.5	12.3	6.8	3.9	1.8	0.8	0.1	
30	92.1	80.8	65.5	50.5	31.4	18.8	10.0	5.4	3.0	1.3	0.4		
20	78.7	68.7	55.0	41.6	25.0	14.4	7.4	3.8	2.0	0.8			
10	60.2	52.0	40.7	29.7	17.0	9.1	4.3	2.1	1.0				

(E)\* SOIL LOSS FROM WIND EROSION IN TONS PER ACRE PER YEAR JANUARY, 1998  
 C = 150  
 I = 134

SURFACE - K =0.90

(L) (V)\*\* - FLAT SMALL GRAIN RESIDUE IN POUNDS PER ACRE

UNSHeltered	0	250	500	750	1000	1250	1500	1750	2000	2250	2500	2750	3000
DISTANCE													
IN FEET													
10000	180.9	163.4	140.0	117.5	83.2	60.6	38.0	24.9	16.5	9.4	5.5	1.2	0.7
8000	180.9	163.4	140.0	117.5	83.2	60.6	38.0	24.9	16.5	9.4	5.5	1.2	0.7
6000	180.9	163.4	140.0	117.5	83.2	60.6	38.0	24.9	16.5	9.4	5.5	1.2	0.7
4000	180.9	163.4	140.0	117.5	83.2	60.6	38.0	24.9	16.5	9.4	5.5	1.2	0.7
3000	180.9	163.4	140.0	117.5	83.2	60.6	38.0	24.9	16.5	9.4	5.5	1.2	0.7
2000	178.9	161.5	138.3	115.9	81.8	59.4	37.2	24.3	16.0	9.1	5.3	1.2	0.6
1000	170.8	153.9	131.3	109.4	76.5	54.8	33.9	21.8	14.3	7.9	4.5	1.0	0.5
800	165.3	148.7	126.6	105.0	73.0	51.8	31.8	20.3	13.1	7.2	4.1	0.9	0.5
600	158.6	142.4	120.8	99.7	68.7	48.2	29.3	18.5	11.8	6.4	3.5	0.8	0.4
400	147.8	132.3	111.6	91.2	62.1	42.7	25.5	15.7	9.9	5.2	2.8	0.6	
300	141.5	126.4	106.2	86.4	58.3	39.6	23.4	14.2	8.9	4.6	2.4	0.2	
200	131.2	116.9	97.6	78.6	52.3	34.7	20.2	12.0	7.3	3.7	1.9	0.2	
150	120.9	107.4	89.0	71.0	46.5	30.2	17.2	10.0	6.0	2.9	1.5	0.1	
100	111.8	98.9	81.5	64.4	41.5	26.3	14.7	8.3	4.9	2.3	1.1	0.1	
80	106.2	93.8	77.0	60.4	38.6	24.1	13.3	7.4	4.3	2.0	1.0	0.1	
60	96.7	85.0	69.2	53.7	33.7	20.5	11.0	6.0	3.4	1.5	0.7	0.1	
50	90.9	79.8	64.7	49.8	30.8	18.5	9.8	5.2	2.9	1.3	0.4		
40	85.4	74.7	60.2	46.0	28.1	16.5	8.6	4.5	2.5	1.0	0.3		
30	76.6	66.8	53.3	40.2	24.1	13.7	7.0	3.5	1.9	0.7			
20	66.0	57.1	45.1	33.3	19.4	10.6	5.2	2.5	1.3	0.5			
10	50.5	43.3	33.4	23.9	13.3	6.7	3.1	1.4	0.7				

\* NOTE: SOIL LOSS FOR VALUES WHERE 'E' IS LESS THAN 0.1 OR GREATER THAN 440.0 ARE NOT SHOWN; OTHER VALUES NOT SHOWN ARE INVALID

\*\* NOTE: VALUES SHOWN ARE FLAT SMALL GRAIN EQUIVALENT, NOT 'V'

**APPLICATION FOR PERMIT  
DNCS ENVIRONMENTAL SOLUTIONS**

**VOLUME III: ENGINEERING DESIGN AND CALCULATIONS  
SECTION 9: SETTLEMENT CALCULATIONS**

**TABLE OF CONTENTS**

<b>Section No.</b>	<b>Title</b>	<b>Page</b>
1.0	INTRODUCTION .....	III.9-1
1.1	Description.....	III.9-1
2.0	DESIGN CRITERIA .....	III.9-1
3.0	FOUNDATION SOILS SETTLEMENT .....	III.9-2
4.0	WASTE SETTLEMENT CALCULATIONS .....	III.9-9
6.0	CONCLUSION.....	III.9-15

**LIST OF FIGURES**

<b>Figure No.</b>	<b>Title</b>	<b>Page</b>
III.9.1	SETTLEMENT POINTS.....	III.9-4

**LIST OF TABLES**

<b>Table No.</b>	<b>Title</b>	<b>Page</b>
III.9.1	SETTLEMENT AND ANGULAR DISTORTION OF FOUNDATION SOILS BETWEEN POINTS, CROSS SECTION A-A' .....	III.9-6
III.9.2	SETTLEMENT AND ANGULAR DISTORTION OF FOUNDATION SOILS BETWEEN POINTS, CROSS SECTION B-B' .....	III.9-8
III.9.3	TOTAL SETTLEMENT AND ANGULAR DISTORTION BETWEEN POINTS, CROSS SECTION A-A' .....	III.9-11
III.9.4	TOTAL SETTLEMENT AND ANGULAR DISTORTION BETWEEN POINTS, CROSS SECTION B-B' .....	III.9-13
III.9.5	TOTAL SETTLEMENT AND ANGULAR DISTORTION BETWEEN POINTS, CROSS SECTION A-A' .....	III.9-16
III.9.6	TOTAL SETTLEMENT AND ANGULAR DISTORTION BETWEEN POINTS, CROSS SECTION A-A' .....	III.9-18

**APPLICATION FOR PERMIT  
DNCS ENVIRONMENTAL SOLUTIONS**

**VOLUME III: ENGINEERING DESIGN AND CALCULATIONS  
SECTION 9: SETTLEMENT CALCULATIONS**

**LIST OF ATTACHMENTS**

<b>Attachment No.</b>	<b>Title</b>
III.9.A	SUMMARY OF GEOTECHNICAL LABORATORY TESTING RESULTS
III.9.B	QIAN, XUEDE; KOERNER, ROBERT M.; AND GRAY, DONALD H. 2002. <i>GEOTECHNICAL ASPECTS OF LANDFILL DESIGN AND CONSTRUCTION</i> . NEW YORK: PRENTICE HALL.
III.9.C	CODUTO, DONALD P. 1998. <i>GEOTECHNICAL ENGINEERING PRINCIPLES AND PRACTICES</i> . NEW JERSEY: PRENTICE HILL.
III.9.D	SHARMA, HARI .D. AND SANGEETA P. LEWIS. 1994. <i>WASTE CONTAINMENT SYSTEMS, WASTE STABILIZATION AND LANDFILLS: DESIGN AND EVALUATION</i> . NEW YORK: JOHN WILEY AND SONS.
III.9.E	STEPHENS, DANIEL B.; HSU, KUO-CHIN; PRIEKSAT, MARK A.; ANKENY, MARK D.; BLANDFORD, NEIL; ROTH, TRACY L.; KELSEY, JAMES A.; WHITWORTH, JULIA R. 1997. A COMPARISON OF ESTIMATED AND CALCULATED EFFECTIVE POROSITY. <i>HYDROGEOLOGY JOURNAL</i> (1998) 6:156–165.

**APPLICATION FOR PERMIT  
DNCS ENVIRONMENTAL SOLUTIONS**

**VOLUME III: ENGINEERING DESIGN AND CALCULATIONS  
SECTION 9 SETTLEMENT CALCULATIONS**

**1.0 INTRODUCTION**

DNCS Environmental Solutions (DNCS Facility) is a proposed Surface Waste Management Facility for oil field waste processing and disposal services. The proposed DNCS Facility is subject to regulation under the New Mexico Oil and Gas Rules, specifically 19.15.36 NMAC, administered by the Oil Conservation Division (OCD). The Facility has been designed in compliance with 19.15.36 NMAC, and will be constructed and operated in compliance with a Surface Waste Management Facility Permit issued by the OCD. The Facility is owned by, and will be constructed and operated by, DNCS Properties, LLC.

**1.1 Description**

The DNCS site is comprised of a 562-acre  $\pm$  tract of land located south of NM 529 in portions of Section 31, Township 17 South, Range 33 East; and in the northern half of Section 6, Township 18 South, Range 33 East, Lea County, NM. A portion of the 562-acre tract is a drainage feature that will be excluded from development. The drainage feature includes a 500-ft setback and totals 67 acres  $\pm$ . The DNCS Facility will include two main components; a liquid oil field waste Processing Area (177 acres  $\pm$ ), and an oil field waste Landfill (318 acres  $\pm$ ); therefore the DNCS Facility comprises 495 acres  $\pm$ . Oil field wastes are anticipated to be delivered to the DNCS Facility from oil and gas exploration and production operations in southeastern NM and west Texas. The Site Development Plan provided in the **Permit Plans, Sheet 3**, identifies the locations of the Processing Area and Landfill facilities.

**2.0 DESIGN CRITERIA**

The slope of the final cover, liner and leachate collection piping after settlement must be consistent with the performance specifications for leachate collection and stormwater control. That is, the final cover and leachate collection system must allow adequate stormwater to runoff to the management controls, and to convey generated leachate such that the head on the high density polyethylene (HDPE) flexible membrane liner (FML) does not exceed 12 inches (30 centimeters).

### 3.0 FOUNDATION SOILS SETTLEMENT

The methodology for estimating floor potential settlement involves selecting points on the landfill floor surface, computing the settlement at each point, and evaluating the resultant change in surface elevation. Points were conservatively selected from a cross-section where the waste and fill material is thickest. Qian et al. (2002), present a method to determine landfill foundation settlement that evaluates elastic, primary, and secondary settlement. The foundation soils at the DNCS site are predominately a mixture of sand with varying amounts of fines and clay. Recent laboratory testing evaluated a mixture of sands and silty sands (i.e., USCS Classifications SM, SC) in the excavation area. **Attachment III.9.A** provides a summary of the laboratory testing results compiled from samples at applicable depths from geotechnical borings installed on-site. Since the foundation soils consist of silty sands, very sandy clays and a mixture of sands and silty sands, elastic settlement is conservatively assumed for this calculation. The elastic settlement is estimated using equation 12.20 from **Attachment III.9.B, p. 469**.

$$Z_e = \left( \frac{\Delta\sigma}{M_s} \right) H_o$$

Where:

- Z<sub>e</sub>** = elastic settlement of soil layer (ft)
- H<sub>o</sub>** = initial thickness of soil layer (ft)
- Δσ** = increment of vertical effective stress, lb/ft<sup>2</sup>
- M<sub>s</sub>** = constrained modulus of soil, lb/ft<sup>2</sup>

The constrained modulus is provided in equation 12.21 from **Attachment III.9.B, p. 470**.

$$M_s = \frac{E_s(1 - \nu_s)}{(1 + \nu_s)(1 - 2\nu_s)}$$

Where:

- M<sub>s</sub>** = constrained modulus of soil, lb/ft<sup>2</sup>
- E<sub>s</sub>** = elastic modulus of soil (lb/ft<sup>2</sup>) **Attachment III.9.B, p. 310**  
E<sub>s</sub> was interpolated from the data from Table 9.5, p. 310 (**Attachment III.9.B**) for CL, MH, GC, SC soils between 85% and 95% standard Proctor dry density to determine E<sub>s</sub> for 90% as specified in the subgrade soils. E<sub>s</sub> = (800 psi + 1,500 psi)/2 = 1,150 psi x 144 in<sup>2</sup>/ft<sup>2</sup> = 165,600 lb/ft<sup>2</sup>.
- ν<sub>s</sub>** = Poisson's ratio for soil = 0.39, which was found using the same method to estimate the elastic modulus of soil.

Settlement is estimated at the select locations (Points A1 through A40, and Points B1 through B26) shown on the landfill cross-sections (**Figure III.9.1**). An example calculation is demonstrated at point A21 on Cross Section A-A', with a total overburden depth of 159.03 ft. (final cover + intermediate cover + waste + protective soil layer).

### **Point A21**

#### *Elastic Foundation Soil Settlement*

Thickness of Waste = 153.03 ft. (assume entire thickness of waste from intermediate cover to top of protective soil layer; this provides a conservative analysis)

Unit Weight of Soil = 110 lb/ft<sup>3</sup> Dry Density

Unit Weight of Waste = 74 lb/ft<sup>3</sup>

$\Delta\sigma =$  (waste effective stress) + (protective soil layer effective stress) + (intermediate cover effective stress) + (final cover effective stress)

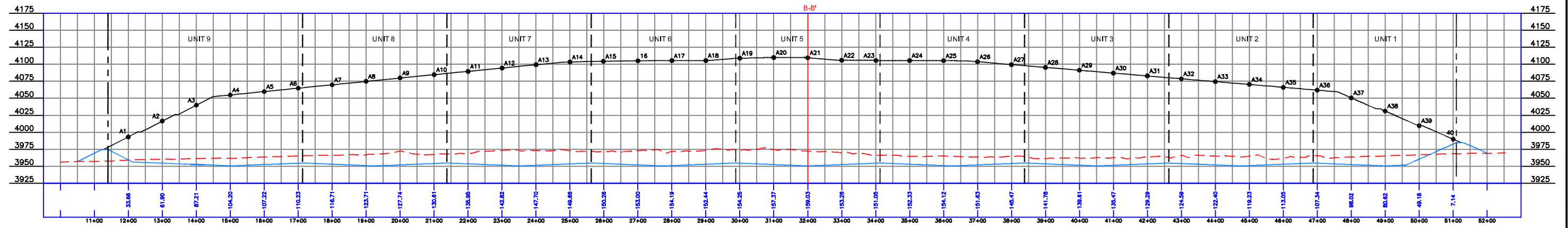
$$\Delta\sigma = (153.03 \text{ ft})(74 \text{ lb/ft}^3) + (2 \text{ ft})(110 \text{ lb/ft}^3) + (1 \text{ ft})(110 \text{ lb/ft}^3) + (3.0 \text{ ft})(110 \text{ lb/ft}^3) = 11,984.22 \text{ lb/ft}^2$$

$$M_s = \frac{165,600 \text{ lb/ft}^2 (1 - 0.39)}{(1 + 0.39)(1 - 2 * 0.39)} = 330,333.55 \text{ lb/ft}^2$$

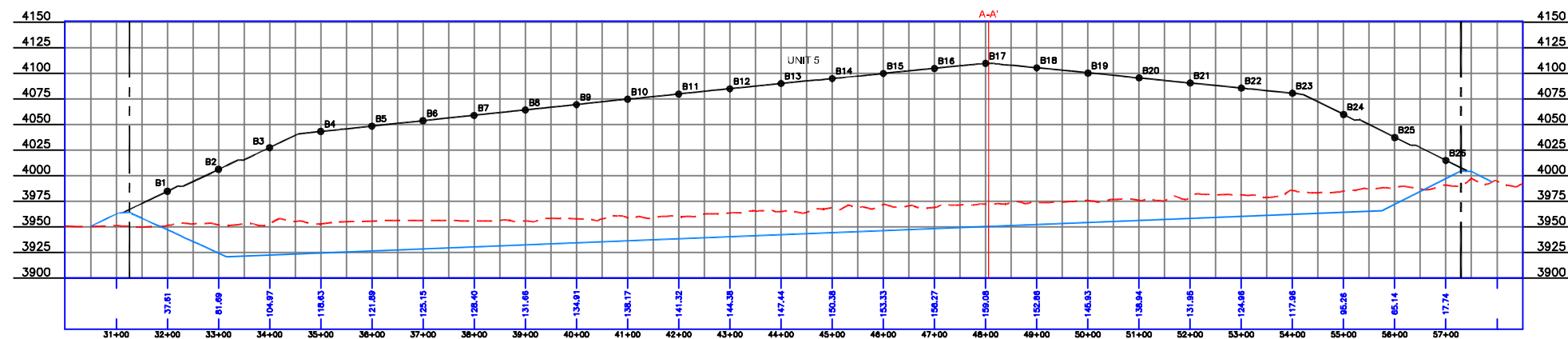
H<sub>o</sub> = 153.03 ft. the full thickness of the compressible CL, MH, GC, SC soils; the compressible soil is considered incompressible at the depth of 45 ft.

$$Z_e = \left( \frac{11,984.22}{330,333.55} \right) 45 \text{ ft} = 1.63 \text{ ft}$$

Settlement between points A21 and A22 = 1.57 ft. – 1.63 ft. = - 0.06 ft.



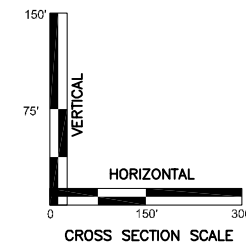
CROSS SECTION A-A'



CROSS SECTION B-B'

**LEGEND**

- LIMIT OF WASTE
- - - CELL BOUNDARY
- - - EXISTING GRADE
- BASE GRADE
- FINAL GRADE
- B3 SETTLEMENT POINT LOCATION



**SETTLEMENT POINTS**

DNCS ENVIRONMENTAL SOLUTIONS  
LEA COUNTY, NEW MEXICO



213 S. Camino del Pueblo  
Bernalillo, New Mexico, USA  
Phone: 505-867-6990  
Fax: 505-867-6991

DATE: 11/04/2013	CAD: SETTLEMENT PTS.dwg	PROJECT #: 542.01.01
DRAWN BY: JMC	REVIEWED BY: DRT	FIGURE III.9.1
APPROVED BY: IKG	gei@gordonenvironmental.com	

Change in slope of base grade:

Elevation of base grade at point A21 = Approximately 3,950.53 ft.

Updated elevation of base grade at point 22 = 3,952.53 ft. – 0.06 ft. = 3,952.47 ft.

$$\text{Updated base grade slope} = \frac{(3,952.47 \text{ ft} - 3,950.53 \text{ ft})}{100 \text{ ft}} \times 100 = 1.94\%$$

Change in base grade slope = 2.0% - 1.94% = 0.06%

The angular distortion between points A21 and A22 is determined as follows:

$$\text{Distortion} = \frac{(\text{Settlement}_{A13} - \text{Settlement}_{A14})}{\text{distance}} * 100$$

$$\text{Distortion} = \frac{(1.57 \text{ ft} - 1.63 \text{ ft})}{100 \text{ ft}} * 100 = - 0.06\%$$

A summary of potential foundation soils settlement is provided in **Tables III.9.1** and **III.9.2**. The angular distortion between each point is calculated as above. The maximum angular distortion of the foundation soils on the floor (i.e., settlement points A2 to A38 and B3 to B24) of the landfill is 0.26% between points A2 and A3 on Cross-Section A-A'. The minimum slope on the landfill floor; perpendicular to the leachate collection pipe is approximately 1.86% after settlement. Additionally, the minimum slope of the leachate collection pipe is 1.86% to the leachate collection sump. These slopes are adequate and will ensure that the design and performance standards for the leachate collection system will be met.

**TABLE III.9.1**  
**Settlement and Angular Distortion of Foundation Soils Between Points**  
**Cross Section A-A'**  
**DNCS Environmental Solutions**

Point Location	Total Settlement (feet)	Distance Between Points (feet)	Angular Distortion (%)	Distortion Direction	Design Base grade Elevation (feet)	Design Slope Between Point Locations (%)	Updated Base grade Elevation (feet)	Updated Slope Between Point Locations (%)
A1	0.276	100	0.378	▼	3959.52	22.00	3959.24	21.90
A2	0.653	100	0.255	▼	3954.55	2.00	3953.90	1.88
A3	0.909	100	0.171	▼	3952.55	2.00	3951.64	1.92
A4	1.080	100	0.030	▼	3950.55	2.00	3949.47	1.86
A5	1.110	100	0.030	▼	3952.53	2.00	3951.42	2.00
A6	1.141	100	0.065	▼	3954.53	2.00	3953.39	1.97
A7	1.206	100	0.071	▼	3953.05	2.00	3951.84	1.99
A8	1.277	100	0.041	▼	3951.05	2.00	3949.77	1.97
A9	1.317	100	0.029	▼	3952.03	2.00	3950.71	1.99
A10	1.346	100	0.054	▼	3954.03	2.00	3952.68	1.98
A11	1.400	100	0.069	▼	3953.55	2.00	3952.15	1.98
A12	1.469	100	0.049	▼	3951.55	2.00	3950.08	1.98
A13	1.518	100	0.020	▼	3951.53	2.00	3950.01	1.97
A14	1.538	100	0.006	▼	3953.53	2.00	3951.99	1.99
A15	1.544	100	0.028	▼	3954.05	2.00	3952.51	1.98
A16	1.572	100	0.012	▼	3952.05	2.00	3950.48	1.98
A17	1.584	100	-0.018	▲	3951.03	2.00	3949.45	1.99
A18	1.566	100	0.018	▼	3953.03	2.00	3951.46	2.00
A19	1.584	100	0.031	▼	3954.55	2.00	3952.97	1.99
A20	1.616	100	0.017	▼	3952.55	2.00	3950.93	1.99
A21	1.633	100	-0.058	▲	3950.55	2.00	3948.92	1.94
A22	1.574	100	-0.022	▲	3952.53	2.00	3950.96	1.96
A23	1.552	100	0.013	▼	3954.53	2.00	3952.98	1.99
A24	1.565	100	0.018	▼	3953.05	2.00	3951.48	1.99
A25	1.583	100	-0.025	▲	3951.05	2.00	3949.47	1.96

**Notes:**

Points Correspond to **Figure III.9.1**

▲ = potential upward distortion

▼ = potential downward distortion

Elevations based on NM State Plan Coordinate System

**TABLE III.9.1**  
**Settlement and Angular Distortion of Foundation Soils Between Points**  
**Cross Section A-A'**  
**DNCS Environmental Solutions**

Point Location	Total Settlement (feet)	Distance Between Points (feet)	Angular Distortion (%)	Distortion Direction	Design Base grade Elevation (feet)	Design Slope Between Point Locations (%)	Updated Base grade Elevation (feet)	Updated Slope Between Point Locations (%)
A26	1.558	100	-0.062	▲	3952.03	2.00	3950.47	2.02
A27	1.496	100	-0.037	▲	3954.03	2.00	3952.53	1.98
A28	1.459	100	-0.022	▲	3953.55	2.00	3952.09	2.02
A29	1.437	100	-0.042	▲	3951.55	2.00	3950.11	2.02
A30	1.395	100	-0.062	▲	3951.53	2.00	3950.13	2.01
A31	1.333	100	-0.047	▲	3953.53	2.00	3952.20	2.03
A32	1.285	100	-0.022	▲	3954.05	2.00	3952.76	2.01
A33	1.263	100	-0.032	▲	3952.05	2.00	3950.79	2.03
A34	1.231	100	-0.062	▲	3951.03	2.00	3949.80	2.00
A35	1.169	100	-0.058	▲	3953.03	2.00	3951.86	1.96
A36	1.111	100	-0.094	▲	3954.55	2.00	3953.44	2.08
A37	1.018	100	-0.175	▲	3952.55	2.00	3951.53	2.14
A38	0.842	100	-0.317	▲	3950.55	2.00	3949.71	1.81
A39	0.525	100	-0.509	▲	3960.42	22.00	3959.89	22.49
A40	0.016				3982.62	22.00	3982.60	

**Notes:**

Points Correspond to **Figure III.9.1**

▲ = potential upward distortion

▼ = potential downward distortion

Elevations based on NM State Plan Coordinate System

**TABLE III.9.2**  
**Settlement and Angular Distortion of Foundation Soils Between Points**  
**Cross Section B-B'**  
**DNCS Environmental Solutions**

Point Location	Total Settlement (feet)	Distance Between Points (feet)	Angular Distortion (%)	Distortion Direction	Design Base grade Elevation (feet)	Design Slope Between Point Locations (%)	Updated Base grade Elevation (feet)	Updated Slope Between Point Locations (%)
B1	0.341	100	0.511	▼	3947.12	22.75	3946.61	22.47
B2	0.853	100	0.235	▼	3924.37	22.75	3924.14	22.65
B3	1.088	100	0.138	▼	3922.42	2.00	3922.28	2.10
B4	1.225	100	0.033	▼	3924.42	2.00	3924.39	2.00
B5	1.258	100	0.033	▼	3926.42	2.00	3926.39	2.00
B6	1.291	100	0.033	▼	3928.42	2.00	3928.39	2.00
B7	1.324	100	0.033	▼	3930.42	2.00	3930.39	2.00
B8	1.357	100	0.033	▼	3932.42	2.00	3932.39	2.00
B9	1.389	100	0.033	▼	3934.42	2.00	3934.39	2.00
B10	1.422	100	0.032	▼	3936.42	2.00	3936.39	2.00
B11	1.454	100	0.031	▼	3938.42	2.00	3938.39	2.00
B12	1.485	100	0.031	▼	3940.42	2.00	3940.39	2.00
B13	1.516	100	0.030	▼	3942.42	2.00	3942.39	2.00
B14	1.545	100	0.030	▼	3944.42	2.00	3944.39	2.00
B15	1.575	100	0.030	▼	3946.42	2.00	3946.39	2.00
B16	1.605	100	0.028	▼	3948.42	2.00	3948.39	1.97
B17	1.633	100	-0.063	▲	3950.42	2.00	3950.36	1.99
B18	1.570	100	-0.070	▲	3952.42	2.00	3952.35	2.00
B19	1.501	100	-0.070	▲	3954.42	2.00	3954.35	2.00
B20	1.430	100	-0.070	▲	3956.42	2.00	3956.35	2.00
B21	1.360	100	-0.070	▲	3958.42	2.00	3958.35	2.00
B22	1.289	100	-0.071	▲	3960.42	2.00	3960.35	1.84
B23	1.219	100	-0.229	▲	3962.42	2.00	3962.19	1.93
B24	0.990	100	-0.304	▲	3964.42	2.00	3964.12	1.70
B25	0.686	100	-0.604	▲	3972.14	25.00	3971.54	25.52
B26	0.082				3997.15	25.00	3997.07	

**Notes:**

Points Correspond to **Figure III.9.1**

▲ = potential upward distortion

▼ = potential downward distortion

Elevations based on NM State Plan Coordinate System

#### 4.0 WASTE SETTLEMENT CALCULATIONS

The methodology to estimate waste settlement involves selecting key points on the final cover surface, computing the settlement at each point, and evaluating the resultant change in surface elevation. Points were selected from Cross-Sections A-A' and B-B' (**Figure III.9.1**). Qian et al. (2002; **Attachment III.9.B**) present a method developed by Sowers (1973) for determining settlement in landfills. This method is based on developed soils consolidation theory, which relates settlement to layer thickness and changes in void ratio.

The primary settlement is estimated using equation 12.4 (**Attachment III.9.B, p. 449**):

$$\Delta H_c = C_c \frac{H_o}{1 + e_o} \log \frac{\sigma_i}{\sigma_o}$$

Where:

- $\Delta H_c$  = primary settlement
- $C_c/(1+e_o) = 0.006$  (**Attachment III.9.C, p. 393,  $D_r = 80\%$** )
- $H_o$  = initial thickness of the waste layer before settlement (assume entire thickness of waste from intermediate cover to the top of protective soil layer; this provides a conservative analysis) [**Figure III.9.1**] = 153.03 ft.
- $\sigma_o$  = previously applied pressure in waste layer (assumed to equal the compaction pressure = 1,000 lbs/ft<sup>2</sup>)
- $\sigma_i$  = total overburden pressure applied at the mid-level of the waste layer (lbs/ft<sup>2</sup>)

Long-term secondary settlement is estimated by equation 12.10 (**Attachment III.9.B, p.451**):

$$\Delta H_s = C_a \frac{H_o}{1 + e_o} \log \frac{t_2}{t_1}$$

Where:

- $\Delta H_s$  = secondary settlement
- $C_a = \frac{1}{3} [C_c/(1+e_o)] = 0.002$  (**Attachment III.9.C, p. 393**)
- $H_o$  = waste thickness at start of secondary settlement = H-H<sub>c</sub> (**Figure III.9.1**)
- $t_1$  = starting time of secondary settlement (1 year)
- $t_2$  = ending time of secondary settlement = Assume 30 years

Settlement is estimated at the key locations (Points A1 through A40 and Points B1 through B26) shown on the landfill Cross-Sections A-A' and B-B' (**Figures III.9.1**). An example calculation is demonstrated at point A21, the location of maximum waste depth for Cross-Sections A-A' (i.e., 153 ft).

## **Point A21**

### *Primary Waste Settlement*

Maximum Thickness of Waste = 153.03 ft.

$$\Delta H_c = C_c \frac{H_o}{1 + e_o} \log \frac{\sigma_i}{\sigma_o}$$

Where:

$$C_c / (1 + e_o) = 0.006 \text{ (Attachment III.9.C, p. 393, } D_r = 80\%)$$

$$H_o = 153.03 \text{ ft.}$$

$$\sigma_o = 1,000 \text{ lbs/ft}^2 \text{ (Typical compaction of waste as found in New Mexico)}$$

$$\sigma_i = 0.5[(153.03 \text{ ft.})(74 \text{ lbs/ft}^3) + 4.0 \text{ ft. (110 lbs /ft}^2)] = 5,882.11 \text{ lbs/ft}^2$$

$$\Delta H_c = 0.006 \times 153.03 \times \log \frac{5,882.11 \frac{\text{lbs}}{\text{ft}}}{1,000 \frac{\text{lbs}}{\text{ft}^2}}$$

$$\Delta H_c = 0.71 \text{ ft.}$$

### *Secondary Waste Settlement*

$$H_o = 153.03 \text{ ft.} - 0.71 \text{ ft.} = 152.32 \text{ ft.}$$

$$\Delta H_s = 0.002 \times 152.32 \log \frac{30 \text{ years}}{1 \text{ years}} = 0.45 \text{ ft}$$

$$\text{Total waste settlement} = 0.71 \text{ ft.} + 0.45 \text{ ft.} = 1.16 \text{ ft.}$$

The maximum final settlement of waste is the sum of primary and secondary settlement at point A21. The waste settlement is 0.71 ft. + 0.45 ft. = 1.16 ft, which has nominal impact on the corresponding calculations for slope, runoff, etc. A summary of potential waste settlement is provided in **Tables III.9.3 and III.9.4.**

**TABLE III.9.3**  
**Waste Settlement and Angular Distortion Between Points**  
**Cross Section A-A'**  
**DNCS Environmental Solutions**

Point Location	Total Settlement (feet)	Distance Between Points (feet)	Angular Distortion (%)	Distortion Direction
A1	0.10	100	0.19	▼
A2	0.29	100	0.20	▼
A3	0.49	100	0.15	▼
A4	0.63	100	0.03	▼
A5	0.66	100	0.03	▼
A6	0.69	100	0.06	▼
A7	0.75	100	0.07	▼
A8	0.81	100	0.04	▼
A9	0.85	100	0.03	▼
A10	0.88	100	0.05	▼
A11	0.93	100	0.07	▼
A12	1.00	100	0.05	▼
A13	1.04	100	0.02	▼
A14	1.06	100	0.01	▼
A15	1.07	100	0.03	▼
A16	1.10	100	0.01	▼
A17	1.11	100	-0.02	▲
A18	1.09	100	0.02	▼
A19	1.11	100	0.03	▼
A20	1.14	100	0.02	▼
A21	1.16	100	-0.06	▲
A22	1.10	100	-0.02	▲
A23	1.08	100	0.01	▼
A24	1.09	100	0.02	▼
A25	1.11	100	-0.02	▲

**Notes:**

Points Correspond to **Figure III.9.1**

▲ = potential upward distortion

▼ = potential downward distortion

Elevations based on NM State Plan Coordinate System

**TABLE III.9.3**  
**Waste Settlement and Angular Distortion Between Points**  
**Cross Section A-A'**  
**DNCS Environmental Solutions**

Point Location	Total Settlement (feet)	Distance Between Points (feet)	Angular Distortion (%)	Distortion Direction
A26	1.08	100	-0.06	▲
A27	1.02	100	-0.04	▲
A28	0.99	100	-0.02	▲
A29	0.96	100	-0.04	▲
A30	0.92	100	-0.06	▲
A31	0.87	100	-0.04	▲
A32	0.82	100	-0.02	▲
A33	0.80	100	-0.03	▲
A34	0.77	100	-0.06	▲
A35	0.71	100	-0.05	▲
A36	0.66	100	-0.08	▲
A37	0.58	100	-0.15	▲
A38	0.43	100	-0.24	▲
A39	0.19	100	-0.20	▲
A40	0.00			

**Notes:**

Points Correspond to *Figure III.9.1*

▲ = potential upward distortion

▼ = potential downward distortion

Elevations based on NM State Plan Coordinate System

**TABLE III.9.4**  
**Waste Settlement and Angular Distortion Between Points**  
**Cross Section B-B'**  
**DNCS Environmental Solutions**

Point Location	Total Settlement (feet)	Distance Between Points (feet)	Angular Distortion (%)	Distortion Direction
B1	0.12	100	0.32	▼
B2	0.44	100	0.20	▼
B3	0.64	100	0.12	▼
B4	0.77	100	0.03	▼
B5	0.80	100	0.03	▼
B6	0.83	100	0.03	▼
B7	0.86	100	0.03	▼
B8	0.89	100	0.03	▼
B9	0.92	100	0.03	▼
B10	0.95	100	0.03	▼
B11	0.98	100	0.03	▼
B12	1.01	100	0.03	▼
B13	1.04	100	0.03	▼
B14	1.07	100	0.03	▼
B15	1.10	100	0.03	▼
B16	1.13	100	0.03	▼
B17	1.16	100	0.03	▼
B18	1.09	100	-0.06	▲
B19	1.03	100	-0.07	▲
B20	0.96	100	-0.07	▲
B21	0.89	100	-0.07	▲
B22	0.82	100	-0.07	▲
B23	0.76	100	-0.07	▲
B24	0.56	100	-0.20	▲
B25	0.31	100	-0.25	▲
B26	0.02	100	-0.29	▲

**Notes:**

Points Correspond to **Figure III.9.1**

▲ = potential upward distortion

▼ = potential downward distortion

Elevations based on NM State Plan Coordinate System

## 5.0 SOIL COVER SETTLEMENT CALCULATIONS

The final cover soil layer consisting of vegetative, barrier, and intermediate cover layers will also experience nominal consolidation due to its own weight. The method for evaluating settlement of the soil cover and cushion layers is based on equation B.2 (**Attachment III.9.D, p. 569**).

### *Primary Soil Settlement*

$$\Delta H_p = C_c \frac{H_p}{1 + e_s} \log \frac{P_o + \Delta P}{P_o}$$

$$C_c / (1 + e_o) = 0.006 \text{ (**Attachment III.9.C, p. 393, } D_r = 80\%**)}$$

Thickness of Soil = H = 3.0 feet of final cover + 1 foot of intermediate cover soil + 2 feet of protective soil layer = 6 ft.

Unit Weight of Soil = 110 lb/ft<sup>3</sup> Dry Density

$$\Delta P = (3.0 \text{ ft.}) (110 \text{ lb/ft}^3) + (1 \text{ ft.}) (110 \text{ lb/ft}^3) + (2.0 \text{ ft.}) (110 \text{ lb/ft}^3) = 660.0 \text{ lb/ft}^2$$

$$P_o = \frac{H}{2} (110 \text{ lb/ft}^3) = 3.0(110) = 330 \text{ lb/ft}^2$$

$$\Delta H_p = (0.006)(6.0 \text{ ft.}) \log \left( \frac{330 \frac{\text{lbs}}{\text{ft}^2} + 660 \frac{\text{lbs}}{\text{ft}^2}}{330 \frac{\text{lbs}}{\text{ft}^2}} \right)$$

$$\Delta H_p = 0.017 \text{ ft}$$

### *Secondary Soil Cover Settlement*

$$\Delta H_s = C_s \frac{H_o}{1 + e_s} \log \frac{t_2}{t_1}$$

$$C_\alpha = \frac{1}{3} [C_c / (1 + e_o)] = 0.002 \text{ (**Attachment III.9.C, p. 393**)}$$

$$H_o = 6.0 \text{ ft.} - 0.017 \text{ ft.} = 5.98 \text{ ft.}$$

$$\Delta H_s = 0.002 (5.98 \text{ ft.}) \log \frac{30}{1} = 0.018 \text{ ft}$$

The maximum settlement of the final cover is the sum of primary and secondary settlement at point A21. The soil final cover layer settlement is equal to 0.017 ft. + 0.018 ft. = 0.035 ft. The maximum angular distortion at the level of the top of final cover occurs between points A11 and A12 and equals 0.07%. Therefore, after conservative assumptions for settlement, the minimum slope of the final cover (5% grade) will be  $5\% - 0.07\% = 4.93\%$ , which has nominal impacts on the slope and runoff calculations.

## 6.0 CONCLUSION

Settlement projections have been calculated for the landfill foundation, the waste mass and for the landfill final soil cover. Settlement estimates include elastic deformation and both primary and secondary consolidation in the foundations soils, in the waste, and in the cover materials. The greatest value of projected settlement in both the foundation soils and in the waste occurs where the waste thickness is greatest (Point A21).

The maximum final settlement of the landfill foundation, waste mass and landfill cover is the sum of primary and secondary settlement at point A21. The foundation soil settlement is equal to 1.63 ft, the waste settlement is equal to 0.71 ft. + 0.45 ft. = 1.16 ft, and the final cover layer settlement is calculated at 0.035 ft. Maximum total settlement that could occur on the final cover of the landfill is the sum of the foundation soil, waste, and cover settlement (i.e.: 1.63 ft + 1.16 ft + 0.035 ft = 2.82 ft). The methodology used to determine settlement at point A21 was used to find the settlement of points A1-A40 for Cross-Section A-A', and points B1-B26 for Cross-Section B-B'. The total settlement for the points on Cross-Sections A-A' and B-B' and the angular distortion between them, is provided on **Table III.9.5** through **Table III.9.6**.

The slope of the final cover, liner and leachate collection pipe after settlement is adequate and consistent with the performance specifications for the leachate collection system and stormwater controls and the regulatory standards.

**TABLE III.9.5**  
**Total Settlement and Angular Distortion Between Points**  
**Cross Section A-A'**  
**DNCS Environmental Solutions**

Point Location	Total Settlement (feet)	Distance Between Points (feet)	Angular Distortion (%)	Distortion Direction	Design Final grade Elevation (feet)	Design Slope Between Point Locations (%)	Updated Final grade Elevation (feet)	Updated Slope Between Point Locations (%)
A1	0.408	100	0.566	▼	3993.19	25.00	3992.78	24.43
A2	0.974	100	0.457	▼	4016.45	25.00	4015.48	24.54
A3	1.431	100	0.319	▼	4039.76	25.00	4038.33	24.68
A4	1.749	100	0.057	▼	4054.75	5.00	4053.00	4.94
A5	1.807	100	0.058	▼	4059.75	5.00	4057.94	4.94
A6	1.864	100	0.125	▼	4064.76	5.00	4062.90	4.88
A7	1.989	100	0.136	▼	4069.76	5.00	4067.77	4.86
A8	2.124	100	0.079	▼	4074.76	5.00	4072.64	4.92
A9	2.203	100	0.056	▼	4079.77	5.00	4077.57	4.94
A10	2.259	100	0.105	▼	4084.64	5.00	4082.38	4.90
A11	2.364	100	0.136	▼	4089.50	5.00	4087.14	4.86
A12	2.500	100	0.097	▼	4094.37	5.00	4091.87	4.90
A13	2.597	100	0.039	▼	4099.23	5.00	4096.63	4.96
A14	2.636	100	0.012	▼	4103.19	5.00	4100.55	4.99
A15	2.648	100	0.055	▼	4104.31	5.00	4101.66	4.95
A16	2.703	100	0.024	▼	4105.05	5.00	4102.35	4.98
A17	2.727	100	-0.035	▲	4105.22	5.00	4102.49	5.04
A18	2.692	100	0.036	▼	4105.47	5.00	4102.78	4.96
A19	2.728	100	0.063	▼	4108.80	5.00	4106.07	4.94
A20	2.791	100	0.033	▼	4109.92	5.00	4107.13	5.03
A21	2.824	100	-0.116	▲	4109.58	5.00	4106.76	4.88
A22	2.708	100	-0.044	▲	4105.79	5.00	4103.08	4.96
A23	2.664	100	0.026	▼	4105.58	5.00	4102.92	5.03
A24	2.690	100	0.036	▼	4105.38	5.00	4102.69	5.04
A25	2.725	100	-0.050	▲	4105.17	5.00	4102.44	4.95

**Notes:**

Points Correspond to **Figure III.9.1**

▲ = potential upward distortion

▼ = potential downward distortion

Elevations based on NM State Plan Coordinate System

**TABLE 9.5**  
**Total Settlement and Angular Distortion Between Points**  
**Cross Section A-A'**  
**DNCS Environmental Solutions**

Point Location	Total Settlement (feet)	Distance Between Points (feet)	Angular Distortion (%)	Distortion Direction	Design Final grade Elevation (feet)	Design Slope Between Point Locations (%)	Updated Final grade Elevation (feet)	Updated Slope Between Point Locations (%)
A26	2.676	100	-0.123	▲	4103.66	5.00	4100.98	4.88
A27	2.553	100	-0.073	▲	4099.50	5.00	4096.95	4.93
A28	2.479	100	-0.043	▲	4095.33	5.00	4092.85	4.96
A29	2.436	100	-0.082	▲	4091.16	5.00	4088.72	4.92
A30	2.355	100	-0.121	▲	4087.00	5.00	4084.65	4.88
A31	2.233	100	-0.092	▲	4082.82	5.00	4080.59	4.91
A32	2.141	100	-0.043	▲	4078.63	5.00	4076.49	4.96
A33	2.099	100	-0.061	▲	4074.45	5.00	4072.35	4.94
A34	2.037	100	-0.119	▲	4070.26	5.00	4068.22	4.88
A35	1.918	100	-0.109	▲	4066.08	5.00	4064.16	4.89
A36	1.809	100	-0.177	▲	4061.89	5.00	4060.08	4.82
A37	1.632	100	-0.323	▲	4050.57	25.00	4048.94	24.68
A38	1.309	100	-0.555	▲	4031.17	25.00	4029.86	24.45
A39	0.755	100	-0.704	▲	4009.60	25.00	4008.85	24.30
A40	0.050				3989.76	25.00	3989.71	

**Notes:**

Points Correspond to **Figure III.9.1**

▲ = potential upward distortion

▼ = potential downward distortion

Elevations based on NM State Plan Coordinate System

**TABLE III.9.6**  
**Total Settlement and Angular Distortion Between Points**  
**Cross Section B-B'**  
**DNCS Environmental Solutions**

Point Location	Total Settlement (feet)	Distance Between Points (feet)	Angular Distortion (%)	Distortion Direction	Design Final grade Elevation (feet)	Design Slope Between Point Locations (%)	Updated Final grade Elevation (feet)	Updated Slope Between Point Locations (%)
B1	0.497				3984.73	25.00	3984.23	
B2	1.329	100	0.832	▼	4006.06	25.00	4004.73	24.17
B3	1.764	100	0.435	▼	4027.38	25.00	4025.62	24.57
B4	2.026	100	0.262	▼	4043.05	5.00	4041.02	24.74
B5	2.089	100	0.063	▼	4048.31	5.00	4046.22	4.94
B6	2.152	100	0.063	▼	4053.56	5.00	4051.41	4.94
B7	2.216	100	0.063	▼	4058.82	5.00	4056.60	4.94
B8	2.280	100	0.064	▼	4064.07	5.00	4061.79	4.94
B9	2.344	100	0.064	▼	4069.33	5.00	4066.99	4.94
B10	2.408	100	0.064	▼	4074.58	5.00	4072.17	4.94
B11	2.470	100	0.062	▼	4079.74	5.00	4077.27	4.94
B12	2.531	100	0.061	▼	4084.79	5.00	4082.26	4.94
B13	2.592	100	0.061	▼	4089.85	5.00	4087.26	4.94
B14	2.651	100	0.059	▼	4094.80	5.00	4092.15	4.94
B15	2.710	100	0.059	▼	4099.74	5.00	4097.03	4.94
B16	2.769	100	0.059	▼	4104.68	5.00	4101.91	4.94
B17	2.825	100	0.057	▼	4109.50	5.00	4106.67	4.94
B18	2.700	100	-0.125	▲	4105.28	5.00	4102.58	4.88
B19	2.562	100	-0.138	▲	4100.35	5.00	4097.79	4.86
B20	2.423	100	-0.139	▲	4095.36	5.00	4092.94	4.86
B21	2.285	100	-0.138	▲	4090.36	5.00	4088.07	4.86
B22	2.149	100	-0.137	▲	4085.37	5.00	4083.22	4.86
B23	2.013	100	-0.136	▲	4080.38	5.00	4078.37	4.86
B24	1.580	100	-0.432	▲	4059.68	25.00	4058.10	4.57
B25	1.031	100	-0.550	▲	4037.29	25.00	4036.26	24.45
B26	0.139	100	-0.892	▲	4014.89	25.00	4014.75	24.11

**Notes:**

Points Correspond to **Figure III.9.1**

▲ = potential upward distortion

▼ = potential downward distortion

Elevations based on NM State Plan Coordinate System

**APPLICATION FOR PERMIT  
DNCS ENVIRONMENTAL SOLUTIONS**

**VOLUME III: ENGINEERING DESIGN AND CALCULATIONS  
SECTION 9: SETTLEMENT CALCULATIONS**

**ATTACHMENT III.9.A  
SUMMARY OF GEOTECHNICAL LABORATORY TESTING RESULTS**

**ATTACHMENT III.9.A**  
**Soils Laboratory Analyses Summary**  
**DNCS Environmental Solutions**

Sample Number <sup>1</sup>	Sample Depth (ft bgs)	USCS Class <sup>2</sup>	Grain Size Distribution			Atterberg Limits <sup>3</sup> LL - PI	Natural Dry Density (PCF)	Natural Moisture <sup>4</sup> (%)	Standard Proctor		Permeability (cm/sec)	Porosity (%)
			Pass #4 (%)	Pass #40 (%)	Pass #200 (%)				Max. Dry Density (PCF)	Optimum Moisture (%)		
B3-5	5-6.5	SP-SC	100	98	9.0			2.8				
B3-20	20-21.5	SC	100	93	13.0			4.7				
B3-35SS	35-36.5	SC	100	97	14.0			4.6				
B3-35CC	35-40	SP-SC	99	95	11.0			2.2	121.1	11.7		
B3-50.25BR	50.25-50.75	SC	100	94	47.1	32-18	112.3	7.6			9.72E-07	32.1
B3-65	65-66	SC	100	77	18.0			11.6				
B3-85	85-90	CL	100	88	82.1	38-24	112.3	3.3			1.01E-07	32.1
B3-115	115-120	SC	100	66	21.0			12.8				
B3-130	130-135	SC	100	62	20.0			8.7				
B3-145	145-150	SC	100	75	31.0			7.4				
B4-0	0-5	SP-SC	99	92	8.0			11.4				
B4-15	15-20	SP-SC	100	98	7.3			6.8				
B4-30CC	30-35	SP-SC	100	98	7.9			4.8	119.9	12.1		
B4-30SS	30-31.5	SP-SC	100	98	8.9			4.9				
B4-55BR	55-55.75	CL	100	88	85.0	42-19	100.8	9.7			7.89E-07	39.1
B4-80	80-85	SC	100	80	27.0			13.9				
B4-100	100-105	SC	100	83	34.0			13.8				
B4-120	120-125	CL	100	95	93.7	38-23	100.9	2.9				39.0
B4-145	145-150	SC	100	83	34.0			7.9				

Notes:

Blank field indicates test not conducted

<sup>1</sup> See Figure IV.2.6 for locations of borings and Attachment IV.2.A for boring logs.

<sup>2</sup> Unified Soil Classification System: SM = silty sand; SP = poorly graded sand; SC = clayey sand; ML = low-plasticity silt; CL = low-plasticity clay; CH = high-plasticity clay

<sup>3</sup> LL = liquid limit; PI = plasticity index; NV = non viscous; NP = non plastic

<sup>4</sup> Gravimetric basis

R = remolded sample; I = in-situ sample; (DS) = direct shear test on sample X

Combined Samples used for Standard Proctor on Boreholes 3,4,5

For Porosity a Specific Gravity of 165.4 PCF was used; where Porosity =  $1 - (\text{Natural Dry Density} / \text{Specific Gravity})$

**ATTACHMENT III.9.A**  
**Soils Laboratory Analyses Summary**  
**DNCS Environmental Solutions**

Sample Number <sup>1</sup>	Sample Depth (ft bgs)	USCS Class <sup>2</sup>	Grain Size Distribution			Atterberg Limits <sup>3</sup> LL - PI	Natural Dry Density (PCF)	Natural Moisture <sup>4</sup> (%)	Standard Proctor		Permeability (cm/sec)	Porosity (%)
			Pass #4 (%)	Pass #40 (%)	Pass #200 (%)				Max. Dry Density (PCF)	Optimum Moisture (%)		
<b>B5-10</b>	10-15'	SC	98	87	13.0			4.2				
<b>B5-25</b>	25-30	SP-SC	98	92	11.0			0.7				
<b>B5-30CC</b>	30-35	SP-SC	100	97	8.8			4.3	123.3	9.9		
<b>B5-30SS</b>	30-31.5	SP-SC	99	88	11.0			4.8				
<b>B5-45</b>	45-50	SP-SC	100	85	7.2			6.1				
<b>B5-70SS</b>	70-70.5	CL	100	93	84.4	41-22	90.6	13.1				45.2
<b>B5-80</b>	80-85	SC	100	66	19.0			12.2				
<b>B5-90</b>	90-95	SC	100	69	22.0			12.5				
<b>B5-105</b>	105	SC	100	67	21.0			14.4				
<b>B5-125</b>	125-130	SC	100	59	27.0			6.6				
<b>B5-145</b>	145-150	CL	100	90	85.5	36-21	107.2	8.4			7.54E-07	35.2
<b>B6-0</b>	0-5	SP	100	99	3.7			2.1				
<b>B6-7</b>	07-13'	SC	100	93	15.0			7.0				
<b>B6-13</b>	13-27	SC	88	70	21.0			3.5				
<b>B6-20</b>	20-40	SC	95	83	14.0			4.1	118.2	11.0		
<b>B6-27</b>	27-48	SC	97	86	16.0			4.0				
<b>B6-60</b>	60-75	SC	100	90	32.9	25-11	106.2	3.1			1.13E-05	35.1

Notes:

Blank field indicates test not conducted

<sup>1</sup> See **Figure IV.2.6** for locations of borings and **Attachment IV.2.A** for boring logs.

<sup>2</sup> Unified Soil Classification System: SM = silty sand; SP = poorly graded sand; SC = clayey sand; ML = low-plasticity silt; CL = low-plasticity clay; CH = high-plasticity clay

<sup>3</sup> LL = liquid limit; PI = plasticity index; NV = non viscous; NP = non plastic

<sup>4</sup> Gravimetric basis

R = remolded sample; I = in-situ sample; (DS) = direct shear test on sample X

Combined Samples used for Standard Proctor on Boreholes 3,4,5

For Porosity a Specific Gravity of 165.4 PCF was used; where Porosity = 1 - (Natural Dry Density / Specific Gravity)

**APPLICATION FOR PERMIT  
DNCS ENVIRONMENTAL SOLUTIONS**

**VOLUME III: ENGINEERING DESIGN AND CALCULATIONS  
SECTION 9: SETTLEMENT CALCULATIONS**

**ATTACHMENT III.9.B**

**QIAN, XUEDE; KOERNER, ROBERT M.; AND GRAY, DONALD H. 2002.  
*GEOTECHNICAL ASPECTS OF LANDFILL DESIGN AND CONSTRUCTION.*  
NEW YORK: PRENTICE HALL.**

# GEOTECHNICAL ASPECTS OF LANDFILL DESIGN AND CONSTRUCTION

**Xuede Qian**

*Geotechnical Engineering Specialist  
Michigan Department of Environmental Quality*

**Robert M. Koerner**

*H. L. Bowman Professor of Civil Engineering, Drexel University  
Director, Geosynthetic Research Institute*

**Donald H. Gray**

*Professor of Civil and Environmental Engineering  
The University of Michigan*



PRENTICE HALL  
Upper Saddle River, New Jersey 07458

TABLE 6.5 Index Properties of Solid Waste

Source	Unit Weight		Volumetric Moisture Content	Porosity	Void Ratio
	lb/ft <sup>3</sup>	kN/m <sup>3</sup>			
Rovers and Farquhar (1973)	59	9.3	0.16	-	-
Fungaroli (1979)	63	9.9	0.05	-	-
Wigh (1979)	73	11.5	0.08	-	-
Walsh and Kinman (1979)	90	14.1	0.17	-	-
Walsh and Kinman (1981)	89	14.0	0.17	-	-
Schroeder et al. (1984a, b)	-	-	0.28	0.52	1.08
Owels et al. (1990)	40 to 90	6.3 to 14.1	0.10 to 0.20	0.40 to 0.50	0.67 to 1.0
Schroeder et al. (1994a, b)	-	-	0.29	0.67	2.03
Zornberg et al. (1999)	64 to 95	10 to 15	0.30	0.49 to 0.62	1.02 to 1.65

Based on its constituent composition the average moisture content of the solid waste shown in Table 6.4 can be calculated as follows:

$$\begin{aligned}
 w_d &= [(60.0)(10.4) + (50.0)(19.1) + (20.0)(34.6) + (10.0)(6.0) + (15.0)(5.0) \\
 &\quad + (15.0)(9.5) + (2.0)(4.0) + (2.0)(7.2) + (8.0)(2.8) + (3.0)(1.4)]/100 \\
 &= (624 + 955 + 692 + 60 + 75 + 142.5 + 8 + 14.4 + 22.4 + 4.2)/100 \\
 &= 2597.5/100 \\
 &= \underline{26.0\%}
 \end{aligned}$$

Thus, the average dry gravimetric moisture content of the solid waste shown in Table 6.4 is 26.0%.

More information about the moisture content of solid waste can be found in Table 6.5. It should be noted that the values of moisture content listed in Table 6.5 are calculated on a volume basis and differ from those calculated on a weight basis, which is more common to geotechnical analyses.

#### 6.4 POROSITY OF MUNICIPAL SOLID WASTE

Porosity is defined as the ratio of the volume of voids to the total volume occupied by a solid waste or soil. Void ratio is defined as the ratio of the volume of voids to the volume of solids. Porosity can be related to the void ratio by using the relationships

$$n = \frac{e}{1 + e} \quad (6.7)$$

and

$$e = \frac{n}{1 - n} \quad (6.8)$$

where  $n$  = porosity of solid waste; and  
 $e$  = void ratio of solid waste.

The porosity of MSW varies typically from 0.40 to 0.67 depending on the compaction and composition of the waste. For comparison, a typical compacted clay liner material will have a porosity of about 0.40. Table 6.5 shows a summary of the index properties of municipal solid waste, which includes initial volumetric moisture content, initial porosity, initial void ratio and unit weight data.

### 6.5 HYDRAULIC CONDUCTIVITY OF MUNICIPAL SOLID WASTE

Proper assessment of the hydraulic conductivity of municipal solid waste is important in the design of leachate collection systems and in leachate recirculation planning particularly for bioreactor landfills (see Chapter 15). The hydraulic conductivity can be measured using a field leachate pumping test and a large-scale percolation test in test pits or by using large-diameter permeameters in the laboratory.

Hydraulic conductivity measured in test pits at several landfills in Canada by Landva and Clark (1990) is plotted against unit weight in Figure 6.3. The values shown are based on an intermediate stage of water level recession, after the flow had stabilized and before any debris could clog the voids. The measured coefficients of hydraulic conductivity ( $1.0 \times 10^{-3}$  to  $4.0 \times 10^{-2}$  cm/sec) correspond to those associated with clean sand and gravel. Qian (1994) used three-year field data from an active landfill in the state of Michigan to develop a relationship between precipitation and leachate volume from a primary leachate collection system with time. With this information, the hydraulic conductivity of the waste can be calculated based on the water travel time, hydraulic gradient, and waste thickness. The hydraulic conductivity calculated in this way was estimated to be about  $9.2 \times 10^{-4}$  to  $1.1 \times 10^{-3}$  cm/sec. Table 6.6 summarizes the hydraulic conductivity of different types of MSW taken from the

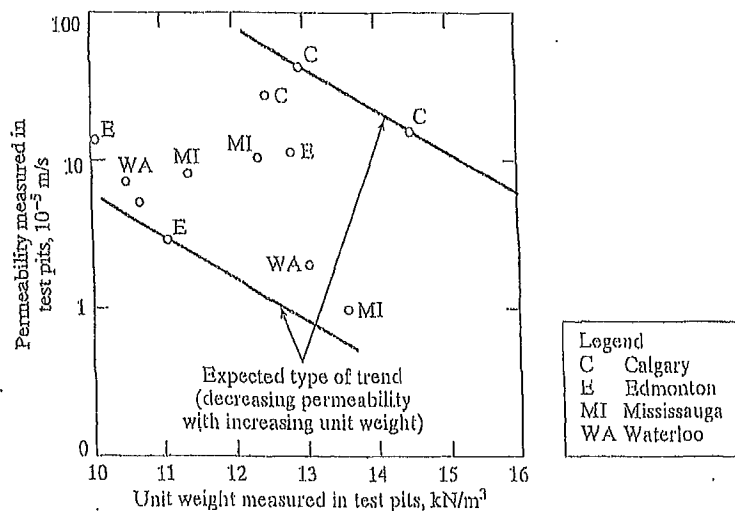
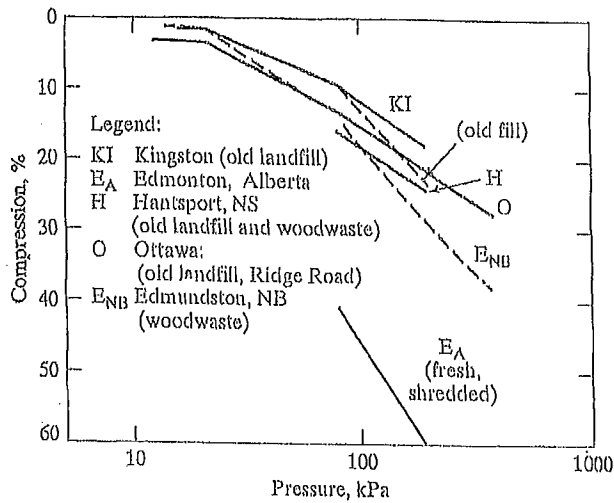


FIGURE 6.3 Unit Weight and Permeability (from Percolation) as Measured in Landfill Test Pits (Landva and Clark, 1990)

FIGURE 6.9 Compressive Strain versus Log Pressure for Various Landfills in Canada (Landva and Clark, 1990)

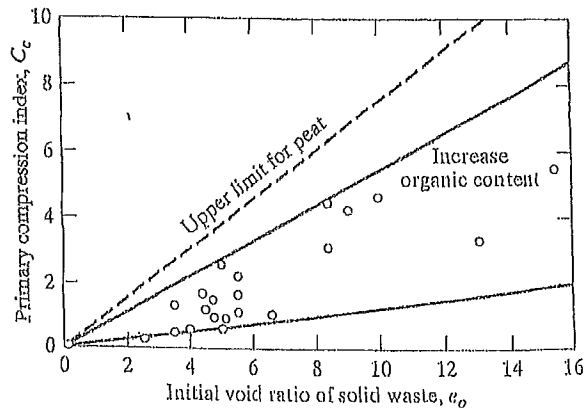


Legend:  
 KI:  $C_c' = 0.17$  ( $p = 20 - 200$  kPa)    O:  $C_c' = 0.21$  ( $p = 100 - 400$  kPa)  
 EA:  $C_c' = 0.35$  ( $p = 80 - 200$  kPa)    ENB:  $C_c' = 0.36$  ( $p = 100 - 400$  kPa)  
 H:  $C_c' = 0.22$  ( $p = 80 - 200$  kPa)

cans; the lower values are for the less resilient materials. The maximum  $C_c$  for peat is about one-third greater than the maximum observed for waste fills.

Landva and Clark (1990) found that the coefficient of secondary consolidation,  $C_{\alpha}$ , (the gradient of the compression versus log time relationship) was in the range 0.2 to 3.0 percent per log cycle time, depending on the type of waste involved. Field testing results using a settlement platform (Keene, 1977) showed that the coefficient of secondary consolidation,  $C_{\alpha}$ , varies between 0.014 and 0.034. Too few tests have been carried out for any firm relationship to be established between the value of  $C_{\alpha}$  and the type of waste, but it does appear that  $C_{\alpha}$  increases with increasing organic content. Sowers (1973) pointed that the coefficient of secondary consolidation,  $C_{\alpha}$ , is also a

FIGURE 6.10 Compressibility of MSW Landfills (Sowers, 1973)



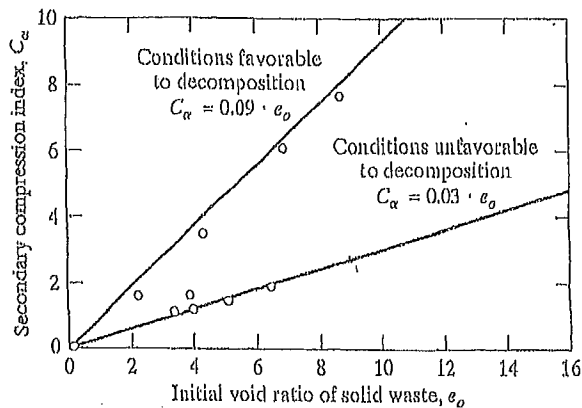


FIGURE 6.11 Secondary Compression of MSW Landfills (Sowers, 1973)

function of the void ratio, as shown in Figure 6.11. For any given void ratio, there is a large range in  $C_{\alpha}$ , related to the potential for physico-chemical and bio-chemical decay. The value is high if the organic content subject to decay is large and the environment is favorable: namely, warm, moist, with fluctuating water table that pumps fresh air into the fill. The value is low for more inert materials and an unfavorable environment. More research and data are necessary before this relationship can be defined more closely.

The most widely reported compressibility parameter is the modified secondary compression index ( $C'_{\alpha}$ ). The reported values of  $C'_{\alpha}$  range from 0.001 to 0.59. The lowest value represents the compressibility of a landfill that had been subjected to dynamic compaction. For typical landfills the lower limit of  $C'_{\alpha}$  is generally around 0.01 to 0.03. This compares to 0.005 to 0.02 for common clays (Holtz and Kovacs, 1981). Fassett et al. (1994) observed that the typical upper limit of  $C'_{\alpha}$  appears to be approximately 0.1.

According to Yen and Scanlon (1975), the settlement rate of waste increases with depth, hence larger values of  $C'_{\alpha}$  should be associated with thicker fills. They observed that this effect leveled off at about 90 ft. and suggested that conditions within the landfill at great depths limit the biological activity to anaerobic decomposition, which is much slower than the aerobic decomposition believed to occur in shallower fills.

The values of  $C_{\alpha}$  and  $C'_{\alpha}$ , like  $C_c$  and  $C'_{c1}$ , are dependent on the values used for  $e_0$  or  $H_0$ . The value of  $C'_{\alpha}$  is also dependent on stress level, time, and on how the origin of time is selected. The waste placement or filling period for landfills is often long and should be taken into consideration for settlement rate analyses (Yen and Scanlon, 1975). The zero time selection has a large impact on  $C'_{\alpha}$  particularly during earlier phases of a landfill (Fassett et al., 1994).

An additional problem with determining  $C'_{\alpha}$  is the fact that this parameter is generally not constant. Edgers (1992) presents settlement log-time data from 22 case histories (shown in Figure 6.12). The majority of the curves show a relatively flat slope (i.e. low  $C'_{\alpha}$  values) at small times, but at larger times the slope greatly increases (Figure 6.13). They attributed the higher slopes in the later stages of compression to increasing decomposition, but it may simply be an artifact of the log-time scale. It is

$d$  = diameter of perforated hole or width of perforated slot on the pipe, in or m; and

$n$  = number of perforated holes or slots per row per foot of pipe.

Pipe stiffness is measured according to ASTM D2412 (Standard Test Method for External Loading Properties of Plastic Pipe by Parallel-Plate Loading). The elastic modulus of the pipe material depends on the type of resin and formulation being used. Three formulas that can be used to calculate pipe stiffness are

$$PS = \frac{E \cdot I}{0.149 \cdot r^3} \quad (9.24)$$

$$PS = 0.559 \cdot E \cdot (t/r)^3 \quad (9.25)$$

and 
$$PS = 4.47 \cdot \frac{E}{(SDR - 1)^3} \quad (9.26)$$

where  $PS$  = pipe stiffness, lb/in<sup>2</sup> or kN/m<sup>2</sup>;

$E$  = elastic modulus of the pipe material, lb/in<sup>2</sup> or kN/m<sup>2</sup>;

$I$  = moment of inertia of the pipe wall per unit length,

$I = t^3/12$ , in<sup>4</sup>/in = in<sup>3</sup> or m<sup>4</sup>/m = m<sup>3</sup>;

$r$  = mean radius of pipe, in or m;

$t$  = wall thickness of pipe, in or m; and

$SDR$  = standard dimension ratio, the same as the dimension ratio.

The allowable deflection ratios for a typical commercial polyethylene pipe are listed in Table 9.4.

Deflections of buried flexible pipe are commonly calculated using Equation 9.16 or 9.21. These equations use the soil reaction modulus,  $E'$ , as a surrogate parameter for soil stiffness. It should be noted that the values of  $E'$  in Table 9.3 only apply for soil fills of less than 50 ft (15 m). However, megafills built over leachate collection pipes often exceed 150 ft (46 m) in height. The soil reaction modulus is not a directly measurable soil parameter; instead it must be determined by back-calculation using observed pipe deflections. Research by Selig (1990) showed that  $E'$  is a function of the bedding condition and overburden pressure. Selig's studies were carried out to seek a correlation between the soil reaction modulus and soil stiffness parameters such as

TABLE 9.4 Allowable Deflection Ratio of Polyethylene Pipe

SDR	Allowable Deflection Ratio
11	2.7%
13.5	3.4%
15.5	3.9%
17	4.2%
19	4.7%
21	5.2%
26	6.5%
32.5	8.1%

Young's modulus of soil,  $E_s$ , and the constrained modulus of soil,  $M_s$ , where  $E_s$  and  $D_s$  are related through Poisson's ratio of soil,  $\nu_s$ , by

$$M_s = \frac{E_s \cdot (1 - \nu_s)}{(1 + \nu_s)(1 - 2 \cdot \nu_s)} \quad (9.27)$$

where  $M_s$  = constrained modulus of soil, lb/ft<sup>2</sup> or kN/m<sup>2</sup>;  
 $E_s$  = elastic modulus of soil, lb/ft<sup>2</sup> or kN/m<sup>2</sup>; and  
 $\nu_s$  = Poisson's ratio of soil.

The studies and analyses by Neilson (1967), Allgood and Takahashi (1972), and Hartely and Duncan (1987) indicated that for

$$E' = k \cdot M_s \quad (9.28)$$

the value of  $k$  may vary from 0.7 to 2.3. Using  $k = 1.5$  as a representative value and  $\nu_s = 0.3$ , in addition to combining Equations 9.27 and 9.28 yields the following relationship between the elastic modulus of the pipe and soil (Selig, 1990):

$$E' = 2 \cdot E_s \quad (9.29)$$

The values of elastic parameters,  $E_s$  and  $\nu_s$ , can be found in Table 9.5 according to different percents of density from a standard Proctor compaction test (ASTM D698).

TABLE 9.5 Elastic Soil Parameters (Selig, 1990)

Soil Type	Stress Level		85% Standard Density			95% Standard Density		
			$E_s$		$\nu_s$	$E_s$		$\nu_s$
	psi	kPa	psi	MPa		psi	MPa	
SW, SP, GW, GP	1	7	1,300	9	0.26	1,600	11	0.40
	5	35	2,100	14	0.21	4,100	28	0.29
	10	70	2,600	18	0.19	6,000	41	0.24
	20	140	3,300	23	0.19	8,600	59	0.23
	40	280	4,100	28	0.23	13,000	90	0.25
	60	420	4,700	32	0.28	16,000	110	0.29
GM, SM, ML, and GC, SC with < 20% fines	1	7	600	4	0.25	1,800	12	0.34
	5	35	700	5	0.24	2,500	17	0.29
	10	70	800	6	0.23	2,900	20	0.27
	20	140	850	6	0.30	3,200	22	0.29
	40	280	900	6	0.38	3,700	25	0.32
	60	420	1,000	7	0.41	4,100	28	0.35
CL, MH, GC, SC	1	7	100	1	0.33	400	3	0.42
	5	35	250	2	0.29	800	6	0.35
	10	70	400	3	0.28	1,100	8	0.32
	20	140	600	4	0.25	1,300	9	0.30
	40	280	700	5	0.35	1,400	10	0.35
	60	420	800	6	0.40	1,500	10	0.38

Table 12.2 Comparison of Settlement and Construction Period (Yen and Scanlon, 1975)

Range of Fill Depth $H_f$ , feet, (meter)	Average Construction Period, $t_c$ (month)	Total Time Required for Construction and Settlement (months)	Approximate Time Required for Settlement to Complete (month)
40 to 80 (12 to 24)	12	113	101
40 to 80 (12 to 24)	72	324	252
80 to 100 (24 to 30)	12	245	233
80 to 100 (24 to 30)	72	310	238

Used with permission of ASCE.

## 12.4 ESTIMATION OF LANDFILL SETTLEMENT

The usual laboratory tests for soil consolidation testing are not well suited for obtaining accurate consolidation parameters for solid waste that has a heterogeneous composition and extremely large particle sizes. By analyzing the field settlement data from some large-scale pilot landfill cells, Sowers (1973) proposed an alternative method to estimate the amount of the landfill settlement. In recent years, this method has been revised and refined several times by other investigators.

The settlement of solid waste includes primary settlement and long-term secondary compression. The total amount of settlement is given by the expression

$$\Delta H = \Delta H_c + \Delta H_\alpha \quad (12.3)$$

where  $\Delta H$  = total settlement of solid waste;  
 $\Delta H_c$  = primary settlement of solid waste;  
 $\Delta H_\alpha$  = long-term secondary settlement of solid waste.

### 12.4.1 Settlement of New Solid Waste

Based on the procedure proposed by Sowers (1973), the equations that follow can be used to calculate the settlement for new landfilled solid waste. The *Initial primary settlement* is given by

$$\Delta H_c = C_c \cdot \frac{H_0}{1 + e_0} \cdot \log \frac{\sigma_1}{\sigma_0} \quad (12.4)$$

or

$$\Delta H_c = C'_c \cdot H_0 \cdot \log \frac{\sigma_1}{\sigma_0} \quad (12.5)$$

where  $\Delta H_c$  = primary settlement;  
 $e_0$  = initial void ratio of the waste layer before settlement;  
 $H_0$  = initial thickness of the waste layer before settlement;  
 $C_c$  = primary compression index (recall Figure 6.10);  
 $C'_c$  = modified primary compression index,  $C'_c = 0.17 \sim 0.36$ ;  
 $\sigma_0$  = previously applied pressure in the waste layer (assumed equal to the compaction pressure,  $\sigma_0 = 1,000 \text{ lb/ft}^2$  or  $48 \text{ kN/m}^2$ );  
 $\sigma_1$  = total overburden pressure applied at the mid level of the waste layer.

The previous compaction pressure applied on the solid waste layer during placement with compaction equipment is assumed to be 1,000 lb/ft<sup>2</sup> (48 kN/m<sup>2</sup>) based on 1973 compaction efforts for municipal solid waste landfills. In other words, the waste that has been placed in the landfill is essentially incompressible at normal pressure below 1,000 lb/ft<sup>2</sup> (48 kN/m<sup>2</sup>) due to the preconsolidation effect caused by previous compaction of the material. The value of the previously applied pressure,  $\sigma_o$ , should be changed during estimation of settlement if the compaction effort is much lower or higher than 1,000 lb/ft<sup>2</sup> (48 kN/m<sup>2</sup>) for a specific landfill project. Indeed, current practices of using waste compactors in the 100 to 150 U.S. tons (900 to 1,300 kN) range will significantly increase the value of  $\sigma_o$ .

The *long-term secondary settlement* can be obtained from

$$\Delta H_\alpha = C_\alpha \cdot \frac{H_o}{1 + e_o} \cdot \log \frac{t_2}{t_1} \quad (12.6)$$

or

$$\Delta H_\alpha = C'_\alpha \cdot H_o \cdot \log \frac{t_2}{t_1} \quad (12.7)$$

where  $\Delta H_\alpha$  = long-term secondary settlement;  
 $e_o$  = initial void ratio of the waste layer before settlement;  
 $H_o$  = initial thickness of the waste layer before settlement;  
 $C_\alpha$  = secondary compression index (recall Figure 6.11);  
 $C'_\alpha$  = modified secondary compression index,  $C'_\alpha = 0.03 \sim 0.1$ ;  
 $t_1$  = starting time of the time period for which long-term settlement of the layer is desired,  $t_1 = 1$  month;  
 $t_2$  = ending time of the time period for which long-term settlement of the layer is desired.

Because a standard consolidation test method for solid waste has not yet been developed, the selection of waste compression indices are mainly based on experience and limited field data. The value of the primary compression index  $C_c$  can be selected from Figure 6.10 based on the initial void ratio and organic content of the solid waste. The value of the secondary compression index  $C_\alpha$  can be selected from Figure 6.1.1 based on the initial void ratio of the waste and the decomposition conditions.

Generally, the initial void ratio of municipal solid waste placed in a landfill after compaction is quite difficult to determine, and hence the values of the primary compression index  $C_c$  and the secondary compression index  $C_\alpha$  cannot be estimated readily for settlement analysis. Accordingly, an alternative approach has been used in engineering practice—namely, the use of a “modified” primary compression index  $C'_c$  and a “modified” secondary compression index  $C'_\alpha$ . Based on experience, the value of the modified primary compression index  $C'_c$  varies from 0.17 to 0.36, and the value of the modified secondary compression index  $C'_\alpha$  varies from 0.03 to 0.1 for municipal solid waste (depending on the initial compaction effort and composition of the solid waste). The value of the modified secondary compression index  $C'_\alpha$  for common clay ranges from 0.005 to 0.02. Therefore, the secondary settlement for municipal solid waste is approximately five to six times that of common clay.

### 12.4.2 Settlement of Existing Solid Waste

The following equations can be used to calculate the settlement of an existing solid waste landfill caused by vertical expansion (Chapter 14) or other additional extra loading, such as a light structure on a raft foundation.

The *primary settlement* is obtained by

$$\Delta H_c = C_c \cdot \frac{H_o}{1 + e_o} \cdot \log \frac{\sigma_o + \Delta\sigma}{\sigma_o} \quad (12.8)$$

or

$$\Delta H_c = C'_c \cdot H_o \cdot \log \frac{\sigma_o + \Delta\sigma}{\sigma_o} \quad (12.9)$$

where  $\Delta H_c$  = primary settlement;  
 $e_o$  = initial void ratio of the waste layer before settlement;  
 $H_o$  = initial thickness of the waste layer of the existing landfill;  
 $C_c$  = primary compression index;  
 $C'_c$  = modified primary compression index,  $C'_c = 0.17 \sim 0.36$ ;  
 $\sigma_o$  = existing overburden pressure acting at the mid level of the waste layer;  
 $\Delta\sigma$  = increment of overburden pressure due to vertical expansion or other extra load.

The *long-term secondary settlement* is given by

$$\Delta H_\alpha = C_\alpha \cdot \frac{H_o}{1 + e_o} \cdot \log \frac{t_2}{t_1} \quad (12.10)$$

or

$$\Delta H_\alpha = C'_\alpha \cdot H_o \cdot \log \frac{t_2}{t_1} \quad (12.11)$$

where  $\Delta H_\alpha$  = secondary settlement;  
 $e_o$  = initial void ratio of the waste layer before starting secondary settlement;  
 $H_o$  = initial thickness of the waste layer before starting secondary settlement;  
 $C_\alpha$  = secondary compression index;  
 $C'_\alpha$  = modified secondary compression index,  $C'_\alpha = 0.03 \sim 0.1$ ;  
 $t_1$  = starting time of the secondary settlement. It is assumed to be equal to the age of the existing landfill for vertical expansion project;  
 $t_2$  = ending time of the secondary settlement.

(e.g., temperature within landfill and oxygen reaching the waste) still is not entirely clear. These functions should be used with caution in engineering practice and should be supported by additional testing data and research.

## 12.7 ESTIMATION OF LANDFILL FOUNDATION SETTLEMENT

If the landfill is underlain by a soil layer, particularly a thick layer of soft, fine-grained soil, consolidation settlements may be large. In these cases, design analyses should consider settlement of the foundation clay layer. Both primary consolidation and long-term secondary settlement should be considered. Calculations are performed using conventional equations from soil mechanics theory and a time frame at least equal to the active life and postclosure care period of the landfill.

Excessive settlement of an underlying foundation clay layer will affect the performance of a landfill liner and leachate collection system. The purposes of analyzing the settlement of a foundation clay layer and overlying landfill liner and leachate collection/removal system are as follows:

- (i) Tensile strain induced in the liner system and leachate collection and removal system must be limited to a minimum allowable tensile strain for the components of these two systems. The compacted clay liner usually has the smallest allowable tensile strain value between 0.1% and 1.0% and an average allowable tensile strain of 0.5%.
- (ii) Post-settlement grades of the landfill cell subbase and the leachate collection pipes must be sufficient to maintain leachate performance to prevent grade reversal and leachate ponding in accordance with the rule requirements.

### 12.7.1 Total Settlement of Landfill Foundation

The total settlement of landfill foundation soil can be divided into three portions: elastic settlement, primary consolidation settlement, and secondary consolidation settlement. The settlement of sandy soils includes only elastic settlement. The settlement of clayey soils includes all three types of settlements. The total settlement of clayey soil is equal to the sum of the elastic settlement and the primary and secondary settlements. Because the permeability of clay is quite low, it takes a long time to complete the whole process of consolidation settlement. The settlement of clayey soil is usually much larger than the settlement of sandy soils.

Because the settlement of sandy soils includes only elastic settlement, the settlement of sand layer can be calculated from the Elastic Settlement equation, which is

$$Z_e = (\Delta\sigma/M_s)H_o \quad (12.20)$$

where  $Z_e$  = elastic settlement of soil layer, ft or m;  
 $H_o$  = initial thickness of soil layer, ft or m;  
 $\Delta\sigma$  = increment of vertical effective stress, lb/ft<sup>2</sup> or kN/m<sup>2</sup>;  
 $M_s$  = constrained modulus of soil, lb/ft<sup>2</sup> or kN/m<sup>2</sup>.

The constrained modulus is given by

$$M_s = \frac{E_s(1 - \nu_s)}{(1 + \nu_s)(1 - 2\nu_s)} \quad (12.21)$$

where  $M_s$  = constrained modulus of soil, lb/ft<sup>2</sup> or kN/m<sup>2</sup>;  
 $E_s$  = elastic modulus of soil, see Table 9.5, lb/ft<sup>2</sup> or kN/m<sup>2</sup>;  
 $\nu_s$  = Poisson's ratio of soil, see Table 9.5.

The *primary consolidation settlement* is given by

$$Z_c = C_r \cdot \frac{H_{oi}}{1 + e_{oi}} \cdot \log \frac{p_c}{\sigma_o} + C_c \cdot \frac{H_o}{1 + e_{oi}} \cdot \log \frac{\sigma_o + \Delta\sigma}{p_c} \quad (12.22)$$

where  $Z_c$  = primary consolidation settlement of clay layer, ft or m;  
 $H_o$  = initial thickness of clay layer, ft or m;  $= 2 \text{ ft}$   
 $e_{oi}$  = initial void ratio of clay layer;  
 $C_r$  = recompression index;  
 $C_c$  = primary compression index.  
 $\sigma_o$  = initial vertical effective stress, lb/ft<sup>2</sup> or kN/m<sup>2</sup>;  
 $p_c$  = preconsolidation pressure, lb/ft<sup>2</sup> or kN/m<sup>2</sup>;  
 $\Delta\sigma$  = increment of vertical effective stress, lb/ft<sup>2</sup> or kN/m<sup>2</sup>.

The *secondary compression settlement* is given by

$$Z_\alpha = C_\alpha \cdot \frac{H_{os}}{1 + e_{os}} \cdot \log \frac{t_2}{t_1} \quad (12.23)$$

where  $Z_\alpha$  = long-term secondary compression settlement, ft or m;  
 $e_{os}$  = initial void ratio of clay layer before starting secondary consolidation settlement;  
 $C_\alpha$  = secondary consolidation compression index;  
 $H_{os}$  = initial thickness of clay layer before starting secondary consolidation settlement, ft or m;  
 $t_1$  = starting time of the time period for which long-term settlement of the layer is desired;  
 $t_2$  = ending time of the time period for which long-term settlement of the layer is desired.

The total settlement of clay layer includes three portions: elastic settlement, primary consolidation settlement, and secondary consolidation settlement. These three types of settlement for clayey soil layers can be calculated from Equations 12.20, 12.22, and 12.23, respectively. The total settlement of clayey soil at point  $i$  can be determined from the equation

$$Z_i = (Z_e)_i + (Z_c)_i + (Z_\alpha)_i \quad (12.24)$$

where  $Z_i$  = total settlement of points  $i$ ;  
 $(Z_e)_i$  = elastic settlement of point  $i$ ;  
 $(Z_c)_i$  = primary consolidation settlement of point  $i$ ;  
 $(Z_\alpha)_i$  = secondary consolidation settlement of point  $i$ .

**APPLICATION FOR PERMIT  
DNCS ENVIRONMENTAL SOLUTIONS**

**VOLUME III: ENGINEERING DESIGN AND CALCULATIONS  
SECTION 9: SETTLEMENT CALCULATIONS**

**ATTACHMENT III.9.C**

**CODUTO, DONALD P. 1998.**

***GEOTECHNICAL ENGINEERING PRINCIPLES AND PRACTICES.***

**NEW JERSEY: PRENTICE HALL.**

# **Geotechnical Engineering**

## **Principles and Practices**

**Donald P. Coduto**

*Professor of Civil Engineering  
California State Polytechnic University, Pomona*

PRENTICE HALL, Upper Saddle River, NJ 07458

where:

$(N_1)_{60}$  = corrected SPT  $N$ -value, as defined in Chapter 3

$C_p$  = grain size correction factor

$C_A$  = aging correction factor

$C_{OCR}$  = overconsolidation correction factor

$D_{50}$  = grain size at which 50 percent of the soil is finer (mm) as defined in Section 4.4

$t$  = age of soil (time since deposition in years). If no age information data is available, use  $t = 100$  yr.

OCR = overconsolidation ratio, as defined in Chapter 11. If no information is available to assess the OCR, use a value of 2.

$q_c$  = cone resistance (kg/cm<sup>2</sup> or ton/ft<sup>2</sup>), as defined in Chapter 3

$Q_c$  = compressibility factor

= 0.91 for highly compressible sands

= 1.00 for moderately compressible sands

= 1.09 for slightly compressible sands

For purposes of solving this formula, a sand with a high fines content or a high mica content is "highly compressible," whereas a pure quartz sand is "slightly compressible."

$\sigma'_z$  = vertical effective stress (lb/ft<sup>2</sup>; kPa), as defined in Chapter 10

Many people confuse relative density with relative compaction. The latter is defined in Chapter 6. Although the names are similar, and they measure similar properties, these two parameters are numerically different. In addition, some people in other professions use the term "relative density" to describe what we call specific gravity! Geotechnical engineers should never use the term in this way.

Table 4.5 presents typical values of  $e_{min}$  and  $e_{max}$  for various sandy soils. These are not intended to be used in lieu of laboratory or in-situ tests, but could be used to check test results or for preliminary analyses.

**TABLE 4.5** TYPICAL VALUES OF  $e_{min}$  AND  $e_{max}$  (Hough, 1969; Adapted by permission of John Wiley and Sons, Inc.)

Soil Description	$e_{min}$ (dense)	$e_{max}$ (loose)
Equal spheres (theoretical values)	0.35	0.92
Clean, poorly graded medium sand (Ottawa, Illinois)	0.50	0.80
Clean, fine-to-medium sand	0.40	1.0
Uniform inorganic silt	0.40	1.1
Silty sand	0.30	0.90
Clean fine-to-coarse sand	0.20	0.95
Micaceous sand	0.40	1.2
Silty sand and gravel	0.14	0.85

**TABLE 11.3** TYPICAL CONSOLIDATION PROPERTIES OF SATURATED NORMALLY CONSOLIDATED SANDY SOILS AT VARIOUS RELATIVE DENSITIES (Adapted from Burmister, 1962)

Soil Type	$C_c / (1+e_0)$					
	$D_r = 0\%$	$D_r = 20\%$	$D_r = 40\%$	$D_r = 60\%$	$D_r = 80\%$	$D_r = 100\%$
Medium to coarse sand, some fine gravel (SW)	-	-	0.005	-	-	-
Medium to coarse sand (SW/SP)	0.010	0.008	0.006	0.005	0.003	0.002
Fine to coarse sand (SW)	0.011	0.009	0.007	0.005	0.003	0.002
Fine to medium sand (SW/SP)	0.012	0.010	0.008	0.006	0.004	0.003
Fine sand (SP)	0.015	0.013	0.010	0.008	0.005	0.003
Fine sand with trace fine to coarse silt (SP-SM)	-	-	0.011	-	-	-
Fine sand with little fine to coarse silt (SM)	0.017	0.014	0.012	0.009	0.006	0.003
Fine sand with some fine to coarse silt (SM)	-	-	0.012	-	-	-

For saturated overconsolidated sands,  $C_c / (1+e_0)$  is typically about one-third of the values listed in Table 11.3, which makes such soils nearly incompressible. Compacted fills can be considered to be overconsolidated, as can soils that have clear geologic evidence of preloading, such as glacial tills. Therefore, many settlement analyses simply consider the compressibility of such soils to be zero. If it is unclear whether a soil is normally consolidated or overconsolidated, it is conservative to assume it is normally consolidated.

Very few consolidation tests have been performed on gravelly soils, but the compressibility of these soils is probably equal to or less than those for sand, as listed in Table 11.3.

Another characteristic of sands and gravels is their high hydraulic conductivity, which means any excess pore water drains very quickly. Thus, the rate of consolidation is very fast, and typically occurs nearly as fast as the load is applied. Thus, if the load is due to a fill, the consolidation of these soils may have little practical significance.

However, there are at least two cases where consolidation of coarse-grained soils can be very important and needs more careful consideration:

1. Loose sandy soils subjected to dynamic loads, such as those from an earthquake. They can experience very large and irregular settlements that can cause serious damage. Kramer (1996) discusses methods of evaluating this problem.



**APPLICATION FOR PERMIT  
DNCS ENVIRONMENTAL SOLUTIONS**

**VOLUME III: ENGINEERING DESIGN AND CALCULATIONS  
SECTION 9: SETTLEMENT CALCULATIONS**

**ATTACHMENT III.9.D**

**SHARMA, HARI .D. AND SANGEETA P. LEWIS. 1994.  
*WASTE CONTAINMENT SYSTEMS, WASTE STABILIZATION  
AND LANDFILLS: DESIGN AND EVALUATION.*  
NEW YORK: JOHN WILEY AND SONS.**

---

# WASTE CONTAINMENT SYSTEMS, WASTE STABILIZATION, AND LANDFILLS: DESIGN AND EVALUATION

---

**HARI D. SHARMA, PH.D., P.E.**

Chief Engineer and Director  
EMCON Associates  
San Jose, California

**SANGEETA P. LEWIS, P.E.**

Project Manager  
CH<sub>2</sub>M Hill  
Oakland, California



A Wiley-Interscience Publication

**JOHN WILEY & SONS, INC.**

New York / Chichester / Toronto / Brisbane / Singapore

## **APPENDIX B**

---

### **SETTLEMENT ANALYSES**

---

Landfill settlement analyses include both foundation and refuse settlements. Foundation settlements are important in designing appropriately graded LCRSs, since these are typically gravity-flow systems. Refuse settlements are important in final cover design and estimating final landfill capacity. Estimating refuse settlements has also been critical in designing vertical landfill expansions and structures constructed on closed landfills.

Foundation settlement analyses for landfills follow the same principle as traditional geotechnical engineering settlement analyses. In this appendix we therefore focus on refuse settlements. For ease in reference, however, a brief discussion of foundation settlements is provided. The reader is referred to introductory geotechnical engineering textbooks if explanation is required on soil settlement and consolidation theories.

#### **B.1 FOUNDATION SETTLEMENT**

##### **B.1.1 Mechanisms**

For cohesive soils, settlement is characterized by the following three mechanisms:

- Immediate settlement following load application
- Consolidation settlements, which occur gradually as excess pore pressure caused by the applied loads are dissipated
- Secondary compression of the soil skeleton

Consolidation and secondary compression occur over several years and are theoretically never complete.

For granular soils, settlement is caused primarily by the compression of the soil skeleton as the particles rearrange due to the applied loads. Due to the relatively high permeability of granular soils, excess pore pressures induced by the applied load are assumed to dissipate in a very short period of time, and settlement is assumed to occur within a short period following load application; this is sometimes called immediate settlement.

### B.1.2 Calculation of Settlement

For cohesive soils the total amount of consolidation settlement can be calculated using the following equation:

$$s = \Delta H = \frac{\Delta e}{1 + e_0} H_t \quad (\text{B.1})$$

where  $s$  = settlement

$\Delta H$  = change in height of layer

$\Delta e$  = change in void ratio

$e_0$  = initial void ratio

$H_t$  = layer thickness

Equation (B.1) can be modified as follows to suit the parameters obtained from a consolidation test:

$$s = \Delta H = \frac{C_c H_t}{1 + e_0} \left( \log \frac{P_0 + \Delta P}{P_0} \right) \quad (\text{B.2})$$

where  $C_c$  = consolidation index or compression index

$P_0$  = initial stress

$\Delta P$  = change in stress

For an infinite layer of soil, the change in stress is relatively easy to calculate and is typically equal to the change in applied load or overburden. However, since most aboveground landfills may be considered embankment loads, the subsurface stress distribution may be calculated using the influence chart shown in Figure B.1 for embankments of infinite length (Osterberg, 1957; U.S. Dept. of the Navy, 1982).

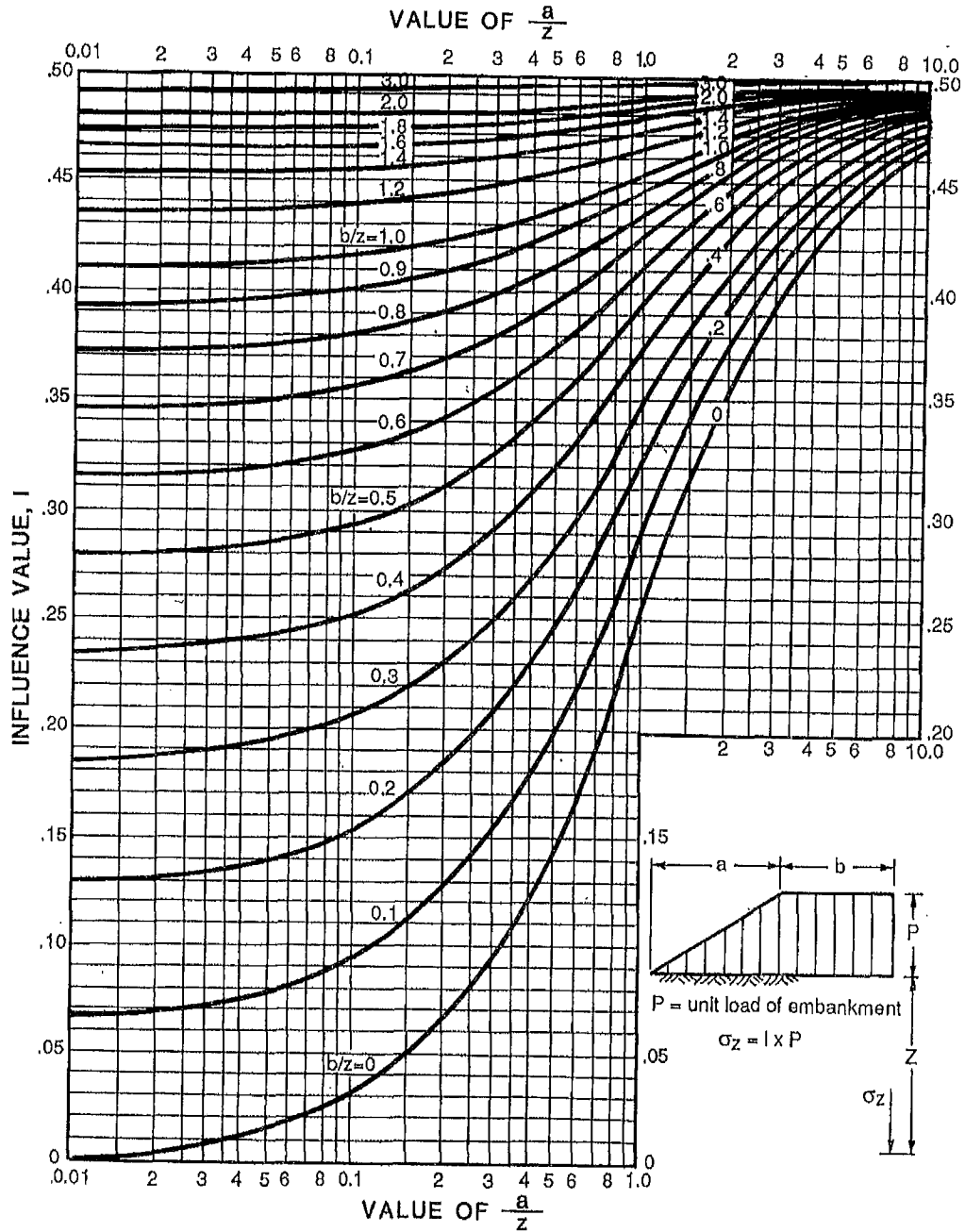


Figure B.1 Influence value for vertical stress under embankment load of infinite length. (From U.S. Dept. of the Navy, 1982.)

**B.1.3 Liquefaction**

**B.1.3.1 Liquefaction Potential.** In seismic regions, significant foundation settlements may also occur due to liquefaction of loose to medium-dense saturated cohesionless soils. Liquefaction is defined as a process where high shear deformations, typically induced by seismic activity, results in a progressive buildup of pore pressure. With limited drainage during the short period that the shear load is in-

**APPLICATION FOR PERMIT  
DNCS ENVIRONMENTAL SOLUTIONS**

**VOLUME III: ENGINEERING DESIGN AND CALCULATIONS  
SECTION 9: SETTLEMENT CALCULATIONS**

**ATTACHMENT III.9.E**

**STEPHENS, DANIEL B.; HSU, KUO-CHIN; PRIEKSAT, MARK A.; ANKENY, MARK  
D.; BLANDFORD, NEIL; ROTH, TRACY L.; KELSEY, JAMES A.; WHITWORTH,  
JULIA R. 1997. A COMPARISON OF ESTIMATED AND CALCULATED EFFECTIVE  
POROSITY. *HYDROGEOLOGY JOURNAL* (1998) 6:156–165.**

---

# A comparison of estimated and calculated effective porosity

Daniel B. Stephens · Kuo-Chin Hsu  
Mark A. Prieksat · Mark D. Ankeny  
Neil Blandford · Tracy L. Roth · James A. Kelsey  
Julia R. Whitworth

**Abstract** Effective porosity in solute-transport analyses is usually estimated rather than calculated from tracer tests in the field or laboratory. Calculated values of effective porosity in the laboratory on three different textured samples were compared to estimates derived from particle-size distributions and soil-water characteristic curves. The agreement was poor and it seems that no clear relationships exist between effective porosity calculated from laboratory tracer tests and effective porosity estimated from particle-size distributions and soil-water characteristic curves. A field tracer test in a sand-and-gravel aquifer produced a calculated effective porosity of approximately 0.17. By comparison, estimates of effective porosity from textural data, moisture retention, and published values were approximately 50–90% greater than the field calibrated value. Thus, estimation of effective porosity for chemical transport is highly dependent on the chosen transport model and is best obtained by laboratory or field tracer tests.

**Résumé** La porosité effective dans les analyses de transport de soluté est habituellement estimée, plutôt que calculée à partir d'expériences de traçage sur le terrain ou au laboratoire. Les valeurs calculées de la porosité effective au laboratoire sur trois échantillons de textures différentes ont été comparées aux estimations provenant de distributions de taille de particules et de courbes caractéristiques sol-eau. La concordance était plutôt faible et il semble qu'il n'existe aucune relation claire entre la porosité effective calculée à partir des expériences de traçage au laboratoire et la porosité effective estimée à partir des distributions de taille de parti-

cules et de courbes caractéristiques sol-eau. Une expérience de traçage de terrain dans un aquifère de sables et de graviers a fourni une porosité effective calculée d'environ 0,17. En comparaison, les estimations de porosité effective de données de texture, de teneur en eau et les valeurs publiées étaient environ 50 à 90% plus fortes que la valeur calibrée sur le terrain. Ainsi, l'estimation de la porosité effective pour le transport en solution dépend fortement du modèle de transport utilisé et est préférable lorsqu'elle est obtenue à partir d'expériences de traçage de laboratoire ou de terrain.

**Resumen** La porosidad efectiva en el análisis del transporte de solutos se suele estimar, en lugar de calcularse a partir de ensayos de trazadores en el campo o el laboratorio. Los valores calculados de la porosidad efectiva en el laboratorio en tres muestras de distintas texturas se compararon con las estimaciones realizadas a partir de las distribuciones de tamaño de partículas y de las curvas características suelo-agua. El ajuste fue bastante pobre y parece que no existe una relación clara entre los valores de la porosidad efectiva calculados mediante los tres métodos. Un ensayo de trazadores en el campo, en un acuífero formado por arenas y gravas, dio lugar a un valor de porosidad efectiva calculado de 0.17. Las estimaciones realizadas a partir de los datos de textura, humedad retenida y valores publicados eran entre un 50–90 por ciento mayores que el valor calibrado en el ensayo de campo. Así, la estimación del valor de la porosidad efectiva para el transporte químico depende mucho del modelo de transporte seleccionado y es mejor si se obtiene a partir de ensayos de laboratorio o de campo.

---

Received, March 1997  
Revised, August 1997  
Accepted, August 1997

Daniel B. Stephens (✉) · Kuo-Chin Hsu · Mark A. Prieksat  
Mark D. Ankeny · Neil Blandford · Tracy L. Roth  
James A. Kelsey  
Daniel B. Stephens and Associates, Inc., 6020 Academy Road  
NE, Albuquerque, New Mexico 87109, USA  
Fax: + 505-822-8877  
e-mail: dbsteph@dbstephens.com

Julia R. Whitworth  
New Mexico Institute of Mining and Technology, Socorro,  
New Mexico 87801, USA

**Key words** laboratory experiments measurements · tracer tests · unconsolidated sediments · numerical modeling

## Introduction

Modeling the transport of contaminants in groundwater has become a common and sometimes routine task for many practitioners in the field of hydrogeology over the past 15 years. Usually, hydraulic conductivity, and to a much lesser extent dispersivity, are the focus of field and laboratory data-collection efforts for models

that are based on the advection–dispersion equation (ADE). A third hydraulic parameter required for transport modeling is effective porosity. For aquifer simulations, it has become common practice to estimate effective porosity from one's experience or the literature.

Effective porosity is generally defined for solute transport as that portion of the soil or rock through which chemicals move, or that portion of the media that contributes to flow (Fetter 1993; Domenico and Schwartz 1990). Horton et al. (1987) added some confusion by defining effective porosity as that part of the pore space where velocity is greater than the average fluid velocity. However, its in simplest and traditional form, effective porosity  $n_e$  is

$$n_e = \frac{q}{v} \quad (1)$$

where  $v$  is the mean velocity of a conservative tracer and  $q$  is the specific discharge, or Darcy velocity (e.g., Bear and Verruijt 1987). It is well recognized that effective porosity is less than the total porosity, because, even if the medium is fully saturated, not all of the water-filled pores are interconnected or contribute to flow. Therefore, terms such as mobile and immobile water or dead-end pores are also used in reference to the definition of effective porosity. In fact, Luckner and Schestakow (1991) equate effective porosity and mobile water content. In this paper we review some of the methods to derive effective porosity in the laboratory and field and assess their validity.

Determining effective porosity from tracer tests is not common practice. Field tracer tests are rare because of their expense, duration, and the impacts of the tracer on the aquifer may not be tolerated by regulators. Laboratory tracer tests are uncommon because the core samples are small and potentially unrepresentative of the aquifer at the scale of interest. Furthermore, laboratory cores are almost always vertical and perpendicular to the bedding, whereas aquifer flow and transport are predominantly horizontal; consequently, column tracer tests may poorly reproduce field conditions. Another reason that effective porosity is not often evaluated is that it has a small range of variability compared with hydraulic conductivity and dispersivity. Nevertheless, in the application of transport models, which in practice is often driven by environmental regulation and litigation, a need exists to justify the data that go into transport models with some type of measurement.

For the above reasons, effective porosity is most often obtained from other measured parameters, such as specific yield, or total porosity minus specific retention or residual water content. For example, Bear (1972, p. 484) defines effective porosity as the drainable porosity or the total porosity minus the field capacity. He indicates that for conditions of homogeneous soils and deep water tables, specific yield and effective porosity are identical. Practitioners in hydrogeology have been

attracted to this apparent identity, and they estimate effective porosity from the convenient relationship between particle size and specific yield, shown in *Figure 1*, that is included in most standard textbooks. Although effective porosity has been assigned two different definitions, many assume that the resulting two values are numerically equivalent. Unfortunately, many appear to have forgotten the caution issued by Bear (1972, p. 8) not to confuse effective porosity defined in the context of transport with effective porosity that pertains to drainage and capillary processes. Despite the obvious distinction, effective porosity defined by the latter is often used in simulating groundwater contamination and seems to have gained acceptance as a surrogate for the transport effective porosity without much challenge. For example, Boutwell et al. (1986) state “Most transport equations use effective porosity which does not include dead-end and unconnected pores. Effective porosity approximately equals specific yield.”

The purpose of this article is to evaluate the reliability of methods in estimating effective porosity from drainage and capillary measurements as well as particle size. Column tracer experiments were conducted in the laboratory to determine effective porosity, and these results were compared with estimates of effective porosity derived from soil–water characteristic curves and particle size. The second part of this article compares results of a field tracer test, where effective porosity was obtained by model calibration, to estimates of effective porosity derived from soil–water characteristic curves and particle size.

## Calculating Effective Porosity for Transport

Effective porosity as required in groundwater transport models can be determined by laboratory and field techniques. Approaches to making these determinations are presented here, but the scope of the article precludes a comprehensive historical review or critique of

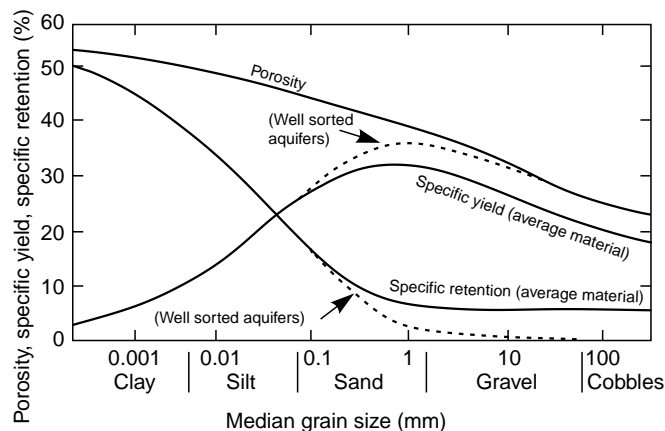


**Fig. 1** Relationship between median grain size and water-storage properties of alluvium

all methods available. Such a thorough review has not been published to our knowledge, although excellent discussions of effective porosity in transport processes are in Norton and Knapp (1977), de Marsily (1986), Peyton et al. (1985), and elsewhere.

### Laboratory Methods

For traditional solute-transport modeling, effective porosity ( $n_e$ ) can be defined as the ratio between Darcy flux and seepage velocity, where  $q$  is experimental Darcy flux and  $v$  is seepage velocity (Eq. (1)). Laboratory apparatus for evaluating transport consists of a column packed with the media to be tested, fittings to maintain a constant flow rate through the column, fittings to inject tracers into the upstream end of the column, and a means to collect samples of outflow periodically for chemical analyses. Darcy flux can be calculated directly from the steady flow rate and column diameter, but seepage velocity depends on the conceptual transport model chosen.

If it is assumed that transport is a chemical and physical equilibrium process, solute transport can be modeled with a single porosity model described by the ADE

$$R \frac{\partial c}{\partial t} + v_i \frac{\partial c}{\partial x_i} = \frac{\partial}{\partial x_i} \left( D_{ij} \frac{\partial c}{\partial x_j} \right) \quad i, j = 1, 2, 3 \quad (2)$$

where  $R$  is the retardation factor,  $c$  is the solute concentration,  $v_i$  is the seepage velocity component in the  $x_i$  direction, and  $D_{ij}$  is the component of the dispersion coefficient tensor. This model assumes that degradation and chemical production are not significant. The mobile-flow pore space is represented by a single effective porosity and is used to estimate seepage velocity. Advective and diffusive processes are active within the pore space designated as effective porosity.

If it is assumed that there is no retardation, then the traditional column-testing approach can utilize the analytical solution of a one-dimensional version of Eq. (2) with constant inlet concentration,  $c_0$ , and zero initial concentration

$$\frac{c}{c_0} = \frac{1}{2} \left[ 1 \pm \operatorname{erf} \left( \frac{x - vt}{2\sqrt{Dt}} \right) \right] \quad (3)$$

where  $\operatorname{erf}$  is the error function. The relative concentration point ( $c/c_0 = 0.5$ ) describes solute moving at the average velocity and for a nonreactive tracer  $c/c_0 = 0.5$  should occur when one pore volume of solution has flowed from the column. Using the measured elapse time,  $t_{0.5}$  at  $c/c_0 = 0.5$ , the known column length,  $L$ , and experimental Darcy flux,  $q$ , the effective porosity can be calculated as

$$n_e = \frac{L}{t_{0.5} q} \quad (4)$$

This approach is similar to determining  $n_e$  with Eq. (1), because  $L/t_{0.5}$  is essentially the average solute velocity

eluting from the column. Luckner and Schestakow (1991) describe a three-step tracer test in short columns designed explicitly to quantify effective porosity.

Shackelford (1995) proposed a cumulative mass approach to derive effective porosity from breakthrough curves. A cumulative mass ratio (CMR) is calculated from

$$\text{CMR} = \frac{\sum \Delta m}{V_p c_0} = \frac{R_d}{2P_L} [(\xi_4 - \xi_2) \operatorname{erfc}(\xi_1) + (\xi_4 + \xi_2) \exp(\xi_2) \operatorname{erfc}(\xi_3)] \quad (5)$$

where

$$\xi_1 = \frac{R_d - T}{2\sqrt{\frac{TR_d}{P_L}}}; \quad \xi_2 = P_L; \quad \xi_3 = \frac{R_d + T}{2\sqrt{\frac{TR_d}{P_L}}};$$

and  $\xi_4 = \frac{TP_L}{R_d}$  (6)

$T$  is the number of pore volumes of flow,  $R_d$  is the retardation factor, and  $P_L$  is the column Péclet number. The CMR is plotted vs  $T$  and the slope of the plot during steady-state transport is unity, given by

$$\lim_{T \rightarrow \infty} \frac{d(\text{CMR})}{dT} = \lim_{T \rightarrow \infty} \frac{1}{2} [\operatorname{erfc}(\xi_1) + \exp(\xi_2) \operatorname{erfc}(\xi_3)] = 1 \quad (7)$$

The unit slope is plotted to determine the  $x$ -axis intercept and is designated as  $T_0$  representing the retardation factor  $R_d$ . The measured value of  $T_0$  for a nonreactive tracer ( $R_d = 1$ ) represents the ratio of  $n_e/n$ . Thus, effective porosity is derived by multiplying this ratio by the total porosity.

Kinetic adsorption and heterogeneous flow regions cause chemical and physical non-equilibrium, respectively. Two-site/two-region transport models (van Genuchten and Wagenet 1989) have been proposed to describe non-equilibrium phenomenon. The two-site/two-region model can be described in dimensionless form as

$$\beta R \frac{\partial C_1}{\partial T} + \frac{\partial C_1}{\partial Z} = \frac{1}{P} \frac{\partial^2 C_1}{\partial Z^2} + \omega(C_1 - C_2) \quad (8)$$

$$(1 - \beta) R \frac{\partial C_2}{\partial T} = \omega(C_1 - C_2) \quad (9)$$

where  $\beta$  is the partition coefficient,  $P$  is the Péclet number (defined as  $vL/D$ ),  $C_1$  is the concentration at equilibrium site,  $C_2$  is the concentration at non-equilibrium site, and  $\omega$  is a dimensionless mass transfer coefficient. For the two-region model when  $R = 1$ ,  $\beta$  is the ratio of the mobile-water region to total porosity. The pore space is divided into two parts, the mobile-water region, where equilibrium processes occur, and the immobile region, where non-equilibrium processes occur. Both advection and diffusion occur in the mobile region, but only first-order kinetic processes occur in the immobile region. Toride et al. (1995) present a versatile

software program, CXTFIT, for evaluating solute breakthrough curves. The program optimizes the parameters by fitting curves to measured data for a range of conceptual models, including the mobile/immobile water model presented in *Eqs. (8) and (9)*.

Breakthrough curves obtained from laboratory column tests can be described by a one-dimensional version of *Eq. (2)*, where  $v$  and  $D$  are viewed as constants or by *Eqs. (8) and (9)*. The decision to apply the equilibrium or non-equilibrium model may be judged using selection criteria presented by Carrera et al. (1990). The complex non-equilibrium model may be more representative of the soil system, but the equilibrium model is generally easier to use.

However, extrapolation of column-test results to field scales is still viewed with some skepticism. Therefore, several methods for determining effective porosity from field solute-transport experiments are presented.

### Field Methods

Effective porosity can be obtained from field-scale well-tracer tests, in which a tracer is injected into a well and is pumped back from either the same injection well or from another well. For example, Hall et al. (1991) propose a method to estimate effective porosity in a homogeneous confined aquifer dominated by steady-state horizontal advective transport with a constant hydraulic gradient. They use Darcy's equation, with an added effective-porosity term from *Eq. (1)*.

$$V = \frac{KI}{n_e} \quad (10)$$

and a version of the equation for the drift and pump-back test described by Leap and Kaplan (1988).

$$V = \frac{(Qt/\pi n_e b)^{1/2}}{d} \quad (11)$$

where  $K$  is the horizontal hydraulic conductivity;  $I$  is the horizontal hydraulic gradient;  $Q$  is pumping rate during recovery of tracer,  $t$  is the time elapsed from the start of pumping until the center of mass of the tracer is recovered;  $b$  is the aquifer thickness; and  $d$  is the time elapsed from the injection of tracer until the center of the mass of tracer is recovered. From *Eqs. (11) and (12)*, effective porosity can be calculated as

$$n_e = \frac{\pi b K^2 I^2 d^2}{Qt} \quad (12)$$

A single-well borehole dilution test (Drost et al. 1968; Halevy et al. 1967; Grisak et al. 1977) can be conducted by injection and subsequent withdrawal of a tracer in a single well through a zone isolated by dual packers. Seepage velocity  $v$  can be calculated as

$$v = -\frac{V}{\beta A t} \ln\left(\frac{c}{c_0}\right) \quad (13)$$

where  $V$  is volume of the borehole interval with verti-

cal cross-sectional area  $A$ ,  $\beta$  is a geometric factor ranging from 0.5–4.0,  $t$  is time,  $c$  is recovered tracer concentration, and  $c_0$  is the concentration of introduced tracer. Effective porosity can then be calculated from *Eq. (1)* if specific discharge can be calculated from hydraulic conductivity  $K$  and hydraulic gradient  $I$ .

Two-well tests can be performed in both confined and unconfined aquifers (Gaspar and Oncescu 1972). One well is pumped at a constant flow rate  $Q$ , and when the flow rate is at a quasi-steady state, a tracer is injected into the other well at distance  $L$  from the pumping well. The concentration recovered from the pumping well is recorded over time. For a horizontal confined aquifer with thickness  $D$ , the effective porosity is calculated as

$$n_e = \frac{Qt_i}{\pi L^2 D} \quad (14)$$

where  $t_i$  is the travel time of the tracer between the injection and pumping wells. For an unconfined aquifer with negligible natural gradient, effective porosity can be calculated as

$$n_e = \frac{Qt_i}{\pi L^2 \left( h - \frac{Q}{4\pi k h} \right)} \quad (15)$$

where  $h$  is the hydraulic head in the well where the tracer was introduced. This method is effective if the wells span the thickness of the aquifer layer and if  $L \gg h$  (Halevy and Nir 1962).

Another approach is to use solute-breakthrough data obtained from field tracer tests to calibrate the transport parameters of the model. However, since the numerical solution to most field-scale problems of non-reactive transport is non-unique (Molson and Frind 1990), the information obtained from model calibration may be valid only for the conceptual model used during calibration. Effective porosity is then a calibrated value that gives the best fit to measured solute breakthrough.

### Laboratory Tracer Tests

Three soil materials (sand, silica flour, and a mixture of 75% fine sand and 25% silica flour) were chosen for testing. The sand, silica flour, and mixture columns were hand packed in the laboratory. Soil columns for the solute-breakthrough tests and hydraulic-properties tests were packed concurrently into a column comprised of brass cylinders to ensure that both columns would have similar physical and hydrologic characteristics.

Brass cylinders approximately 5 cm in diameter were cut to lengths of approximately 5 and 10 cm. The columns were prepared by securing one 5-cm-length and one 10-cm-length of brass cylinder together, end to end, using tape. The air-dry soil material was then poured

into the cylinder while gently tapping and shaking the cylinder, to insure uniform settling and packing, until the column was full. The cylinders were separated and trimmed flat on the ends. The 10-cm section was used for the solute-transport and breakthrough analysis, and the 5-cm portion was used for hydraulic-properties testing.

The repacked samples were placed in permeameters, and saturated hydraulic conductivities,  $K_s$ , were determined using constant and falling-head methods. Values of  $K_s$  are shown in *Table 1*. Soil-water characteristics for drainage were determined using hanging-column, pressure-plate, and thermocouple psychrometer analysis. Data from the moisture-retention analyses, shown in *Figure 2*, were fit using the RETC computer code (van Genuchten et al. 1991), and the results are shown in *Table 1*. The total porosity is equal to the saturated water content,  $\theta_s$ , and is very close to the calculated porosity value obtained using the dry bulk density and an assumed particle density of  $2.65 \text{ g/cm}^3$ .

Recognizing that the pressure potential used to determine residual moisture content will affect the moisture-retention analysis (Stephens and Rehfeldt 1985; Corey 1994), residual water contents ( $\theta_r$ ) were determined by using pressure potentials of  $-0.33 \text{ bar}$  (Ahuja 1989) and  $-15 \text{ bar}$  (*Table 1*).

Solute breakthrough tests, using a tritium tracer, were performed on the 10-cm-long repacked soil columns; results are shown in *Table 2*. The columns were oriented vertically and the flow direction was upward. A  $0.05\text{-M}$  calcium sulfate-water solution was delivered from a reservoir to the columns using a peristaltic pump. The soil columns were periodically removed from the system and weighed to determine the extent of saturation. When the column weights were constant, the columns were considered to be saturated. Outflow solution was collected, using fraction collectors, for several days to determine column fluxes. After column fluxes had been determined, a tritium solute was then introduced into the influent solution. Activity of outflow samples and samples of the influent solutions were determined using a scintillation counter.

Solute-breakthrough data were analyzed using the CXTFIT (version 2.0) code (Toride et al. 1995). Both equilibrium and non-equilibrium models were fit to the tritium-breakthrough results. Effluent samples were assumed to represent flux-averaged concentrations. Because tritium approximates a conservative tracer, the retardation factor was set to 1 for all fitting procedures. The program was allowed to fit all other parameters, i.e., in the equilibrium model, mean pore velocity and dispersion are fitted, and in the non-equilibrium model two additional parameters,  $\beta$  and  $\omega$ , are fitted. Measured data and fitted curves are shown in *Figure 3*. Calculated values of pore velocity and dispersion coefficient determined by fitting the equilibrium and non-equilibrium models are shown in *Table 3*. For the non-equilibrium model,  $v = v_m$ , the velocity through the mobile pores.

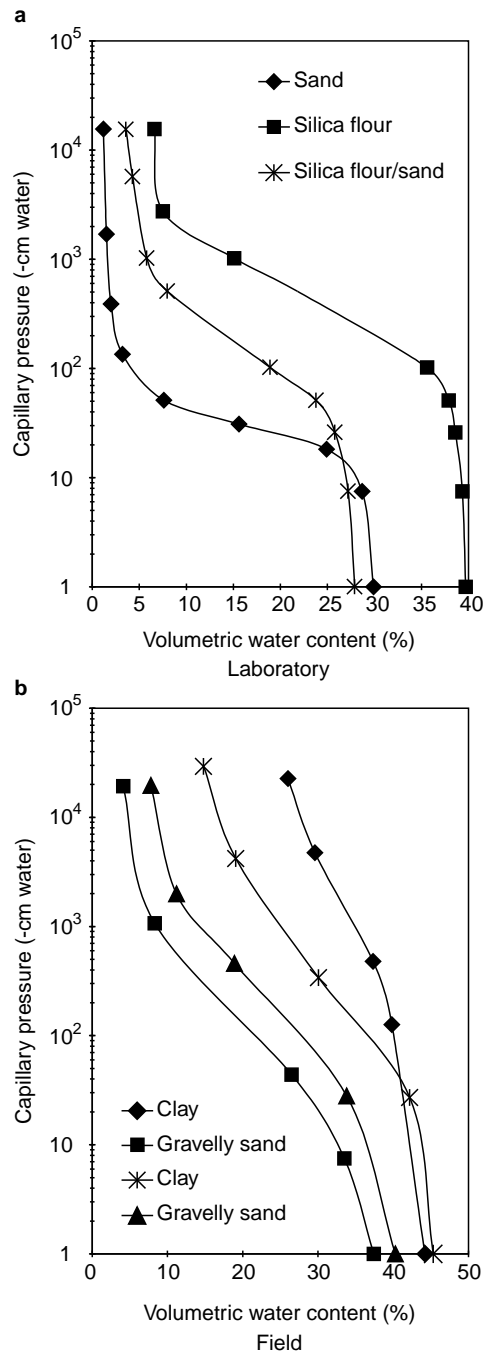


**Fig. 2a,b** Curves of soil-water characteristics

Effective porosity is calculated from *Eq. (1)* knowing  $q$  from the experimental flow rate (*Table 2*) and  $v$  obtained by analyses of the breakthrough curve using the CXTFIT program (*Table 3*). For the non-equilibrium model, one could presume that  $\beta$ , the mobile water content/porosity ratio, multiplied by the total porosity would also represent effective porosity.

Cumulative effluent solute mass was also measured for each column and the data were analyzed to compute effective porosity with Shackleford's cumulative-mass approach (*Eqs. (5)–(7)*).

**Table 1** Laboratory hydraulic properties of soils used in the laboratory tracer tests and soils from the field site

Soil type	$b$ (g/cm <sup>3</sup> )	$K_s$ (cm/sec)	$\theta_r$ (-1/3 bar) (cm <sup>3</sup> /cm <sup>3</sup> )	$\theta_r$ (-15 bar) (cm <sup>3</sup> /cm <sup>3</sup> )	$\theta_s$ (cm <sup>3</sup> /cm <sup>3</sup> )	$d_{50}$ (mm)
Sand	1.86	$5.2 \times 10^{-3}$	0.024	0.011	0.300	0.13
Silica	1.60	$1.6 \times 10^{-5}$	0.263	0.066	0.397	0.024
Sand/Silica Mixture	1.94	$4.6 \times 10^{-5}$	0.124	0.036	0.279	0.091
Field 1 – Clay	1.48	$2.0 \times 10^{-8}$	0.387	0.279	0.442	0.0065
Field 2 – Gravelly Sand	1.66	$1.6 \times 10^{-3}$	0.157	0.046	0.374	8.7
Field 3 – Sandy Clay	1.45	$2.3 \times 10^{-6}$	0.307	0.163	0.453	0.038
Field 4 – Gravelly Sand	1.58	$4.7 \times 10^{-4}$	0.215	0.093	0.403	2.7

$b$ : Bulk density  
 $K_s$ : Saturated hydraulic conductivity  
 $\theta_r$ : Residual water content  
 $\theta_s$ : Saturated water content  
 $d_{50}$ : Median grain size  
Porosity

**Table 2** Laboratory tracer test conditions

Soil Type	Flow rate, Q (cm <sup>3</sup> /hr)	Inlet Pulse Duration (hr)	Column Cross Section, A (cm <sup>2</sup> )	Column Length, L (cm)	Darcy flux, q (cm/hr)
Sand	24.40	12.35	42.21	10.045	0.578
Silica	19.79	21.5	42.21	9.124	0.469
Sand/Silica Mixture	16.89	13.1	42.21	9.737	0.400

**Table 3** Transport parameters from laboratory experiments

Soil Type	Equilibrium Model		Non-Equilibrium Model			
	$v$ (cm/hr)	D (cm <sup>2</sup> /hr)	$v$ (cm/hr)	D (cm <sup>2</sup> /hr)	$\beta$	$\omega$
Sand	1.339	7.76	5.621	2.24	0.2665	1.556
Silica	1.139	12.29	1.674	6.60	0.3221	0.1612
Sand/Silica Mixture	1.15	2.197	18.67	$6.6 \times 10^{-3}$	0.068	6.16

$v$  = Pore-water velocity  
D = Hydrodynamic dispersion coefficient  
 $\beta = \theta_m/\theta$ , where  $\theta_m$  is the volumetric water content of mobile liquid phase and  $\theta$  is total water content  
 $\omega = \alpha L/\theta v$ , where L is characteristic length, and  $\alpha$  is a first-order kinetic rate coefficient

**Table 4** Estimated and calculated effective porosity in soil columns

Soil Type	Calculated			Estimated		
	Equilibrium Model	Non-Equilibrium Model	Cumulative Mass Approach	Particle Size	$n-\theta_r$ (0.3b)	$n-\theta_r$ (15b)
Sand	0.431	0.102	0.248	0.32	0.276	0.289
Silica	0.412	0.280	0.159	0.20	0.134	0.331
Sand/Silica Mixture	0.348	0.021	0.261	0.30	0.155	0.243

Table 4 summarizes the laboratory measured and estimated effective-porosity results. The equilibrium-model parameters resulted in effective porosity values that were greater than the total porosity (Table 1) for each soil and were deemed to be unreasonable. The non-equilibrium model gave the best fit to the experimental breakthrough data. However, the calculated effective porosity represented only approximately 33, 70, 7% of the saturated water content for the sand, silica,

and sand/silica mix, respectively. The cumulative-mass approach provided estimates of effective porosity that appear intuitively more reasonable, inasmuch as the effective porosity comprises approximately 83, 40, and 93% of the saturated water content for the sand, silica, and sand/silica mix.

The  $\beta$  parameter from the non-equilibrium model (Table 3), when multiplied by total porosity,  $\theta_s$  (Table 1), gives  $\theta_m$ , the mobile water content. The respec-

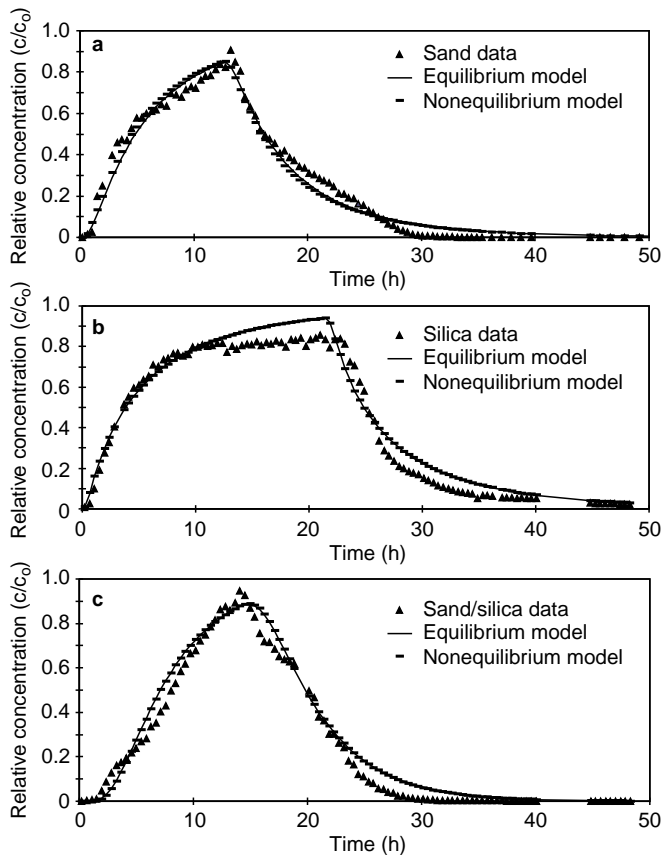


**Fig. 3** Observed and fitted tritium breakthrough concentration for fine sand, silica flour, and sand/silica mixture

tive values of  $\theta_m$  are 0.08 for sand, 0.128 for silica, and 0.02 for the sand/silica mix. The mobile water content is similar to the effective porosity calculated by *Eq. (1)*, except for silica. The reason for the poor agreement for silica is not clear.

Among the methods to estimate effective porosity of a specific soil, significant variability is evident. The estimated effective porosity from particle size (i.e., *Fig. 1*) tends to be most similar to effective porosity calculated by the cumulative-mass approach. The estimated effective porosity based on porosity minus the 0.33-bar water content gives reasonable agreement with calculated values from cumulative-mass approach, except for the sand/silica mix. The estimated effective porosity calculated as porosity minus the 15-bar water content gives fair agreement to effective porosity calculated for the sand and the sand/silica mix from the cumulative-mass approach; but for silica, porosity minus 15-bar water content overestimates the values from cumulative-mass approach by more than 100% and is actually closer to the effective porosity calculated from the non-equilibrium model.

Due to the scatter in calculated values of effective porosity for each soil, it is not possible to discern which model provided the most accurate estimate of effective porosity. The value of effective porosity appears to be

dependent on the conceptual model chosen for transport. Wide scatter also exists in the estimated values of effective porosity. Consequently, it is not possible based on these experiments to establish any relationship between estimated and calculated effective porosity, even for homogeneous soil.

Sources of uncertainty also exist in the analysis of the tracer experiments. For example, at the low Péclet numbers (0.9–5.2) in these short-column tests, the breakthrough curves are probably sensitive to boundary conditions. In the usual application of the equilibrium models, instead of obtaining  $v$  by fitting, one assumes that  $v$  is known from  $q/\theta_s$  (Parker 1984). However, this would preclude us from obtaining effective porosity from *Eq. (1)*. Likewise, the velocity can be specified in the non-equilibrium model and effective porosity calculated from  $\beta\theta_s$ . Unfortunately, without constraints on more parameters, the calculated values of effective porosity from the popular code CXTFIT vary considerably. Perhaps special tracer tests, such as those described by Luckner and Schestakow (1991), would provide more definitive calculations of effective porosity in the laboratory.

### Field Tracer Test

A groundwater reclamation system constructed to remediate contamination at the Tucson International Airport Superfund site (in Arizona, USA) afforded an opportunity to determine effective porosity in the field. The reclamation well field, which began operation in 1987, consists of extraction wells that pump contaminated water to a treatment plant where sulfuric acid is added to the treated water prior to reinjection. Sulfate in excess of background concentrations was considered as a conservative tracer in groundwater. Groundwater monitor wells were sampled periodically as part of the routine system performance assessment. A portion of the reclamation system consisting of the area near injection well R-5 and monitor well M-6 was used for analyzing the breakthrough data. This area and a geologic cross section are shown in *Figure 4*.

Effective porosity was obtained by calibrating a numerical flow and transport model. The flow code MODFLOW (McDonald and Harbaugh 1988) was used to generate the transient hydraulic-head field in two dimensions in the plan view (*Fig. 4*). The mesh consisted of grid blocks of 37 rows  $\times$  31 columns having dimensions of 25  $\times$  25 feet. The injection-rate history is known from available metering records; rates ranged from 50–392 gpm. Hydraulic conductivity is 40 feet/day throughout this local domain and is consistent with the regional-scale conductivity field generated by geostatistical analysis of numerous well tests in the area. The storage coefficient is 0.25. The comparison of the model predicted and measured hydraulic head in the monitor well M-6 is presented in *Figure 5*.

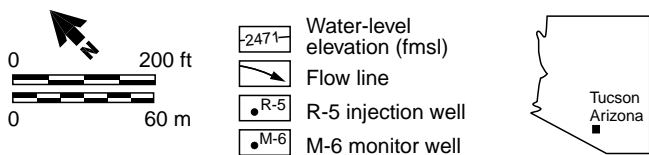
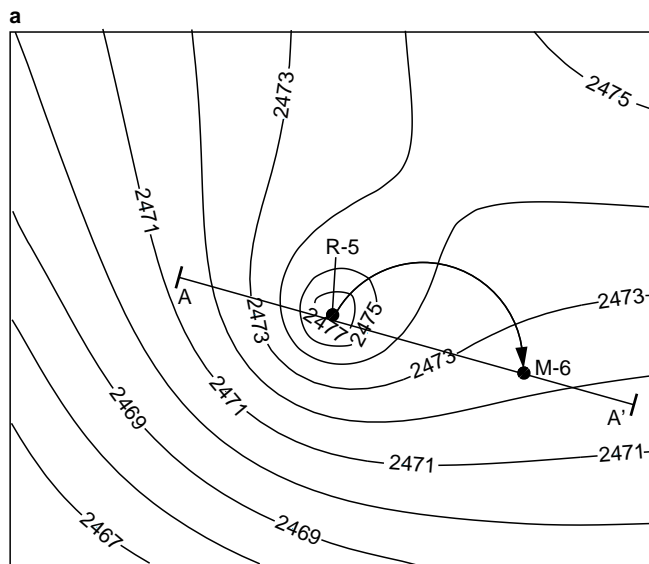


**Fig. 4** **a** Water-level elevations and **b** geologic cross section through recharge well R-5 and monitor well M-6, Tucson International Airport Superfund Site, Arizona, USA

For transport, the solute-transport code SURFACT (Hydrogeologic, Inc. 1996) was used which accepted as input the velocity field produced by MODFLOW. Effective porosity was obtained in a trial-and-error process by adjusting the model-assigned effective porosity until a best fit to observed sulfate data was obtained. As part of the calibration process, longitudinal and

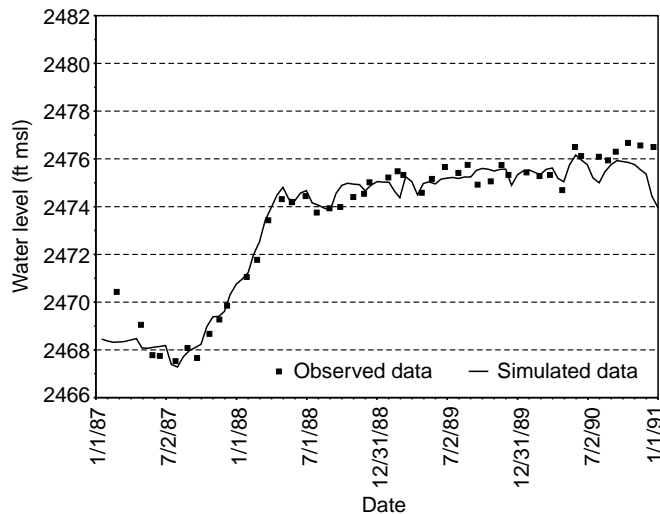


**Fig. 5** Observed and predicted water levels in monitor well M-6

transverse dispersivity were also adjusted. The calibration criterion was the minimization of the root mean squared error in concentration

$$RMS = \left[ \frac{1}{n} \sum_{i=1}^n (c_m - c_s)_i^2 \right]^{0.5} \tag{16}$$

where  $n$  is the number of monitoring data,  $c_m$  is the measured concentration, and  $c_s$  is the simulated concentration. The results are shown in *Figure 6*, which demonstrates that there is no unique solution, that the breakthrough curves are much more sensitive to effective porosity than dispersivity ratio, and that the best fit

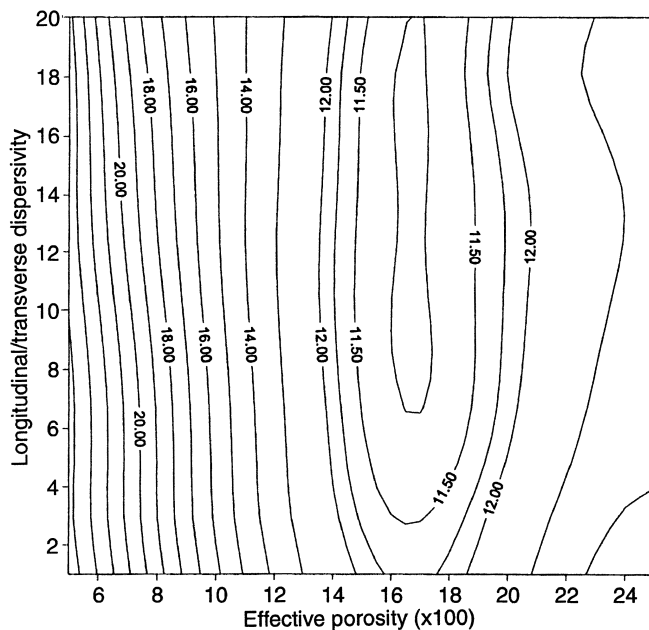


**Fig. 6** RMS error from numerical simulation of sulfate breakthrough

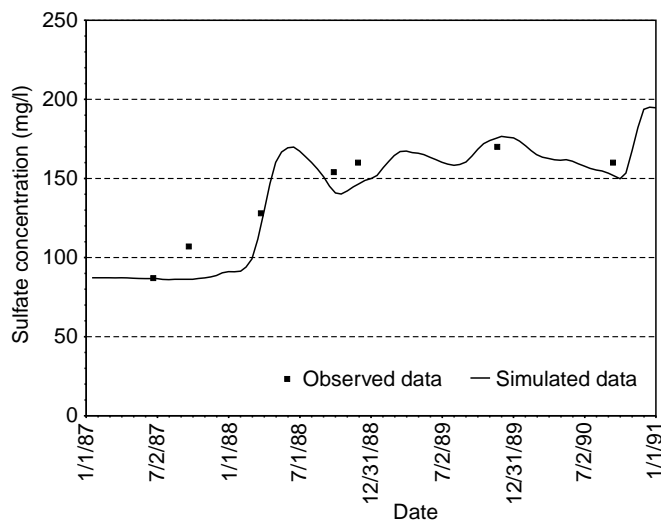


**Fig. 7** Observed and predicted sulfate concentrations

to the measured concentration occurs when effective porosity is approximately 0.17. *Figure 7* shows the observed and simulated concentration history for the monitor well.

For comparison, the effective porosity also was inferred using *Figure 1* and estimated median particle size, based on geologic logs of the injection well. The aquifer consists of alluvium that is predominantly sand and gravel, with some layers of silt and clay (*Fig. 4*). Assuming transport occurs primarily in the gravelly sand, the effective porosity is estimated to be 0.32, based on a qualitative evaluation of soil texture. Measured physical properties from two core samples of similar gravelly sand field soils are given in *Table 1*. The measured median particle size by sieve analysis was used in *Figure 1* to determine specific yield. The estimated effective porosity is approximately 0.31.

The effective porosity was also estimated from measured soil-water characteristic curves on two samples of similar sand-and-gravel aquifer material from nearby borings (*Table 1*). For these samples effective porosity, estimated as porosity minus the 15-bar water content, ranges from 0.30–0.32. These values are consistent with effective porosity estimated from the specific yield determined with *Figure 1*, based on soil texture characterized both qualitatively from the geologic description and quantitatively from sieve analysis.

Groundwater models have also been constructed to simulate the regional transport of organic solvents over an area that encompasses this field tracer study area, as well as a plume one mile wide and five miles long. Each of the modelers estimated the effective porosity as 0.25, using professional judgment applied to the predominantly gravelly sand composition of the aquifer (Hargis and Montgomery 1982; Mock 1985; CH2M Hill 1987).

*Table 5* summarizes the effective porosity values obtained at the field site. The estimates are approximately 50–90% greater than the measurements obtained from

**Table 5** Estimated and calculated effective porosity at field site

Method		Effective Porosity
Calculated	Field Tracer Test	0.17
Estimated	Geologic Logs	0.32
	Measured Particle Size	0.31
	$n-\theta_r$ (15b)	0.32
	Mock (1985)	0.25
	CH2M Hill (1987)	0.25
	Hargis (1982)	0.25

the field tracer test. One practical implication of this result is that the predicted length of the regional TCE plume by the regional transport model using the smaller effective porosity would be at least 1.5 times longer than a plume predicted with the estimated, larger effective porosity.

## Conclusion

A comparison of estimated and calculated effective porosity was done in this study. Calculated effective porosity from tracer tests in the laboratory is highly dependent on the chosen conceptual transport model and fitting approach. No consistent agreement was observed between estimated effective porosity and values calculated from laboratory tracer tests. Estimation methods tend to overestimate the transport effective porosity in a field tracer test conducted in a layered aquifer composed predominantly of gravelly sand. Effective porosity for transport cannot be reliably estimated from particle size and specific yield or from measurements of soil-water retention.

Field tracer tests provide the most direct method for obtaining effective porosity, but often they are relatively expensive and time-consuming. However, as in the case study here, model calibration may be a cost-effective approach to determine effective porosity using existing monitor-well time-series data.

**Acknowledgment** We are grateful to R. Bowman, Geoscience Department, New Mexico Institute of Mining Technology, Socorro, New Mexico, for conducting the laboratory tracer-breakthrough experiments and for his helpful suggestions in the interpretation of data.

## References

- Ahuja LR, Cassel DK, Bruce RR, Barnes BB (1989) Evaluation of spatial distribution of hydraulic conductivity using effective porosity data. *Soil Sci Soc Am J* 148:404–411
- Bear J (1972) *Dynamics of fluids in porous media*. Elsevier, New York
- Bear J, Verruijt A (1987) *Modeling groundwater flow and pollution*. Reidel, Dordrecht

- Boutwell SH, Brown SM, Roberts BR, Atwood DF (1986) Modeling remedial actions at uncontrolled hazardous waste sites. Neyes Publications, Park Ridge, New Jersey
- CH2M-Hill (1987) Draft: assessment of the relative contribution to groundwater contamination from potential sources in the Tucson Airport area, Tucson, Arizona, EPA contract no. 68-01-7251, CH2M Hill, Santa Ana, California
- Carrera J, Samper J, Galarza G, Medina A (1990) An approach to process identification: application to solute transport through clays. In: ModelCARE 90: calibration and reliability in groundwater modeling. IAHS Publ 195:231-240
- Corey AT (1994) Mechanics of immiscible fluids in porous media. Water Resource Publication, Fort Collins, Colorado
- Marsily G de (1986) Quantitative hydrogeology: groundwater hydrology for engineers. Academic Press, San Diego, California
- Domenico PA, Schwartz FW (1990) Physical and chemical hydrogeology. Wiley, New York
- Drost W, Klotz D, Koch A, Moser M, Neumaier F, Rauer W (1968) Point dilution methods of investigating groundwater flow by means of radioisotopes. Water Resour Res 4:125-146
- Fetter CW (1993) Contaminant hydrogeology. MacMillan, New York
- Gaspar E, Oncescu M (1972) Radioactive tracers in hydrology. Elsevier, New York
- Grisak GE, Merriott WF, Williams DW (1977) A fluoride borehole dilution apparatus for groundwater velocity measurements. Can Geotech J 14:554-561
- Halevy E, Nir A (1962) The determination of aquifer parameters with the aid of radioactive tracers. J Geophys Res 67 (6): 403
- Halevy E, Moser H, Zellhofer O, Zuber A (1967) Borehole dilution techniques: a critical review. In: Isotopes in Hydrology, IAEA Proc Series, IAEA, Vienna
- Hall SH, Luttrell SP, Cronin WE (1991) A method for estimating effective porosity and ground-water velocity. Ground Water 29:171-174
- Hargis and Montgomery (1982) Digital simulation of contaminant transport in the regions aquifer systems, Tucson Report no. TR-C.4
- Horton R, Thompson ML, McBride JF (1987) Method of estimating the travel time of noninteracting solutes through compacted soil material. Soil Sci Soc Am J 51:48-53
- Hydrogeologic, Inc. (1996) MS-VNS users manual
- Leap DI, Kaplan PG (1988) A single-well tracing method for estimating regional advective velocity in a confined aquifer: theory and preliminary laboratory verification. Water Resour Res 24 (3): 993-998
- Luckner L, Schestakow WM (1991) Migration processes in the soil and groundwater zone. Lewis Publishers, Chelsea, Michigan
- McDonald MG, Harbaugh AW (1988) A modular three-dimension finite-difference groundwater flow model. USGS Open File Rep 83-875
- Mock PA, Travers BC, Williams CK (1985) Results of the Tucson Airport area remedial investigation, phase I, vol II. Tucson Report TR-B.1., pp 88-89
- Molson JW, Frind EO (1990) Perspectives on non-uniqueness in three-dimension transport simulations of biodegrading organic contaminants. In: ModelCARE 90: calibration and reliability in groundwater modeling. IAHS Publ 195:341-350
- Norton D, Knapp R (1977) Transport phenomena in hydrothermal systems: the nature of porosity. Am J Sci 277:913-936
- Parker JC (1984) Analysis of solute transport in column tracer studies. Soil Sci Soc Am J 48 (4): 719
- Peyton GR, Gibb JR, LeFaivre MH, Ritchey JD (1985) On the concept of effective porosity and its measurement in saturated fine-grained porous materials. In: Proc 2nd Canadian/American Conference of Hydrology, National Water Well Association, Dublin, Ohio
- Shackelford CD (1995) Cumulative mass approach for column testing. J Geotech Eng: 696-703
- Stephens DB, Rehfeldt KR (1985) Evaluation of closed-form analytical models to calculate conductivity in a fine sand. Soil Sci Soc Am J 49:12-19
- Toride N, Leij FJ, van Genuchten MTh (1995) The CXTFIT code for estimating transport parameters from laboratory and field tracer experiments. Version 2.0. U.S. Salinity Laboratory Research Rep no. 137
- van Genuchten MTh, Wagenet RJ (1989) Two-site/two-region models for pesticide transport and degradation: theoretical development and analytical solutions. Soil Sci Soc Am J 53:1303-1310
- van Genuchten MTh, Leij FJ, Yates SR (1991) The RETC code for quantifying the hydraulic functions of unsaturated soils. U.S. Salinity Laboratory Research Rep, 83 pp

**APPLICATION FOR PERMIT  
DNCS ENVIRONMENTAL SOLUTIONS**

**VOLUME III: ENGINEERING DESIGN AND CALCULATIONS  
SECTION 10: EVAPORATION CALCULATIONS**

**TABLE OF CONTENTS**

<b>Section No.</b>	<b>Title</b>	<b>Page</b>
1.0	INTRODUCTION .....	III.10-1
1.1	Description .....	III.10-1
2.0	DESIGN CRITERIA .....	III.10-1
3.0	EVAPORATION POND DESIGN.....	III.10-2
3.1	Design Criteria .....	III.10-4
3.2	Design Concepts.....	III.10-5
3.3	Water Balance Modeling.....	III.10-6
3.4	Mechanical Evaporator Lateral Drift Analysis .....	III.10-9
4.0	SUMMARY .....	III.10-11

**LIST OF FIGURES**

<b>Figure No.</b>	<b>Title</b>	<b>Page</b>
III.10.1	EVAPORATION POND WATER BALANCE FLOW DIAGRAM .....	III.10-7
III.10.2	EVAPORATION POND MECHANICAL EVAPORATOR LOCATIONS .....	III.10-8
III.10.3	EFFECT OF HUMIDITY AND TEMPERATURE ON DRIFT .....	III.10-13

**LIST OF TABLES**

<b>Table No.</b>	<b>Title</b>	<b>Page</b>
III.10.1	EVAPORATOR WATER BALANCE.....	III.10-3
III.10.2	INFLUENCE OF DROPLET SIZE ON DRIFT DISTANCE.....	III.10-10
III.10.3	LATERAL DRIFT AT VARIOUS WINDSPEEDS .....	III.10-10
III.10.4	DRIFTSIM ANALYSIS RESULTS.....	III.10-12

**APPLICATION FOR PERMIT  
DNCS ENVIRONMENTAL SOLUTIONS**

**VOLUME III: ENGINEERING DESIGN AND CALCULATIONS  
SECTION 10: EVAPORATION CALCULATIONS**

**LIST OF ATTACHMENTS**

<b>Attachment No.</b>	<b>Title</b>
III.10.A	EFFECTS OF MAJOR VARIABLES ON DRIFT DISTANCES OF SPRAY DROPLETS
III.10.B	DRIFTSIM: PREDICTING DRIFT DISTANCE OF SPRAY DROPLETS AND RESULTING EVAPORATION

**APPLICATION FOR PERMIT  
DNCS ENVIRONMENTAL SOLUTIONS**

**VOLUME III: ENGINEERING DESIGN AND CALCULATIONS  
SECTION 10: EVAPORATION CALCULATIONS**

**1.0 INTRODUCTION**

DNCS Environmental Solutions (DNCS Facility) is a proposed Surface Waste Management Facility for oil field waste processing and disposal services. The proposed DNCS Facility is subject to regulation under the New Mexico Oil and Gas Rules, specifically 19.15.36 NMAC, administered by the Oil Conservation Division (OCD). The Facility has been designed in compliance with 19.15.36 NMAC, and will be constructed and operated in compliance with a Surface Waste Management Facility Permit issued by the OCD. The Facility is owned by, and will be constructed and operated by, DNCS Properties, LLC.

**1.1 Description**

The DNCS site is comprised of a 562-acre  $\pm$  tract of land located south of NM 529 in portions of Section 31, Township 17 South, Range 33 East; and in the northern half of Section 6, Township 18 South, Range 33 East, Lea County, NM. A portion of the 562-acre tract is a drainage feature that will be excluded from development. The drainage feature includes a 500-ft setback and totals 67 acres  $\pm$ . The DNCS Facility will include two main components; a liquid oil field waste Processing Area (177 acres  $\pm$ ), and an oil field waste Landfill (318 acres  $\pm$ ); therefore the DNCS Facility comprises 495 acres  $\pm$ . Oil field wastes are anticipated to be delivered to the DNCS Facility from oil and gas exploration and production operations in southeastern NM and west Texas. The Site Development Plan provided in the **Permit Plans, Sheet 3**, identifies the locations of the Processing Area and Landfill facilities.

**2.0 DESIGN CRITERIA**

The Processing Area will include evaporation ponds for the disposal of Produced Water. The area and volume of the lined portion of each evaporation pond is 1.88 acres of water surface with a capacity of 9.5 acre-feet (ft). DNCS will include a total of twelve ponds which will provide a total of 22.56 surface acres for evaporation of 114 total acre-ft of pond capacity.

## **2.1 General Site Conditions**

The site terrain is gently sloping toward the west with sparse vegetation. The macro-climate of the DNCS area is classified by the Koppen Climate Classification System as a “BSk”, which indicates a semi-arid steppe with much of the characteristics of a desert. Meteorological climatic data was obtained from the Western Regional Climate Center for pan evaporation at Lake Avalon and precipitation at the Hobbs FAA Airport weather stations which are the closest reporting points for these two data sets.

The evaluation of climate data for these nearby weather stations indicates that they are relatively similar and will likely provide reasonable precipitation estimates for the site (**Table III.10.1**). Climatic data available for the Lake Avalon weather station includes pan evaporation for for the years of record from 1914 through 1979. The Hobbs FAA Airport weather station includes precipitation for the years of record from 1942 through 2006. The Lake Avalon pan evaporation data was used to estimate monthly evaporation values at the DNCS site. The observed pan evaporation values were scaled by a factor of 0.7 to represent actual pond evaporation. The average monthly evaporation and precipitation data used for design of the DNCS evaporation ponds is summarized in **Table III.10.1**. Considering this climatic data, the annual evaporation exceeds annual precipitation on average by over six times.

The predominant wind directions for the site are from the south and southeast, with an average annual wind speed of 11 miles per hour (mph). The maximum sustained wind speed conservatively used for facility design is 14 mph.

## **3.0 EVAPORATION POND DESIGN**

This section provides the engineering analyses and technical details to support design of the evaporation ponds for the DNCS Facility with an average evaporation rate of 1,000 bbl per pond. While maintaining potential drift within the pond boundary.

**Table III.10.1  
Evaporator Water Balance  
DNCS Environmental Solutions**

	January	February	March	April	May	June	July	August	September	October	November	December	Total
Rainfall	0.42	0.40	0.41	0.46	1.64	1.63	2.32	2.35	2.45	1.19	0.55	0.55	<b>14.37</b>
Pan Evaporation	4.49	5.33	9.42	12.36	14.31	15.16	14.14	12.33	9.25	7.26	4.68	4.20	<b>112.93</b>
Actual Evaporation	3.14	3.73	6.59	8.65	10.02	10.61	9.90	8.63	6.48	5.08	3.28	2.94	<b>79.05</b>
NET	-2.72	-3.33	-6.18	-8.19	-8.38	-8.98	-7.58	-6.28	-4.03	-3.89	-2.73	-2.39	<b>-64.68</b>
Net Evaporation (bbl/pond)	4,526	5,536	10,278	13,615	13,923	14,928	12,595	10,439	6,690	6,469	4,531	3,972	<b>107,501</b>

Notes:

1. Rainfall obtained from Hobbs FAA Airport and is average monthly rainfall from 1942-2006.
2. Input is the maximum Monthly Produced water that can be introduced to Evaporation Ponds based on Water Balance.
3. Evaporation rates obtained from Lake Avalon, New Mexico from 1914 -1979.
4. Actual Evaporation rates represent 70% of reported Pan Evaporation rate.
5. Pond surface area 1.928 acres
9. Based on the Hobbs Wind Rose, the wind speed in this area is below 14 mph 63% of the time.

295

bbl/day

**Mechanical Evaporation Analysis**

Mechanical Evaporation Rate <sup>1</sup>	1-ME	2	3	4	5	6	7	8	9	12	18	24
10	216	432	648	864	1,080	1,296	1,512	1,728	1,944	2,592	3,888	5,184
20	432	864	1,296	1,728	2,160	2,592	3,024	3,456	3,888	5,184	7,776	10,368
30	648	1,296	1,944	2,592	3,240	3,888	4,536	5,184	5,832	7,776	11,664	15,552
40	864	1,728	2,592	3,456	4,320	5,184	6,048	6,912	7,776	10,368	15,552	20,736
50	1,080	2,160	3,240	4,320	5,400	6,480	7,560	8,640	9,720	12,960	19,440	25,920
60	1,296	2,592	3,888	5,184	6,480	7,776	9,072	10,368	11,664	15,552	23,328	31,104

Notes:

1. Mechanical Evaporation Rate in Gallons per Minute
2. Evaporation rate per Mechanical Evaporator (ME) expressed in bbls per day
3. Wind Speed <14 MPH                      63                      % of Time
4. US Barrel =                                      42                      Gallons

**Minimum Anticipated Mechanical Evaporation Potential**

Evaporation by month	January	February	March	April	May	June	July	August	September	October	November	December	Annual BBL	BBL/Day
3-ME @ 10GPM (1-Pond)	20,088	18,144	20,088	19,440	20,088	19,440	20,088	20,088	19,440	20,088	19,440	20,088	236,520	648
6-ME @ 10GPM (2-Ponds)	40,176	36,288	40,176	38,880	40,176	38,880	40,176	40,176	38,880	40,176	38,880	40,176	473,040	1,296
9-ME @ 10GPM	60,264	54,432	60,264	58,320	60,264	58,320	60,264	60,264	58,320	60,264	58,320	60,264	709,560	1,944
12-ME @ 10GPM (2-Ponds)	80,352	72,576	80,352	77,760	80,352	77,760	80,352	80,352	77,760	80,352	77,760	80,352	946,080	2,592
18-ME @ 10GPM (4-Ponds)	120,528	108,864	120,528	116,640	120,528	116,640	120,528	120,528	116,640	120,528	116,640	120,528	1,419,120	3,888
24-ME @ 10GPM (4-Ponds)	160,704	145,152	160,704	155,520	160,704	155,520	160,704	160,704	155,520	160,704	155,520	160,704	1,892,160	5,184

## 3.1 Design Criteria

### 3.1.1 Design Regulations

Regulations relevant to the design of the evaporation ponds presented here in Section 3.0 are summarized below.

#### *Key Regulatory Agencies and Documents:*

**New Mexico Oil Conservation Division (OCD):** Title 19 Natural Resources and Wildlife, Chapter 15 Oil and Gas, Part 36 Surface Waste Management Facilities, Section 17 Specific Requirements Applicable to Evaporation, Storage, Treatment and Skimmer Ponds, specifically B(12) which indicates that “*The maximum size of an evaporation or storage pond shall not exceed 10 acre-feet*”.

**New Mexico Office of the State Engineer (NMOSE):** Title 19 Natural Resources and Wildlife, Chapter 25 Administration and Use of Water – General Provisions, Part 12 Dam Design, Construction and Dam Safety, Section 7 Definitions, H. Dams, (2) Non-Jurisdictional Dam which indicates that “*Any dam less than or equal to 10 feet in height and having storage less than or equal to 10 acre-feet of water. The state engineer does not regulate the design, construction and operation of a non-jurisdictional dam...*” exempting this facility’s structures from this rule.

### 3.1.2 Project Design Criteria

Design criteria relevant to the analyses presented here in Section 3.0 are summarized below.

#### *Geometry:*

**Process Operations:** Design evaporation capacity of 1,000 barrels per day (bbl/d) of produced water per pond, with potential expansion capacity to 9,000 bbl/d.

**Evaporation Pond Storage Capacity:** Less than 10 acre-ft per pond, with potential expansion to 12 ponds. Developing an ultimate pond design configuration resulted in a 9.5 acre-foot pond capacity with a surface water area of 82,000 square feet (ft) and measuring 410 ft x 200 ft.

**Maximum Evaporative Surface Area:** for twelve ponds would be 984,000 square ft or 22.56 acres.

**Process Design Life:** 50 years.

#### *Produced Water Properties:*

**Design Volumetric Flow Rate:** 12,000 bbl/d or 350 gallons per minute (gpm).

### ***System Requirements:***

**Evaporation Pond Liner System:** Double layer liner system as follows (top to bottom): (1) upper (secondary) 60 mil HDPE geomembrane liner; (2) leak detection system consisting of a 200 mil HDPE geonet; (3) lower (primary) 60 mil HDPE geomembrane liner; underlain by (4) a density controlled compacted subgrade.

**Leak Detection System:** The leak detection system will meet the following requirements:(1) constructed with a bottom slope of at least two percent; (2) constructed with a 200 mil HDPE geonet with a transmissivity of  $1 \times 10^{-3} \text{ m}^2/\text{sec}$  or greater; (3) constructed of materials that are chemically resistant to the waste and leachate; (4) designed and operated to minimize clogging during the active life; and (5) constructed with sumps and liquid removal methods (i.e., pumps).

## **3.2 Design Concepts**

This section presents the general evaporation pond design concepts with the technical aspects of these concepts discussed in detail in the following sections.

The DNCS Properties, LLC. Facility is designed for start-up operations at 3,000 bbl/d routinely, with a potential to expand to 12,000 bbl/d on average. The design produced water flows from the Settling Tanks will be discharged to the evaporation ponds. The average design flow rates associated with the start-up and ultimate production rates are 88 and 350 gallons per minute (gpm), respectively.

The evaporation pond system is designed for construction in phases. Phase I includes 4 ponds, each with a surface dimension of 410 ft by 200 ft (i.e. 1.88 acres), designed to evaporate the inflows associated with the average receipt of 3,000 bbl/d. Similarly, Phase II includes an additional 4 ponds with the same dimensions designed to evaporate the flows associated with an additional 4,000 bbl/d of produced water received routinely. All ponds are designed and constructed to provide contingency storage with an additional 3.5 ft of freeboard (above the required design capacities). Pond berms with a minimum crest width of 15 ft are designed between ponds to allow access to all sides of the ponds, as well as operation and maintenance of the evaporation equipment. Two leak detection system (LDS) sumps have been included in the design of each evaporation pond. Liquids collected in the LDS sumps will be pumped using a mobile pump, and returned to the evaporation ponds.

In order to improve performance of the evaporation pond system (i.e., enhance the evaporative capabilities), the design includes implementation of a mechanical evaporation system. The evaporators will be placed and sized to maximize evaporation and minimize the potential for wind-drift beyond the extents of the lined evaporation pond area. A continuous liner is designed over the entire evaporation pond area, including over the separation berms. A textured geomembrane will be extrusion welded on top of the berms between pond cells to facilitate access (i.e., pedestrian or ATV).

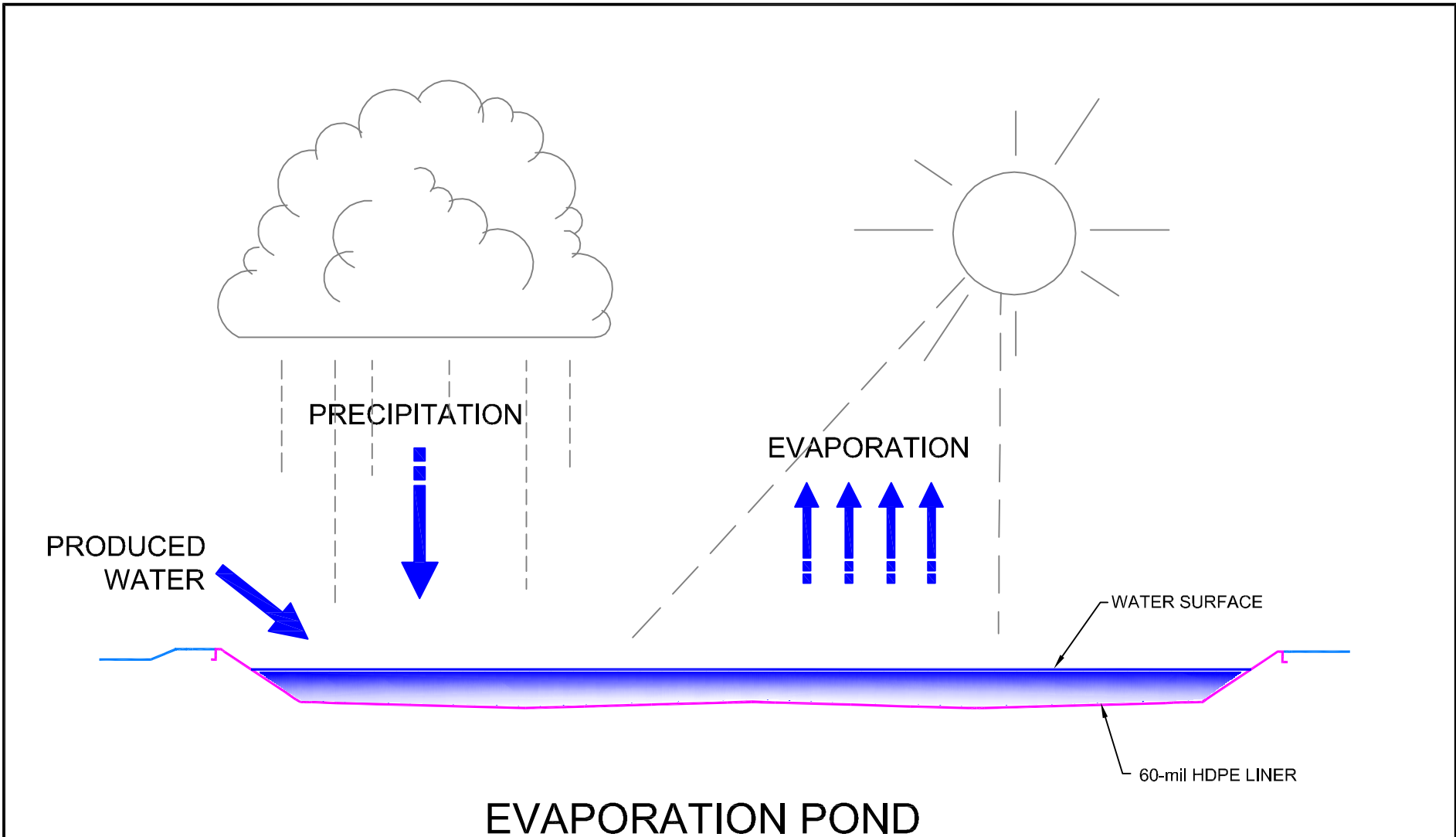
### **3.3 Water Balance Modeling**

A probabilistic water balance model was developed to assist in determining the evaporation potential of the pond system (i.e., required evaporative surface area). Water balance calculations were performed (See **Table III.10.1**).

The following water balance components were considered: (1) the amount of Produced Water entering the pond system from the Settling Tanks, (2) water entering the pond system through meteoric precipitation, and (3) the amount of water released to the atmosphere through evaporation.

Precipitation values are likely to exhibit largest variations, and were therefore treated as stochastic inputs (i.e., probabilistic), while the other parameters were treated as deterministic variables. **Figure III.10.1** presents the process flow diagram for the evaporation pond water balance.

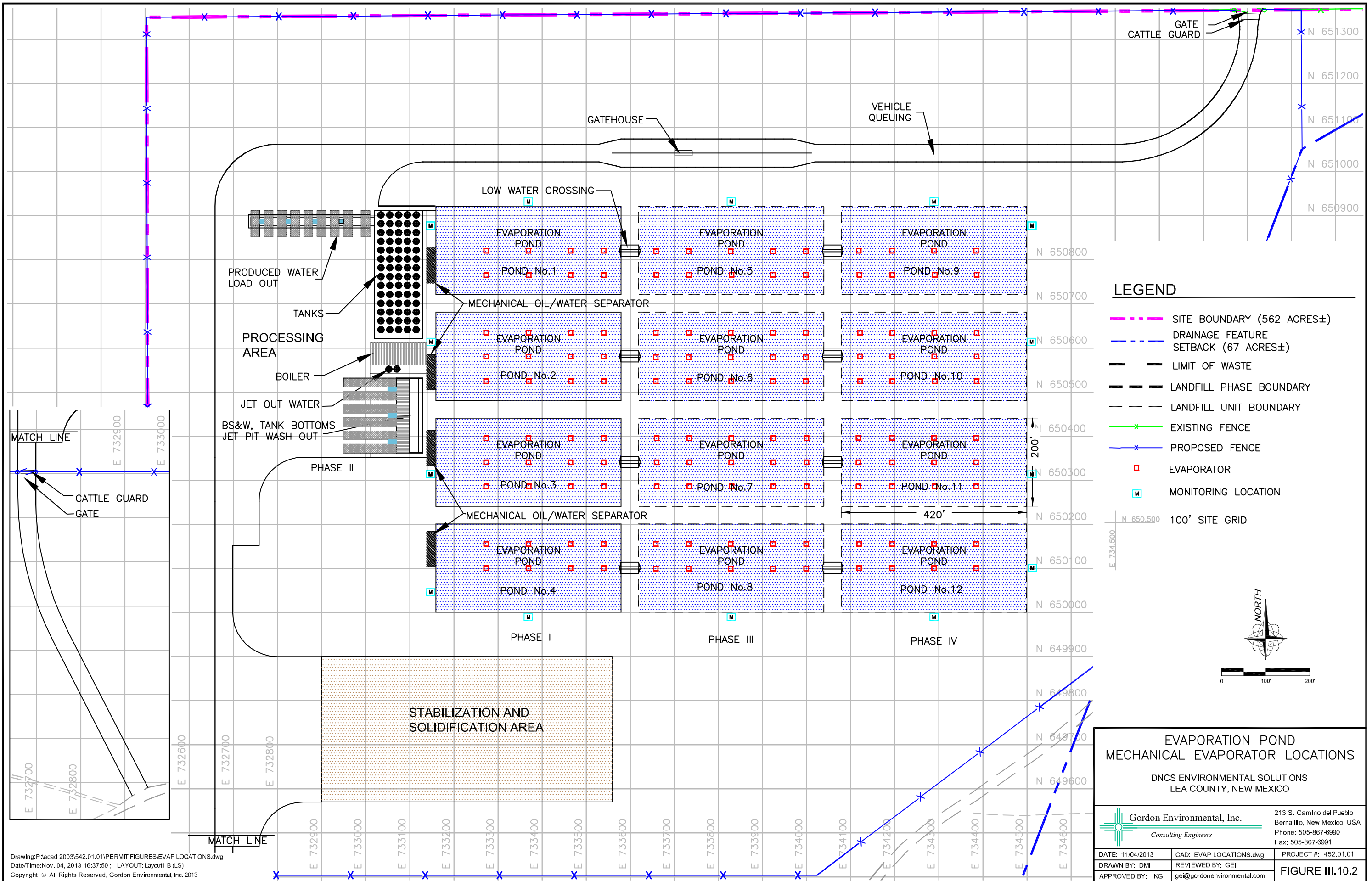
Preliminary analyses revealed a prohibitively large evaporation area for extreme precipitation events when considering evaporation losses solely from the pond surface. To reduce the required evaporative area, subsequent analyses included a mechanical evaporation system resulting in enhanced evaporation losses. All evaporators will be located at points within the ponds (as depicted in **Figure III.10.2**) to minimize the probability of wind-drift blowing the produced water beyond the lined evaporation pond area.



# EVAPORATION POND

<b>EVAPORATION POND WATER BALANCE FLOW DIAGRAM</b> DNCS ENVIRONMENTAL SOLUTIONS LEA COUNTY, NEW MEXICO		
 <b>Gordon Environmental, Inc.</b> <i>Consulting Engineers</i>		213 S. Camino del Pueblo Bernalillo, New Mexico, USA Phone: 505-867-6990 Fax: 505-867-6991
DATE: 11/04/2013	CAD: EVAPORATION.dwg	PROJECT #: 542.01.01
DRAWN BY: DMI	REVIEWED BY: GEI	
APPROVED BY: IKG	gei@gordonenvironmental.com	<b>FIGURE III.10.1</b>

Drawing: P:\acad 2003\542.01.01\PERMIT FIGURES\EVAPORATION.dwg  
 Date/Time: Nov. 04, 2013-16:47:51 : LAYOUT: A (LS)  
 Copyright © All Rights Reserved, Gordon Environmental, Inc. 2013



- LEGEND**
- - - SITE BOUNDARY (562 ACRES±)
  - - - DRAINAGE FEATURE
  - - - SETBACK (67 ACRES±)
  - LIMIT OF WASTE
  - LANDFILL PHASE BOUNDARY
  - LANDFILL UNIT BOUNDARY
  - x - EXISTING FENCE
  - x - PROPOSED FENCE
  - EVAPORATOR
  - M MONITORING LOCATION
  - - - 100' SITE GRID



**EVAPORATION POND  
MECHANICAL EVAPORATOR LOCATIONS**

DNCS ENVIRONMENTAL SOLUTIONS  
LEA COUNTY, NEW MEXICO

<b>Gordon Environmental, Inc.</b> <i>Consulting Engineers</i>		213 S. Camino del Pueblo Bernalillo, New Mexico, USA Phone: 505-867-6990 Fax: 505-867-6991
DATE: 11/04/2013	CAD: EVAP LOCATIONS.dwg	PROJECT #: 452.01.01
DRAWN BY: DMI	REVIEWED BY: GEI	<b>FIGURE III.10.2</b>
APPROVED BY: IKG	gei@gordonenvironmental.com	

Drawing: P:\acad 2003\542.01.01\PERMIT FIGURES\EVAP LOCATIONS.dwg  
 Date/Time: Nov. 04, 2013-16:37:50 ; LAYOUT: Layout-B (LS)  
 Copyright © All Rights Reserved, Gordon Environmental, Inc. 2013

The results of the water balance for each pond were calculated assuming the average annual rainfall; the percentage of the an average day when the wind speed is under 12 mph when the mechanical evaporators will be running; limiting the mechanical evaporators to no more than 10 gpm flow rate through the evaporators (even though extensive experience with this equipment indicated a greater evaporative expectation); and an input of 1,000 bbl/d of Produced Water. Based on these assumptions, the required number of mechanical evaporators per pond to evaporate 1,000 bbl/d was estimated to be three. The conservative assumption was made to discount the surface evaporation potential from the pond. due to the micro-climate created by the mechanical evaporators **Table III.10.1** details the evaporation potential per pond and identifies the additional evaporation potential that may be available based on extensive industry experience with the mechanical evaporators.

The influence of dissolved solids in the process water flow to the evaporation ponds may affect pond evaporation. It will be important to collect field evaporation measurements during the early years of pond operations to confirm the adequacy of this initial design. These field measurements will assist in refining expansion design of the evaporation ponds for an increase to 12,000 bbl/d average evaporation potential.

### **3.4 Mechanical Evaporator Lateral Drift Analysis**

The proposed mechanical evaporators were analyzed for drift potential to ensure that all of the mist generated in the evaporation process would remain within the area of the lined pond. The objective of this analysis was to determine at what distance the suspended solids would fall out with a given wind speed, droplet diameter and known level of Total Suspended Solids (TDS).

The higher the TDS the less lateral distance traveled and time the water droplet spends suspended in the air. For this analysis an 8% total TDS saturation was assumed. The proposed mechanical evaporator makes 150 micron water droplet particle sizes. This analysis assumes that the droplet particle size would be 100 microns for the drift calculations. Based on **Table III.10.2** the time required for a 100 micron particle size to fall 10 ft is 10 seconds in a 3 mph wind.

**TABLE III.10.2  
Influence of Droplet Size on Potential Drift Distance  
DNCS Environmental Solutions**

<b>Droplet Diameter (Microns)</b>	<b>Type of droplets</b>	<b>Time required to fall 10 feet</b>	<b>Lateral distance Droplets travel in falling 10 feet in a 3 mph wind</b>
5	Fog	66 minutes	3 miles
20	Very fine spray	4.2 minutes	1,100 feet
<b>100</b>	<b>Fine spray</b>	<b>10 seconds</b>	<b>44 feet</b>
150	Evaporator Standard	9 seconds	39 feet
240	Medium spray	6 seconds	28 feet
400	Course spray	2 seconds	8.5 feet
1,000	Fine rain	1 second	4.7 feet

The proposed mechanical evaporator propels the water droplets 15 ft in the air resulting in a 15 ft anticipated fall height for the water droplet particles generated. In this 3 mph wind the water droplet could drift 66 ft before falling back into the pond. Drift particles can travel up to 17 ft per mph in a strong wind (<12 mph). **Table III.10.3** provides a summary of anticipated lateral drift at different wind speeds for water droplets with an 8% TDS.

**TABLE III.10.3  
Lateral Drift at Various Windspeeds  
DNCS Environmental Solutions**

<b>Wind Speed MPH</b>	<b>Lateral Drift Ft @ 8% TDS</b>
2 MPH	31ft
4 MPH	62ft
6 MPH	93ft
8 MPH	125ft
10 MPH	155ft
12 MPH	187ft
14 MPH	219ft

An analysis was performed with DRIFTSIM a computer modeling program (**Attachment III.10.B**) that predicts the drift distance of spray droplets. This program was developed by Ohio State University, Food Agriculture, and Biological Engineering Department in coordination with the United States Department of Agriculture, Agricultural Research Service. The results from this model, utilizing a low TDS liquid (assuming greater drift), a 12 mph maximum wind speed (maximum average sustained wind speed onsite) and variable humidity's at various temperatures confirmed that based on the anticipated 150 micron droplet size, all lateral drift will fall back into the lined pond area. **Table III.10.4** and **Figure III.10.3** provide a summary of the output from this analysis.

The majority of the strong winds at this location come from the southeast direction. Given the layout of the evaporation ponds, the proposed mechanical evaporators could operate in up to 14 mph wind before the automation would need to shut the machines down relative to concerns that drift might escape the lined ponds.

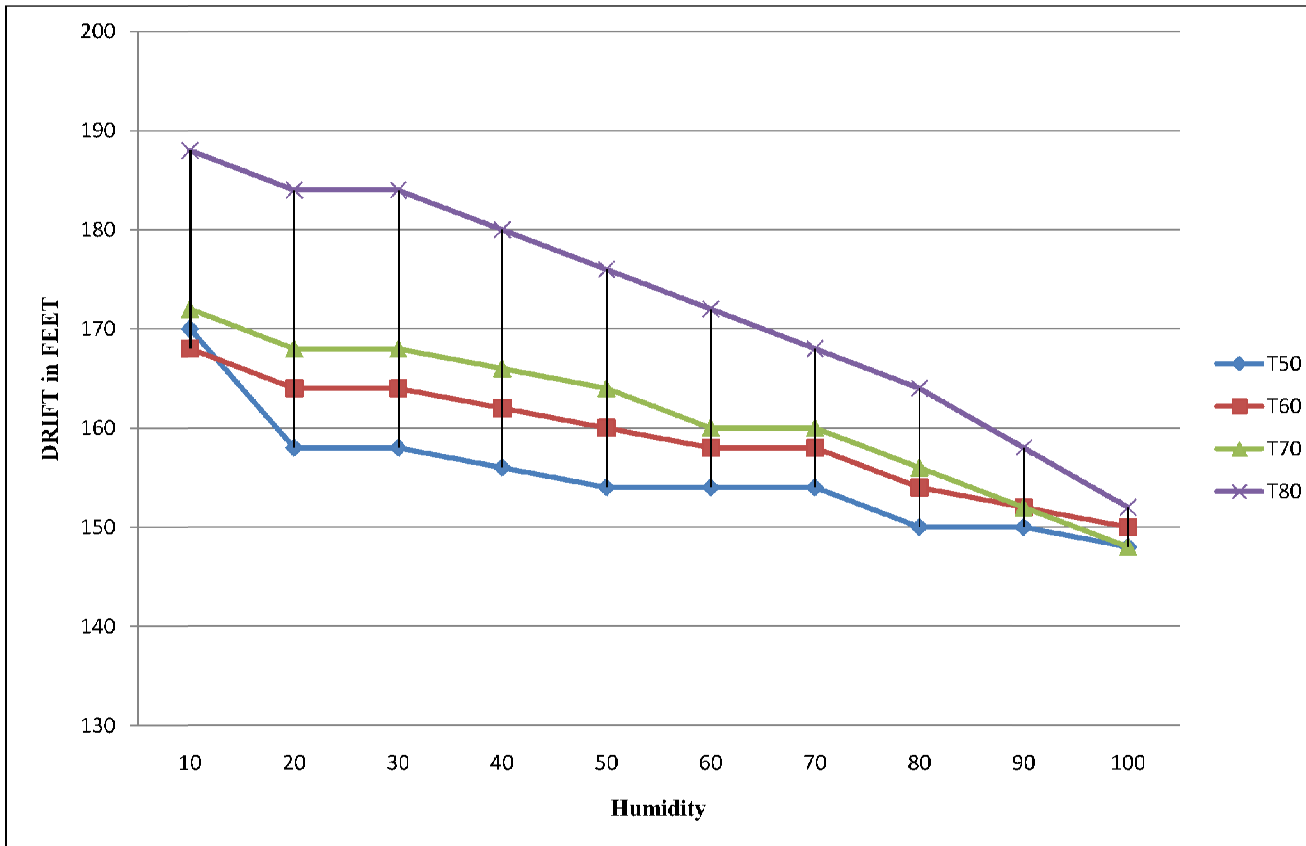
The mechanical evaporators will be controlled by a weather station with software designed to monitor wind speed and control (start and stop) the equipment to optimize evaporation hours and minimize the potential for freezing during cold periods. This weather station will also control for wind speed and direction to minimize any potential for over spray and drift situations on windy days.

#### **4.0 SUMMARY**

The proposed evaporation ponds with mechanical evaporators will be able to evaporate the proposed volumes of Produced Waters that are anticipated for receipt in the various phases of this facility's development. The potential for drift can be managed to ensure that all materials remain within the lined area of the evaporation ponds.

**TABLE III.10.4  
DRIFTSIM Analysis Results  
DNCS Environmental Solutions**

<b>Temp</b>	<b>Drop Diameter</b>	<b>Humidity</b>	<b>Drift</b>	<b>Drift</b>
50	150	10	170	85
50	150	20	158	79
50	150	30	158	79
50	150	40	156	78
50	150	50	154	77
50	150	60	154	77
50	150	70	154	77
50	150	80	150	75
50	150	90	150	75
50	150	100	148	74
60	150	10	168	84
60	150	20	164	82
60	150	30	164	82
60	150	40	162	81
60	150	50	160	80
60	150	60	158	79
60	150	70	158	79
60	150	80	154	77
60	150	90	152	76
60	150	100	150	75
70	150	10	172	86
70	150	20	168	84
70	150	30	168	84
70	150	40	166	83
70	150	50	164	82
70	150	60	160	80
70	150	70	160	80
70	150	80	156	78
70	150	90	152	76
70	150	100	148	74
80	150	10	188	94
80	150	20	184	92
80	150	30	184	92
80	150	40	180	90
80	150	50	176	88
80	150	60	172	86
80	150	70	168	84
80	150	80	164	82
80	150	90	158	79
80	150	100	152	76



## EFFECT OF HUMIDITY AND TEMPERATURE ON DRIFT

DNCS ENVIRONMENTAL SOLUTIONS  
LEA COUNTY, NEW MEXICO



Gordon Environmental, Inc.

Consulting Engineers

213 S. Camino del Pueblo  
Bernalillo, New Mexico, USA  
Phone: 505-867-6990  
Fax: 505-867-6991

DATE: 11/04/2013	CAD: DRIFT GRAPH.dwg	PROJECT #: 542.01.01
DRAWN BY: MLH	REVIEWED BY: MRH	
APPROVED BY: IKG	gek@gordonenvironmental.com	FIGURE III.10.3

**APPLICATION FOR PERMIT  
DNCS ENVIRONMENTAL SOLUTIONS**

**VOLUME III: ENGINEERING DESIGN AND CALCULATIONS  
SECTION 10: EVAPORATION CALCULATIONS**

**ATTACHMENT III.10.A  
EFFECTS OF MAJOR VARIABLES ON DRIFT DISTANCES OF  
SPRAY DROPLETS**

ohioline.ag.ohio-state.edu -- your Link to Information, News, and Education



# FactSheet

Extension

## Ohio State University Extension Fact Sheet

### Food, Agricultural, and Biological Engineering

590 Woody Hayes Drive, Columbus, Ohio 43210

---

# Effect of Major Variables on Drift Distances of Spray Droplets

AEX-525-98

---

#### Author

##### H. Erdal Ozkan

Professor  
The Ohio State University  
Food, Agricultural and Biological Engineering Department  
590 Woody Hayes Drive  
Columbus, OH 43210

---

Pesticide applications are required to ensure an adequate and high quality supply of many agricultural crops. Due to concerns for production costs, safety, and the environment, it is important to maximize the pesticide deposit on the target. One of the major problems challenging pesticide applicators is spray drift, which is defined as movement of pesticides by wind from the application site to an off-target site.

Spray drift occurs wherever liquid sprays are applied. Although complete elimination of spray drift is impossible, problems can be reduced significantly if the pesticide applicator is aware of major factors which influence drift, and takes precautions to minimize their influence on off-target movement of droplets.

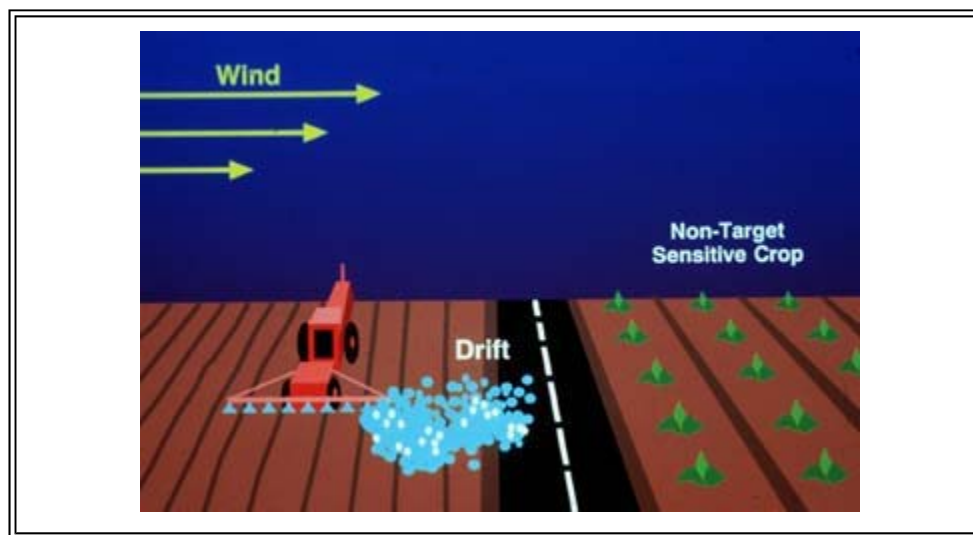
Drift is influenced by many factors that usually may be grouped into one of the following categories: 1) Spray characteristics, 2) Equipment and application techniques used, 3) Weather, and 4) Operator care and skill. A general discussion of these factors can be found in another publication by Ozkan (1991). In this publication, you will find specific information on how much influence some of these major factors

have on the drift distances of spray droplets.

The factors that significantly influence off-target movement of droplets are wind velocity and direction, droplet size and density, and distance from the atomizer to the target. Other factors that influence drift include droplet velocity and direction of discharge from the atomizer, volatility of the spray fluid, relative humidity, ambient temperature, and atmospheric turbulence intensity. Many scientists have conducted field tests to study influence of these variables on spray drift. Unfortunately, field tests have the limitation that weather conditions cannot be controlled and the variables that influence spray drift may interact and vary during a test. Computer simulations can allow determination of the effects of different values of variables such as droplet size and velocity, relative humidity, and wind velocity on spray drift. One such computer model was developed by Reichard et al.(1992a) in Ohio for modeling the effects of several variables on spray drift. Using the computer program, individual or mean droplet trajectories were determined for different values of several variables listed above. Experiments were also conducted to verify the accuracy of the computer model in predicting drift distances of water droplets in a wind tunnel. These tests revealed that the computer model can be used to accurately calculate spray drift distances for a wide range of spray droplet sizes and wind velocities (Reichard et. al., 1992b).

The major drift factors included in this publication are droplet size, wind velocity, relative humidity, ambient temperature, droplet discharge height, and initial droplet velocity. Although turbulence intensity is a major factor which influence drift, data related to this variable was not included in this publication because it is not something pesticide applicators can assess easily, and its magnitude can vary rapidly unlike the changes in other atmospheric conditions such as relative humidity and temperature. The affect of turbulence intensity on drift distances of droplets is discussed in the publication by Reichard et. al. (1992a). A turbulence intensity of 20% was assumed for all the computer simulation results reported in this publication,.

Although the accuracy of the drift data produced by computer simulation has been validated, one has to be cautious when drawing conclusions from the data presented in this publication. Due to the many variables that influence spray drift, it is extremely difficult to precisely predict drift distances of droplets for field conditions. Some of the variables that affect drift distances, such as wind turbulence, velocity and direction can vary considerably while a droplet is drifting. It is common for terrain and vegetation (size and density) to vary over the path of a drifting droplet and these influence local wind velocity and direction. The drift distance data presented in this publication are only valid for the constant conditions specified. The data presented are useful in comparing the relative effects of several factors on drift distances, but are not intended to precisely model variable field conditions.





**Spray drift is the reason for the discoloration of part of the wheat crop shown in this photograph. The size of the area affected by drift and its severity depend on how adverse the weather conditions are and poor decisions made by the operator of the sprayer.**

### **Droplet Size, Wind Velocity and Relative Humidity**

Droplet size and wind velocity are the two most influential factors affecting drift. Relative humidity influences the evaporation rate of a droplet and hence its size, flight time, velocity and drift distance. Table 1 and Figure 1 show the simulated mean drift distances for various sizes of water droplets (50-200 micron diameter), wind velocities (2-8 mph), relative humidities (20-80%), and 75 degrees F ambient temperature. (Additional data are included in Tables in the publication by Zhu et al., 1994). Unless otherwise indicated, all simulated drift distances discussed in this publication are for droplets discharged downward with 65 ft/second (45 mph) velocity toward a target 18 inches below the point of discharge.



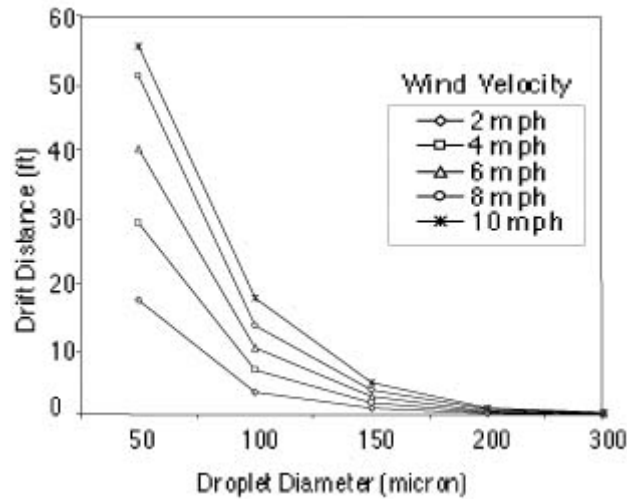


**Figure 1. Effect of droplet diameter and wind velocity on drift distances of water droplets directed downward at 65 ft/second toward a target 18 inches below discharge point (Temperature = 75 degrees F; Relative Humidity = 60%).**

**Table 1. Effect of wind velocity and relative humidity on drift distances of droplets directed downward with initial velocity of 65 ft/second toward target 18 inches below discharge point. (Temperature = 75 degrees F; turbulence intensity = 20%)**

Initial droplet size (microns)	Wind velocity (mph)	20	40	60	80
20	2	3.03*	3.72*	6.41*	15.29*
20	4	6.00*	6.47*	10.24*	21.45*
20	6	6.57*	7.66*	11.87*	23.23*
20	8	7.96*	8.97*	13.29*	26.42*
20	10	8.99*	10.58*	15.06*	30.10*
50	2	10.70*	12.10	17.20*	25.30*
50	4	18.70*	21.00*	28.80*	41.70*
50	6	26.50*	30.00*	40.00*	55.60*
50	8	34.30*	38.20*	50.90*	69.00*
50	10	37.60*	42.00*	55.32*	87.24*
100	2	3.44	3.41	3.37	3.30
100	4	6.87	6.81	6.71	6.58
100	6	10.30	10.20	10.05	9.85
100	8	13.72	13.61	13.39	13.14
100	10	17.94	17.77	17.48	17.05
150	2	0.92	0.92	0.92	0.91

150	4	1.83	1.82	1.82	1.82
150	6	2.74	2.74	2.73	2.71
150	8	3.67	3.66	3.62	3.60
150	10	4.78	4.78	4.75	4.77
200	2	0.20	0.20	0.20	0.20
200	4	0.38	0.38	0.38	0.38
200	6	0.55	0.55	0.55	0.55
200	8	0.75	0.75	0.75	0.75
200	10	0.96	0.96	0.96	0.96
300	2	0.05	0.05	0.05	0.05
300	4	0.10	0.10	0.10	0.10
300	6	0.15	0.15	0.15	0.15
300	8	0.21	0.21	0.21	0.21
300	10	0.26	0.26	0.26	0.26
* Droplet completely evaporated before deposition.					

Water droplets with 50 micron diameter and smaller are highly susceptible to drift. All droplets 50 micron diameter and smaller completely evaporated before they reached 18 inches below point of discharge for wind velocities between 2.0 and 10.0 mph and relative humidities (RH) between 20 and 80% (Table 1). The mean drift distances of small droplets increased rapidly with increased wind velocity. For example, with 60% RH, 50 micron diameter droplets were displaced 17.2, 28.8, 40.0, 50.9, and 55.3 ft before they completely evaporated when wind velocities were 2, 4, 6, 8, and 10 mph, respectively.

The mean drift distances of 50 micron diameter water droplets and smaller increased with increased relative humidity because high relative humidity increased the lifetimes of the volatile droplets. Although both evaporated completely before deposition, the mean drift distances of 50 micron diameter droplets were greater than for 20 micron diameter droplets with the same relative humidity and wind velocity. This occurs because 50 micron diameter droplets have 15.6 times more volume and hence longer life than 20 micron diameter droplets. With 10 mph wind velocity and 60% RH, 20 and 50 micron diameter droplets drifted 15.1 and 55.3 ft downwind from the discharge point, respectively.

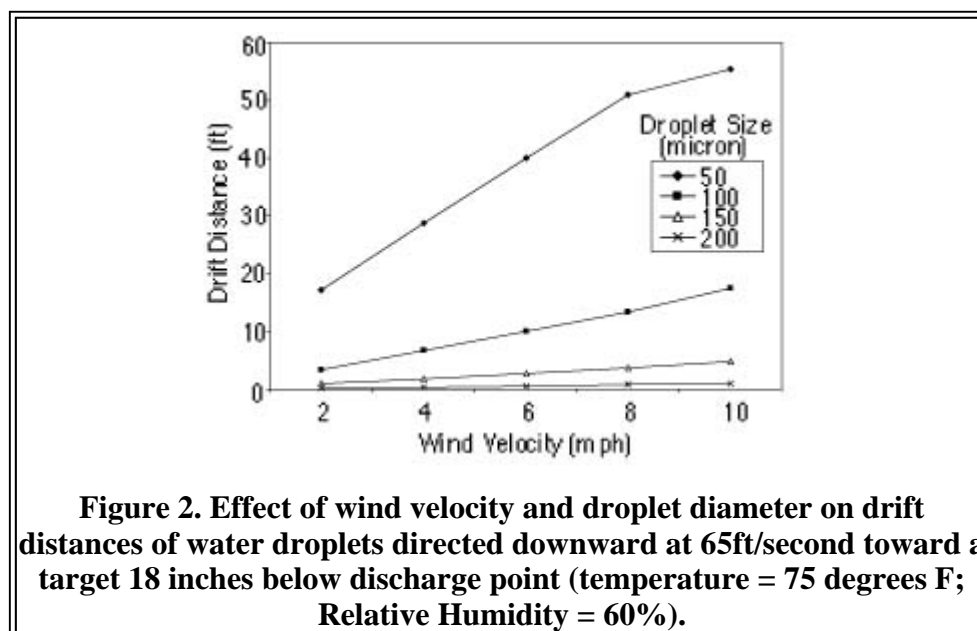
Most nozzles used for applying pesticides produce a large portion of the spray volume in 100 micron diameter droplets and larger. For example, our measurements of spray droplets from an XR 8002 VS nozzle (Spraying Systems Co., Wheaton, IL 60189) with 0.2 gpm flow rate when operated at 40 psi indicated that about 75% of the total spray volume was in droplets 100 micron diameter and larger. Computer simulation results indicate that all 100 micron and larger diameter water droplets reached 18 in below point of discharge at wind velocities up to 10 mph regardless of the relative humidity. However, due to affecting the evaporation rate, and hence droplet size, relative humidity significantly influenced the drift distances of 50 micron diameter droplets before they evaporated. With wind velocity of 10 mph, the mean drift distances of 50 micron diameter water droplets increased from 37.6 to 87.2 ft as relative humidity increased from 20% to 80%.

Data in Table 1 indicate that drift distances of droplets 200 micron diameter and larger are much less than for 100 micron diameter. For example, with 10 mph wind velocity and 60% RH, the mean drift

distance of 100 micron diameter droplets was about 18 times that of 200 micron diameter droplets (0.96 ft versus 17.48 ft). The mean drift distances of 200 micron diameter droplets were 0.20, 0.38, 0.55, 0.75, and 0.96 ft for wind velocities of 2, 4, 6, 8, and 10 mph, respectively. Relative humidity over a range of 20-80% had very little influence on the drift distances of 200 micron diameter droplets. The mean drift distances of all droplets 200 micron diameter and larger did not exceed 0.96 ft with wind velocities up to 10.0 mph.

Figure 1 illustrates the effect of water droplet size (50-300 micron diameter) on mean drift distance for wind velocities of 2.0, 4.0, 6.0, 8.0, and 10.0 mph, and 60% RH at 75 degrees F. All droplets 100 micron diameter or larger reached 18 in below point of discharge and deposited. The mean drift distances of the droplets increased with increased wind velocity but decreased as initial droplet size increased. The amount of droplet displacement that can be tolerated depends on several factors including the crop and surrounding area, and the pest control agent. If the target is a row crop that is sprayed from a nozzle centered over each row, then small amounts of droplet displacement by wind can result in large portions of the spray missing the target. It is also common for gusts with velocities two or more times the mean wind velocity to occur while spraying. Figure 1 indicates that drift is far less likely to be a problem when spraying with 200 micron diameter and larger droplets.

Figure 2 illustrates the simulated effect of wind velocities up to 10.0 mph on the mean drift distances for 100, 150, 200, and 300 micron diameter water droplets at 60% RH. Figure 2 and Table 1 both indicate that the influence of wind velocity on drift distance increases as droplet size decreases. Figure 2 shows that there is a nearly linear relationship between mean drift distance and wind velocity for each droplet size. The rate of change in drift distance with change in wind velocity was much greater for 100 than 200 micron diameter droplets. For example, over a range of 2 to 10 mph wind velocity the drift distances of 100 and 200 micron diameter droplets increased 1.8 and 0.01 ft per mph increase in wind velocity respectively.



Some spray carriers are oil or nonvolatile liquids. If the nonvolatile droplet density is close to the density of water, drift distances would be similar to drift distances in Table 1 for water droplets with 80% RH. Droplets 50 micron diameter or smaller can have very long drift distances with 100% RH. For example, the mean drift distances of 10 micron diameter droplets are beyond 650 ft with wind velocities of 5.5 mph and higher. For many pesticide applications, a small portion of the mixture is nonvolatile.

For small droplets that are still airborne when all of the water evaporates, there is potential for the small nonvolatile portion remaining to drift very long distances.

## Temperature and Relative Humidity

Pesticides are applied over wide ranges of temperatures and relative humidities which influence the evaporation rates of droplets. Since evaporation of liquid from a droplet decreases its mass, it also influences the drift distance of the droplet. Table 2 shows the effects of temperatures (50, 68, and 86 degrees F) on droplet diameters at the end of droplet flights, and mean drift distances for water droplets with initial diameters ranging from 50 to 300 micron, wind velocities of 1 to 22 mph and 50% RH.

<b>Table 2. Effect of temperature and wind velocity on droplet size at the end of flight of various size water droplets discharged downward at 65 ft/second toward a target 18 inches below point of discharge. (Relative humidity = 50%)</b>							
<b>Initial Droplet size (micron)</b>	<b>Wind Velocity (mph)</b>	<b>Final Droplet Size (micron) and Drift Distance (ft)</b>					
		<b>Temperature (degrees F)</b>					
		<b>50</b>		<b>68</b>		<b>86</b>	
		<b>DS#</b>	<b>DD##</b>	<b>DS#</b>	<b>DD##</b>	<b>DS#</b>	<b>DD##</b>
50	1.1	0.0	11.58*	0.0	9.84*	0.0	9.74*
50	5.6	0.0	53.14*	0.0	32.8*	0.0	23.52*
50	11.1	0.0	105.94*	0.0	61.34*	0.0	41.32*
50	22.4	0.0	208.61*	0.0	117.75*	0.0	75.76*
70	1.1	59.4	5.18	43.6	6.30	0.0	12.50*
70	5.6	59.2	26.14	42.7	32.14	0.0	38.70*
70	11.1	59.0	52.48	41.9	64.61	0.0	70.19*
70	22.4	58.8	105.94	40.4	132.18	0.0	132.51*
100	1.1	96.7	2.13	93.7	2.13	88.7	2.36
100	5.6	96.7	10.53	93.7	10.73	88.7	11.64
100	11.1	96.7	19.48	93.7	21.48	88.6	23.39
100	22.4	96.6	42.97	93.5	43.62	88.3	47.56
150	1.1	149	0.59	148	0.59	147	0.59
150	5.6	149	2.72	148	2.85	147	2.98
150	11.1	149	5.58	148	5.74	147	6.04
150	22.4	149	11.97	148	12.27	147	12.82
200	1.1	200	0.13	199	0.13	199	0.13
200	5.6	200	0.56	199	0.56	199	0.56
200	11.1	200	1.18	199	1.18	199	1.18
200	22.4	200	2.69	199	2.69	199	2.69
300	1.1	300	0.03	300	0.03	299	0.03
300	11.1	300	0.33	300	0.33	299	0.33

300	22.4	300	0.69	300	0.69	299	0.69
* Droplet completely evaporated before deposition.							
# DS - Droplet diameter (micron) at end of flight.							
## DD - drift distance (ft).							

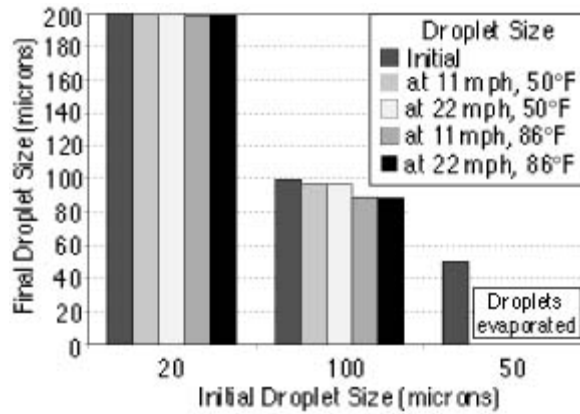
Table 2 indicates that ambient temperature had more influence on droplet sizes at end of flights for smaller droplets than larger droplets. For 70 micron diameter droplets, 5.6 mph wind velocity, and 50% RH, the mean droplet sizes at end of flights were 59.2, 42.7, and zero micron for ambient temperatures of 50, 68, and 86 degrees F, respectively. For 200 micron diameter droplets and the same conditions, the mean droplet sizes at times of deposition were 200, 199, and 199 micron. Over a temperature range of 50-86 degrees F, the volumes of 100 and 200 micron diameter water droplets changed about 20.9 and 1.5% respectively during flights when wind velocity was 1.1 m/s.

Table 2 also shows that wind velocities up to 22.4 mph had greater influence on droplet size change during flight on smaller than on larger droplets. For 70 micron diameter droplets at 68 degrees F and 50% RH, the droplet diameters at deposition were 43.6 and 40.4 micron with wind velocities of 1.1 and 22.4 mph, respectively. The 70 micron diameter water droplets lost 76 and 81% of their volume during flights with wind velocities of 1.1 and 22.4 mph, respectively. For 200 micron diameter droplets with the same conditions, the final droplet sizes at time of deposition were 199 micron for all wind velocities over a range of 1.1 to 22.4 mph.

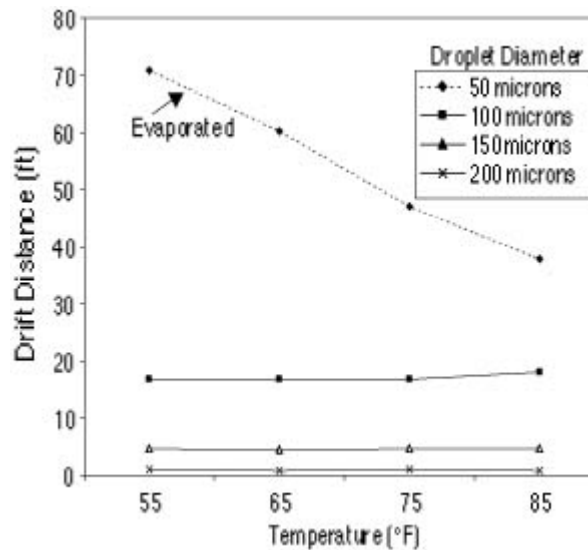
Temperature can affect evaporation rate during flight and hence droplet size and drift distance. Because smaller droplets have greater surface area to volume ratios and longer flight times than larger droplets, temperature has greater influence on the drift distances of smaller droplets. With wind velocity of 5.6 mph and relative humidity of 50%, 50 micron diameter water droplets drifted 53.1 and 23.5 ft before completely evaporating at temperatures of 50 and 86 degrees F, respectively. With the same conditions, 100 micron diameter droplets drifted 10.5 and 11.6 ft before deposition at temperatures of 50 and 86 degrees F, respectively. Ambient temperatures within the range of 50 and 86 degrees F had very little influence on drift distances of 200 micron diameter and larger water droplets when wind velocity varied from 1.1 to 22.4 mph.

Figure 4 illustrates the simulated mean drift distances for 50, 100 and 200 micron diameter water droplets with 10 mph wind velocity, 50% RH and ambient temperatures of 55, 65, 75, and 85 degrees F. The curve for 50 micron droplets shows that drift distance decreased as temperature increased. The 50 micron diameter droplets completely evaporated before deposition. Small droplets tend to travel at speed close to wind velocity. When temperature, and hence evaporation rate increases, their travel distance over their lifetime tends to decrease. The curve for 100 micron diameter droplets shows that drift distance before deposition increased with increased temperature. The drift distance tended to increase with increased temperature because increased temperature resulted in faster evaporation rate, smaller droplet size and increased travel distance before deposition. Temperature over the range of 50 to 86 degrees F had little influence on drift distances of 200 micron diameter droplets. The data used to produce the curves on Figure 3 are presented in Table 3.





**Figure 3. Effect of temperature and wind velocity on droplet sizes at the end of flight of 50, 100 and 200 micron diameter water droplets discharged down at 65 ft/second toward a target 18 inches below nozzle (RH=50%).**



**Figure 4. Mean drift distances for 50, 100 and 200 micron diameter water droplets with 10 mph wind velocity, 50% RH and ambient temperatures of 55, 65, 75 , and 85 degrees F.**

**Table 3. Effect of wind velocity and temperature on drift distances of droplets directed downward with initial velocity of 65 ft/second toward target 18 inches below discharge point. (Relative humidity = 50%; Turbulence intensity = 20%)**

Initial Droplet size (micron)	Wind velocity (mph)	Drift Distance (ft)			
		Temperature (degrees F)			
		55	65	75	85
20	2	4.24*	4.47	4.64	4.79*
20	4	7.23*	7.33*	7.71*	7.79*

20	6	10.07*	9.20*	9.22*	9.07
20	8	12.82*	11.33*	10.42*	10.38*
20	10	15.55*	13.27*	11.92*	11.44
50	2	15.73*	14.97*	13.51*	12.60*
50	4	29.55*	26.39*	22.00*	18.82*
50	6	43.28*	37.87*	30.19*	25.18*
50	8	56.91*	49.21*	38.73*	31.79*
50	10	70.92*	60.31*	46.97*	37.90*
100	2	3.35	3.34	3.53	3.63
100	4	6.69	6.71	7.03	7.23
100	6	10.03	10.05	10.58	10.82
100	8	13.37	13.40	14.08	14.44
100	10	16.74	16.76	16.73	18.10
150	2	0.94	0.92	0.96	0.94
150	4	1.85	1.82	1.91	1.88
150	6	2.77	2.73	2.85	2.81
150	8	3.69	3.64	3.78	3.76
150	10	4.64	4.56	4.75	4.70
200	2	0.21	0.20	0.21	0.20
200	4	0.39	0.39	0.39	0.38
200	6	0.57	0.54	0.58	0.54
200	8	0.74	0.76	0.78	0.74
200	10	0.98	0.95	0.96	0.93
* Droplet completely evaporated before deposition.					

Table 4 shows the mean drift distances for water droplets with initial diameters (25-300 micron), ambient temperatures (55-85 degrees F), relative humidities (20-100%), and 10 mph wind velocity. At low temperature (55 degrees F) and high relative humidity (80%), 50 micron diameter droplets were able to reach 18 in below their discharge point but traveled about 120 ft downwind before depositing. Table 4 indicates that relative humidity has little influence on drift distances of 150 micron diameter and larger droplets. This is because the flight times of these droplets are short. With wind velocity of 10 mph, 200 micron diameter droplets were only displaced over a range of less than 1 foot (0.93 to 0.98 ft) for the ranges of relative humidity and ambient temperature.

<b>Table 4. Effect of relative humidity and ambient temperature on mean drift distances of various size water droplets directed downward at 65 ft/second toward a target 18 inches below point of discharge. (Wind velocity = 10 mph)</b>						
<b>Droplet size (micron)</b>	<b>Ambient temp. (degrees F)</b>	<b>Drift distances (ft)</b>				
		<b>Relative humidity (%)</b>				
		<b>20</b>	<b>40</b>	<b>60</b>	<b>80</b>	<b>100</b>

25	55	17.93*	20.37*	29.76*	56.43*	381.60
25	65	14.67*	16.63*	23.53*	43.18*	377.97
25	75	12.58*	14.41*	19.94*	37.95*	391.31
25	85	11.41*	12.77*	17.81*	33.25*	400.12
50	55	63.32*	60.87*	60.87*	119.73	76.78
50	65	48.21*	53.93*	63.82*	93.51*	76.05
50	75	37.58*	42.00*	55.32*	87.24*	78.82
50	85	30.81*	34.40*	44.81*	73.93*	80.34
100	55	16.90	16.82	16.63	16.43	16.20
100	65	16.97	16.88	16.64	16.36	15.99
100	75	17.94	17.77	17.48	17.05	16.46
100	85	18.55	18.28	17.88	17.34	16.55
150	55	4.65	4.64	4.62	4.62	4.59
150	65	4.58	4.57	4.56	4.54	4.50
150	75	4.78	4.78	4.72	4.72	4.66
150	85	4.76	4.73	4.70	4.64	4.58
200	55	0.98	0.98	0.95	0.95	0.95
200	65	0.95	0.95	0.94	0.94	0.94
200	75	0.96	0.96	0.96	0.96	0.96
200	85	0.93	0.93	0.93	0.93	0.93
300	55	0.98	0.98	0.95	0.95	0.95
300	65	0.95	0.95	0.94	0.94	0.94
300	75	0.96	0.96	0.96	0.96	0.96
300	85	0.93	0.93	0.93	0.93	0.93
* Droplet completely evaporated before deposition.						

Figure 5 illustrates the effect of relative humidity on mean drift distances of 25, 50, 100 and 200 micron size water droplets for 10 mph wind velocity. The ambient temperature was 65 degrees F for the simulations. The mean drift distances of 25 and 50 micron diameter water droplets, before complete evaporation, increased with increased relative humidity over the range of 20 to 80%. For the same conditions, but with 100% RH, 50 micron diameter droplets deposited 18 in below and 76 ft downwind from the point of discharge while 25 micron diameter droplets drifted beyond 378 ft. There was no change in drift distance of 200 micron diameter water droplets over the 10 to 80% range of relative humidity.



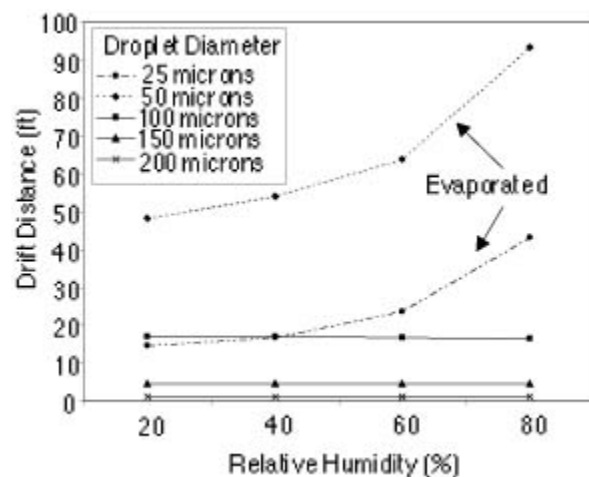


**Figure 5. The effect of relative humidity on mean drift distances of 25, 50, 100 and 200 micron size water droplets for 10 mph wind velocity. (The ambient temperature= 65 degrees F).**

### Droplet Discharge Height

Agricultural pesticides are applied with a very wide range of nozzle heights above targets. Nozzle height depends on several factors including the sprayer setup, target and operating conditions. Table 5 shows the effects of discharge height (0.5-3.0 ft), droplet diameter (50-300 micron) and wind velocity (2.0-10.0 mph) on mean drift distances of water droplets directed downward with initial velocity of 65 ft/seconds. Relative humidity and ambient temperature were 50% and 70 degrees F, for all simulations. The mean drift distances of 50 micron diameter and smaller droplets were nearly constant with each wind velocity for the discharge height range of 0.5 to 3.0 ft. This occurs because these droplets have short life times and do not travel downward far enough to deposit before completely evaporating.

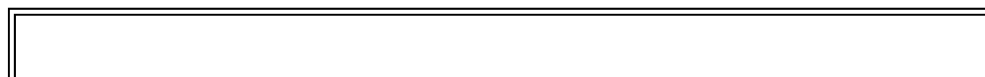
Initial Droplet size (micron)	Wind velocity (mph)	Drift distances (ft)					
		Nozzle height (ft)					
		0.5	1	1.5	2	2.5	3.0
50	2	0.43*	13.87*	14.02*	14.14*	14.22*	13.97*
50	4	14.28*	23.51*	23.72*	23.80*	23.83*	23.98*
50	6	19.96*	32.92*	33.41*	33.65*	33.78*	33.76*
50	8	25.61*	42.32*	43.18*	43.40*	43.39*	43.73*
50	10	31.20*	51.48*	52.29*	52.89*	53.37*	53.43*
100	2	0.50	1.50	3.37	5.40	7.51	9.85
100	4	0.99	2.99	6.76	10.82	15.02	19.72
100	6	1.48	4.47	10.15	16.23	22.54	29.62
100	8	1.98	5.97	13.51	21.63	30.05	39.51

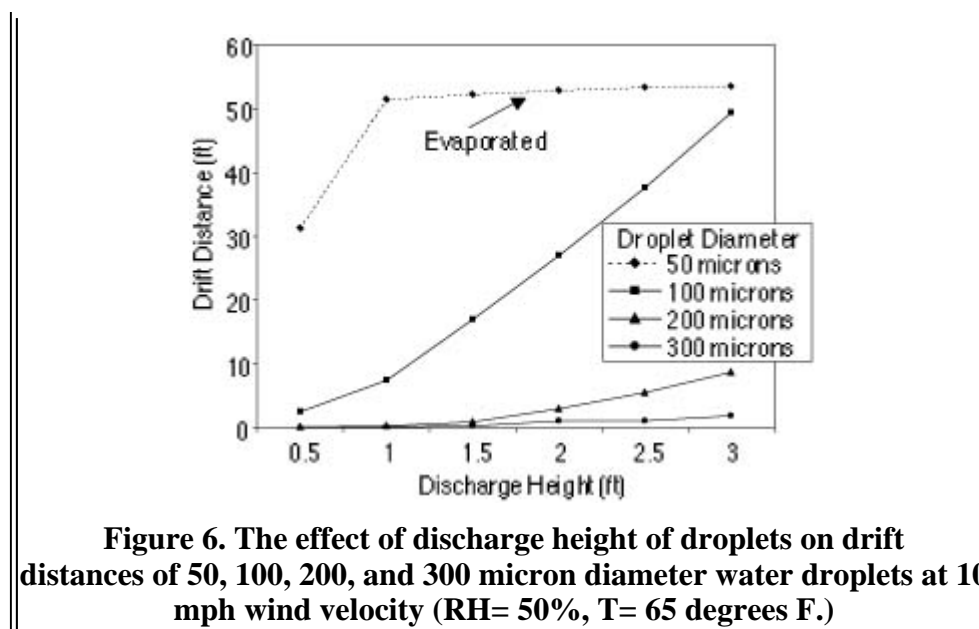
100	10	2.49	7.47	16.91	27.06	37.59	49.40
150	2	0.04	0.29	0.92	1.80	2.77	3.76
150	4	0.07	0.57	1.82	3.57	5.50	7.49
150	6	0.11	0.86	2.73	5.34	8.25	11.23
150	8	0.16	1.15	3.63	7.12	11.01	14.99
150	10	0.19	1.43	4.55	8.92	13.78	18.75
200	2	0.02	0.07	0.20	0.61	1.13	1.76
200	4	0.03	0.14	0.38	1.19	2.24	3.51
200	6	0.05	0.20	0.55	1.76	3.34	5.23
200	8	0.06	0.27	0.75	2.37	4.48	7.01
200	10	0.08	0.34	0.93	2.98	5.63	8.79
300	2	0.00	0.01	0.05	0.11	0.20	0.38
300	4	0.02	0.05	0.10	0.24	0.41	0.79
300	6	0.02	0.07	0.15	0.35	0.62	1.17
300	8	0.02	0.08	0.21	0.46	0.80	1.56
300	10	0.04	0.12	0.26	1.04	1.04	1.97
* Droplet completely evaporated before deposition.							

Increased discharge height resulted in increased drift distances for 100 micron diameter and larger water droplets (Table 5). For example, with 10 mph wind velocity and 65 ft/second initial droplet velocity, when discharge height increased from 0.5 to 3.0 ft, the mean drift distance of 200 and 300 micron diameter droplets increased from 2.49 to 49.40 ft and 0.08 to 8.79 ft, respectively. When the discharge height increased from 0.5 to 3.0 ft, the mean drift distance of 100 micron diameter droplets increased from 1.98 to 39.51 ft and kept increasing until the discharge height of 10 ft is reached. When the discharge height is increased beyond 10 ft, the drift distance remained constant (217 ft) because the 100 micron diameter water droplets completely evaporated before deposition.

When simulations for large size droplets were performed, results indicated that if the discharge height becomes too large, even the large droplets have tendency to drift under high wind velocity conditions. For example, the mean drift distance of 1000 micron diameter droplets was 5 ft for wind velocity and discharge height of 22 mph and 10 ft, respectively. Computer simulation also indicated that the mean drift distances of 1000 and 2000 micron diameter droplets were 57 and 19 ft, respectively, before impaction 13 ft below the point of discharge for 22 mph wind velocity, 50% relative humidity, and zero mph initial droplet velocity.

Figure 6 illustrates the effect of discharge height of droplets on the mean drift distances of 50, 100, 200, and 300 micron diameter water droplets for 10 mph wind velocity, 50% RH and 65 degrees F. The graph shows that increasing discharge height above 0.5 ft had no affect on the mean drift distance of 50 micron diameter droplets because they completely evaporated before depositing. However, increasing discharge height of 100 micron diameter and larger droplets affects their mean drift distances. Changes in discharge heights have less effect on mean drift distances as droplet size increases above 200 micron diameter.





### Initial Droplet Velocity

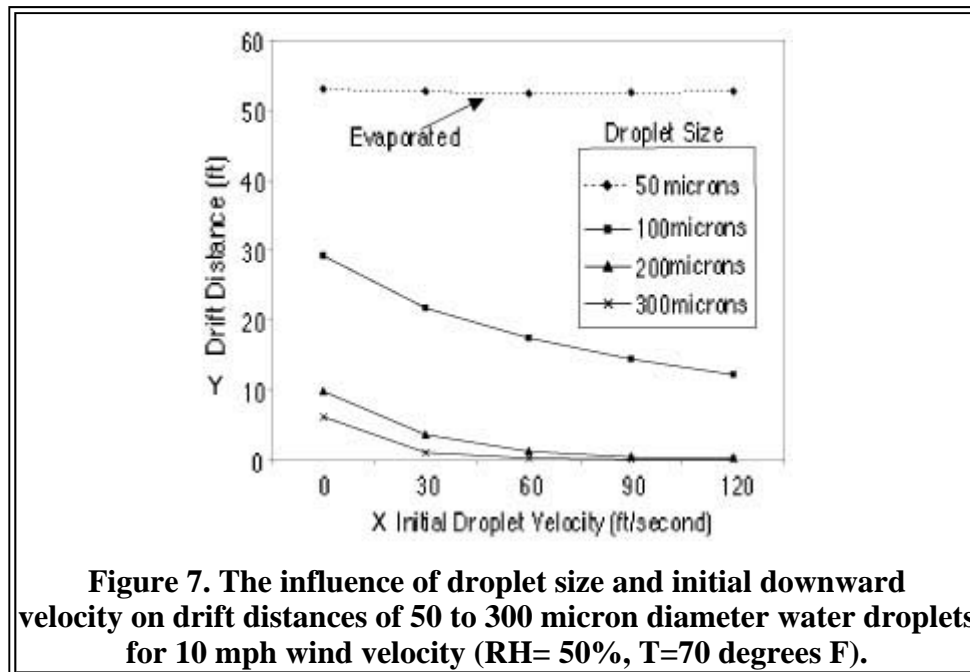
Pesticides are applied with many different types of nozzles. The velocity of droplets delivered by nozzles depends on the configuration of the nozzle, and operating pressure. Table 6 shows the effects of initial droplet velocity (0-120 ft/second) and wind velocity (2.5-10.0 mph) on the mean drift distances of various size water droplets directed downward toward a target 1.5 ft below the point of discharge. Relative humidity and ambient temperature were 50% and 70 degrees F, for all simulations. The data indicate that increasing the initial downward droplet velocity can decrease the mean drift distances before deposition of 75 micron diameter and larger droplets. When spray is directed downward from a nozzle centered over a row of plants, for example, it is important to maximize spray deposition on the target. Even for 30 ft/second initial droplet velocities, the drift distances of 100 micron diameter and smaller water droplets would be excessive when spraying row crops if the droplets were exposed to crosswinds with velocities of only 1 mph. Also, for many applications where the spray is exposed to crosswinds, the drift distances of 200 micron diameter droplets would be excessive for droplets directed downward with slow velocities. For example, the mean drift distances of 200 micron diameter droplets in 2.5 mph crosswinds are 2.4 and 0.9 ft for droplets directed downward with 0 and 30 ft/sec velocities, respectively. When wind velocity was 10 mph, the mean drift distance of 200 micron diameter droplets decreased from 9.88 to 0.28 ft as the initial downward droplet velocity increased from 0 to 120 ft/s. Some applicators use large droplets to reduce spray drift potential. With no initial downward droplet velocity (zero ft/second) and 18 in discharge height, the mean drift distances of 1000 micron diameter droplets were 0.24, 0.63, 1.08, and 1.62 ft when wind velocities were 2.5, 5.0, 7.5, and 10.0 mph, respectively. With 60 ft/sec instead of 0 m/s initial velocity, the mean drift distance of the 1000 micron diameter drops was only 0.04 ft when wind velocity was 10 mph. Table 6 also illustrates that initial droplet velocities had no effect on drift distances of 50 micron diameter water droplets. None of the 50micron diameter and smaller droplets reached 18 in below the point of discharge before complete evaporation for a range of initial droplet velocities from zero to 120 ft/second and wind velocities from 2.5 to 10.0 mph.

**Table 6. Effect of initial droplet velocity and wind velocity on drift distances of various size water droplets directed downward toward a target 18 inches below point of droplet discharge. (Temperature: 70 degrees F;**

Relative Humidity = 50%)						
Droplet size (micron)	Wind velocity (mph)	Drift Distances (ft)				
		Initial Droplet Velocity (ft/second)				
		0	30	60	90	120
50	2.5	16.50*	16.42*	16.40*	16.53*	16.50*
50	5.0	28.80*	28.74*	28.62*	28.67*	28.67
50	7.5	40.76*	40.73	40.74	40.70	40.54*
50	10.0	52.98*	52.70*	52.43*	52.48*	52.67*
75	2.5	17.86	13.05	11.35	10.29	9.09
75	5.0	33.83	25.82	22.19	20.03	18.31
75	7.5	49.58	38.64	33.03	29.74	27.17
75	10.0	65.28	52.26	44.00	39.49	36.01
100	2.5	5.39	5.39	4.37	3.64	3.06
100	5.0	14.51	10.79	8.75	7.26	6.10
100	7.5	21.84	16.25	13.11	10.88	9.12
100	10.0	29.25	21.75	17.51	14.48	12.15
150	2.5	3.64	2.05	1.26	0.73	0.39
150	5.0	7.34	4.10	2.49	1.45	0.76
150	7.5	11.07	6.19	3.73	2.15	1.12
150	10.0	14.83	8.34	5.00	2.87	1.49
200	2.5	2.36	0.89	0.31	0.13	0.07
200	5.0	4.82	1.79	0.58	0.25	0.15
200	7.5	7.34	2.72	0.89	0.82	0.20
200	10.0	9.88	3.72	1.20	0.52	0.28
300	2.5	1.39	0.24	0.08	0.04	0.03
300	5.0	2.91	0.49	0.15	0.08	0.5
300	7.5	4.56	0.76	0.22	0.12	0.07
300	10.0	6.23	1.06	0.31	0.17	0.11
500	2.5	0.67	0.08	0.03	0.01	0.00
500	5.0	1.52	0.16	0.05	0.03	0.03
500	7.5	2.49	0.25	0.09	0.05	0.03
500	10.0	3.58	0.34	0.11	0.06	0.04
1000	2.5	0.24	0.03	0.00	0.00	0.00
1000	5.0	0.63	0.05	0.03	0.01	0.00
1000	7.5	1.08	0.08	0.03	0.03	0.01
1000	10.0	1.62	0.11	0.04	0.03	0.03

\* Droplet completely evaporated before deposition.

Figure 7 illustrates the influence of droplet size and initial downward velocity on drift distances of 50 to 300 micron diameter water droplets for 10 mph wind velocity. The relative humidity and ambient temperature were 50% and 70 degrees F for all simulations. As evident from the data presented on Figure 7, for 10 mph wind velocity, drift distances are greatly influenced by both droplet size and the initial downward velocity of the droplet. The drift distances of 100 micron diameter and larger droplets decreased with increased initial droplet velocity. Figure 7 also illustrates the large difference in drift distances between 100 and 200 micron diameter water droplets.



## Conclusions

The following conclusions are based on the computer simulations of mean drift distances of water droplets within the range of variables discussed in this publication.

1. Changes in wind velocity, discharge height, ambient temperature and relative humidity had much greater influence on the drift distances of droplets 100 micron diameter or less than on 200 micron diameter and larger droplets. For droplets that did not evaporate before deposition, there was a nearly linear relationship between wind velocity and drift distance.
2. With 100% RH, 10 micron diameter droplets drifted beyond 650 ft when wind velocity exceeded 5.5 mph.
3. Droplets 50 micron diameter and smaller completely evaporated before reaching 18 inches below the discharge point, regardless of initial velocity, for relative humidities 60% and lower and temperatures between 55 and 85 degrees F. Also, the mean drift distances of these droplets increased with increased droplet size.
4. Mean drift distances of 100 micron diameter and larger droplets increased with increased wind velocity and discharge height, but decreased with increased droplet size and discharge velocity.
5. Drift distances of water droplets as large as 200 micron diameter were influenced by initial

droplet velocity and height of discharge.

6. 6. For 10 mph wind velocity, 20% turbulence intensity, 50% RH, 70 degrees F ambient temperature, 60 ft/second initial downward droplet velocity and 18 inches discharge height, the mean drift distances of 100, 200, and 500 micron diameter droplets were 17.5, 1.2, and 0.11 ft, respectively.
7. 7. The drift potential of 200 micron diameter droplets is considerably less than for 100 micron diameter droplets. Unless some means such as shields or air jets are used, drift reduction techniques should be directed toward reducing the portion of spray volume contained in droplets less than 200 micron diameter for applications where minimizing drift is important. For some applications, such as with high nozzles and slow initial downward velocity and high wind velocity, droplets larger than 200 micron diameter may be needed to satisfactorily reduce drift.

## Acknowledgment

Most of the information presented in this publication was adapted from the following publication.

Zhu, H., D.L. Reichard, R.D. Fox, R.D. Brazee and H.E. Ozkan. 1994. Simulation of drift of discrete sizes of water droplets from field sprayers. Transactions of the ASAE 37(5):1401-1407.

## References

Ozkan, H.E. 1991. Reducing spray drift. OSU Extension Bulletin 816. Ohio State University Extension, Columbus, Ohio.

Reichard, D.L., H. Zhu, R.D. Fox and R.D. Brazee. 1992a. Computer simulation of spray drift that influence spray drift. Transactions of the ASAE 35(5):1401-1407.

Reichard, D.L., H. Zhu, R.D. Fox and R.D. Brazee. 1992b. Wind tunnel evaluation of a computer program to model spray drift. Transactions of the ASAE 35(3):755-758.

---

NOTE: Disclaimer - This publication may contain pesticide recommendations that are subject to change at any time. These recommendations are provided only as a guide. It is always the pesticide applicator's responsibility, by law, to read and follow all current label directions for the specific pesticide being used. Due to constantly changing labels and product registrations, some of the recommendations given in this writing may no longer be legal by the time you read them. If any information in these recommendations disagrees with the label, the recommendation must be disregarded. No endorsement is intended for products mentioned, nor is criticism meant for products not mentioned. The author and Ohio State University Extension assume no liability resulting from the use of these recommendations.

---

All educational programs conducted by Ohio State University Extension are available to clientele on a nondiscriminatory basis without regard to race, color, creed, religion, sexual orientation, national origin, gender, age, disability or Vietnam-era veteran status.

Keith L. Smith, Associate Vice President for Ag. Adm. and Director, OSU Extension.

TDD No. 800-589-8292 (Ohio only) or 614-292-1868

---

| [Ohioline](#) | [Search](#) | [Fact Sheets](#) | [Bulletins](#) |

**APPLICATION FOR PERMIT  
DNCS ENVIRONMENTAL SOLUTIONS**

**VOLUME III: ENGINEERING DESIGN AND CALCULATIONS  
SECTION 10: EVAPORATION CALCULATIONS**

**ATTACHMENT III.10.B  
DRIFTSIM: PREDICTING DRIFT DISTANCE OF SPRAY DROPLETS  
AND RESULTING EVAPORATION**



# DRIFTSIM—Predicting Drift Distances of Spray Droplets

**Heping Zhu and Robert D. Fox**

Agricultural Engineers

USDA-ARS

Application Technology Research Unit

Wooster, OH 44691

**H. Erdal Ozkan**

Professor and Extension Agricultural Engineer

Food, Agricultural, and Biological

Engineering Department

The Ohio State University

Columbus, OH 43210

## Introduction

Spray drift, movement of pesticide droplets through air during or after application to a site other than the intended targets of application, is one of the most critical problems pesticide applicators have to deal with. For example, three-fourths of agriculture-related complaints investigated by the Ohio Department of Agriculture involved drift issues; two-thirds of the total complaints in a five-year period brought to the attention of Iowa Department of Agriculture were related to drift problems; about one-third of court cases due to spray misapplications reported by a major insurance company involved drift damages. Drift problems will become even more critical in the future when farmers use more genetically modified crops which restrict use of non-selective herbicides because even a small amount of these herbicides can cause serious damage to neighboring crops.

Although complete elimination of spray drift is impossible, problems can be minimized if chemicals are applied with the proper equipment and methods under favorable weather conditions. Increased awareness of environmental quality and better understanding of the causes of spray drift can help operators make reasonable judgments for safer, more efficient applications.

Factors that significantly influence off-target movement of droplets are wind velocity and direction, droplet size and density, and distance from the atomizer to the target. Other factors that influence drift include droplet velocity, and direction of discharge from the atomizer, volatility of the spray fluid, relative humidity, ambient temperature, and atmospheric turbulence intensity. Many scientists have conducted field tests to study

influence of these variables on spray drift. Unfortunately, field tests have the limitation that weather conditions cannot be controlled and the variables that influence spray drift may interact and vary during a test.

Computer simulations can allow determination of effects of different variables such as droplet size and velocity, relative humidity, and wind velocity on spray drift. One such computer model or commercially available computational fluid dynamics (CFD) program was evaluated by Reichard et al. (1992) in Ohio for modeling the effects of several variables on spray drift. Experiments were conducted to verify the accuracy of the computer model in predicting drift distances of water droplets in a wind tunnel with a single size droplet generator. These tests revealed that the computer model could be used to accurately calculate spray drift distances for a wide range of spray droplet sizes and wind velocities. With the computer model, individual or mean droplet trajectories were determined for different values of several variables listed above (Zhu et al., 1994). However, the model is very expensive and requires special operator skills and a high-speed computer with a large memory space to operate. It also takes long time to calculate a drift distance even for a single simulation condition.

DRIFTSIM is a simplified and user-friendly version of a computer model developed with a visual BASIC language program to interpolate values from a large database of drift distances originally calculated from the CFD model evaluated by Reichard et al. (1992). Detailed information on DRIFTSIM is given in a publication by Zhu et al. (1995). DRIFTSIM can be used to determine effects of major drift-causing factors on the mean drift distances up to 656 feet from the release point for individual water droplets or classes of droplets. These factors or variables used in DRIFTSIM are listed in Table 1, with the limiting values acceptable to DRIFTSIM.

<b>Table 1. Variables and their ranges used in DRIFTSIM program</b>				
Variable	Range			
	American Unit		Metric Unit	
Wind velocity	0-22	mph	0-10	m/s
Droplet size	10-2000	Micron ( $\mu\text{m}$ )	10-2000	$\mu\text{m}$
Droplet velocity	0-110	mph	0-50	m/s
Discharge height	0-6.5	ft	0-2.0	m
Temperature	50-86	$^{\circ}\text{F}$	10-30	$^{\circ}\text{C}$
Relative humidity	10-100	%	10-100	%

Turbulence intensity is another important factor indicating how much the wind velocity varies about the mean. It can vary considerably in field conditions, but based on the frequency of nearly 20% turbulence intensity observed in many of the field measurements conducted in Ohio, a constant value of 20% turbulence intensity was used in DRIFTSIM for all calculations.

For classes of droplets in this version of DRIFTSIM, the upper-limit log normal (ULLN) method (Goering and Smith, 1978) was used to calculate the drop-size distribution produced by a nozzle. The ULLN method used three size measurements,  $D_{V,1}$ ,  $D_{V,5}$ , and  $D_{V,9}$  to estimate the volume of spray in droplets less than a selected droplet size. The  $D_{V,1}$ ,  $D_{V,5}$ , and  $D_{V,9}$  for the droplet size spectra produced by a specific nozzle can be measured with most modern droplet sizing instruments. DRIFTSIM computes the drift distance for the average of lower and upper droplet size for each size class. It also computes the portion of spray in each size class.

## Terms used in DRIFTSIM program

**Single size droplets:** For the program to calculate a mean drift distance of a given size droplets with other variables

**Array of droplets (DVs):** For the program to calculate drift distances with the portion of volume for many size classes of droplets by entering  $D_{v,1}$ ,  $D_{v,5}$  and  $D_{v,9}$

**$D_{v,1}$ :** Droplet diameter such that 10% of total liquid volume that is in droplets smaller than  $D_{v,1}$  (micron or  $\mu\text{m}$ )

**$D_{v,5}$ :** Droplet diameter such that 50% of total liquid volume that is in droplets smaller than  $D_{v,5}$  (micron or  $\mu\text{m}$ )

**$D_{v,9}$ :** Droplet diameter such that 90% of total liquid volume that is in droplets smaller than  $D_{v,9}$  (micron or  $\mu\text{m}$ )

**Array of droplets (nozzle):** For the program to calculate drift distances with the portion of volume for many size classes of droplets by selecting nozzle type [**Note:** In DRIFTSIM, data is available for only a limited number of nozzles]

**Temperature:** Ambient air temperature during spray operation ( $^{\circ}\text{F}$  in American unit or  $^{\circ}\text{C}$  in Metric unit)

**Relative humidity:** Relative humidity of ambient air (%)

**Wind velocity:** Wind speed at nozzle level during the spray application (mph in American unit or m/s in Metric unit)

**Discharge height:** Nozzle orifice height above the ground (ft in American unit or m in Metric unit)

**Droplet velocity:** Velocity of droplets near the outlet of the nozzle orifice (mph in American unit or m/s in Metric unit)

**Droplet diameter:** Droplet diameter near the outlet of the nozzle orifice (micron or  $\mu\text{m}$ )

**Operating pressure:** Liquid pressure acting on the nozzle orifice (psi or kPa)

## Operating DRIFTSIM

To operate DRIFTSIM, minimum requirements for a computer are Pentium PC with a CD drive, MS-Windows version 3.1 or later, 8 MB of memory, 30 MB free hard drive space, and a mouse.

DRIFTSIM is compact enough to fit on a CD. It can be operated from either a CD or a computer hard drive. DRIFTSIM automatically starts running when the CD containing DRIFTSIM is inserted in the CD drive of the computer. To operate the program from the computer hard drive, DRIFTSIM files and program should be first copied onto the hard drive, and then the user should execute DRIFTSIM.exe file to start the program. The program may run somewhat faster from a hard drive than a CD.

After the program starts, it gives three on-screen boxes for choosing units and droplet size types and entering values of simulation variables. A selection of units or droplet size types can be changed at any time during the operation without needing to exit the program. To change the value of any variable, simply click on the input area next to the variable, and enter a value that is within the acceptable range defined in Table 1. Only two screens appear during the whole calculation process: input and result screens.

## Steps to run DRIFTSIM from a CD

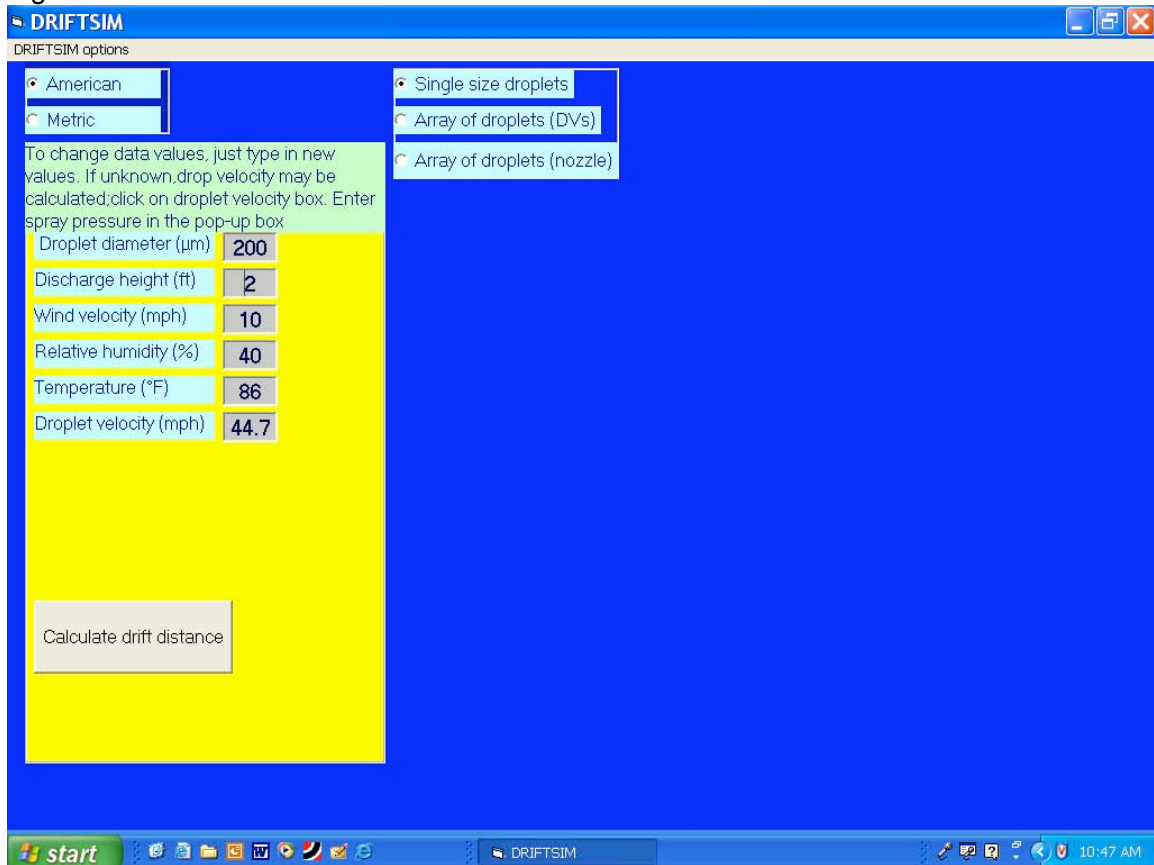
- (1) Insert CD in the computer.
- (2) Introductory information for DRIFTSIM as shown in Figure 1 appears on the screen.

Figure 1



- (3) Click on the “*Start Driftsim*” box. Three on-screen boxes for choosing and entering simulation conditions appear on the screen as shown in Figure 2. [**Note:** initial values for drift variables shown on the screen are built into DRIFTSIM. These values are only examples, not recommended values.]

Figure 2

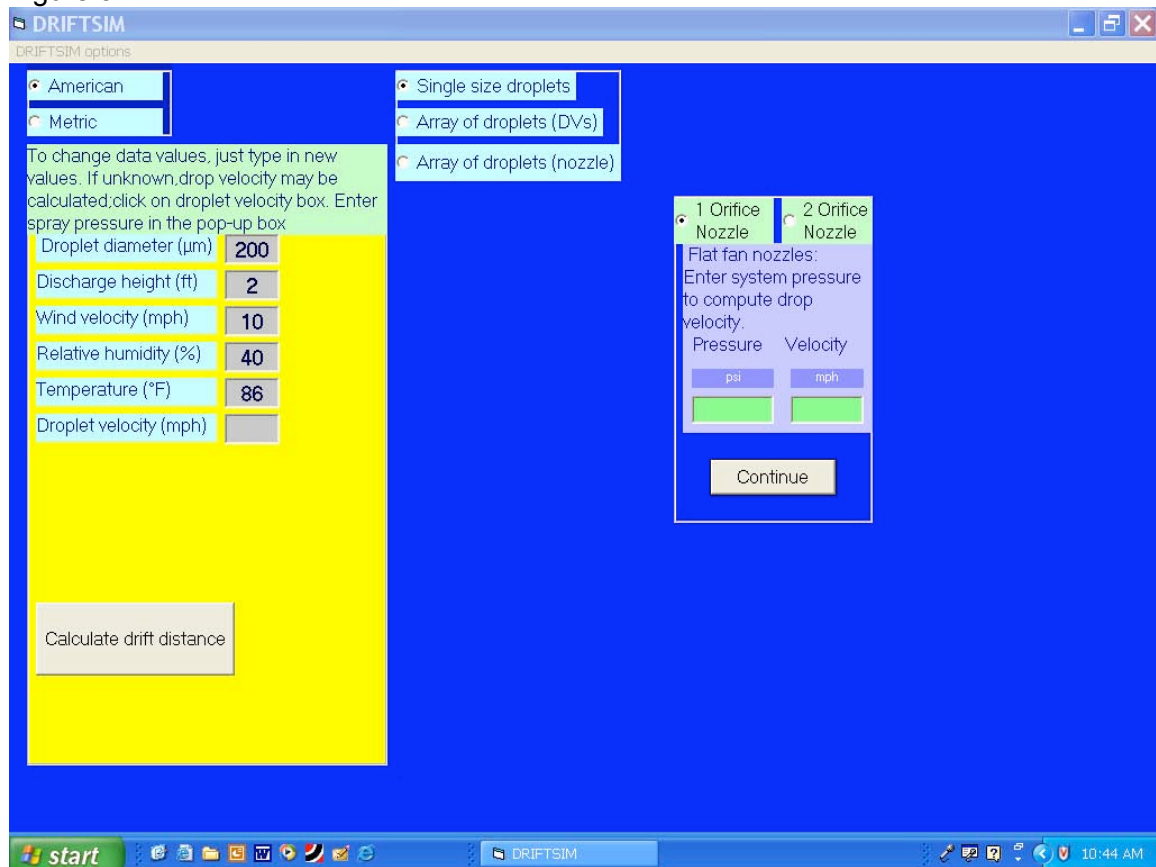


- (4) Select either "American" or "Metric" unit for calculation.
- (5) Select one of the three choices as a type of input for the droplet size: "Single size droplets", "Array of droplets (DVs)", or "Array of droplets (nozzle)".
- (6) For "Single size droplets", follow steps (7) to (11); for "Array of droplets (DVs)", follow steps (12) to (17); for "Array of droplets (nozzle)", follow steps (19) to (23).

**[Note:** Steps (7) to (11) are for "Single size droplets" only]

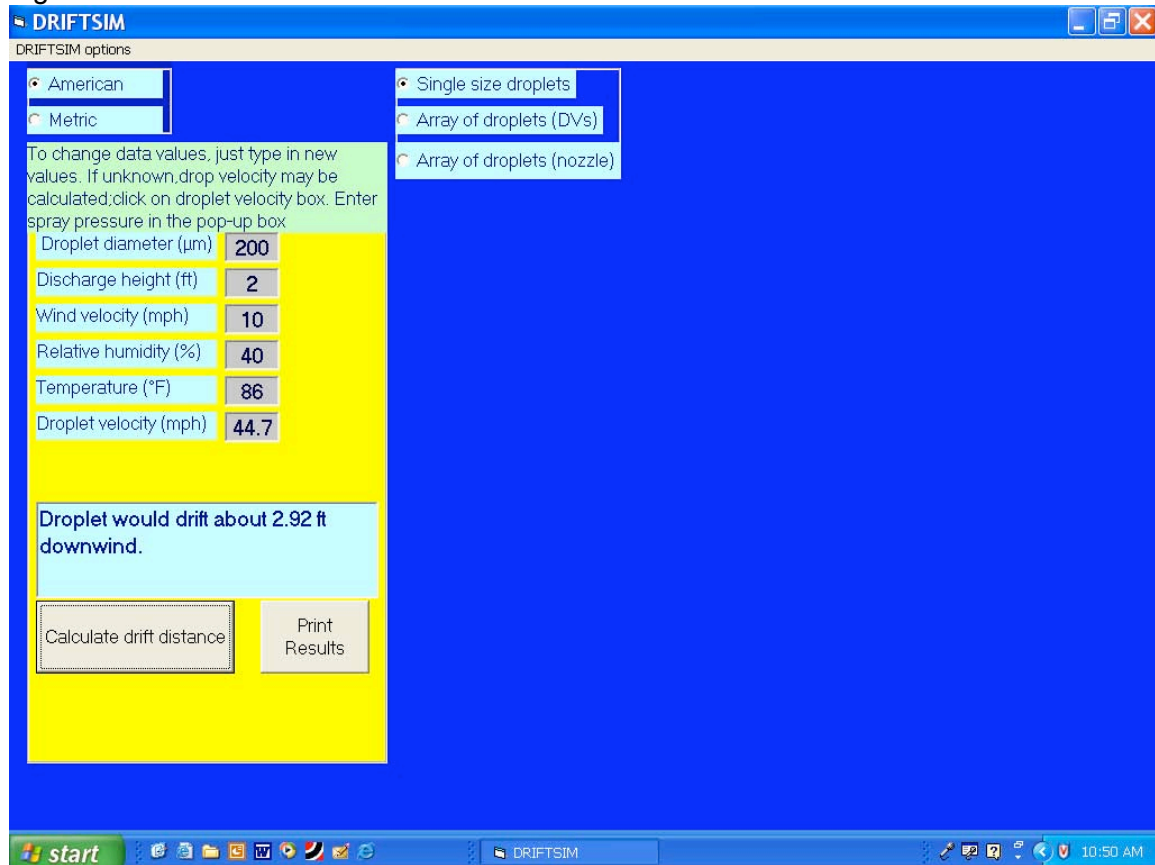
- (7) Enter or change values for "Droplet diameter", "Wind velocity", "Discharge height", "Droplet velocity", "Temperature", "Relative humidity" for inputs of variables. The value of "Droplet velocity" can be entered either by the user, or automatically by the program once the user enters a value for the operating pressure on the box which pops up on the screen as shown in Figure 3 after the user empties the "Droplet velocity" box. A red error message appears in the box under the variables if the value of an individual variable is outside the range defined in Table 1.

Figure 3



- (8) Click on "Compute drift distance" to obtain the results on the screen as shown in Figure 4.

Figure 4

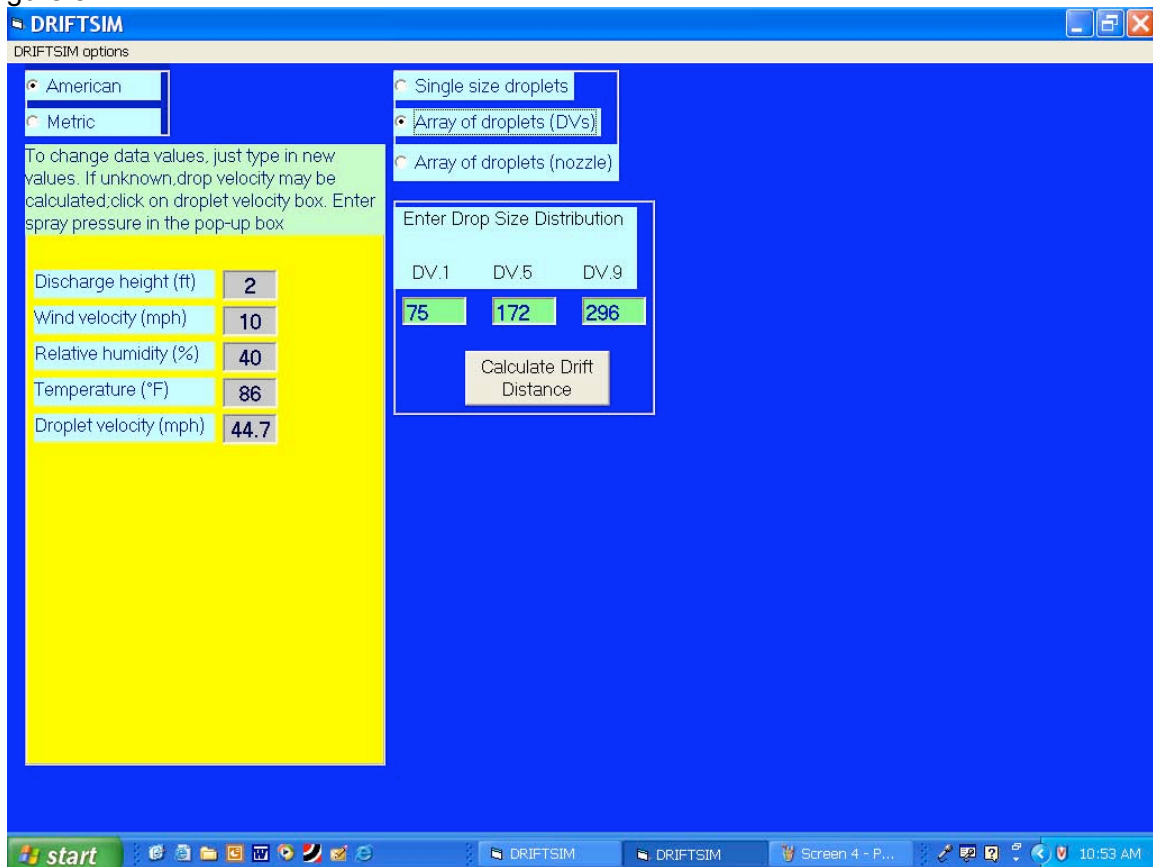


- (9) Click on "Print results" if you want to get a printout of input variables and the result.
- (10) To continue running DRIFTSIM with a new or revised set of inputs for the "single size droplet", repeat steps (7) to (10).
- (11) When you are done with all the simulations, exit DRIFTSIM by clicking on the **X** at the upper right corner of the window on the screen.

**[Note:** Steps (12) to (17) are for "Array of droplets (DVs)" only]

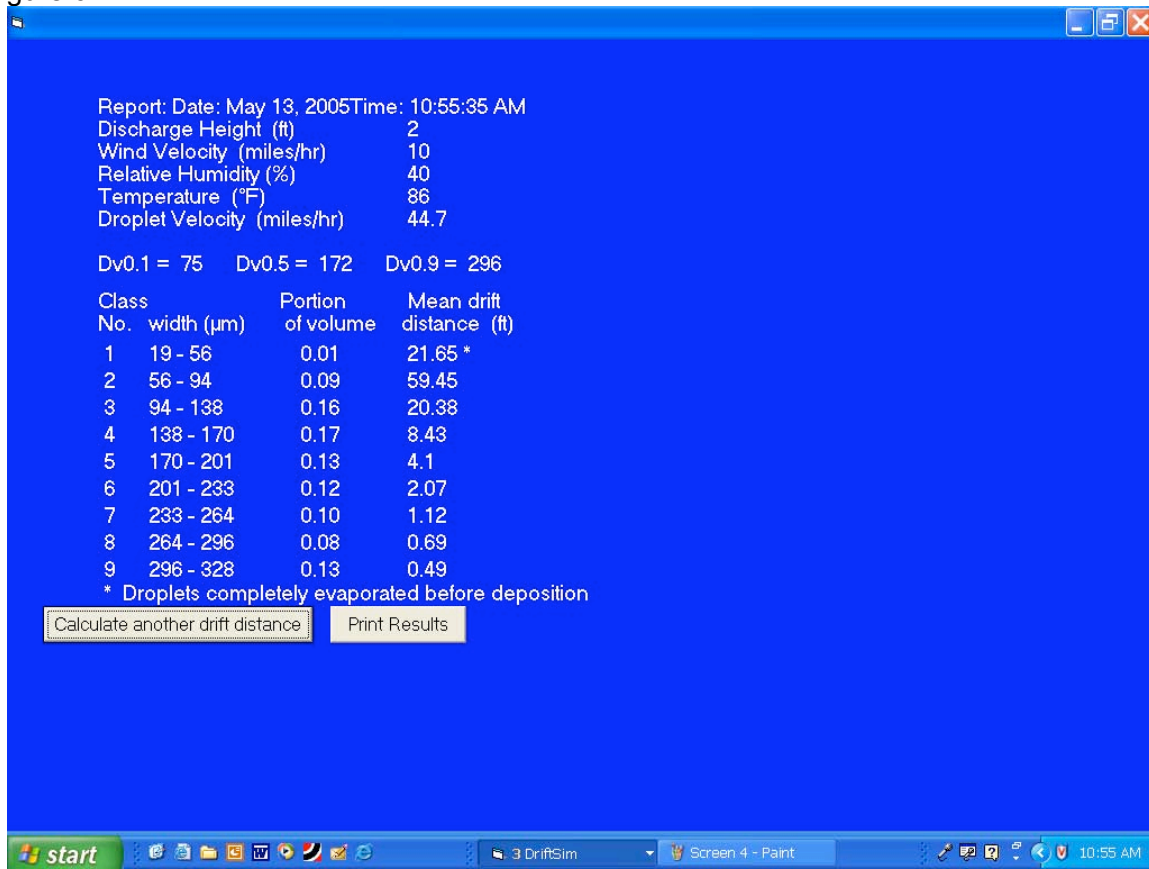
- (12) After choosing "Array of droplets (DVs)", a new box for droplet size distribution appears on the screen as shown in Figure 5.

Figure 5



- (13) Enter " $D_{v,1}$ ", " $D_{v,5}$ " and " $D_{v,9}$ " values in boxes.
- (14) Enter or change values for "Wind velocity", "Discharge height", "Droplet velocity", "Temperature" and "Relative humidity".
- (15) Click on "Calculate Drift Distance". Drift distances of 9 size classes of droplets along with the portion of the spray volume corresponding to each size class appear on the screen as shown in Figure 6. Error message appears on this screen if " $D_{v,1}$ ", " $D_{v,5}$ " and " $D_{v,9}$ " values are not reasonable.

Figure 6

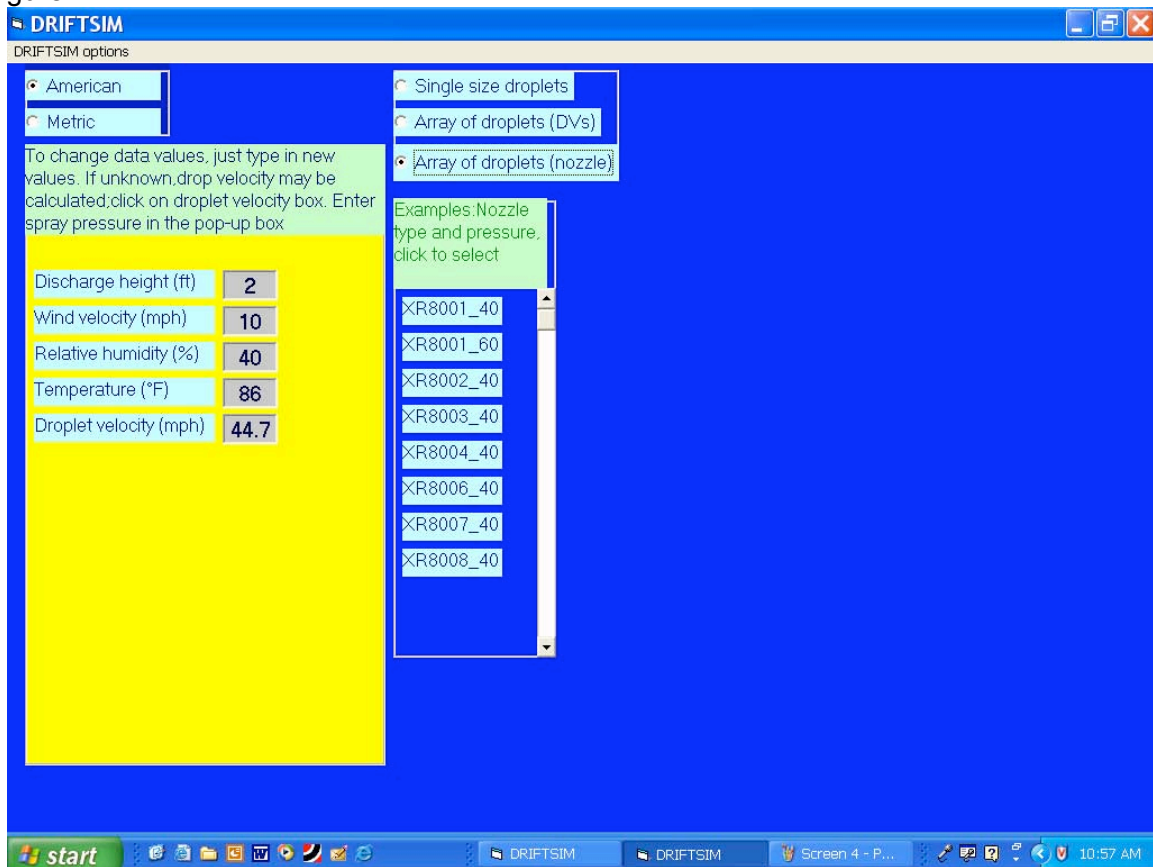


- (16) Click on either “*Print Results*” to get a printout of the results, or “*Calculate another drift distance*” to repeat steps (13) to (16) for a revised or new set of inputs.
- (17) When you are done with all the simulations, exit DRIFTSIM by clicking on the **X** at the upper right corner of the window on the screen.

**[Note:** Steps (18) to (23) are for “*Array of droplets (nozzle)*” only]

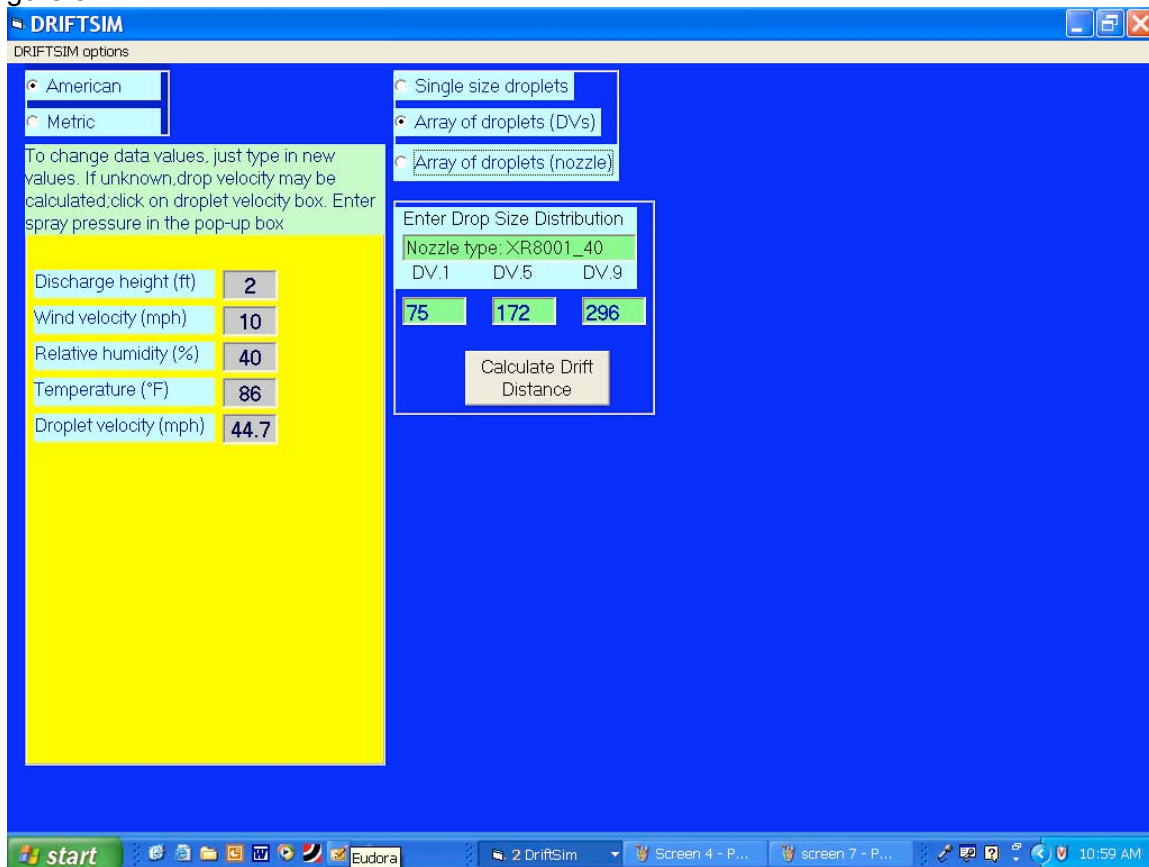
- (18) After choosing “*Array of droplets (nozzle)*”, a new box with a list of several nozzles appears on the screen as shown in Figure 7.

Figure 7



- (19) Click on one of nozzle choices, then " $D_{v,1}$ ", " $D_{v,5}$ " and " $D_{v,9}$ " values automatically appear in boxes for the nozzle chosen, as shown in Figure 8.

Figure 8



- (20) Enter or change values for “*Wind velocity*”, “*Discharge height*”, “*Droplet velocity*”, “*Temperature*”, and “*Relative humidity*”.
- (21) Click on “*Calculate Drift Distance*”. Drift distances of 9 size classes of droplets along with the portion of the spray volume corresponding to each size class appear on the screen as the same as step (15). Error message appears on this screen if “ $D_{v,1}$ ”, “ $D_{v,5}$ ” and “ $D_{v,9}$ ” values are not reasonable.
- (22) Click on either “*Print Results*” to get a printout of the results, or “*Calculate another drift distance*” to repeat steps (18) to (22) for a revised or new set of inputs.
- (23) When you are done with all the simulations, exit DRIFTSIM by clicking on the **X** at the upper right corner of the window on the screen.

## Steps to run DRIFTSIM from a computer hard drive

To operate DRIFTSIM from a hard drive, the user should copy both DRIFTSIM subdirectory and all contents in the subdirectory, except AUTORUN.INF and Browsercall.exe, from the CD to the hard drive [**Note:** the subdirectory name must be DRIFTSIM; otherwise, the program will not work]. After the copying process is completed, go to DRIFTSIM subdirectory in the hard drive and click on DriftSim.exe file. DRIFTSIM introductory page should appear on the screen. Then follow steps (3) to (23) above to run the program.

## References

- Goering, C.E. and D.B. Smith. 1978. Equations for droplet size distributions in sprays. Transactions of ASAE 21(2): 209-216.
- Reichard, D.L., H. Zhu, R.D. Fox and R.D. Brazee. 1992. Wind tunnel evaluation of a computer program to model spray drift. Transactions of the ASAE 35(3):755-758.
- Zhu, H., D.L. Reichard, R.D. Fox, R.D. Brazee and H.E. Ozkan. 1994. Simulation of drift of discrete sizes of water droplets from field sprayers. Transactions of the ASAE 37(5):1401-1407.
- Zhu, H., D.L. Reichard, R.D. Fox, H.E. Ozkan and R.D. Brazee. 1995. DRIFTSIM, a program to estimate drift distances of spray droplets. Applied Engineering in Agriculture 11 (3): 365-369.

This manual, as well as other information on spray drift, is available at Ohio State University Extension's web site "Ohioline" (<http://ohioline.osu.edu>) by clicking on "Search" and entering "DRIFTSIM" or "spray drift" in the search box.

OSU Extension embraces human diversity and is committed to ensuring that all educational programs conducted by Ohio State University Extension are available to clientele on a nondiscriminatory basis without regard to race, color, age, gender identity or expression, disability, religion, sexual orientation, national origin, or veteran status.

Keith L. Smith, Associate Vice President for Agricultural Administration and Director, OSU Extension

TDD No. 800-589-8292 (Ohio only) or 614-292-1868

**APPLICATION FOR PERMIT  
DNCS ENVIRONMENTAL SOLUTIONS**

**VOLUME III: ENGINEERING DESIGN AND CALCULATIONS  
SECTION 11: WAVE ACTION CALCULATIONS**

**TABLE OF CONTENTS**

<b>Section No.</b>	<b>Title</b>	<b>Page</b>
1.0	INTRODUCTION .....	III.11-1
1.1	Description .....	III.11-1
2.0	DESIGN CRITERIA .....	III.11-1
3.0	CALCULATION .....	III.11-2
4.0	SUMMARY .....	III.11-3

**LIST OF ATTACHMENTS**

<b>Attachment No.</b>	<b>Title</b>
III.11.A	<i>LOW COST SHORE PROTECTION: A GUIDE FOR ENGINEERS AND CONTRACTORS</i> (U.S. ARMY CORPS OF ENGINEERS 2004)
III.11.B	<i>WATER-RESOURCES ENGINEERING</i> (LINSLEY & FRANZINI 1979)

**APPLICATION FOR PERMIT  
DNCS ENVIRONMENTAL SOLUTIONS**

**VOLUME III: ENGINEERING DESIGN AND CALCULATIONS  
SECTION 11: WAVE ACTION CALCULATIONS**

**1.0 INTRODUCTION**

DNCS Environmental Solutions (DNCS Facility) is a proposed Surface Waste Management Facility for oil field waste processing and disposal services. The proposed DNCS Facility is subject to regulation under the New Mexico Oil and Gas Rules, specifically 19.15.36 NMAC, administered by the Oil Conservation Division (OCD). The Facility has been designed in compliance with 19.15.36 NMAC, and will be constructed and operated in compliance with a Surface Waste Management Facility Permit issued by the OCD. The Facility is owned by, and will be constructed and operated by, DNCS Properties, LLC.

**1.1 Description**

The DNCS site is comprised of a 562-acre  $\pm$  tract of land located south of NM 529 in portions of Section 31, Township 17 South, Range 33 East; and in the northern half of Section 6, Township 18 South, Range 33 East, Lea County, NM. A portion of the 562-acre tract is a drainage feature that will be excluded from development. The drainage feature includes a 500-ft setback and totals 67 acres  $\pm$ . The DNCS Facility will include two main components; a liquid oil field waste Processing Area (177 acres  $\pm$ ), and an oil field waste Landfill (318 acres  $\pm$ ); therefore the DNCS Facility comprises 495 acres  $\pm$ . Oil field wastes are anticipated to be delivered to the DNCS Facility from oil and gas exploration and production operations in southeastern NM and west Texas. The Site Development Plan provided in the **Permit Plans, Sheet 3**, identifies the locations of the Processing Area and Landfill facilities.

**2.0 DESIGN CRITERIA**

The purpose of the Wave Action Calculations presented herein is to provide the wave height and run-up for the evaporation ponds proposed for the DNCS Processing Area. The DNCS Processing Area is planned to include 12 evaporation ponds, approximately 420 feet (ft) in

length and 200 ft in width, each with a capacity of approximately 9.5 acre-ft. These calculations assume a pond length of 420 ft and a conservative wind speed of 75 miles per hour (mph). Wave height and run-up must be less than the 3.5 ft of freeboard provided in the pond design. The methodology applied for determining wave height and run-up in reservoirs for the Wave Action Calculations is provided in two documents, *Low Cost Shore Protection: A Guide for Engineers and Contractors* (U.S. Army Corps of Engineers 2004; **Attachment III.11.A**); and *Water-Resources Engineering* (Linsley & Franzini 1979; **Attachment III.11.B**).

### 3.0 CALCULATION

The fastest-mile wind speed for a 25-year return period was obtained from Figure 16 in **Attachment III.11.A**. The fastest mile wind speed is approximately 75 mph for the DNCS site vicinity.

Wave height in a pond is estimated using the following equation (i.e., page 166, Equation 7-4, **Attachment III.11.B**):

$$Z_w = 0.034 (V_w)^{1.06} F^{0.47}$$

Where:

$Z_w$  = height of wave (feet)

$V_w$  = wind speed (mph) = 75 mph

$F$  = fetch length (miles) = 420 feet/5,280 feet/mile = 0.080 miles

Therefore:  $Z_w = 0.034 (75 \text{ mph})^{1.06} (0.080 \text{ miles})^{0.47}$

$$Z_w = 0.034 (97.2) (0.30)$$

$$Z_w = 0.99 \text{ feet} = \text{height of wave in pond due to a 75 mph wind}$$

The height of wave runup for a smooth (i.e., HDPE liner) surface can be obtained from Table 11 in **Attachment III.11.A**. As shown on Table 11,  $R = 1.75H$  for a 2.5H:1V smooth slope and  $R = 1.50H$  for a 4.0H:1V smooth slope. Interpolating between these two values, a value of  $R = 1.68H$  is obtained for a 3.0H:1V smooth slope. Therefore:

Wave Runup =  $1.68H = 1.68 (0.99 \text{ ft}) = 1.66 \text{ ft}$  for a 3H:1V smooth sideslope.

Total: Wave height + Wave runup = 0.99 ft + 1.66 ft = 2.65 ft

#### **4.0 SUMMARY**

When considering a 75 mph wind across the length of a pond, a wave height of 0.99 ft is obtained. This wave will cause a runup of approximately 1.66 ft on the pond sideslope. The ponds have been design with a minimum freeboard of 3.5 ft, which will provide adequate protection against the combined potential impact of waves, wave runup, and simultaneous rainfall event (i.e., 25 year, 24 hour rainfall = 4.9 inches).

**APPLICATION FOR PERMIT  
DNCS ENVIRONMENTAL SOLUTIONS**

**VOLUME III: ENGINEERING DESIGN AND CALCULATIONS  
SECTION 11: WAVE ACTION CALCULATIONS**

**ATTACHMENT III.11.A**

***LOW COST SHORE PROTECTION: A GUIDE FOR ENGINEERS AND  
CONTRACTORS (U.S. ARMY CORPS OF ENGINEERS 2004)***

# LOW COST SHORE PROTECTION

*... a Guide for Engineers and Contractors*

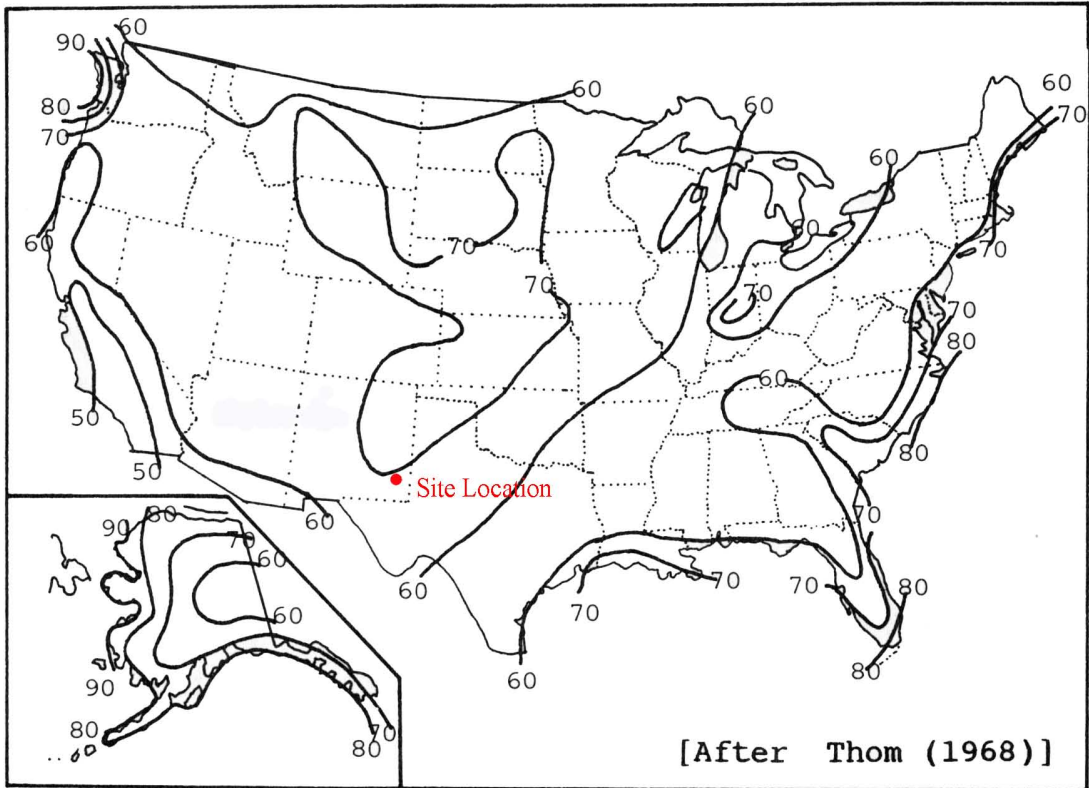


Figure 15 Fastest-Mile Wind Speeds: 10-year Return Period

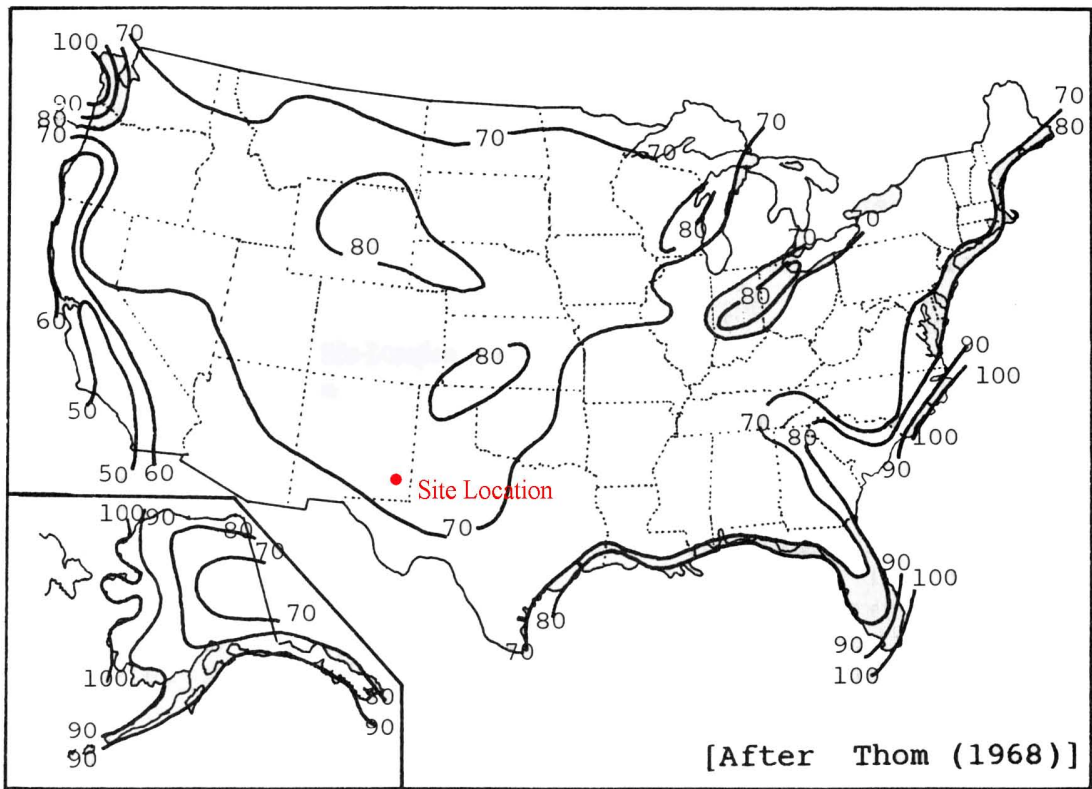


Figure 16 Fastest-Mile Wind Speeds: 25-year Return Period



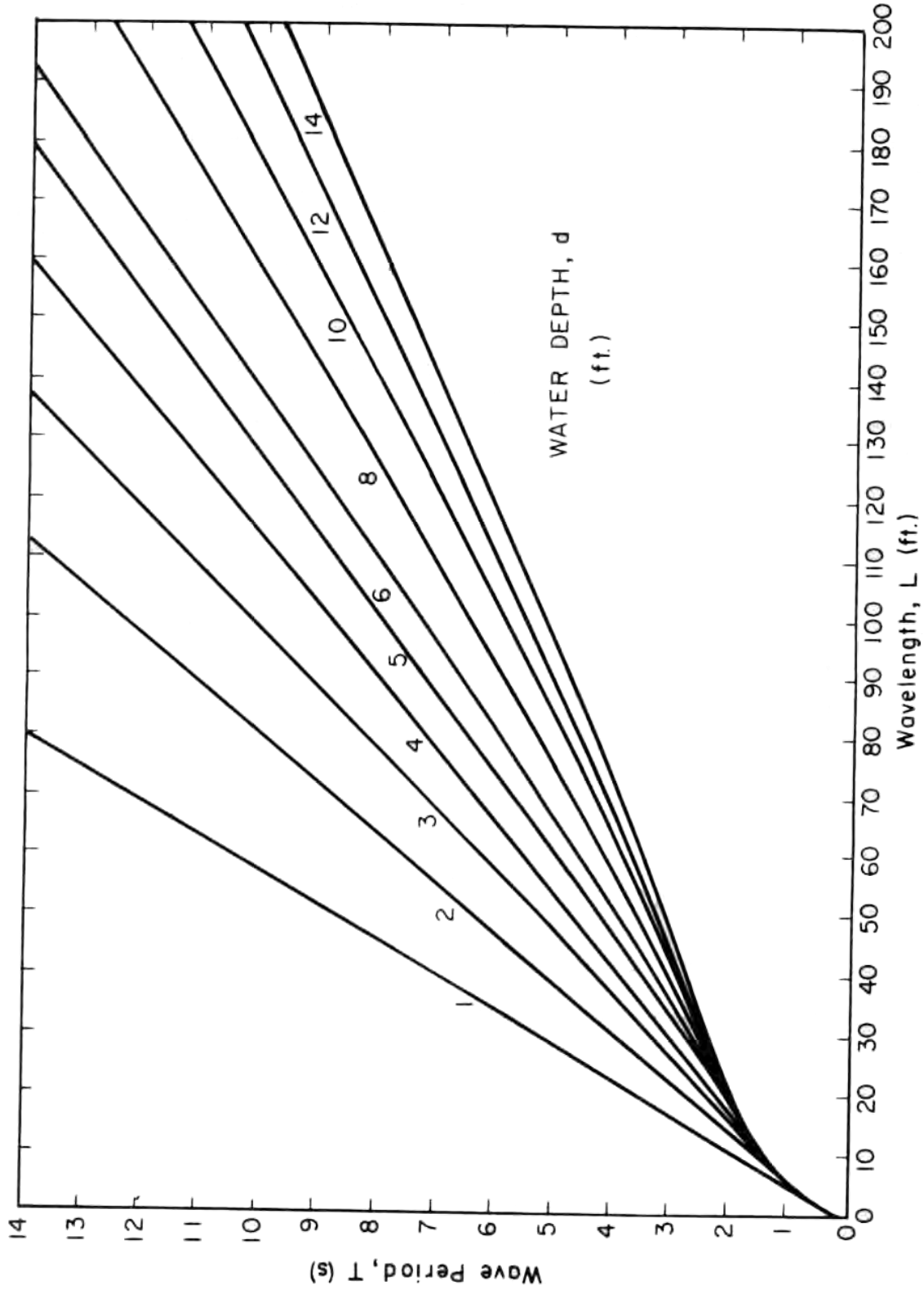


Figure 26 Local Wavelength Given Depth and Period  
 [After Giles and Eckert (1979)]

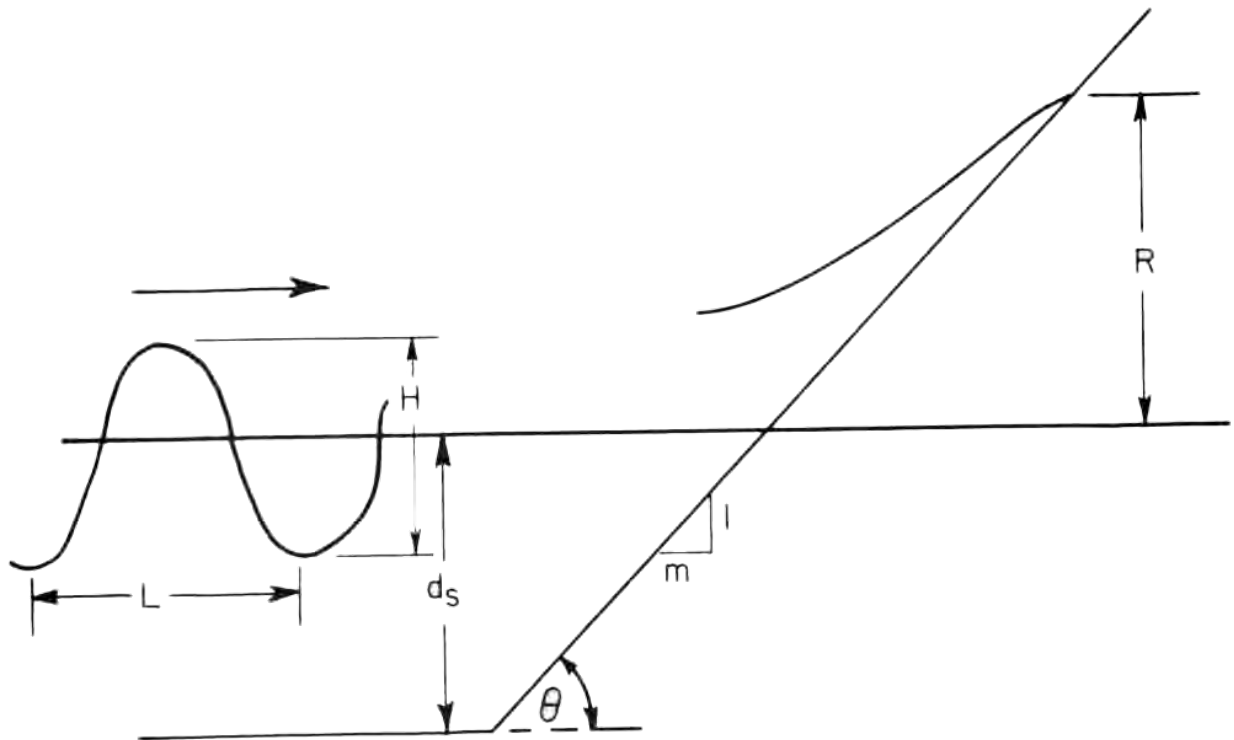


Figure 27 Wave Runup Definition Sketch

For STEPPED slopes, Stoa (1979) recommends using 70 to 75 percent of the smooth slope runup if the risers are vertical, and 86 percent if the edges are rounded.

A rough approximation of the runup height can be obtained from Table 11. However, the values in the table tend to represent the upper bound of the available data and may result in over design. Equations (13) and (14) or the methods given in Stoa (1978) and (1979) are recommended.

If it is impossible or undesirable to build a structure to the recommended height, a splash apron should be provided at the top of the structure. These are generally constructed of rock and they prevent the ground at the top from being eroded and undermining that portion of the structure.

### Environmental Factors

Many different materials can be used to construct shore protection structures, including rock, concrete, timber, metal and plastics. The choice often depends on the desired permanence of the protection. Durable materials usually cost considerably more than shorter-lived materials used for temporary protection. The choice of materials is important because the coastal environment is a harsh testing ground for all man-made structures. Aside from wave forces, which are formidable in and of themselves, a host of chemical, biological and other factors can degrade structural materials. A brief review of these follows.

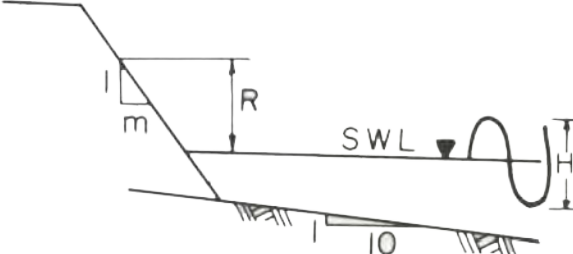
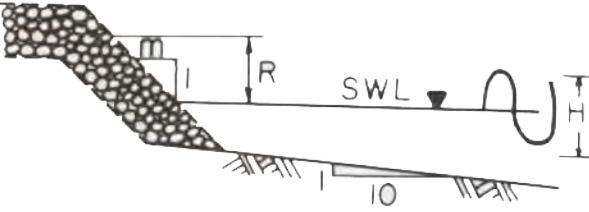
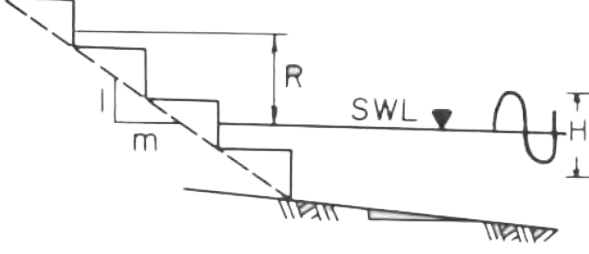
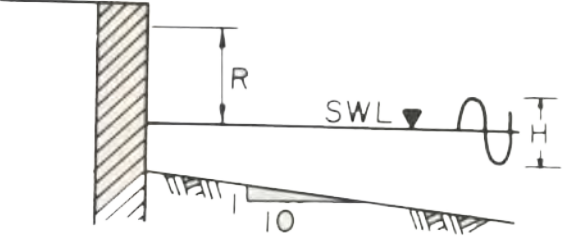
 <p>SMOOTH FACE</p>	<p><u>m</u></p> <p>1.5</p> <p>2.5</p> <p>4.0</p>	<p><u>R</u></p> <p>2.25H</p> <p>1.75H</p> <p>1.50H</p>
 <p>ROUGH FACE</p>	<p><u>m</u></p> <p>1.5</p> <p>2.5</p> <p>4.0</p>	<p><u>R</u></p> <p>1.25H</p> <p>1.00H</p> <p>0.75H</p>
 <p>STEPPED FACE</p>	<p><u>m</u></p> <p>1.5</p>	<p><u>R</u></p> <p>2.00H</p>
 <p>VERTICAL FACE</p>	<p><u>m</u></p> <p>—</p>	<p><u>R</u></p> <p>2.00H</p>

Table 11 Wave Runup Heights

**APPLICATION FOR PERMIT  
DNCS ENVIRONMENTAL SOLUTIONS**

**VOLUME III: ENGINEERING DESIGN AND CALCULATIONS  
SECTION 11: WAVE ACTION CALCULATIONS**

**ATTACHMENT III.11.B  
*WATER-RESOURCES ENGINEERING*  
(LINSLEY & FRANZINI 1979)**

# WATER-RESOURCES ENGINEERING

THIRD EDITION

Ray K. Linsley

*Professor Emeritus of Hydraulic Engineering  
Stanford University*

*Partner, Linsley, Kraeger Associates*

Joseph B. Franzini

*Professor of Civil Engineering  
Associate Chairman, Department of Civil Engineering  
Stanford University*

**McGraw-Hill Book Company**

New York St. Louis San Francisco Auckland Bogotá Düsseldorf  
Johannesburg London Madrid Mexico Montreal New Delhi Panama  
Paris São Paulo Singapore Sydney Tokyo Toronto

by ordinary earth-moving methods would be expensive unless the excavated sediment has some sales value.

**7-9 Wind setup and waves in reservoirs** Earth dams must have sufficient freeboard above maximum pool level so that waves cannot wash over the top of the dam. Waves in reservoirs may also damage shoreline structures and embankments adjacent to the water and interfere with navigation. Part of the design of any reservoir is an estimate of wind setup and wave height.

Wind setup is the tilting of the reservoir water surface caused by the movement of the surface water toward the leeward shore under the action of the wind. This current of surface water is a result of tangential stresses between the wind and the water and of differences in atmospheric pressure over the reservoir. The latter, however, is, typically, a smaller effect. As a consequence of wind setup, the reservoir water surface is above normal still-water level on the leeward side and below the still-water level on the windward side. This results in hydrostatic unbalance, and a return flow at some depth must occur. The water-surface slope which results is that necessary to sustain the return flow under conditions of bottom roughness and cross-sectional area of flow which exist. Wind setup is generally larger in shallow reservoirs with rough bottoms.

Wind setup may be estimated from

$$Z_s = \frac{V_w^2 F}{1400d} \quad (7-3)$$

where  $Z_s$  is the rise in feet (meters) above still-water level,  $V_w$  is the wind speed in miles (kilometers) per hour,  $F$  is the *fetch* or length of water surface over which the wind blows in miles (kilometers), and  $d$  is the average depth of the lake along the fetch in feet (meters). In SI metric units, the constant in the denominator becomes 63,200.

Equation (7-3) is modified<sup>1</sup> from the original equation developed by Dutch engineers on the Zuider Zee. Additional information and techniques are given in other references.<sup>2</sup> Wind-setup effects may be transferred around bends in a reservoir and the value of  $F$  used may be somewhat longer than the straight-line fetch.

When wind begins to blow over a smooth surface, small waves, called capillary waves, appear in response to the turbulent eddies in the wind stream. These waves grow in size and length as a result of the continuing push of the wind on the back of the waves and of the shearing or tangential force between the wind and the water. As the waves grow in size and length, their speed increases until they move at speeds approaching the speed of the wind. Because growth of a wave depends in part upon the difference between wind speed and wave speed, the growth rate approaches zero as the wave speed approaches the wind speed.

<sup>1</sup> T. Saville, Jr., E. W. McClendon, and A. L. Cochran, Freeboard Allowances for Waves in Inland Reservoirs, *J. Waterways and Harbors Div., ASCE*, pp. 93-124, May, 1962.

<sup>2</sup> Shore Protection, Planning and Design, *Tech. Rept. 3*, 3d ed., U.S. Army Coastal Engineering Research Center, June, 1966.

The duration of the wind and the time and direction from which it blows are important factors in the ultimate height of a wave. The variability of the wind and the amazingly complex and yet to be fully understood response of the water surface to the wind lead to a wave pattern that is a superposition of many waves. The pattern is often described by its energy distribution or spectrum. The growth of wind waves as a function of fetch, wind speed, and duration can be calculated from knowledge of the mechanism of wave generation and use of collected empirical results.<sup>1</sup> The duration of the wind and the fetch play an important role because a wave may not reach its ultimate height if the wave passes out of the region of high wind or strikes a shore during the growth process. The depth of water also plays a key role, tending to yield smaller and shorter waves in deep water.

Wave-height data gathered at two major reservoirs<sup>2</sup> confirm the theoretical and experimental data for ocean waves if a modified value of fetch is used. The derived equation is

$$z_w = 0.034V_w^{1.06}F^{0.47} \quad (7-4)$$

<sup>1</sup> W. J. Pierson, Jr., and R. W. James, *Practical Methods for Observing and Forecasting Ocean Waves*, U.S. Navy Hydrographic Office Pub. 603, 1955 (reprinted 1960).

<sup>2</sup> T. Saville, Jr., E. W. McClendon, and A. L. Cochran, *Freeboard Allowances for Waves in Inland Reservoirs*, *J. Waterways and Harbors Div.*, ASCE, pp. 93-124, May, 1962.

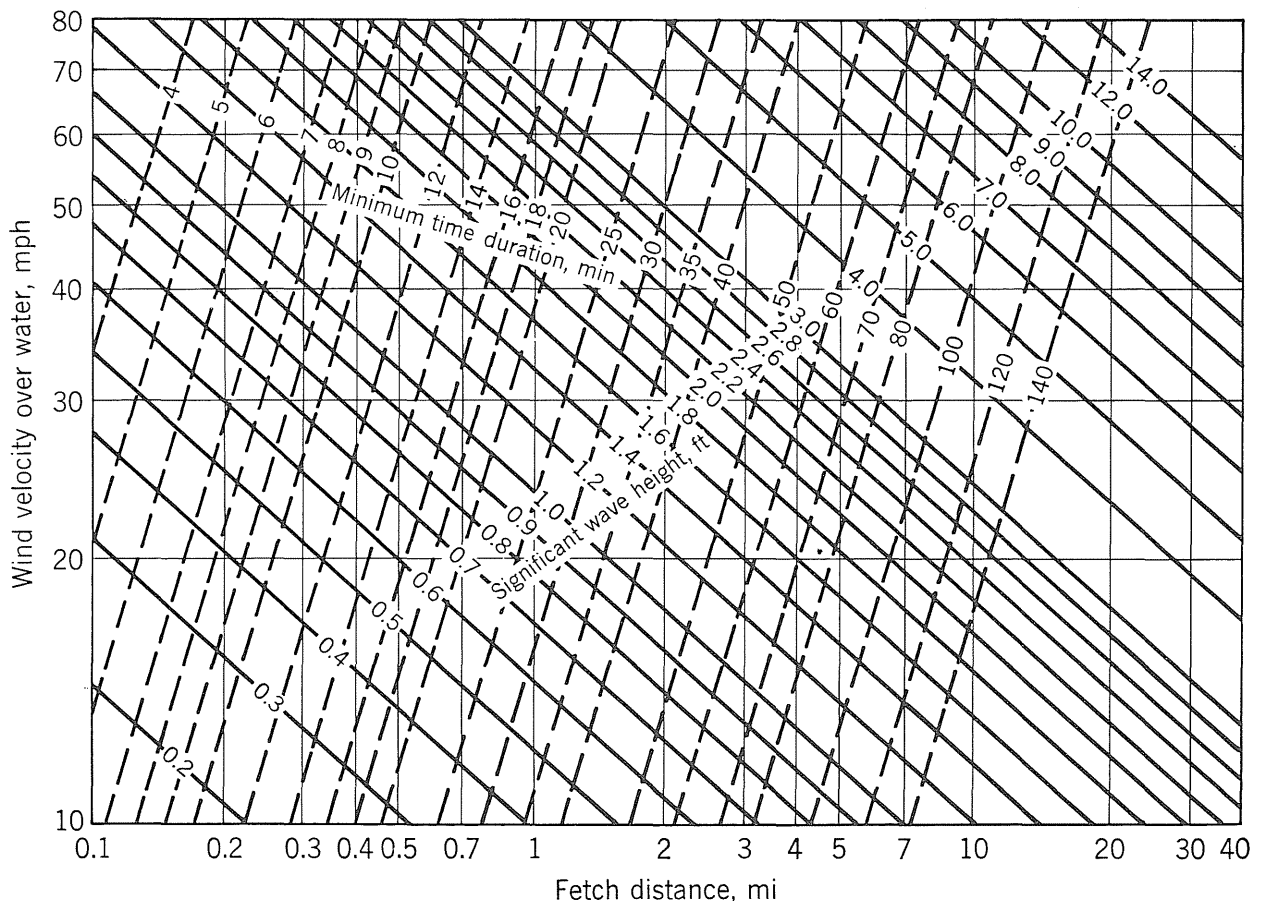


**Figure 7-14** Significant wave heights and minimum wind durations (from Saville, McClendon, and Cochran). For metric version see Appendix B.

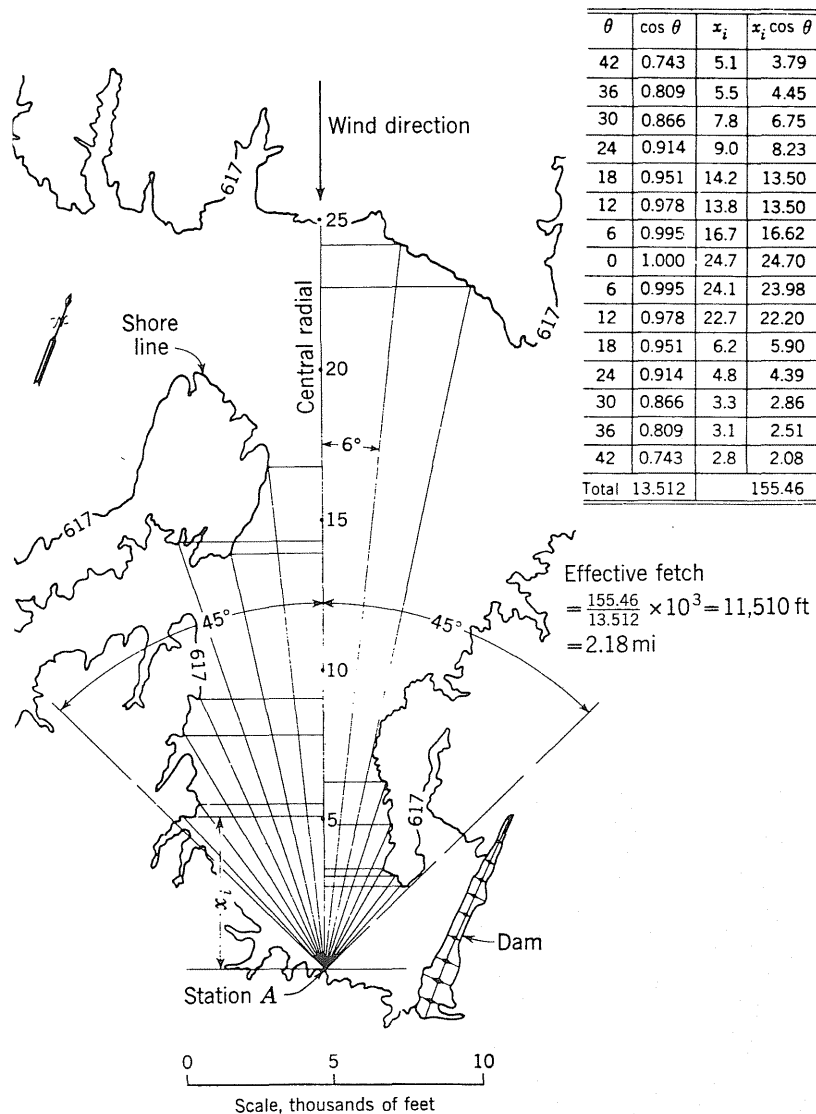


Figure 7-15 Computation of effective fetch. (Modified from Saville, McClendon, and Cochran)

where  $z_w$  is the average height in feet (meters) of the highest one-third of the waves and is called the *significant wave height*,  $V_w$  is the wind velocity in miles (kilometers) per hour about 25 ft (7.6 m) above the water surface, and  $F$  is the fetch in miles (kilometers). In SI metric units the coefficient becomes 0.005. The equation is shown graphically in Fig. 7-14<sup>1</sup> together with lines showing the minimum duration of wind required to develop the indicated wave height. Figure 7-15 shows the method of computing the effective fetch for a narrow reservoir.

Since the design must be made before the reservoir is complete, wind data over land must generally be used. Table 7-2 gives ratios of wind speed over land to those over water and may be used to correct observed wind to reservoir conditions. Waves are critical only when the reservoir is near maximum levels. Thus in selecting the critical wind speed for reservoirs subject to seasonal fluctuations,

<sup>1</sup> A graph for the solution of Eq. (7-4) in SI metric units is given in Appendix B-1.

**Table 7-2 Relationship between wind over land and that over water. (After Saville, McClendon, and Cochran)**

Fetch, mi (km)	0.5 (0.8)	1 (1.6)	2 (3.2)	4 (6.5)	6 (9.7)	8 (12.9)
$V_{\text{water}}/V_{\text{land}}$	1.08	1.13	1.21	1.28	1.31	1.31

only winds which can occur during the season of maximum pool levels should be considered. The direction of the wind and the adopted fetch must also be the same.

The height of the significant wave is exceeded about 13 percent of the time. If a more conservative design is indicated, a higher wave height may be chosen. Table 7-3 gives ratios of  $z'/z_w$  for waves of lower exceedance.

When a wave strikes a land slope, it will *run up* the slope to a height above its open-water height. The amount of run-up depends on the surface. Figure 7-16 shows the results of small-scale experiments<sup>1</sup> on smooth slopes and rubble mounds. Height of run-up  $z_r$  is shown as a ratio  $z_r/z_w$  and is dependent on the ratio of wave height to wavelength (wave steepness). Wavelength  $\lambda$  for deep-water waves may be computed from

$$\lambda = 5.12t_w^2 \text{ ft} \quad \text{or} \quad \lambda = 1.56t_w^2 \text{ m} \quad (7-5)$$

where the wave period  $t_w$  is given by

$$t_w = 0.46V_w^{0.44}F^{0.28} \quad (7-6)$$

For shallow-water waves other length relations are appropriate.<sup>2</sup> In metric units the coefficient of Eq. (7-6) becomes 0.32. The curves for rubble mounds represent extremely permeable construction, and for more typical riprap on earth embankments the run-up may be somewhat higher, depending on both the permeability and the relative smoothness of the surface.

<sup>1</sup> T. Saville, Jr., Wave Run-up on Shore Structures, *Trans., ASCE*, Vol. 123, pp. 139–158, 1958; R. Y. Hudson, Laboratory Investigation of Rubble-mound Breakwaters, *Trans. ASCE*, Vol. 126, Part IV, pp. 492–541, 1962.

<sup>2</sup> Shore Protection, Planning and Design, *Tech. Rept. 3*, 3d ed., U.S. Army Coastal Engineering Research Center, June, 1966.

**Table 7-3 Percentage of waves exceeding various wave heights greater than  $z_w$ . (After Saville, McClendon, and Cochran)**

$z'/z_w$	1.67	1.40	1.27	1.12	1.07	1.02	1.00
Percentage of waves $> z'$	0.4	2	4	8	10	12	13

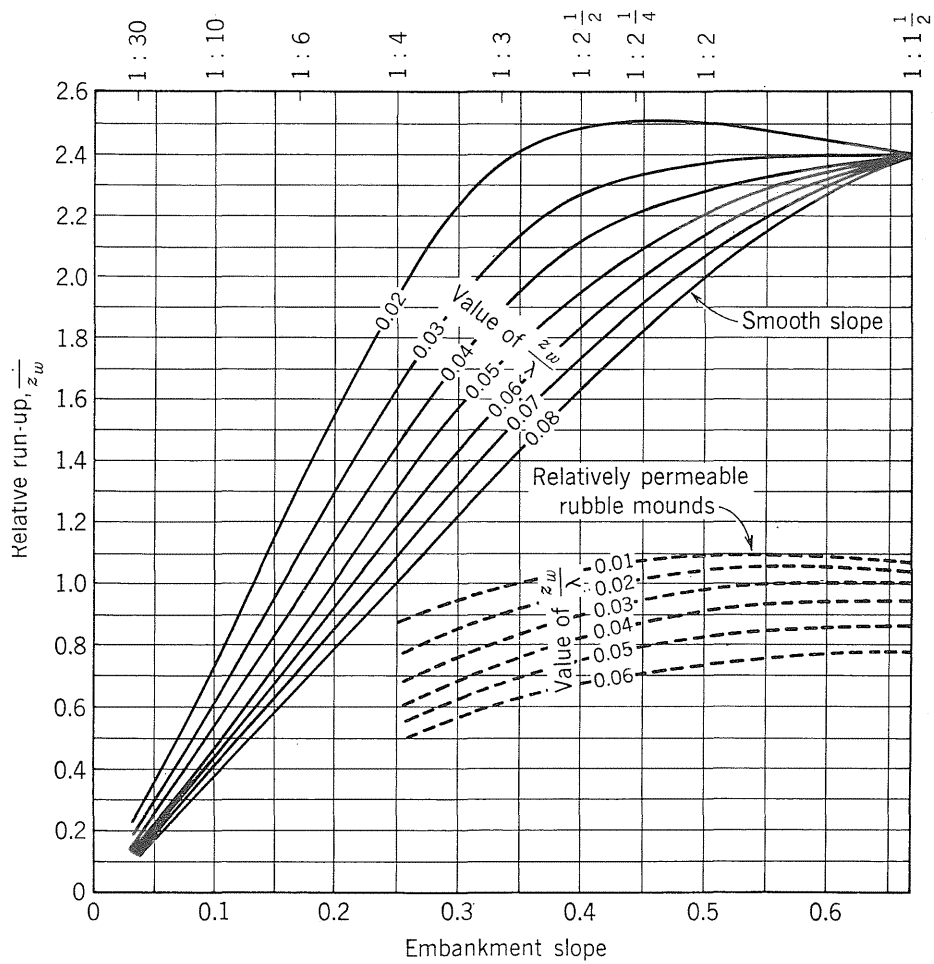


**Figure 7-16** Wave run-up ratios versus wave steepness and embankment slopes. (From Saville, McClendon, and Cochran)